Number of papers published in the Acdemic Year 2023-24

S.No	Title of paper	Name of the author/s	Department of the teacher	Name of journal	ISSN number	Link to the recognition in UGC enlistment of the Journal
1	Ultrasound-Assisted Synthesis of Defective MOF-801 for the Adsorptive Removal of Cationic Dyes	Dr. P. Kiran Kumar	Chemistry	Iranian Journal of Chemistry and Chemical Engineering	1021-9986	https://doi.org/10.30492/ijcce.2023.563407.5637
2	A Systematic Investigation on Elaeocarpus Sylvestris Leaf Extract Capped Cuo Nanoparticles as Reducing Agent and Their Antioxidant Activity.	Dr. J. Laxmi Mangamma	Chemistry	Colloid and polymer science	1435-1536	https://doi.org/10.1007/s00396-023-05159-1
3	Green generation of zinc oxide nanoparticles by flower extract of orange jasmine for photodegradation of pollutant and antimicrobial activities	Dr. J. Laxmi Mangamma	Chemistry	Biomass Conversion and Biorefinery	2190-6823	http://dx.doi.org/10.1007/s13399-024-05408-5
4	Facile green fabrication of magnetite nanoparticles using an aqueous flower extract of Murraya paniculata (L) Jack for an efficient removal of organic dye pollutant, antibacterial activities.	Dr. J. Laxmi Mangamma	Chemistry	Inorganic Chemistry Communications	1387-7003	https://www.sciencedirect.com/science/article/pii/S1387700324002739
5	Green synthesis of CuO nanorods using Jatropha podagrica leaf extract for dye degradation and antibacterial applications	Dr. J. Laxmi Mangamma	Chemistry	Nanotechnology for Environmental Engineering	2365-6387	https://doi.org/10.1007/s41204-024-00372-x
6	Green synthesis of CuO nanorods using Jatropha podagrica leaf extract for dye degradation and antibacterial applications	Sri G. Venkatesh	Chemistry	Nanotechnology for Environmental Engineering	2365-6387	https://doi.org/10.1007/s41204-024-00372-x
7	An eco-friendly and sustainable method for producing Fe3O4 nanoparticles using Jatropha podagrica leaf extract for efficient dye degradation and antibacterial uses	Sri G. Venkatesh	Chemistry	Colloid and polymer science	1435-1536	https://doi.org/10.1007/s00396-023-05187-x
8	A green and sustainable approach to the fabrication of ZnO nanoparticles via Jatropha podagrica leaf extract for effective dye degradation and antibacterial applications	Sri G. Venkatesh	Chemistry	Hybrid Advances	2773-207X	https://doi.org/10.1016/j.hybadv.2023.100110
9	Trace Elemental and Heavy Metal Levels in Frequently Consumed Local Vegetables of Three Chronic Kidney Disease-Prevalent Villages	Sri G. Narayana Murthy	Botany	Biological Trace Element Research	1559-0720	https://doi.org/10.1007/s12011-023-03761-6
10	Elemental levels in frequently consumed local leafy vegetables from three villages with chronic kidney disease prevalence,	Sri G. Narayana Murthy	Botany	Journal of Food Composition and Analysis	1096-0481	https://doi.org/10.1016/j.jfca.2023.105868
11	Analysis of a Wild Leafy Vegetable (Premnalatifolia Roxb.) Samples for Essential Trace Elements usingICP-MS Technique	Sri G. Narayana Murthy	Botany	International Journal of Scientific Engineering and Research (IJSER)	2347-3878	https://drive.google.com/file/d/16tW3--PDaNhMl7c-f6H2GQUeIDcRZRFv/view?usp=sharing

12	Kedarnath Agarwal ki kavitaon mein samajik yathaarth bodh	Dr. S. Suryavathi	Hindi	sahityaakaash		https://drive.google.com/file/d/1bRpRZ4m2CIzmIg1vS-gLRZrkU-_F0OO-/view?usp=drivesdk
13	Hindi upanyason mein kinnar jeevan ki traasadi	Dr. S. Suryavathi	Hindi	samshodhak	2394-5990	https://drive.google.com/file/d/1bRJHW1upb5T7apgQLAXydLwxeemHP5lb/view?usp=drivesdk
14	Screening of in-vitro Antidiabetic Potentials from the protein extracts of Stomopneustes variolaris	Dr V.Ratna Bharathi	Zoology	Uttara Pradesh Journal of Zoology	0256-971X	https://mbimph.com/index.php/UPJOZ/issue/view/261
15	Diversity and abundance of avifauna in Kondakarla Ava lake, Andhra Pradesh, India	Dr V.Ratna Bharathi	Zoology	Journal of emerging technologies and innovative research	2349-5162	https://www.jetir.org/trackauthorhome.php?a_rid=527120
16	MHD Hybrid Nanofluid Flow over a Stretching/Shrinking Sheet with Skin Friction: Effects of Radiation and Mass Transpiration	Sri A. Krishna Rao	Mathematics	Magnetochemistry	2312-7481	http://doi.org/10.3390/magnetochemistry9050118
17	Nonlinear Analysis of Cross Rolls of Electrically Conducting Fluid an Applied Magnetic Field with Rotation	Sri A. Krishna Rao	Mathematics	Processes	2227-9717	https://doi.org/10.3390/pr11071945
18	Orthonormal Eigenfunction Expansions for Iterative Bounded Value Problems on Time Scales	Sri A. Krishna Rao	Mathematics	Library Progress International	2320-317X	www.bpasjournals.com
19	Green synthesis of CuO nanorods using Jatropha podagrica leaf extract for dye degradation and antibacterial applications	Dr. P. Kiran Kumar	Chemistry	Nanotechnology for Environmental Engineering	2365-6387	https://doi.org/10.1007/s41204-024-00372-x

Ultrasound-Assisted Synthesis of Defective MOF-801 for the Adsorptive Removal of Cationic Dyes

Penmethsa, Kiran Kumar; Sunkara, Satya Veni*[+]

Department of Chemistry, Jawaharlal Nehru Technological University Kakinada (JNTUK) Kakinada-533003, Andhra Pradesh, INDIA

ABSTRACT: *Defective MOF-801 (Zirconium-fumarate metal-organic framework) was de novo synthesized using environmentally friendly ultrasound-assisted synthesis. The effect of the modulator on the crystallinity, morphology, density of missing linkers, pore volume, and the specific surface area (BET) of synthesized MOF-801 was studied using two modulators, acetic acid, and formic acid, in different quantities. The MOF-801 sample (MOF-801-100FA) was applied to investigate the adsorptive removal of two cationic dyes viz Crystal Violet (CV) and Methylene Blue (MB) from an aqueous solution in a single system. MOF-801-100FA was found to be more effective in removing MB dye than CV dye. The maximum equilibrium adsorption capacity was 30.4 mg/g and 18.9 mg/g with MB and CV dyes having an initial concentration of 50 mg/L. Langmuir and Freundlich isotherm models were the best fit for adsorption data based on linear regression analysis. The best kinetic model for the adsorption was pseudo-second-order kinetics (R^2 = 0.9975 for CV dye and 0.9998 for MB dye). The effect of dye concentration, contact time, MOF dose, and pH of dye solution on the adsorption of dyes was also investigated. The study showed that defective MOF-801-100FA is an efficient adsorbent for the removal of CV and MB dyes from aqueous solution*.

KEYWORDS: *MOF-801; Ultrasound-assisted; Cationic dyes; Crystal violet; Methylene blue; Adsorptive removal.*

INTRODUCTION

Dyes are widely used in paper, pharmaceutical, printing, food, textile, and plastic industries. During the dyeing process, lakhs of tons of dyes are lost to effluents. Dye-containing wastewater is harmful to the environment and threatens human and animal health. Therefore, removing the dyes from wastewater before releasing them into the water stream is an essential and challenging task. Although several methods are good at removing dyes from contaminated water, adsorptive removal is one of the best options due to ease of operation, high performance, and low cost of application. Many adsorbents were used for the adsorptive removal of dyes [1-5]. MOFs are employed for the removal of these dyes from aqueous solutions as they possess unique characteristics compared to conventional adsorbents [6-8].

*****To whom correspondence should be addressed.*

+ *E-mail: dr.satyapurna@gmail.com*

1021-9986/2023/10/3293-3305 13/$/6.03

Metal-Organic Frameworks (MOFs) are porous coordination polymers having three-dimensional network structures constructed by coordination-driven self-assembly of inorganic polynuclear clusters known as secondary building units (SBUs) and multitopic organic linkers. The modulator synthesis strategy is used for the synthesis of crystalline MOFs as in the absence of a modulator, mostly amorphous MOF is obtained. Usually, the synthesis of MOF takes place using higher amounts of monotopic acids as modulators which compete with linkers for the coordination of metal ions. It is well-known that a higher concentration of modulators induces structural defects in MOFs. The density of structural defects depends on the nature and concentration of the modulator used in the synthesis. Many of the synthesized MOFs are known to have structural defects. The study of structural defects is of paramount importance as they influence the properties of MOFs [9-12].

MOF-801 is one of the most widely studied metal-organic frameworks. It has exceptional hydrothermal stability. It is the smallest member of Zirconium-based metal-organic frameworks first reported by *Wißmann et al*., (2012) [13]. It is one of the commercially available Zirconium MOFs. Many potential applications of MOF-801 were reported in the literature. It was used in hydrogen and water storage [14], water harvesting from the air [15], photocatalytic degradation of methyl violet 2B [16], removal of fluoride [17], arsenite, and arsenate [18], Chromium (VI) ions [19, 20], nanoscale drug delivery [21], and separation of propylene/propane mixture [22].

Compared to traditional energy sources, ultrasound provides unusual reaction conditions wherein very high temperatures and pressure are generated quickly due to cavitation. There are several reports in the literature about the application of ultrasound irradiation for a large variety of syntheses [23-25]. Soon after the first ultrasound-assisted synthesis of MOFs reported by *Qiu et al*., (2008) [26], many reports were published in the literature about the successful preparation of nano/microporous MOFs. Only a few reports in the literature describe the ultrasonic-assisted synthesis of Zirconium-based MOFs [16, 27]

In the present study, a series of four defective MOF-801 samples were *de novo* synthesized using rapid and environmentally friendly ultrasonic-assisted synthesis. The *de novo* synthesized MOF samples were characterized by various characterization methods and their specific surface area (BET) values were determined. The role of two modulators on the density of missing linkers in the synthesized MOFs was analyzed based on the ThermoGravimetric Analysis (TGA) plots. It was found that the defective MOF-801-100FA carries a negative charge at basic pH and hence can accommodate the cationic dyes. The cationic dyes, MB and CV, possessing positive charge are selectively adsorbed through electrostatic interactions by MOF-801-100FA with a negative charge. The presence of these cationic dyes in aqueous solution is not desirable as they are biohazard substances, and potentially carcinogenic materials [28, 29]. The adsorptive removal of these dyes by defective MOF-801-100FA was investigated in detail using different adsorption isotherms and kinetic models.

EXPERIMENTAL SECTION

Materials and equipment

All the chemicals purchased from Sigma Aldrich were used as such without purification. Powder X-Ray Diffraction (PXRD) patterns were recorded using monochromatized Cu Kα radiation (λ = 1.5406 Å) on a Bruker D8 Advance diffractometer operated at 40 kV and 40 mA. Field-Emission Scanning Electron Microscopy (FE-SEM) images were obtained on a Supra55 Zeiss instrument. Scanning Electron Microscopy- Energy Dispersive X-ray spectroscopy (SEM-EDX) was recorded at 10 kV acceleration voltage to determine the elemental composition of MOF samples. The Fourier transform infrared (FT-IR) spectra were recorded on an Agilent Cary 660 instrument in the transmission mode (in the 400 cm^{-1} - 4000 cm^{-1} range). ThermoGravimetric Analysis (TGA) measurement was recorded in the air using Perkin Elmer STA 6000 thermal analyzer. Specific surface area (BET) values are obtained from Nitrogen adsorption-desorption isotherms recorded using a BELSORP analyzer at -196 °C. ANM USC 300 Ultrasonic bath was used for ultrasonication. The absorbance of dye solutions in the visible region was determined using a Shimadzu UV-2450 spectrophotometer. The pH of the dye solutions was altered using 0.1 M HCl and 0.1 M NaOH solutions. A digital pH meter (Model 335, Systronics) was used to determine the pH of the solutions.

Synthesis of defective MOF-801 samples

A series of four defective MOF-801 samples were synthesized under optimum reaction conditions at room temperature

Table 1: Optimum reaction conditions for the synthesis of defective MOF-801 samples using ultrasonication

MOF sample	$ZrOCl_2.8H_2O$ (mmol)	Fumaric acid (mmol)	Acetic acid(mL)	Formic acid (mL)	DMF (mL)	Time(h)
MOF-801-70FA	1.5	1.5	0	4.2	12	4
MOF-801-100FA	1.5	1.5	0	6.0	12	4
MOF-801-70AA	1.0	1.0	4.2	0	8	4
MOF-801-100AA	1.0	1.0	6.0	0	8	4

using different amounts of formic acid/ acetic acid modulators as presented in Table 1. MOF-801 samples synthesized with 70 and 100 equivalents of acetic acid with respect to the $ZrOCl_2.8H_2O$ (metal precursor) were named MOF-801-70AA and MOF-801-100AA respectively and with 70 and 100 equivalents of formic acid were named MOF-801-70FA and MOF-801-100FA respectively.

$ZrOCl_2.8H_2O$ was dissolved in DMF, then fumaric acid was added to the solution. After that respective amount of formic acid/acetic acid was added. The reaction mixture was placed in the ultrasonic bath for 4 hours. Ultrasonic irradiation having a frequency of 40 kHz with a power of 150 watts was applied at room temperature. The temperature of the reaction mixture during sonication was monitored and was found to be less than 60 °C even after the reaction time of 4h. The synthesis of MOF-801-100FA was outlined in Scheme 1.

After cooling down to room temperature, the as-synthesized white crystalline MOFs were recovered by filtration. The crystalline materials were washed three times with 10 mL of DMF followed by ethanol (3 x 10 mL) and acetone (3 x 10 mL). The materials were dried overnight at room temperature and then activated by heating at 100 °C under vacuum for 8 h.

Adsorption study

Removal of two cationic dyes, MB, and CV, from single dye solutions by adsorption, was studied using as-synthesized MOF-801-100FA as the adsorbent. The adsorption of MB and CV dyes from aqueous solution in a single system was investigated using the dye solutions having different initial concentrations, varying the pH of dye solutions, taking different MOF doses, and varying the contact time of MOF with the dye solutions. Adsorption studies were carried out at a temperature of 28 ± 2 °C. Standard solutions of the dyes were prepared by dissolving 1000 mg of the dye in 1000 mL of distilled water. A set of standard solutions for each dye was prepared using the stock solutions. The absorbance maximum of dye solutions at 590 nm for CV and 665 nm for MB was measured and calibration curves were plotted for each of the dye solutions. 50 mL of each dye solution in a single system was used to study the adsorption. The dye solution and MOF-801-100FA were mixed using a magnetic stirrer at 300 rpm. The adsorption efficiency, Q_e (mg/g), was calculated using Equation (1):

$$Q_e = \frac{V\,(C_o - C_e)}{M}, \quad (1)$$

Where C_o (mg/L) was the initial dye concentration, and C_e (mg/L) was the dye concentration at equilibrium. V (L) was the volume of the dye solution, and M (g) is the mass of MOF-801-100FA. 20 mg of MOF-801-100FA was added to each of the 50 mL dye solutions having a concentration of 5, 10, 20, 30, 40, and 50 mg/L. After the time interval of 12 hours, the absorbance of each solution was measured and the C_e values were determined from the absorbance values using the calibration curves.

The percentage removal of dyes was calculated using Equation (2):

$$\text{Percentage removal} = \frac{(C_o - C_e)}{C_o} \times 100\%, \quad (2)$$

Adsorption isotherms were described using Freundlich, Langmuir, and Temkin adsorption isotherm models.

Freundlich adsorption isotherm is expressed as Equation (3):

$$\ln Q_e = \ln K_F + \frac{1}{n} \ln C_e \quad (3)$$

Here, K_F is the Freundlich constant, and n is the constant whose value indicates the favourability of the adsorption process.

The value of 1/n provides information about the usability of the adsorbent over the concentration range of the dye solution.

Langmuir isotherm is represented by Equation (4):

$$\frac{C_e}{Q_e} = \frac{C_e}{Q_m} + \frac{1}{Q_m K_L} \quad (4)$$

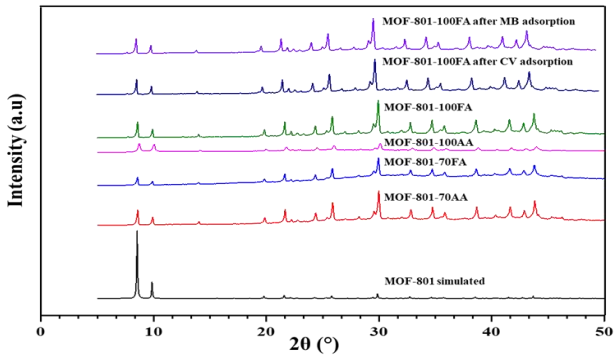

Fig. 1: PXRD patterns of MOF-801 simulated, MOF-801-70AA, MOF-801-70FA, MOF-801-100AA, MOF-801-100FA and MOF-801-100FA after CV adsorption, and MOF-801-100FA after MB adsorption

Here, Q_e is the maximum adsorption capacity (mg/g) of the adsorbent (MOF-801-100FA) with the highest concentration of dye (100 mg/L) used in the adsorption experiment, and K_L is the Langmuir adsorption constant.
Temkin isotherm is given by Equation (5):

$$Q_e = \frac{RT}{B_T} \ln C_e + \frac{RT}{B_T} \ln K_T \quad (5)$$

Here, B_T is the adsorption heat constant (J) and K_T is the equilibrium binding constant (L/ mg)

Adsorption kinetics

For the kinetic study, 50 mL of CV or MB dye solution having a concentration of 5 mg/L and 20 mg of MOF-801-100FA as adsorbent was used. At the desired time (t), the dye solution was withdrawn and the absorbance was measured. Q_t (mg/g), dye amount adsorbed at time t, was obtained by Equation (6):

$$Q_t = \frac{V(C_o - C_t)}{M} \quad (6)$$

Here, C_t (mg/L) is the dye concentration at time t (min).
To study the kinetics in the adsorption process, three kinetic models, pseudo-first-order, pseudo-second-order, and Intraparticle diffusion were used. These three models are expressed as Equations (7), (8), and (9):
Pseudo-first-order kinetics,

$$\ln(Q_e - Q_t) = \ln Q_e + k_1 t \quad (7)$$

Pseudo-second-order kinetics,

$$\frac{t}{Q_t} = \frac{1}{k_2 Q_e^2} + \frac{1}{Q_e} t \quad (8)$$

Intraparticle diffusion kinetics,

$$Q_t = k_i t^{1/2} + C \quad (9)$$

Here, k_1 (min^{-1}), k_2 (g/mg min) and k_i ($mg/g\ min^{1/2}$) are the rate constants for pseudo-first-order, pseudo-second-order, and intraparticle diffusion respectively. C is the intraparticle diffusion constant.

Desorption of MOF

The MB dye and CV dye adsorbed-MOFs were separated from the respective dye solutions by centrifugation (6000 rpm for 20 min). Thereafter, the MOFs were washed with methanol several times until no violet color in the methanol solution while washing the CV-loaded MOF and no blue color in methanol solution while washing the MB-loaded MOF was observed. Finally, the recovered MOFs were activated by drying under vacuum at 100 °C for 8 h. The adsorption-desorption process was performed for five consecutive cycles.

RESULTS AND DISCUSSION

Characterization of defective MOF-801 samples

The as-synthesized crystalline MOFs were characterized using different characterization techniques. The Powder X-Ray Diffraction (PXRD) patterns of the synthesized materials were compared with simulated patterns of MOF-801 in Fig. 1 [30]. The synthesized materials' peaks fit well with the simulated MOF-801. The characteristic peaks positioned around $2\theta = 8.5^o$ and 9.8^o in the PXRD patterns indicate the successful synthesis of MOF-801 samples. The presence of sharp peaks suggests that highly crystalline MOF-801 samples were obtained. The effect of the modulator's type and concentration on the MOF's crystallinity was evident in Fig.1. With the increase in the concentration of the formic acid modulator from 70 equivalents to 100 equivalents, there is an increase in the intensity of the peaks indicating the increase in the crystallinity of the MOF. Such a trend is not observed with the acetic acid modulator. Under identical reaction conditions, the highest crystallinity was observed with 70 equivalents of acetic acid in MOF-801-70AA amongst MOF-801-70AA, and MOF-801-100AA. Among the synthesized MOFs, sharp and high-intensity peaks are observed in MOF-801-100FA. A comparison between PXRD patterns before and after adsorption by MOF-801-100FA indicates that the MOF framework was intact even after the adsorption of CV and MB dyes.

The morphology of the samples was characterized by FE-SEM. The FE-SEM images were presented in Fig. 2. With the increase in the concentration of acetic acid,

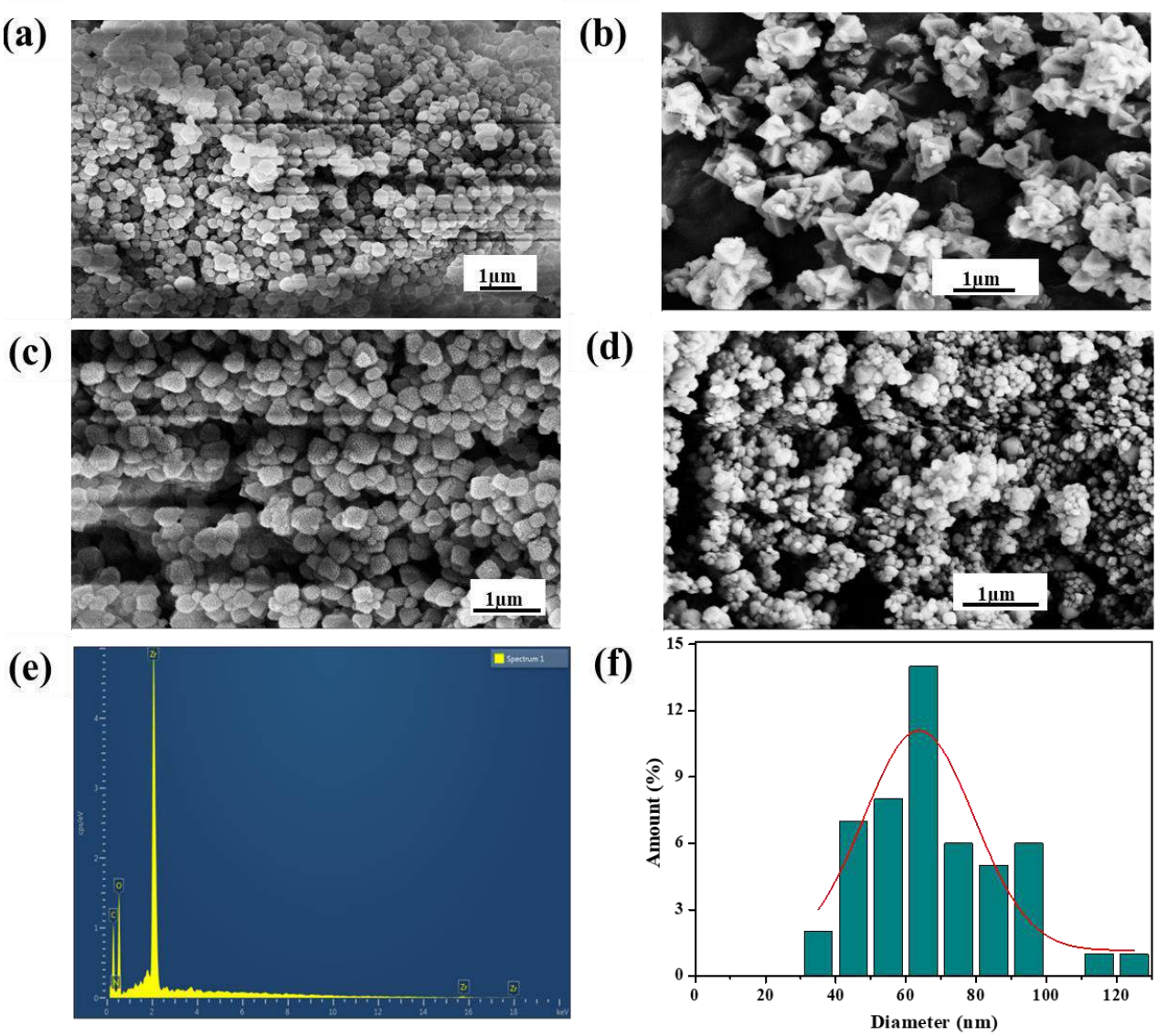

Fig. 2: FE-SEM images of MOF-801-70AA (a), MOF-801-100A (b), MOF-801-70FA (c), MOF-801-100FA (d), SEM-EDX spectrum of MOF-801-100FA (e), and Particle size distribution of MOF-801-100FA particles from SEM images (f)

an increase in the size of the particles was observed. Whereas the particle size decreased with the increase in the concentration of formic acid modulator from 70 to 100 equivalents. The SEM-EDX spectrum of MOF-801-100FA was given in Fig. 2. Zirconium (Lα= 2.042 keV), carbon (kα = 0.277 keV), and oxygen (kα = 0.525 keV) were identified in the spectrum based on the energies of the emitted X-rays from these elements. Particles of MOF-801-100FA are cubic with an average diameter of 68.1 nm as determined from the size of 50 particles using ImageJ. A histogram fitted with Gaussian distribution of the size of the MOF-801-100FA particles was presented in Fig. 2.

The FT-IR spectra of the MOF-801 samples were found in Fig. 3. The bands at 491 cm^{-1} and 660 cm^{-1} could be assigned to the asymmetric stretching vibration of Zr-(OC) and bending vibration of $Zr_6(OH)_4O_4$ cluster respectively. Absorption bands observed at 796 cm^{-1}, 987 cm^{-1}, and 1210 cm^{-1} could be assigned to C-H vibrations. Strong absorption bands observed at 1402 cm^{-1} and 1578 cm^{-1} were ascribed to the symmetrical stretching and asymmetrical stretching vibrations of the carboxylic group of the fumaric acid linker [31].

Nitrogen adsorption-desorption isotherms of activated MOF-801 samples were presented in Fig. 4. All the isotherms

Table 2: Comparison of the specific surface areas determined from N_2 sorption isotherms of MOF-801samples

MOF-801 sample	BET area (m^2/g)	Pore volume (cm^3/g)	Mean pore diameter (Å)
MOF-801-100FA	699	0.31	17.86
MOF-801-70FA	578	0.39	26.8
MOF-801-100AA	224	0.13	23.9
MOF-801-70AA	234	0.20	34.7

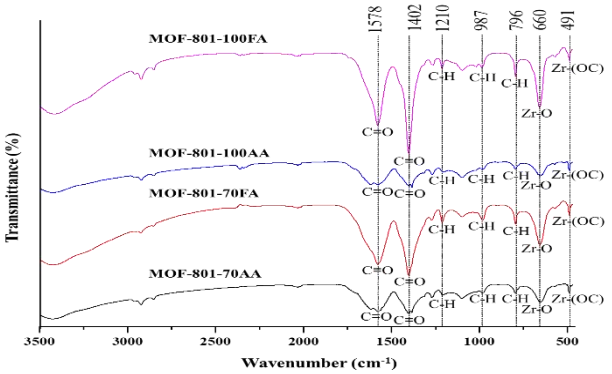

Fig. 3: FT-IR spectra of MOF-801-70AA, MOF-801-70FA, MOF-801-100AA, MOF-801-100FA

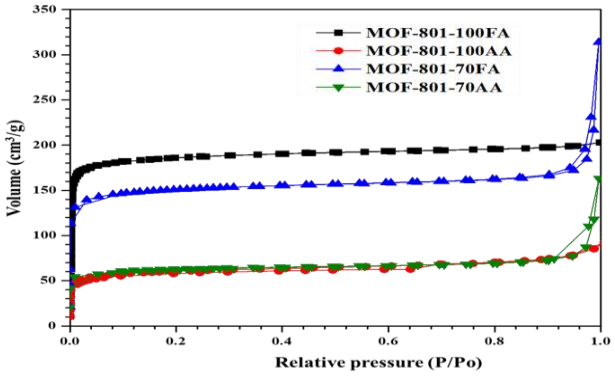

Fig. 4: Nitrogen adsorption-desorption isotherms of MOF-801-70AA, MOF-801-70FA, MOF-801-100AA, and MOF-801-100FA

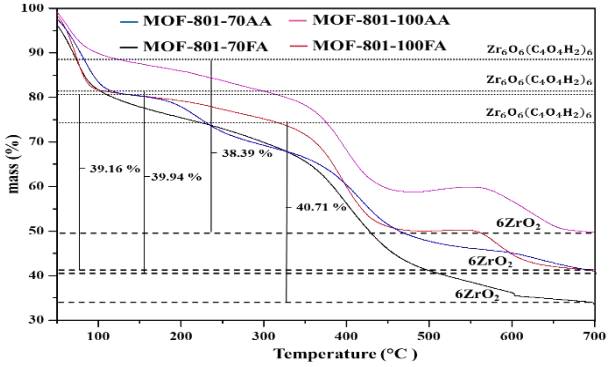

Fig. 5: The TG curves of MOF-801-70AA, MOF-801-70FA, MOF-801-100AA, and MOF-801-100FA

are type-1 based on IUPAC classification. They indicate that the materials are microporous. Among the MOF-801 samples, MOF-801-100FA has the highest specific surface area (BET area) of 699 m^2/g. The BET area, pore volume, and mean pore diameter of the MOF-801 samples were presented in Table 2.

Thermogravimetric analysis curves of the defective MOF-801 samples were presented in Fig. 5. All the synthesized MOFs exhibited almost similar shapes of TGA curves. Either Acetic acid or formic acid modulator has produced no appreciable changes in the shapes of TGA curves. As reported in the literature there are three distinct mass loss steps in the TGA curves [14]. In the first step occurring below 120 °C mass loss was due to the evaporation of water molecules occluded in the pores. The mass loss in the second step occurring at 250-400°C could be attributed to the decomposition of the linker molecules. The last step occurring at around 550-680 °C can be assigned to the decomposition of carboxylate ions coordinated to zirconium cations releasing carbon dioxide. Assuming that the mass loss occurring between 250 and 680 °C is due to the decomposition of the linker, the formation of ZrO_2 as the final product after heating of MOF-801 in the air is given by the following Equation (10):

$$Zr_6O_6(C_4O_4H_2)_6 + 18O_2 \rightarrow 6ZrO_2 + 24CO_2 + 6H_2O \quad (10)$$

Based on the stoichiometry of the Equation, from one formula unit of $Zr_6O_6(C_4O_4H_2)_6$, six moles of ZrO_2 are obtained. Assuming that 100 g of initial $Zr_6O_6(C_4O_4H_2)_6$ was taken, the mass of the solid residue ZrO_2 should be 55.7 g corresponding to a relative mass loss of 44.3%. The recorded mass losses for the MOF samples were below the theoretical value. For MOF-801-70AA, MOF-801-100AA, MOF-801-70FA and MOF-801-100FA the observed mass losses were 39.94%, 38.39%, 40.71% and 39.16% respectively. According to the recent study on defective MOF-801, the deviation of the mass loss from the theoretical value in the region of 250 and 680 °C is proportional to the number of missing linkers in its structure [32].

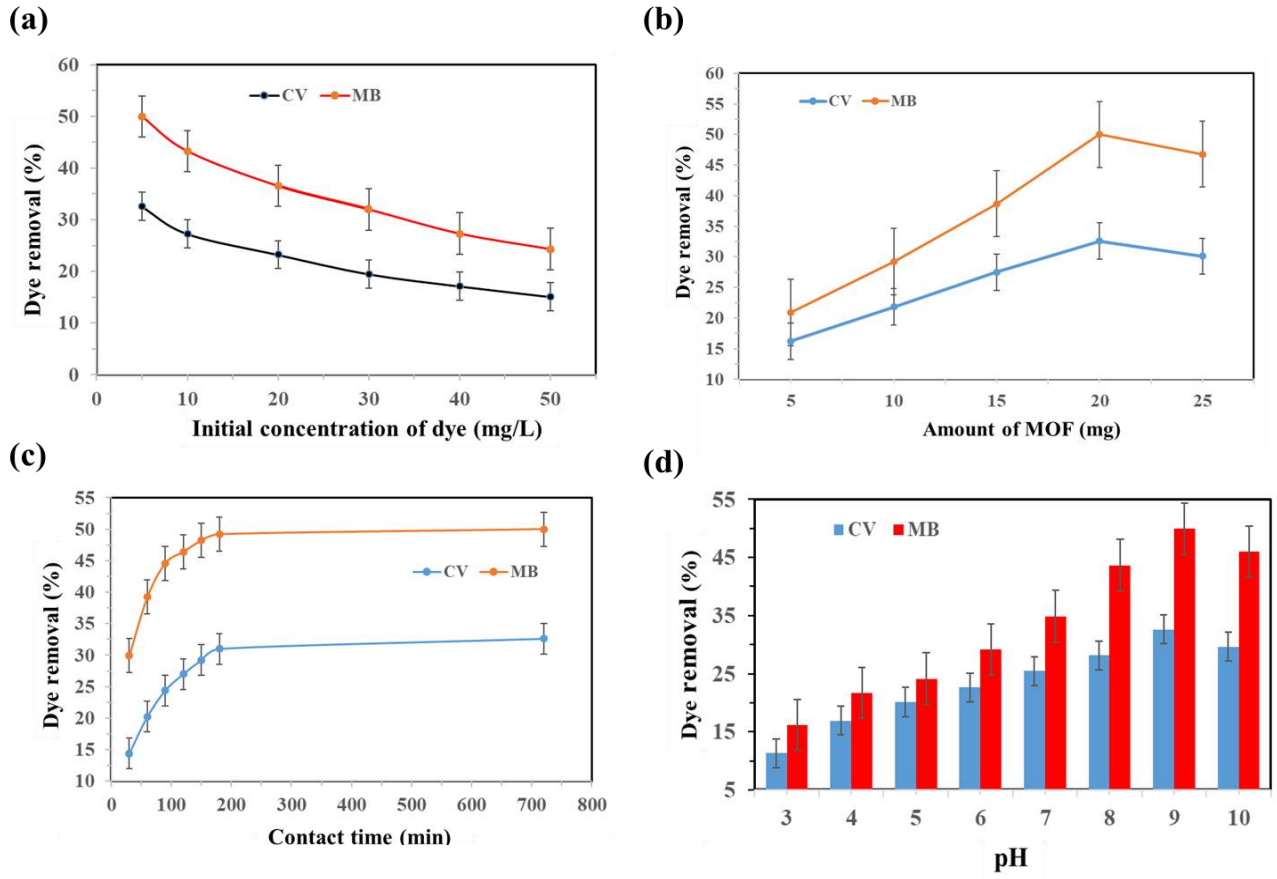

***Fig. 6: Factors affecting the adsorption of CV and MB dyes onto MOF-801-100FA. The initial concentration of dye (a), amount of MOF-801-100FA* (b), *contact time* (c), *and pH of the dye solution* (d)**

Applying the same analogy to the present study suggests that the synthesized MOFs have missing-linker defects. Other reported studies also support our findings that there are missing-linker defects in the *de novo* synthesized MOF-801 frameworks [9, 33]. From the mass loss changes, it is evident that there were significant changes in the density of missing linkers with the amount of acetic acid and formic acid modulators used in the synthesis of MOF-801.

Effect of initial dye concentration

Taking 20 mg of MOF-801-100FA adsorbent, the adsorption experiments were carried out by varying the initial concentration of CV and MB dyes in the range of 5-50 mg/L. The equilibrium time for adsorption was 12h. The effect of the initial concentration of dyes on the adsorption by MOF-801-100FA was shown in Fig. 6(a). The percentage removal of CV dye decreased from 32.6% to 15.10% and MB dye from 50% to 24.32% with an increase in the initial concentration of dye from 5 mg/L to 50 mg/L. As reported in the earlier study, the decrease in the percentage removal of dye can be attributed to the saturation of adsorption sites with the initial dye concentration of 5 mg/L [34].

Effect of MOF-801-100FA dose

The effect of the MOF-801-100FA dose on the percentage removal of CV and MB dyes in the adsorption experiments was shown in Fig. 6(b). Adsorption experiments were conducted by adding a MOF-801-100FA dose of 5,10,15,20, and 25 mg to each 50 mL of 5 mg/L CV and MB dye solutions. Maximum dye removal percentage was achieved with 20 mg of MOF dose as it has a large surface area. The percentage removal of CV dye increased from 16.21% to 32.6% and MB dye increased from 20.9% to 50% with the increase in the dose of MOF-801-100FA from 5 mg to 20 mg.

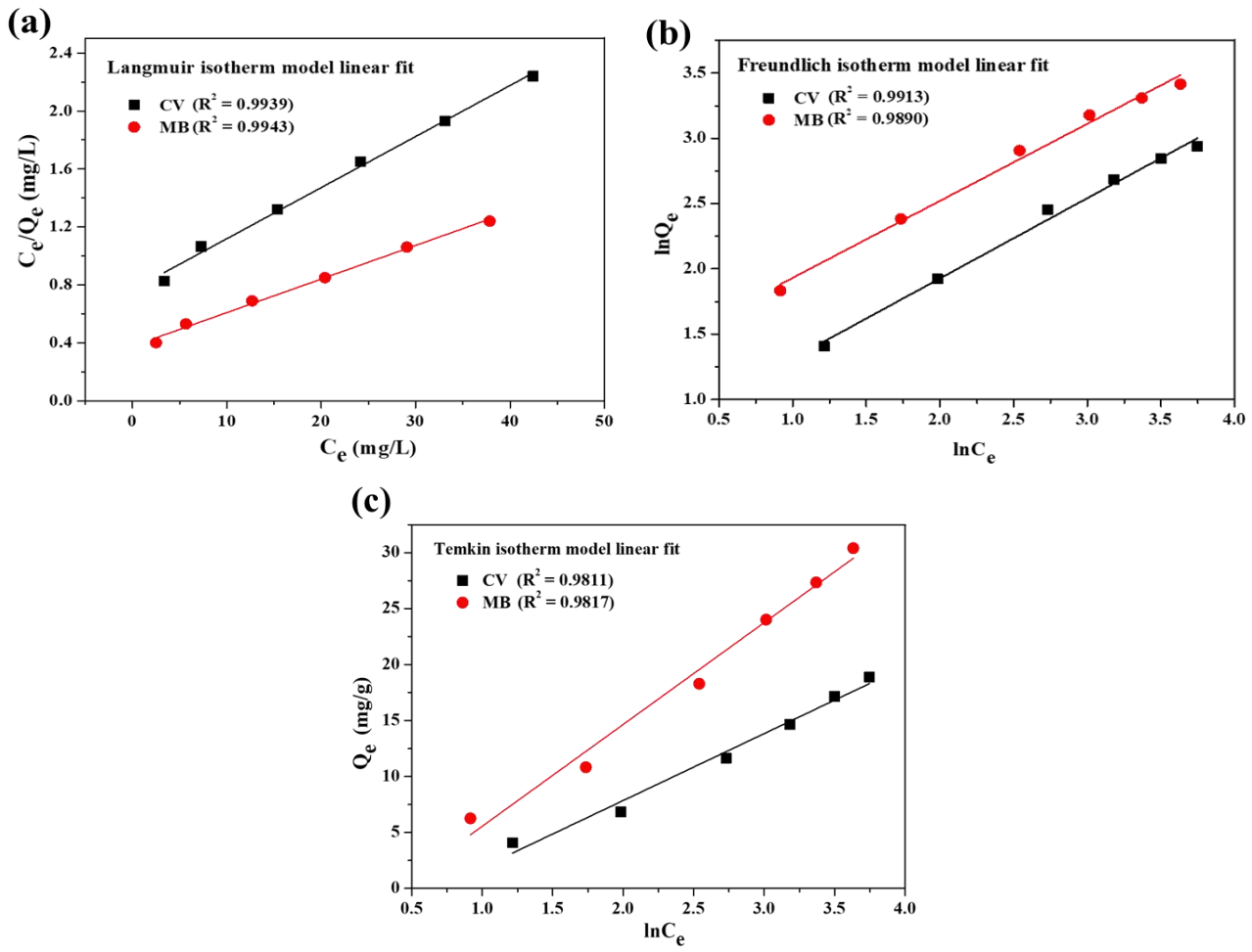

Fig. 7: Plot of linear fitting Langmuir isotherm model (a), Freundlich isotherm model* (b)*, and Temkin isotherm model* (c) *for CV and MB adsorption

Effect of contact time

The effect of contact time on the adsorption of CV and MB dyes was studied by fixing the maximum contact time at 12 hours. The variation in the percentage of dye removal with the contact time was shown in Fig. 6(c). The maximum CV and MB dye removal percentage achieved was found to be 32.6% and 50% respectively. After an initial rise in the percentage of dyes adsorbed onto the MOF-801-100FA surface, there was a slowdown in the percentage of dyes adsorbed with contact time. The extent of adsorption of dyes decreases with an increase in contact time due to the decrease in the number of active sites on the surface of MOF-801-100FA.

Effect of pH

The effect of pH of the dye solutions on the adsorptive removal of dyes by the MOF-801-100FA was studied by performing the adsorption experiments with 50 ml of CV and MB dyes having a concentration of 5 mg/L, and 20 mg of MOF-801-100FA at a temperature of 30 ± 2 °C for a contact time of 12 hours. The change in percentage removal of CV and MB dyes by MOF-801-100FA with the change in the pH of dye solutions from 3.0 to 10.0 was shown in Fig. 6(d). An increase in the percentage removal with the increase in pH of the dye solutions from 3.0 to 9 was observed. Maximum adsorption of dyes was observed at a pH of 9.0. The isoelectric point of MOF was found to be 6.5. Above this pH value, the MOF surface carries a negative charge and readily binds with the cationic dyes, CV and MB, existing in positive form through electrostatic interactions. The possible mechanism for the adsorption of CV and MB dyes by MOF adsorbent is via electrostatic interaction [6, 35].

Table 3: Isotherm parameters for adsorption of CV and MB dyes on MOF-801-100 FA

Dye	$Q_{e,exp}$ (mg/g)	Freundlich isotherm			Langmuir isotherm			Temkin isotherm		
		n	K_F (mg/g)	R^2	Q_m (mg/g)	K_L (L/mg)	R^2	B_T (J)	K_T (L/mg)	R^2
CV	18.88	2.01	0.6991	0.9913	28.37	0.0460	0.9939	421	0.50	0.9811
MB	37.84	1.69	3.83	0.9890	43.14	0.0614	0.9943	277	0.68	0.9817

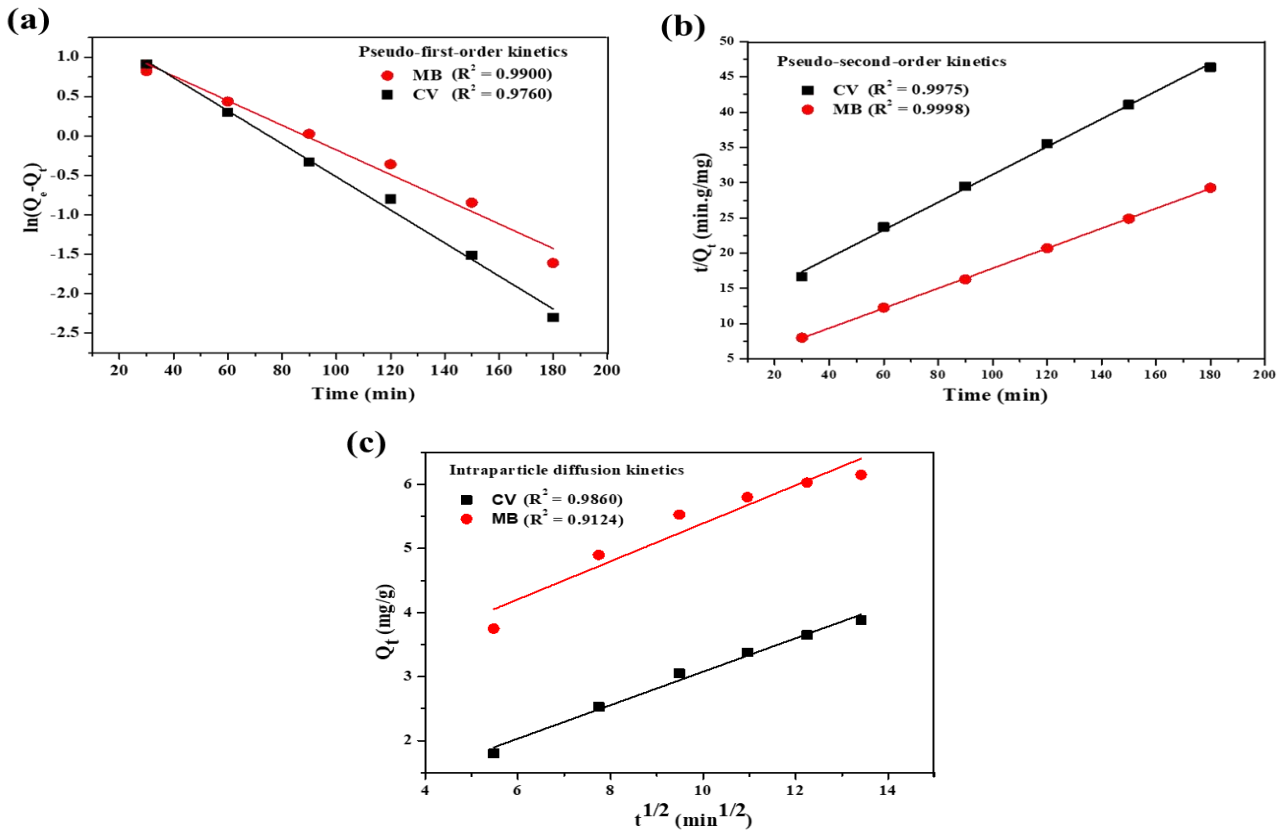

Fig. 8: Plot of linear fitting of pseudo-first-order kinetics model* (a), *pseudo-second-order kinetics model* (b), *and Intraparticle diffusion kinetics model* (c) *for CV and MB adsorption

Adsorption isotherms

Three adsorption isotherm models, Freundlich, Langmuir, and Temkin were used to determine the adsorption performance of MOF-801-100FA. Adsorption isotherm models were applied to get information about the mechanism of adsorption, evaluation of the performance of the adsorption process, and capacity of MOF-801-100FA as an adsorbent. Equations (3), (4), and (5) were used to represent these three adsorption isotherms. The isotherm data obtained for CV and MB dyes was fitted to the three models to determine the best fit for the adsorption data. Linear plots for Freundlich, Langmuir, and Temkin isotherms were shown in Fig. 7. The adsorption isotherm parameters for the three models were given in Table 3.

Based on the correlation coefficient (R^2) values, the Langmuir model (R^2 = 0.9939 for CV dye adsorption, and 0.9943 for MB dye adsorption) was the best fit compared to Freundlich (R^2 = 0.9913 for CV dye adsorption, and 0.9890 for MB dye adsorption) and Temkin (R^2 = 0.9811 for CV dye adsorption, and 0.9817 for MB dye adsorption) models.

The separation factor (R_L), an important characteristic of the Langmuir adsorption isotherm, was calculated using Equation (11):

$$R_L = \frac{1}{1+K_L C_o} \quad (11)$$

Here, C_o (mg/L) is the highest initial dye concentration and K_L is the Langmuir constant.

Table 4: Kinetic parameters for adsorption of CV and MB dyes on MOF-801-100 FA

Dye	C_o(mg/L)	$Q_{e,exp}$(mg/g)	Pseudo-first-order model			Pseudo-second-order model			Intraparticle diffusion model		
			$Q_{e,cal}$ (mg/g)	k_1(min^{-1})	R^2	$Q_{e,cal}$(mg/g)	k_2 (g/mg. min)	R^2	k_i (mg/g. $min^{1/2}$)	C	R^2
CV	5	4.08	4.003	0.0156	0.9760	5.08	0.00338	0.9975	0.2612	0.47	0.9860
MB	5	6.25	4.850	0.0210	0.9900	7.06	0.0054	0.9998	0.2965	2.42	0.9124

Table 5: Comparison with other MOF adsorbents for adsorption of CV and MB dyes

Dye	MOF adsorbent	Adsorption capacity (mg/g)	Reference
CV	MOF-801-100FA	18.90	Present work
	Fe-BDC	9.29	[34]
	$Cu_3(BTC)_2$	0.29	[37]
	H_2dtoaCu	165.83	[38]
	IFMC-2	2.40	[39]
	Cd-based	221.00	[40]
	Zn-based	54.50	[41]
	BUT-29	832.00	[42]
MB	MOF-801-100FA	30.40	Present work
	MIL-101(Fe)	58.82	[43]
	UiO-66-NO_2	41.70	[44]
	UiO-66-10%Ca	50.25	[45]
	MOF-235	187.00	[46]
	Fe-BDC MOF	8.65	[47]
	UiO-66	91.00	[48]
	ZIF-8	522.95	[49]

With the highest concentration of dye (50 mg/L) used in the adsorption experiment, the calculated value of R_L for CV was 0.303, and 0.246 for MB. The adsorption process was favorable as the obtained R_L values were between 0 and 1 [34]. From the linear plots of the Freundlich Isotherm model, the value of 1/n was found to be 0.497 for CV dye and 0.592 for MB dye. The obtained 1/n values indicate that the adsorbent applies to the entire CV and MB dye concentrations range. However, due to the small difference in R^2 values in Langmuir and Freundlich models, it is not clear whether adsorption occurred on a homogeneous or heterogeneous surface. The results obtained from linearized isotherm models are inconclusive. To overcome the limitations of the linearized models and to select the optimum adsorption isotherm model, nonlinear regression analysis must be applied [36].

Kinetics studies

Adsorption data were analyzed using three kinetic models, pseudo-first-order, pseudo-second-order, and intraparticle diffusion. These three models were represented by Equations (7), (8), and (9). The linear plots for the three models were presented in Fig. 8, and their corresponding kinetic parameters were listed in Table 4. Linear regression coefficient (R^2)

Values indicate that the pseudo-second-order kinetic model is the best fit for the adsorption data. The value of R^2 (0.9975 for CV dye adsorption, and 0.9998 for MB dye adsorption) for the pseudo-second-order kinetic plot is higher than the R^2 values of linear plots of the other two kinetics models. The pseudo-second-order rate constants were determined to be 3.378 x 10^{-3} g/mg min and 5.40 x 10^{-3} g/mg min for the adsorption of CV dye and MB dyes respectively. The results indicate that the adsorptive removal of CV and MB dyes from aqueous solution by MOF-801-100FA was due to chemisorption. The adsorption capacity of MOF-801-100FA for the adsorption of CV and MB dyes was compared with other MOF adsorbents as shown in Table 5.

Recyclability of adsorbent

To assess the recyclability of MOF-801-100FA, a desorption and regeneration experiment was conducted. A slight decrease in the adsorption capacity of MOF-801-100FA was observed with increasing cycle number. After five consecutive adsorption-desorption cycles, 81% of the initial MB dye removal efficiency and 74% of the initial CV dye removal efficiency was retained. The study shows that MOF-801-100FA has good recycling ability and could be used as a potential adsorbent for the removal of MB and CV dyes from aqueous solution.

CONCLUSIONS

In the present work, we demonstrated the energy-efficient and green *de novo* synthesis of defective MOF-801 samples using ultrasonication at room temperature. Among the four synthesized samples, MOF-801-100FA was highly crystalline with high specific surface area (BET area) of 699 m^2/g. TGA analysis revealed that the MOF-801-100FA sample was defective due to the missing linkers in the framework structure. The MOF was tested to remove two cationic dyes, CV and MB, from the aqueous solution by adsorption. The obtained adsorption data best fit the Langmuir and Freundlich isotherm models. Nonlinear regression analysis must be used to determine the optimum adsorption isotherm as the results obtained from linearized isotherm models are inconclusive. The adsorption kinetics was best described by the pseudo-second-order kinetics model. The MOF was found to have a higher adsorption efficiency toward MB dye. The maximum equilibrium adsorption capacity was 30.4 mg/g and 18.9 mg/g with MB and CV dyes having an initial concentration of 50 mg/L. The maximum adsorption of dyes was observed at a pH of 9. MOF-801-100FA was regenerated for the removal of CV and MB dyes with significant efficiency after five cycles. It is a promising adsorbent for the removal of these cationic dyes from aqueous solution.

Received : Dec.14, 2022 ; Accepted : Apr.17, 2023

REFERENCES

[1] Dutta S., Gupta B., Srivastava S.K., Gupta A.K., Recent Advances on the Removal of Dyes from Wastewater Using various Adsorbents: A Critical Review, *Materials Advances*, **21**: 4497-4531 (2021).

[2] Liang H., Hu X., Preparation of Magnetic Cellulose Nanocrystal- Modified Diatomite for Removal of Methylene Blue from Aqueous Solutions, *Iran. J. Chem. Chem. Eng. (IJCCE)*, **41(3)**: 787-798 (2022).

[3] Sakha P., Mahmoud Z., Tohid S.T., Mahdi K., Neural Network, Isotherm, and Kinetic Study for Wastewater Treatment Using Populus alba's Prund Material, *Iran. J. Chem. Chem. Eng. (IJCCE)*, **40(6)**: 1868-1881 (2021).

[4] Mohammad-Rezaei R., Khalilzadeh B., Rahimi F., Moradi S., Shahlaei M., Derakhshankhah H., Jaymand M., Simultaneous Removal of Cationic and Anionic Dyes from Simulated Industrial Effluents Using a Nature-Inspired Adsorbent, *Environ. Res.*, **214(3)**: 113966 (2022).

[5] Mohammad-Rezaei R., Khalilzadeh B., Rahimi F., Rezaee P., Arab S.S., Derakhshankhah H., Jaymand M., Simultaneous Removal of Cationic Dyes from Simulated Industrial Wastewater Using Sulfated Alginate Microparticles, *J. Mol. Liq.*, **363**: 119880 (2022).

[6] Beydaghdari M., Saboor F.H., Babapoor A., Karve V.V., Asgari M., Recent Advances in MOF-Based Adsorbents for Dye Removal from the Aquatic Environment, *Energies.*, **15(6)**: 2023 (2022).

[7] Fu M., Deng X., Wang S-Q., Yang F., Lin L-C., Zaworotko M.J., Dong Y., Scalable Robust Nano-Porous Zr-Based MOF Adsorbent with High-Capacity for Sustainable Water Purification, *Sep. Purif. Techno*., **288**: 120620 (2022).

[8] Au V.K-M., Recent Advances in the Use of Metal-Organic Frameworks for Dye Adsorption, *Front. Chem*., **8**: 70821 (2020).

[9] Xiang W., Zhang Y., Chen Y., Liu C-J., Tu X., Synthesis, Characterization, and Application of Defective Metal-Organic Frameworks: Current Status and Perspectives, *J. Mater. Chem. A*., **8**: 21526-21546 (2020).

[10] Choi J., Lin L-C., Grossman J.C., Role of Structural Defects in the Water Adsorption Properties of MOF-801, *J. Phys. Chem. C*., **122**: 5545-5552 (2018).

[11] Bai Y., Dou Y., Xie L-H, Rutledge W., Li J-R., Zhou H-C., Zr-Based Metal-Organic Frameworks: Design, Synthesis, Structure, and Applications, *Chem. Soc. Rev*., **45**: 2327-2367 (2016).

[12] Cao Y., Mi X., Li X., Wang B., Defect Engineering in Metal-Organic Frameworks as Futuristic Options for Purifica- Tion of Pollutants in an Aqueous Environment, *Front. Chem*., **9**: 673738 (2021).

[13] Wißmann G., Schaate A., Lilienthal S., Bremer I., Schneider A.M., Behrens P., Modulated Synthesis of Zr-Fumarate MOF, *Microporous Mesoporous Mater*., **152**: 64-70 (2012).

[14] Butova V.V., Pankin I.A., Burachevskaya O.A., Vetlitsyna-Novikova K.S., Soldatov A.V., New Fast Synthesis of MOF-801 for Water and Hydrogen Storage: Modulator Effect and Recycling Options, *Inorganica Chimica Acta*., **514**: 120025 (2021).

[15] Kim H., Yang S., Rao S.R., Narayanan S., Kapustin E.A., Furukawa H., Umans A.S., Yaghi O.M., Wang E.N., Water Harvesting from Air with Metal-Organic Frameworks Powered by Natural Sunlight, *Science*, **356**: 430-434 (2017).

[16] Saidi M., Benomara A., Mokhtari M., Boukli-Hacene L., Sonochemical Synthesis of Zr-fumaric Based Metal-Organic Framework (MOF) and Its Performance Evaluation in Methyl Violet 2B Decolorization by Photocatalysis, *React Kinet Mech Catal*., **131**: 1009-1021 (2020).

[17] Ke F., Peng C., Zhang T., Zhang M., Zhou C., Cai H., Zhu J., Wan X., Fumarate-Based Metal-Organic Frameworks as a New Platform for Highly Selective Removal of Fluoride from Brick Tea, *Sci Rep*., **8**: 939 (2018).

[18] Prabhu S.M., Srinivasarao K., Park C.M., Sasaki. K., Synthesis of Modulator-Driven Highly Stable Zirconium- Fumarate Frameworks and Mechanistic Investigations of their Arsenite and Arsenate Adsorption from Aqueous Solutions, *Cryst. Eng. Comm*., **21**: 2320-2332 (2019).

[19] Yoo J., Ryu U., Kwon W., Choi K.M., A Multi-Dye Containing MOF for the Ratiometric Detection and Simultaneous Removal of $Cr_2O_7^{2-}$ in the Presence of Interfering Ions, *Sens Actuators B: Chem*., **283**: 426-433 (2019).

[20] Zheng M., Zhao X., Wang K., She Y., Gao Z., Highly Efficient Removal of Cr(VI) on a Stable Metal-Organic Framework Based on Enhanced H-Bond Interaction, *Ind. Eng. Chem. Res*., **58**: 23330-23337 (2019).

[21] Lázaro I.A., Haddad S., Rodrigo-Muñoz J.M., , Forgan R.S., Surface-Functionalization of Zr-Fumarate MOF for Selective Cytotoxicity and Immune System Compatibility in Nanoscale Drug Delivery, *ACS Appl. Mater. Interfaces*., **10**: 31146-3115 (2018).

[22] Lacomi P., Formalik F., Marreiros J., Shang J., Justyna R., Mohmeyer A., Behrens P., Ameloot R., Kuchta B., Llewellyn P.L., Role of Structural Defects in the Adsorption and Separation of C3 Hydrocarbons in Zr-Fumarate- MOF (MOF-801), *Chem. Mater*., **31**: 8413-8423 (2019).

[23] Rouhani M., Ramazani A., Joo S.W., Novel, Fast and Efficient One-Pot Sonochemical Synthesis of 2-Aryl-1,3,4- Oxadiazoles, *Ultrason Sonochem*., **21(1)**: 262-267 (2014).

[24] Rouhani M., Ramazani A., Joo S.W., Ultrasonics in Isocyanide-Based Multicomponent Reactions: A New, Efficient and Fast Method for the Synthesis of Fully Substituted 1,3,4-Oxadiazole Derivatives under Ultrasound Irradiation, *Ultrason Sonochem*., **22**: 391-396 (2014).

[25] Ramazani A., Rouhani M., Joo S.W., Catalyst-Free Sonosynthesis of Highly Substituted Propenamide Derivatives in Water, *Ultrason Sonochem*., **28**: 393-399 (2016).

[26] Qiu L-G., Li Z-Q., Wu Y., Wang W., Xu T., Jiang X., Facile Synthesis of Nanocrystals of Microporous Metal-Organic Framework by an Ultrasonic Method and Selective Sensing of Organoamines, *Chem. Comm*., **31**: 3642-3644 (2008).

[27] Jahan I., Rupam T.H., Palash M.L., Rocky K.A., Saha B.B., Energy Efficient Green Synthesized MOF-801 for Adsorption Cooling Applications, *J. Mol. Liq*., **345**: 117760 (2022).

[28] Mani S., Bhargava R.N., Exposure to Crystal Violet, Its Toxic, Genotoxic and Carcinogenic Effects on Environment and Its Degradation and Detoxification for Environmental Safety, *Rev. Environ. Contam. Toxicol*., **237**: 71-104 (2016).

[29] Khan I., Saeed K., Zekker I., Zhang B., Hendi A.H., Ahmad A., Ahmad S., Zada N., Ahmad H., Shah L.A., Shah T., Khan I., Review on Methylene Blue: Its Properties, Uses, Toxicity and Photodegradation, *Water* **14**: 242 (2022).

[30] Furukawa H., Gándara F., Zhang Y-B., Jian J., Queen W.L., Hudson M.R., Yaghi O.M., Water Adsorption in Porous Metal-Organic Frameworks and Related Materials, *J Am. Chem Soc*., **136**: 4369-4381 (2014).

[31] Ren J., Musyoka N.M., Langmi H.W., North B.C., Mathe M., Pang W., Wang M., Walker J., In-Situ IR Monitoring of the Formation of Zr-Fumarate MOF, *Appl. Surf Sci*., **404**: 263-267 (2017).

[32] Prasetya N., Li K., Synthesis of Defective MOF-801 *via* an Environmentally Benign Approach for Diclofenac Removal from Water, *Sep. Purif. Techno*., **301**: 122024 (2022).

[33] Shearer G.C., Chavan S., Bordiga S., Svelle S., Olsbye U., Lillerud K.P., Defect Engineering: Tuning the Porosity and Composition of the Metal-Organic Framework UiO-66, *Chem. Mater*., **28**: 3749-3761 (2016).

[34] Soni S., Bajpai P.K., Bharti D., Mittal J., Arora C., Removal of Crystal Violet from Aqueous Solution Using Iron Based Metal Organic Framework, *Desalination Water Treat*., **205**: 386-399 (2020).

[35] Khan M.S., Khalid M., Shahid M., What Triggers Dye Adsorption by Metal Organic Frameworks? The Current Perspectives, *Mater. Adv*., **1**: 1575-1601 (2020).

[36] Tonk S., Rápó E., Linear and Nonlinear Regression Analysis for the Adsorption of Remazol Dye by Romanian Brewery Waste By-Product, Saccharomyces Cerevisiae, *Int. J. Mol. Sci*., **23(19)**: 11827 (2022).

[37] Loera-Serna S., Garcia-Ortiz J., Ortiz E., Dyes Adsorption on $Cu_3(BTC)_2$ Metal-Organic Framework. Advanced Materials, *TechConnect Briefs*, **1**: 331-334 (2016).

[38] Li X., Zheng L., Huang L., Zheng O., Lin Z., Guo L., Qiu B., Chen G., Adsorption Removal of Crystal Violet from Solution Using a Metal-Organic Frameworks Material, Copper Coordination Polymer with Dithiooxamide, *J. Appl. Polym. Sci*., **129**: 2857-2864 (2013).

[39] Qin J-S., Zhang S-R., Du D-Y., Shen P., Bao S-J., Lan Y-Q., Su Z-M., A Microporous An-ionic Metal-Organic Framework for Sensing Luminescence of Lanthanide (III) Ions and Selective Absorption of Dyes by Ionic Exchange, *Chem. Eur. J*., **20**: 5625-5630 (2014).

[40] Chand S., Elahi S.M., Pal A., Das M.C., A New Set of Cd(II)-coordination Polymers with Mixed Ligand of Dicarboxy- Late and Pyridyl Substituted Diaminotriazine: Selective Sorption Towards CO_2 and Cationic Dye, *Dalton Trans*., **46**: 9901-9911 (2017).

[41] Zhang J., Li F., Sun Q., Rapid and Selective Adsorption of Cationic Dyes by a Unique Metal-Organic Framework with Decorated Pore Surface, *Appl. Surf. Sci*., **440**: 1219-1226 (2018).

[42] Yang Q., Wang B., Chen Y., Xie Y., An Anionic In(III)-Based Metal-Organic Framework with Lewis Basic Sites for the Selective Adsorption and Separation of Organic Cationic Dyes, *Chin. Chem. Lett*., **30**: 234-238 (2019).

[43] Eltaweil A.S., El-Monaem E.M., Omer A.M, Khalifa R.E., El-Latif, M.M.A., El-Subruiti G.M., Efficient Removal of Toxic Methylene blue (MB) dye from Aqueous Solution Using a Metal-Organic Framework (MOF) MIL-101(Fe): Isotherms, Kinetics, and Thermodynamic Studies, *Desalination Water Treat.*, **189**: 395-407 (2020).

[44] Dinh H.T., Tran N.T., Trinh D.X., Investigation into the Adsorption of Methylene Blue and Methyl Orange by UiO-66-NO_2 Nanoparticles, *J. Anal. Methods Chem*., **2021**: 1-10 (2021).

[45] Amery N.Al., Abid H.R., Wang S., Liu S., Removal of Methylene Blue (MB) by Bimetallic Metal Organic Framework Framework, *J. Appl. Mat. and Tech*., **2**: 36-49 (2020).

[46] Haque E., Jun W.J., Jhung S.H., Adsorptive Removal of Methyl Orange and Methylene Blue from Aqueous Solution with a Metal-Organic Framework Material, Iron Terephthalate, *J. Hazard Mater*., **185**: 507-511 (2011).

[47] Arora C., Soni S., Sahu S., Mittal J., Kumar P., Bajpai P.K., Iron Based Metal Organic Framework for Efficient Removal of Methylene Blue dye from Industrial Waste, *J. Mol. Liq*., **284**: 343-352 (2019).

[48] Mohammadi A.A., Alinejad A., Kamarehie B., Javan S., Ghaderpoury A., Ahmadpour M., Ghaderpoori M., Metal- Organic Framework Uio-66 for Adsorption of Methylene Blue dye from Aqueous Solutions, *Int. J. Environ. Sci. Technol*., **14**: 1959-1968 (2017).

[49] Al-Wasidi A.S., Alzahrani I.I.S., Naglah A.M., El-Desouky M.G., Khalil M.A., El-Bindary A.A., El-Bindary M.A., Effective Removal of Methylene Blue From Aqueous Solution and Using Metal-Organic Framework; Modeling Analysis, Statistical Physics Treatment DFT Calculations, *Chemistry Select*, **6**: 11431-11447 (2021).

Colloid and Polymer Science
https://doi.org/10.1007/s00396-023-05159-1

ORIGINAL CONTRIBUTION

A systematic investigation on *Elaeocarpus sylvestris* leaf extract capped CuO nanoparticles as reducing agent and their antioxidant activity

Tejaswini G[1,2] · Laxmi Mangamma J[3] · Durga Praveena V[2] · Manga Raju I[4] · Meher Baba G[5] · Bhagya Lakshmi K[6]

Received: 16 June 2023 / Revised: 25 July 2023 / Accepted: 3 August 2023

Abstract

Recently, the role of plant-based nanoparticles as sustainable catalysts has emerged as a new field in material science. As a result of their wide applicability, bio-designed nanocatalysts have dominated the present study. At this juncture, this study gives the rapid and systematic procedure for the formation of an aqueous *Elaeocarpus sylvestris* plant leaf extract–capped copper oxide nanoparticles (ESCuO NPs). A benign method has been established for the fabrication of ESCuO nanoparticles that which serves as an innocuous, renewable, and mild reducing agent. Vivid spectrochemical and optical experimental investigation supported the formation of the ESCuO particles. Based on TEM investigation, the produced ESCuO NPs had spherical shape and an average size of 53 nm. The phytochemicals were used as a reducing agent internally without the use of harmful chemicals or extremely high temperatures. The derived ESCuO NPs have been employed as a powerful catalyst to reduce 4-nitrophenol. Furthermore, rate constants for different doses were calculated. The antioxidant efficiency of synthesized ESCuO NPs was determined. This study illustrates the way for cutting-edge synthesis of CuO NPs with numerous applications.

Keywords *Elaeocarpus sylvestris* · CuO nanoparticles · 4-Nitrophenol · Antioxidant activity · Reducing agent

Introduction

As a result of the industrial revolution and the quick development of technology, all types of industries often discharge massive amounts of dangerous chemicals into the air, water, and land, wreaking havoc on the ecosystem. Emerging contaminants are being released into water bodies as a result of the industrial revolution. These new toxins pose dangers to ecosystems and human health, necessitating creative treatment strategies. More specifically, 4-nitrophenol is a straightforward organic aromatic molecule that is widely employed in the production of numerous goods needed in current society, including colors, pesticides, and medications [1]. However, toxic chemicals like 4-nitrophenol are not only harmful but also anthropogenic and hindering in nature, so its reduction is a crucial challenge.

Additionally, 4-nitrophenol and its by-products are utilized to create pesticides, insecticides, and herbicides that pose a harm to both the environment and people [2].

In this connection, the significant challenge of reduction of 4-nitrophenol has been performed with the application of nanotechnology with their specific characteristic properties recently [3]. There is a plethora of effective research on the use of nanoparticles to reduce 4-nitrophenol. Metal nanoparticles have many uses in the biological, electrochemical, and medicinal domains because of their distinctive features, such as substantial surface area relative to volume ratios and significant surface energies related to their bulk molecules [4–7]. There are various types of metal oxide nanoparticles, but copper oxide nanoparticles are of particular interest due to their potential for usage in both science and industry. Due

✉ Tejaswini G
tejagara@gcrjy.ac.in

1 Department of Chemistry, Acharya Nagarjuna University, Guntur 522510, India

2 Department of Chemistry, Government College (A), Rajamahendravaram 533105, AP, India

3 Department of Chemistry, Govt. Degree College, Chodavaram, AP, India

4 Ward Sanitation & Environment Secretary, Public Health Department, GVMC, Visakhapatnam 530004, AP, India

5 Department of Chemistry, ONGC, Rajamahendravaram 533106, AP, India

6 SRR & CVR Government Degree College (A), Vijayawada 520010, AP, India

to their biocidal qualities, CuO has drawn attention and may be used effectively in a variety of biomedical applications, including illness treatment, drug delivery, cellular delivery, and biomedical imaging [8]. CuO NPs are employed as heterogeneous catalysts in the pharmaceutical industry as drug delivery, antioxidant, anticancer, and therapeutic agents [9]. The extremely unique crystal shapes and large surface areas of copper oxide NPs make them extremely excellent antibacterial particles [10].

Like other nanoparticles, CuO NPs can be produced through chemical and physical methods; however, current research has begun to recognize green CuO nanoparticles due to the green revolution in all fields. To prevent hazardous chemicals and an abrasive environment when using chemical methods and a laborious procedure while using physical methods, a green protocol for the production of CuO NPs has been established. As a result, the biological technique for producing CuO NPs is receiving greater attention because it is simple to use, easy to handle, does not require cell culture, and is environmentally benign [11]. Thus, using plant extracts for the synthesis of CuO NPs has already been reported for *Gloriosa superba* [12], *Aloe barbadensis* [13], *Malva sylvestris* [14], and *Carica papaya* [15].

In the current study, *Elaeocarpus sylvestris* plant leaf extract is used as a green source for producing copper oxide nanoparticles in a sustainable manner. The *Elaeocarpus sylvestris* plant has uttermost priority both in the spiritual purpose and scientific research. This plant belongs to the Elaeocarpaceae (Rudraksha) family. These are subtropical and long-leaved evergreen shrubs and trees. The research on this plant reveals that phytochemicals like alkaloids, terpenoids, and flavonoids are present, as reported by Amit Dadhich [16]. The antioxidant activity of this plant was reported by Amalia Indah Prihantini et al. [17]. This shows its action towards depression, stress, pain in the nerve, anxiety, palpitation, migraine, asthma, hypertension, and alleviations related to the liver and arthritis traditionally [18–22]. CuO NPs have been synthesized employing plant leaf extract from *Elaeocarpus sylvestris* for the first time. The current study investigates the environmentally friendly synthesis of CuO NPs and characterizes them using various microscopic and spectroscopic methods and tested its reduction activity of 4-nitrophenol and antioxidant activities.

Experimental methods

Reagents

The chemicals utilized in this research were of superior quality, conforming to analytical grade specifications. $Cu(NO_3)_2.3H_2O$, NaOH, 4-nitrophenol, $NaBH_4$, ethanol, and DPPH (1,1-diphenyl-2-picrylhydrazyl) were obtained from Merck and employed without any refinement. The *Elaeocarpus sylvestris* tree leaves were piled up near the Lord Shiva temple, Bommuru, Rajahmundry. Double-distilled water was utilized throughout all synthetic procedures.

Green protocol description of ESCuO nanoparticles

The fabrication of nanoparticles takes place through a variety of methods and approaches. A facile green protocol through the coprecipitation method has substantially emerged recently. Natural (plant biomolecule) capping, stabilizing, and reducing agents are being employed to accomplish CuO NPs by avoiding perilous reagents [23, 24]. Irrespective of all plant particles, leaves are a good extract yielding part through the coprecipitation method.

Elaeocarpus sylvestris leaf extract preparation

The fabrication of ESCuO NPs was executed by using *Elaeocarpus sylvestris* leaf extract as a green source operator. *Elaeocarpus sylvestris* tree leaves were washed to remove the dust particles. To dry these leaves, they were kept in the shade for 15 days. Subsequently, a fine green powder of the dried leaves was obtained by using ultra household mixer. In order to create the 1% aqueous leaf extract, 100 ml of distilled water was combined with 1 g of finely powdered leaves. For 20–25 min, the aqueous mixture was heated to 60 °C while being constantly stirred. Then, to obtain a clear solution free of any particles, the brown aqueous leaf extract was filtered through Whatman No. 1 filter paper. The filtrate was then kept at 4 °C.

Elaeocarpus sylvestris–functionalized CuO nanoparticle synthesis

By using an environmentally friendly source, such as an aqueous solution of *Elaeocarpus sylvestris* leaf extract, the coprecipitation process was used to create *Elaeocarpus sylvestris*–functionalized CuO nanoparticles. A typical synthesis technique involved dissolving 1.87 g of $Cu(NO_3)_2.3H_2O$ in 90 mL of distilled water. At room temperature, the solution is a clear blue color after being thoroughly mixed for 20 to 25 min. The reaction mixture volume was then increased to 100 mL by adding 10 mL of aqueous leaf extract, which caused it to turn dark green. Then, it was stirred for 15 min to get sonicated well with the mixture. Later, the temperature was raised to 80 °C and maintained for up to 1 h, and an intense green color was observed. Accordingly, 1 M 10 mL NaOH was added dropwise, and soon after addition, the mixture turned dark brown, which indicated the formation of *Elaeocarpus sylvestris*–functionalized CuO NPs as per literature [25].

The workup procedure included washing 2–3 times using distilled water and later two times with ethanol. The prepared CuO NPs precipitate was kept in the oven at 40 °C for drying overnight.

Elaeocarpus sylvestris–functionalized CuO nanoparticle instrumentation

The fabrication of nanoparticles in any way requires a firm footing through instrumental (optical, spectral, and microscopic) techniques. Likewise, ESCuO NPs were put forward through diversified characterization and analytical techniques. These helped us to estimate specific properties of synthesized material to be studied in an accurate scalable manner which is rapid and reliable to understand the obtained results. Here, a variety of instruments and analytical methods, including UV–visible spectroscopy as well as FTIR, X-RD, SEM, EDAX, and TEM-SAED instruments, are used to examine the bio-orchestrated CuO NPs. Shimadzu UV-2600 in the range of 200–800 nm was used for determination of absorbance of *Elaeocarpus sylvestris* leaf extract and synthesized ESCuO NPs. The FTIR spectra of ESCuO NPs were recorded using Bruker FTIR Alpha spectrometer in the range of 400–4000 cm^{-1}, and standard KBr pellet method is employed. PANalytical X pert pro diffractometer at 0.02°/s scan rate using Cu-k1 radiation ($\lambda = 1.54061$) was used to obtain the powder X-ray diffraction (XRD) patterns. XRD was used to determine the crystallinity of the synthesized ESCuO NPs. FESEM (FE-SEM model JEOL 6390LA/ OXFORD XMX N) at an accelerating voltage of 0.5 to 30 kV with magnification × 300,000 equipped with energy-dispersive X-ray spectroscopy (EDAX) of resolution 136 eV detector area 30 mm^2 is used to investigate the morphology and elemental composition of ESCuO NPs. HRTEM (HR-TEM model JEOL/JEM 2100) at an accelerating voltage of 200 kV with point resolution 0.23 nm and lattice resolution 0.14 nm equipped with selected area electron diffraction patterns (SAED) is used to investigate the size and shape of the synthesised ESCuO NPs. The HRTEM images of various resolutions of the nanoparticles are collected.

Reduction of 4-nitrophenol by ESCuo NPs

Here, normally used procedure has been employed as per literature [26]. Commonly, 25 mL of an aqueous solution of 4-nitrophenol was taken in a RB flask for 10 min while stirring to ensure good mixing. Ten milligrams of synthesized NPs made from copper oxide were then added to the reactant at 2.5 mM. Then, to decrease 4-nitrophenol at room temperature, 0.25 M $NaBH_4$ that had been dissolved in a 25-mL aqueous solution was mixed into the reaction solution. The mixture was a deep yellow color, and it was allowed to mix thoroughly through stirring until it became colorless. The colorless reaction mixture indicated the complete reduction of 4-nitrophenol. Frequently obtained samples of the reaction mixture, then a UV–visible spectrophotometer was utilized to check if the reaction had finished. Additionally, the outcomes were analyzed with and without $NaBH_4$.

Antioxidant potentiality

The "DPPH (1,1-diphenyl-2-picrylhydrazyl) scavenging test" is a technique used to investigate the synergistic effect of antioxidant molecules on capped CuO NPs as well as their effectiveness as antioxidants. The ESCuO NPs have been employed for conducting the experiment. It was calculated using the DPPH free radical scavenging potential method and measured according to the procedure described by Dobrucka [27]. An aliquot of 3 mL of 0.004% DPPH solution in ethanol and 0.1 mL of ESCuO NPs at various concentrations (100, 200, 300, 400, 500 µg/mL) were mixed, which were shielded from light. The DDPH reagent was made 24 h before and kept out of the light. Each mixture was left for 30 min; using the Shimadzu UV-2600 spectrometer, changes in absorbance intensity were measured at 517 nm. After which DPPH scavenging activity was calculated from using the equation given here, the findings were estimated as an amount of scavenging of a control blank with the absorption value of the investigated materials calculated at 517 nm.

$$Radical\ Scavenging\ activity(\%) = \frac{A_{control\ blank} - A_{sample} \times 100}{A_{control\ blank}} \quad (1)$$

Results and discussion

The hydroxyl and carboxyl groups found in *Elaeocarpus sylvestris* leaves are the best green sources to act as reducing, stabilizing, and capped operators for CuO NPs, according to the remarkable results achieved by several instrumental approaches. The biosynthesized ESCuO NPs are apt for further catalytic applications as their metabolites constitute amino, hydroxyl, and carboxyl functional groups.

UV–visible spectroscopy

Figure 1 depicts the comparative UV–Vis spectrum of both an aqueous solution of *Elaeocarpus sylvestris* leaf extract and the synthesized ESCuO NPs. In Fig. 1a, the absorption of the specified signal at 232 nm was observed for the aqueous leaf extract of *Elaeocarpus sylvestris*. Whereas the absorbance at 232 nm is related to the benzoyl ring system of π—π^* *or* n—π^* transitions, these are demonstrating that polyphenols

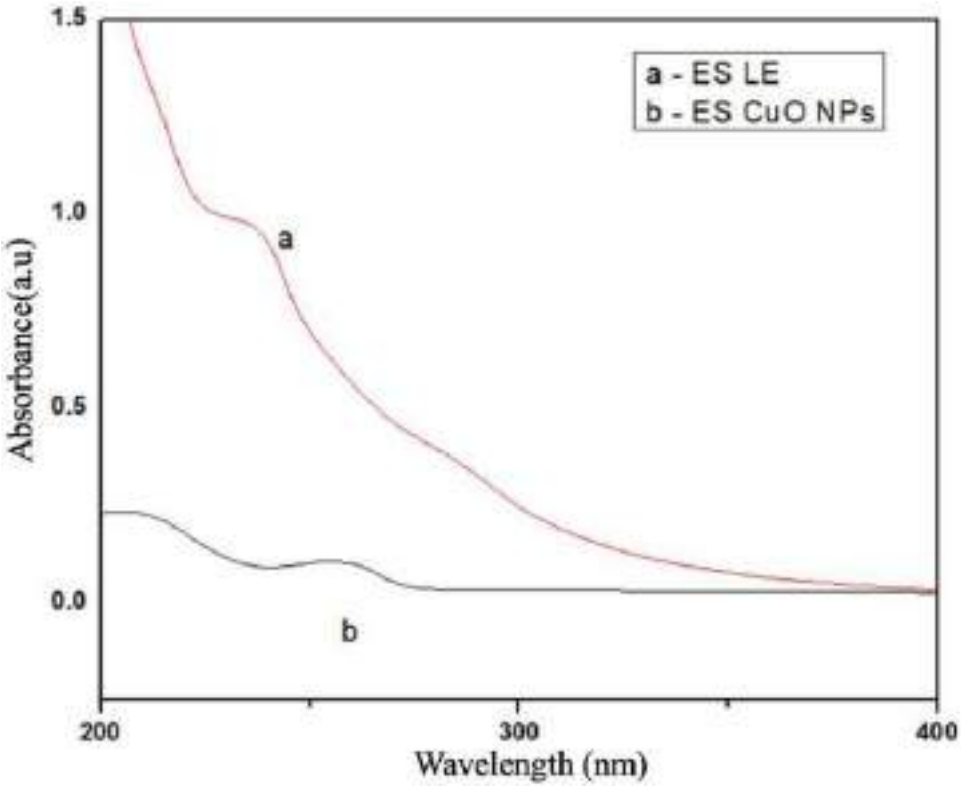

Fig. 1 UV–visible spectrum of **a** ES leaf extract and **b** ESCuO NPs

are some of the constituent phytochemicals in the *Elaeocarpus sylvestris* leaf extract [28]. Figure 1b gives the UV–visible spectrum of ESCuO NPs. Now, the drawn spectrum revealed the absorption peaks at 225 and 262 nm. The peak at 225 nm is attributed to the plant constituents [29], and the peak at 262 indicates the formation of ESCuO nanoparticles [28, 30].

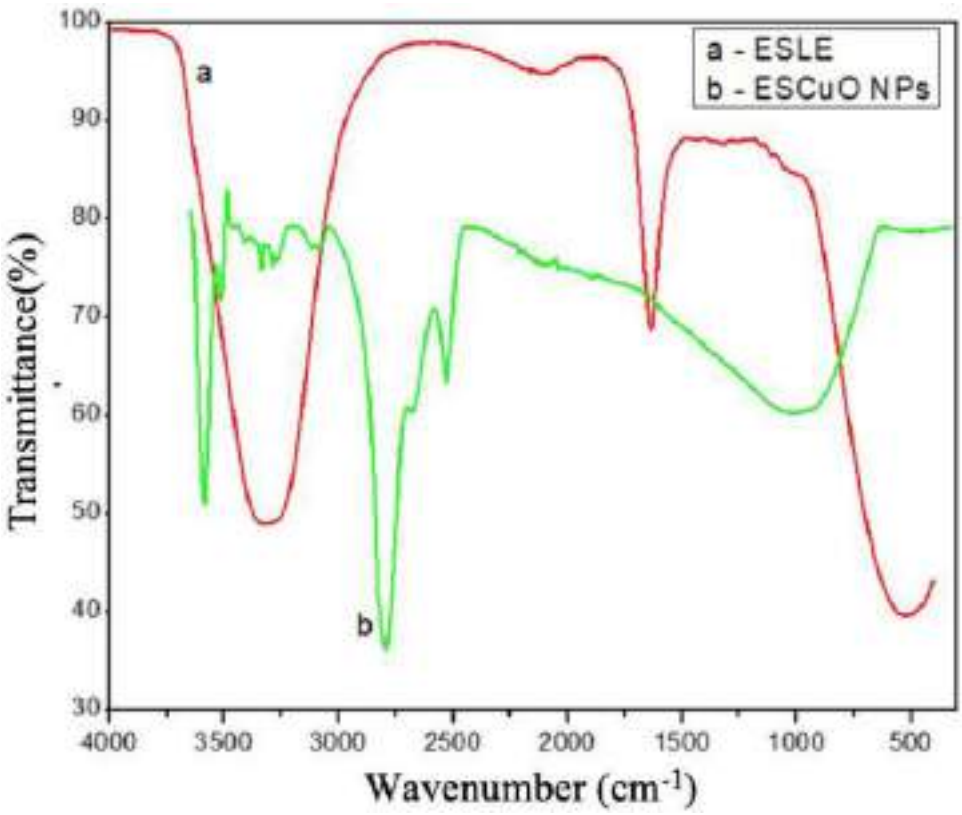

Fig. 2 FTIR spectra of **a** ES leaf extract and **b** ESCuO NPs

FT-IR

The important constituents responsible for the capping, stabilizing, and reducing of synthesized ESCuO nanoparticles are corroborated through FTIR. In this context, the functional group particulars of the plant and of synthesized ESCuO nanoparticles were investigated and depicted in Fig. 2. The FTIR spectrum of the employed biosource is shown in Fig. 2(a). The obtained spectra expressed the key functional groups through its characteristic ranges corresponding to the values of 3323.90, 2107.53, 1634.43, and 531.44 cm^{-1}, respectively. The spectrum shows value at 3323.9 cm^{-1} confirmed the -OH bond stretching vibration robustly. However, plant literature reveals that there is no compound with N–H functional group. Actually, the employed biosource contains ellagic acid, gallic acid, methyl gallate as major constituents with -OH and -COOH groups [31]. Given to the bending vibration of group -OH explicitly is 1634.43 cm^{-1}. Another intense peak at 2106.33 cm^{-1} is ascertained to C = O in biomolecules. The single intensity peak below 900 is 531.55 cm^{-1} and is due to the bending vibrations of C–C aromatic ring.

Moreover, the FTIR analysis of green-synthesized ESCuO NPs in Fig. 2b exhibited a shift in the transmittance intensity values compared to the spectra of biosource employed. Besides, it confirms the surface functionalization of bio-source of *Elaeocarpus sylvestris* on the green-synthesized CuO NPs. The FTIR image depicts the peak values at 3795.67, 2801.95, 2661.75, 990, and 583 cm^{-1}, respectively. One of the prominent peaks, called OH stretching, shifted purposefully from 3323.9 cm^{-1} to 3795.67 cm^{-1}, indicating that the phenolic -OH of the biosource is tightly bound to the CuO NPs. The stretching frequencies of the C–C and aromatic groups were assigned values of 2801.95 and 2661.75 cm^{-1}, respectively, while the C-O bond of the plant's components was given a value of 990 cm^{-1}. It is interesting to note that the Cu–O bond's stretching vibrations are represented by the other band at 583 cm^{-1}. Therefore, the above results confirmed the typical role of biocomponents of plant such as substituting carboxylic acids and reducing sugars, polyphenols, and proteins which are acted as best in functionalization and stabilization of ESCuO NPs [25, 26].

XRD

The crystal structure of ESCuO NPs was confirmed by XRD. Here, diffraction patterns of ESCuO NPs were obtained and presented in Fig. 3. Green CuO NPs have been shown to have prominent diffraction peaks that demonstrated their crystalline nature at various peak positions. The observed peak positions at 2θ = 32.59°, 35.61°, 38.78°, 48.82°, 53.54°, 58.37°, 61.60°, 66.31°, 68.15°, 72.46°, and 75.30° were ascertained to corresponding hkl planes (110), (111), (200), (202), (020), (202), (113), (311), (220), and (400) [32]. These are highly compatible with the cupric oxide nanoparticle JCPDS Standard No. 01–080-0076. Finally, it validates the monoclinic phase, face-centered cubic structure of CuO NPs. As per previous reports, the presence of diffraction peaks between 35 and 39° designated the formation of CuO NPs. Fifty-three nanometer is the average size of CuO NPs as measured by Debye–Scherrer's formula [33].

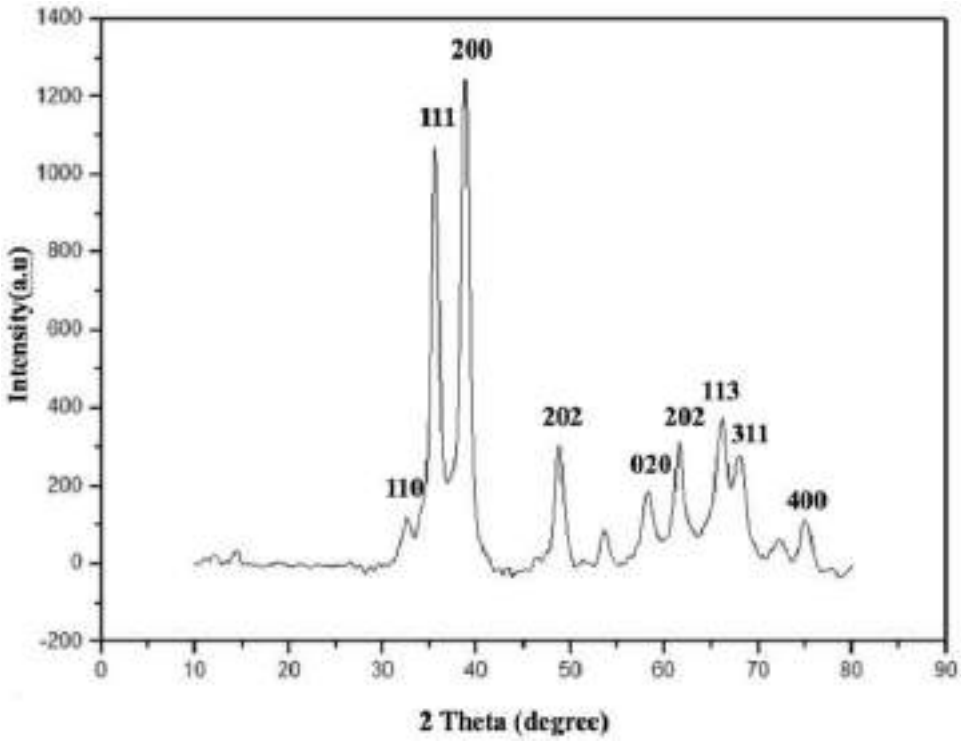

Fig. 3 XRD pattern of ESCuO NPs

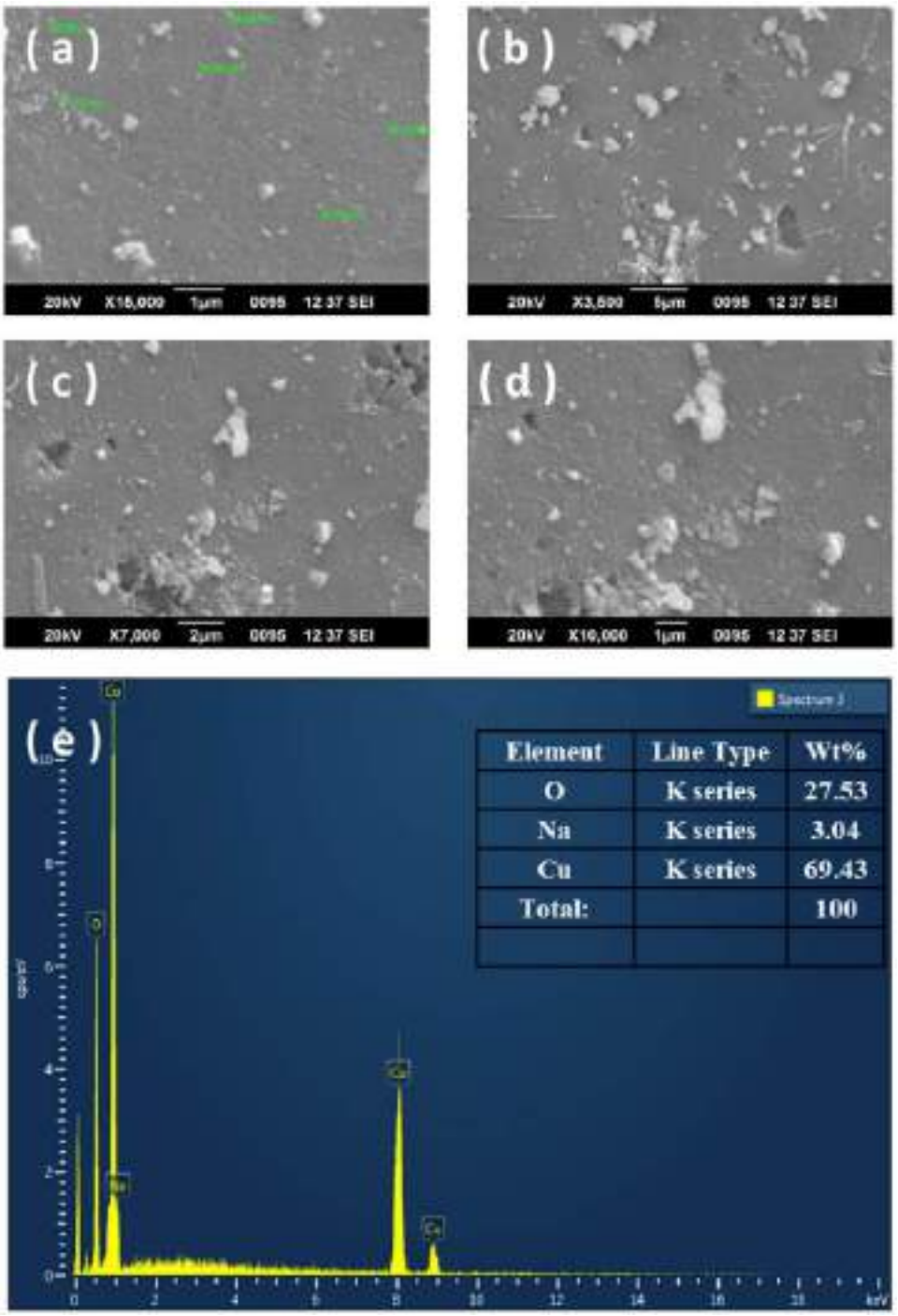

Fig. 4 **a**–**d** SEM pictures of ESCuO NPs; **e** EDX spectra of ESCuO NPs

$$D = k\lambda/\beta cos\theta$$

SEM

The interpretation of surface texture of orchestrated ESCuO NPs was carried out through the SEM microscopic technique. Figure 4a–d displays SEM images of ESCuO NPs. Moreover, the SEM pictures represented in Fig. 4 reveal the defined spherical morphology of the orchestrated CuO NPs. The observed pictures showed that the ESCuO NPs had nearly spherical morphologies and were agglomerated and monodispersed. The chemical composition of the *Elaeocarpus sylvestris* extract is surface linked to this variance in particle shape and size distribution [34, 35]. In addition to that, the high surface energy of ESCuO nanoparticles caused little aggregation. This character developed because the water medium served as the source of the synthesis process

[36–38]. Small nuclear particles actively self-aggregate and oriented in a way to form larger spheres explicitly. In addition to this, the SEM micrographs were like shattered pieces (agglomerated particles) on a rough surface. Figure 4e displays the chemical composition of the produced NPs being examined by the EDX method. Only two powerful signals, Cu and O, contribute significantly to the spectrum, with weight percentages of 69.43 and 27.53, respectively. Additionally, the presence of significant concentrations of Cu and O with sharp peaks points to the stability and quality of the synthesized ESCuO NPs. Sodium was another signal that was seen and had a very low intensity (3%). Interestingly, there is an unlabeled peak with less intensity which is ascribed to carbon (0.01%) according to Sone et al. [39]. According to him, the carbon film used to support the CuO samples as well as leaf-based organic compounds that emerged from the aqueous extract could be ascribed for the presence of C found in the powder. Figure 4b depicts the needle-shaped and layered flakes that were visible on the surface. The findings showed that the ESCuO NPs were functionalized by the *Elaeocarpus sylvestris* leaf extract biomolecules in a significant way.

TEM

Figure 5a–e depicts the micrographs of the synthesized ESCuO NPs. The spherical morphological distribution of orchestrated ESCuO NPs with sizes in various ranges between 9–25 nm is explicitly depicted in Fig. 5. The TEM micrographs illustrate that the particles are scattered, and some appear to be well coated with the leaf extract of *Elaeocarpus sylvestris*. The different magnifications of TEM images declare that very small particles below 25 nm are observed [36, 40]. The mean particle size was characterized by "Image J software (National Institute of Health, Bethesda, MD, USA)," and it was 53.99 nm. Correspondingly, the obtained value is in accordance with the crystallite size attained by the Debye–Scherrer equation using XRD. The bright diffraction rings are observed in the "selected area electron diffraction (SAED)" phenomenon of orchestrated ESCuO NPs in Fig. 5f. The areas with white and black dots revealed the hydrophilic and hydrophobic characteristics of CuO nanoparticles, respectively. The well-organized and arranged location of the lattice planes in CuO nanoparticles has been demonstrated by the fringes that appeared [36, 41]. The polycrystalline nature of the CuO nanoparticles has been found to be consistent with the appearance of white spots and rings in dark nature [36, 42].This showed that the CuO NPs are polycrystalline in nature. It is further confirmed that the particles are finely crystallized. The SAED image's diffused ring dot pattern fits the XRD pattern, demonstrating the monoclinic structure of the synthesized ESCuO nanoparticles.

Reduction of 4-nitrophenol using ESCuO NPs

4-Nitrophenol can be reduced by different metal, metal oxide, and bimetallic nanoparticles like Au, Ag, Pt, Pd, and Au–Ag. Eventually, all the aforementioned metals and metal oxides are cost-effective, and some are harmful, but the literature says green-synthesized CuO nanoparticles are also used as reducing agents in organic reactions [43]. Nevertheless, CuO NPs are eco-friendly, bioactive, and commercially viable. Here, ESCuO NPs act as blistering agents

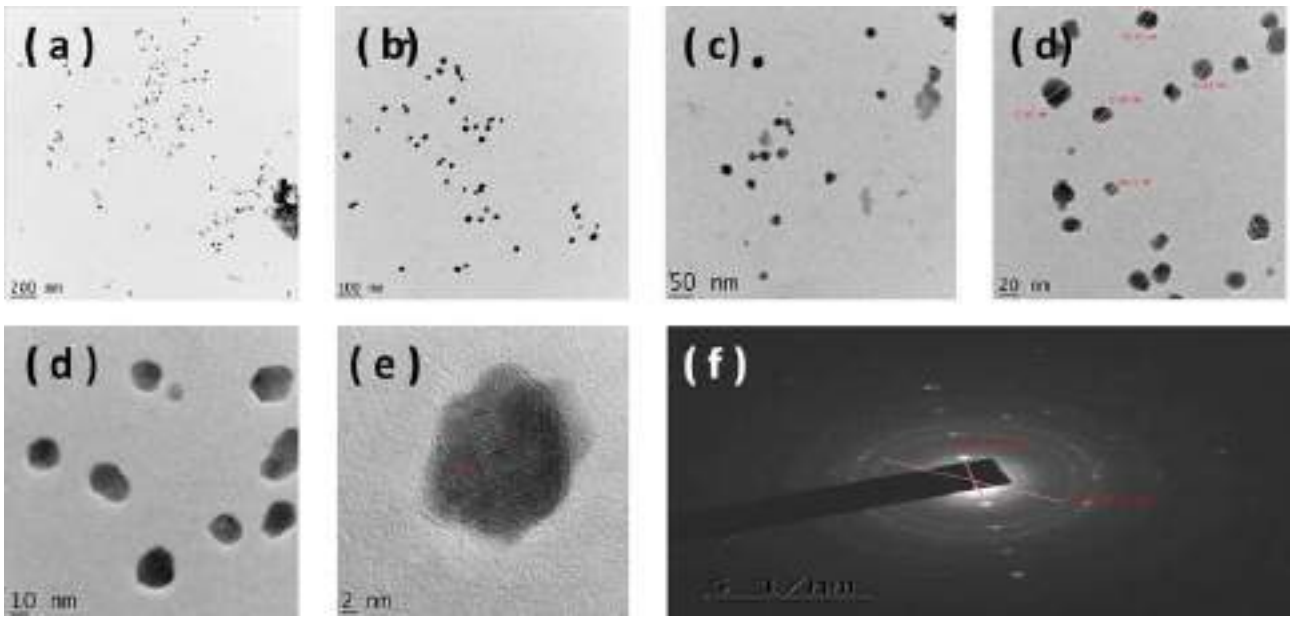

Fig. 5 **a–e** TEM images of ESCuO NPs; **f** SAED of ESCuO NPs

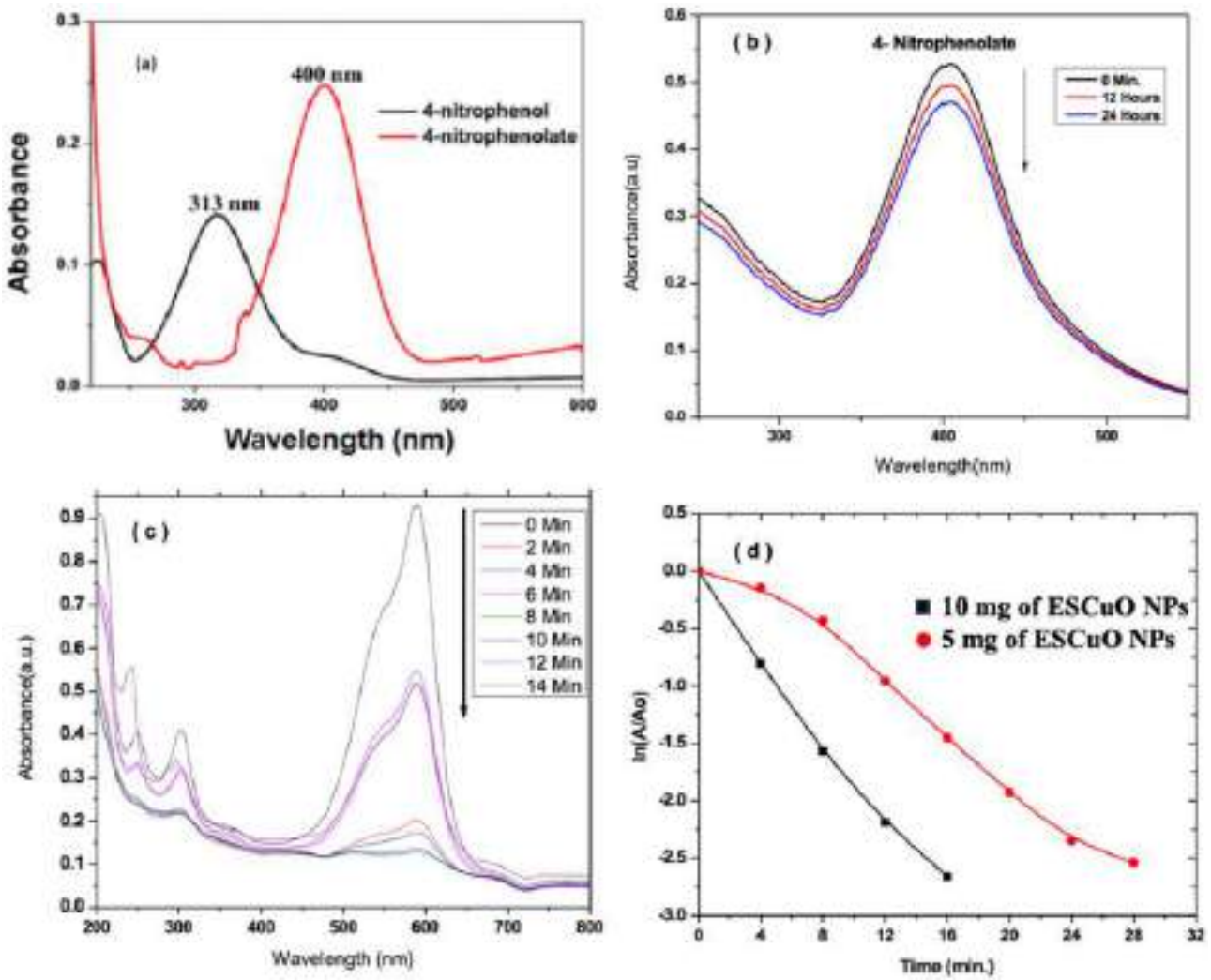

Fig. 6 **a** A schematic representation of conversion of para-nitrophenol to para-aminophenol by ESCuO NPs and $NaBH_4$. **b** 4-Nitrophenol reduction with ES leaf extract and $NaBH_4$ without ESCuO NPs. **c** 4-Nitrophenol reduction by ESCuO NPs and $NaBH_4$. **d** Kinetics of reduction

and an efficient reducing agents for removal of hazardous 4-nitrophenol. Figure 6a denotes the schematic representation of conversion of para-nitrophenol to para-aminophenol by ESCuO NPs and $NaBH_4$.

In the presence of $NaBH_4$ as a reducing agent, the performance of the as-synthesized ESCuO NPs as a catalyst was evaluated against 4-nitrophenol reduction [14]. The conversion of 4-nitrophenol into 4-aminophenol is depicted in Fig. 6. In the absence of $NaBH_4$, UV–vis absorbance of p-nitrophenol showed a peak at about 313 nm. However, when $NaBH_4$ was added to the p-NP solution, the peak at 313 nm vanished, and a new, strong peak at about 400 nm emerged. During the reduction process, a weakly yellowish-orange p-nitrophenolate solution formed from 4-nitrophenol transforms into a strong yellowish-orange p-nitrophenolate ion in alkaline conditions [26]. The UV–Vis absorbance of the p-nitrophenol and $NaBH_4$ mixture without a catalyst was the source of the initial, strong spectrum. Following the addition of the catalyst, the peak at 400 nm began to progressively fade while a new peak at about 313 nm began to emerge, signifying the transformation of the

Table 1 The kinetic parameters determined during the conversion of para-nitrophenol to para-aminophenol by ESCuO NPs

S. no	CuO NPs in (mg)	Rate constant (min^{-1})	R^2	Time required for reduction of 4-nitrophenol (min)
1	5	0.1477	0.9834	24
2	10	0.1596	0.9718	14

Table 2 The antioxidant activity of ESCuO NPs

Sl. no	CuO NPs in (µg/mL)	DPPH (%) (mean ± S.D)
1	100	59.45 ± 0.03
2	200	59.56 ± 0.01
3	300	60.33 ± 0.02
4	400	60.44 ± 0.02
5	500	61.21 ± 0.03

p-nitrophenolate ion into the p-aminophenol, as shown in Fig. 6b. Based on the appearance of the absorbance peak at about 400 nm in the presence of the ESCuO NPs as a catalyst, the amount of time needed to convert 4-nitrophenol completely was calculated [30]. When the 10 mg ESCuO NPs as a catalyst was added, the entire conversion of 4-nitrophenol into aminophenol took place in 14 min (Fig. 6c), whereas there was no change when the catalyst was not present.

The rate constant (k) of reduction of 4-nitrophenol using different doses of ESCuO NPs was determined (Fig. 6d) (Table 1). The kinetic analysis results showed that the data best fit with pseudo-first-order. The rate constant of the reaction obtained from the slope of a plot Fig. 6d depicts that the rate of catalytic reduction of 4-nitrophenol is the significant for the ESCuO catalyst synthesized using *Elaeocarpus sylvestris* leaf extract based on the literature. The reason for the higher rate constants when there is a greater concentration of ESCuO nanoparticles is because there is a corresponding increase in the quantity of reactive sites available for the reduction of 4-nitrophenol [26]. Figure 6c exhibits 4-nitrophenol reduction by ESCuO NPs and $NaBH_4$. Figure 6d depicts the kinetics of reduction followed.

Antioxidant activity

Free radicals are created in biological systems when biomolecules interact with molecular oxygen [44]. Numerous studies have looked at the antioxidant activity of many different types of natural and manmade substances [45]. The DPPH scavenging assay is thought to be the most used technique for examining a material's antioxidant capacity. The antioxidant activity of ESCuO NPs was investigated as its capacity to reduce the stable nitrogen radical DPPH, which causes gradual decrease in absorbance at 517 nm, with increase in concentration of ESCuO NPs. This further confirms the free radical scavenging activity of ESCuO NPs. Hence, ESCuO NPs were used as radical scavenger and DPPH was used as the radical source. The color of the DPPH solution changed from deep violet to pale yellow in the presence of ESCuO NPs. The antioxidant efficiency CuO nanoparticles and green-synthesized CuO nanoparticles are compared by Naz et al. [46] which confirms that there is definite enhancement in its efficiency due to the capping of plant biomolecules [47]. Here, various concentrations of samples were prepared (100, 200, 300, 400, and 500 µg/mL) and placed these samples in a dark condition for half an hour after the addition of DPPH free radical. Then, after, samples were analyzed using spectrophotometer, and percentage of efficiency values shown in the table were calculated using the formula (Eq. 1).

These results showed that the antioxidant efficiency of ESCuO NPs is dose-dependent (Table 2). All values represented in the tables are the average ± SD of the results of two separately conducted experiments. Figure 7 shows the free radical scavenging activity of ESCuO NPs, which exhibits up to 61.21 ± 0.03% in 500 µg/mL concentration of ESCuO NPs.

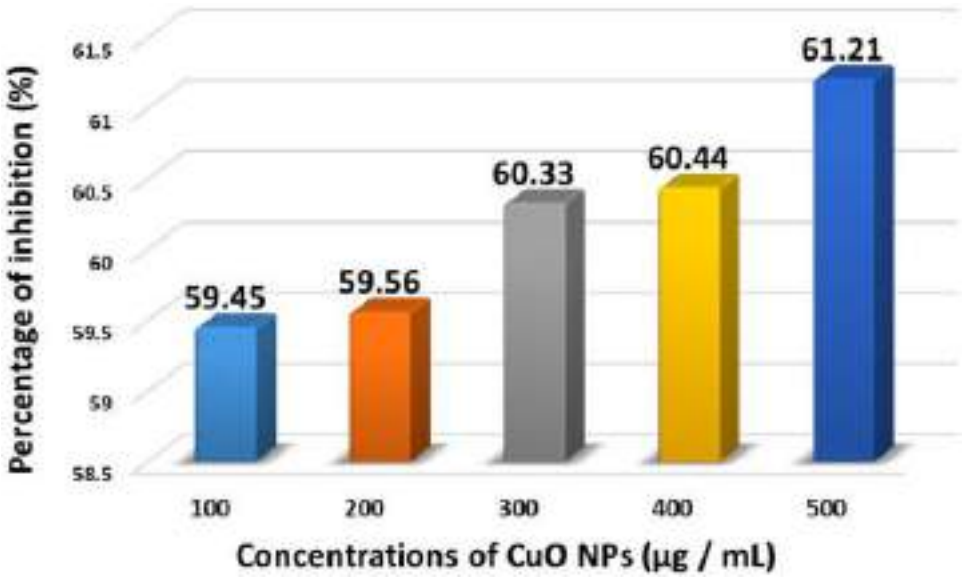

Fig. 7 Free radical scavenging activity of ESCuO NPs

Conclusion

Finally, a novel, simple, and green method is established in a promising and sustainable way for the production of CuO nanoparticles. To escape from regular chemical methods and their toxicity, an environmentally friendly substitute is the need of the hour. This green protocol with *Elaeocarpus sylvestris* leaf extract became successful in this way. The fabricated particles are corroborated with respective instrumental analysis. The findings revealed that the formed particles have a spherical shape with a 53-nm size and a face-centered cubic structure. SEM pictures have defined spherical morphology of the orchestrated ESCuO NPs. The EDAX spectrum showed the elemental percentage of Cu and O are 69.43 and 27.53, respectively. ESCuO NPs with sizes in various ranges between 9 and 25 nm is explicitly depicted by TEM instrument. In general, CuO nanoparticles are cheaper than other metal oxides. The ESCuO NPs shown efficient catalytic activity in the conversion of para nitrophenol to para aminophenol. The rate constant (k) of reduction of 4-nitrophenol using different doses of ESCuO NPs was determined, and for 5 mg and 10 mg of ESCuO NPs, rate constants are 0.1477 and 0.1596 and reduction takes place within 24 and 14 min, respectively. Therefore, the ESCuO NPs show efficient catalytic activity in the conversion of para-nitrophenol to para-aminophenol. Furthermore, it proves ESCuO NPs have promising antioxidant potentiality and show the free radical scavenging activity exhibits up to $61.21 \pm 0.03\%$ in 500 µg/mL concentration of ESCuO NPs. Therefore, ESCuO NPs act as a good catalyst for elimination of organic pollutants. In future perspective, the study gives the new pathway in a variety of applications, including biomedicine and catalysis.

Author contribution Tejaswini wrote the manuscript, Laxmi Mangamma prepared the tables, Praveena prepared the figures, Manga Raju and Meher Baba collected the data, and Bhagya Lakshmi K reviewed the manuscript.

Availability of data and materials Not applicable.

Declarations

Ethical approval Not applicable.

Competing interests The authors declare no competing interests.

References

1. Zhao B, Mele G, Pio I, Li J, Palmisano L, Vasapollo G (2010) Degradation of 4-nitrophenol (4-NP) using Fe–TiO2 as a heterogeneous photo-Fenton catalyst. J Hazard Mater 176(1–3):569–574, ISSN 0304–3894, https://doi.org/10.1016/j.jhazmat.2009.11.066
2. Kaur J, Singh J, Rawat M (2019) An efficient and blistering reduction of 4-nitrophenol by green synthesized silver nanoparticles. SN Appl Sci 1:1060. https://doi.org/10.1007/s42452-019-1088-x
3. Anjum M, Miandad R, Waqas M, Gehany F, Barakat MA (2019) Remediation of wastewater using various nano-materials. Arabian J Chem 12(8):4897–4919, ISSN 1878–5352, https://doi.org/10.1016/j.arabjc.2016.10.004
4. Tejaswini G, Lakshmi Kishore P, Naga Lakshmi V, Bhagya Lakshmi KA (2022) Comprehensive Review on Green Synthetic Approaches and Applications of 3d-Series Metal Oxide Nanoparticles. Asian J Chem 34(10):2478–2488. https://doi.org/10.14233/ajchem.2022.23904
5. Tejaswini G, Lakshmi Kishore P, Kiran Kumar P et al (2023) Bio Designed ZnO Nanoparticles with Leaves of Elaeocarpus Sylvestris and Investigation of Photocatalyst for Dye Degradation and Antimicrobial applications. Arab J Sci Eng. https://doi.org/10.1007/s13369-023-07944-0
6. Siddiqui S, Goddard RH, Bielmyer-Fraser GK (2015) Comparative effects of dissolved copper and copper oxide nanoparticle exposure to the sea anemone, Exaiptasia pallida. Aquat Toxicol 160:205–213
7. Barabadi H, Alizadeh Z, Rahimi MT et al (2019) "Nanobiotechnology as an emerging approach to combat malaria: a systematic review", Nanomedicine: Nanotechnology. Biology and Medicine 18:221–233
8. Vaidehi D, Bhuvaneshwari V, Bharathi D, Sheetal BP (2018) Antibacterial and photocatalytic activity of copper oxide nanoparticles synthesized using Solanum lycopersicum leaf extract. Mater Res Expr 5(8):085403
9. Amin F, Fozia KB, Alotaibi A, Qasim M, Ahmad I, Ullah R, Bourhia M, Gul A, Zahoor S, Ahmad R (2021) Green Synthesis of Copper Oxide Nanoparticles Using Aerva javanica Leaf Extract and Their Characterization and Investigation of In Vitro Antimicrobial Potential and Cytotoxic Activities. Evidence-based complementary and alternative medicine : eCAM 2021:5589703. https://doi.org/10.1155/2021/5589703
10. Perreault F, Melegari SP, Da Costa CH, de Oliveira Franco Rossetto AL, Matias WG (2012) Genotoxic effects of copper oxide nanoparticles in neuro 2A cell cultures. Sci Ge Total Environ 441:117–124
11. Nations S, Long M, Wages M, Maul JD, Theodorakis CW, Cobb GP (2015) Subchronic and chronic developmental effects of copper oxide (CuO) nanoparticles on Xenopus laevis. Chemosphere 135:166–174
12. Naika HR, Lingaraju K, Manjunath K, Kumar D, Nagaraju G, Suresh D, Nagabhushana H (2015) Green synthesis of CuO nanoparticles using Gloriosa superba L. extract and their antibacterial activity. J Taibah Univ Sci 9(1):7–12, ISSN 1658–3655. https://doi.org/10.1016/j.jtusci.2014.04.006
13. Gunalan S, Sivaraj R, Venckatesh R (2012) Aloe barbadensis Miller mediated green synthesis of mono-disperse copper oxide nanoparticles: optical properties. Spectrochim Acta A Mol Biomol Spectrosc 97:1140–1144. https://doi.org/10.1016/j.saa.2012.07.096
14. Benhammada A, Trache D (2022) Green synthesis of CuO nanoparticles using Malva sylvestris leaf extract with different copper precursors and their effect on nitrocellulose thermal behavior. J Therm Anal Calorim 147:1–16. https://doi.org/10.1007/s10973-020-10469-5
15. Sankar R, Manikandan P, Malarvizhi V, Fathima T, Shivashangari KS, Ravikumar V (2014) Green synthesis of colloidal copper oxide nanoparticles using Carica papaya and its application in photocatalytic dye degradation. Spectrochim Acta Part A Mol Biomol Spectrosc 121:746–750
16. Dadhich A, Rishi A, Sharma G, Chandra S (2013) Phytochemicals of elaeocarpus with their therapeutic value: A review. Intern J Pharma Bio Sci 4

17. Prihantini A, Tachibana S, Itoh K (2015) Antioxidant Active Compounds from Elaeocarpussylvestris and their Relationship between Structure and Activity. Procedia Environ Sci 28:758–768. https://doi.org/10.1016/j.proenv.2015.07.089
18. Wu L, Wu J, Chen SP, Li ZJ, Zhang J, Yuan E, Hu JW (2019) Chemical Constituents of the Twigs of Elaeocarpus sylvestris. Chem Nat Comp. 55. https://doi.org/10.1007/s10600-019-02679-7
19. Prasannan P, Jeyaram Y, Pandian A, Raju R, Sekar S (2020) A Review on Taxonomy, Phytochemistry, Pharmacology, Threats and Conservation of Elaeocarpus L. (Elaeocarpaceae). Botan Rev 86. https://doi.org/10.1007/s12229-020-09229-9
20. Jang BK, Chi LW, Cho JS, Lee CH (2020) Preliminary screening to assess the antimicrobial activities of extracts of evergreen woody species from South Korea against Staphylococcus aureus. Journal of Plant Biotechnology. Korean Soc Plant Biotechnol. https://doi.org/10.5010/jpb.2020.47.1.090
21. Bae S, Kim SY, Do MH, Lee CH, Song YJ (2017) 1,2,3,4,6-Penta-O-galloyl-ß-D-glucose, a bioactive compound in Elaeocarpus sylvestris extract, inhibits varicella-zoster virus replication. Antiviral Res 144:266–272, ISSN 0166–3542. https://doi.org/10.1016/j.antiviral.2017.06.018
22. To KP, Kang SC, Song YJ (2013) The extract of Elaeocarpus sylvestris inhibits human cytomegalovirus immediate early gene expression and replication in vitro. Mole Med Rep 9. https://doi.org/10.3892/mmr.2013.1824
23. Sharma D, Kanchi S, Bisetty K (2019) Biogenic synthesis of nanoparticles: A review. Arabian J Chem 12(8):3576–3600, ISSN 1878–5352. https://doi.org/10.1016/j.arabjc.2015.11.002
24. Chakraborty N, Banerjee J, Chakraborty P, Banerjee A, Chanda S, Ray K, Acharya K, Sarkar J (2022) Green synthesis of copper/copper oxide nanoparticles and their applications: a review. Green Chem Lett Rev 15(1):187–215. https://doi.org/10.1080/17518253.2022.2025916
25. Veisi H, Karmakar B, Tamoradi T et al (2021) Biosynthesis of CuO nanoparticles using aqueous extract of herbal tea (Stachys Lavandulifolia) flowers and evaluation of its catalytic activity. Sci Rep 11:1983. https://doi.org/10.1038/s41598-021-81320-6
26. Nasrollahzadeh M, Maham M, Sajadi SM (2015) Green synthesis of CuO nanoparticles by aqueous extract of Gundelia tournefortii and evaluation of their catalytic activity for the synthesis of N-monosubstituted ureas and reduction of 4-nitrophenol. J Coll Inter Sci 455:245–253, ISSN 0021–9797, https://doi.org/10.1016/j.jcis.2015.05.045
27. Dobrucka R (2018) Antioxidant and Catalytic Activity of Biosynthesized CuO Nanoparticles Using Extract of Galeopsidis herba. J Inorg Organomet Polym 28:812–819. https://doi.org/10.1007/s10904-017-0750-2
28. Ssekatawa K, Byarugaba DK, Angwe MK, Wampande EM, Ejobi F, Nxumalo E, Maaza M, Sackey J, Kirabira JB (2022) Phyto-Mediated Copper Oxide Nanoparticles for Antibacterial, Antioxidant and Photocatalytic Performances. Frontiers in Bioengineering and Biotechnology. https://doi.org/10.3389/fbioe.2022.820218
29. Tejaswini G, Beebi S, Baba GM et al (2023) Elaeocarpus Sylvestris mediated green approach for fabrication of magnetite nanoparticles: Antimicrobial and antioxidant potentialities. Appl Nanosci. https://doi.org/10.1007/s13204-023-02785-7
30. Bordbar M, Sharifi-Zarchi Z, Khodadadi B (2017) Green synthesis of copper oxide nanoparticles/clinoptilolite using Rheum palmatum L. root extract: high catalytic activity for reduction of 4-nitro phenol, rhodamine B, and methylene blue. J Sol-Gel Sci Technol 81:724–733. https://doi.org/10.1007/s10971-016-4239-1
31. Hostnik G, Tošović J, Štumpf S, Petek A, Bren U (2022) The influence of pH on UV/Vis spectra of gallic and ellagic acid: A combined experimental and computational study. Spectrochimica Acta Part A: Mole Biomole Spectros 267(2):120472, ISSN13861425. https://doi.org/10.1016/j.saa.2021.120472
32. Alhalili Z (2022) Green synthesis of copper oxide nanoparticles CuO NPs from Eucalyptus Globoulus leaf extract: Adsorption and design of experiments. Arabian J Chem 15(5):103739, ISSN 1878–5352. https://doi.org/10.1016/j.arabjc.2022.103739
33. Patterson AL (1939) The Scherrer formula for X-ray particle size determination. Phys Rev 56:978–982
34. Ganesan K, Jothi VK, Natarajan A, Rajaram A, Ravichandran S, Ramalingam S (2020) Green synthesis of Copper oxide nanoparticles decorated with graphene oxide for anticancer activity and catalytic applications. Arabian J Chem 13(8):6802–6814, ISSN 1878–5352. https://doi.org/10.1016/j.arabjc.2020.06.033
35. Sebeia N, Jabli M, Ghanmi H, Ghith A, Saleh TA (2019) Effective Dyeing of Cotton Fibers Using Cynomorium Coccineum L. Peel Extracts: Study of the Influential Factors Using Surface Response Methodology. J Nat Fibers 1–13
36. Velsankar K, RM AK, Preethi R, Muthulakshmi V, Sudhahar S (2020) Green synthesis of CuO nanoparticles via Allium sativum extract and its characterizations on antimicrobial, antioxidant, antilarvicidal activities. J Environ Chem Eng 104123. https://doi.org/10.1016/j.jece.2020.104123
37. Antonoglou O, Lafazanis K, Mourdikoudis S, Vourlias G, Lialiaris T, Pantazaki A, Dendrinou-Samara C (2019) Biological relevance of CuFeO2 nanoparticles: Antibacterial and anti-inflammatory activity, genotoxicity, DNA and protein interactions. Mater Sci Eng: C 99:264–274, ISSN 0928–4931. https://doi.org/10.1016/j.msec.2019.01.112
38. Shao F, Yang A, Yu DM, Wang J, Gong X, Tian HX (2018) Biosynthesis of Barleria gibsoni leaf extract mediated zinc oxide nanoparticles and their formulation gel for wound therapy in nursing care of infants and children. J Photochem Photobiol B: Biol 189:267–273, ISSN 1011–1344. https://doi.org/10.1016/j.jphotobiol.2018.10.014
39. Sone BT, Diallo A, Fuku XG, Gurib-Fakim A, Maaza M (2020) Biosynthesized CuO nano-platelets: Physical properties & enhanced thermal conductivity nanofluidics. Arabian J Chem 13(1):160–170, ISSN 1878–5352. https://doi.org/10.1016/j.arabjc.2017.03.004
40. Nasrollahzadeh M, Sajadi SM, Rostami-Vartooni A, Hussin SM (2016) Green synthesis of CuO nanoparticles using aqueous extract of Thymus vulgaris L. leaves and their catalytic performance for N-arylation of indoles and amines. J Colloid Interface Sci 466:113–119
41. Khan ZUH, Sadiq HM, Shah NS, Khan AU, Muhammad N, Hassan SU, Zakir A (2019) Greener synthesis of zinc oxide nanoparticles using Trianthema portulacastrum extract and evaluation of its photocatalytic and biological applications. J Photochem Photobiol B: Biol 192:147–157, ISSN 1011–1344. https://doi.org/10.1016/j.jphotobiol.2019.01.013
42. Velsankar K, Sudhahar S, Parvathy G, Kaliammal R (2020) Effect of cytotoxicity and aAntibacterial activity of biosynthesis of ZnO hexagonal shaped nanoparticles by Echinochloa frumentacea grains extract as a reducing agent. Materials Chemistry and Physics 239:121976, ISSN 0254-0584. https://doi.org/10.1016/j.matchemphys.2019.121976
43. Mejía YR, Reddy Bogireddy NK (2022) Reduction of 4-Nitrophenol Using Green-Fabricated Metal Nanoparticles. RSC Adv 12(29):18661–18675. https://doi.org/10.1039/D2RA02663E
44. Yasin A, Fatima U, Shahid S, Mansoor S, Inam H, Javed M, Iqbal S, Alrbyawi H, Somaily HH, Pashameah RA et al (2022) Fabrication of Copper Oxide Nanoparticles Using Passiflora edulis Extract for the Estimation of Antioxidant Potential and Photocatalytic Methylene Blue Dye Degradation. Agronomy 12(10):2315. https://doi.org/10.3390/agronomy12102315

45. Brand-Williams W, Cuvelier ME, Berset C (1995) Use of a free radical method to evaluate antioxidant activity. LWT - Food Sci Technol 28(1):25–30, ISSN 0023–6438. https://doi.org/10.1016/S0023-6438(95)80008-5
46. Naz S, Gul A, Zia M, Javed R (2023) Synthesis, biomedical applications, and toxicity of CuO nanoparticles. Appl Microbiol Biotechnol 107(4):1039–1061. https://doi.org/10.1007/s00253-023-12364-z
47. Ramasubbu K, Padmanabhan S, Al-Ghanim KA, Nicoletti M, Govindarajan M, Sachivkina N, Rajeswari VD (2023) Green synthesis of copper oxide nanoparticles using Sesbania grandiflora leaf extract and their evaluation of anti-diabetic, cytotoxic, anti-microbial, and anti-inflammatory properties in an in-vitro approach. Fermentation 9(4):332. https://doi.org/10.3390/fermentation9040332

Biomass Conversion and Biorefinery
https://doi.org/10.1007/s13399-024-05408-5

ORIGINAL ARTICLE

Green generation of zinc oxide nanoparticles by flower extract of orange jasmine for photodegradation of pollutant and antimicrobial activities

J. Laxmi Mangamma[1,2] · **Keloth Basavaiah**[1]

Received: 24 November 2023 / Revised: 29 January 2024 / Accepted: 5 February 2024

Abstract
In this paper, the complex problem of eliminating dye in polluted water and inhibiting the growth of microbes was discussed. The main aim of this paper is to synthesize plant-mediated zinc oxide nanoparticles by using an aqueous flower extract of orange jasmine or *Murraya paniculata* (L.) Jack *(*FM ZnO NPs) as reducing and ligating agents in the co-precipitated method. UV-DRS, UV–Vis, FTIR, TEM, XRD, EDS, FESEM, XPS, and BET techniques were employed to confirm the prepared FM ZnO NPs. Absorption of FM ZnO NPs showed a wavelength of 354 nm, band gap value of 3.22 eV, Zn–O bond vibration was at 580 cm^{-1}, and type IV adsorption isotherm was shown by BET. The synthesized FM ZnO NPs are hexagonal as revealed by SEM, with average crystallite and TEM sizes of 28.7 nm and 57.21 nm. The FM ZnO NPs used for photocatalytic activity under UV irradiation were investigated and the percentage (%) of degradation of CV by FM ZnO NPs was found to be 95%. The synthesized ZnO NPs were evaluated against pathogenic bacteria *Enterococcus faecalis* and *Pseudomonas aeruginosa* and also tested on antifungal bacteria *Aspergillus niger* and *Penicillium chrysogenum*. Among these, gram-positive *Enterococcus faecalis* (14 mm) and *Aspergillus niger* (15 mm) were efficiently inhibited at a concentration of 10 µg/mL by synthesized NPs. The current work illustrates the revolutionary method of manufacturing green ZnO NPs using a new green source and its wide range of applications.

Keywords Plant-mediated synthesis · Zinc oxide nanoparticles · Pollutant · Antifungal · Pathogenic bacteria

1 Introduction

Human health is now the primary determinant of human sustainability and continued development, and it is intimately correlated with the availability of resources for clean water. There is a severe lack of safe drinking water, particularly in developing nations, as a result of several dangerous substances seeping into freshwater bodies and the absence of affordable techniques for water filtration. Among all, synthetic dyes are seriously hazardous and major environmental pollutants due to their solubility in water. In the toxicological dye chemistry, about 40,000 to 50,000 tons are discharged into water leading to water pollution. Crystal violet is a synthetic cationic vibrant colored dye used in textile industries, staining agents in laboratories, and paints. Instead of many uses, it is carcinogenic, causes skin irritation [1], kidney failure, and permanent blindness, and damages mucous membranes and the gastrointestinal tract [2]. All of the researchers have found it quite difficult to come up with creative, environmentally friendly ways to remove the dyes from wastewater. It was discovered that nanomaterials were a potential material for wastewater dye removal. It was well recognized that these materials may be used in a variety of industries, including environmental remediation, biomedical, mechanical, pharmaceutical, electrical, bioengineering, biotechnology, and cosmetic [3, 4]. Nanotechnology plays a role in the efficient removal of organic dyes from contaminated water and the capacity to inhibit bacteria growth [5].

Nanotechnology has continuously progressed in producing nanodevices using different chemical, physical, and biological methods. Particularly, plant-mediated biological methods are easily adaptable for the synthesis of

✉ J. Laxmi Mangamma
laxmichemistry1@gmail.com

[1] Department of Chemistry, Andhra University, Visakhapatnam, India

[2] Government Degree College, Chodavaram, Visakhapatnam, India

customized nanoparticles [6, 7] with various metal oxide nanoparticles like CuO, Fe_3O_4, NiO, and ZnO being synthesized [8, 9]. Among all, ZnO NPs are prominent as they are used extensively in the field of food additives, packaging materials [10], solar cells, optoelectronic laser devices [11], gas sensors [12], pyroelectricity, luminescent materials, pigments, UV shielding materials [13], and pollutant degradation [14] protective agents in sunscreen products and cosmetics [15]. It also has significant use in biological applications [16]. ZnO NPs synthesized by various researchers by using plant extracts are *Brassica oleracea* var. botrytis leaf extract [17], aqueous leaf extract of *Dolichos Lablab* [18], *Moringa oleifera* gum[19], *Jatropha podagrica* leaf extract[20], and leaves of Elaeocarpus *Sylvestris* [21], *Hardwickia binata* leave extract [22], and pomegranate peel extract [23].

For the first time, a quick method using flowers from *Murraya paniculata* (L.) Jack (orange jasmine*)* has been established to prepare green ZnO NPs. Here, flower extract acts as a ligating agent. This plant family is Rutaceae, widely distributed from South Asia to Australia. These plant extracts are astringent and stimulating. Orange jasmine is used in traditional medicine in the treatment of headaches, abdominal pain, and dysentery [24]. Extensive research on this plant illuminated multiple pharmacological effects including anti-nociceptive, antioxidant, antidiabetic, antimicrobial, antioxidant, and analgesic activities due to the presence of various natural compounds like coumarins, indole naphthoquinone alkaloids (murrapanine) [25], phenols, terpenoids and hexa methoxy flavonoids [26]. 3,5,7,3′,4′,5′-hexamethoxy flavone, and murrayaculatine flavonoids were extracted from fresh flowers of *Murraya paniculata* (L.) Jack [27]. In a pioneering effort, ZnO NPs are successfully prepared using flower extract of *Murraya paniculata* (L.) Jack containing diverse phenolic and phytochemicals (act as ligating and enhanced stability) to achieve well-defined shapes and sizes. The diversification is achieved by selecting new and unique plant sources for synthesizing nanoparticles without the use of harmful chemicals. The present flower extract *Murraya paniculata* (L.) Jack plant extracts allow additional advantages such as productivity, tailored for specific applications, and reduced cost. The key constituents present in the flower extract of *Murraya paniculata* (L.) Jack may play a key role in the bio-reduction of metal salt. The as-synthesized FM ZnO NPs were tested as photocatalysts for the degradation of crystal violet dye in aqueous solution. As the green source has various antimicrobial properties, the synergistic effect of green synthesized FM ZnO NP antimicrobial activity is *evaluated against both gram-positive bacteria (Enterococcus faecalis) and gram-negative bacteria (Pseudomonas aeruginosa) employing the agar well diffusion method.*

2 Materials and methods

Flowers of orange jasmine were collected from the botanical garden of the VSK Government Degree College, Visakhapatnam, Andhra Pradesh, India. Zinc acetate dihydrate $Zn(OOCCH_3)_2.2H_2O$ (98% PURITY), sodium hydroxide (NaOH), and crystal violet (CV) from Merck in India were used without purification. Milli Q-water was utilized in these experiments.

2.1 Orange jasmine flower extract preparation

Fresh flowers are collected and rinsed thoroughly with milli-Q water. These flowers were then dried under shaded for 18 days until completely dry. Dried flowers were ground well into a fine powder using a grinder. One gram of the powdered flower sample was placed in a 250-mL flask, and 100 mL of milli-Q water was added. This mixture was heated at 60 °C for 30 min, yielding a brilliant brown solution. The solution was filtered through Whatman grade 1 filter paper to eliminate particulate matter, and the resultant solution was stored in a refrigerator at 4 °C for synthesis of FM ZnO NPs.

2.2 Synthesis of ZnO NPs using flower extract of orange jasmine

During the synthesis, processing parameters such as pH, temperatures, and concentrations of flower extract and precursor are to be kept under consideration. In an established process, 0.2 g of Zn $(CH_3COO)_2$, 10 mL solution of 1% flower extract of *Murraya paniculata* (L.) Jack using water as a solvent, and 80 mL Milli-Q water were taken in a flask. Then the combination was agitated in a water bath and subsequently heated to 70 °C for the time of 60 min which led to form a yellowish white–colored solution. Following this, 1 M NaOH drop was added to complete the precipitation of FM ZnO NPs at pH 12. The resultant solution underwent multiple washes and was subjected to centrifugation at 8000 rpm, and the white solid was formed after vacuum drying at 60 °C for 12 h shown in Fig. 1. A white precipitate was used for the characterization.

2.3 Characterization of synthesized FM ZnO NPs

Synthesized FM ZnO NPs were characterized by various analytical techniques. An Instrument employed to assess the wavelength of FM ZnO NPs used a modal Schimadzu-2450 double beam spectrophotometer (wavelength range of 90–700 nm). FT-IR spectra of flower extract and FM ZnO NPs were characterized by FT-IR (Model, Make Bruker). An energy-dispersive spectrum (EDS) equipped with Zeiss

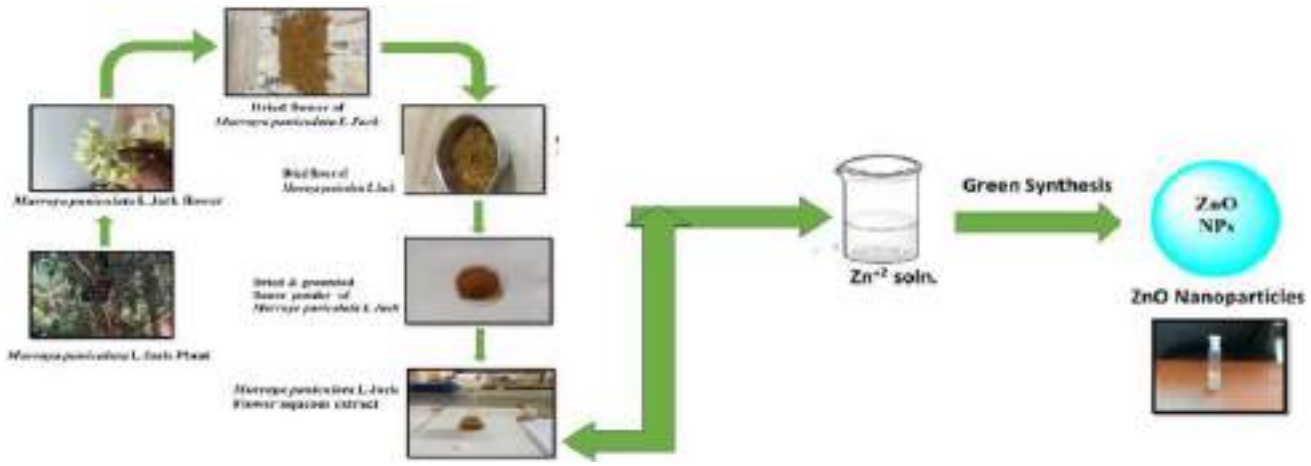

Fig. 1 Procedure for fabrication of FM ZnO NPs

Ultra-60 modal (SEM) scanning electron microscopy was used to identify the elemental composition and morphology. X-ray diffractometer (XRD) (functioning at 45 kV and 40 mA made by PANalytical X'pert) patterns of FM ZnO NPs were observed. FM ZnO NPs were examined by the model FEITECNAI G2 S-Twin (TEM) transmission electron microscopy with an accelerating voltage of 200 kV utilized to determine the size and morphology of FM ZnO NPs. Pore size, pore volume, and surface area determined by N_2 adsorption–desorption of FM ZnO NPs were investigated by instrument quanta chrome Nova 2200E. The prepared FM ZnO NPs were tested on bacterial strains and fungal strains by well diffusion method.

3 Results and discussion

The direct evidence for the formation of ZnO NPs is in Fig. 2. The UV–Vis absorption spectra of aqueous flower extract and FM ZnO NPs are in Fig. 2a; the aqueous flower extract of *Murraya paniculata* (L.) Jack has bands at 290 and 340 nm, which are attributed to the occurrence of natural products in an orange jasmine extract. A well-defined absorption peak at 354 nm [28] points to the formation of ZnO NPs in Fig. 2b and is attributed to the efficient scattering and light absorption. The absence of flower extract peaks in the prepared NPs suggests the involvement of phytochemicals in the process of reduction and encapsulation [18].

The diffuse reflectance spectra of synthesized ZnO NPs are depicted in Fig. 3. The Kubelka–Munk equation was used to calculate the band gap value of ZnO NPs and found to be 3.22 eV which is near to bulk ZnO (~3.37 eV) [29] due to flower extract that modifies the surface of the nanoparticles.

The complete picture of the different functional groups and their structural information is given through the transmittance intensities of *Murraya paniculata* (L.) Jack flower extract and prepared FM ZnO NPs in their FTIR spectra exhibited in Fig. 4.Figure 4 represents the FTIR spectrum of an aqueous flower extract and synthesized FM ZnO NPs.

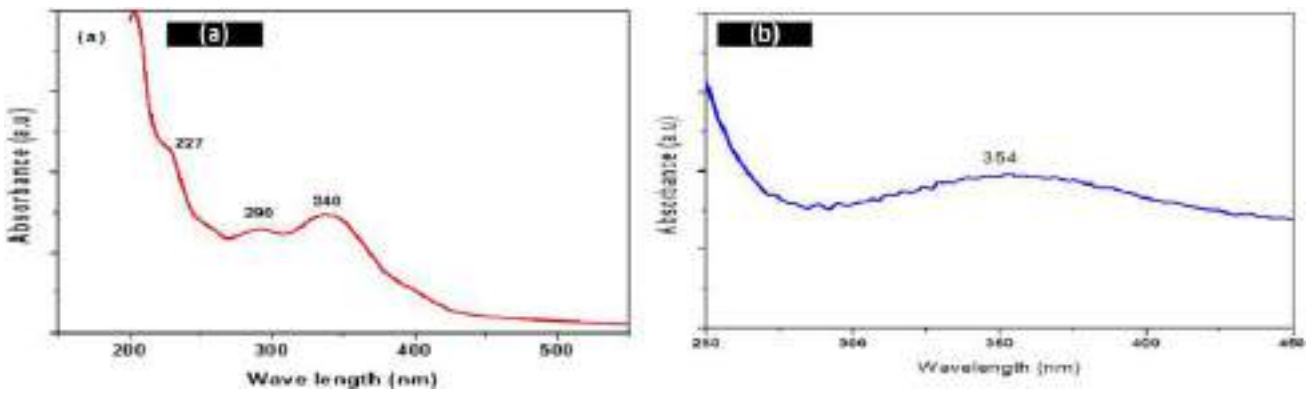

Fig. 2 UV–Vis absorption of (**a**) flower extract of *Murraya paniculata* (L.) Jack, **b** synthesized FM ZnO NPs

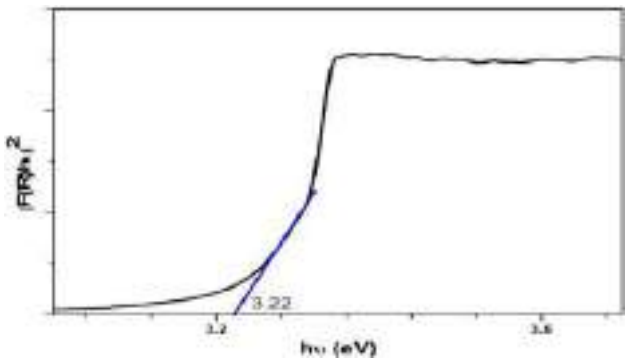

Fig. 3 UV-DRS spectrum of fabricated FM ZnO NPs

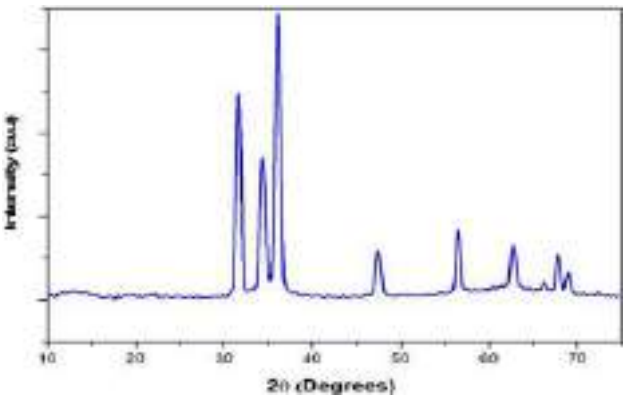

Fig. 5 Powder XRD patterns of synthesized FM ZnO NPs

The FTIR spectrum of the *Murraya paniculata* (L.) Jack, an aqueous flower extract, exhibited characteristic stretching frequencies at 3348, 2162, 1995, 1636, 1437, 1118, 1042, 889, and 634 cm^{-1} respectively. The broad peak at 3348 cm^{-1} is attributed to the OH stretching of phenolic compounds in flower extract. Carbonyl stretching in proteins causes the peak at 1636 cm^{-1}, which can be the amide band of proteins. The presence of CO groups is indicated by the peaks at 1118 and 1042 cm^{-1} in Fig. 4a. The additional peak at 580 was observed in Fig. 4b of FM ZnO NPs due to the vibration of Zn–O and also occur shifting of peaks in FM ZnO NPs [30].

Figure 5 represents the XRD spectra of ZnO. X-ray diffraction peaks obtained at 31.79°, 34.41°, 36.21°, 47.45°, 56.56°, 62.81°, 66.35°, 67.94°, 69.08°, 72.56°, and 76.95° correspond to (100), (002), (101), (102), (110), (103), (200), (112), (201), (004), and (202) planes that confirmed the presence of ZnO NPs [31]. The XRD results for fabricated NPs well agreement with standards (JCPDS No. 36–1451). The robust crystalline structure is evidenced by well-defined narrow peaks; the absence of other peaks shows the purity of the NPs. $D = k\lambda/\beta\cos\theta$ Scherrer equation was used to determine the grain size. Here, D stands for the crystal size, λ represents the wavelength of X-ray radiation ($\lambda = 0.15406$ nm) for Cu Kα, k is the shape factor (typically taken as 0.9), β corresponds to the full width at half maximum (FWHM), and θ represents the diffraction angle. The computed average crystallite size of the NPs is 28.7 nm.

FESEM images showed the hexagonal surface morphology of ZnO NPs pictured in Fig. 6a–b. Notice that most of the ZnO NPs have a large surface area and are highly agglomerated which is typical in green synthesis. The energy dispersive X-ray spectrum (EDS) depicted in Fig. 6c provides valuable information about elemental composition detected at specific signals of zinc atoms at 1 keV, 8.7 keV, and 9.6 keV along with the single peak of oxygen atom at 0.5 keV in the ZnO NPs.

TEM images depicted in Fig. 7a–b confirmed the shape and average size of synthesized FM ZnO NPs that were found to be hexagonal morphology with a size of 57.21 nm which was calculated by ImageJ through that histogram

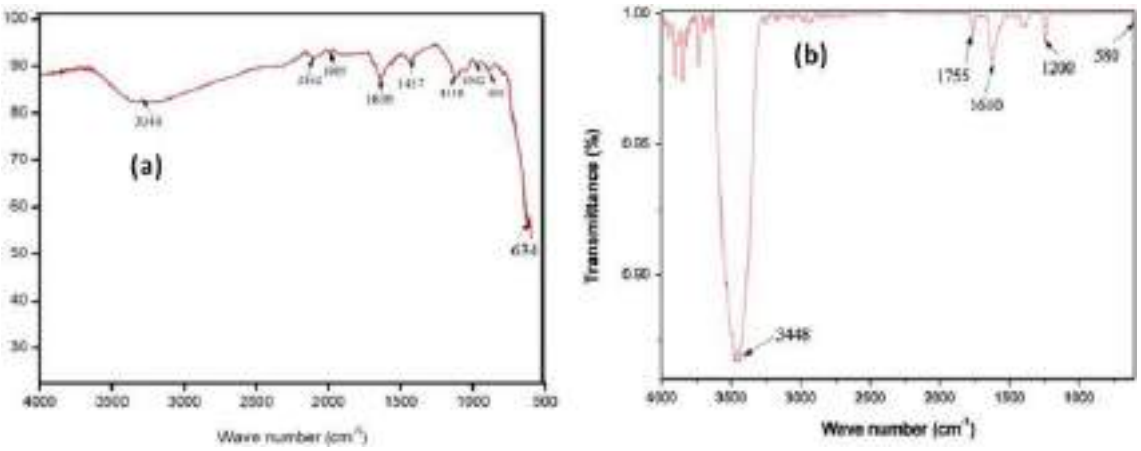

Fig. 4 **a** FTIR spectrum of *Murraya paniculata* (L.) Jack flower powder and (**b**) FTIR spectrum of FM ZnO NPs

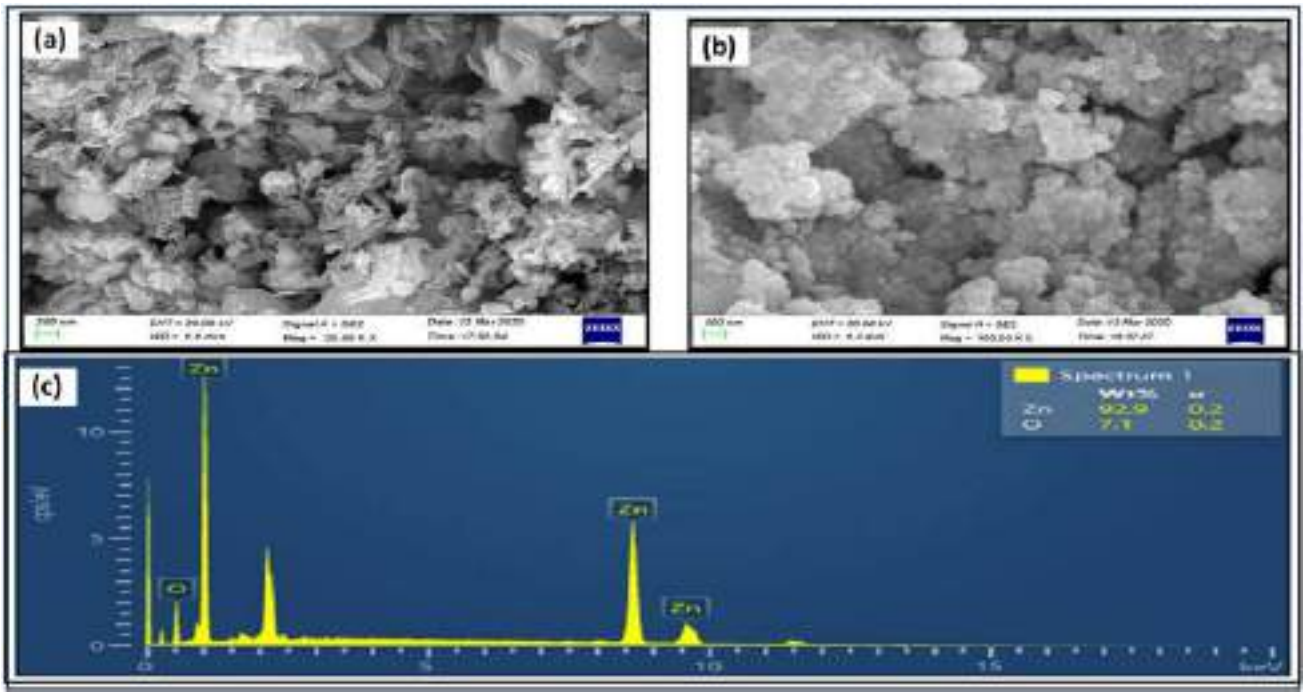

Fig. 6 **a**, **b** FESEM micrograph of green synthesized FM ZnO NPs in different magnifications, **c** EDS spectrum of synthesized FM ZnO NPs

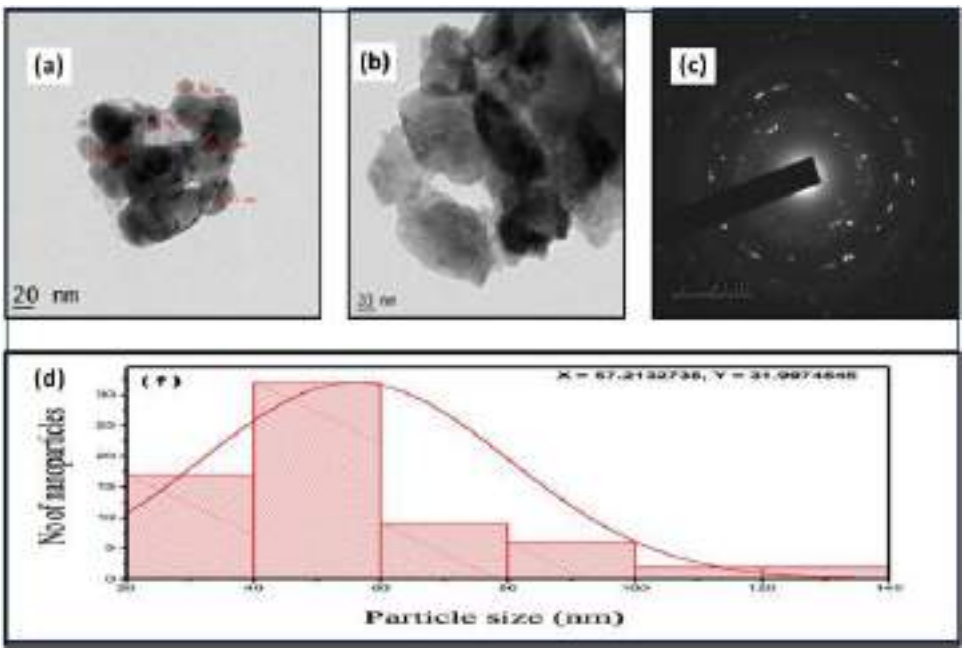

Fig. 7 **a**, **b** TEM images, **c** SAED pattern, **d** histogram of the size distribution of synthesized FM ZnO NPs

being established shown in Fig. 7d. Here, the particle size is greater than calculated crystallite size from XRD. Ring-like patterns are shown in Fig. 7c by SAED (selected area diffraction) indicating nanocrystalline nature [32].

The oxidation states and chemical composition of the elements of FM ZnO NPs were analyzed by XPS. As can be seen in Fig. 8a, the entire spectrum confirmed the presence of FM ZnO NPs capped by organic moieties, which coincides with the EDS findings. For the composition and surface electronic structure of FM ZnO NPs, X-ray photoelectron spectroscopy was employed. The peaks of Zn, O, and C elements in the XPS spectrum can be clearly observed. The detected C 1 s peak originates from the flower extract of carbon species capped on the samples.

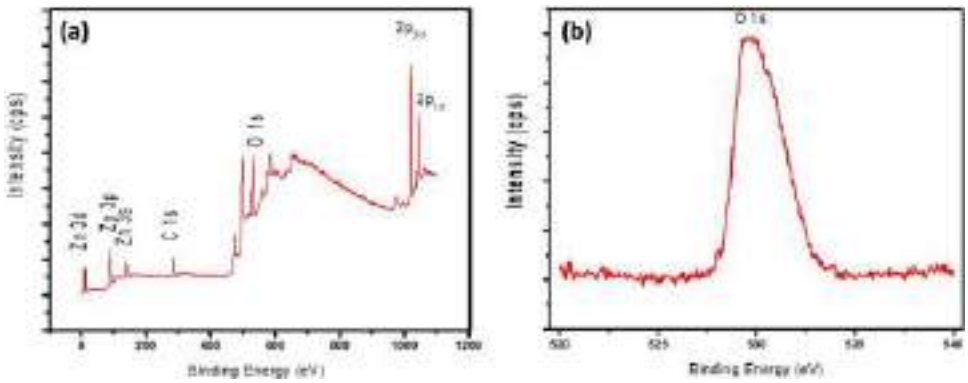

Fig. 8 XPS spectra of synthesized FM ZnO NPs

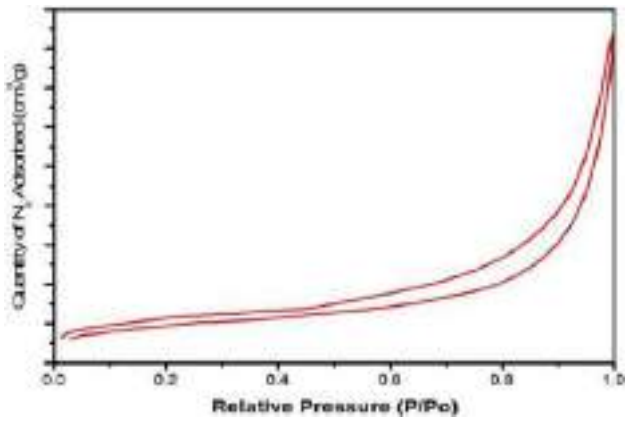

Fig. 9 BET plot for synthesized FM ZnO NPs

As reported in above Fig. 8a, the survey on XPS spectrum shows prominent peaks due to the presence of Zn 2p3/2 (1021.8 eV), Zn 2p1/2 (1044.6 eV), Zn 3 s, Zn 3p, and Zn 3d, core levels recognized along with other characteristic peaks of the O 1 s (530 eV) shown in Fig. 8b and C 1s (284.60 eV) levels. The spin orbit splitting between Zn 2p3/2 (1021.8 eV) and Zn 2p1/2 (1044.6 eV) was reported for photoelectrons excited from Zn^{+2} ions in the ZnO crystal lattice. All these binding energies are well agreed [33].

BET surface technique was used to investigate the surface structure of synthesized FM ZnO NPs. The results of BET in Fig. 9 suggest pore diameter, surface area, and pore volume, and the synthesized FM ZnO NPs were determined to be 1.66 nm, 5.84 m^2/g, and 0.0205 cm^3/g, respectively. The adsorption–desorption isotherm shows type IV indicates the mesoporous structure and maximum relative pressure (P/P_0); about 4.80 m^2/g of nitrogen was adsorbed that provides slit-shaped pores [34].

3.1 Plausible mechanism for the synthesis of FM ZnO NPs

The murayyaculatine present in an aqueous flower extract of *Murraya paniculata* (L.) Jack acted as a ligating agent during the synthesis of FM ZnO NPs. Murrayaculatine contains $–COO^-$ group acted as a capping agent as shown in Fig. 10.

3.2 Photocatalytic degradation of crystal Violet (CV)

Initially, synthesized FM ZnO NPs were used for blank experiments that were carried out without irradiation and showed no removal of CV dye. Additionally, there was no degradation observed without the catalyst in UV–visible light. The impact of pH, catalyst dosage, and concentration of the dye on the photodegradation of CV was explored in this study.

FM ZnO NP solution containing dye varied the pH between 3 and 11. The mixture solution was subjected to stirring for 30 min. After every 30 min, 5 mL of aliquots was taken and analyzed by UV–Vis spectroscopy. The absorbance data presented in Fig. 11a showed that significant degradation of the rate of CV was maximum at pH = 10. The optimum catalyst dosage can be determined by altering the FM ZnO NP quantity from 25 mg, 50 mg, and 75 mg in CV dye solution. As expressed in Fig. 11a–d, it was observed that degradation is maximum at 75 mg. This increases the number of hydroxyl radicals, and more number of dye pollutants get adsorbed on the catalyst surface which finally enhances the rate of photocatalytic degradation. But beyond 75 g of catalyst dosage, the photocatalytic activity decreased due to an increase in turbidity of solution due to which penetration of light is restricted after this maximum; the absorption intensity of CV solution at 664 nm decreased as the reaction time progressed. Figure 11b indicates the plot between the C_t/C_o of CV dye and time "t" (min). The kinetics of the photocatalytic degradation of CV could be described by pseudo-first-order kinetics and kinetic parameters shown in Table 1.

Various CV dye concentrations with increments of 5 (5,10, 15 mg/L solution) on the removal efficiency of FM ZnO NPs (75 mg) at pH = 10 were investigated. Table 2 shows the UV–Vis absorption spectra of 5 mg/L to

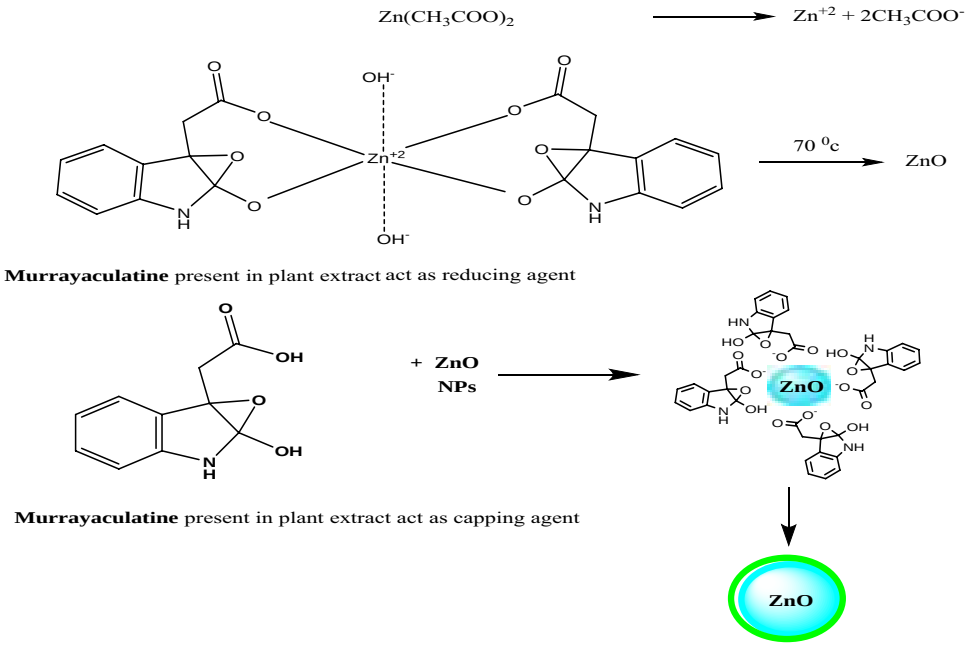

Fig. 10 Plausible reduction mechanism for the formation of FM ZnO NPs

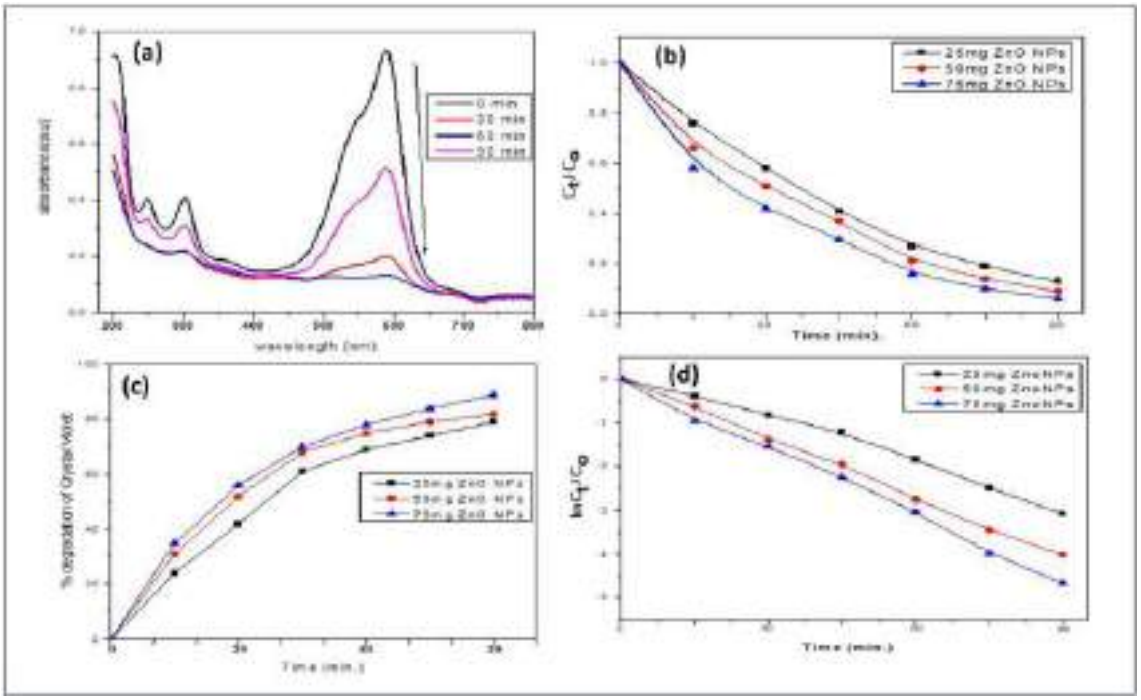

Fig. 11 **a** Spectra of CV dye degradation, **b** CV dye degradation using different dosages of catalyst. **c** % of CV dye degradation, **d** first-order rate kinetics of CV dye degradation in the presence of FM ZnO NPs

15 mg/L CV solution at different time intervals. The intensity of the CV solution maximum at 590 nm and decreased as the reaction time was progressed. The percentage (%) of degradation of 5 mg/L, 10 mg/L, and 15 mg/L CV by FM ZnO NPs was found to be 94.92%, 91.75%, and 82.56% respectively. The photocatalytic degradation kinetics of CV are described by pseudo-first-order kinetics.

$$In\left(C_t/C_0\right) = -kt \tag{1}$$

Table 1 Calculated kinetic parameters from photocatalytic degradation of CV dye at different amounts of the catalyst FM ZnO NPs at constant pH = 10

S. no	Amount of the catalyst FM ZnO NPs (mg)	Calculated rate constant (min^{-1})	Value of R^2	Time for photodegradation (min)
1	25	0.00995	0.9944	90
2	50	0.0172	0.9991	90
3	75	0.02372	0.9995	90

Table 2 The kinetic parameters obtained from photocatalytic degradation of different concentrations of CV dye using a constant amount of 75 mg of FM ZnO NPs at pH = 10

Sample number	Concentration of CV dye (mg/L)	Calculated rate constant (min^{-1})	R^2 value	Time for completion of photodegradation (min)
1	5	0.03318	0.9837	90
2	10	0.02041	0.9938	90
3	15	0.01186	0.9957	90

In the mechanism of the photocatalytic degradation of CV, the ZnO NPs are irradiated with a UV-light source leading to the formation of electron–hole pairs ($e^- + h^+$). Electrons (e^-) in the conduction band are scavenged by oxygen (O_2) molecules leading to the formation of superoxide anion $\bullet O_2^-$ and simultaneous protonation produces OOH • radicals. In the further steps, holes (h+) in the valence band react with either H_2O or OH^- to produce an active species such as hydroxyl radicals $OH^\bullet$ and superoxide anion $^\bullet O_2^-$, or highly active $OH^\bullet$ radical oxidizes CV dye to form CO_2, H_2O, and nontoxic products (Fig. 12).

3.3 Antibacterial efficacy

The antimicrobial efficacy of FM ZnO NPs was carried out against pathogenic organisms such as MTCC 439 *Enterococcus faecalis* and MTCC 424 *Pseudomonas aeruginosa* with nutrient agar medium in agar well diffusion method. Sterilize the medium and seed with the respective strains of bacteria and aseptically transfer them into each petri dish. The FM ZnO NPs were freshly dissolved in distilled H_2O and put to the tests with standard (ciprofloxacin, 5 µg/mL) and varying concentrations of 10 µg/mL, 5 µg/mL, and 2.5 µg/mL were used and introduced in petri dishes containing strains. The results of these tests were run in triplicate, and the mean and standard deviation were calculated. The activity diameter of the zone of inhibition was determined for each of the previously

Table 3 Comparison of the photocatalytic degradation of ZnO NPs in the present work with previous works

Green materials	Dye	Light source	Irradiation time (min)	Degradation efficiency (%)	Reference
Murraya paniculata (L.) Jack extract	**Crystal violet**	**UV light**	**90**	**94.92**	**Present work**
Sageretia thea aqueous extract	**Crystal violet**	**UV light**	**8 h**	**40.65**	[35]
Delonix Elata leaf extract	**Crystal violet**	**UV light**	**90**	**86**	[36]
Moringa oleifera peel extract	**Crystal violet**	**UV light**	**70**	**94**	[37]

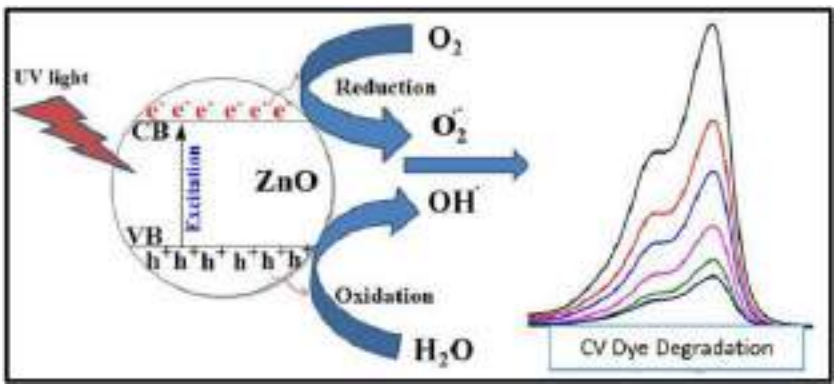

Fig. 12 Schematic diagram for the possible photocatalytic mechanism of FM ZnO NPs towards CV dye degradation

where "C_0" is the concentration of CV without FM ZnO NPs, "C_t" is the concentration of CV with FM ZnO NPs at different time intervals, and k is the first-order rate constant. The degradation efficiency of the as-prepared FM ZnO NPs was compared with that of recently reported ZnO NPs in Table 3.

stated samples using the HiMedia antibiotic zone scale, as shown in Fig. 13. Table 4 shows the observations and findings.

It is evident from Table 4 that the inhibition was dose-dependent. As indicated in Table 3, the test findings were expressed as means and standard deviation (SD) of the zone of inhibition values. From these values, it is evident that for both bacterial strains, FM ZnO NPs did not exhibit a zone of inhibition at a dose of 2.5 µg/mL. Similarly, FM ZnO NPs do not show activity against *Pseudomonas aeruginosa*, and 12.67 ± 0.58 mm against *Enterococcus faecalis* at 5 µg/mL concentration. Both strains have shown significant zone of inhibition values as 11 ± 0.58 mm and 14.67 ± 0.58 mm at 10 µg/mL. These values conclude that MIC (minimum inhibitory concentration) values for the FM ZnO NPs against *Pseudomonas aeruginosa* and *Enterococcus faecalis* were 5 µg/mL and 10 µg/mL respectively. Two bacterial strain outcomes demonstrated that FM ZnO NPs exhibited potent antibacterial activity.

3.4 Antifungal activity

The antifungal activity of FM ZnO NPs was investigated against pathogenic organisms MTCC 282 *Aspergillus niger* and MTCC 5108 *Penicillium chrysogenum* by agar-well diffusion method. Sterilized potato dextrose agar medium was seeded with the respective strains transferred aseptically in a petri dish. The FM ZnO NPs were freshly dissolved with distilled H_2O and carried out at varied concentrations (1, 2, and 3). The samples and standard (fluconazole) were placed in a 6 mm diameter well of petri plates and were incubated at 28 ± 3 °C for about 24 h. The activity diameter was measured using the HiMedia antibiotic zone scale and inhibition zone results depicted in Table 5 and inhibition shown in Fig. 14.

It revealed that the inhibition was concentration-dependent. Table 3 exhibits the test results in means and standard deviation (SD) of the zone of inhibition values. From these values, it is evident that both organisms exhibited equal values of zone of inhibition at a dose of 2.5 µg/mL. Similarly, FM ZnO NPs showed zone of inhibition value is 11 ± 0.58 against *Aspergillus niger* and 12.67 ± 0.58 value against *Penicillium chrysogenum* at 5 µg/mL concentration. Both strains have shown significant zone of inhibition values as 15.67 ± 0.58 mm and 11.67 ± 0.58 mm at 10 µg/mL. These values declared that MIC (minimum inhibitory concentration) values for the FM ZnO NPs have the same value as 2.5 µg/mL for both organisms. The outcomes demonstrated that FM ZnO NPs exhibited efficient antifungal activity.

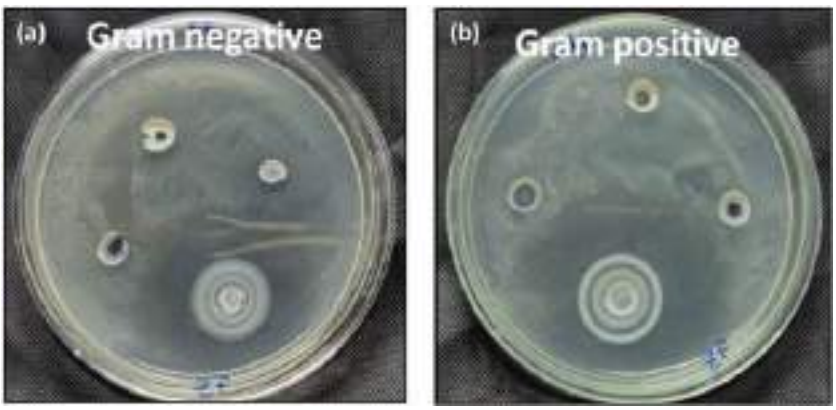

Fig. 13 Antibacterial activity of synthesized FM ZnO NPs against (**a**) gram-negative bacteria and (**b**) gram-positive bacteria

Table 4 Inhibition values of FM ZnO NPs against bacteria stains

Test organism	FM ZnO NPs			Ciprofloxacin (standard)
Con. (µg/mL)	**10**	**5**	**2.5**	**5**
Pseudomonas aeruginosa	**11 ± 0.58**	**0**	**0**	**38.67 ± 0.58**
Enterococcus faecalis	**14.67 ± 0.58**	**12.67 ± 0.58**	**0**	**38 ± 1.0**

Table 5 Inhibition values from the antifungal activity of FM ZnO NPs

Test organism	FM ZnO NPs			Fluconazole (standard)
Con. (µg/mL)	**10**	**5**	**2.5**	**5**
Aspergillus niger	**15.67 ± 0.58**	**11 ± 0.58**	**9 ± 0.58**	**14.67 ± 0.58**
Penicillium chrysogenum	**11.67 ± 0.58**	**12.67 ± 0.58**	**9 ± 0.58**	**30 ± 1.0**

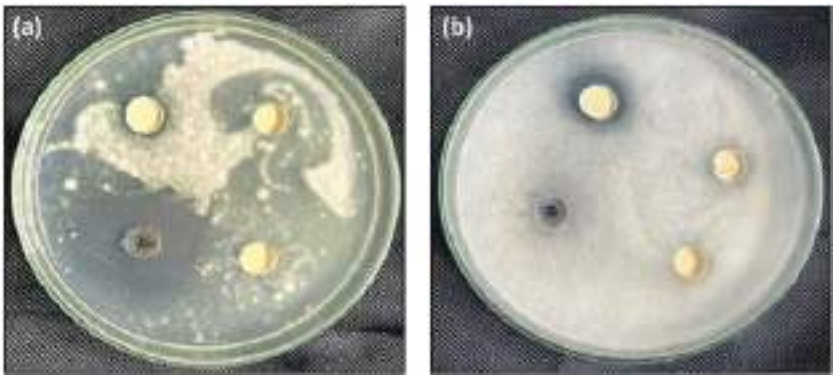

Fig. 14 Antifungal activity of synthesized FM ZnO NPs **a** *Aspergillus niger*, **b** *Penicillium chrysogenum*

4 Conclusion

In this study, an aqueous flower extract of *Murraya paniculata* (L.) Jack has alkaloids, phenolic acid, flavonoids, tannins, terpenoids, and carbohydrate active functional groups which act as ligating to the formation of NPs. The synthesized NPs were characterized by different analytical techniques which conformed to the Zn–O bond, hexagonal shape of NPs, the average size of 57 nm, and high crystallinity. The band gap value of FM ZnO NPs is found to be 3.22 eV. The observed H4 type hysteresis loop of surface area was 5.84 m^2/g eased by the BJH method. Catalytic and antibacterial application of as-synthesized ZnO NPs was reported. The synthesized NPs have more potential for photocatalytic activity towards CV dye removal from 94.92% within 90 min and followed first-order kinetics. It is observed that potent antibacterial efficacy towards gram-positive *Enterococcus faecalis* than gram-negative *Pseudomonas aeruginosa*. In addition to that, efficient anti fungal activity against *Aspergillus niger* was achieved using 10 µg/ml and 5 µg/ml concentrations of synthesized nanoparticles. The novel plant extracts allow additional advantages such as productivity, tailored for specific applications, and reduced cost. In this present research, synthesized ZnO NPs showed outstanding adsorption for eliminating crystal violet dye and moderately inhibited the growth of gram-positive, gram-negative, and anti-fungal microbes.

Acknowledgements The authors express sincere gratitude to Dr. P. L Kishore, I. Manga Raju, students and faculty of Dr. VSK GDC, Visakhapatnam and GDC, Chodavaram Chemistry Department.

Author contribution Laxmi Mangamma J. wrote the manuscript, and Keloth Basavaiah reviewed the manuscript.

Data availability This declaration is "not applicable."

Declarations

Ethical approval This declaration is "not applicable."

Competing interests The authors declare no competing interests.

References

1. Mittal A, Mittal J, Malviya A, Kaur D (2010) Gupta VK (2010) Adsorption of hazardous dye crystal violet from wastewater by waste materials. J Colloid Interface Sci 343(2):463–473. https://doi.org/10.1016/j.jcis.2009.11.060
2. Awadallah-F A, Al-Muhtaseb SA (2016) Removal of crystal violet from wastewater using resorcinol-formaldehyde carbon xerogels. Sep Sci Technol 51(3):403–415. https://doi.org/10.1080/01496395.2015.1112398
3. Shaba EY, Jacob JO, Tijani JO et al (2021) A critical review of synthesis parameters affecting the properties of zinc oxide nanoparticle and its application in wastewater treatment. Appl Water Sci 11:48. https://doi.org/10.1007/s13201-021-01370-z
4. Faisal S, Jan H, Shah SA, Shah S, Khan A, Akbar MT, Rizwan M, JanWajidullah F, Akhtar N, Khattak A, Syed S (2021) ACS Omega 6(14):9709–9722. https://doi.org/10.1021/acsomega.1c00310
5. Kouhbanani MAJ, Mosleh-Shirazi S, Beheshtkhoo N, Kasaee SR, Nekouian S, Alshehery S, Kamyab H, Chelliapan S, Ali MA, Amani AM (2023) Investigation through the antimicrobial activity of electrospun PCL nanofiber mats with green synthesized Ag–Fe nanoparticles. J Drug Deliv Sci Technol 85:104541. https://doi.org/10.1016/j.jddst.2023.104541. (**ISSN 1773-2247**)
6. Kamyab H, Chelliapan S, Tavakkoli O, Mesbah M, Khan Bhutto J, Khademi T, Kirpichnikova I, Ahmad A, ALjohani AA (2022) A review on carbon-based molecularity-imprinted polymers (CBMIP) for detection of hazardous pollutants in aqueous solutions. Chemosphere. 308(part3):136471. https://doi.org/10.1016/j.chemosphere.2022.136471. (**ISSN0045-6535**)
7. Albrecht MA, Evans CW, Raston CL (2006) Green chemistry and the health implications of nanoparticles. Green Chem 8:417–432. https://doi.org/10.1039/B517131H
8. Tejaswini G, Lakshmi Kishore P, Naga Lakshmi V, Bhagya Lakshmi K (2022) A comprehensive review on green synthetic approaches and applications of 3D-series metal oxide nanoparticles. Asian J Chem 34:2478–2488. https://doi.org/10.14233/ajchem.2022.23904
9. LaxmiMangamma J, Rama Devi D, VidyaSagar PSR, Ramesh Babu M, Basavaiah K (2022) Review on plant mediated green synthesis of magnetite nanoparticles for pollution abatement, biomedical and electronic applications. Asian J Chem 34(5):1047–1054
10. Al-Naamani L, Dobretsov S, Dutta J (2016) Chitosan-zinc oxide nanoparticle composite coating for active food packaging applications. Innov Food Sci EmergingTechnol 38:231–237. https://doi.org/10.1016/j.ifset.2016.10.010
11. Sankapal BR, Gajare HB, Karade SS, Salunkhe RR, Dubal DP (2016) Zinc oxide encapsulated carbon nanotube thin films for energy storage applications. Electrochim Acta 192:377–384. https://doi.org/10.1016/j.electacta.2016.01.193

12. Kumar R, Al-Dossary O, Kumar G, Umar A (2015) Zinc oxide nanostructures for NO 2 gas–sensor applications: a review. Nano-Micro Lett 7:97–120. https://doi.org/10.1007/s40820-014-0023-3
13. Kumar SG, Rao KK (2015) (2015) Zinc oxide based photocatalysis: tailoring surface-bulk structure and related interfacial charge carrier dynamics for better environmental applications. RSC Adv 5:3306–3351. https://doi.org/10.1039/C4RA13299H
14. Hatamie A, Khan A, Golabi M, Turner AP, Beni V, Mak WC, Sadollahkhani A, Alnoor H, Zargar B, Bano S (2015) Zinc oxide nanostructure-modified textile and its application to biosensing, photocatalysis, and as antibacterial material. Langmuir 31:10913–10921. https://doi.org/10.1021/acs.langmuir.5b02341
15 Khalafi T, Buazar F, Ghanemi K (2019) Phycosynthesis and enhanced photocatalytic activity of zinc oxide nanoparticles toward organosulfur pollutants. Sci Rep 9:6866. https://doi.org/10.1038/s41598-019-43368-3
16. Kamyab H, Chelliapan S, Hayder G, Yusuf M, Mahdi Taheri M, Rezania S, Hasan M, Kumar Yadav K, Khorami M, Farajnezhad M, Nouri J (2023) Exploring the potential of metal and metal oxide nanomaterials for sustainable water and wastewater treatment: a review of their antimicrobial properties. Chemosphere 335:139103. https://doi.org/10.1016/j.chemosphere.2023.139103. (**ISSN 0045-6535**)
17. Manojkumar U, Kaliannan D, Srinivasan V, Balasubramanian B, Kamyab H, HaiderMussa Z, Palaniyappan J, Mesbah M, Chelliapan S, Palaninaicker S (2022) Green synthesis of zinc oxide nanoparticles using Brassica oleracea var. botrytis leaf extract: photocatalytic, antimicrobial and larvicidal activity. Chemosphere 323:138263. https://doi.org/10.1016/j.chemosphere.2023.138263
18. Kahsay MH, Tadesse A, RamaDevi D, Belachew N, Basavaiah K (2019) Green synthesis of zinc oxide nanostructures and investigation of their photocatalytic and bactericidal applications. RSC Adv 9(63):36967–36981. https://doi.org/10.1039/C9RA07630A
19 Manikandan V, Balasubramanian B, Bharti B et al (2022) Development of ZnO/MOGAC nanocomposites for enhanced photocatalytic removal of PO_4^{3-} and NO_3- ions from wastewater under various light irradiations. Biomass Conv Bioref. https://doi.org/10.1007/s13399-021-02173-7
20. Golthi V, Kommu J, Ramesh AV (2023) A green and sustainable approach to the fabrication of ZnO nanoparticles via *Jatropha podagrica* leaf extract for effective dye degradation and antibacterial applications. Colloid Polym Sci. https://doi.org/10.1007/s00396-023-05187-x
21. Tejaswini G, Lakshmi Kishore P, Kiran Kumar P et al (2023) Bio designed ZnO nanoparticles with leaves of elaeocarpus sylvestris and investigation of photocatalyst for dye degradation and antimicrobial applications. Arab J Sci Eng. https://doi.org/10.1007/s13369-023-07944-0
22 Manimegalai P, Selvam K, Loganathan S et al (2023) Green synthesis of zinc oxide (ZnO) nanoparticles using aqueous leaf extract of *Hardwickia binata*: their characterizations and biological applications. Biomass Conv Bioref. https://doi.org/10.1007/s13399-023-04279-6
23 Shaban AS, Owda ME, Basuoni MM et al (2022) *Punica granatum* peel extract mediated green synthesis of zinc oxide nanoparticles: structure and evaluation of their biological applications. Biomass Conv Bioref. https://doi.org/10.1007/s13399-022-03185-7
24. Kjanijou M, Jiraungkoorskul K, Kosai P, Jiraungkoorskul W (2012) Effect of Murraya paniculata leaf extract against Culex quinquefasciatus larva. Asian J Biol Sci 5(4):201–208. https://doi.org/10.3923/ajbs.2012.201.208
25. Wu T-S, Liou M-J, Lee C-J, Jong T-T, McPhail AT, McPhail DR, Lee K-H (1989) Structure and synthesis of murrapanine, a novel skeletal indolenaphthoquinone alkaloid and cytotoxic principal from Murraya paniculata var. omphalocarpa. Tetrahedron Lett 30:6649–6652. https://doi.org/10.1016/S0040-4039(00)70641-1
26. Wiart C, Chapter 8 - Antiparasitic Asian medicinal plants in the Clade Malvids, Editor(s): Christophe Wiart (2021) Medicinal plants in Asia and Pacific for parasitic infections, Academic Press, pp 233–348, ISBN 9780128168110. https://doi.org/10.1016/B978-0-12-816811-0.00008-1
27. Wu T-S, Chan Y-Y, Leu Y-L, Huang S-C (1994) A flavonoid and indole alkaloid from flowers of Murraya paniculata. Phytochemistry 37:287–288. https://doi.org/10.1016/0031-9422(94)85045-3
28 Raha S, Ahmaruzzaman Md (2022) ZnO nanostructured materials and their potential applications; progress, challenges and perspectives. Nano scale Adv 4:8. https://doi.org/10.1039/D1NA00880C
29. Varadavenkatesan T, Lyubchik E, Pai S, Pugazhendhi A, Vinayagam R, Selvaraj R (2019) Photocatalytic degradation of rhodamine B by zinc oxide nanoparticles synthesized using the leaf extract of Cyanometra ramiflora. J Photochem Photobiol B Biol 199:111621. https://doi.org/10.1016/j.jphotobiol.2019.111621. (**ISSN 1011–1344**)
30 El-Khawaga AM, Elsayed MA, Gobara M et al (2023) Green synthesized ZnO nanoparticles by *Saccharomyces cerevisiae* and their antibacterial activity and photocatalytic degradation. Biomass Conv Bioref. https://doi.org/10.1007/s13399-023-04827-0
31. Jamdagni P, Khatri P, Rana JS (2016) Green synthesis of zinc oxide nanoparticles using flower extract of Nyctanthes arbortristis and their antifungal activity. J King Saud Univ-Sci 30(2):168–175. https://doi.org/10.1016/j.jksus.2016.10.002
32. Abdelbaky AS, Mohamed AMHA, Sharaky M et al (2023) Green approach for the synthesis of ZnO nanoparticles using *Cymbopogon citratus* aqueous leaf extract: characterization and evaluation of their biological activities. Chem Biol Technol Agric 10:63. https://doi.org/10.1186/s40538-023-00432-5
33. Mahana A, Mehta SK (2021) Potential of *Scenedesmus*-fabricated ZnO nanorods in photocatalytic reduction of methylene blue under direct sunlight: kinetics and mechanism. Environ Sci Pollut Res 28:28234–28250. https://doi.org/10.1007/s11356-021-12682-7
34. Khan M, Ware P, Shimpi N (2021) Synthesis of ZnO nanoparticles using peels of *Passiflora foetida* and study of its activity as an efficient catalyst for the degradation of hazardous organic dye. SN Appl Sci 3:528. https://doi.org/10.1007/s42452-021-04436-4
35. Khalil AT, Hameed S, Afridi S, Mohamed HEA, Shinwari ZK (2021) *Sageretia thea* mediated biosynthesis of metal oxide nanoparticles for catalytic degradation of crystal violet dye. Mater Today: Proceedings 36:397–400. https://doi.org/10.1016/j.matpr.2020.04.687
36. Karthik P, Ravichandran S, Mukkannan A, Rajesh J (2022) Plant-mediated biosynthesis of zinc oxide nanoparticles from Delonix Elata: a promising photocatalyst for crystal violet degradation. Inorg Chem Commun 146:110122. https://doi.org/10.1016/j.inoche.2022.110122
37. Surendra TV, Roopan SM, Al-Dhabi NA, Arasu MV, Sarkar G, Suthindhiran K (2016) Vegetable peel waste for the production of ZnO nanoparticles and its toxicological efficiency, antifungal, hemolytic, and antibacterial activities. Nanoscale Res Lett 11:1–10. https://doi.org/10.1186/s11671-016-1750-9

Inorganic Chemistry Communications 162 (2024) 112290

Contents lists available at ScienceDirect

Inorganic Chemistry Communications

journal homepage: www.elsevier.com/locate/inoche

Short communication

Facile green fabrication of magnetite nanoparticles using an aqueous flower extract of *Murraya paniculata (L) Jack* for an efficient removal of organic dye pollutant, antibacterial activities

J. Laxmi Mangamma [a,b,*], Keloth Basavaiah [a]

[a] Department of Inorganic and Analytical Chemistry, Andhra University, Visakhapatnam, India
[b] Government Degree College, Chodavaram, Visakhapatnam, India

ARTICLE INFO

Keywords:
Plant mediated synthesis
Magnetite nanoparticles
Organic dye pollutant
Antimicrobial

ABSTRACT

This article reports, the plant-mediated synthesis of Magnetite nanoparticles achieved by utilising an aqueous flower extract of Murraya paniculata (L) Jack (FMPM NPs). The active compounds are phenols, alkaloids, flavones and terpenoids in the aqueous flower extract of Murraya paniculata act as ligating agents to synthesize novel green superparamagnetic magnetite nanoparticles by the coprecipitation method. As prepared FMPM NPs have been characterized by a range of spectroscopic and microscopic techniques. All spectroscopic and microscopic results confirmed the occurrence of pure FMPM NPs. Fourier transform-infrared spectroscopy (FTIR) shows the presence of a Fe-O bond and the band gap was found to be 2.57 eV for FMPM NPs. The surface area of the synthesized nanoparticles was 70.31 m^2/g evaluated by BET analysis. The elemental analysis has been performed by the XPS technique. The XRD pattern revealed the crystal size of 14.12 nm of FMPM NPs. TEM images show the spherical shaped FMPM NPs with an average particle size of 11.58 nm. SEM results clearly show spherically shaped FMPM NPs. The superparamagnetic character of FMPM NPs is revealed by the VSM curve and saturation magnetization (Ms) value of 58 emu/g. FMPM NPs used for photocatalytic activity, tested against gram positive, gram negative and antifungal bacteria. As prepared FMPM NPs, showed 93 % removal efficiency of Fast sulphon black-F dye pollutant. Moreover, FMPM NPs efficiently inhibit the growth of Enterococcus faecalis and Penicillium chrysogenum. The current research is for the fabrication of magnetite nanoparticles utilising novel green source and examining their applications.

1. Introduction

Recent past, synthesis and applications of functional metal oxide [1,2], mixed metal oxides [3,4] and nano composites [5,6] have received great importance owing to their unique physio-chemical, electrical, thermal, and optical properties than their bulk counterpart because of their high surface area and small size [1]. Especially, superparamagnetic metal oxide nanoparticles, with small size and aggregate free nanoparticles have been employed for biomedical applications [2]. Among, all the superparamagnetic metal oxide nanoparticles, the magnetite nanoparticles (Fe_3O_4 NPs) have emerged as a potential material for biomedical, catalysis, high density storage and optoelectrics applications [2].

Many approaches have been adopted for the fabrication of size and shape-controlled Fe_3O_4 NPs such as hydrothermal, microemulsion, sono chemical, solvothermal, electrochemical, co-precipitation, and sol–gel techniques [7–13]. These were not suitable for biomedical applications due to the use of dangerous chemicals like sodium borohydride, toluene and dimethyl formamide. Therefore, it is highly required to synthesize Fe_3O_4 NPs via green synthetic approaches utilising biological materials such as fungi, bacteria, yeast and plant extracts. However, the synthesis of nanoparticles using fungi, and bacteria have limitations such as handling of microbes and large-scale industrial production [14]. Among all biological synthetic approaches, the plant mediated synthesis has emerged as a potential approach due to its simple, green, facile, cost effective, large scale industrial production and suitability for biomedical applications.

Moreover, in plant mediated synthesis of nanoparticles, phytochemicals present in plant extracts can act as both reducing and ligating agent for the preparation of size, shape controlled and aggregate free

* Corresponding author at: Department of Inorganic and Analytical Chemistry, Andhra University, Visakhapatnam, India.
E-mail address: laxmichemistry1@gmail.com (J. Laxmi Mangamma).

https://doi.org/10.1016/j.inoche.2024.112290
Received 7 November 2023; Received in revised form 7 March 2024; Accepted 10 March 2024
Available online 11 March 2024

Fe_3O_4 NPs. Furthermore, these NPs are synthesized without using an external oxidizing and reducing agents. The active biomolecules capped Fe_3O_4 NPs have enhanced biomedical activities than conventionally prepared Fe_3O_4 NPs [15]. This is due to the synergetic effect of Fe_3O_4 NPs and bioactive molecules in the plant extracts. Numerous plant extracts have been employed for the preparation of Fe_3O_4 NPs are *Jatropha podagrica* aqueous leaf extract [16] *Chlorella vulgaris* extract [17] aqueous leaf extract of *Elaeocarpus Sylvestris* [18], aqueous leaf extract Zanthoxylum armatum DC [19], pod extract of Dolchos lablab L [20], Rhus coriarja seed extract [21], Prunus serrulate leaf extract [22], Menthapulegium L.leaf extract [23] and pomegranate leaves extract [24] (see Tabel 1).

Murraya paniculata (L) Jack is a family of Rutaceae [25] and is cultivated in gardens for smelling flowers [26]. It is available in India and employed as an herbal medicine to treat dysentery, cough and diarrhoea. The phytochemical studies reveal that *Murraya paniculata* contains alkaloids, flavonoids, essential oils and coumarins [27]. Recently, published an article by use of this flower extract for the preparation of ZnO nanoparticles [28]. With this awareness, the research aimed to adopt an eco-conscious method for the preparation of magnetite by utilising the flower extract of *Murraya paniculata (L) Jack*. Moreover, the diverse phytochemicals present in plant extract played a role in the formation of stabilised nanoparticles. Maximising to investigation of the capabilities of different plant species is essential to synthesising nanoparticles of additional advantages like enhancing yield, ease of synthesis, scalability, rapid, cost-effective, size, and morphology are specialised properties suitable for specific applications. Here, aqueous plant extracts are used due to biocompatibility, nontoxic solvent and preserves bioactive compounds [29]. We report for the first time the synthesis of FMPM NPs utilising flower extract of *Murraya paniculata (L) Jack* for an efficient removal of organic dye pollutant and antimicrobial activities. FMPM NPs were also investigated against *Enterococcus faecalis, Pseudomonas aeruginosa, Aspergillusniger* and *Penicilliumchrysogenum.*

2. Experimental methods

2.1. Chemicals and reagents

All analytical grade chemicals i.e, Ferrous sulphate heptahydrate, Ferric chloride hexa hydrate, Ammonia, Millie Q water, Ethanol, and Fast Sulphon black-F (FSB) were from Merck utilized for these experiments. *Murraya paniculata* flowers were collected from Dr V. S. Krishna Government Degree College, Botanical Garden Visakhapatnam, Andhra Pradesh, India. Sources of strains Enterococcus faecalis, Pseudomonas aeruginosa Aspergillusniger, Penicilliumchrysogenum collected from IMTECH, Chandigarh, India.

Table 1
Study of magnetite nanoparticles with literature.

Plant extract	Average particle size (nm)	Crystallite size	Structure	Reference
Murraya paniculata (L) flower	14.12	11.58	Spherical	Present work
Jatropha podagrica leaves	15.57	14.10	Hexagonal Cubic and rod shaped	[16]
Zanthoxylum Armatum DC leaves	17	20.7	Spherical	[19]
Sargassum Muticum	18	17–25	Spherical	[14]
Pomegranate leaves	45–60	56	Spherical	[24]

2.2. Preparation of an aqueous flower extract of Murraya paniculata

Murraya paniculata flowers were collected from plant, then washed with water and shade dried for 20 days. Dried flowers were grounded into fine powder stored in an airtight container for further use. Prepared 1 % aqueous flower extract, and 1 g of flower powder taken in Erlen Meyer flask.100 mL distilled water was added and heated at 60° for 20 min. The extract was subsequently cooled and filtered through Whatman paper shown in Fig. 1 resulting filtrate was preserved at 4 °C for the preparation of magnetite nanoparticles.

2.3. Preparation of Fe_3O_4NPs using an aqueous flower extract of Murraya paniculata

In this process, optimised temperature, pH levels, concentration of flower extract and concentration of precursors. With an established procedure, FMPM NPs were prepared by co-precipitation method by utilising an aqueous flower extract of *Murraya paniculata*. In the standard procedure, dissolving 2:1 M ratio of $FeCl_3{\cdot}6H_2O$ (0.11 g) and $FeSO_4{\cdot}7H_2O$ (0.556 g) in 90 mL of distilled water and subjected to 10 min of stirring. Then heated to 80 °C with constant stirring for 10 min. Afterwards, 10 mL of a 1 % aqueous flower extract of *Murraya paniculata* was introduced to the mixture and it proceeded at 80 °C for 30 min under continuous stirring. Finally,7 mL of 25 % ammonia was added slowly and pH adjusted to 10. The mixture solution was turned into a black precipitate which indicates the formation of FMPM NPs. The FMPM NPs precipitate was separated by external magnetite washed periodically with ethanol and Milli-Q water and finally dried.

2.4. Characterization of FMP Fe_3O_4 NPs

Various techniques have been used to characterise the synthesised FMPM NPs. A SCHIMADZU-2450 (Make, SCHIMADZU, Japan) double beam spectrophotometer of the wavelength range of 190–700 nm was used to measure FMPM NPs made from *Murraya paniculata (L) Jack* flower extract. The FT-IR spectra of *Murraya paniculata (L) Jack* extract and FMPM NPs were carried out by utilising an FT-IR spectrophotometer (Model, Make Bruker). Scanning Electron Microscopy (SEM), (FE-SEM, Zeiss Ultra-60) with an energy dispersive spectrum (EDS), as well as a PANalyticalX'pert X-Ray Diffractometer (XRD) performed at 40 mA and 45 kV, the morphology and elemental analysis of produced FMPM NPs were studied. Transmission electron microscopy (TEM model FEI TECNAI G2 S-Twin) with a 200 kV accelerating voltage was used to determine the size and morphology of FMPM NPs. To determine the magnetic characteristics of FMPM NPs, a Vibrating sampling magneto meter (VSM) was used (Lake Shore Cryotronics, Inc., Idea-VSM, model 7410, USA). Thermogravimetric/differential thermal analysis (TGA derivative) was used to examine the FMPM NPs thermal characteristics (NETZSCH STA 449 F3 Jupiter). Prepared FMPM NPs were investigated against two bacteria and also against two fungi **(**MTCC 439) *Enterococcus faecalis***,** **(**MTCC 424) *Pseudomonas aeruginosa* and also against two fungi *Aspergillus niger* (MTCC 282) *Penicillium chrysogenum* (MTCC 5108).

3. Results and discussion

UV–Vis spectral investigation confirms the formation and stability of FMPM NPs in an aqueous colloidal solution. Fig. 2**a** shows that the peaks at 290 nm and 341 nm were found in an extract of *Murraya paniculata (L) Jack* and the highest absorbance band was located at a wavelength of 355 nm indicating that $FeCl_3$ had been reduced to FMPM NPs. Fig. 2**b** shows the band gap at 2.57 eV.

Murraya paniculata (L) Jack extract was subjected to FT-IR analysis to identify the functional groups and forecast their role in the formation of FMPM NPs. The FT-IR spectra of an extract of *Murraya paniculata (L) Jack* is depicted in the figure (Fig. 2**c**). The significant absorption band at 3348 cm^{-1} is attributed to the alcohol and phenolic compound O—H

Fig. 1. A *Murraya paniculata* flower **b** Dried grounded flower powder of *Murraya paniculata* **c.** Aqueous extract of *Murraya paniculata* flower powder.

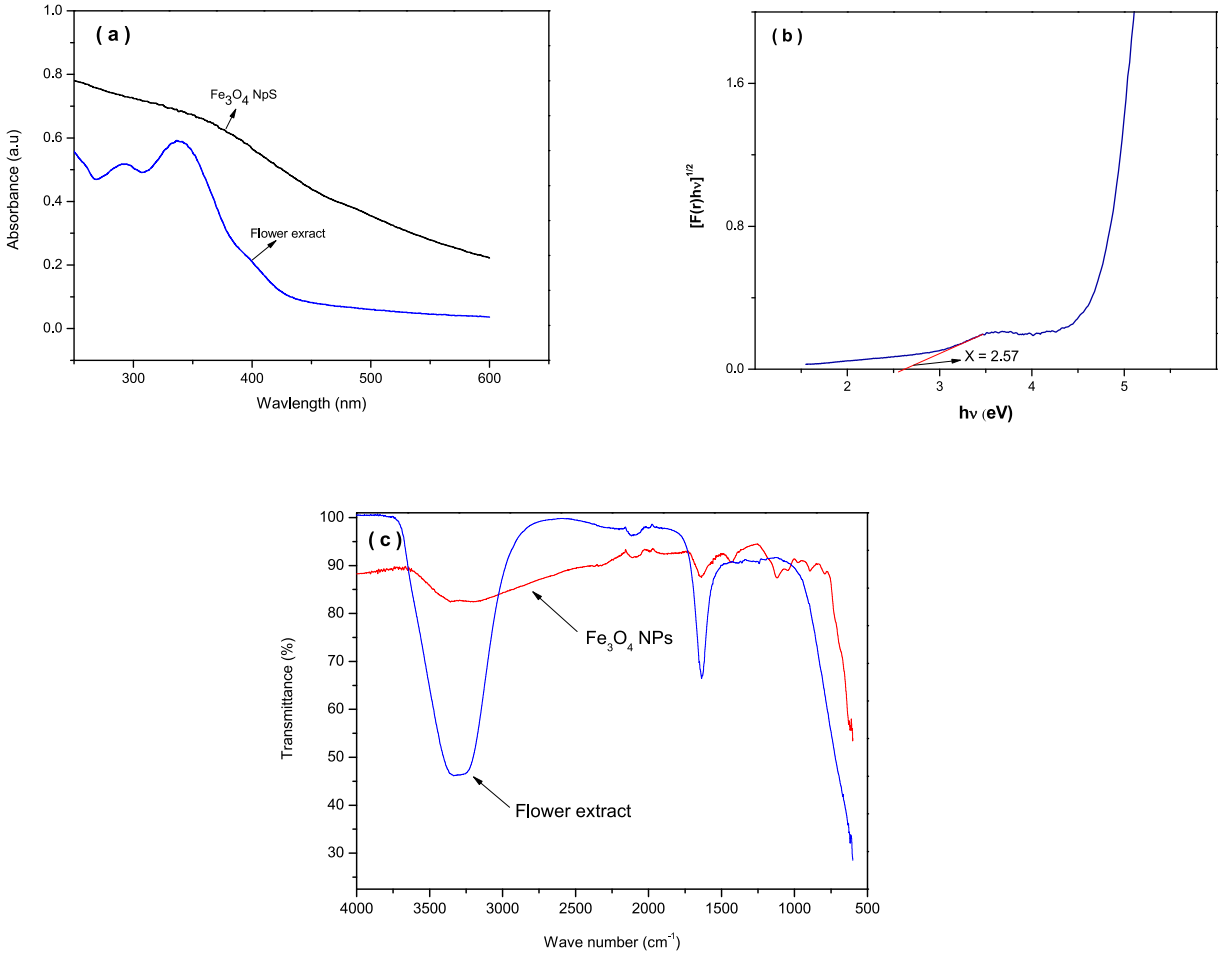

Fig. 2. A. UV–Visible Spectra of Murraya paniculata (L) Jack flower aqueous extract and FMPM NPs. **b.** UV–Vis diffuse reflectance (%R) spectra of FMPM NPs. **c.** FTIR spectra of FMPM NPs.

stretching band. The peak at 1636 cm^{-1} is due to CO stretching groups in ketones, aldehydes, and carboxylic acids in plant extracts [30]. The Fe—O band is characteristic of the production of FMPM NPs, which has absorption bands ranging from 418 to 549 cm^{-1} [31].

The XRD patterns of FMPM NPs are shown in Fig. 3**a**. The diffraction peaks observed indices are (022), (122), (025), (210), and (230). The planes are responsible for the peaks at $\theta = 30.100^0$, 35.470^0, 43.140^0, 57.120^0, and 62.570^0, respectively. All the peaks of XRD are clearly in line with the reported JCPDS file no. 89-6466 and can be indexed to XRD results clearly shows that formation and there were no impurity peaks found [32]. Pure FMPM NPs with Orthorhombic structure. The Debye-Scherrer equation $D = K / \text{Cos}\ \theta$ [12]. was used to compute the crystal size of 14.12 ± 0.02 nm of the produced nanoparticles. An XRD pattern shows that the bio-route iron oxide nanoparticles are crystalline.

A VSM technique was used to analyse the magnetic behaviour of synthetic FMPM NPs made with an aqueous flower extract of *Murraya paniculata (L) Jack*. Fig. 3**b** shows the magnetization curve for the produced FMPM NPs. With a saturation magnetization (Ms) value of (0.5831) 58 emu/g at room temperature, the magnetization curve displays superparamagnetic behaviour with a sigmoidal shape and no hysteresis loop [33].

In the TGA/DTA study, when heated from 40 to 750 °C the FMPM NPs produced with an aqueous flower extract of *Murraya paniculata (L) Jack* lost 10 % of their weight overall. There were two stages to the weight loss process. At 40 to 170 °C, surface water and volatile components were removed from the nanoparticles (2.7 % loss). Weight loss of 7.30 percent was recorded in the second phase from 170 to 750 °C as shown in Fig. 3**c** which showed that biomolecules around the nanoparticles degraded rapidly [34,35].

Pore volume and surface area of FMPM NPs were determined using liquid nitrogen temperature, N_2 adsorption and desorption isotherms with exact pore size determination (Brunauer-Emmett-Teller, BET). The

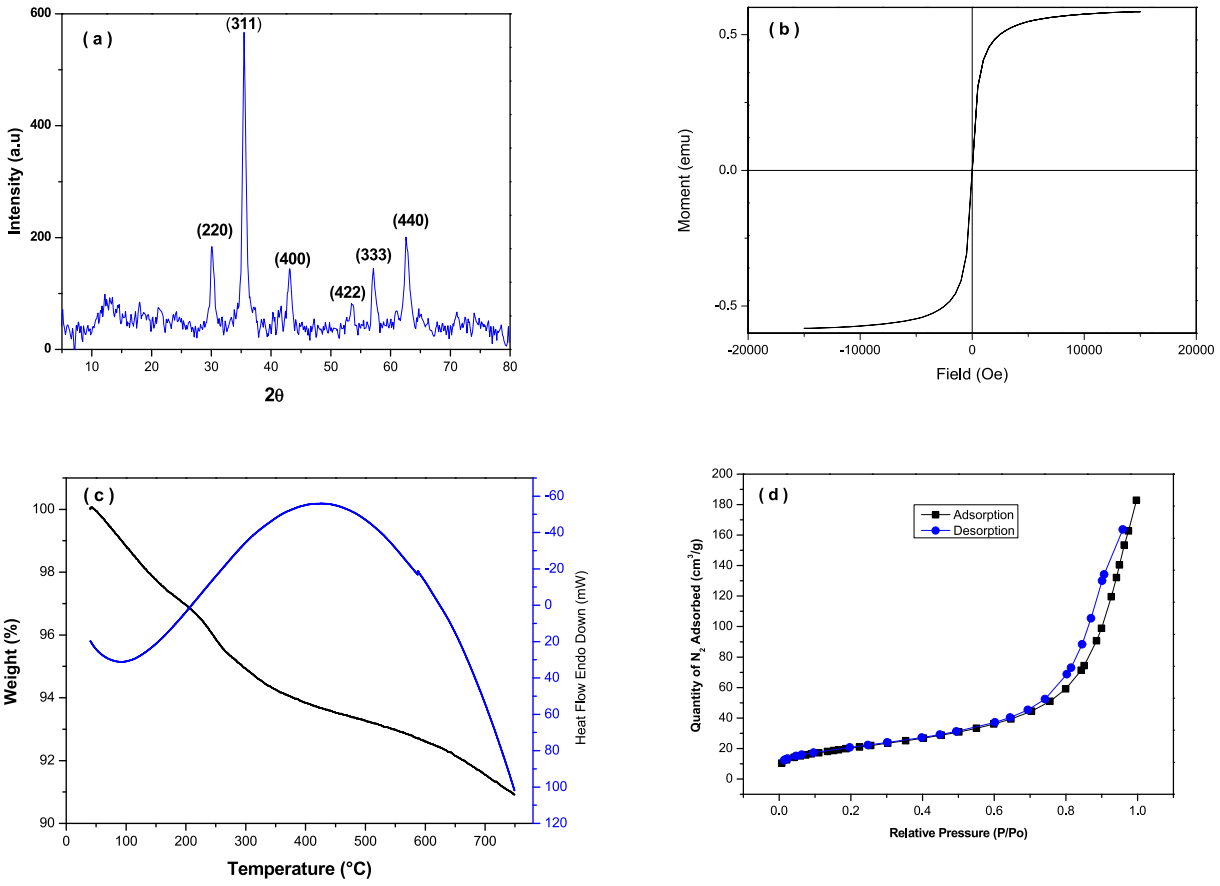

Fig. 3. A XRD powder diffraction pattern **b.** Room temperature magnetization curve **c.** TGA and derivative TGA **d.** Brunauer–Emmett–Teller (BET) surface area analysis plot of FMPM NPs.

graphs of BET analysis are shown in Fig. 3**d.** TYPE IV indicates mesoporous adsorption–desorption isotherm is seen for the produced iron oxide nanoparticles [36]. The surface area, pore volume, and pore diameter of the synthesised FMPM NPs were determined to have a large surface area of 70.31 m^2/g, 0.27 cm^3 /g, and 3.35 nm, respectively. The adsorption–desorption isotherm shows that at maximum relative pressure (P/P_0), about 76.01 cm^3/g of nitrogen was adsorbed which shows slit-shaped pores [37]. The hysteresis pattern reveals that the condensation took place between a value of 0.5 and a value of 0.99.

To determine more about the morphology of FMPM NPs, FE-SEM and TEM were used. FE-SEM images are shown in Fig. 4 **(a-c)**, showing the FMPM NPs indicating uniformly dispersed small spherical-shaped particles as well as intriguing rod-shaped particles.

The elemental composition and stoichiometry of the produced FMPM NPs were determined by EDS analysis, as shown in Fig. 4 **d.** The presence of elemental Iron (Fe) and Oxygen (O)confirms the formation

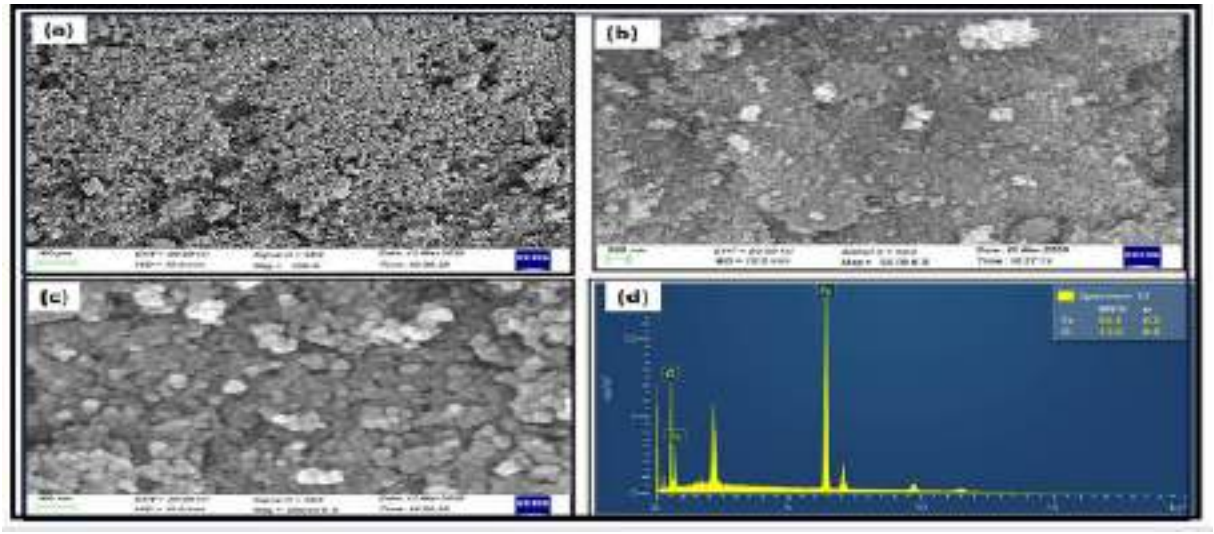

Fig. 4. A-c SEM images at different magnifications and **d.** EDX spectrum of FMPM NPs.

of FMPM NPs [20]. The presence of additional Carbon peaks in the EDS spectrum ascribed that the phytochemicals act as capping agents for FMPM NPs.

TEM images Fig. 5 clearly reveal that the spherical shaped FMPM NPs with average size of 11.58 nm. FMPM NPs show a ring-like diffraction pattern which demonstrates (Fig. 5**e**) the polycrystalline nature.

XPS spectrum of prepared FMPM NPs. seen in Figure Fig. 6. As reported above Fig. 6**a**, shows wide scan XPS spectra. In contrast, the Fe2p XPS spectrum depicts a prominent peak at 708 eV in Fig. 6**b**, which corresponds to the FMPM NPs generated utilising the green synthesis method including extracts from Eichhorniacrassipes [38], Magnetospirillummagneticum Strain RSS-1 [39], and agro-waste [40]. The XPS spectra of FMPM NPs are shown in Fig. 6 **b**, spectral lines at 708 eV correspond to Fe^{2+} and Fe^{3+} [41].

Iron exhibits peaks in the energy range of about 706 to 708 eV, hence the absence of these peaks demonstrates the purity of magnetite nanoparticles. Fig. 6 **(c-d)** of O(1 s) peaks observed at 533.3 eV corresponds to O—H and C—O bonds and peaks detected at 283 eV signature peak in the *Murraya paniculata (L) Jack* flower extract could be attributed to C═O linkage in the phenyl ring of biomolecules. The presence of Fe2p and O(1 s) indicates a Fe-O bond in magnetite nanoparticles. The outcomes are in line with those obtained by employing mango peel extract to generate iron nanoparticles [38].

3.1. Plausible mechanism for synthesis of FMPM NPs

The green source, *Murraya paniculata (L) Jack* flower has been found to contain 60 different chemicals. Chemical components of the flower were discovered by chromatographic methods, and their structures were clarified by spectroscopic methods [42]. The *Murraya paniculata (L) Jack* flower has a flavone called 3,5,7,3′,4′,5′- hexamethoxyflavone [43]. Root bark and flower extracts of *Murraya paniculata (L) Jack* produced the indole alkaloids murrayacarine and murrayaculatine [44]. Eight flavonoids were found in M. paniculata leaves [45].

Fig. 7 depicts a potential process for the generation of FMPM NPs utilising the flower extract *Murraya paniculata (L) Jack*. It's composed of *Murraya paniculata (L) Jack* aqueous flower extract, Fe (II) and Fe (III).

3.2. Investigation of antimicrobial activity of FMPM NPs

The Agar well diffusion method was used to test the antibacterial activity of FMPM NPs by employing 24 h cultures with medium (Nutrient Agar) in an autoclave set to 120 °C. Each sterilised petri dish was filled with 20 mL of the medium, which had been seeded aseptically with the strains of bacteria for that dish. Various amounts of the test substances were tested after they had been reconstituted with the solvent. Samples, distilled water, and Ciprofloxacin were all put into a well with a diameter of 6 mm. A petri dish was kept at 37 °C for 12 h. As a positive control, used a standard solution that had 5 μg/mL in it. The HiMedia antibiotic zone scale was used to figure out the zone (Table 2**)**.

The Agar well diffusion method was carried out to determine the antifungal activity of FMPM NPs by employing 24 h cultures with medium (Potato Dextrose Agar). This was sterilized by autoclaving at 120 °C (15 psi) for 30 min. Then medium with fungi strains was aseptically transferred into the sterilized petri dish. The FMPM NPs were freshly soluble in distilled water and tested at different concentrations along with standard (Fluconazole) were placed in a 6 mm diameter well and Results are represented in Table 3**.**

The antimicrobial activity of the FMPM NPs were concentration dependent, the inhibition activity increase in concentration and the activity was also increased (Fig. 8**)** which is compared with standard antibiotic Ciprofloxacin**.** The FMPM NPs showed a moderate zone of inhibition (ranging 10 −15 mm) against the tested pathogens at 2.5, 5 and 10 μg/mL concentrations. FMPM NPs inhibition (ranging 10–15 mm) was observed at 2.5 μg/mL for gram positive concentration of iron oxide nanoparticles.

Similarly, the inhibition activity of the FMPM NPs was compared with standard Fluconazole. The FMPM NPs showed moderate to high zones of inhibition (ranging from 9 to 26 mm) observed for pathogens at 2.5, 5 and 10 μg/mL concentrations. Inhibition (ranging 11–26 mm) was observed at 10 μg/mL of FMPM NPs.

3.3. Removal of Fast sulfan black F from contaminated water by using FMPM NPs

Contaminated water containing FSB removed by FMPM NPs.

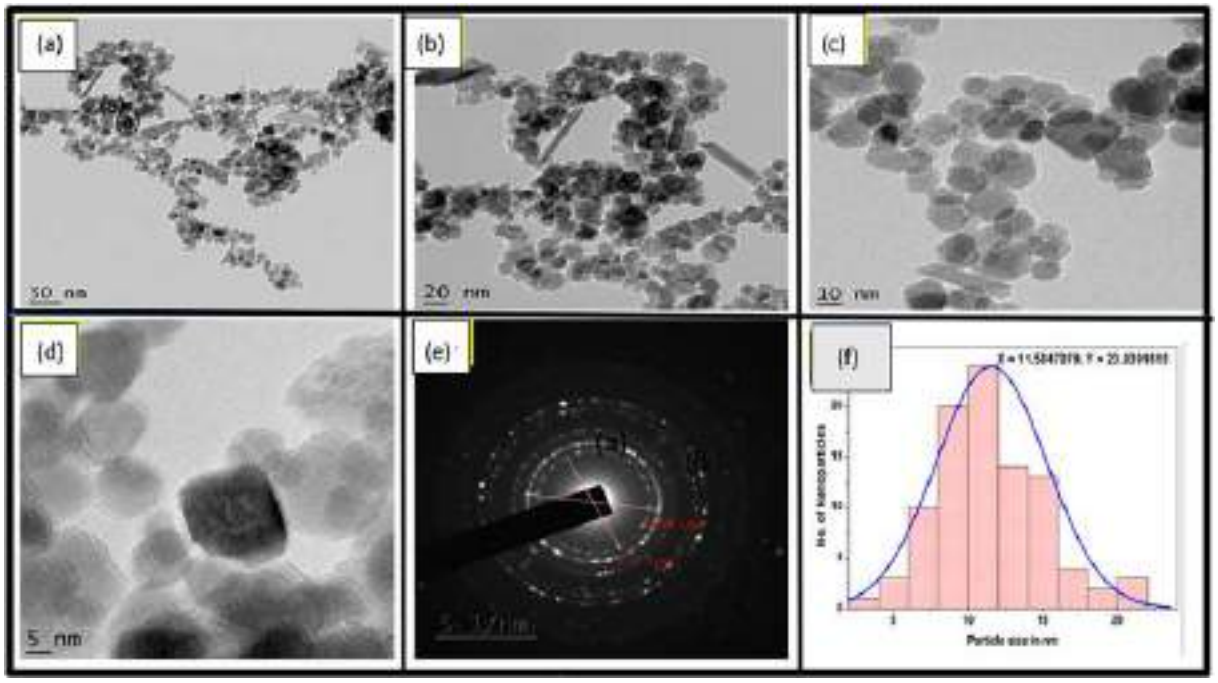

Fig. 5. A-d TEM images **e** SAED pattern and **f** Size distribution histogram of FMPM NPs.

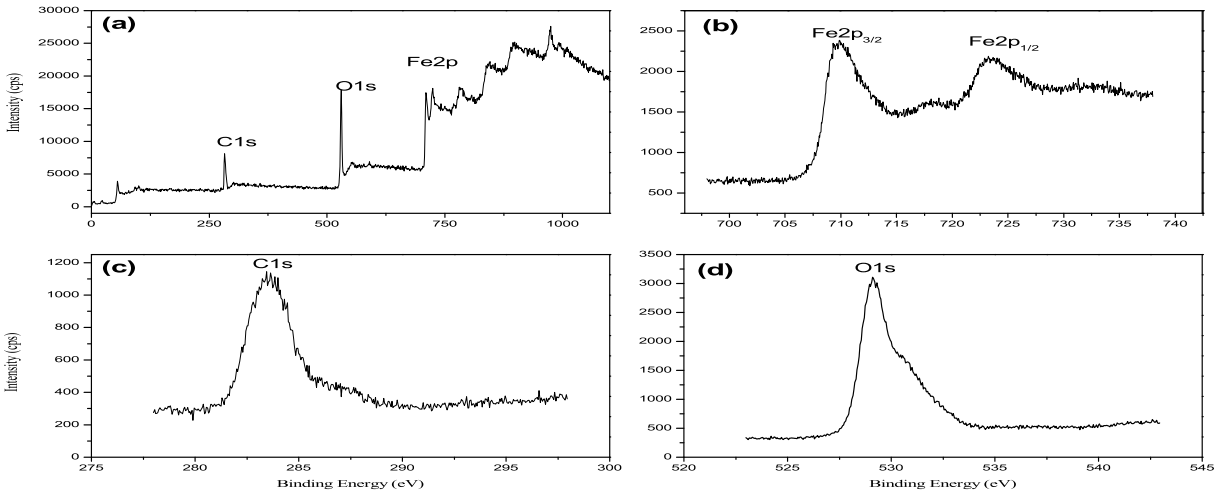

Fig. 6. XPS spectra of synthesized FMPM NPs.

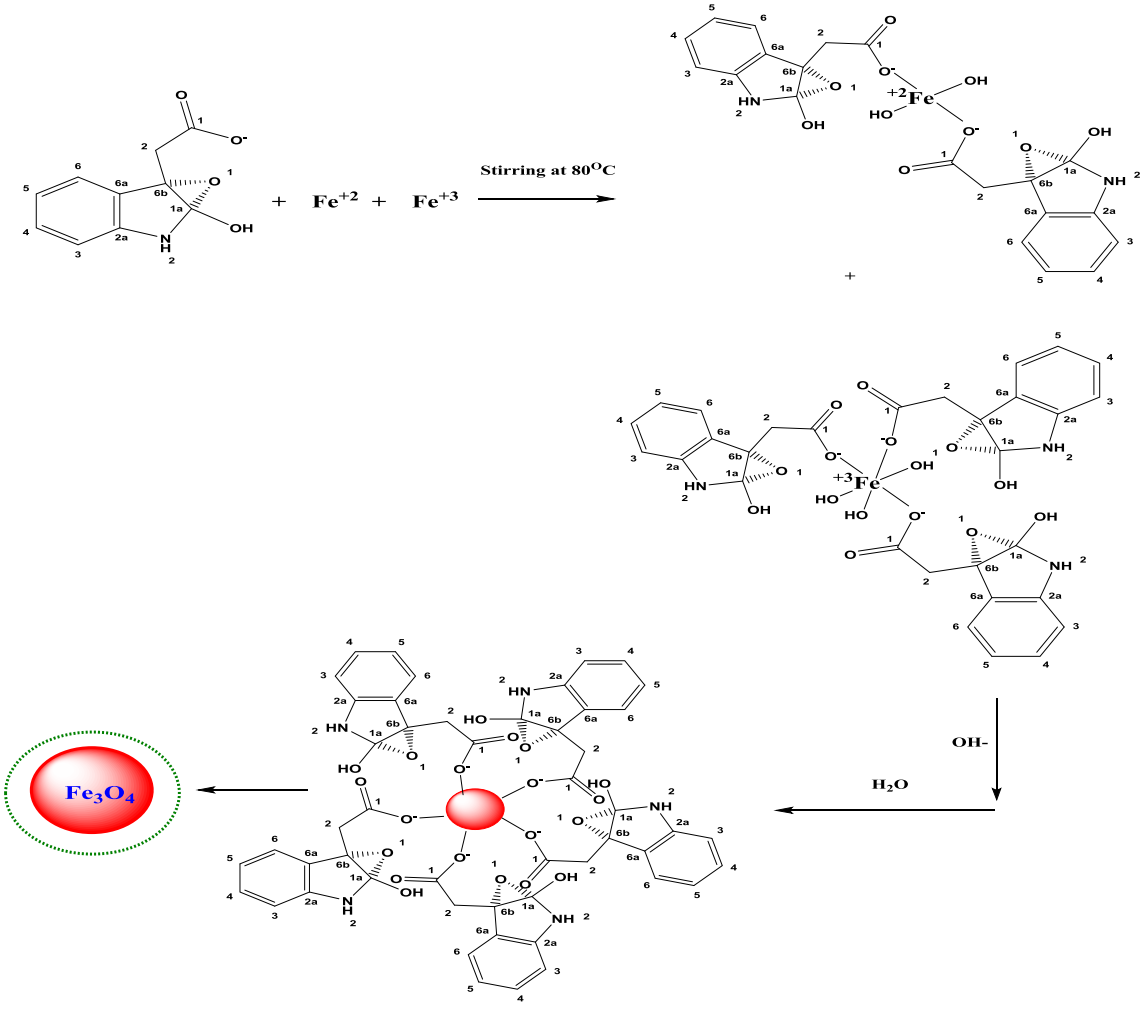

Fig. 7. A proposed mechanism of synthesized FMPM NPs.

Removal efficiency was investigated by varying dye, FMPM NPs concentrations and pH. Langmuir and Freundlich adsorption isotherms were used as model equilibrium adsorption isotherms, results from two typical kinetic models were examined for improved understanding of the adsorption process.

3.4. Effect of FSB concentration

It is note that the effect of FSB concentration is dependent on the close relationship between dye concentrations and porous nature of FMPM NPs surface. The FSB dye was made at various doses (5, 10, 15, and 20 mg/L). 50 mg of FMPM NPs were added to the dye solution and

Table 2
Antibacterial activity comparison results of synthesized FMPM NPs.

Name	Enterococcus faecalis	Pseudomonas aeruginosa
Shape	Round	Rod
Gram Reaction	Gram positive	Gram - negative
MTCC No.	MTCC 439	MTCC 424
FMP Fe_3O_4 NPs 10 μg/mL	11 mm	10 mm
FMP Fe_3O_4 NPs 5 μg/mL	11 mm	0
FMP Fe_3O_4 NPs 2.5 μg/mL	12 mm	0
Ciprofloxacin	30 mm	24 mm

Table 3a
Antifungal activity synthesized FMPM NPs.

Name	Aspergillus niger	Penicillium chrysogenum
MTCC No.	MTCC 282	MTCC 5108
FMP Fe_3O_4 NPs 10 μg/mL	11 mm	26 mm
FMP Fe_3O_4 NPs 5 μg/mL	9 mm	16 mm
FMP Fe_3O_4 NPs 2.5 μg/mL	0 mm	10 mm
Fluconazole	18 mm	32 mm

Table 3b
Langmuir, Freundlich adsorption isotherms parameters.

Isotherm models	Parameters		
Langmuir Isotherm	Q_0 (mg/g)	b_L(L/mg)	R^2
	6.62	0.105	0.9583
Freundlich Isotherm	1/n	k_f ($mg^{1-1/n}$ $L^{1/n}$ g^{-1})	R^2
	0.179	10.39	0.8948

the mixture was agitated until equilibrium was reached. A UV–Visible spectrophotometer was used to measure the amount of dye that remained after centrifugation. As the original dye concentration was increased, the dye removal effectiveness declined. This could be because the adsorption sites on the FMPM NPs surface were saturated [46] as shown in Fig. 9**a**.

3.5. Effect of pH

When it comes to the adsorption of FSB on the surface of FMPM NPs, it was decided to test the influence of pH on dye removal by making dye solutions with a pH range of 2 to 7. The adsorption of FSB dye on FMPM NPs was examined at dosages of 50 mg and contact times of 40 min. Fig. 9 **b** shows that lowering the pH of the dye solution improved effectiveness in FSB dye removal. To remove 93 % of the initial dye concentration (5 mg/L), the dye removal efficiency was set at pH = 4. The electrostatic attraction between the positively charged FMP Fe_3O_4 NPs adsorbent and the anionic FSB dye is thought to be responsible for FSB dye adsorption on FMPM NPs.

3.6. Effect of adsorbent dosage on adsorption

A dye concentration of 5 mgL^{-1}, pH = 4 was maintained to study the impact of adsorbent dose on dye adsorption. The starting adsorbent concentration was varied from 10, 20, 30, 40 and 50 mg, with all other experimental parameters being constant. Results (Fig. 9 **c**) showed that as the adsorbent dosage rose, dye removal efficiency improved. More surface area means increased binding sites for the adsorption of the target FSB dye on FMPM NPs, which could be explained by more surface area being available.

3.7. Adsorption isotherms

When testing adsorbents for the removal of FSB from contaminated water, adsorption isotherms were used to see how effective they were. Langmuir and Freundlich's isotherms were used to interpret the quantitative results.

3.8. Langmuir isotherm

Adsorbed molecules on the same side can't interact with each other after adsorption equilibrium is attained. The Langmuir isotherm is mathematically defined by Eq. (1).

$$Ce/qe = 1/K_L q\max + Ce/q\max \quad (1)$$

"Ce" stands for the equilibrium concentration of the FSB in the

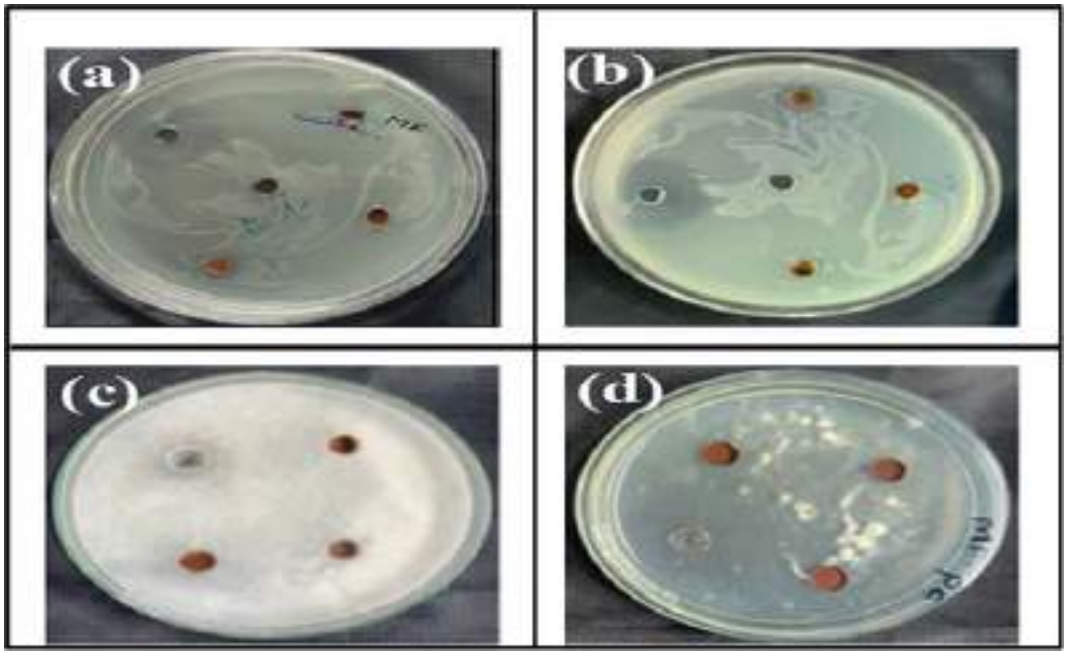

Fig. 8. A-b antimicrobial activity for the two bacterial strains and **c-d** antifungal activity for the two fungal strains.

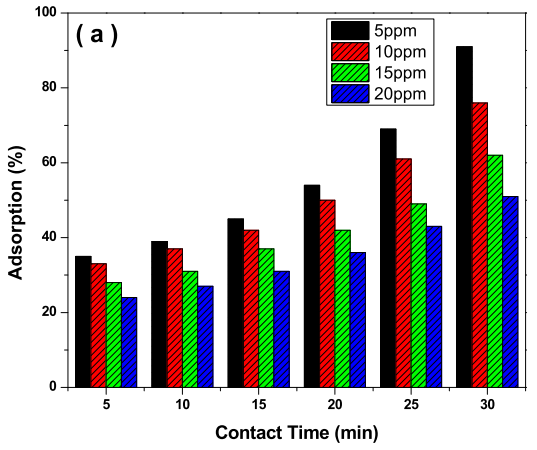

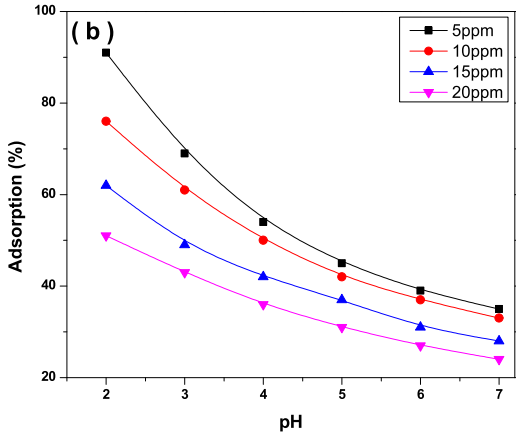

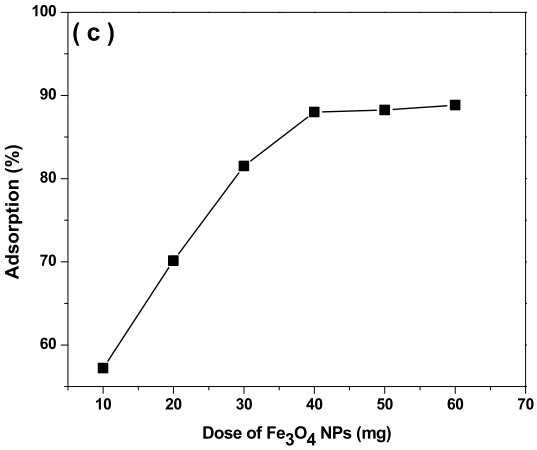

Fig. 9. **A** Percent of dye removal by FMPM NPs at an initial concentration of FSB dye **b** pH of solution **c** Dose of FMPM NPs adsorbent.

aqueous solution (mg/L), and "K_L" stands for Langmuir equilibrium constant (L/mol), maximum adsorption capacity "q_{max}" is of the adsorbent, i.e. FMPM NPs (mg/g), and "q_e" stands for the amount of the FSB adsorbed. Eq. (2) can also express the Langmuir isotherm as an equilibrium parameter, a dimensionless constant.

$$R_L = 1/\ (1 + K_L C_0) \tag{2}$$

where 'K_L' stands for Langmuir constant and 'C_o' stands for the highest initial concentration of the dye (mgL^{-1}).

3.9. Freundlich isotherm

Freundlich isotherm establishes an empirical relationship between the concentrations of a solute on the adsorbent surface and the concentration of that same solute in the liquid with which the adsorbent comes into contact. Eq. (3) is the Freundlich isotherm linear equation.

$$\log q_e = \log K_F + 1/n \log Ce \tag{3}$$

There is a constant 'K_F' in the Freundlich equation and 'n' is the adsorption intensity that indicates the amount of dye adsorbed per unit weight of adsorbent (mg/g). FSB is more readily adsorbed on FMPM NPs adsorption intensity 'n' value exceeds 1[47].

Fig. 10 **a** shows that the ability of aqueous flower extract of *Murraya paniculata (L) Jack* capped Fe_3O_4 NPs to remove dye depends on the concentration of FSB at the beginning of the reaction, as the initial dye concentration rises, so the removal capacity also increases. As shown in Fig. 10 **b, c**, data analysis shows that the Langmuir model fits better than the Freundlich model for FSB dye adsorption on aqueous flower extract of *Murraya paniculata (L) Jack* capped Fe_3O_4 NPs, as the R^2 values in the Langmuir model are considerably closer to one.

3.10. Recyclability experiment

The reusability of magnetite for the removal of FSB was carried out five times. Removed the FSB from the FMPM NPs that had been attached to the dye adsorption. An external magnet was employed to collect an aqueous flower extract of *Murraya paniculata (L) Jack* capped Fe_3O_4 NPs, which were then used for up to five cycles of the FSB adsorption experiment. After five cycles the removal efficiency was found to be 79 % shown in Fig. 11.

4. Conclusion

There were no harmful compounds used as capping agents during the synthesis of FMPM NPs, which made them extremely stable. This has been confirmed by UV–Vis spectroscopy, FT-IR, XRD, SEM with EDS, VSM, XPS, BET and thermo gravimetric analysis. FMPM NPs band gap was 2.57 eV. The average crystal size of iron oxide nanoparticles, as determined by XRD, was 14.12 nm and 11.58 nm using TEM. The extremely large surface area of the synthesized nanoparticles was determined to be 70.31 m^2/g by the BJH method showing H4 type of hysteresis loop. The elemental analysis performed by the XPS technique confirmed the oxidation states and elements of synthesised magnetite nanoparticles. Furthermore, the saturation magnetization (Ms) value of

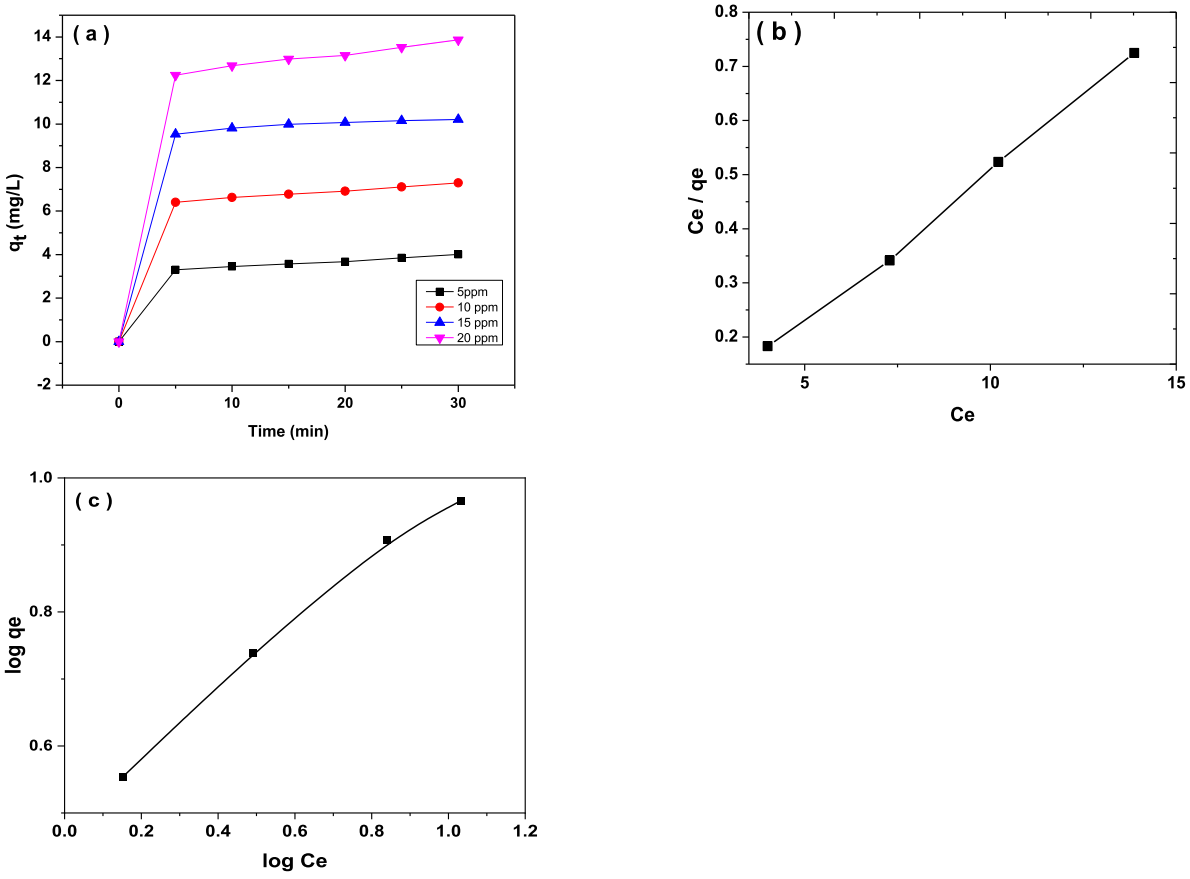

Fig. 10. Plots of **a** The amount of dye adsorbed at various concentration of FSB **b** Langmuir isotherm **c** Freundlich isotherm.

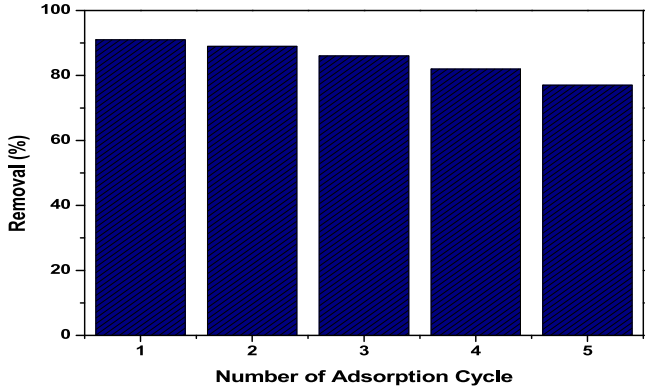

Fig. 11. The recyclability of the FMPM NPs in the FSB remova.

58 emu/g for *Murraya paniculata (L) Jack* capped Fe_3O_4 NPs revealed by VSM indicated superparamagnetic behaviour. FMPM NPs are more potent for adsorption studies of FSB dye removal within 40 min. The iron oxide nanoparticle's antibacterial and antifungal activities were found to be highly effective. According to the findings of this study, *Murraya paniculata (L) Jack* capped Fe_3O_4 NPs could be an effective treatment for gram-positive *Enterococcus faecalis* bacteria and *Penicillium chrysogenum* fungi of synthesized magnetite nanoparticles. Novel plant extracts follow additional advantages of outstanding adsorption for removal of FSB and effectively inhibit the gram-positive and antifungal microbes. It's possible to expand the research to include preclinical studies in relevant animal models, as well as nanomedicine applications.

CRediT authorship contribution statement

J. Laxmi Mangamma: . Keloth Basavaiah: Supervision, Validation, Writing – review & editing.

Declaration of competing interest

The authors declare that they have no known competing financial interests or personal relationships that could have appeared to influence the work reported in this paper.

Data availability

The authors do not have permission to share data.

Acknowledgement

The authors express sincere gratitude to Dr P.L Kishore, I. Manga Raju, students and faculty of Dr VSK GDC Visakhapatnam.

References

[1] G. Tejaswini, P.L. Kishore, V.N. Lakshmi, A comprehensive review on green synthetic approaches and applications of 3 d-series metal oxide, Nanoparticles 34 (10) (2022) 2478–2488, https://doi.org/10.14233/ajchem.2022.23904.
[2] J.L. Mangamma, D.R. Devi, P.S.R.V. Sagar, M.R. Babu, K. Basavaiah, Review on plant mediated green synthesis of magnetite nanoparticles for pollution abatement, biomedical and electronic applications, Asian J. Chem. 34 (2022) 1047–1054, https://doi.org/10.14233/ajchem.2022.23650.
[3] T. Dippong, E.A. Levei, I.G. Deac, I. Petean, O. Cadar, Int. J. Mol. Sci. 23 (6) (2022) 3097, https://doi.org/10.3390/ijms23063097.
[4] M. Ştefănescu, T. Dippong, M. Stoia, et al., Study on the obtaining of cobalt oxides by thermal decomposition of some complex combinations, undispersed and

dispersed in SiO2 matrix, J. Therm. Anal. Calorim. 94 (2008) 389–393, https://doi.org/10.1007/s10973-008-9111-2.
[5] T. Dippong, E.A. Levei, C. Leostean, O. Cadar, Impact of annealing temperature and ferrite content embedded in SiO2 matrix on the structure, morphology and magnetic characteristics of (Co0. 4Mn0. 6Fe2O4) δ (SiO2) 100-δ nanocomposites, J. Alloy. Compd. 868 (2021) 159203, https://doi.org/10.1016/j.jallcom.2021.159203.
[6] T. Dippong, E.A. Levei, F. Goga, O. Cadar, Influence of Mn2+ substitution with Co2 + on structural, morphological and coloristic properties of MnFe2O4/SiO2 nanocomposites, Mater. Charact. 172 (2021) 110835, https://doi.org/10.1016/j.matchar.2020.110835.
[7] A.C.B. Jesus, J.D. Jesus, R.J.S. Lima, K.O. Moura, J.M.A. Almeida, J.G.S. Duque, C. T. Meneses, Synthesis and magnetic interaction on concentrated Fe3O4 nanoparticles obtained by the co-precipitation and hydrothermal chemical methods, Ceram. Int. 46 (8) (2020) 11149–11153, https://doi.org/10.1016/j.ceramint.2020.01.135.
[8] G. Asab, E.A. Zereffa, T. Abdo Seghne, Synthesis of silica-coated Fe3O4 nanoparticles by microemulsion method: Characterization and evaluation of antimicrobial activity, Int. J. Biomater. (2020), https://doi.org/10.1155/2020/4783612.
[9] Y. Mizukoshi, T. Shuto, N. Masahashi, S. Tanabe, Preparation of superparamagnetic magnetite nanoparticles by reverse precipitation method: contribution of sonochemically generated oxidants, Ultrason. Sonochem. 16 (4) (2009) 525–531, https://doi.org/10.1016/j.ultsonch.2008.12.017.
[10] S.M. Fotukian, A. Barati, M. Soleymani, A.M. Alizadeh, Solvothermal synthesis of CuFe2O4 and Fe3O4 nanoparticles with high heating efficiency for magnetic hyperthermia application, J. Alloy. Compd. 816 (2020) 152548, https://doi.org/10.1016/j.jallcom.2019.152548.
[11] E. Sohouli, E.M. Khosrowshahi, P. Radi, E. Naghian, M. Rahimi-Nasrabadi, F. Ahmadi, Electrochemical sensor based on modified methylcellulose by graphene oxide and Fe3O4 nanoparticles: application in the analysis of uric acid content in urine, J. Electroanal. Chem. 877 (2020) 114503, https://doi.org/10.1016/j.jelechem.2020.114503.
[12] T. Dippong, E.A. Levei, I.G. Deac, I. Petean, G. Borodi, O. Cadar, Sol-gel synthesis, structure, morphology and magnetic properties of Ni0.6Mn0.4Fe2O4 nanoparticles embedded in SiO2 matrix, Nanomaterials 11 (2021) 3455, https://doi.org/10.3390/nano11123455.
[13] T. Dippong, D. Toloman, M. Dan, E.A. Levei, O. Cadar, Structural, morphological and photocatalytic properties of Ni-Mn ferrites: influence of the Ni: Mn ratio, J. Alloy. Compd. 913 (2022) 165129, https://doi.org/10.1016/j.jallcom.2022.165129.
[14] A.C. Paiva-Santos, A.M. Herdade, C. Guerra, D. Peixoto, M. Pereira-Silva, M. Zeinali, F. Veiga, Plant-mediated green synthesis of metal-based nanoparticles for dermopharmaceutical and cosmetic applications, Int. J. Pharm. 597 (2021) 120311, https://doi.org/10.1016/j.ijpharm.2021.120311.
[15] M. Mahdavi, F. Namvar, M.B. Ahmad, R. Mohamad, Green biosynthesis and characterization of magnetic iron oxide (Fe3O4) nanoparticles using seaweed (Sargassum muticum) aqueous extract, Molecules 18 (5) (2013) 5954–5964, https://doi.org/10.3390/molecules18055954.
[16] V. Golthi, J. Kommu, An eco-friendly and sustainable method for producing Fe_3O_4 nanoparticles using Jatropha podagrica leaf extract for efficient dye degradation and antibacterial uses, Hybrid Adv. 4 (2023) 100110, https://doi.org/10.1016/j.hybadv.2023.100110.
[17] T.S. AlGarni, M.H. Ali, A.M. Al-Mohaimeed, Green biosynthesis of Fe3O4 nanoparticles using Chlorella vulgaris extract for enhancing degradation of 2, 4 dinitrophenol, J. King Saud Univ.-Sci. 35 (1) (2023) 102426, https://doi.org/10.1016/j.jksus.2022.102426.
[18] G. Tejaswini, S. Beebi, G.M. Baba, G. Sanyasinaidu, K.B. Lakshmi, E laeocarpus Sylvestris mediated green approach for fabrication of magnetite nanoparticles: antimicrobial and antioxidant potentialities, Appl. Nanosci. 1–14 (2023), https://doi.org/10.1007/s13204-023-02785-7.
[19] A.V. Ramesh, D. Rama Devi, S. Mohan Botsa, K. Basavaiah, Facile green synthesis of Fe_3O_4 nanoparticles using aqueous leaf extract of Zanthoxylum armatum DC. for efficient adsorption of methylene blue, J. Asian Ceram. Soc. 6 (2) (2018) 145–155, https://doi.org/10.1080/21870764.2018.1459335.
[20] K. Basavaiah, M.H. Kahsay, D. RamaDevi, Green synthesis of magnetite nanoparticles using aqueous pod extract of Dolichos lablab L for an efficient adsorption of crystal violet, Emergent Mater. 1 (2018) 121–132, https://doi.org/10.1007/s42247-018-0005-1.
[21] A.A. Barzinjy, D.A. Abdul, F.H. Hussain, S.M. Hamad, Green synthesis of the magnetite (Fe3O4) nanoparticle using Rhus coriaria extract: a reusable catalyst for efficient synthesis of some new 2-naphthol bis-Betti bases, Inorganic Nano-Met. Chem. 50 (8) (2020) 620–629, https://doi.org/10.1080/24701556.2020.1723027.
[22] H. Şengönül, O. Demircan, Synthesis and characterization of Fe3O4 nanoparticles using Prunus serrulata Leaf Extract, BioNanoScience 13 (4) (2023) 1944–1954, https://doi.org/10.1007/s12668-023-01174-2.
[23] A. Bouafia, S.E. Laouini, Green synthesis of iron oxide nanoparticles by aqueous leaves extract of Mentha Pulegium L.: effect of ferric chloride concentration on the type of product, Mater. Lett. 265 (2020) 127364, https://doi.org/10.1016/j.matlet.2020.127364.
[24] C. Prasad, S. Karlapudi, P. Venkateswarlu, I. Bahadur, S. Kumar, Green arbitrated synthesis of Fe3O4 magnetic nanoparticles with nanorod structure from pomegranate leaves and Congo red dye degradation studies for water treatment, J. Mol. Liq. 240 (2017) 322–328, https://doi.org/10.1016/j.molliq.2017.05.100.
[25] D. Joshi, K.J. Gohil, A brief review on Murraya paniculata (Orange jasmine): pharmacognosy, phytochemistry and ethanomedicinal uses, J. Pharmacopuncture 26 (1) (2023) 10, https://doi.org/10.3831/KPI.2023.26.1.10.
[26] N.S. Dosoky, P. Satyal, T.P. Gautam, W.N. Setzer, Composition and biological activities of Murraya paniculata (L.) Jack Essential Oil from Nepal, Medicines 3 (1) (2016) 7, https://doi.org/10.3390/medicines3010007.
[27] I. Paul, S. Ghosh, K. Acharya, P.B.S. Bhadoria, Bioactivities of Phenylpropanoids Extracted from Ephemeral Flowers of Medicinal Woody Species Murraya paniculata (Linn.) Jack. J. Biologically Active Products Nat. 12(4) (2022) 353–365. R.A. Nyquist, Interpreting infrared, Raman, and nuclear magnetic resonance spectra, Vol. 2. Academic Press, 2001. doi:10.1080/22311866.2022.2125903.
[28] J.L. Mangamma, K. Basavaiah, Green generation of zinc oxide nanoparticles by flower extract of orange jasmine for photodegradation of pollutant and antimicrobial activities, Biomass Convers. Biorefin. 1–11 (2024), https://doi.org/10.1007/s13399-024-05408-5.
[29] M. Khan, T. Khan, S. Wahab, M. Aasim, T.A. Sherazi, M. Zahoor, S.I. Yun, Solvent based fractional biosynthesis, phytochemical analysis, and biological activity of silver nanoparticles obtained from the extract of Salvia moorcroftiana, PLoS One 18 (10) (2023) e0287080.
[30] J. Shao, S. Zhou, Z. Jiang, T. Chi, J. Ma, M. Kuo, L. Jia, Warfarin and coumarin-like Murraya paniculata extract down-regulate EpCAM-mediated cell adhesion: individual components versus mixture for studying botanical metastatic chemopreventives, Sci. Rep. 6 (1) (2016) 30549, https://doi.org/10.1038/srep30549.
[31] Y.P. Yew, K. Shameli, M. Miyake, N. Kuwano, N.B. Bt Ahmad Khairudin, S.E. Bt Mohamad, K.X. Lee, Green synthesis of magnetite (Fe 3 O 4) nanoparticles using seaweed (Kappaphycus alvarezii) extract, Nanoscale Res. Lett. 11 (2016) 1–7, https://doi.org/10.1186/s11671-016-1498-2.
[32] I.P. Sari, Y. Yulizar, Green synthesis of magnetite (Fe3O4) nanoparticles using Graptophyllum pictum leaf aqueous extract, in: IOP Conference Series: Materials Science and Engineering, Vol. 191, No. 1. IOP Publishing, 2017, p. 012014, April. https://doi.org/10.1088/1757-899X/191/1/012014.
[33] M.D. Nguyen, H.V. Tran, S. Xu, T.R. Lee, Fe3O4 nanoparticles: structures, synthesis, magnetic properties, surface functionalization, and emerging applications, Appl. Sci. 11 (23) (2021) 11301, https://doi.org/10.3390/app112311301.
[34] T. Tatarchuk, A. Shyichuk, J. Lamkiewicz, J. Kowalik, Inversion degree, morphology and colorimetric parameters of cobalt aluminate nanopigments depending on reductant type in solution combustion synthesis, Ceram. Int. 46 (10) (2020) 14674–14685, https://doi.org/10.1016/j.ceramint.2020.02.269.
[35] S. Mashjoor, M. Yousefzadi, H. Zolgharnain, E. Kamrani, M. Alishahi, Organic and inorganic nano-Fe3O4: alga Ulva flexuosa-based synthesis, antimicrobial effects and acute toxicity to briny water rotifer Brachionus rotundiformis, Environ. Pollut. 237 (2018) 50–64, https://doi.org/10.1016/j.envpol.2018.02.036.
[36] A. Mirzaei, K. Janghorban, B. Hashemi, S.R. Hosseini, M. Bonyani, S.G. Leonardi, G. Neri, Synthesis and characterization of mesoporous α-Fe2O3 nanoparticles and investigation of electrical properties of fabricated thick films, Process. Appl. Ceram. 10 (4) (2016) 209–217, https://doi.org/10.2298/PAC1604209M.
[37] S. Guo, Z. Dan, N. Duan, G. Chen, W. Gao, W. Zhao, Zn (II), Pb (II), and Cd (II) adsorption from aqueous solution by magnetic silica gel: preparation, characterization, and adsorption, Environ. Sci. Pollut. Res. 25 (2018) 30938–30948, https://doi.org/10.1007/s11356-018-3050-7.
[38] Y. Yi, Y. Wei, P.E. Tsang, Z. Fang, Aging effects on the stabilisation and reactivity of iron-based nanoparticles green synthesised using aqueous extracts of Eichhornia crassipes, Environ. Sci. Pollut. Res. 26 (2019) 28361–28371, https://doi.org/10.1007/s11356-019-06006-z.
[39] H. Shimoshige, Y. Nakajima, H. Kobayashi, K. Yanagisawa, Y. Nagaoka, S. Shimamura, T. Maekawa, Formation of core-shell nanoparticles composed of magnetite and samarium oxide in Magnetospirillum magneticum strain RSS-1, PLoS One 12 (1) (2017) e0170932.
[40] M. Stan, I. Lung, M.L. Soran, C. Leostean, A. Popa, M. Stefan, A.S. Porav, Removal of antibiotics from aqueous solutions by green synthesized magnetite nanoparticles with selected agro-waste extracts, Process Saf. Environ. Prot. 107 (2017) 357–372, https://doi.org/10.1016/j.psep.2017.03.003.
[41] B.D. Yirsaw, M. Megharaj, Z. Chen, R. Naidu, Reduction of hexavalent chromium by green synthesized nano zero valent iron and process optimization using response surface methodology, Environ. Technol. Innov. 5 (2016) 136–147, https://doi.org/10.1016/j.eti.2016.01.005.
[42] T.S. Wu, Y.Y. Chan, Y.L. Leu, S.C. Huang, A flavonoid and indole alkaloid from flowers of Murraya paniculata. doi: 10.1016/0031-9422(94)85045-3.
[43] T.S. Wu, M.J. Liou, T.T. Jong, Y.J. Chen, J.S. Lai, Indole alkaloids and coumarins from the root bark of Murraya paniculata var. omphalocarpa, Phytochemistry 28 (10) (1989) 2873–2874, https://doi.org/10.1016/S0031-9422(00)98115-9.
[44] T. Kinoshita, K. Firman, Myricetin 5, 7, 3′, 4′, 5′-pentamethyl ether and other methylated flavonoids from Murraya paniculata, Phytochemistry 45 (1) (1997) 179–181, https://doi.org/10.1016/S0031-9422(96)00853-9.
[45] R.J. Ferracin, M.F.D.G. da Silva, J.B. Fernandes, P.C. Vieira, Flavonoids from the fruits of Murraya paniculata, Phytochemistry 47 (3) (1998) 393–396, https://doi.org/10.1016/S0031-9422(97)00598-0.
[46] Z. Eren, F.N. Acar, Adsorption of reactive black 5 from an aqueous solution: equilibrium and kinetic studies, Desalination 194 (1–3) (2006) 1–10, https://doi.org/10.1016/j.desal.2005.10.022.
[47] N. Mohammadi, H. Khani, V.K. Gupta, E. Amereh, S. Agarwal, Adsorption process of methyl orange dye onto mesoporous carbon material–kinetic and thermodynamic studies, J. Colloid Interface Sci. 362 (2) (2011) 457–462, https://doi.org/10.1016/j.jcis.2011.06.067.

Nanotechnology for Environmental Engineering
https://doi.org/10.1007/s41204-024-00372-x

ORIGINAL PAPER

Green synthesis of CuO nanorods using *Jatropha podagrica* leaf extract for dye degradation and antibacterial applications

Venkatesh Golthi[1,2,3] · Jayarao Kommu[1,3] · Kiran Kumar Penmethsa[2] · J. Laxmi Mangamma[2]

Received: 12 January 2024 / Accepted: 22 April 2024

Abstract

A sturdy eco-friendly synthesis technique was applied, utilizing leaf extract from the Buddha Belly plant (*Jatropha podagrica*) as a capping agent, to produce copper oxide nanorods (CuO NRs). Analysis of HR-TEM and SEM images confirmed that these NRs exhibit a rod-like shape and possess a monoclinic crystalline structure with an average size of 8–14 nm. The FT-IR spectrum displayed characteristic vibration modes related to the Cu–O bond between 433 and 526 cm^{-1}. The photocatalytic efficiency of the NRs was tested by exposing them to sunlight in the presence of Rhodamine B (RhB) and Crystal Violet (CV) dyes. Remarkably, the NRs degraded 95–97% of the dyes within 1–2 h. When employing 150 µL of the NRs in a well diffusion method, inhibitory zones measuring 14, 16, 13, and 11 mm were noted against *Bacillus coagulans, Staphylococcus aureus, Escherichia coli,* and *Klebsiella pneumoniae,* respectively. This study demonstrates that JP-CuO NRs effectively remove dyes from aqueous solutions and kill bacteria.

Graphical Abstract

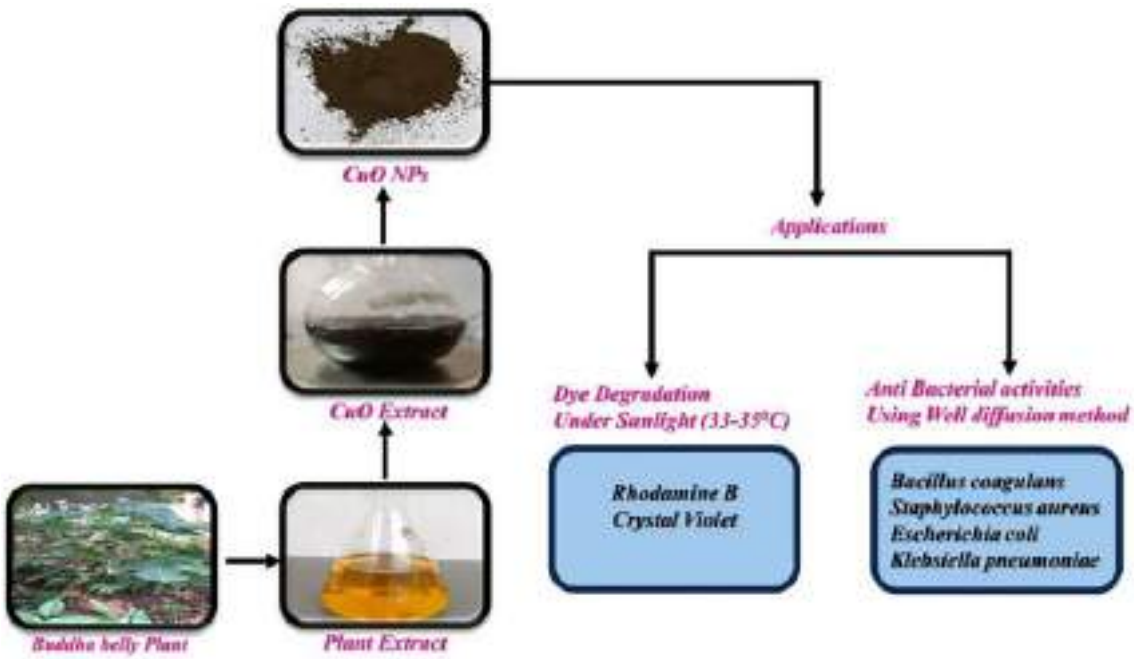

Keywords CuO nanorods · *Jatropha podagrica* plant · Dye degradation · Antimicrobial activity

Extended author information available on the last page of the article

Introduction

In today's world, there has been a consistent rise in industrial activity and population numbers, leading to the introduction of various new pollutants into water bodies. Notably, industries such as textiles, paper, leather, and printing are major sources of harmful dye effluents, posing serious ecological and health risks [1]. Dyes like Rhodamine B (RhB) and Crystal Violet (CV) are particularly concerning due to their potential ingestion hazards for both humans and animals, as well as their ability to cause skin, eye, and respiratory irritation [2]. Additionally, the reemergence of infectious diseases and the increasing prevalence of antibiotic resistance in various pathogenic bacteria are significant global public health challenges. Enterococcus, Staphylococcus, and Streptococcus, closely related species of harmful microorganisms, are responsible for a wide range of infections and diseases, contributing to the urgency of addressing these issues [3].

In recent decades, there has been notable progress in nanotechnology. A key focus in material science has been the development of nanoparticles (NPs) with adjustable morphology, allowing for precise control over their shape, size, and arrangement [4]. Extensive research has been dedicated to exploring their wide-ranging applications, spanning chemical and biological sensing, medical therapeutics, antimicrobial and antibacterial agents, and drug delivery systems [5]. Additionally, these NPs hold promise in fields like wastewater treatment, energy-efficient devices, optics, optoelectronics, electrochemistry, and catalysis [6]. Among the various types of antioxidant metal oxide NPs, CuO NPs have garnered considerable interest due to their cost-effectiveness, ready availability of copper salt, potent antioxidant properties, and low toxicity towards living cells, ensuring the safety of CuO NPs [7]. The antioxidant effectiveness of CuO NPs is influenced by various factors, including their inherent characteristics, crystal structure, chemical composition, surface charge, particle size, surface coating, and how they are dispersed. Additionally, CuO NPs exhibit a range of valuable physical attributes, including electron correlation effects, spin dynamics, a high dielectric constant, and the potential for high-temperature superconductivity [8–10]. In the industrial field, they are commonly employed as p-type semiconductors with a specific bandgap range of 1.21–2.51 eV, contributing to the design and manufacture of batteries, solar cells, gas sensors, and catalysts [11–13]. In today's context, CuO NPs serve as heterogeneous catalysts and play roles in biomedicine, functioning as antioxidants, drug delivery carriers, and imaging agents [14–17]. In the past, various physical and chemical processes have been employed in the synthesis of CuO NPs, offering the ability to produce particles tailored to specific preferences [18]. Nevertheless, these production techniques come with several drawbacks, including potentially harmful organic solvents, expensive reagents, challenges in isolating the NPs, and lengthier processing times [19]. Plant-mediated synthesis has emerged as a promising alternative within this range of methods due to its straightforwardness, environmentally friendly nature, user-friendliness, cost-effectiveness, adaptability for large-scale industrial production, and applicability in the biomedical field [20]. Plant extracts contain phytochemicals that serve dual roles as both reducing and capping agents, enabling the creation of CuO NPs with precise control over size and shape, and the prevention of aggregation, all without the necessity for external oxidizing, reducing, or capping agents [21, 22].

This study aimed to demonstrate the antioxidant activity of CuO nanorods (NRs) synthesized using *Jatropha podagrica* leaf extract (JP) as a sustainable source for the effective removal of organic dye pollutants. JP is a widely recognized native medicinal plant with a history of being employed to address a range of health conditions, such as ulcers, scabies, injuries, and fever. It also has beneficial properties such as anti-tumorigenic, antioxidant, and antibacterial capabilities [23]. The study first examined the JP leaves for specific phytochemical components, such as tannins, glycol flavones, proanthocyanidins, and phenolic acids [24, 25]. The leaf extract of *Jatropha podagrica* is safe, a critical consideration in the formulation of nanorods [24]. We have recently published an article outlining the incorporation of this plant extract in the synthesis of ZnO and Fe_3O_4 nanoparticles [26, 27]. These phytochemicals play a vital role in synthesizing JP-CuO NRs, acting as both capping agents and stability enhancers, surpassing what conventional chemical synthesis methods can achieve [24]. Additionally, the various phenolic acids in these phytochemicals help achieve well-defined sizes and shapes for the JP-CuO NRs, surpassing green-synthesized nanoparticles (As illustrated in Table 1). To harness the full potential of undiscovered plant species, it is crucial to identify fresh and distinctive plants for synthesizing nanorods. This strategy enables researchers to broaden the spectrum of nanorods that can be efficiently stabilized by uncovering new proteins and phytochemicals from plant sources that have not been investigated before. Additionally, these newfound plant species might present supplementary benefits, such as enhanced productivity, lowered costs, or specialized characteristics suitable for specific applications. The JP-CuO NRs were notable for having a negatively charged surface, which gave them outstanding degrading abilities for removing the dyes Rhodamine B (RhB) and Crystal Violet (CV). The antibacterial activity of these JP- CuO NRs was tested against both Gram-positive (*Bacillus coagulans, Staphylococcus aureus*) and Gram-negative (*Escherichia coli, Klebsiella pneumoniae*) bacteria.

Table 1 Contrasting the average size and structure of JP-CuO NRs in this study about findings from prior research

Material of plants	Average particle size	Structure	Implementation	References
Jatropha podagrica leaf extract	8–14 nm	Rod-like shape	Dye degradation and antibacterial applications	Present work
Eucalyptus globoulus leaf extract	88 nm	Spherical shape	Dye degradation	[28]
Abelmoschus esculentus fruit extract	20 nm	Spherical shape	Cytotoxicity and photocatalytic applications	[29]
malva sylvestris leaf extract	19–26 nm	Spherical shape	Thermal decomposes kinetics	[30]
Calotropis procera leaf extract	20–80 nm	Spherical shape	Photodegradation, antibacterial and antioxidant	[31]
Syzygium alternifolium fruit extract	17.5 nm	Spherical shape	Antiviral activity	[32]
Panicum sumatrense grains extract	20 nm	Rectangular in shape	Biological applications	[33]

Materials and methods

Materials

Preparation of CuO NRs using JP leaf extract

Jatropha podagrica (JP) plant leaves were freshly collected, washed with warm water, and rinsed with deionized. The leaves were then dried in the shade for 25 days until completely dehydrated. The dried leaves were then ground into a fine powder. One gram of the powder was added to a 500 mL glass beaker with 200 mL of deionized water. The mixture was heated at 80 °C for 30 min on a heating mantle, resulting in a deep golden-yellow solution. The solution was first filtered to remove solid particles, and then it underwent centrifugation to obtain a pure extract solution. This extract was subsequently stored in a refrigerator at a temperature of 4 °C for future use.

Synthesis of JP-CuO NRs

A conventional environmentally friendly method was used to synthesize CuO nanorods (NRs). First, 1 g of $Cu(SO_4)_2{\cdot}5H2O$ was dissolved in 90 mL of distilled water. After thorough mixing for 25–30 min at room temperature, the solution turned a clear blue color. Then, 10 mL of aqueous leaf extract was added, increasing the volume to 100 mL and turning the solution green. This mixture was sonicated vigorously for 10–15 min to ensure proper mixing. Next, the temperature was raised to 80 °C and maintained for up to 1 h, resulting in a deep green color. Then, 1 M NaOH (10 mL) was gradually added dropwise, causing the mixture to turn a dark brown color. To remove suspended particles, the mixture was dispersed in deionized water and centrifuged at 7000 rpm. The dark brown particles obtained were washed repeatedly with deionized water to eliminate impurities and achieve the ultimate product. The resulting dark brown solid was subsequently subjected to vacuum drying at 70 °C for 8 h in an oven. Lastly, the material underwent fine grinding with a mortar and pestle, preparing it for subsequent characterization [34].

JP-CuO NRs as efficient photocatalysts for Rhodamine B (RhB) and crystal violet (CV) dye degradation

The evaluation of the photocatalytic efficiency of JP-CuO NRs in degrading RhB and CV dyes was carried out utilizing naturally available UV radiation from sunlight. Initially, solutions of 100 mL containing 1 ppm of RhB and CV dyes were prepared and mixed with 0.01 g of JP-CuO NRs in separate containers. These mixtures were then stirred in darkness for an hour to stabilize the solutions and prevent any adsorption–desorption processes. After stabilization, the solutions were exposed to sunlight for 4 h, specifically from 11 AM to 3 PM, with outdoor temperatures ranging from 33 to 35 °C. Continuous magnetic stirring was employed to maintain a pH level of 10 during this time. At predefined intervals, consistent samples were collected from each dye solution, and the NRs were separated by centrifugation at 8000 rpm. The absorption of RhB and CV dyes at 540 nm and 580 nm was determined using a UV–visible spectrophotometer. The extent of photocatalytic degradation and the corresponding rate constants were calculated based on these measurements.

$$\text{Degradation rate } (\%) = \left(\left(A_0 - A\right)/A_0\right) \times 100$$

$$\ln A_0/A = kt$$

In this context, "A_0" denotes the starting concentration, "A" represents the concentration after the degradation process, "k" stands for the degradation rate constant, and "t" indicates the duration of exposure to sunlight. [35, 36].

Exploration of antibacterial activity of JP-CuO NRs

The antibacterial properties of JP-CuO NRs were evaluated in 24 h bacterial cultures (*Bacillus coagulans, Staphylococcus aureus, Escherichia coli, and Klebsiella pneumoniae*) using the Agar-Well diffusion method. The nutrient agar medium was sterilized for approximately 30 min at 120 °C using an autoclave to prepare it. Each sterile petri dish was then filled with 20 mL of the medium, and the respective bacterial strains were introduced under aseptic conditions. The plates were left at room temperature until the agar solidified. A sterile borer created a single 6 mm diameter well in each plate. Test substances, control (distilled water), and a standard drug were added to the 6 mm wells after being freshly dissolved in distilled water at concentrations of 1, 2, and 3. The petri plates were then incubated at 37 °C for 12 h, and the inhibition results are depicted in Fig. 8. A standard solution with a concentration of 5 g/mL served as a positive control. The diameter of the inhibitory zone was determined using the HiMedia antibiotic zone scale. All experiments were conducted in triplicate, yielding consistent results [37].

Characterization of JP-CuO NRs

Various analytical methods were utilized to ascertain the crystalline structure of CuO nanorods. To investigate the optical properties, UV–Vis diffuse reflectance/absorbance spectroscopy was conducted on the synthesized samples. A Shimadzu (2450—SHIMADZU) spectrophotometer equipped with a diffuse reflectance accessory was used at room temperature, with $BaSO_4$ serving as a reference material. Measurements were taken over the wavelength range of 200–800 nm. Fourier transform infrared spectra (FT-IR) for the samples were obtained using a Thermo Nicolet iS50 spectrometer, covering a frequency range from 4000 to 400 cm^{-1} in transmission mode with high-quality KBr pellets. X-ray diffraction (XRD) measurements were carried out using a Bruker Kappa Apex II instrument over a 2θ range of 0 to 90°. This instrument employed CuKα radiation (with a wavelength of $\lambda = 1.54060$ Å) at 40 kV and 35 mA, with a scanning rate of 0.2 s. The CuO nanorods were characterized using scanning electron microscopy (SEM) and high-resolution transmission electron microscopy (HRTEM) to investigate their surface morphology, elemental composition, and microstructure. SEM analyses were conducted using a Jeol 6390LA/ OXFORD XMX N apparatus equipped with energy-dispersive X-ray (EDX) spectroscopy. The acceleration voltage for SEM imaging ranged from 0.5 to 30 kV. For a more in-depth examination of the nanorods' microstructure and particle size, HRTEM was employed. HRTEM analyses were performed using a JEOL/JEM 2100 instrument operated at an applied voltage of 200 kV. Carbon-copper grids were used for sample preparation, allowing for precise particle size determination. Furthermore, SAED images were acquired using the HRTEM instrument to further elucidate the nanorods' crystal structure.

Results and discussions

UV–Vis spectroscopy studies

Figure 1 displays the UV–Vis absorption spectra of the leaf extract of JP and synthetic CuO NRs. The leaf extract contains various phytochemicals, such as alkaloids, flavonoids, phenolic acids, tannins, glycol flavones, and proanthocyanidins, which absorb light at 280 nm and 351 nm (π-π* and n-π* transitions) [23]. The JP-CuO NRs have a distinct absorption peak at 273 nm, but not at 280 or 351 nm. This suggests that the phytochemicals in the leaf extract play a key role in reducing, binding, and encapsulating JP-CuO NRs during the synthesis process [38, 39].

FTIR analysis of the synthesized JP-CuO NRs

The functional groups included in the synthesized JP-CuO NRs were identified, and their chemical composition was ascertained, using Fourier transform infrared (FTIR) spectroscopy. The FTIR analysis of the plant extract (Fig. 2) shows a significant peak at approximately 3500 cm^{-1}, indicating the presence of phenolic groups. Moreover, observable peaks at 1178 and 1042 cm^{-1} correspond to vibrational characteristics of polyphenolic molecules within the plant extract [24]. The FTIR spectrum of the CuO NRs (Fig. 2) shows absorption peaks in the range of 4000–400 cm^{-1}. The peaks between 433 and 526 cm^{-1} correspond to the stretching frequency of the Cu–O bond [28]. Furthermore, the emergence of peaks between 1117 and 1032 cm^{-1} underscores aspects related to chemical bonding, the crystalline nature of the material, and the relative intensities of IR bands linked to polyphenolic compounds [40]. The symmetric stretching of the aliphatic amino group is suggested by the presence of a peak at 1384 cm^{-1} [41]. Notably, the peak observed at 1630 cm^{-1} corresponds to the C=C stretching indicative of aromatic compounds [42]. Additionally, the peaks between 2852 and 2923 cm^{-1} are characteristic of –CH stretching vibrations typically associated with aldehyde groups [43]. Finally, the absorption band at 3432 cm^{-1} signifies the –OH stretching vibration inherent to phenolic groups [44]. These distinctive peaks within the IR spectrum provide valuable insights into the purity and compositional characteristics of the biosynthesized CuO NRs.

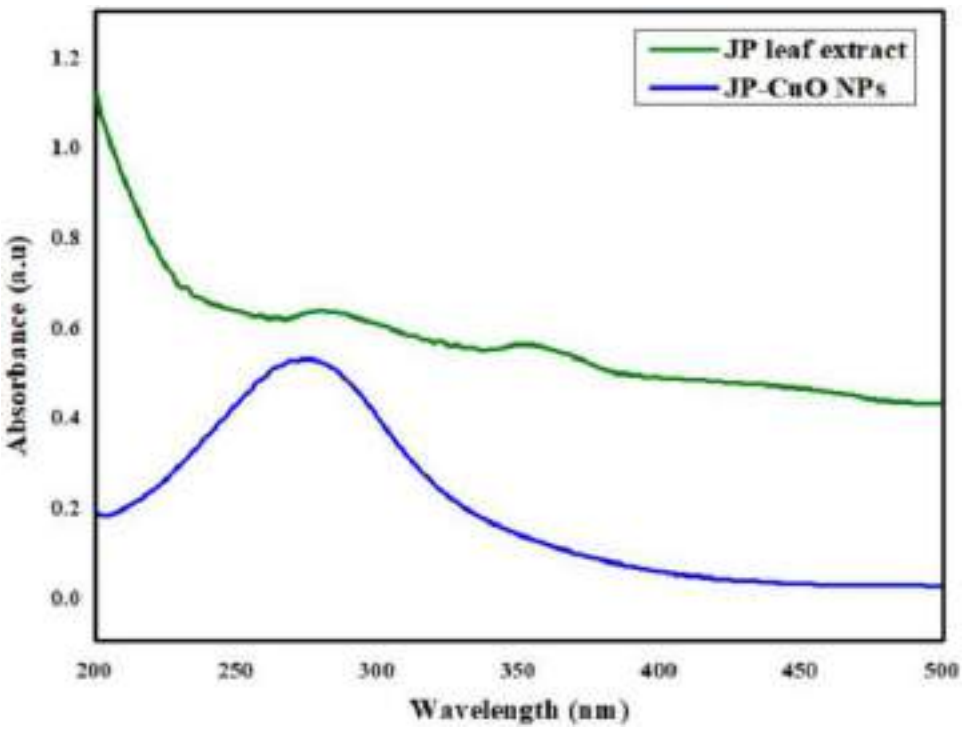

Fig. 1 UV–Vis Spectra of JP-CuO NRs and JP leaf extract

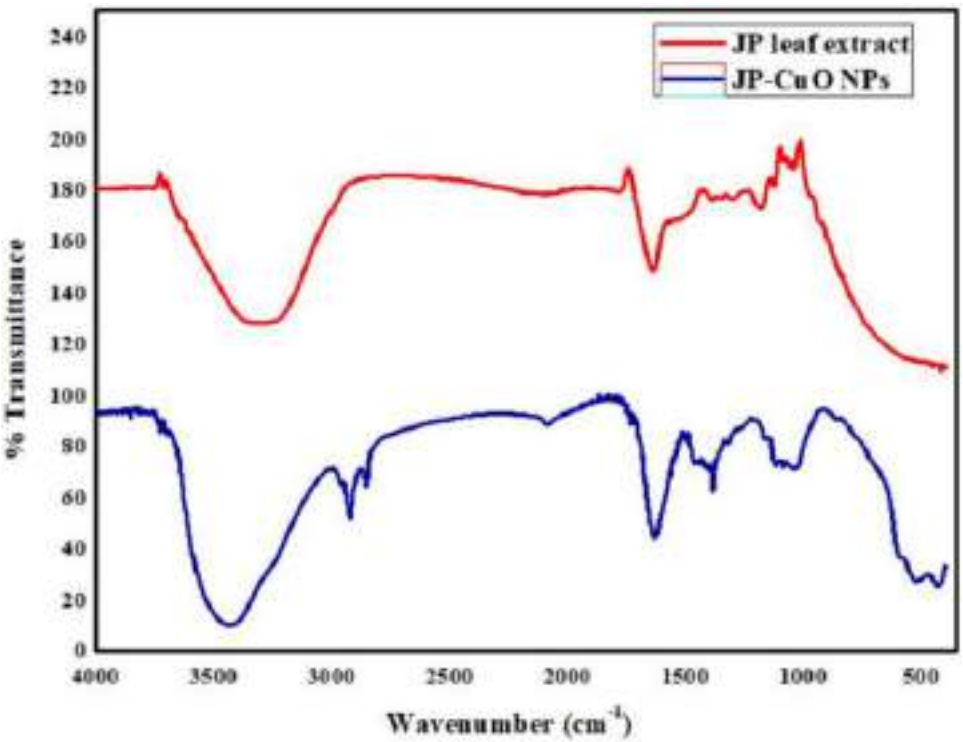

Fig. 2 FTIR spectra of JP-CuO NRs and JP extract

XRD analysis of JP-CuO NRs

The XRD analysis, as depicted in Fig. 3, unveiled discernible peaks that are indicative of CuO NRs at various angles. These angles include 32.67°, 35.66°, 38.85°, 48.77°, 53.87°, 58.21°, 61.65°, 66.24°, 68.19°, 75.23°, and 77.18°. These particular peaks corresponded to distinct crystal lattice planes, specifically (100), (002), (111), (202), (020), (-202), (113), (311), (-113), (-311), and (004) respectively. According to earlier studies, the presence of diffraction

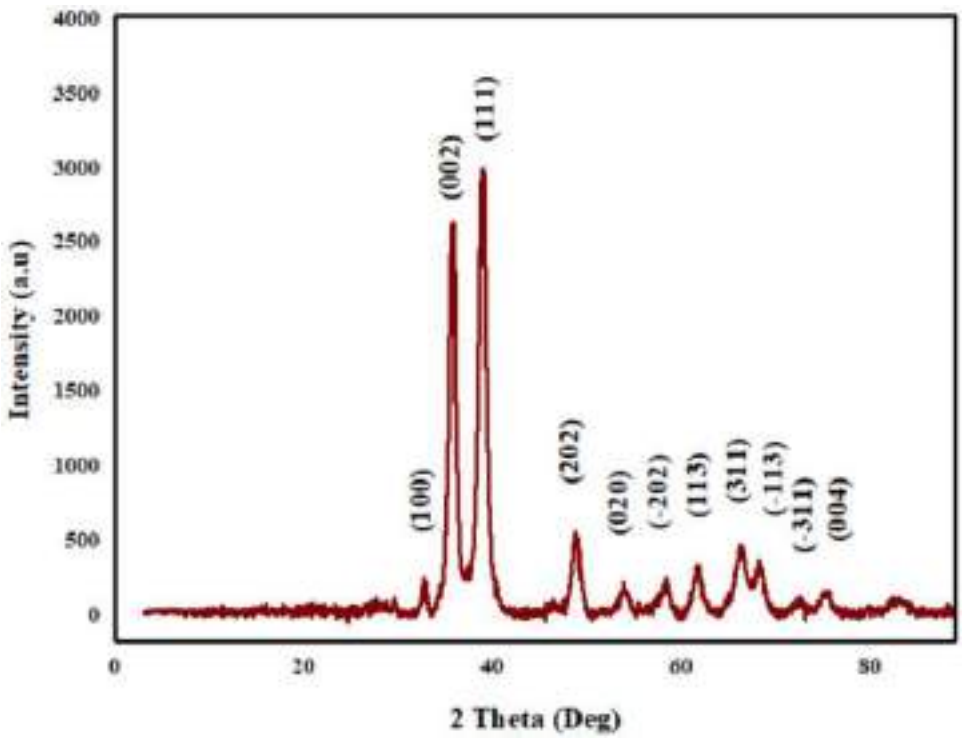

Fig. 3 XRD patterns of CuO NRs using an aqueous leaf extract of *Jatropha podagrica*

peaks falling within the range of 35 to 39° is indicative of CuO NRs formation (JCPDS Standard No. 01–080-0078). It's worth noting that the intensity of the (002) and (111) peaks suggested a monoclinic crystalline structure [45]. The sharp and well-defined diffraction peaks in the XRD pattern of the JP-CuO NRs indicate that they have a strong crystalline structure. The absence of other peaks confirms that the NRs are pure. The most prominent peaks observed between 35 and 39 °C for JP-CuO NRs were utilized to calculate the average crystallite size, which was determined to be 8.2 nm employing the Debye–Scherrer equation [46].

$$D = k\lambda/\beta\cos\theta$$

where D is the crystal size, λ is the wavelength of X-ray radiation (0.15406 nm for Cu Kα), k is the shape factor (usually assumed to be 0.9), β is the full width at half maximum (FWHM) of the diffraction peak, and θ is the diffraction angle.

SEM–EDX analysis of JP-CuO NRs

The surface properties of the generated CuO NRs were analyzed using a SEM. As shown in Fig. 4a and b, the particles exhibited a predominantly rod-like shape, forming clusters and appearing well-dispersed [44]. Some particle clustering was evident, likely due to the presence of phenolic compounds derived from the JP plant, which acted as a capping agent. Furthermore, the high surface energy of JP-CuO NRs resulted in minimal aggregation, which was attributed to the water medium serving as the synthesis source. To identify the chemical elements, present in the CuO NRs, an EDX analysis was performed on a densely populated area of the sample (Fig. 4c)**.** The EDX spectrum showed significant peaks at 0.9, 8, and 8.9 keV, corresponding to copper atoms. A single peak at 0.5 keV was also observed, corresponding to oxygen atoms. Figure 4c exhibited distinct and strong signals for Cu and O atoms, with a weight percentage of 84.57% and 15.43%, respectively. The absence of other peaks indicates that the CuO NRs are of high purity.

TEM analysis of JP-CuO NRs

High-resolution transmission electron microscopy (HR-TEM) was used to study the size, shape, and structure of the JP-CuO NRs in detail. HR-TEM images showed the nanorod structure at different magnifications are shown in Fig. 5a–c. HR-TEM images revealed CuO nanorods with a diameter of around 10–14 nm and a length of 100–200 nm (Fig. 5a and b). The selected area electron diffraction pattern (SAED) of the JP-CuO NRs is portrayed in Fig. 5d. The SAED pattern indicated the presence of polycrystalline NRs in the JP-CuO sample [47].

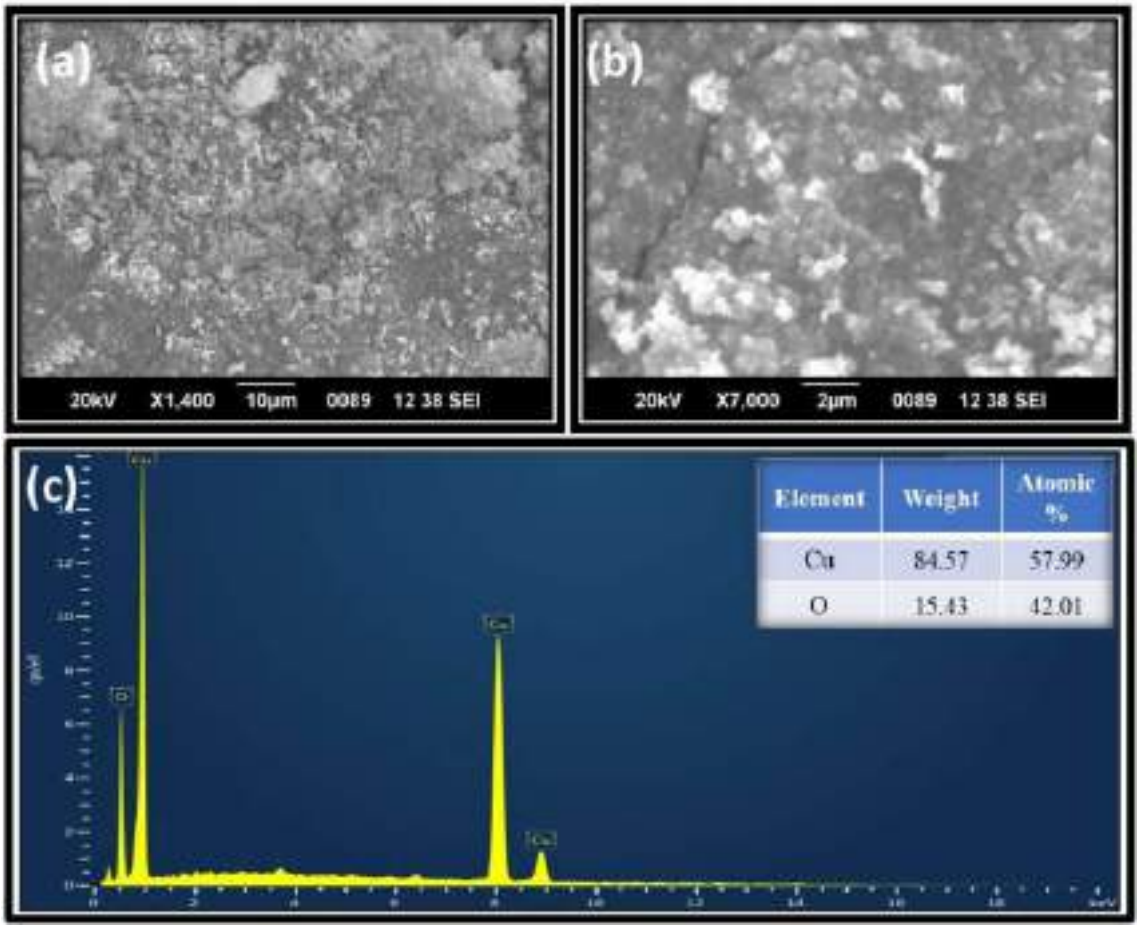

Fig. 4 **a** and **b** SEM images of JP-CuO NRs various magnifications and **c** EDX spectra of JP-CuO NRs

A photocatalytic degradation of RhB and CV dyes by the fabricated JP-CuO NRs

The JP-CuO catalyst was utilized to illustrate the photocatalytic removal of RhB and CV dyes in an environment of bright sunlight. RhB and CV dye degradation are shown in Figs. 6 and 7 across two distinct periods of 120 min and 60 min, respectively. These results also show that these dyes have separate wavelength ranges at 540 nm and 580 nm. The UV–Visible spectrometer was used to measure the RhB and CV dye degradation at regular intervals of 30 min and 15 min respectively. Degradation efficiencies of 95% and 97% were achieved for RhB and CV dyes, respectively. The degradation efficiency of the as-prepared JP-CuO NRs was compared with that of recently reported CuO nanoparticles in Tables 2, 3. The results of this work suggest that JP-CuO NRs have a lot of potential as a catalyst for rapidly breaking down organic contaminants by photocatalysis. The significant rates of degradation shown together with the apparent impact of different pH settings on the removal process spotlight the potential utility of JP-CuO NRs in resolving a variety of problems with water pollution brought on by organic pollutants. As a result, our findings suggest promising opportunities for using JP-CuO NRs to address environmental contamination problems.

The method shown below demonstrates how electrons and holes affect dye deterioration [35, 48].

$$CuO + h\nu \rightarrow e^- + h^+$$

$$\text{Absorption of } O_2 : O_2 + e^- \rightarrow O_2^{-\cdot}$$

$$\text{Water Ionization} : H_2O \rightarrow OH^- + H^+$$

$$\text{Superoxide protonation} : O_2^{-\cdot} + H^+ \rightarrow HOO^{\cdot}$$

$$HOO^{\cdot} + e^- \rightarrow HO_2^-$$

$$HOO^- + H^+ \rightarrow H_2O_2$$

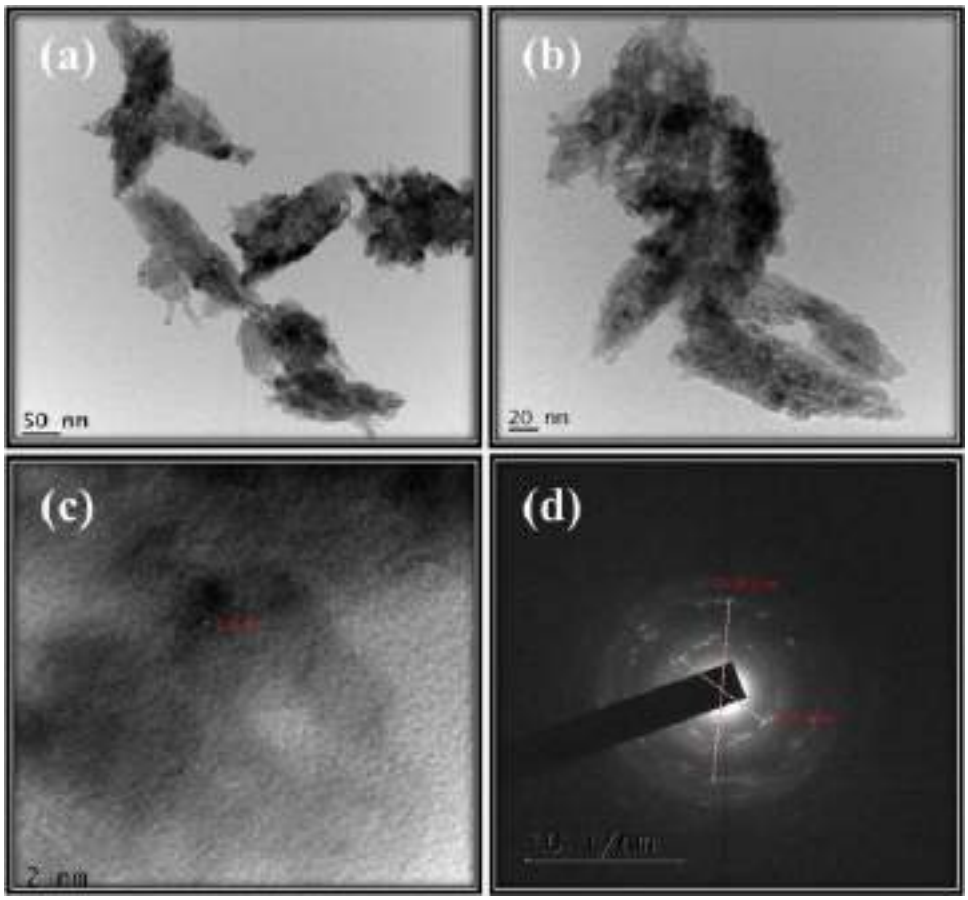

Fig. 5 **a**–**c** HR-TEM images JP-CuO NRs, and **d** SAED patterns

$$H_2O_2 + e^- \rightarrow OH^- + OH^{\cdot}$$

$$H_2O + h^+ \rightarrow H^+ + OH^{\cdot}$$

$$\text{Dyes} + OH^{\cdot} \rightarrow \text{Removal product}$$

The OH radical stated is a very strong oxidant that is quite successful in causing a variety of dyes, including RhB and CV, to degrade.

Anti-bacterial activities of synthesized JP-CuO NRs

JP-CuO NRs were evaluated for their efficacy against both Gram-positive (*Bacillus coagulans* and *Staphylococcus aureus*) and Gram-negative (*Escherichia coli* and *Klebsiella pneumoniae*) bacteria using the well diffusion method. Figure 8 illustrates the results of the zone inhibition test, displaying the diameters of the inhibition zones (in mm) surrounding each well containing the JP-CuO NRs. The most positive outcomes were noted with inhibition zones measuring 14, 16, 13, and 11 mm against *Bacillus coagulans, Staphylococcus aureus, Escherichia coli,* and *Klebsiella pneumoniae*, respectively, at a concentration of 150 µL, in comparison to the standard drug, as outlined in Table 4. [50, 51].

The results of the study showed that Gram-positive bacteria were more susceptible to JP-CuO NRs than Gram-negative bacteria**.** The variation in sensitivity can be explained by the significant presence of a dense peptidoglycan layer in the cell wall of Gram-positive bacteria, providing a small physical barrier that offers protection. In contrast, Gram-negative bacteria possess both lipopolysaccharide and peptidoglycan, rendering them more resistant to the effects of JP-CuO NRs**.**

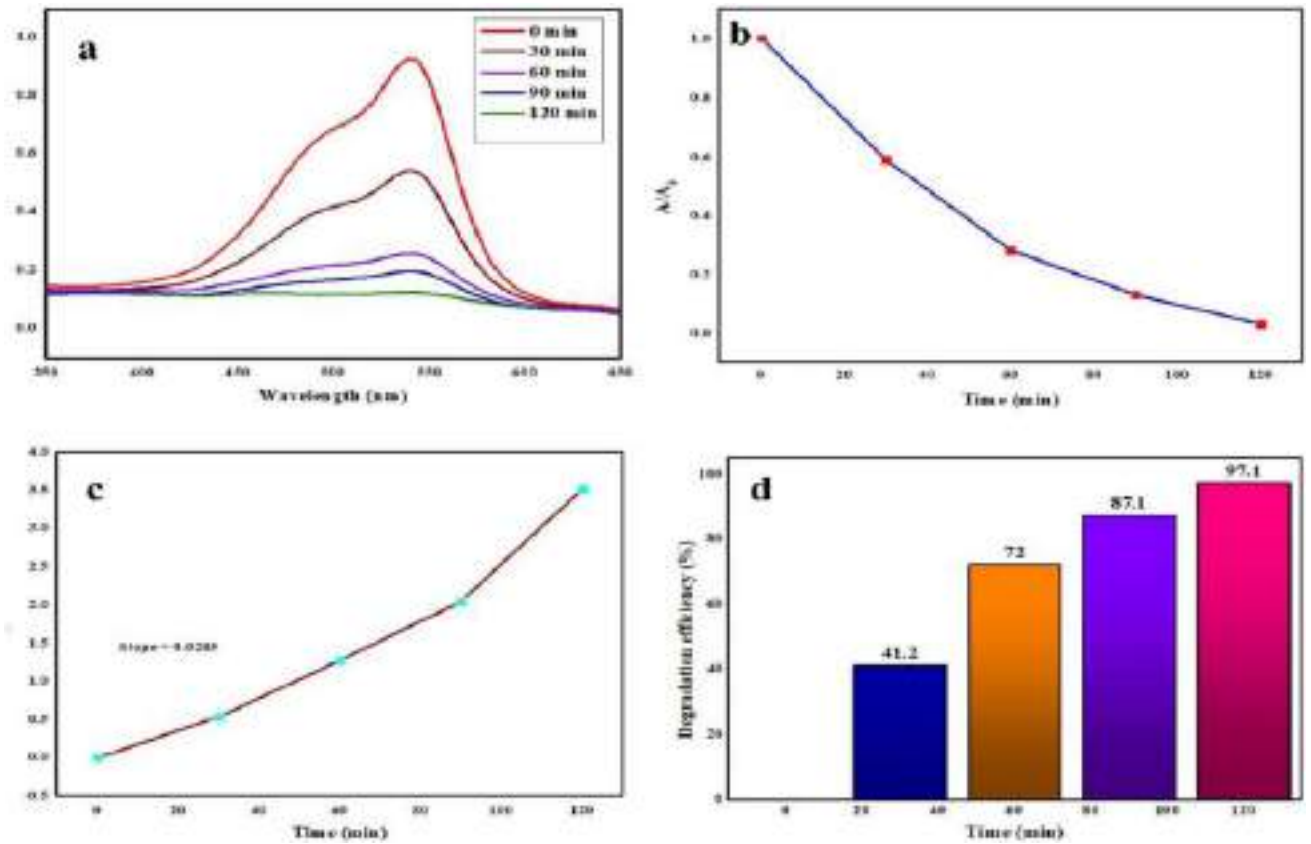

Fig. 6 **a** UV–vis absorbance spectra of RhB dye under UV (sunlight) illumination over JP-CuO NRs as a function of time, **b** the progression of RhB dye degradation during consecutive time intervals, **c** the kinetics of RhB dye degradation presented as a first-order linear plot with ln A_0/A as a function of time, and **d** a column chart representing the distribution of RhB dye degradation across different time intervals

Conclusions

We have developed a green method for making copper oxide nanorods (CuO NRs) using *Jatropha podagrica* leaf extract as a capping agent. The NRs were also effective photocatalysts, breaking down Rhodamine B (RhB) and Crystal Violet (CV) dyes in sunlight with degradation rates of 95–97% within 120 and 60 min, respectively. We also tested the NRs against Gram-positive (*Bacillus coagulans* and *Staphylococcus aureus*) and Gram-negative (*Escherichia coli* and *Klebsiella pneumoniae*) bacteria, and they produced inhibition zones of 14, 16, 13, and 11 mm, respectively, at a concentration of 150 µL. These results suggest that JP-CuO NRs could be used to clean up water pollution and develop powerful antibacterial agents.

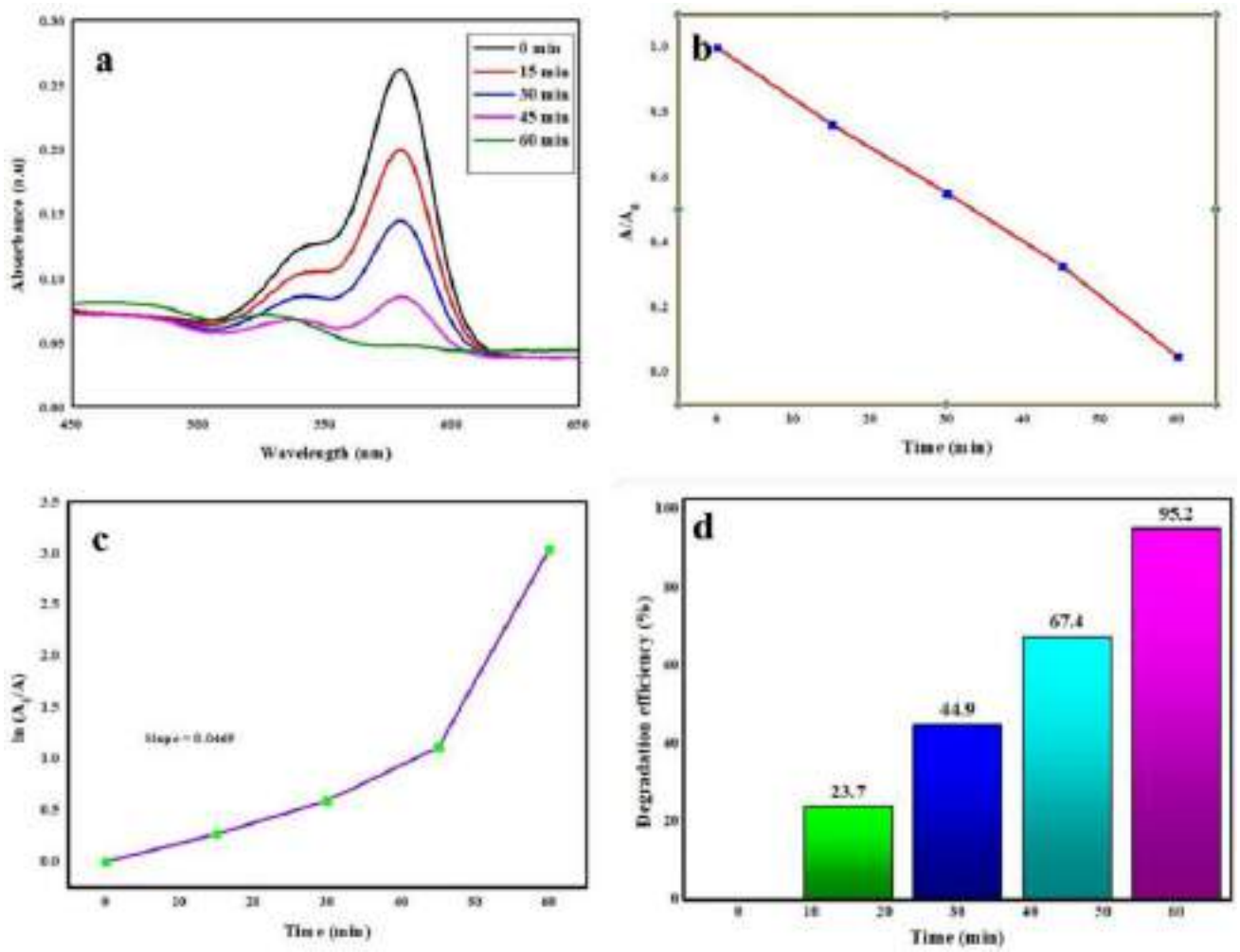

Fig. 7 **a** UV–vis absorbance spectra of CV dye under UV (sunlight) illumination over JP-CuO NRs as a function of time, **b** the progression of CV dye degradation during consecutive time intervals, **c** the kinetics of CV dye degradation presented as a first-order linear plot with ln A_0/A as a function of time, and **d** a column chart representing the distribution of CV dye degradation across different time intervals

Table 2 Lists the materials required to prepare the JP-CuO NRs

Chemical name	Supplier name	Purity (%)	Usage
Copper (II) sulfate pentahydrate ($Cu(SO_4)_2{\cdot}5H_2O$)	Merk, India	98	Reagent for the preparation of CuO NRs
Sodium hydroxide (NaOH)	Merk, India	99	Precipitating agent for the preparation of CuO NRs
Milli Q-water	Merk, India	100	Solvent
Bacillus coagulans	Aadhya Biosciences Pvt. Ltd Visakhapatnam, India	100	Well diffusion method
Staphylococcus aureus	Aadhya Biosciences Pvt. Ltd Visakhapatnam, India	100	Well diffusion method
Escherichia coli	Aadhya Biosciences Pvt. Ltd Visakhapatnam, India	100	Well diffusion method
Klebsiella pneumoniae	Aadhya Biosciences Pvt. Ltd Visakhapatnam, India	100	Well diffusion method
Jatropha podagrica leaves	Government Degree College Chodavaram, India	100	Capping and stabilized agent for the CuO NRs

Table 3 Comparison of the photocatalytic degradation of JP-CuO NRs in the present work with previous works

Green materials	Dye	Light source	Irradiation time (min)	Degradation efficiency (%)	References
Jatropha podagrica leaf extract	Rhodamine B	Sunlight	120	95	Present work
	Crystal violet		60	97	
Ferulago angulate boiss extract	Rhodamine B	UV light	150	83	[48]
Citrus aurantifolia leaf extract	Rhodamine B	UV light	120	91	[35]
Ruellia tuberosa root extract	Crystal Violet	Sunlight	120	90	[36]
Sida acuta leaf extract	Crystal Violet	Sunlight	100	87	[49]

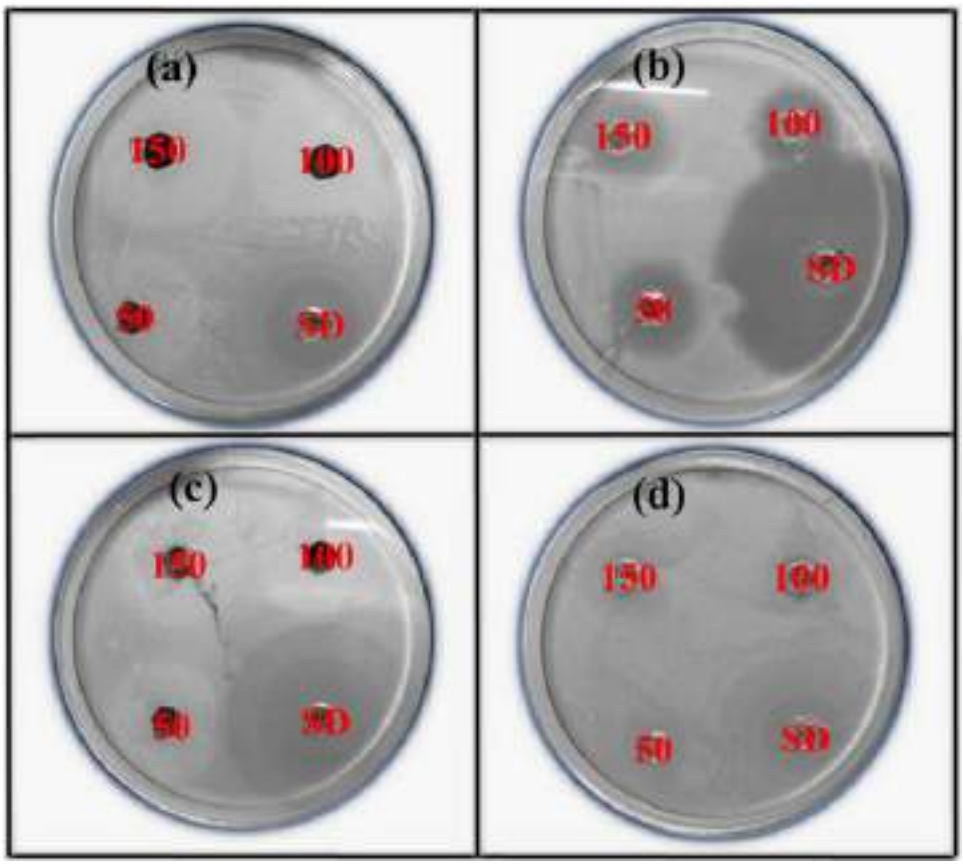

Fig. 8 Antibacterial activity of CuO NRs synthesized using *Jatropha podagrica* leaf extract for **a** *Bacillus coagulans*, **b** *Staphylococcus aureus*, **c** *Escherichia coli*, and **d** *Klebsiella pneumoniae*

Table 4 Zone of inhibition at various concentrations of JP-CuO NRs

Name	*Bacillus coagulans*	*Staphylococcus aureus*	*Escherichia coli*	*Klebsiella pneumoniae*
Shape	Round	Round	Round	Round
Gram reaction	Gram-positive	Gram-positive	Gram-negative	Gram-negative
50 µL	11 mm	14 mm	11 mm	10 mm
100 µL	13 mm	15 mm	12 mm	10 mm
150 µL	14 mm	16 mm	13 mm	11 mm
Antibiotic	30 mm	32 mm	30 mm	26 mm

Acknowledgements The authors express sincere gratitude to Dr. K. Basavaiah, professor in the Department of Analytical Chemistry at Andhra University, Visakhapatnam, Andhra Pradesh, India, for generously facilitating UV-Vis spectroscopy for characterizations

Authors contributions Venkatesh Golthi wrote the manuscript and prepared the tables, J Laxmi Mangamma collected the data, Kiran Kumar Penmethsa prepared the figures, and Jayarao Kommu reviewed the manuscript.

Funding The authors did not receive any funding for this research work.

Availability of data and materials This declaration is "not applicable".

Declarations

Ethical approval This declaration is "not applicable".

Conflict of interest There are no conflicts to declare.

References

1. Lee KM, Lai CW, Ngai KS, Juan JC (2016) Recent developments of zinc oxide based photocatalyst in water treatment technology: a review. Water Res 88:428–448. https://doi.org/10.1016/j.watres.2015.09.045
2. Jain R, Mathur M, Sikarwar S, Mittal A (2007) Removal of the hazardous dye rhodamine B through photocatalytic and adsorption treatments. J Environ Manage 85(4):956–964. https://doi.org/10.1016/j.jenvman.2006.11.002
3. Jones N, Ray B, Ranjit KT, Manna AC (2008) Antibacterial activity of ZnO nanoparticle suspensions on a broad spectrum of microorganisms. FEMS Microbiol Lett 279(1):71–76. https://doi.org/10.1111/j.1574-6968.2007.01012.x
4. Mayeen A, Shaji LK, Nair AK, Kalarikkal N (2018) Morphological characterization of nanomaterials. In: Characterization of nanomaterials, pp. 335–364. Woodhead Publishing. https://doi.org/10.1016/B978-0-08-101973-3.00012-2
5. Fatima F, Siddiqui S, Khan WA (2021) Nanoparticles as novel emerging therapeutic antibacterial agents in the antibiotics resistant era. Biol Trace Elem Res 199:2552–2564. https://doi.org/10.1007/s12011-020-02394-3
6. Veloso RC, Souza A, Maia J, Ramos NMM, Ventura J (2021) Nanomaterials with high solar reflectance as an emerging path towards energy-efficient envelope systems: a review. J Mater Sci. https://doi.org/10.1007/s10853-021-06560-3
7. Naz S, Gul A, Zia M, Javed R (2023) Synthesis, biomedical applications, and toxicity of CuO nanoparticles. Appl Microbiol Biotechnol 107(4):1039–1061. https://doi.org/10.1007/s00253-023-12364-z
8. Karthikeyan NR, Philip J, Raj B (2008) Effect of clustering on the thermal conductivity of nanofluids. Mater Chem Phys 109(1):50–55. https://doi.org/10.1016/j.matchemphys.2007.10.029
9. Agarwal R, Verma K, Agrawal NK, Duchaniya RK, Singh R (2016) Synthesis, characterization, thermal conductivity and sensitivity of CuO nanofluids. Appl Therm Eng 102:1024–1036. https://doi.org/10.1016/j.applthermaleng.2016.04.051
10. Oruç Ç, Altındal A (2017) Structural and dielectric properties of CuO nanoparticles. Ceram Int 43(14):10708–10714. https://doi.org/10.1016/j.ceramint.2017.05.006
11. Vidyasagar CC, Arthoba Naik Y, Venkatesha TG, Viswanatha R (2012) Solid-state synthesis and effect of temperature on optical properties of CuO nanoparticles. Nano-Micro Lett 4:73–77. https://doi.org/10.1007/BF03353695
12. Langmar O, Ganivet CR, Schol P, Scharl T, De La Torre G, Torres T, Guldi DM (2018) Improving charge injection and charge transport in CuO-based p-type DSSCs–a quick and simple precipitation method for small CuO nanoparticles. J Mater Chem C 6(19):5176–5180. https://doi.org/10.1039/C8TC00769A
13. Jiang T, Bujoli-Doeuff M, Farré Y, Pellegrin Y, Gautron E, Boujtita M, Odobel F (2016) CuO nanomaterials for p-type dye-sensitized solar cells. RSC Adv 6(114):112765–112770. https://doi.org/10.1039/C6RA17879K
14. Letchumanan D, Sok SP, Ibrahim S, Nagoor NH, Arshad NM (2021) Plant-based biosynthesis of copper/copper oxide nanoparticles: an update on their applications in biomedicine, mechanisms, and toxicity. Biomolecules 11(4):564. https://doi.org/10.3390/biom11040564
15. Das D, Nath BC, Phukon P, Dolui SK (2013) Synthesis and evaluation of antioxidant and antibacterial behavior of CuO nanoparticles. Colloids Surf, B 101:430–433. https://doi.org/10.1016/j.colsurfb.2012.07.002
16. Gholamali I, Hosseini SN, Alipour E, Yadollahi M (2019) Preparation and characterization of oxidized starch/CuO nanocomposite hydrogels applicable in a drug delivery system. Starch-Stärke 71(3–4):1800118. https://doi.org/10.1002/star.201800118
17. Perlman O, Weitz IS, Azhari H (2015) Copper oxide nanoparticles as contrast agents for MRI and ultrasound dual-modality imaging. Phys Med Biol 60(15):5767. https://doi.org/10.1088/0031-9155/60/15/5767
18. Muthuvel A, Jothibas M, Manoharan C (2020) Synthesis of copper oxide nanoparticles by chemical and biogenic methods: photocatalytic degradation and in vitro antioxidant activity. Nanotechnol Environ Eng 5:1–19. https://doi.org/10.1007/s41204-020-00078-w
19. Murugan B, Rahman MZ, Fatimah I, Lett JA, Annaraj J, Kaus NHM, Sagadevan S (2023) Green synthesis of CuO nanoparticles for biological applications. Inorg Chem Commun. https://doi.org/10.1016/j.inoche.2023.111088
20. Cuong HN, Pansambal S, Ghotekar S, Oza R, Hai NTT, Viet NM, Nguyen VH (2022) New frontiers in the plant extract mediated biosynthesis of copper oxide (CuO) nanoparticles and their potential applications: a review. Environ Res 203:111858. https://doi.org/10.1016/j.envres.2021.111858
21. Yugandhar P, Vasavi T, Devi UM, P., & Savithramma, N. (2017) Bioinspired green synthesis of copper oxide nanoparticles from *Syzygium alternifolium* (Wt.) Walp: characterization and evaluation of its synergistic antimicrobial and anticancer activity. Appl Nanosci 7:417–427. https://doi.org/10.1007/s13204-017-0584-9
22. Sathiyavimal S, Vasantharaj S, Veeramani V, Saravanan M, Rajalakshmi G, Kaliannan T, Pugazhendhi A (2021) Green chemistry route of biosynthesized copper oxide nanoparticles using Psidium guajava leaf extract and their antibacterial activity and effective removal of industrial dyes. J Environ Chem Eng 9(2):105033. https://doi.org/10.1016/j.jece.2021.105033
23. Bhaskarwar BHUSHAN, Itankar PRAKASH, Fulke ABHAY (2008) Evaluation of antimicrobial activity of medicinal plant Jatropha podagrica (Hook). Rouman Biotechnol Lett 13(5):3873–3877
24. Thomas S (2016) Pharmacognostic and phytochemical constituents of leaves of Jatropha multifida Linn. and Jatropha podagrica Hook. J Pharmacognosy Phytochem 5(2):243–246
25. Panzu NN, Lengbiye EM, Domondo A, Inkoto CL, Muanyishay CL, Gbolo BZ, Mpiana PT (2020) A review on the Bioactivity and Phytochemistry of Jatropha podagrica Hook Euphorbiaceae. Discov Phytomed 7(4):186–194
26. Golthi V, Kommu J, Ramesh AV (2023) A green and sustainable approach to the fabrication of ZnO nanoparticles via *Jatropha podagrica* leaf extract for effective dye degradation and antibacterial applications. Colloid Polym Sci. https://doi.org/10.1007/s00396-023-05187-x
27. Golthi V, Kommu J (2023) An eco-friendly and sustainable method for producing Fe3O4 nanoparticles using Jatropha podagrica leaf extract for efficient dye degradation and antibacterial uses. Hybrid Adv. https://doi.org/10.1016/j.hybadv.2023.100110
28. Alhalili Z (2022) Green synthesis of copper oxide nanoparticles CuO NPs from Eucalyptus Globoulus leaf extract: adsorption and

design of experiments. Arab J Chem 15(5):103739. https://doi.org/10.1016/j.arabjc.2022.103739
29. Javid-Naderi MJ, Sabouri Z, Jalili A, Zarrinfar H, Samarghandian S, Darroudi M (2023) Green synthesis of copper oxide nanoparticles using okra (Abelmoschus esculentus) fruit extract and assessment of their cytotoxicity and photocatalytic applications. Environ Technol Innov 32:103300. https://doi.org/10.1016/j.eti.2023.103300
30. Benhammada A, Trache D (2022) Green synthesis of CuO nanoparticles using Malva sylvestris leaf extract with different copper precursors and their effect on nitrocellulose thermal behavior. J Therm Anal Calorim 147:1–16. https://doi.org/10.1007/s10973-020-10469-5
31. Shah IH, Ashraf M, Sabir IA, Manzoor MA, Malik MS, Gulzar S, Zhang Y (2022) Green synthesis and characterization of copper oxide nanoparticles using *Calotropis procera* leaf extract and their different biological potentials. J Mol Struct 1259:132696. https://doi.org/10.1016/j.molstruc.2022.132696
32. Yugandhar P, Vasavi T, Jayavardhana Rao Y, Devi UM, P., Narasimha, G., & Savithramma, N. (2018) Cost effective, green synthesis of copper oxide nanoparticles using fruit extract of Syzygium alternifolium (Wt.) Walp., characterization and evaluation of antiviral activity. J Cluster Sci 29:743–755. https://doi.org/10.1007/s10876-018-1395-1
33. Velsankar K, Parvathy G, Mohandoss S, Kumar RM, Sudhahar S (2022) Green synthesis and characterization of CuO nanoparticles using Panicum sumatrense grains extract for biological applications. Appl Nanosci 12(6):1993–2021. https://doi.org/10.1007/s13204-022-02441-6
34. Veisi H, Karmakar B, Tamoradi T, Hemmati S, Hekmati M, Hamelian M (2021) Biosynthesis of CuO nanoparticles using aqueous extract of herbal tea (Stachys Lavandulifolia) flowers and evaluation of its catalytic activity. Sci Rep 11(1):1983. https://doi.org/10.1038/s41598-021-81320-6
35. Rafique M, Tahir MB, Irshad M, Nabi G, Gillani SSA, Iqbal T, Mubeen M (2020) Novel Citrus aurantifolia leaves based biosynthesis of copper oxide nanoparticles for environmental and wastewater purification as an efficient photocatalyst and antibacterial agent. Optik 219:165138. https://doi.org/10.1016/j.ijleo.2020.165138
36. Vasantharaj S, Sathiyavimal S, Saravanan M, Senthilkumar P, Gnanasekaran K, Shanmugavel M, Pugazhendhi A (2019) Synthesis of ecofriendly copper oxide nanoparticles for fabrication over textile fabrics: characterization of antibacterial activity and dye degradation potential. J Photochem Photobiol B Biol 191:143–149. https://doi.org/10.1016/j.jphotobiol.2018.12.026
37. Kumar PV, Shameem U, Kollu P, Kalyani RL, Pammi SVN (2015) Green synthesis of copper oxide nanoparticles using Aloe vera leaf extract and its antibacterial activity against fish bacterial pathogens. BioNanoScience 5:135–139. https://doi.org/10.1007/s12668-015-0171-z
38. Ssekatawa K, Byarugaba DK, Angwe MK, Wampande EM, Ejobi F, Nxumalo E, Kirabira JB (2022) Phyto-mediated copper oxide nanoparticles for antibacterial, antioxidant and photocatalytic performances. Front Bioeng Biotechnol 10:820218. https://doi.org/10.3389/fbioe.2022.820218
39. Hosseini-Koupaei M, Shareghi B, Saboury AA, Davar F, Sirotkin VA, Hosseini-Koupaei MH, Enteshari Z (2019) Catalytic activity, structure and stability of proteinase K in the presence of biosynthesized CuO nanoparticles. Int J Biol Macromol 122:732–744. https://doi.org/10.1016/j.ijbiomac.2018.11.001
40. Andualem WW, Sabir FK, Mohammed ET, Belay HH, Gonfa BA (2020) Synthesis of copper oxide nanoparticles using plant leaf extract of Catha edulis and its antibacterial activity. J Nanotechnol 2020:1–10. https://doi.org/10.1155/2020/2932434
41. Vishveshvar K, Aravind Krishnan MV, Haribabu K, Vishnuprasad S (2018) Green synthesis of copper oxide nanoparticles using Ixiro coccinea plant leaves and its characterization. BioNanoScience 8:554–558. https://doi.org/10.1007/s12668-018-0508-5
42. Velsankar K, Rm AK, Preethi R, Muthulakshmi V, Sudhahar S (2020) Green synthesis of CuO nanoparticles via Allium sativum extract and its characterizations on antimicrobial, antioxidant, antilarvicidal activities. J Environ Chem Eng 8(5):104123. https://doi.org/10.1016/j.jece.2020.104123
43. Singh J, Kumar V, Kim KH, Rawat M (2019) Biogenic synthesis of copper oxide nanoparticles using plant extract and its prodigious potential for photocatalytic degradation of dyes. Environ Res 177:108569. https://doi.org/10.1016/j.envres.2019.108569
44. Nasrollahzadeh M, Sajadi SM, Rostami-Vartooni A (2015) Green synthesis of CuO nanoparticles by aqueous extract of Anthemis nobilis flowers and their catalytic activity for the A3 coupling reaction. J Colloid Interface Sci 459:183–188. https://doi.org/10.1016/j.jcis.2015.08.020
45. Ahamed M, Alhadlaq HA, Khan MM, Karuppiah P, Al-Dhabi NA (2014) Synthesis, characterization, and antimicrobial activity of copper oxide nanoparticles. J Nanomater 2014:17–17. https://doi.org/10.1155/2014/637858
46. Sagadevan S, Vennila S, Marlinda AR, Al-Douri Y, Rafie Johan M, Anita Lett J (2019) Synthesis and evaluation of the structural, optical, and antibacterial properties of copper oxide nanoparticles. Appl Phys A 125:1–9. https://doi.org/10.1007/s00339-019-2785-4
47. Pallela PNVK, Ummey S, Ruddaraju LK, Kollu P, Khan S, Pammi SVN (2019) Antibacterial activity assessment and characterization of green synthesized CuO nano rods using Asparagus racemosus roots extract. SN Appl Sci 1:1–7. https://doi.org/10.1007/s42452-019-0449-9
48. ShayeganMehr E, Sorbiun M, Ramazani A et al (2018) Plant-mediated synthesis of zinc oxide and copper oxide nanoparticles by using ferulago angulata (schlecht) boiss extract and comparison of their photocatalytic degradation of Rhodamine B (RhB) under visible light irradiation. J Mater Sci Mater Electron 29:1333–1340. https://doi.org/10.1007/s10854-017-8039-3
49. Sathiyavimal S, Vasantharaj S, Bharathi D, Saravanan M, Manikandan E, Kumar SS, Pugazhendhi A (2018) Biogenesis of copper oxide nanoparticles (CuONPs) using Sida acuta and their incorporation over cotton fabrics to prevent the pathogenicity of Gram negative and Gram positive bacteria. J Photochem Photobiol, B 188:126–134. https://doi.org/10.1016/j.jphotobiol.2018.09.014
50. Naika HR, Lingaraju K, Manjunath K, Kumar D, Nagaraju G, Suresh D, Nagabhushana H (2015) Green synthesis of CuO nanoparticles using Gloriosa superba L. extract and their antibacterial activity. J Taibah Univ Sci 9(1):7–12. https://doi.org/10.1016/j.jtusci.2014.04.006
51. Nethravathi PC, Kumar MP, Suresh D, Lingaraju K, Rajanaika H, Nagabhushana H, Sharma SC (2015) Tinospora cordifolia mediated facile green synthesis of cupric oxide nanoparticles and their photocatalytic, antioxidant and antibacterial properties. Mater Sci Semicond Process 33:81–88. https://doi.org/10.1016/j.mssp.2015.01.034

Authors and Affiliations

Venkatesh Golthi[1,2,3] · Jayarao Kommu[1,3] · Kiran Kumar Penmethsa[2] · J. Laxmi Mangamma[2]

✉ Venkatesh Golthi
venkatesh@gdcc.ac.in

[1] Andhra University Trans-Disciplinary Research Hub (A.U. TDR-HUB), Visakhapatnam, AP 530003, India

[2] Department of Chemistry, Government Degree College, Chodavaram, AP 531036, India

[3] Department of Chemistry, Wellfare Institute of Science, Technology and Management, Pinagadi, Pendurthi, AP 531173, India

Hybrid Advances 4 (2023) 100110

Contents lists available at ScienceDirect

Hybrid Advances

journal homepage: www.journals.elsevier.com/hybrid-advances

An eco-friendly and sustainable method for producing Fe_3O_4 nanoparticles using *Jatropha podagrica* leaf extract for efficient dye degradation and antibacterial uses

Venkatesh Golthi [a,b,c,*], Jayarao Kommu [a,c]

[a] Andhra University Trans-Disciplinary Research Hub (A.U. TDR-HUB), Visakhapatnam, 530003, AP, India
[b] Department of Chemistry, Government Degree College, Chodavaram, 531036, AP, India
[c] Department of Chemistry, Wellfare Institute of Science, Technology and Management, pinagadi, Pendurthi, 531173, AP, India

ARTICLE INFO

Keywords:
Fe_3O_4 nanoparticles
Jatropha podagrica plant leaves
Antibacterial activities
Dye degradations

ABSTRACT

A green and efficient method was used to synthesize Fe_3O_4 nanoparticles using *Jatropha podagrica* leaf extract (JP- Fe_3O_4 NPs) as a stabilizer. The nanoparticles were characterized using various techniques, including XRD, FT-IR, SEM, SEM-EDX, HR-TEM, and UV–visible spectroscopy. The SEM and HR-TEM images showed that the nanoparticles were spherical, hexagonal, cubic, and rod-shaped, with sizes ranging from 14 to 16 nm. The FT-IR spectrum showed a characteristic peak at 581 cm^{-1}, corresponding to the Fe O bond. The photocatalytic activity of the nanoparticles was tested by degrading Fluorescein sodium (FS) and Crystal violet (CV) dyes in sunlight. The nanoparticles could degrade 92–95 % of the dyes within 1–2 h. The nanoparticles also exhibited potent antimicrobial activity against both gram-positive and gram-negative bacteria. When 150 μL of the nanoparticles were used in a well diffusion method, inhibition zones of 13, 15, 11, and 10 mm were observed against *Bacillus coagulans, staphylococcus aureus, Escherichia coli,* and *Klebsiella pneumoniae*, respectively. This study demonstrates that the synthesized JP- Fe_3O_4 NPs effectively remove dyes from aqueous solutions and have potent antimicrobial properties.

1. Introduction

Over the past two decades, nanotechnology has achieved remarkable progress, spanning a diverse array of applications across biology, medicine, and technology [1]. At the heart of nanotechnology lies the art of synthesizing nanoparticles in varying shapes and dimensions, unlocking a wide spectrum of potential applications. Among the myriad nanoparticle types, magnetic Fe_3O_4 nanoparticles (Fe_3O_4 NPs) hold a distinctive place due to their exceptional characteristics stemming from finite-size and surface effects. These encompass high magnetization, superparamagnetic, and additional anisotropy contributions [2]. A captivating aspect of these Fe_3O_4 NPs is their capacity to relinquish magnetization once an externally applied magnetic field is withdrawn. Moreover, they exhibit attributes such as low toxicity, biocompatibility, and robust magnetic properties, rendering them remarkably suited for deployment in domains such as bioimaging, cancer theragnostic applications, and drug delivery [3]. To optimize the magnetic properties of these NPs, their sizes, and size distributions can be tailored, which, in turn, are influenced by the synthesis method employed. As a result, various synthesis approaches have been developed to produce Fe_3O_4 NPs, all aimed at achieving the desired properties for specific applications.

Fe_3O_4 NPs have been synthesized using various methods, such as hydrothermal [4], microemulsion [5], sonochemical [6], electrochemical [7], sol-gel [8], co-precipitation [4,9], mechanochemical (10), solvothermal [10], and emulsion techniques [11]. However, these approaches have proven unsuitable for biomedical applications due to the inclusion of toxic chemicals like sodium borohydride, dimethyl formamide, hydrazine, and carbon monoxide [12]. Consequently, there is a pressing need to explore biological synthesis approaches for Fe_3O_4 NPs. Among these, plant-mediated synthesis has emerged as a promising option due to its simplicity, eco-friendliness, ease of use, cost-effectiveness, scalability for industrial production, and suitability for biomedical applications [13]. Plant extracts contain phytochemicals that can act as both reducing and capping agents, allowing for the creation of Fe_3O_4 NPs with controlled size, shape, and absence of

* Corresponding author. Andhra University Trans-Disciplinary Research Hub (A.U. TDR-HUB), Visakhapatnam, 530003, AP, India.
E-mail address: venkatesh@gdcc.ac.in (V. Golthi).

https://doi.org/10.1016/j.hybadv.2023.100110
Received 19 August 2023; Received in revised form 10 November 2023; Accepted 14 November 2023
Available online 19 November 2023

Table 1
Contrasting the average particle size and structure of Fe_3O_4 nanoparticles in our study with findings from prior research.

Materials of plant	Average particle size	Structure	Applications	Reference
Jatropha podagrica leaf extract	14–16 nm	Spherical, hexagonal, cubical, and rod shape	Dye degradation and antibacterial applications	Present work
Chlorella vulgaris extract	55.8–172.9 nm	Spherical shape	Degradation of 2,4 dinitrophenol	[19]
Spirogyra hyalina and *Ajuga bracteosa* extracts	36 nm	Spherical and rod-shaped	Anti-bacterial applications	[20]
Prunus serrulata leaf extract	40 nm	Spherical shape	Synthesis and characterization of magnetic nanoparticles	[21]
Natural tannic acid extracted from green tea	23–31 nm	Cubical shape	Investigation of structural, morphological, optical properties, and colloidal stability for gas sensor application	[22]
Menthapulegium L. leaf extract.	22–34 nm	Cubical shape	Synthesis and characterization of magnetic nanoparticles	[23]
Rhus coriaria seed extract	53 nm	Spherical shape	Anti-bacterial and anti-fungal applications	[24]

aggregates, without needing external oxidizing, reducing, and capping agents [14]. Moreover, the bioactive molecules present in plant extracts contribute to the capping process, enhancing the biomedical properties of the resulting Fe_3O_4 NPs beyond those obtained through conventional methods. This synergy between Fe_3O_4 NPs and bioactive plant molecules improves biomedical activities. As a result, numerous extracts of plants have been utilized in preparing Fe_3O_4 NPs using this approach.

In this research, we attempted to produce Fe_3O_4 NPs through a green synthesis method, utilizing *Jatropha podagrica* (JP) plant extract, with a dual focus on efficient organic dye pollutant removal and antioxidant activities. *Jatropha podagrica*, a traditional medicinal plant known for its historical use in treating various conditions like fever, scabies, ulcers, and wounds, exhibits beneficial properties such as anti-tumorigenic, antioxidant, and antibacterial activities [15]. The leaves of this plant were analyzed and found to contain specific phytochemicals, including phenolic acids (such as vanillic, syringic, P-hydroxybenzoic acid, melilotic, *cis*-trans ferulic, *p*-coumaric acid, and phloretic acids), flavonoids

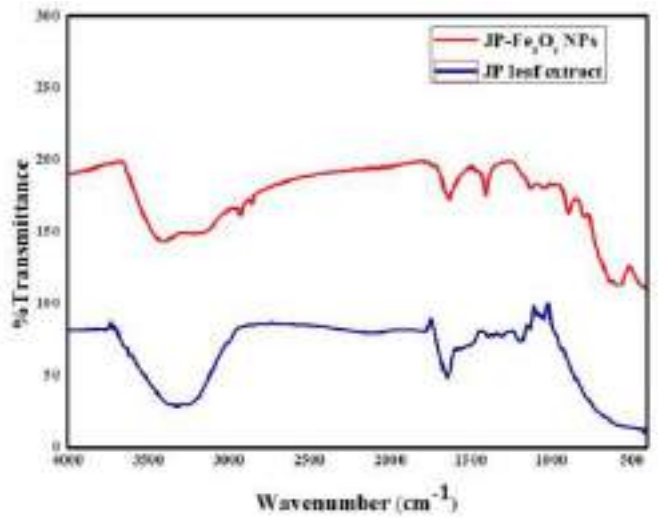

Fig. 2. FTIR spectra of *Jatropha podagrica* leaf extract and *Jatropha podagrica* leaf extract capped Fe_3O_4 NPs.

(e.g., apigenin, acacetin, and luteolin), tannins, glycol flavones, and proanthocyanidins [16,17]. The leaf extract of *Jatropha podagrica* has been demonstrated to be non-toxic, making it a crucial factor to be taken into account when preparing nanoparticles [16]. Recently, we have published an article detailing the utilization of this plant extract in the preparation of ZnO nanoparticles [18]. With this knowledge in mind, the study aimed to adopt an eco-friendly approach by utilizing the leaf extract of *Jatropha podagrica* for the bio-green synthesis of Fe_3O_4 NPs. The naturally occurring chemicals in the extract were essential for the synthesis of JP- Fe_3O_4 NPs. They helped to stabilize the nanoparticles and make them more effective than those synthesized using traditional chemical methods [16]. Additionally, the different types of phenolic acids in the extract helped to create nanoparticles that were well-defined in terms of their size and shape. This is better than other nanoparticles synthesized using green methods (as indicated in Table 1). To fully explore the potential of different plant species, it is important to use new and unique plants for nanoparticle synthesis. This will allow researchers to find new proteins and chemicals from plants that have not been used before to stabilize nanoparticles. Additionally, these new plant species may offer other advantages, such as higher yields, lower costs, or special properties that are useful for specific applications. In this study, the JP-Fe_3O_4 NPs had a negatively charged surface, which made them very good at removing Fluorescein sodium (FS) and Crystal violet (CV) dyes from water. The antibacterial activity of these JP- Fe_3O_4 NPs was tested against both Gram-positive (*Bacillus coagulans, staphylococcus aureus*)

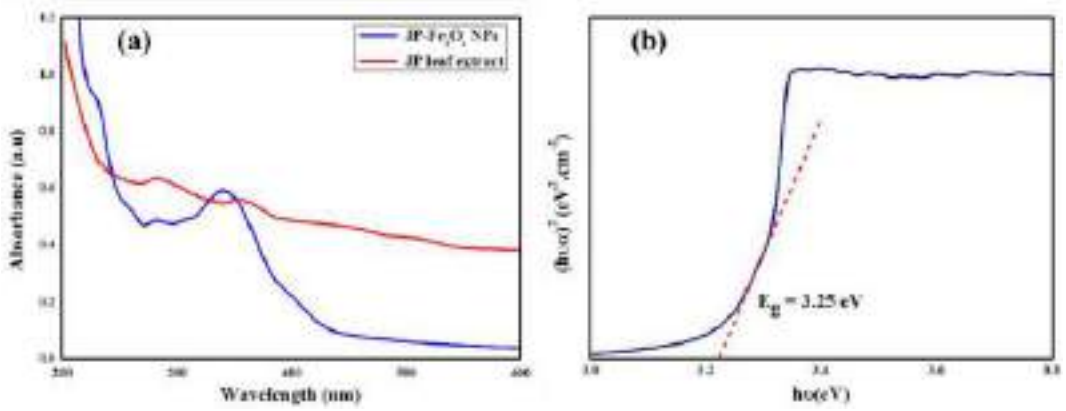

Fig. 1. (a) UV–Vis Spectra of *Jatropha podagrica* leaf extract and JP-Fe_3O_4 NPs and (b) The direct band gap energy of JP-Fe3O4 NPs from using Tauc plot.

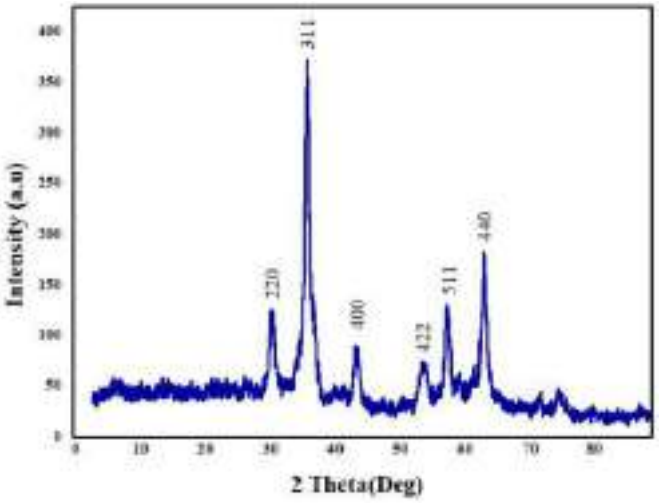

Fig. 3. XRD patterns of Fe_3O_4 NPs using an aqueous leaf extract of *Jatropha podagrica*.

Table 2
Calculating the average particle size of JP-Fe_3O_4 NPs.

Planes	2θ	β	cosθ	Size (nm)
220	31.98	0.492	0.964649	15.6
311	34.63	0.615	0.951218	12.3
400	36.47	0.507	0.928551	14.5
422	47.75	0.464	0.891481	15.3
511	56.82	0.526	0.876517	13.2
440	63.07	0.501	0.851864	13.5
Average size				**14.1**

and Gram-negative (*Escherichia coli, Klebsiella pneumoniae*) bacteria.

2. Materials and methods

2.1. Materials

Raw leaves of *Jatropha podagrica* were collected from the Government Degree College Garden located in Chodavaram, Andhra Pradesh, India. The reagents employed in the experiments, comprising ferric chloride hexahydrate ($FeCl_3{\cdot}6H_2O$), Ammonium Iron (II) sulfate ($(NH_4)_2Fe(SO_4)_2{\cdot}6H_2O$), Aqueous ammonia ($NH_3{\cdot}H_2O$), Fluorescein sodium (FS), and Crystal violet (CV), were purchased from Merck in India and utilized without the need for further purification. Sources of *Bacillus coagulans, staphylococcus aureus, Escherichia coli, and Klebsiella pneumoniae* strains collected from IMTECH, Chandigarh, India. Milli Q-water was employed for all the conducted tests.

2.2. Jatropha podagrica (JP) leaf extract preparation

The JP plant leaves were cleansed using warm water followed by a rinse with Milli-Q water. Subsequently, they were air-dried in shaded conditions for a period of 1 month until they were completely devoid of moisture. Once dried, the leaves were finely ground into a powder. A quantity of 1 g from the powdered sample was then placed in a 250 mL glass beaker along with 100 mL of Milli-Q water. The mixture was subjected to heating at 80 °C for a duration of 30 min, resulting in the formation of a solution with a golden-yellow. The solution was first filtered to remove solid particles, and then it underwent centrifugation to obtain a pure extract solution. This extract was subsequently stored in a refrigerator at a temperature of 4 °C for future use.

2.3. Synthesis of Jatropha podagrica capped Fe_3O_4 nanoparticles (JP-Fe_3O_4 NPs)

In a standard green synthesis procedure, a solution was prepared by dissolving $FeCl_3{\cdot}6H_2O$ (1.11 g) and $(NH_4)_2Fe(SO_4)_2{\cdot}6H_2O$ (0.556 g) in a 2:1 ratio in 90 mL of Milli Q water. The resultant mixture underwent sonication for 15–20 min. Subsequently, the solution was subjected to heating at 80 °C while maintaining continuous stirring for a span of 15 min. Following this step, 10 mL of a 1 % aqueous extract derived from *Jatropha podagrica* leaves was introduced into the reaction mixture, and the reaction was allowed to proceed for 45 min at 80 °C under sustained stirring. The reaction mixture underwent a steady and controlled addition of 5 mL of aqueous ammonia solution, with continuous stirring. This resulted in a change in the mixture, causing the formation of JP-Fe_3O_4 NPs, evident from the appearance of a black precipitate. The resultant JP-Fe_3O_4 NPs precipitate was isolated from the mixture using an external magnet, followed by intermittent washing steps using ethanol and Milli Q water. Finally, the precipitate was dried at room temperature under vacuum conditions [25].

2.4. Photocatalytic potential of JP- Fe_3O_4 NPs for the degradation of FS, and CV dyes

The assessment of the photocatalytic efficacy of JP-Fe_3O_4 NPs in the degradation of FS and CV dyes was conducted using readily available UV radiation from sunlight. Initially, 100 mL solutions containing 1 ppm of FS and CV dyes were combined with 0.01 g of JP-Fe_3O_4 NPs in separate containers. These mixtures were stirred in the dark for an hour to stabilize the solutions and halt any adsorption-desorption processes. Following stabilization, the solutions were exposed to sunlight for 4 h, specifically from 11 a.m. to 3 p.m., with an outdoor temperature ranging from 33 to 35 °C. Continuous magnetic stirring was employed to maintain a pH level of 10 during this time. At predefined intervals, consistent samples were collected from each dye solution, and the NPs were separated by centrifugation at 8000 rpm. A UV spectrometer was utilized to measure the color intensities at 521 nm and 625 nm for the FS and CV dyes, respectively [26].

The degradation rate and degradation constant can be determined utilizing the subsequent formulas.

$$\text{Degradation rate } (\%) = ((A_0 - A) / A_0) \times 100$$

$$\ln A_0/A = kt$$

Here, A_0 refers to the initial concentration of the substance, while A represents the final concentration after the degradation process. The degradation constant is denoted by K, and 't' indicates the amount of time exposed to sunlight.

2.5. Investigation of antibacterial activity of JP-Fe_3O_4 NPs

The study assessed the antibacterial properties of the JP-Fe_3O_4 NPs in 24-h bacterial cultures (*Bacillus coagulans, staphylococcus aureus, Escherichia coli,* and *Klebsiella pneumoniae*) using the Agar-Well diffusion method. To prepare the nutrient agar medium, it was sterilized for approximately 30 min at 120 °C using an autoclave. Each sterile Petri dish was then filled with 20 mL of the medium, and the appropriate bacterial strains were aseptically introduced. The plates were left at room temperature to solidify the agar. A sterile borer was utilized to create a single well with a 6 mm diameter in each plate. Test substances, control (distilled water), and a standard drug were introduced into the 6 mm wells after being freshly dissolved in distilled water (at concentrations of 1, 2, and 3). The petri plates were incubated at 37 °C for 12 h, and the inhibition results are shown in Fig. 10. A standard solution with a concentration of 5 g/mL was used as a positive control. The diameter of the inhibitory zone was determined using the HiMedia antibiotic zone scale. All experiments were conducted in triplicate, and consistent results were obtained [27].

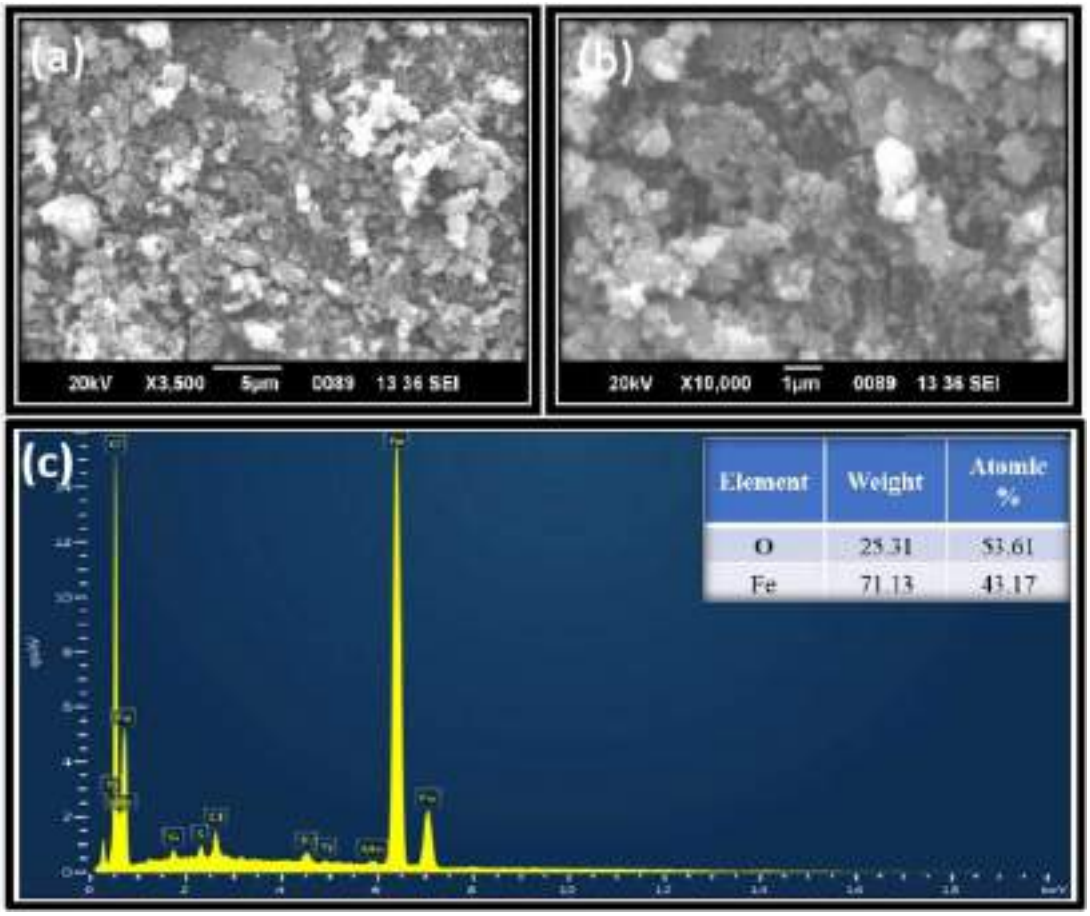

Fig. 4. (a and b) SEM images of Fe_3O_4 NPs capped with *Jatropha podagrica* leaf extract at different magnifications and (c) EDX spectrum of JP-Fe_3O_4 NPs.

2.6. Characterization of JP- Fe_3O_4 NPs

Various analytical methods were employed to elucidate the crystalline structure of JP-Fe_3O_4 NPs. X-ray diffraction (XRD) analyses were conducted using a Bruker Kappa Apex II instrument, operating at 40 kV and 35 mA, with CuKα radiation (λ = 1.54060 Å). The measurement range spanned from 2θ = 0–90°, and the scanning rate was set at 0.2 s. Fourier transform infrared spectra (FT-IR) were acquired using a Thermo Nicolet iS50 spectrometer. The spectra covered a frequency range of 4000–400 cm^{-1} and employed spectroscopic grade KBr pellets in transmission mode. To assess optical properties, UV–vis diffuse reflectance/absorbance spectroscopy was performed on the synthesized samples. A Shimadzu (2450 – SHIMADZU) spectrophotometer with a diffuse reflectance accessory was employed at room temperature. $BaSO_4$ was utilized as a reference material, and measurements spanned the wavelength range of 200–800 nm. The surface characteristics and elemental composition of the JP- Fe_3O_4 NPs were closely examined using scanning electron microscopy (SEM). We utilized the Jeol 6390LA/OXFORD XMX N instrument, which included energy-dispersive X-ray (EDX) spectroscopy. The SEM images were captured with an acceleration voltage of 20 kV. For a more extensive exploration of the microstructure and particle sizes, high-resolution transmission electron microscopy (HRTEM) was employed. We employed the JEOL/JEM 2100 instrument with an operational voltage of 200 kV. The elemental oxidation states of the samples were determined using an Axis Ultra X-ray photoelectron spectroscopy (XPS) instrument, which utilized a monochromatic X-ray source with Al Kα radiation. In addition, we conducted magnetization measurements at room temperature under the influence of applied magnetic fields using a Lakeshore VSM 7410 vibrating sample magnetometer (VSM).

3. Results and discussions

3.1. UV–vis spectroscopy studies

The aqueous leaf extract of *Jatropha podagrica* and synthetic JP-Fe_3O_4 NPs both have UV–Vis absorption spectra that are shown in Fig. 1a. Due to the presence of numerous phytochemicals, including phenolic acids, alkaloids, flavonoids, tannins, proanthocyanidins, and glycol flavones, the leaf extract displays high absorption bands at 280 and 351 nm [15]. In addition, the distinctive absorption band seen at 341 nm in the spectra shows the creation of JP-Fe_3O_4 NPs, principally as a result of the absorption and scattering of light by these NPs [28]. Notably, the lack of the absorption peaks from the leaf extract of *Jatropha podagrica* at 280 and 351 nm in the spectra of JP-Fe_3O_4 NPs suggests that the previously stated phytochemicals play a vital role in reducing and capping the JP-Fe_3O_4 NPs during their formation.

The optical band gap plays a pivotal role in determining the effectiveness of photocatalytic materials. This is because the transition of electronic states from the valence to the conduction band occurs only when the incoming photon possesses an energy equal to or higher than the band gap energy. Tauc and Menth introduced an expression to calculate the optical band gap [29].

$$(h\nu\alpha) = A\,(h\nu\text{-}E_g)^n$$

Here, A represents the absorption constant, α denotes the absorption coefficient, and n is a material-dependent constant (in this study, n is equal to 0.5). The estimated value was 3.25 eV, and the corresponding Tuac plot can be observed in Fig. 1b.

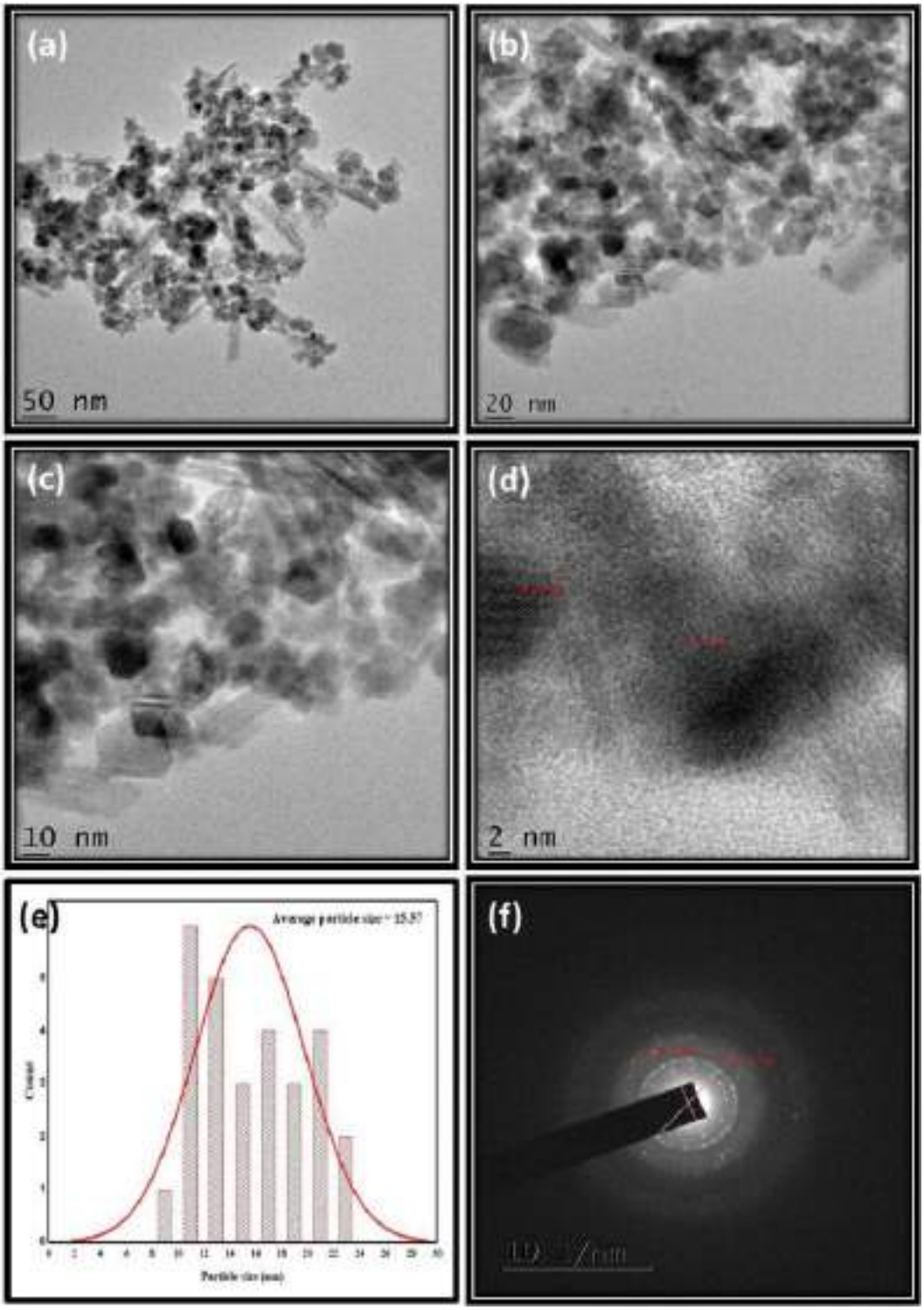

Fig. 5. (a–d) HR-TEM images, (e) Size distribution Histogram of Fe_3O_4 NPs Synthesized with aqueous extract of *Jatropha podagrica* leaves, and (f) SAED pattern.

3.2. FTIR analysis of the synthesized JP-Fe_3O_4 NPs

FTIR spectroscopy was employed for the purpose of identifying the functional groups present within the synthesized JP-Fe_3O_4 NPs and to ascertain their molecular composition. Fig. 2 provides a visualization of the data pertaining to the identified functional groups present both in the plant material and the JP-Fe_3O_4 NPs. The analysis discloses a broad peak appearing around 3322 cm^{-1}, signifying the presence of a phenolic group. Evidenced by the absorption of a broad peak at approximately 1639 cm^{-1}, the identification of aromatic compounds is corroborated. Additionally, discernible peaks at 1178 cm^{-1} and 1042 cm^{-1} denote the existence of amide functional groups and vibrations associated with polyphenolic molecules present in plant extract [16]. Moreover, Fig. 2 exemplifies the analysis of JP-Fe_3O_4 NPs, revealing absorption peaks spanning the range of 400–4000 cm^{-1}. Notably, the peak positioned at 581 cm^{-1} suggests the stretching frequency related to Fe–O bonding [30]. Peaks residing at 1122 cm^{-1}, 887 cm^{-1}, and 795 cm^{-1} provide insights into the chemical bonding, crystalline nature, and relative

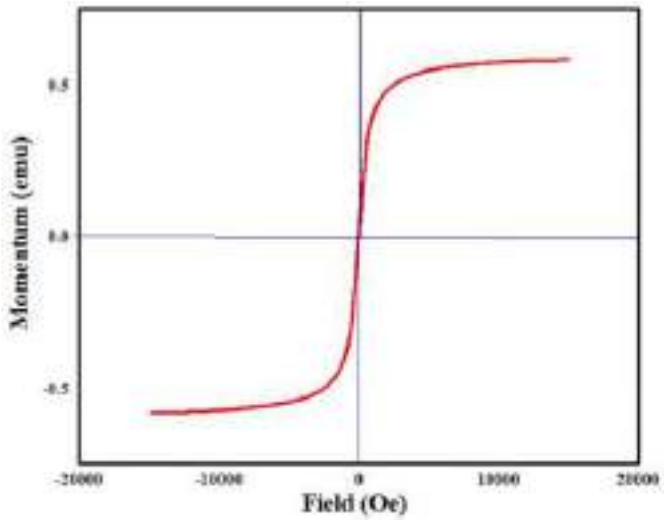

Fig. 6. Magnetization curve of synthesized Fe_3O_4 NPs using aqueous leaf extract of *Jatropha podagrica* at ambient temperature.

intensities of the IR bands associated with polyphenolic groups. The peak at 1400 cm^{-1} could potentially be attributed to the symmetric stretching of carboxyl side groups within the amino acid residues of protein molecules. The presence of a peak in the vicinity of 1627 cm^{-1} likely corresponds to the C═C stretching indicative of aromatic compounds. Prominent absorption bands observed at 3405 cm^{-1}, 2921 cm^{-1}, and 2851 cm^{-1} are indicative of –OH stretching vibrations in phenolic groups and –CH stretching vibrations in aldehyde groups. The presence of these distinctive peaks in the IR spectrum serves to confirm the purity and composition of the biofabricated JP-Fe_3O_4 NPs.

3.3. XRD analysis of the synthesized JP-Fe_3O_4 NPs

The X-ray diffraction analysis (Fig. 3) unveiled distinct JP-Fe_3O_4 NPs peaks at varying angles: 30.56°, 35.94°, 43.58°, 47.75°, 53.88°, 57.55°, and 63.17°. These angles corresponded to diverse crystal lattice planes, namely (220), (311), (400), (422), (511), and (440), respectively. These peaks impeccably matched the reported JCPDS values (File no. 89–6466) and aligned precisely with the crystal lattice parameters (a = 2.7992, b = 9.4097, c = 9.4832). This alignment indicated the absence of any impurity peaks within the patterns [28]. To determine the crystal dimensions of the synthesized NPs, the Debye-Scherrer equation $D = K\lambda/\beta \cos\theta$ was employed. In this equation, D signifies the crystallite size of Fe_3O_4 NPs, λ stands for the wavelength of the X-ray source (λ = 0.1541 nm), β represents the full width at half maximum of the diffraction peak, and θ corresponds to the half-diffraction angle (Bragg angle). Using the Scherrer constant (K = 0.9), the computed average crystal dimensions of JP-Fe_3O_4 NPs were ascertained to be 14.98 nm, as presented in Table 2 below.

3.4. SEM-EDX analysis of synthesized JP-Fe_3O_4 NPs

Surface characteristics of the Bio-synthesized JP-Fe_3O_4 NPs were investigated using an SEM (scanning electron microscope). The micrographs in Fig. 4a and b revealed that the NPs displayed a mixture of shapes, including spherical, hexagonal, cubic, and rod-like structures. Clustering of particles was observed, which is likely attributed to the

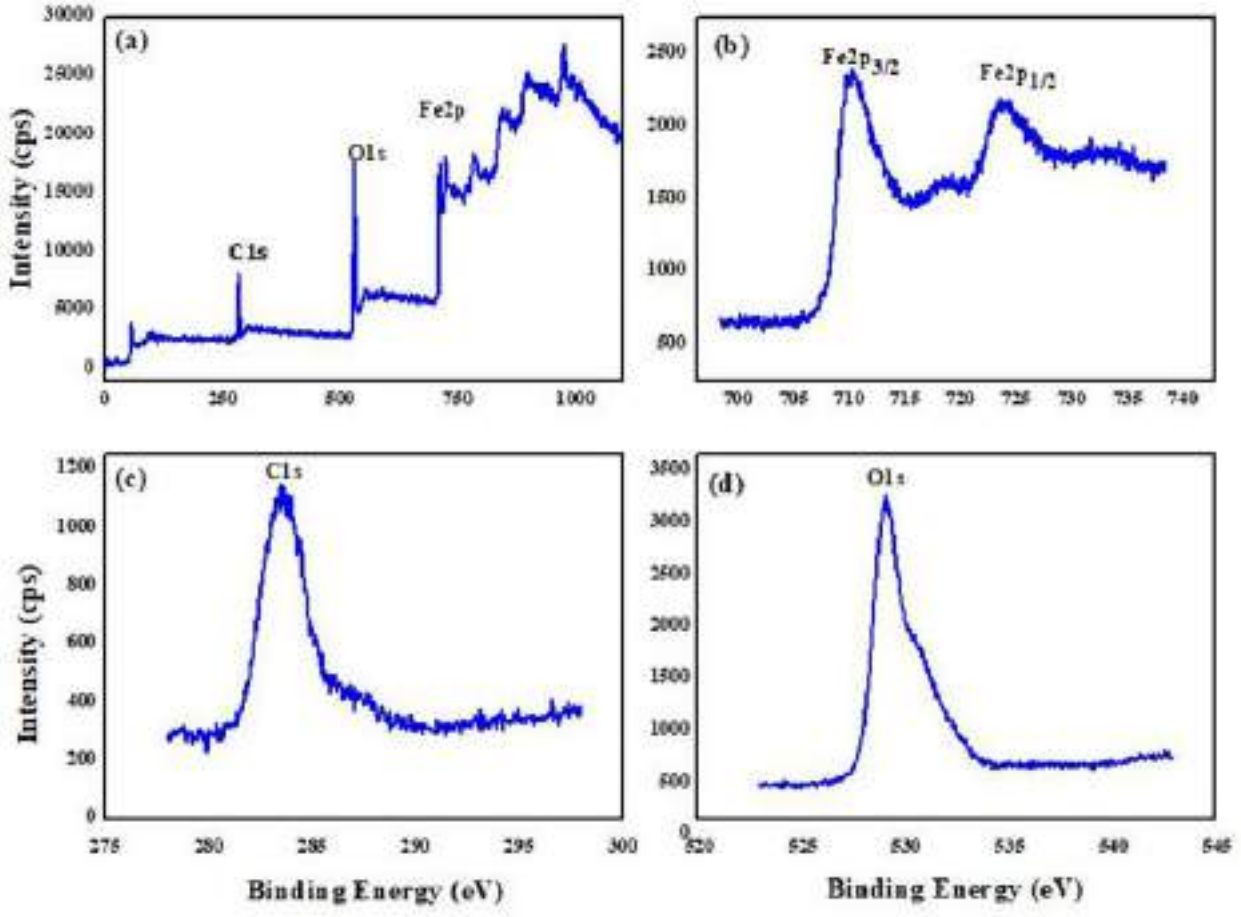

Fig. 7. XPS (a) Survey peaks (b) Fe2p peaks (c) C1s peaks (d) O1s peaks of fabricated Fe_3O_4 NPs using an aqueous leaf extract *Jatropha podagrica*.

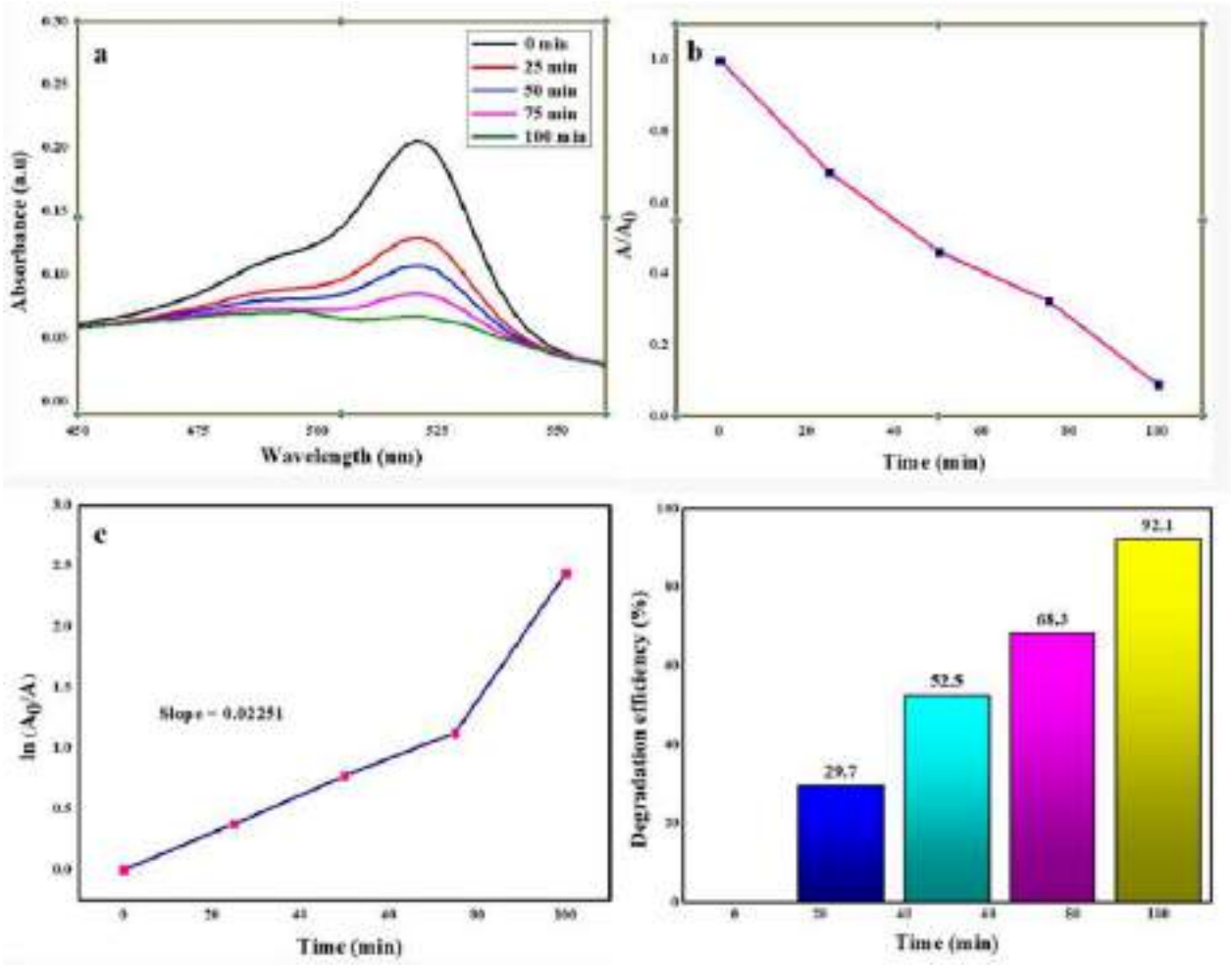

Fig. 8. (a) UV–vis absorbance spectra of FS dye under UV (sunlight) illumination over JP-Fe_3O_4 NPs as a function of time, (b) the progression of FS dye degradation during consecutive time intervals, (c) the kinetics of FS dye degradation presented as a first-order linear plot with ln A_0/A as a function of time, and (d) a column chart representing the distribution of FS dye degradation across different time intervals.

presence of phenolic compounds from the JP plant, acting as a capping agent [31].

To determine the chemical arrangement of the Fe_3O_4 NPs, an EDX (energy-dispersive X-ray spectrum) was obtained from a densely populated area (Fig. 4c). The EDX analysis exhibited prominent signals from Iron atoms at 0.6 keV, 6.4 keV, and 7 keV, respectively, in addition to a single peak corresponding to oxygen atoms at 0.5 keV. Moreover, there were minor peaks indicating the presence of sulfur (S), chlorine (Cl), silicon (Si), titanium (Ti), and Manganese (Mn) atoms, suggesting the contribution of these elements from the biological components that were predominantly associated with the JP-Fe_3O_4 NPs [32].

3.5. TEM analysis of synthesized JP-Fe_3O_4 NPs

The size, configuration, and structure of the synthesized JP-Fe_3O_4 NPs were explored using HR-TEM (high-resolution transmission electron microscopy). TEM images of JP-Fe_3O_4 NPs are shown in Fig. 5(a–d), displaying various magnifications. The TEM image clearly depicts the presence of aggregated free JP-Fe_3O_4 NPs, exhibiting a mixture of spherical, hexagonal, cubic, and rod-like shapes [33,34]. The average particle size of the aggregated free JP-Fe_3O_4 NPs was resolved to be 15.57 nm (Fig. 5e), which aligns with the crystallite size obtained from XRD analysis. This aggregation specifies that the surface of JP-Fe_3O_4 NPs was capped by bioactive molecules, which prevented further particle aggregation.

3.6. Vibrating sample magnetometer (VSM) of JP-Fe_3O_4 NPs

A vibrating sample magnetometer (VSM) was harnessed to delve into the magnetic attributes of the artificially created Fe_3O_4 NPs, which were synthesized through the utilization of an aqueous leaf extract derived from *Jatropha podagrica*. Fig. 6 visually portrays the magnetization curve encapsulating the synthesized JP-Fe_3O_4 NPs. This curve assumes a sigmoidal form bereft of a hysteresis loop, thereby signifying a superparamagnetic nature [35]. At ambient temperature, the JP-Fe_3O_4 NPs manifest a saturation magnetization (Ms) measurement amounting to 0.5831 (58 emu/g). The robust magnetic characteristics exhibited by these JP-Fe_3O_4 NPs facilitate their adept concentration and isolation through the application of a small magnetic force.

3.7. XPS of JP-Fe_3O_4 NPs

X-ray photoelectron spectroscopy (XPS) was engaged to meticulously probe into the chemical composition and oxidation states characterizing the engineered JP-Fe_3O_4 NPs. Illustrated in Fig. 7a is the comprehensive XPS spectrum, which corroborates the existence of JP-Fe_3O_4 NPs encompassed by organic moieties. This outcome aligns harmoniously with the findings derived from the energy-dispersive X-ray (EDX) analysis.

The Fe2p XPS spectrum, showcased in Fig. 7b, prominently exhibits a peak at 708 eV, intricately corresponding to Fe_3O_4 NPs [36–39]. Delving

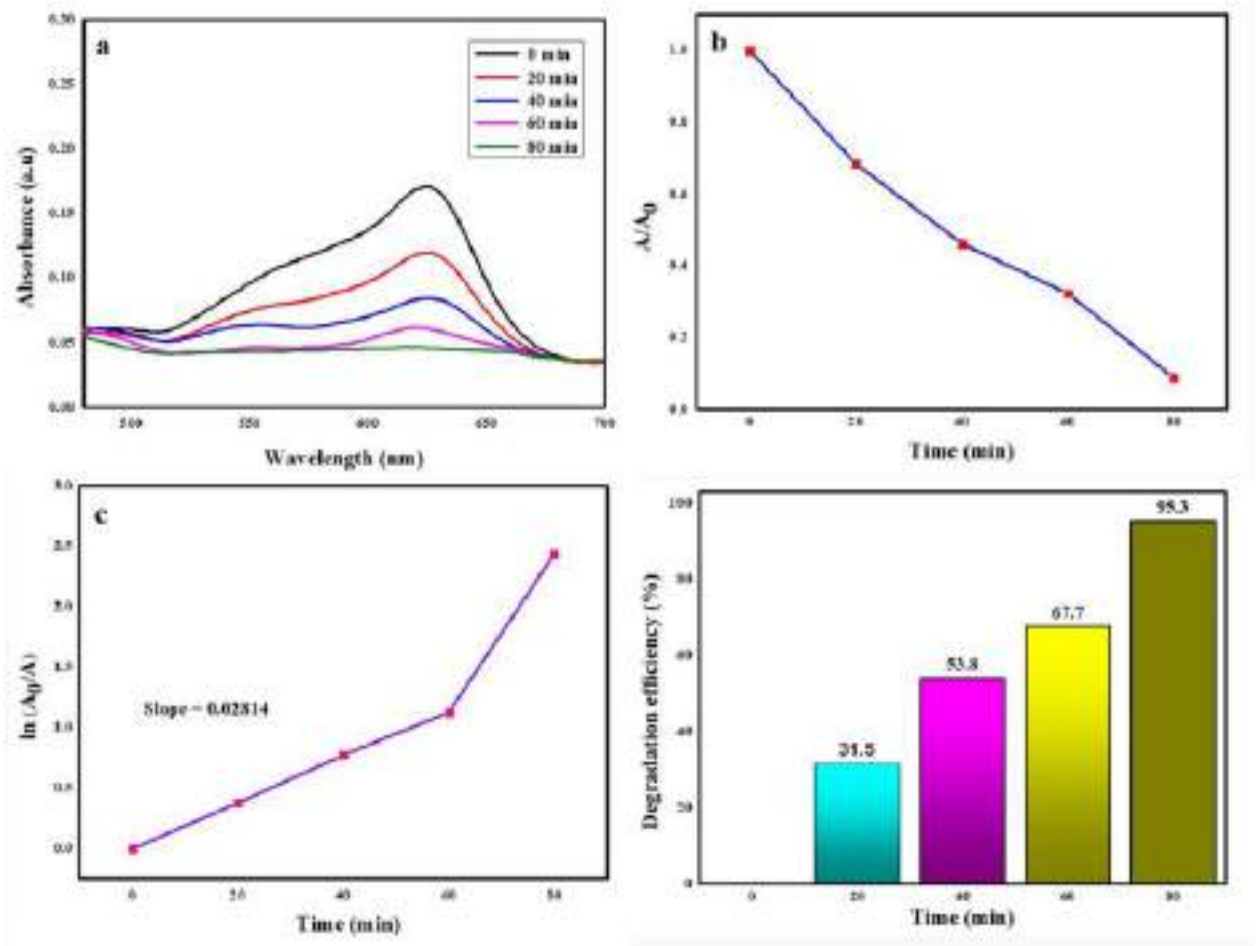

Fig. 9. (a) UV–vis absorbance spectra of CV dye under UV (sunlight) illumination over JP-Fe_3O_4 NPs as a function of time, (b) the progression of CV dye degradation during consecutive time intervals, (c) the kinetics of CV dye degradation presented as a first-order linear plot with ln A_0/A as a function of time, and (d) a column chart representing the distribution of CV dye degradation across different time intervals.

further into the JP-Fe_3O_4 XPS spectra, presented in the same figure, discloses spectral lines situated at 708 eV. This spectral characteristic unequivocally signals the concurrent presence of Fe^{2+} and Fe^{3+} oxidation states [40].

Notably, the discernible absence of peaks spanning the energy spectrum around 706–708 eV, which are conventionally attributed to zero-valent iron, serves to underscore the unadulterated nature of the JP-Fe_3O_4 NPs. This observation elegantly concurs with the findings obtained from X-ray diffraction (XRD) analysis. Moreover, the lack of peaks at 533.8 eV and 534.2 eV serves as additional confirmation, firmly establishing the non-existence of hydrous iron oxides such as $Fe(OH)_3$ [41].

Additionally, the perceptible peaks registering at 283 eV and 533 eV find their attribution to C 1s and O1s, signifying the presence of polyphenols. These peaks serve to substantiate the capping of bioactive molecules upon the surface of the JP-Fe_3O_4 NPs, as displayed in Fig. 7c and d. The oxygen and carbon signature peaks attributed to the *Jatropha podagrica* leaf extract can be attributed to the polyphenolic molecules.

3.8. Photocatalytic degradation of FS and CV dyes by the synthesized JP-Fe_3O_4 NPs

JP-Fe_3O_4 catalyst used under solar irradiation revealed efficient degradation of CV and FS dyes (Figs. 8 and 9), demonstrating high photocatalytic activity [42]. Under sunlight exposure, the degradation of FS and CV dyes proceeded at various speeds, requiring around 100 and 80 min, respectively. The deterioration process was monitored using a UV spectrometer at intervals of 20 and 25 min for FS and CV, respectively, at 521 and 625 nm. The degradation efficiencies for FS and CV dyes were 92 % and 95 %, respectively. In Table 3, a comparison was made between the CV dye degradation efficiency of the JP-Fe_3O_4 NPs and the Fe_3O_4 NPs reported in previous studies. Notably, there has been no prior successful attempt to degrade the FS dye using Fe_3O_4 NPs. These findings underscore the significant promise held by JP-Fe_3O_4 NPs as a robust catalyst, poised to facilitate the highly efficient photocatalytic degradation of organic pollutants. The significant degradation rates found and the impact of pH 10 on the process lead to the conclusion that JP-Fe_3O_4 NPs might be used to treat a variety of water and wastewater streams polluted with organic contaminants. These findings imply that JP-Fe_3O_4 NPs have intriguing opportunities for resolving the problems associated with environmental contamination.

The mechanism shown below demonstrates how holes and electrons contribute to dye deterioration [46].

$Fe_3O_4 + h\nu \rightarrow e^- + h^+$

O_2 absorption: $O_2 + e^- \rightarrow O_2^-$

Ionization of water: $H_2O \rightarrow OH^- + H^+$

Protonation of superoxide: $O_2^{-\cdot} + \rightarrow H^+ \; HOO^{\cdot}$

$HOO^{\cdot} + e^- \rightarrow HO_2^-$

$HOO^- + H^+ \rightarrow H_2O_2$

$H_2O_2 + e^- \; OH^- + \rightarrow OH$

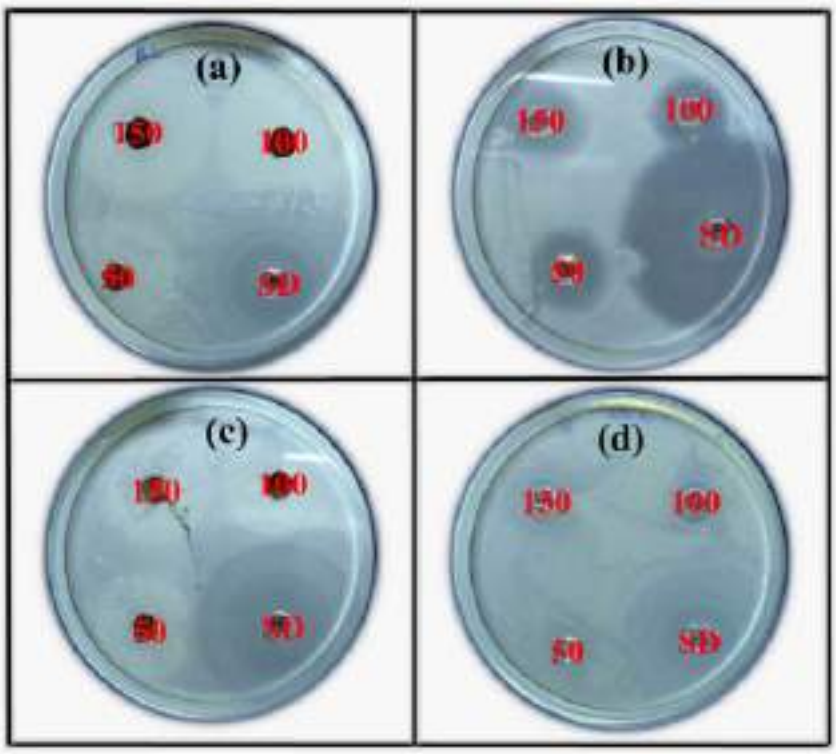

Fig. 10. Antibacterial activity of Fe_3O_4 NPs synthesized using *Jatropha podagrica* leaf extract for (a) *Bacillus coagulans*, (b) *Staphylococcus aureus*, (c) *Escherichia coli*, and (d) *Klebsiella pneumoniae.*

Table 3
Comparison of the photocatalytic degradation of Fe_3O_4 nanoparticles in the present work with previous works.

Synthesis method	Name of the dyes	Removal time (min)	Removal efficiency (%)	Reference
Green method (*Jatropha podagrica* leaf extract)	Crystal violet	80	95	Present work
	Fluorescein sodium	100	93	
Green method (Chlorella vulgari) extract	Crystal violet	90	96.2	[43]
Green method (Dolichos lablab L) pod extraxt	Crystal violet	200	95	[44]
Chemical method (Co-precipitation)	Crystal violet	120	94.7	[45]

$$H_2O + h^+ \rightarrow H^+ + OH$$

$$\text{Dyes} + OH \rightarrow \text{Degradant product}$$

The aforementioned OH radical is a very strong oxidant that is quite successful in breaking down different dyes like FS and CV.

3.9. Anti-bacterial activities of fabricated JP-Fe_3O_4 NPs

The efficiency of JP-Fe_3O_4 NPs as an antibacterial agent was assessed against both Gram-positive bacteria (*Bacillus coagulans, staphylococcus aureus*) and Gram-negative (*Escherichia coli, Klebsiella pneumoniae*) employing the well diffusion method. The results, shown in Fig. 10, indicate the diameter of inhibition zones (in mm) surrounding each well containing the JP-Fe_3O_4 NPs. The most favorable results were observed with 13, 15, 11, and 10 mm inhibition zones observed against *Bacillus coagulans, staphylococcus aureus, Escherichia coli,* and *Klebsiella pneumoniae* at a concentration of 150 μL, comparing the standard drug, as presented in Table 4. Interestingly, the JP-Fe_3O_4 NPs demonstrated better antibacterial activity compared to the reference journals [47,48].

Table 4
Zone of inhibition at various concentrations of JP-Fe_3O_4 NPs.

Name	*Bacillus coagulans*	*Staphylococcus aureus*	*Escherichia coli*	*Klebsiella pneumoniae*
Shape	Round	Round	Round	Round
Gram reaction	Gram-positive	Gram-positive	Gram-negative	Gram-negative
50 μL	10 mm	13 mm	10 mm	9 mm
100 μL	12 mm	14 mm	10 mm	9 mm
150 μL	13 mm	15 mm	11 mm	10 mm
Antibiotic	30 mm	32 mm	30 mm	26 mm

The antimicrobial effect of NPs may occur through various proposed mechanisms, but the primary mechanism by which these particles exhibit antibacterial properties appears to be the induction of oxidative stress via reactive oxygen species (ROS). ROS, which encompasses superoxide radicals (O^{2-}), hydroxyl radicals (–OH), hydrogen peroxide (H_2O_2), and singlet oxygen ($_1O^2$), have the capacity to inflict damage on cellular components such as DNA, proteins, and bacterial cell membranes [49]. In this study, it is suggested that JP-Fe_3O_4 NPs serve as a source of ROS, thereby inhibiting the growth of most pathogenic bacteria. This is achieved through the reaction of Fe^{2+} with oxygen, resulting in the production of hydrogen peroxide (H_2O_2). Subsequently, the H_2O_2 interacts with ferrous irons in what is known as the Fenton reaction, giving rise to hydroxyl radicals that are recognized for their ability to harm biological molecules [50]. Additionally, the small size of JP-Fe_3O_4 NPs may contribute to their antimicrobial effectiveness, as they can interact with bacterial membranes and potentially penetrate the bacterial cell, ultimately hindering bacterial growth [51].

From Tables 4 and it can be observed that Gram-positive bacteria

(*Bacillus coagulans, staphylococcus aureus*) showed higher sensitivity to JP-Fe_3O_4 NPs compared to Gram-negative bacteria (*Escherichia coli, Klebsiella pneumoniae*). This variation in susceptibility could be attributed to the substantial peptidoglycan layer present in the cell wall of Gram-positive bacteria. This layer serves as a robust physical barrier, offering heightened protection. In contrast, Gram-negative bacteria possess both lipopolysaccharides and peptidoglycan, making them more resistant to the effects of JP-Fe_3O_4 NPs [52].

4. Conclusions

In summary, we have successfully utilized an environmentally friendly approach to synthesize Fe_3O_4 nanoparticles by employing *Jatropha podagrica* leaf extract (JP- Fe_3O_4 NPs) as a capping agent. Various analytical techniques were employed to characterize these nanoparticles, confirming their distinctive features, including shapes like spheres, hexagons, cubes, and rods, with sizes ranging from 14 to 16 nm. The JP-Fe_3O_4 NPs have displayed impressive photocatalytic efficiency, effectively breaking down FS and CV dyes in sunlight. These dyes degraded by 92–95 % within 100 and 80 min for FS and CV, respectively. We also assessed their antibacterial properties against both Gram-positive (*Bacillus coagulans, staphylococcus aureus*) and Gram-negative (*Escherichia coli, Klebsiella pneumoniae*) bacterial strains, resulting in inhibition zones of 13,15,11 and 10 mm using 150 µL of nanoparticles. These findings underscore the potential applications of JP-Fe_3O_4 NPs in addressing water pollution challenges and in developing potent antibacterial agents.

Declaration of competing interest

The authors declare that they have no known competing financial interests or personal relationships that could have appeared to influence the work reported in this paper.

Acknowledgment

The authors express sincere gratitude to Dr. K. Basavaiah, professor in the Department of Analytical Chemistry at Andhra University, Visakhapatnam, Andhra Pradesh, India, for generously facilitating UV–Vis spectroscopy for the purpose of characterizations.

References

[1] M. Zain, H. Yasmeen, S.S. Yadav, S. Amir, M. Bilal, A. Shahid, M. Khurshid, Applications of nanotechnology in biological systems and medicine, in: Nanotechnology for Hematology, Blood Transfusion, and Artificial Blood, Elsevier, 2022, pp. 215–235, https://doi.org/10.1016/B978-0-12-823971-1.00019-2.

[2] D.G. Actis, I.J. Bruvera, G.A. Pasquevich, P.M. Zélis, Fixed magnetic nanoparticles: obtaining anisotropy energy density from high field magnetization, J. Magn. Magn Mater. 563 (2022), 169962, https://doi.org/10.1016/j.jmmm.2022.169962.

[3] H. Alijani, A. Noori, N. Faridi, S.Z. Bathaie, M.F. Mousavi, Aptamer-functionalized Fe_3O_4@ MOF nanocarrier for targeted drug delivery and fluorescence imaging of the triple-negative MDA-MB-231 breast cancer cells, J. Solid State Chem. 292 (2020), 121680, https://doi.org/10.1016/j.jssc.2020.121680.

[4] A.C.B. Jesus, J.D. Jesus, R.J.S. Lima, K.O. Moura, J.M.A. Almeida, J.G.S. Duque, C. T. Meneses, Synthesis and magnetic interaction on concentrated Fe_3O_4 nanoparticles obtained by the co-precipitation and hydrothermal chemical methods, Ceram. Int. 46 (8) (2020) 11149–11153, https://doi.org/10.1016/j.ceramint.2020.01.135.

[5] G. Asab, E.A. Zereffa, T. Abdo Seghne, Synthesis of silica-coated Fe_3O_4 nanoparticles by microemulsion method: characterization and evaluation of antimicrobial activity, International journal of biomaterials (2020), https://doi.org/10.1155/2020/4783612, 2020.

[6] M.A. Dheyab, A.A. Aziz, M.S. Jameel, P.M. Khaniabadi, B. Mehrdel, Mechanisms of effective gold shell on Fe_3O_4 core nanoparticles formation using sonochemistry method, Ultrason. Sonochem. 64 (2020), 104865, https://doi.org/10.1016/j.ultsonch.2019.104865.

[7] E. Sohouli, E.M. Khosrowshahi, P. Radi, E. Naghian, M. Rahimi-Nasrabadi, F. Ahmadi, Electrochemical sensor based on modified methylcellulose by graphene oxide and Fe_3O_4 nanoparticles: application in the analysis of uric acid content in urine, J. Electroanal. Chem. 877 (2020), 114503, https://doi.org/10.1016/j.jelechem.2020.114503.

[8] P. Hu, T. Chang, W.J. Chen, J. Deng, S.L. Li, Y.G. Zuo, A.A. Volinsky, Temperature effects on magnetic properties of Fe_3O_4 nanoparticles synthesized by the sol-gel explosion-assisted method, J. Alloys Compd. 773 (2019) 605–611, https://doi.org/10.1016/j.jallcom.2018.09.238.

[9] H. Mohammadi, E. Nekobahr, J. Akhtari, M. Saeedi, J. Akbari, F. Fathi, Synthesis and characterization of magnetite nanoparticles by co-precipitation method coated with biocompatible compounds and evaluation of in-vitro cytotoxicity, Toxicol Rep 8 (2021) 331–336, https://doi.org/10.1016/j.toxrep.2021.01.012.

[10] S.M. Fotukian, A. Barati, M. Soleymani, A.M. Alizadeh, Solvothermal synthesis of $CuFe_2O_4$ and Fe_3O_4 nanoparticles with high heating efficiency for magnetic hyperthermia application, J. Alloys Compd. 816 (2020), 152548, https://doi.org/10.1016/j.jallcom.2019.152548.

[11] C.E. Astete, C.S. Kumar, C.M. Sabliov, Size control of poly (d, l-lactide-co-glycolide) and poly (d, l-lactide-co-glycolide)-magnetite nanoparticles synthesized by emulsion evaporation technique, Colloids Surf. A Physicochem. Eng. Asp. 299 (1–3) (2007) 209–216, https://doi.org/10.1016/j.colsurfa.2006.11.055.

[12] G. Bonsignore, M. Patrone, S. Martinotti, E. Ranzato, "Green" biomaterials: the promising role of honey, J. Funct. Biomater. 12 (4) (2021) 72, https://doi.org/10.3390/jfb12040072.

[13] N. Rani, P. Singh, S. Kumar, P. Kumar, V. Bhankar, K. Kumar, Plant-mediated synthesis of nanoparticles and their applications: a review, Mater. Res. Bull. 112233 (2023), https://doi.org/10.1016/j.materresbull.2023.112233.

[14] J. Singh, T. Dutta, K.H. Kim, et al., 'Green' synthesis of metals and their oxide nanoparticles: applications for environmental remediation, J. Nanobiotechnol. 16 (2018) 84, https://doi.org/10.1186/s12951-018-0408-4.

[15] BHUSHAN Bhaskarwar, PRAKASH Itankar, ABHAY Fulke, Evaluation of antimicrobial activity of medicinal plant *Jatropha podagrica* (Hook), Roumanian Biotechnol. Lett. 13 (5) (2008) 3873–3877.

[16] S. Thomas, Pharmacognostic and phytochemical constituents of leaves of *Jatropha multifida Linn.* and *Jatropha podagrica* Hook, J. Pharmacogn. Phytochem. 5 (2) (2016) 243–246.

[17] N.N. Panzu, E.M. Lengbiye, A. Domondo, C.L. Inkoto, C.L. Muanyishay, B.Z. Gbolo, P.T. Mpiana, A review on the bioactivity and phytochemistry of *Jatropha podagrica hook* (euphorbiaceae), Discov. Phytomed. 7 (4) (2020) 186–194, https://doi.org/10.15562/phytomedicine.2020.150.

[18] V. Golthi, J. Kommu, A.V. Ramesh, A green and sustainable approach to the fabrication of ZnO nanoparticles via *Jatropha podagrica* leaf extract for effective dye degradation and antibacterial applications, Colloid Polym. Sci. (2023) 1–15, https://doi.org/10.1007/s00396-023-05187-x.

[19] T.S. AlGarni, M.H. Ali, A.M. Al-Mohaimeed, Green biosynthesis of Fe3O4 nanoparticles using Chlorella vulgaris extract for enhancing degradation of 2, 4 dinitrophenol, J. King Saud Univ. Sci. 35 (1) (2023), 102426, https://doi.org/10.1016/j.jksus.2022.102426.

[20] M.S. Sharif, H. Hameed, A. Waheed, M. Tariq, A. Afreen, A. Kamal, W. Zaman, Biofabrication of Fe_3O_4 nanoparticles from spirogyra hyalina and ajuga bracteosa and their antibacterial applications, Molecules 28 (8) (2023) 3403, https://doi.org/10.3390/molecules28083403.

[21] H. Şengönül, O. Demircan, Synthesis and characterization of Fe_3O_4 nanoparticles using *Prunus serrulata* leaf extract, BioNanoSci (2023), https://doi.org/10.1007/s12668-023-01174-2.

[22] S. Ananthi, M. Kavitha, E.R. Kumar, A. Balamurugan, Y. Al-Douri, H.K. Alzahrani, N.M. El-Metwaly, Natural tannic acid (green tea) mediated synthesis of ethanol sensor based Fe_3O_4 nanoparticles: investigation of structural, morphological, optical properties and colloidal stability for gas sensor application, Sensor. Actuator. B Chem. 352 (2022), 131071, https://doi.org/10.1016/j.snb.2021.131071.

[23] A. Bouafia, S.E. Laouini, Green synthesis of iron oxide nanoparticles by aqueous leaves extract of Mentha Pulegium L.: effect of ferric chloride concentration on the type of product, Mater. Lett. 265 (2020), 127364, https://doi.org/10.1016/j.matlet.2020.127364.

[24] A.A. Barzinjy, D.A. Abdul, F.H. Hussain, S.M. Hamad, Green synthesis of the magnetite (Fe_3O_4) nanoparticle using Rhus coriaria extract: a reusable catalyst for efficient synthesis of some new 2-naphthol bis-Betti bases, Inorganic and Nano-Metal Chem. 50 (8) (2020) 620–629, https://doi.org/10.1080/24701556.2020.1723027.

[25] V.K. Vg, A.A. Prem, Green synthesis and characterization of iron oxide nanoparticles using Phyllanthus niruri extract, Orient. J. Chem. 34 (5) (2018), https://doi.org/10.13005/ojc/340547.

[26] B. Kumar, K. Smita, L. Cumbal, A. Debut, S. Galeas, V.H. Guerrero, Phytosynthesis and photocatalytic activity of magnetite (Fe_3O_4) nanoparticles using the Andean blackberry leaf, Mater. Chem. Phys. 179 (2016) 310–315.

[27] S.M. Mousavi, S.A. Hashemi, M. Zarei, S. Bahrani, A. Savardashtaki, H. Esmaeili, B. Ramavandi, Data on cytotoxic and antibacterial activity of synthesized Fe_3O_4 nanoparticles using Malva sylvestris, Data Brief 28 (2020), 104929, https://doi.org/10.1016/j.dib.2019.104929.

[28] I.P. Sari, Y. Yulizar, Green synthesis of magnetite (Fe_3O_4) nanoparticles using Graptophyllum pictum leaf aqueous extract, in: IOP Conference Series: Materials Science and Engineering, vol. 191, IOP Publishing, 2017, April, 012014, https://doi.org/10.1088/1757-899X/191/1/012014, 1.

[29] J. Tauc, A. Menth, States in the gap, J. Non-Cryst. Solids 8 (1972) 569–585, https://doi.org/10.1016/0022-3093(72)90194-9.

[30] H. Al-Karagoly, A. Rhyaf, H. Naji, S. Albukhaty, F.A. AlMalki, A.A. Alyamani, S. Aloufi, Green synthesis, characterization, cytotoxicity, and antimicrobial activity of iron oxide nanoparticles using Nigella sativa seed extract, Green Process. Synth. 11 (1) (2022) 254–265, https://doi.org/10.1515/gps-2022-0026.

[31] Javad Safari, Zohre Zarnegar, Hoda Hekmatara, Green synthesis of Fe_3O_4 nanoparticles and Survey their magnetic properties, synthesis and reactivity in inorganic, metal-organic, Nano-Metal Chemistry (2015), https://doi.org/10.1080/15533174.2013.776597.

[32] D.A. Demirezen, Y.Ş. Yıldız, D.D. Yılmaz, Amoxicillin degradation using green synthesized iron oxide nanoparticles: kinetics and mechanism analysis, Environ. Nanotechnol. Monit. Manag. 11 (2019), 100219, https://doi.org/10.1016/j.enmm.2019.100219.

[33] H. Fatima, D.W. Lee, H.J. Yun, K.S. Kim, Shape-controlled synthesis of magnetic Fe 3 O 4 nanoparticles with different iron precursors and capping agents, RSC Adv. 8 (41) (2018) 22917–22923, https://doi.org/10.1039/C8RA02909A(Paper. RSC Adv., 2018, 8, 22917-22923.

[34] S.F. Chin, S.C. Pang, C.H. Tan, Green synthesis of magnetite nanoparticles (via thermal decomposition method) with controllable size and shape. http://hdl.handle.net/10044/1/18318, 2011.

[35] M.D. Nguyen, H.-V. Tran, S. Xu, T.R. Lee, Fe_3O_4 nanoparticles: structures, synthesis, magnetic properties, surface functionalization, and emerging applications, Appl. Sci. 11 (23) (2021) 11301, https://doi.org/10.3390/app112311301.

[36] Y. Yi, Y. Wei, P.E. Tsang, Z. Fang, Aging effects on the stabilisation and reactivity of iron-based nanoparticles green synthesised using aqueous extracts of Eichhornia crassipes, Environ. Sci. Pollut. Res. Int. 26 (27) (2019 Sep) 28361–28371, https://doi.org/10.1007/s11356-019-06006-z.

[37] W. Lu, Y. Shen, A. Xie, W. Zhang, Green synthesis and characterization of superparamagnetic Fe_3O_4 nanoparticles, J. Magn. Magn Mater. 322 (13) (2010) 1828–1833, https://doi.org/10.1016/j.jmmm.2009.12.035.

[38] Ze Lin, Xiulan Weng, Gary Owens, Zuliang Chen, Simultaneous removal of Pb(II) and rifampicin from wastewater by iron nanoparticles synthesized by a tea extract, J. Clean. Prod. 242 (2020), 118476, https://doi.org/10.1016/j.jclepro.2019.118476. ISSN 0959-6526.

[39] Y. Cai, Y. Shen, A. Xie, S. Li, X. Wang, Green synthesis of soya bean sprouts-mediated superparamagnetic Fe_3O_4 nanoparticles, J. Magn. Magn Mater. 322 (19) (2010) 2938–2943, https://doi.org/10.1016/j.jmmm.2010.05.009.

[40] G. Ren, L. Yang, Z. Zhang, B. Zhong, X. Yang, X. Wang, A new green synthesis of porous magnetite nanoparticles from waste ferrous sulfate by solid-phase reduction reaction, J. Alloys Compd. 710 (2017) 875–879, https://doi.org/10.1016/j.jallcom.2017.03.337.

[41] G. Sathishkumar, V. Logeshwaran, S. Sarathbabu, P.K. Jha, M. Jeyaraj, C. Rajkuberan, S. Sivaramakrishnan, Green synthesis of magnetic Fe_3O_4 nanoparticles using Couroupita guianensis Aubl. fruit extract for their antibacterial and cytotoxicity activities, Artif. Cell Nanomed. Biotechnol. 46 (3) (2018) 589–598, https://doi.org/10.1080/21691401.2017.1332635.

[42] A. Kumar, S. Kumari, Parmanand, S.K. Sharma, Constructing the nanomixture of guar gum and Fe_3O_4 for photocatalytic degradation of dyes and heavy metal, J. Mater. Sci. Mater. Electron. (2022) 1–11, https://doi.org/10.1007/s10854-021-07472-3.

[43] P.L. Kiew, N.A. Mohd Fauzi, Shania Aufaa Firdiani, M.K. Lam, L.S. Tan, W.M. Yeoh, Iron oxide nanoparticles derived from Chlorella vulgaris extract: characterization and crystal violet photodegradation studies, Progress in Energy and Environment 24 (2023) 1–10, https://doi.org/10.37934/progee.24.1.110.

[44] M.H. Kahsay, N. Belachew, A. Tadesse, K. Basavaiah, Magnetite nanoparticle decorated reduced graphene oxide for adsorptive removal of crystal violet and antifungal activities, RSC Adv. 10 (57) (2020) 34916–34927, https://doi.org/10.1039/D0RA07061K.

[45] A.V. Samrot, H.H. Ali, J. Selvarani, E. Faradjeva, P. Raji, P. Prakash, Adsorption efficiency of chemically synthesized Superparamagnetic Iron Oxide Nanoparticles (SPIONs) on crystal violet dye, Current Research in Green and Sustainable Chemistry 4 (2021), 100066, https://doi.org/10.1016/j.crgsc.2021.100066.

[46] H. Jiang, Y. Sun, J. Feng, J. Wang, Heterogeneous electro-Fenton oxidation of azo dye methyl orange catalyzed by magnetic Fe_3O_4 nanoparticles, Water Sci. Technol. 74 (5) (2016) 1116–1126, https://doi.org/10.2166/wst.2016.300.

[47] S. Kanagasubbulakshmi, K. Kadirvelu, Green synthesis of iron oxide nanoparticles using Lagenaria siceraria and evaluation of its antimicrobial activity, Def. Life Sci. J. 2 (4) (2017) 422–427, https://doi.org/10.14429/dlsj.2.12277.

[48] V.K. Vg, A.A. Prem, Green synthesis and characterization of iron oxide nanoparticles using Phyllanthus niruri extract, Orient. J. Chem. 34 (5) (2018), https://doi.org/10.13005/ojc/340547.

[49] L. Gabrielyan, H. Badalyan, V. Gevorgyan, A. Trchounian, Comparable antibacterial effects and action mechanisms of silver and iron oxide nanoparticles on Escherichia coli and Salmonella typhimurium, Sci. Rep. 10 (1) (2020), 13145, https://doi.org/10.1038/s41598-020-70211-x.

[50] U.S. Ezealigo, B.N. Ezealigo, S.O. Aisida, F.I. Ezema, Iron oxide nanoparticles in biological systems: antibacterial and toxicology perspective, JCIS Open 4 (2021), 100027, https://doi.org/10.1016/j.jciso.2021.100027.

[51] Z. Vardanyan, V. Gevorkyan, M. Ananyan, H. Vardapetyan, A. Trchounian, Effects of various heavy metal nanoparticles on Enterococcus hirae and Escherichia coli growth and proton-coupled membrane transport, J. Nanobiotechnol. 13 (2015) 1–9, https://doi.org/10.1186/s12951-015-0131-3.

[52] G. Sathishkumar, V. Logeshwaran, S. Sarathbabu, P.K. Jha, M. Jeyaraj, C. Rajkuberan, S. Sivaramakrishnan, Green synthesis of magnetic Fe_3O_4 nanoparticles using Couroupita guianensis Aubl. fruit extract for their antibacterial and cytotoxicity activities, Artif. Cell Nanomed. Biotechnol. 46 (3) (2018) 589–598, https://doi.org/10.1080/21691401.2017.1332635.

Colloid and Polymer Science
https://doi.org/10.1007/s00396-023-05187-x

RESEARCH

A green and sustainable approach to the fabrication of ZnO nanoparticles via *Jatropha podagrica* leaf extract for effective dye degradation and antibacterial applications

Venkatesh Golthi[1,2,3] · Jayarao Kommu[1,3] · A. V. Ramesh[4]

Received: 19 August 2023 / Revised: 13 October 2023 / Accepted: 16 October 2023

Abstract
A robust green synthesis method was employed using *Jatropha podagrica* (Buddha belly plant) leaf extract as a capping agent to prepare ZnO nanoparticles (ZnO NPs). Several analytical techniques such as XRD, SEM, SEM-EDX, HR-TEM, FT-IR, and UV-visible spectroscopy were employed to characterize the green synthesized JP-ZnO NPs. The XRD, SEM, and HR-TEM images proved the presence of spherical nanoparticles having a wurtzite crystalline structure with a size of 12 to 18 nm. The characteristic vibration mode of the Zn-O bond was observed at 430 cm^{-1} in the FT-IR spectrum. The photocatalytic performance of these NPs was evaluated through the degradation of Rhodamine B (RhB), Fluorescein Sodium (FS), and Crystal Violet (CV) dyes in sunlight. Degradation rates of 90–95% were achieved in a time span of 1–2 h. The synthesized ZnO nanoparticles were efficient antimicrobial agents against gram-positive (*Staphylococcus aureus*, *Bacillus coagulans*) and gram-negative (*Klebsiella pneumoniae*, *Escherichia coli*) bacterial strains. Using the well diffusion method, with 150 µL of JP-ZnO nanoparticles, inhibition zones measuring 17, 15, 11, and 10 mm were formed. The current study highlights the efficiency of synthesized JP-ZnO nanoparticles in removing the dyes from aqueous solutions and their efficient antimicrobial properties.

Keywords ZnO nanoparticle · *Jatropha podagrica* plant · Dye degradation · Antioxidant activity

Introduction

In the contemporary world, there has been a continuous increase in industrialization and population growth, leading to the release of various new pollutants into aquatic environments. Specifically, the discharge of noxious dye effluents from industries like textile, paper, leather, and printing poses grave ecological and health hazards [1, 2]. Dyes such as Rhodamine B (RhB), Fluorescein Sodium (FS), and Crystal Violet (CV) pose ingestion risks to humans and animals and induce skin, ocular, and respiratory irritation [3]. In a different context, the recurrence of contagious illnesses and the ongoing evolution of antibiotic resistance in numerous disease-causing bacteria present a significant global public health concern. *Enterococcus*, *Staphylococcus*, and *Streptococcus*, which are closely related species, are harmful microorganisms that are attributed to a diverse range of infections and diseases [4].

In the realm of recent advancements in nanotechnology, nanomaterials play a crucial role due to their significant surface area and volume ratio [5]. This characteristic makes them valuable for applications such as water purification and the creation of novel biocidal substances. Among various types of nanoparticles, zinc oxide nanoparticles (ZnO NPs) possess exceptional optical and electrical characteristics, making them an outstanding choice for *n*-type semiconductor materials [6]. These NPs demonstrate remarkable efficacy in dye degradation [6, 7] and also exhibit antibacterial properties [8, 9], further highlighting their distinctiveness.

✉ Venkatesh Golthi
venkatesh@gdcc.ac.in

1 Andhra University Trans-Disciplinary Research Hub (A.U. TDR-HUB), Visakhapatnam 530003, AP, India

2 Department of Chemistry, Government Degree College, Chodavaram 531036, AP, India

3 Department of Chemistry, Wellfare Institute of Science, Technology and Management, Pinagadi, Pendurthi 531173, AP, India

4 Department of Chemistry, Dr. V.S. Krishna Govt. Degree College, Visakhapatnam 530003, AP, India

Numerous techniques have been documented for the production of ZnO NPs, including hydrothermal [10], precipitation [11], microwave [12], microemulsion [13], solvothermal [14], supercritical water [15], and sol-gel methods [16]. Recent progress in nanotechnology has spurred the rise of sustainable synthesis approaches for generating ZnO NPs [17, 18]. These environmentally synthesized ZnO NPs have garnered substantial interest for their prospective utilization across diverse domains, encompassing dye degradation and antibacterial functionalities. The utilization of these NPs offers a promising solution for addressing environmental challenges associated with dye pollution and combating the spread of drug-resistant bacteria. By harnessing the unique properties of green-synthesized ZnO NPs, researchers aim to explore their efficacy in degrading dyes and inhibiting the growth of pathogenic bacteria, presenting a sustainable and effective approach for environmental and healthcare applications [17–19]. This article delves into the dye degradation and antibacterial activity of ZnO NPs synthesized through green methods, shedding light on their potential as eco-friendly alternatives in addressing pressing global concerns [20–23].

Jatropha podagrica (JP), a traditional medicinal plant, has a history of being utilized for treating various ailments like fever, scabies, ulcers, and wounds. Additionally, it exhibits several beneficial properties including antitumorigenic, antioxidant, and antibacterial activities [24]. The leaves of *Jatropha podagrica* have been analyzed and found to contain specific phytochemicals, namely, flavonoids (such as apigenin, acacetin, and luteolin), phenolic acids (including vanillic, syringic, P-hydroxybenzoic acid, melilotic, cis-trans ferulic, P-coumaric, and phloretic acids), tannins, proanthocyanidins, and glycol flavones [25, 26]. ZnO NPs were successfully produced using leaf extract from the *Jatropha podagrica* plant for the first time. The phytochemicals found within the extract played a crucial and multifaceted role in the *Jatropha podagrica*-capped ZnO nanoparticle (JP-ZnO NP) synthesis, serving both as capping agents and enhancing stability, surpassing that achieved through conventional chemical synthesis methods [25]. Moreover, the presence of diverse phenolic acids within these phytochemicals contributes to achieving well-defined sizes and shapes of ZnO NPs, outperforming analogous green-synthesized counterparts (as depicted in Table 1). To unlock the full potential of unexplored plant species, the selection of new and unique plants for nanoparticle synthesis is imperative. This approach allows researchers to diversify the spectrum of nanoparticles that can be effectively stabilized, achieved through the discovery of novel proteins and phytochemicals derived from previously uninvestigated plant sources. Additionally, these novel plant species may offer additional advantages such as heightened productivity, reduced costs, or specialized attributes suitable for specific applications. In the present research, JP-ZnO nanoparticles displayed a surface with a negative charge, providing them with outstanding adsorption properties for efficiently eliminating Rhodamine B (RhB), Fluorescein Sodium (FS), and Crystal Violet (CV) dyes. Additionally, the antibacterial effectiveness of these manufactured JP-ZnO NPs was evaluated against both Gram-positive bacteria (*Staphylococcus aureus*, *Bacillus coagulans*) and Gram-negative bacteria (*Klebsiella pneumoniae*, *Escherichia coli*).

Table 1 Comparison of the average size and morphology of ZnO nanoparticles in the present work with previous publications

Plant materials	Precursor name	Average size and morphology	Applications	Reference
Jatropha podagrica leaf extract	$Zn(OOCCH_3)_2.2H2O$	12–18 nm and spherical shape	Dye degradation and antibacterial applications	Present work
Calotropis procera extract	$Zn(NO_3)_2.6H2O$	24 nm and spherical shape	Photodegradation of methyl orange	[17]
Solanum torvum L. leaf extract	$Zn(NO_3)_2.6H2O$	28.24 and spherical shape	Toxicological studies	[27]
Simarouba glauca leaf extract	$Zn(NO_3)_2.6H2O$	17–37 nm and hexagonal shape	Antioxidant and antimitotic properties	[28]
Aegle marmelos fruit juice	$Zn(NO_3)_2.6H2O$	17 nm and hexagonal shape	Photodegradation, antibacterial and antioxidant	[29]
Punica granatum leaf extract	$Zn(NO_3)_2.6H2O$	20 nm and spherical shape	Photocatalytic degradation	[30]
Pelargonium zonale leaf extract	$Zn(NO_3)_2.6H2O$	50–60 nm and spherical in shape	Antibacterial activities	[31]
Azadirachta indica leaf extract	$Zn(NO_3)_2.6H2O$	100–200 nm and triangular shape	Antimicrobial activity	[32]
Tetraselmis indica extract	$Zn(OOCCH_3)_2.2H2O$	20–40 nm and spherical shape	Antibacterial, antioxidant, and hemolytic activity	[33]
Aesculus hippocastanum extract	$Zn(OOCCH_3)_2.2H2O$	40 nm and hexagonal shape	Antibacterial activities	[34]
Sechium edule leaf extract	$Zn(OOCCH_3)_2.2H2O$	36.2 nm and spherical shape	Antibacterial and anticancer studies	[35]

Materials and methods

Materials

Fresh *Jatropha podagrica* leaves were picked from the garden of the Government Degree College in Chodavaram, Andhra Pradesh, India. The initial source, zinc acetate dihydrate $Zn(OOCCH_3)_2.2H_2O$ (98% purity), sodium hydroxide (NaOH), Rhodamine B (RhB), Fluorescein Sodium (FS), and Crystal Violet (CV) were acquired from Merck in India and utilized without purification. Milli-Q water was utilized in all of the experiments.

Jatropha podagrica leaf extract preparation

Fresh JP plant leaves were collected and meticulously cleansed using warm water, followed by thorough rinsing with Milli-Q water. These leaves were then dried under shaded conditions for a duration of 25 days until completely dry. Once dry, the leaves were ground into a fine powder using a grinder. Subsequently, 1 g of the powdered sample was placed in a 250-mL glass beaker, and 100 mL of Milli-Q water was added. The blend was subsequently warmed using a heating mantle at 80 °C for 30 min, yielding a brilliant golden-yellow solution. The solution was meticulously sieved using Whatman grade 1 filter paper to eliminate any particulate matter and subsequently subjected to centrifugation at 8000 rpm for 5–10 min to attain a pristine extract solution. The resultant extract was then carefully stored in a refrigerator at 4 °C for subsequent processing [36].

Synthesis of *Jatropha podagrica*-capped ZnO nanoparticles

In a standard eco-friendly synthesis procedure, 10 mL of the aqueous extract derived from JP leaves was blended with 100 mL of a 2 mM aqueous solution containing zinc acetate dihydrate. The amalgamation was subjected to stirring at 80 °C for 30 min, leading to the creation of a vivid yellow solution. Following this, a 1 M solution of sodium hydroxide was meticulously introduced dropwise into the mixture, with uninterrupted agitation at ambient temperature. As a result, the yellow color of the mixture gradually transformed into a yellowish-white suspension, reaching a pH of 12. To purify the suspended particles, they were dispersed in Milli-Q water and then centrifuged at a speed of 8000 rpm. The resultant white particles underwent repeated washing with Milli-Q water to purge impurities and yield the ultimate product. The white solid was then subjected to vacuum drying at 60 °C for 6 h in an oven. Lastly, the material was finely pulverized using a mortar and pestle, rendering it ready for subsequent characterization [36, 37].

Photocatalytic potential of JP-ZnO NPs for the degradation of RhB, FS, and CV dyes

The photocatalytic effectiveness of JP-ZnO NPs against RhB, FS, and CV dyes was assessed using a readily available source of UV radiation — sunlight. In separate containers, 0.01 g of JP-ZnO NPs was blended with 100 mL of 1 ppm solutions of RhB, FS, and CV dyes. To ensure the stability of the solutions against adsorption–desorption phenomena, the reaction mixtures were gently stirred in the absence of light for a duration of 1 h. After stabilization, the solutions were maintained in the sunshine with constant stirring using magnetic stirrers at pH 10. At regular intervals, constant samples were taken from each dye solution and the NPs were separated in a centrifuge at 8000 rpm. A UV spectrometer was used to measure the color intensities at 555 nm, 495 nm, and 590 nm for the RhB, FS, and CV dyes, respectively. The proportion of photocatalytic degradation and rate constants were calculated using the equation below:

$$\text{Degradation rate } (\%) = \left(\left(A_0 - A\right)/A_0\right) \times 100$$

$$\ln A_0/A = kt$$

In the equation, "A_0" symbolizes the initial concentration, while "A" denotes the concentration at the culmination of the degradation process. The degradation constant is denoted by k, and t indicates the duration of sunlight irradiation [38].

Characterization of JP-ZnO NPs

To ascertain the crystalline arrangement of the JP-ZnO NPs, a variety of analytical methodologies were applied. X-ray diffraction (XRD) measurements were carried out across a 2θ range of 0 to 90° using a Bruker Kappa Apex II instrument. The instrument was operated with CuKα radiation ($\lambda = 1.54060$ Å) at settings of 40 kV, 35 mA, and a scanning rate of 0.2 s. Fourier transform infrared spectra (FT-IR) of the samples were captured utilizing a Thermo Nicolet iS50 spectrometer. Spectra were acquired within the frequency span of 4000–400 cm^{-1}, using high-quality KBr pellets in transmission mode. For an in-depth investigation of the optical attributes, UV-Vis diffuse reflectance/absorbance spectroscopy was conducted on the synthesized samples. A Shimadzu (2450 – SHIMADZU) spectrophotometer, equipped with a diffuse reflectance accessory, was deployed under room temperature conditions. $BaSO_4$ was utilized as a reference material, and measurements were executed over the wavelength range of 200–800 nm. The surface topography and elemental composition of the JP-ZnO NPs were

scrutinized through scanning electron microscopy (SEM). The specific apparatus employed was the JEOL 6390LA/OXFORD XMX N, which featured energy-dispersive X-ray (EDX) spectroscopy. SEM images were recorded with an acceleration voltage of 20 kV. For a more comprehensive exploration of the microstructure and particle dimensions, high-resolution transmission electron microscopy (HRTEM) was engaged. The JEOL/JEM 2100 instrument was utilized at an operational voltage of 200 kV. Carbon-copper grids were used for sample preparation, enabling the acquisition of micrographs that facilitated particle size determination. Furthermore, selected area electron diffraction (SAED) images were captured utilizing the HRTEM instrument.

Results and discussions

UV-Vis spectroscopy studies

Figure 1 illustrates the UV-Vis absorption spectra of both JP leaf extract and JP-ZnO NPs. The leaf extract comprises a diverse array of phytochemicals, encompassing alkaloids, phenolic acids, flavonoids, tannins, proanthocyanidins, and glycol flavones. These compounds contribute to pronounced absorption bands at 280 and 351 nm [24]. Additionally, a well-defined absorption peak at 372 nm in the spectra signifies the presence of JP-ZnO NPs, predominantly arising from their capacity to absorb and scatter light [39]. Notably, the absence of absorption peaks at 280 and 351 nm in the JP-ZnO NPs spectra, which were originally observed in the JP leaf extract, implies that these phytochemicals play a pivotal role in the reduction and encapsulation of JP-ZnO NPs during the synthesis process [40].

FTIR analysis of the synthesized JP-ZnO NPs

FTIR spectroscopy was employed to discern the specific functional groups existing within the synthesized NPs and to ascertain their molecular composition. To examine the data concerning functional groups found in the plant (as depicted in Fig. 2), it is evident that a wide peak detected at approximately 3500 cm^{-1} signifies the presence of a phenolic group. Additionally, the identification of aromatic compounds is supported by the absorption of a broad peak around 1639 cm^{-1}. Furthermore, the peaks observed at 1178.39 cm^{-1} and 1042.36 cm^{-1} indicate the existence of amide functional groups and carbonated functional group vibrations within the plant. JP-ZnO NPs were analyzed (as shown in Fig. 2), and their absorption peaks were found to be in the range of 400–4000 cm^{-1}. The peak at 429.08 cm^{-1} indicates the stretching frequency of Zn-O bonding [41]. Peaks observed at 917.20, 901.10, and 795 cm^{-1} can be assigned to carbonate moieties. The occurrence of the symmetric stretching of carboxyl side groups within the amino acid residues of protein molecules is potentially ascribed to

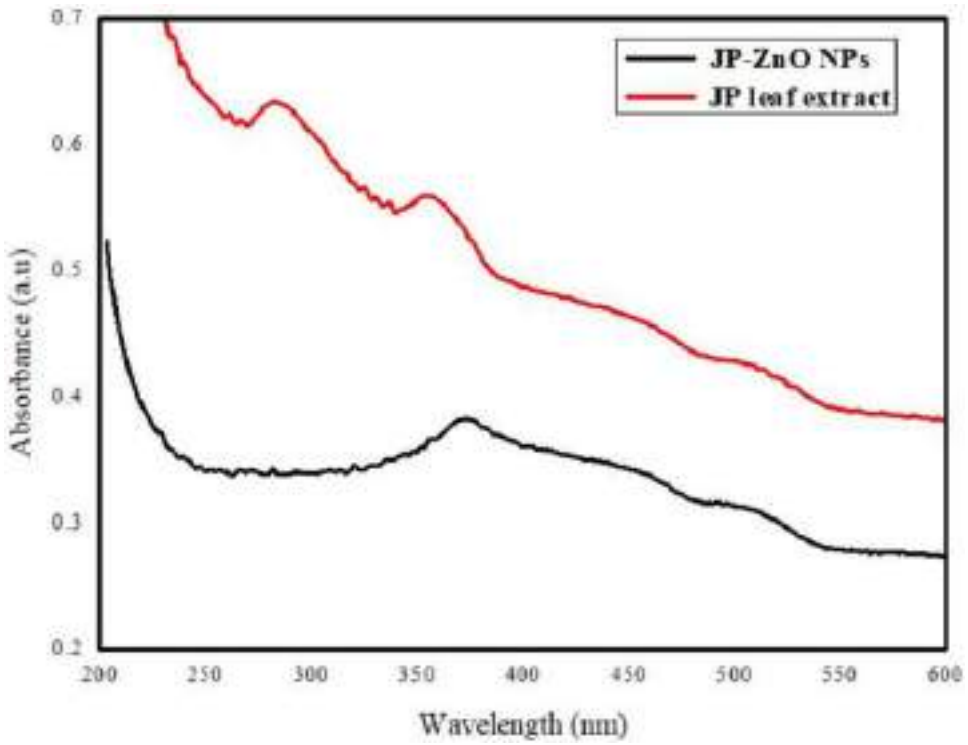

Fig. 1 UV-Vis spectra of *Jatropha podagrica* (JP) leaf extract and *Jatropha podagrica* leaf extract-capped ZnO NPs

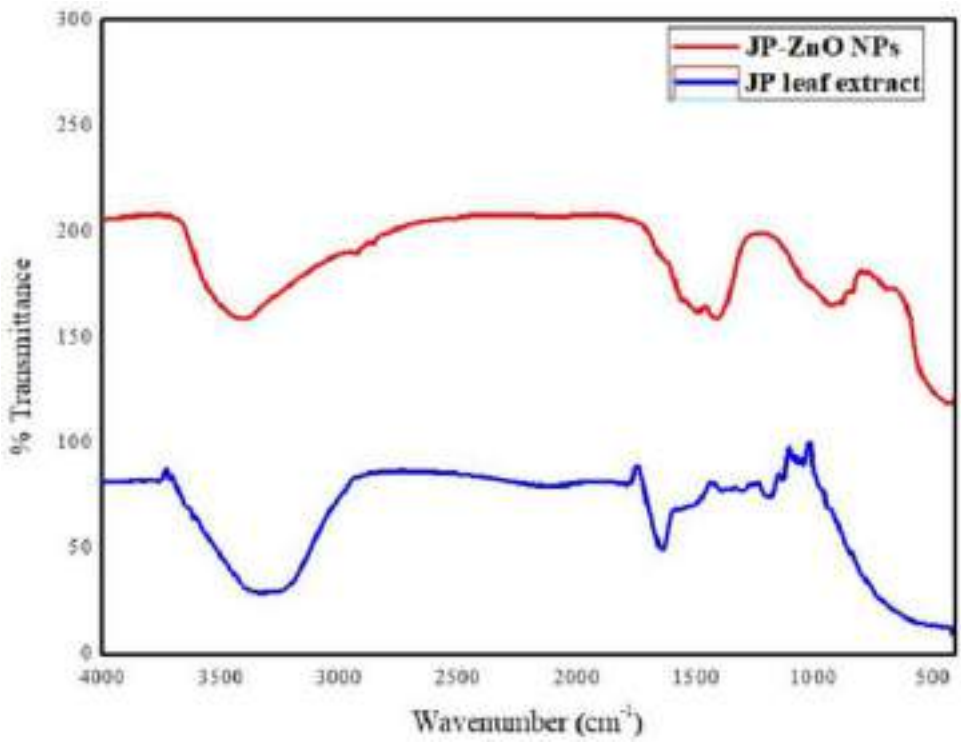

Fig. 2 FTIR spectra of *Jatropha podagrica* leaf extract and *Jatropha podagrica* leaf extract-capped ZnO NPs

the peak at 1410.06 cm^{-1} [42]. The presence of a peak within the 1550- to 1450-cm^{-1} range is likely linked to the C=C stretching of aromatic compounds [43]. Evident and robust absorption bands at 3397.10 and 2923.56 cm^{-1} were identified, signifying the −OH stretching vibration intrinsic to phenolic groups and the −CH stretching vibration characteristic of aldehyde groups [44, 45]. These distinctive peaks within the IR spectrum serve as indicators of the purity and compositional makeup of the biofabricated JP-ZnO NPs.

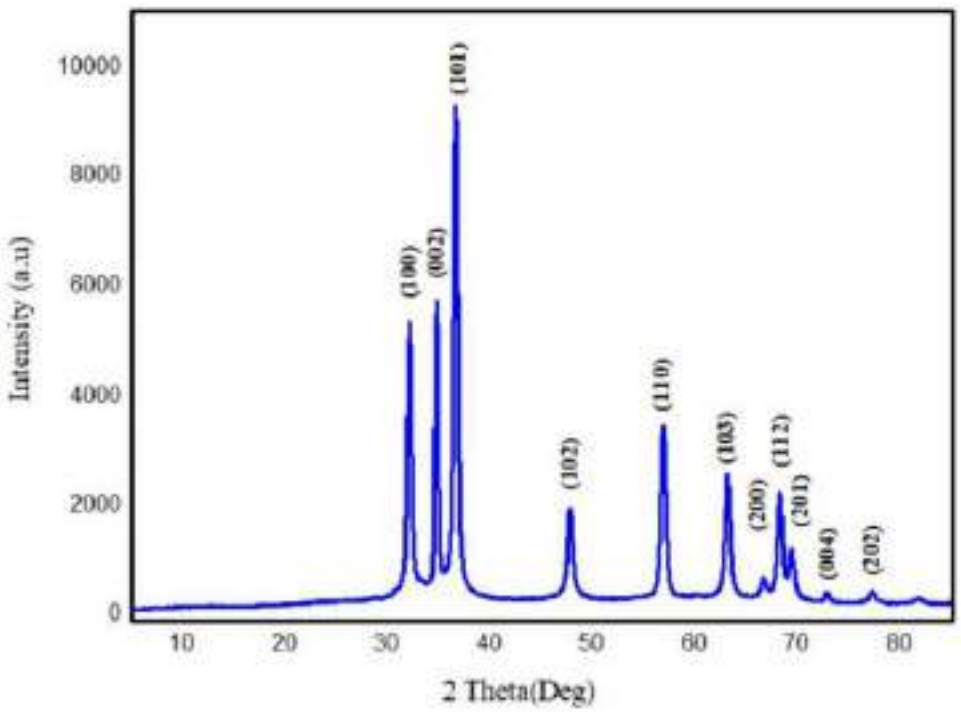

Fig. 3 XRD patterns of ZnO NPs using an aqueous leaf extract of *Jatropha podagrica*

Table 2 The structure and geometric parameters of JP-ZnO NPs

Planes	2θ	β	cosθ	Size (nm)
100	31.98	0.53635	0.96131	14.23869
002	34.63	0.41516	0.954683	18.26832
101	36.47	0.52835	0.949781	14.28094
102	47.75	0.71887	0.914431	10.10545
110	56.82	0.59138	0.879566	11.81562
103	63.07	0.67663	0.852321	10.00707
200	66.68	1.30914	0.835424	5.069625
112	68.17	0.6336	0.828207	10.38434
201	69.28	0.74629	0.82274	8.7581
004	72.76	0.37226	0.805101	17.18142
202	77.18	0.40693	0.781629	15.25936
Average size				**12.30627**

XRD analysis of the synthesized JP-ZnO NPs

The X-ray diffraction analysis, as shown in Fig. 3, revealed distinctive peak characteristic of JP-ZnO at various angles: 31.98°, 34.63°, 36.47°, 47.75°, 56.82°, 63.07°, 66.68°, 68.17°, 69.28°, 72.76°, and 77.18°. These peaks corresponded to different crystal lattice planes, including (100), (002), (101), (102), (110), (103), (200), (112), (201), (004), and (202), respectively. The congruence of these peaks with the established JCPDS Card No. 89–0510 indicated the presence of ZnO NPs in the wurtzite crystalline structure. The well-defined and narrow diffraction peaks attested to a robust crystalline structure, while the absence of other signals verified the purity of the synthesized JP-ZnO NPs. Notably, the intensity of the (002) peak indicated the

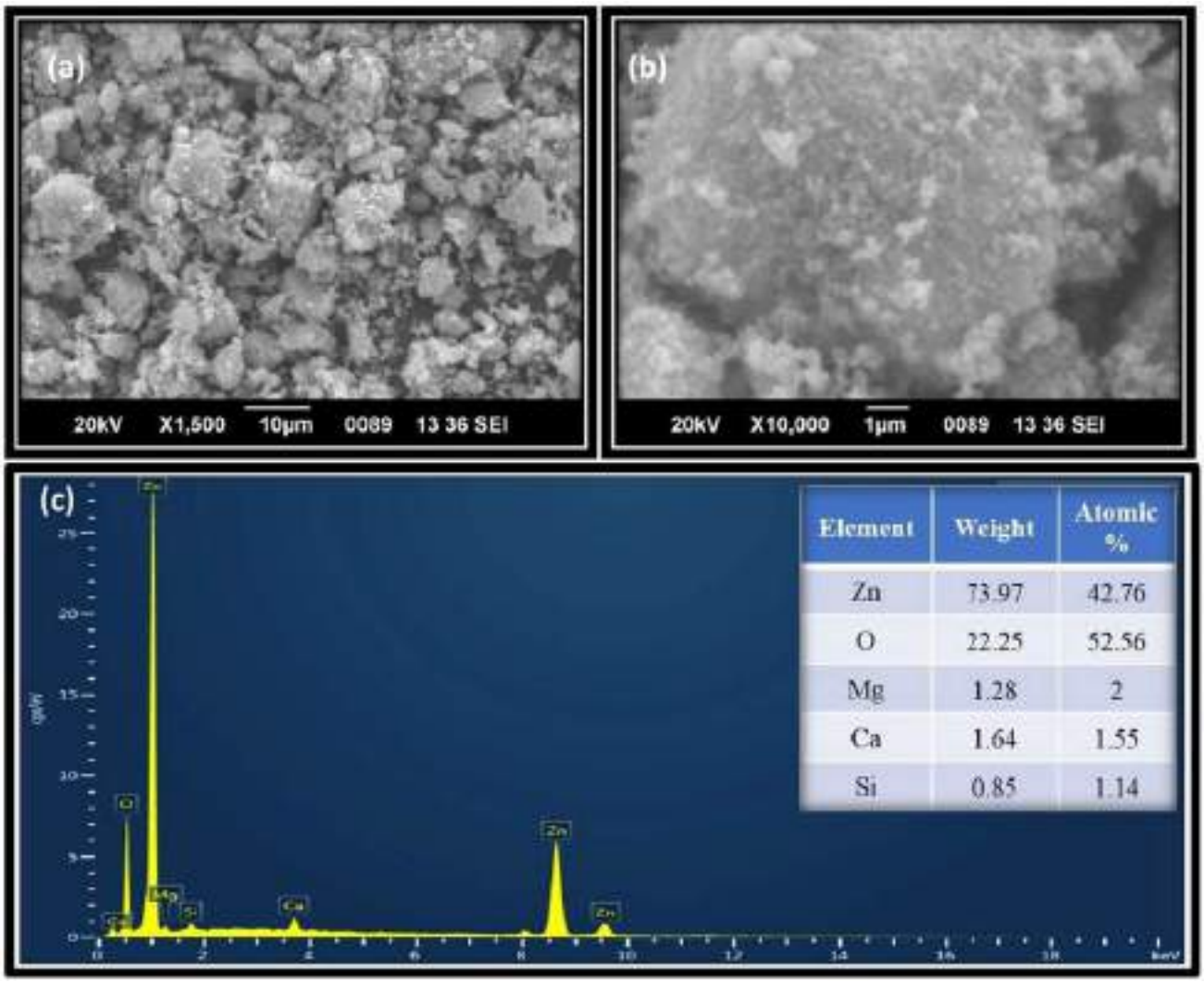

Fig. 4 **a** and **b** SEM images ZnO NPs capped with *Jatropha podagrica* leaf extract different magnifications and **c** EDX spectrum of ZnO NPs

spherical morphology of the particles [46]. To calculate the average grain size of the samples, the Debye-Scherer equation was employed: $D = k\lambda/\beta\cos\theta$. Here, D represents the crystal size, λ stands for the wavelength of X-ray radiation ($\lambda = 0.15406$ nm) for Cu Kα, k is the shape factor (typically taken as 0.9), β denotes the full width at half maximum (FWHM), and θ represents the diffraction angle.

Table 2 represents the structure and geometric parameters of JP-ZnO NPs.

Employing the Debye-Scherer equation, the average size of the crystallites within the JP-ZnO NPs was computed to be 12.30627 nm (Table 2), confirming their nanoscale dimensions.

SEM-EDX analysis of synthesized JP-ZnO NPs

The surface characteristics of the produced JP-ZnO NPs were examined using a scanning electron microscope (SEM). As depicted in Fig. 4(a), (b), the particles exhibited predominantly wurtzite crystalline structure and a spherical shape [47]. Some clustering of particles was observed, likely attributed to the presence of phenolic

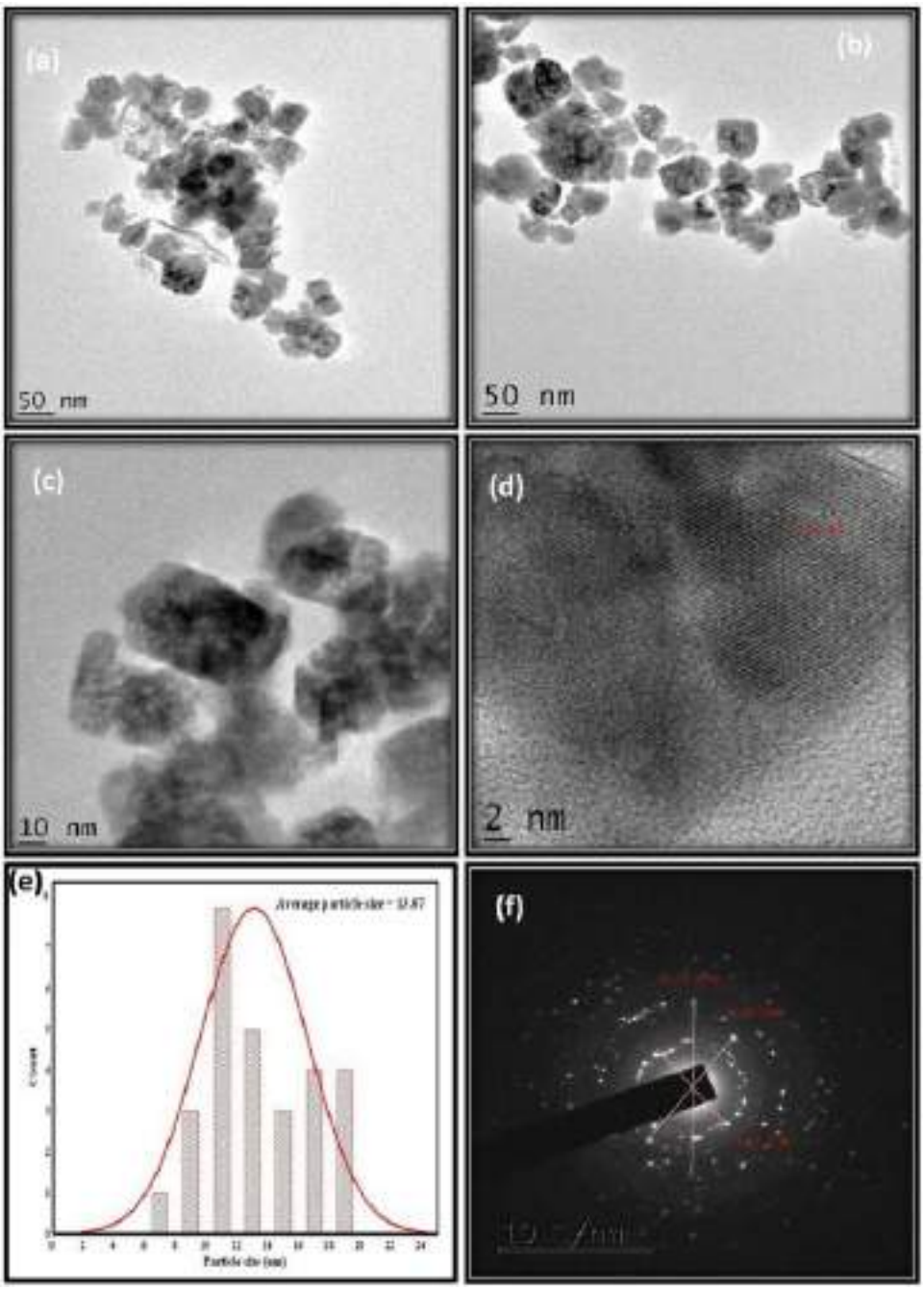

Fig. 5 **a**–**d** HR-TEM images, **e** size distribution histogram of using aqueous *Jatropha podagrica* leaf extract of ZnO NPs, and **f** SAED patterns

compounds from the JP plant, which acted as a capping agent. To determine the chemical constitution of the ZnO NPs, an energy-dispersive X-ray spectrum (EDX) was obtained from a densely populated region (Fig. 4(c)). The EDX spectrum revealed significant signals from zinc atoms at 1 keV, 8.7 keV, and 9.6 keV, respectively, along with a single peak corresponding to oxygen atoms at 0.5 keV. The presence of a negligible amount of carbon atoms confirmed the high purity of the NPs. Additionally, minor peaks representing calcium (Ca), magnesium (Mg), and silicon (Si) atoms were detected, indicating the contribution of these elements from the biological components.

TEM analysis of synthesized JP-ZnO NPs

The dimensions, arrangement, and architecture of the synthesized JP-ZnO NPs underwent meticulous scrutiny through high-resolution transmission electron microscopy (HR-TEM). HR-TEM images at varying magnifications are showcased in Fig. 5(a–c). Scrutinizing these images unveiled that the average size of the JP-ZnO NPs resides within the range of 12–18 nm. Impressively, a measured "*d*" spacing of 0.22 nm harmonized with the *d* values derived from X-ray diffraction (XRD), thereby affirming the ZnO NPs' wurtzite crystalline structure and spherical morphology [48], as visualized in Fig. 5(d). Significantly, Fig. 5(e) underscores that the particle size deduced from the HR-TEM analysis exhibited commendable concurrence with outcomes from the XRD analysis. The selected area electron diffraction pattern (SAED) of the JP-ZnO NPs is portrayed in Fig. 5(f). The SAED pattern indicated the presence of polycrystalline NPs in the JP-ZnO sample.

Plausible mechanism for fabrication of JP-ZnO NPs

Figure 6 provides an illustrative representation of a potential procedure aimed at producing ZnO NPs utilizing a water-based solution derived from the leaves of

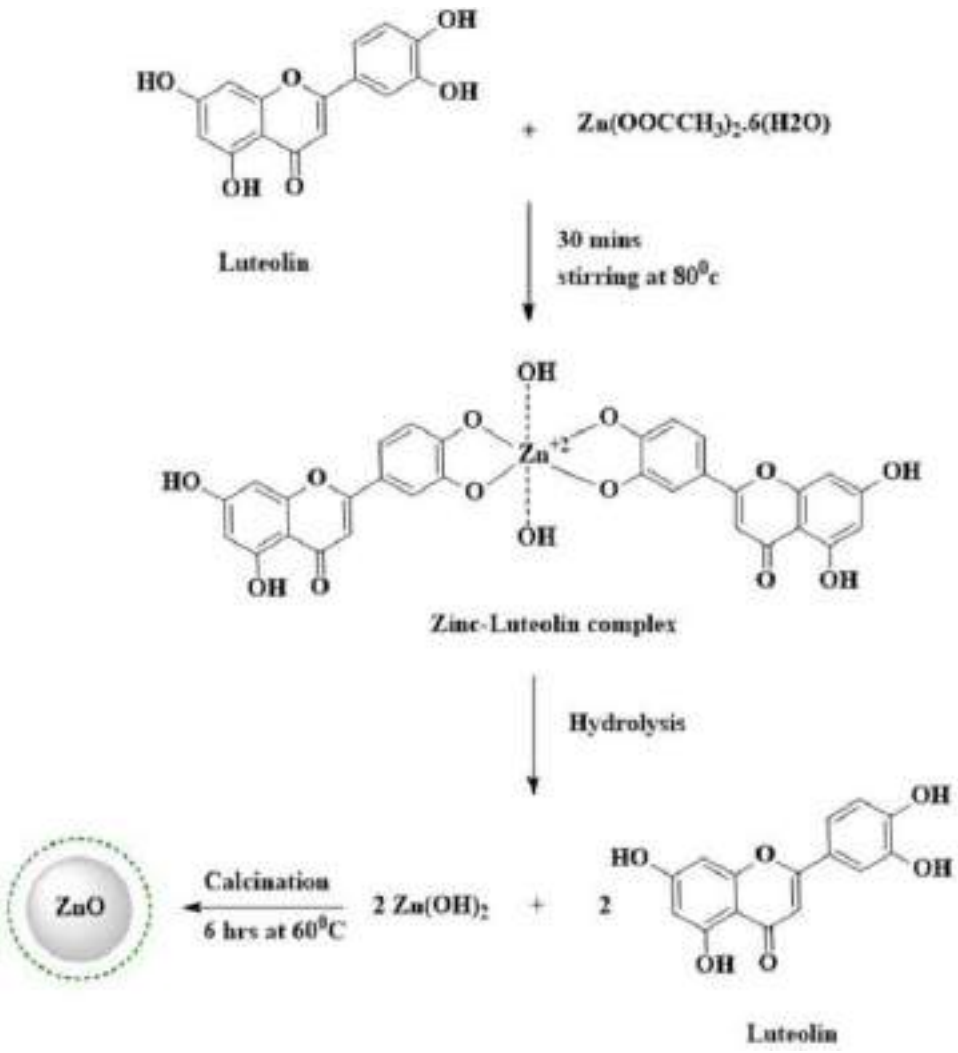

Fig. 6 A proposed mechanism of synthesized ZnO NPs using a *Jatropha podagrica* leaf extract

JP. The procedure involves combining an aqueous leaf extract obtained from JP with zinc acetate hexahydrate ($Zn(OOCCH_3)_2.6H_2O$) within a single aqueous phase. The leaf extract from JP contains a range of constituents, including phenolic acids, flavonoids, tannins, terpenoids, and carbohydrates. These components serve a dual purpose as both reducing and capping agents in the reaction. Notably, a remarkable chemical within the leaf extract is luteolin, which complexes with zinc in the form of Zn^{+2} ions.

This initial complexation is followed by the sequential progression of events. First, there is the conception of zinc hydroxide ($Zn(OH)_2$) via hydrolysis. Subsequently, through a process of calcination, the complex undergoes decomposition [49]. This decomposition process strongly favors the generation of JP-ZnO NPs.

A photocatalytic degradation of RhB, FS, and CV dyes by the fabricated JP-ZnO NPs

To evaluate the photocatalytic activity of prepared JP-ZnO NPs, they were employed as catalysts in the photodegradation of RhB, CV, and FS dyes in sunlight. Figures 7, 8, and 9 demonstrate the degradation of the dyes RhB, FS, and CV under sunlight, occurring at time intervals of 180 min, 90 min, and 60 min, respectively. The UV-visible spectrometer was used to measure the RhB, FS, and CV dye degradation at regular intervals of 30 min, 20 min, and 15 min, respectively. Degradation efficiencies of 95%, 94%, and 90% were achieved for RhB, FS, and CV dyes, respectively. The degradation efficiency of the as-prepared JP-ZnO NPs was compared with that of recently reported ZnO NPs in Table 3.

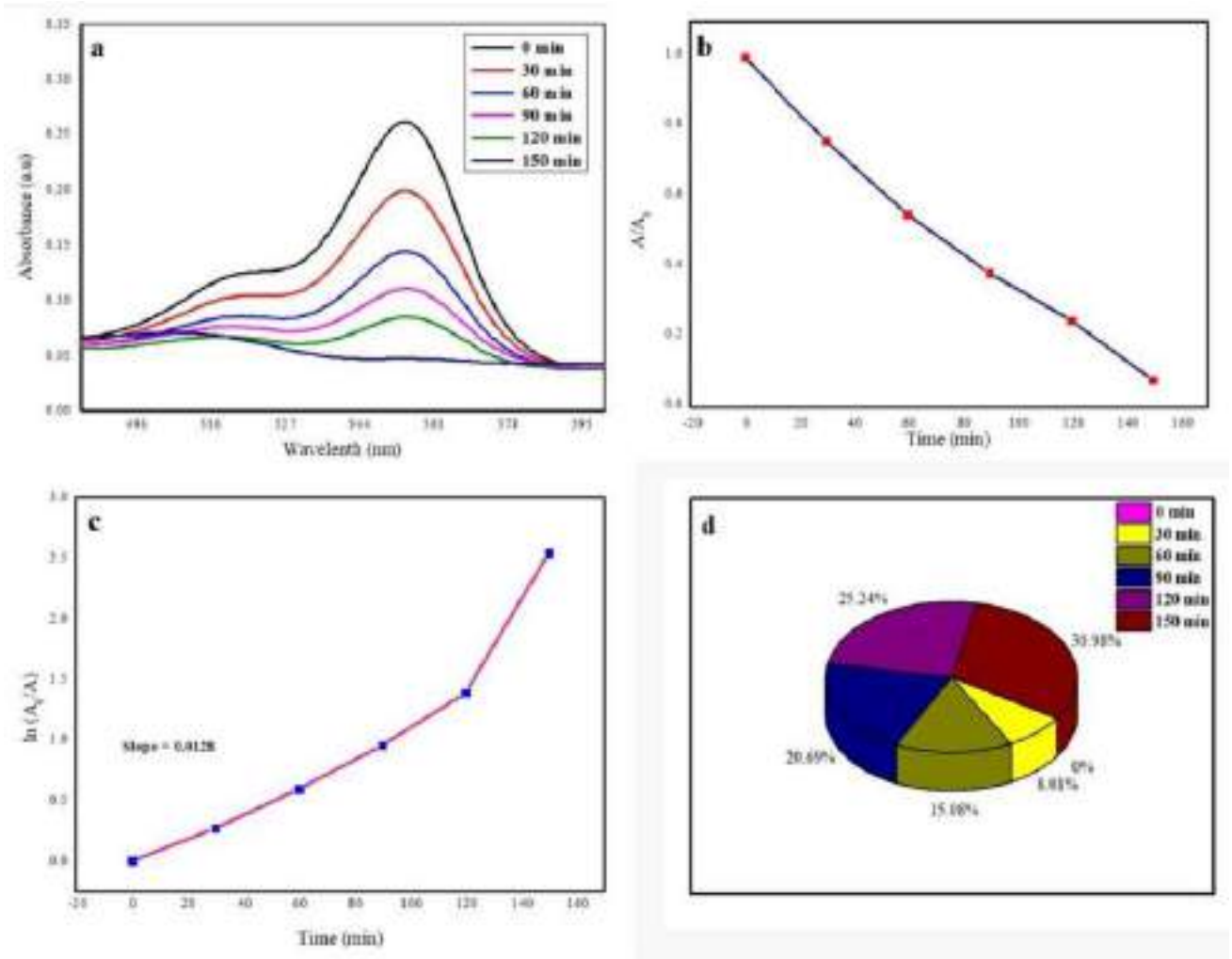

Fig. 7 **a** UV-Vis absorbance spectra of RhB dye under UV (sunlight) illumination over JP-ZnO NPs as a function of time, **b** the progression of RhB dye degradation during consecutive time intervals, **c** the kinetics of RhB dye degradation presented as a first-order linear plot with ln A_0/A as a function of time, and **d** a pie chart representing the distribution of RhB dye degradation across different time intervals

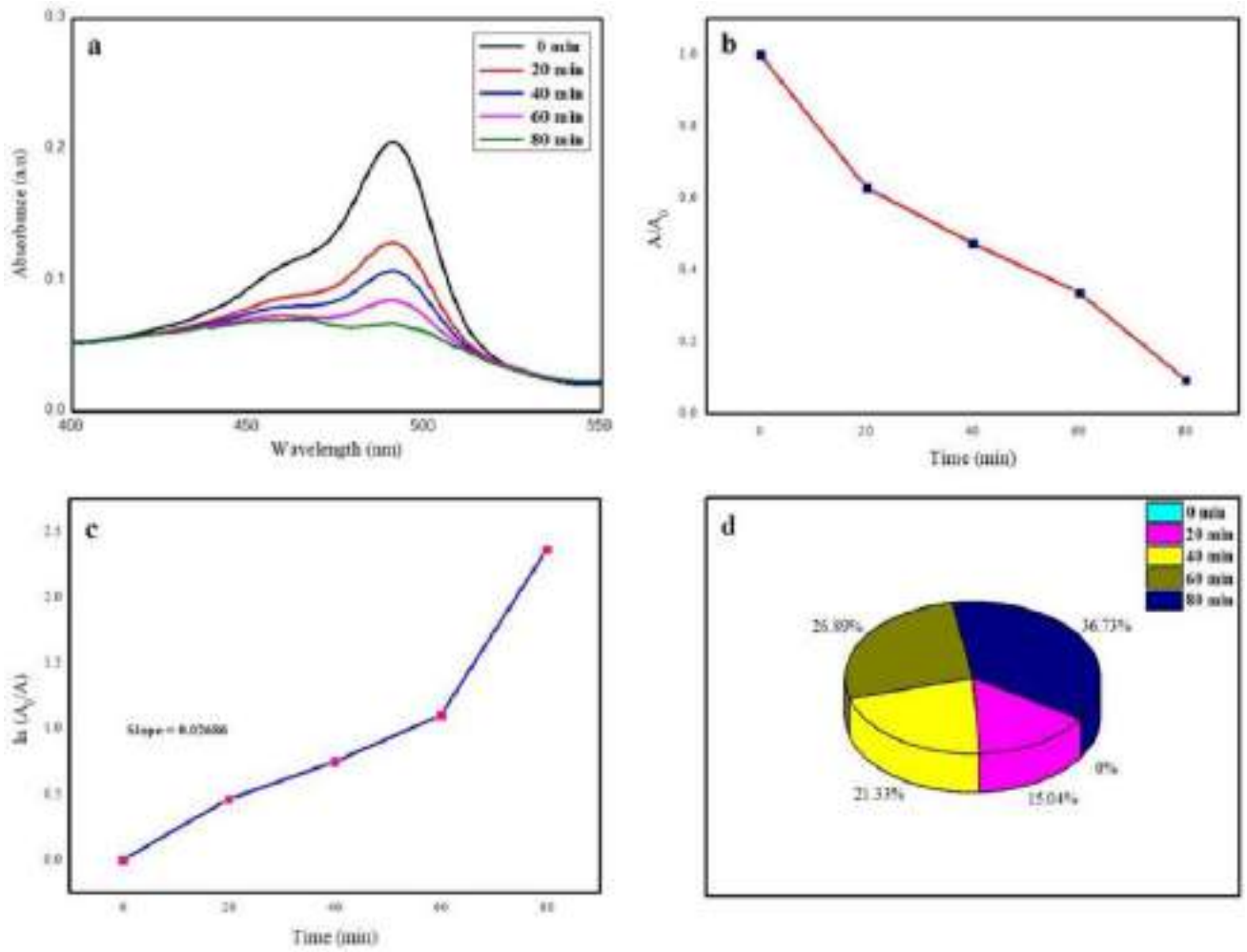

Fig. 8 **a** UV-Vis absorbance spectra of FS dye under UV (sunlight) illumination over JP-ZnO NPs as a function of time, **b** the progression of FS dye degradation during consecutive time intervals, **c** the kinetics of FS dye degradation presented as a first-order linear plot with ln A_0/A as a function of time, and **d** a pie chart representing the distribution of FS dye degradation across different time intervals

The results of this study strongly suggest that JP-ZnO NPs possess significant promise as a material for effectively catalyzing the degradation of organic pollutants through photocatalysis. The remarkable rates of degradation observed, coupled with the observable impact of varying pH conditions on the degradation process, highlight the potential application of JP-ZnO NPs in addressing a wide spectrum of water and wastewater pollution challenges stemming from organic contaminants. These results suggest that JP-ZnO NPs offer promising prospects for addressing environmental pollution challenges.

The following mechanism illustrates how electrons and holes contribute to dye degradation [56]:

$$ZnO + h\nu \rightarrow e^- + h^+$$

O_2 absorption: $O_2 + e^- \rightarrow O_2^-$

Ionization of water: $H_2O \rightarrow OH^- + H^+$

Protonation of superoxide: $O_2^- + H^+ \rightarrow HOO$

$$HOO + e^- \rightarrow HO_2^-$$

$$HOO^- + H^+ \rightarrow H_2O_2$$

$$H_2O_2 + e^- \rightarrow OH^- + OH$$

$$H_2O + h^+ \rightarrow H^+ + OH$$

Dyes + OH. → Degradant product

The aforementioned OH radical is an extremely potent oxidant, highly effective in the degradation of numerous dyes such as RhB, FS, and CV.

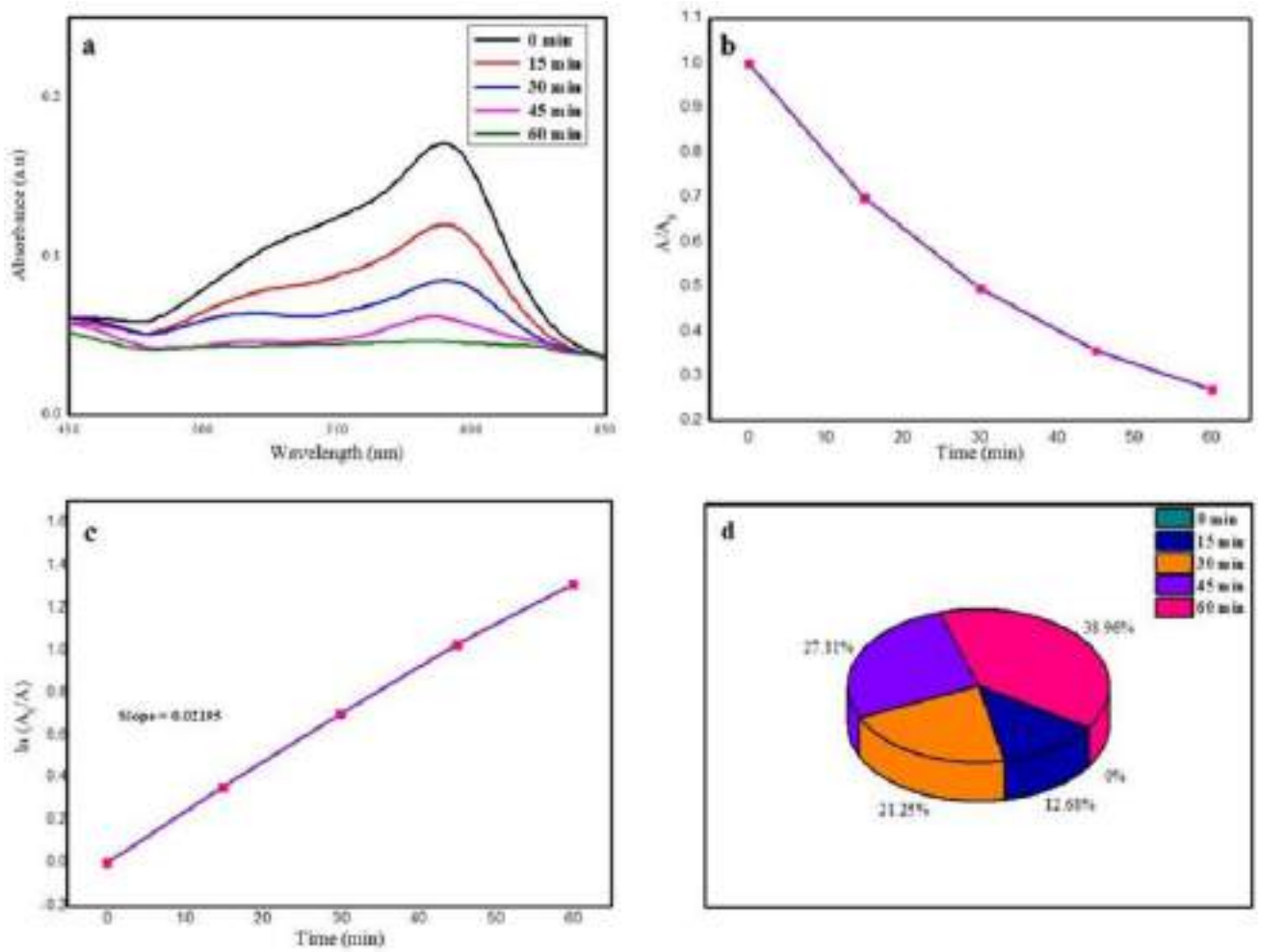

Fig. 9 **a** UV-Vis absorbance spectra of CV dye under UV (sunlight) illumination over JP-ZnO NPs as a function of time, **b** the progression of CV dye degradation during consecutive time intervals, **c** the kinetics of CV dye degradation presented as a first-order linear plot with ln A_0/A as a function of time, and **d** a pie chart representing the distribution of CV dye degradation across different time intervals

Antibacterial activities of synthesized JP-ZnO NPs

The antibacterial effectiveness of JP-ZnO NPs was assessed against both Gram-positive bacteria (*S. aureus*, *B. coagulans*) and Gram-negative bacteria (*K. pneumoniae*, *E. coli*) through the utilization of the well diffusion method. The outcomes of the zone inhibition technique are depicted in Fig. 10, illustrating the diameters of inhibition zones (measured in millimeters) encompassing each well containing the JP-ZnO NP solution. The JP-ZnO NPs prepared for this

Table 3 Comparison of the photocatalytic degradation of ZnO nanoparticles in the present work with previous works

Green materials	Dye	Light source	Irradiation time (min)	Degradation efficiency (%)	Reference
Jatropha podagrica leaf extract	Rhodamine B	Sunlight	150	95	Present work
	Crystal Violet	Sunlight	60	94	
	Fluorescein Sodium	Sunlight	90	90	
Alchemilla vulgaris leaf extract	Rhodamine B	Sunlight	120	75	[50]
Hibiscus sabdariffa L. petal extract	Rhodamine B	Sunlight	300	80.13	[51]
Paraserianthes lophantha leaf extract	Rhodamine B	UV light	180	83	[52]
Moringa oleifera peel extract	Crystal Violet	UV light	70	94	[53]
Delonix elata leaf extract	Crystal Violet	UV light	90	86	[54]
Sageretia thea aqueous extract	Crystal Violet	UV light	8 h	40.65	[55]

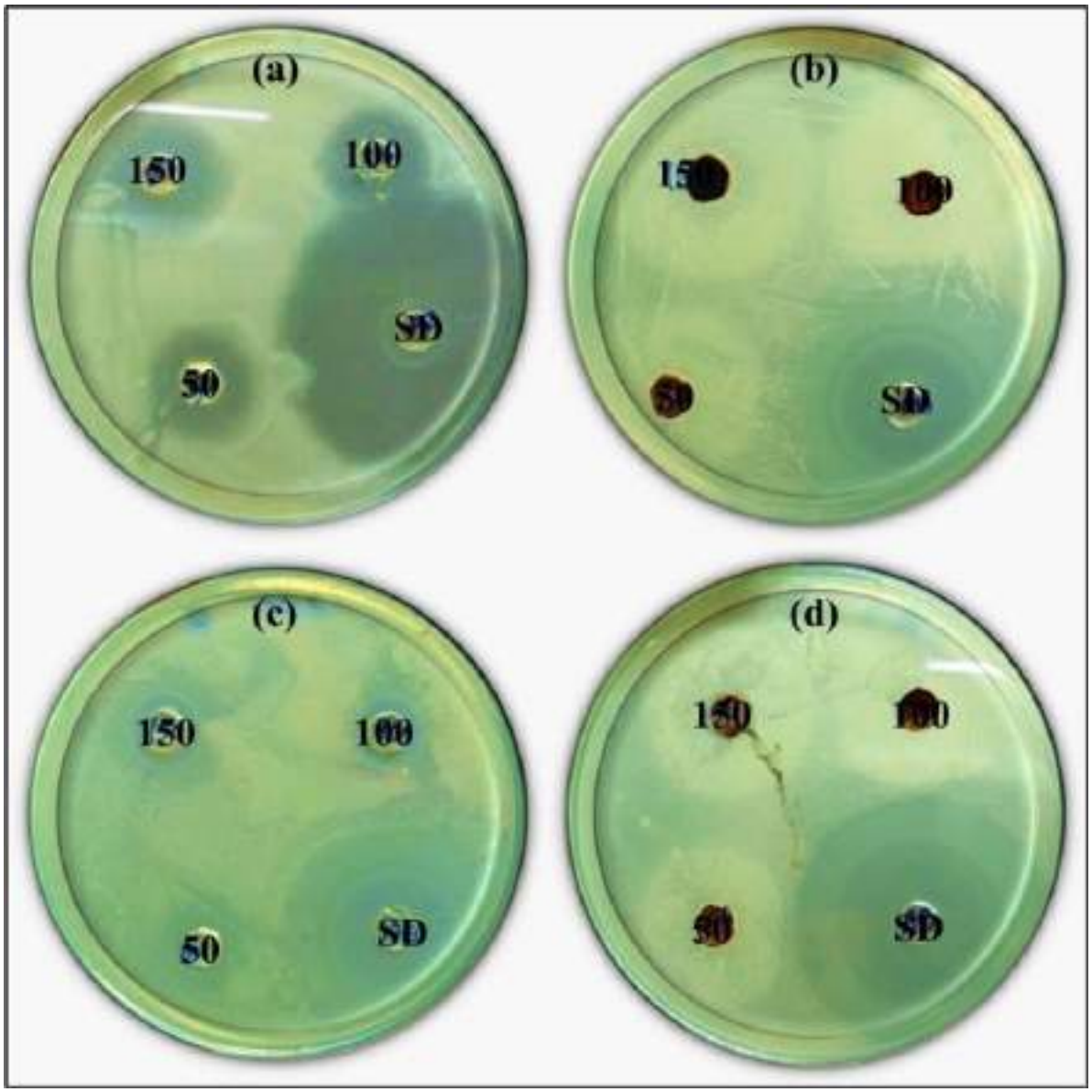

Fig. 10 Antibacterial efficacy of ZnO NPs synthesized using *Jatropha podagrica* leaf extract for **a** *S. aureus*, **b** *B. coagulans*, **c** *K. pneumoniae*, and **d** *E. coli*

study exhibited substantial antibacterial potency against *S. aureus*, *B. coagulans*, *K. pneumoniae*, and *E. coli*. Particularly favorable outcomes were witnessed against *S. aureus* (17 mm), *B. coagulans* (15 mm), *K. pneumoniae* (11 mm), and *E. coli* (10 mm) at a concentration of 150 µL, surpassing the performance of conventional drugs. The plant extract

Table 4 Zone of inhibition at different concentrations of JP-ZnO NPs

Name	*S. aureus*	*B. coagulans*	*K. pneumoniae*	*E. coli*
Shape	Round	Round	Round	Round
Gram reaction	Gram positive	Gram positive	Gram negative	Gram negative
50 µL	15 mm	12 mm	10 mm	10 mm
100 µL	16 mm	13 mm	11 mm	10 mm
150 µL	17 mm	15 mm	13 mm	11 mm
Antibiotic	40 mm	27 mm	40 mm	32 mm

exhibited commendable activity against both Gram-positive and Gram-negative bacteria, resulting in an inhibition zone of 6 mm. At various JP-ZnO NP concentrations, Table 4 shows the zone of inhibition.

From the aforementioned results, the susceptibility of Gram-positive bacteria (*S. aureus*, *B. coagulans*) exhibited a heightened degree of susceptibility to JP-ZnO NPs in contrast to Gram-negative bacteria (*K. pneumoniae*, *E. coli*). This discrepancy in sensitivity can be attributed to the substantial presence of a thick peptidoglycan layer within the cell wall of Gram-positive bacteria, which serves as a robust physical barrier offering shielding and protection. In contrast, Gram-negative bacteria possess both lipopolysaccharide and peptidoglycan, rendering them more resistant to the effects of JP-ZnO NPs [57–59].

Conclusions

In summary, we have successfully employed an eco-friendly method for synthesizing ZnO nanoparticles, using *Jatropha podagrica* leaf extract as a capping agent. Distinct analytical techniques were employed to characterize the nanoparticles which confirmed their wurtzite crystalline structure, spherical shape, and size in the range of 12 to 18 nm. The JP-ZnO nanoparticles have demonstrated a remarkable photocatalytic efficiency, effectively breaking down RhB, FS, and CV dyes under sunlight. The degradation rates of 90–95% were achieved within a time frame of 150, 90, and 60 min for RhB, FS, and CV dyes. We evaluated their antibacterial properties against both gram-positive (*S. aureus*, *B. coagulans*) and gram-negative (*K. pneumoniae*, *E. coli*) bacterial strains. Using 150 µL of nanoparticles, inhibition zones measuring 17, 15, 11, and 10 mm were obtained. These findings highlight the potential applications of JP-ZnO nanoparticles in addressing water pollution challenges and formulating potent antibacterial agents.

Acknowledgements The authors express sincere gratitude to Dr. K. Basavaiah, professor in the Department of Analytical Chemistry at Andhra University, Visakhapatnam, Andhra Pradesh, India, for generously facilitating UV-Vis spectroscopy for the purpose of characterizations.

Author contribution Venkatesh wrote the manuscript and prepared the tables and figures, A. V. Ramesh collected the data, and Jayarao reviewed the manuscript.

Availability of data and materials This declaration is "not applicable" .

Declarations

Ethical approval This declaration is "not applicable".

Competing interests The authors declare no competing interests.

References

1. Lee KM, Lai CW, Ngai KS, Juan JC (2016) Recent developments of zinc oxide based photocatalyst in water treatment technology: a review. Water Res 88:428–448. https://doi.org/10.1016/j.watres.2015.09.045
2. Weber R, Watson A, Forter M, Oliaei F (2011) Review Article: Persistent organic pollutants and landfills — a review of past experiences and future challenges. Waste Manag Res 29(1):107–121. https://doi.org/10.1177/0734242X10390730
3. Jain R, Mathur M, Sikarwar S, Mittal A (2007) Removal of the hazardous dye rhodamine B through photocatalytic and adsorption treatments. J Environ Manage 85(4):956–964. https://doi.org/10.1016/j.jenvman.2006.11.002
4. Jones N, Ray B, Ranjit KT, Manna AC (2008) Antibacterial activity of ZnO nanoparticle suspensions on a broad spectrum of microorganisms. FEMS Microbiol Lett 279(1):71–76. https://doi.org/10.1111/j.1574-6968.2007.01012.x
5. Emami-Karvani Z, Chehrazi P (2011) Antibacterial activity of ZnO nanoparticle on gram-positive and gram-negative bacteria. Afr J Microbiol Res 5(12):1368–1373. https://doi.org/10.5897/AJMR10.159
6. Golmohammadi M, Honarmand M, Ghanbari S (2020) A green approach to synthesis of ZnO nanoparticles using jujube fruit extract and their application in photocatalytic degradation of organic dyes. Spectrochim Acta Part A Mol Biomol Spectrosc 229:117961. https://doi.org/10.1016/j.saa.2019.117961
7. Davar F, Majedi A, Mirzaei A (2015) Green synthesis of ZnO nanoparticles and its application in the degradation of some dyes. J Am Ceram Soc 98:1739–1746. https://doi.org/10.1111/jace.13467
8. Raghupathi KR, Koodali RT, Manna AC (2011) Size-dependent bacterial growth inhibition and mechanism of antibacterial activity of zinc oxide nanoparticles. Langmuir 27(7):4020–4028. https://doi.org/10.1021/la104825u
9. Sirelkhatim A, Mahmud S, Seeni A et al (2015) Review on zinc oxide nanoparticles: antibacterial activity and toxicity mechanism. Nano-Micro Lett 7:219–242. https://doi.org/10.1007/s40820-015-0040-x
10. Maryanti E, Damayanti D, Gustian I (2014) Synthesis of ZnO nanoparticles by hydrothermal method in aqueous rinds extracts of *Sapindus rarak* DC. Mater Lett 118:96–98. https://doi.org/10.1016/j.matlet.2013.12.044
11. Ghorbani HR, Mehr FP, Pazoki H, Rahmani BM (2015) Synthesis of ZnO nanoparticles by precipitation method. Orient J Chem 31(2). https://doi.org/10.13005/ojc/310281
12. Ahammed KR, Ashaduzzaman M, Paul SC et al (2020) Microwave assisted synthesis of zinc oxide (ZnO) nanoparticles in a noble approach: utilization for antibacterial and photo catalytic activity. SN Appl Sci 2:955. https://doi.org/10.1007/s42452-020-2762-8
13. Yıldırım ÖA, Durucan C (2010) Synthesis of zinc oxide nanoparticles elaborated by microemulsion method. J Alloy Compd 506(2):944–949. https://doi.org/10.1016/j.jallcom.2010.07.125
14. Ghoshal T, Biswas S, Paul M, De SK (2009) Synthesis of ZnO nanoparticles by solvothermal method and their ammonia sensing properties. J Nanosci Nanotechnol 9(10):5973–5980. https://doi.org/10.1166/jnn.2009.1290
15. Leybros A, Piolet R, Ariane M, Muhr H, Bernard F, Demoisson F (2012) CFD simulation of ZnO nanoparticle precipitation in a supercritical water synthesis reactor. J Supercrit Fluids 70:17–26. https://doi.org/10.1016/j.supflu.2012.06.001
16. Hasnidawani JN, Azlina HN, Norita H, Bonnia NN, Ratim S, Ali ES (2016) Synthesis of ZnO nanostructures using sol-gel method. Procedia Chem 19:211–216. https://doi.org/10.1016/j.proche.2016.03.095
17. Gawade VV, Gavade NL, Shinde HM, Babar SB, Kadam AN, Garadkar KM (2017) Green synthesis of ZnO nanoparticles by

using *Calotropis procera* leaves for the photodegradation of methyl orange. J Mater Sci: Mater Electron 28:14033–14039. https://doi.org/10.1007/s10854-017-7254-2
18. Rathnasamy R, Thangasamy P, Thangamuthu R et al (2017) Green synthesis of ZnO nanoparticles using *Carica papaya* leaf extracts for photocatalytic and photovoltaic applications. J Mater Sci: Mater Electron 28:10374–10381. https://doi.org/10.1007/s10854-017-6807-8
19. Batra V, Kaur I, Pathania D, Chaudhary V (2022) Efficient dye degradation strategies using green synthesized ZnO-based nanoplatforms: a review. Appl Surf Sci Adv 11:100314. https://doi.org/10.1016/j.apsadv.2022.100314
20. Thi TUD, Nguyen TT, Thi YD, Thi KHT, Phan BT, Pham KN (2020) Green synthesis of ZnO nanoparticles using orange fruit peel extract for antibacterial activities. RSC Adv 10(40):23899–23907. https://doi.org/10.1039/D0RA04926C
21. Raj A, Lawrence RS, Jalees MOHAMMAD, Lawrence KAPIL (2015) Anti-bacterial activity of zinc oxide nanoparticles prepared from *Brassica oleraceae* leaves extract. Int J Adv Res 3(11):322–328
22. Ramesh M, Anbuvannan M, Viruthagiri GJSAPAM (2015) Green synthesis of ZnO nanoparticles using *Solanum nigrum* leaf extract and their antibacterial activity. Spectrochim Acta Part A Mol Biomol Spectrosc 136:864–870. https://doi.org/10.1016/j.saa.2014.09.105
23. Espenti CS, Rama Krishna AG, Rami Reddy YV (2020) Green biosynthesis of ZnO nanomaterials and their anti-bacterial activity by using *Moringa Oleifera* root aqueous extract. SN Appl Sci 2:1424. https://doi.org/10.1007/s42452-020-2945-3
24. Bhaskarwar BHUSHAN, Itankar PRAKASH, Fulke ABHAY (2008) Evaluation of antimicrobial activity of medicinal plant *Jatropha podagrica* (Hook). Rom Biotechnol Lett 13(5):3873–3877
25. Thomas S (2016) Pharmacognostic and phytochemical constituents of leaves of *Jatropha multifida* Linn. and *Jatropha podagrica* Hook. J Pharmacogn Phytochem 5(2):243–246
26. Panzu NN, Lengbiye EM, Domondo A, Inkoto CL, Muanyishay CL, Gbolo BZ, Mpiana PT (2020) A review on the bioactivity and phytochemistry of *Jatropha podagrica* Hook (Euphorbiaceae). Discov Phytomedicine 7(4):186–194. https://doi.org/10.15562/phytomedicine.2020.150
27. Ezealisiji KM, Siwe-Noundou X, Maduelosi B et al (2019) Green synthesis of zinc oxide nanoparticles using *Solanum torvum* (L) leaf extract and evaluation of the toxicological profile of the ZnO nanoparticles–hydrogel composite in Wistar albino rats. Int Nano Lett 9:99–107. https://doi.org/10.1007/s40089-018-0263-1
28. Hemanth Kumar, N.K., Murali, M., Satish, A et al (2020) Bioactive and biocompatible nature of green synthesized zinc oxide nanoparticles from *Simarouba glauca* DC: An Endemic Plant to Western Ghats, India. J Clust Sci 31:523–534. https://doi.org/10.1007/s10876-019-01669-7
29. Mallikarjunaswamy C, Lakshmi Ranganatha V, Ramu R et al (2020) Facile microwave-assisted green synthesis of ZnO nanoparticles: application to photodegradation, antibacterial and antioxidant. J Mater Sci Mater Electron 31:1004–1021. https://doi.org/10.1007/s10854-019-02612-2
30. Singh K, Singh J, Rawat M (2019) Green synthesis of zinc oxide nanoparticles using *Punica granatum* leaf extract and its application towards photocatalytic degradation of Coomassie brilliant blue R-250 dye. SN Appl Sci 1:624. https://doi.org/10.1007/s42452-019-0610-5
31. Vahidi A, Vaghari H, Najian Y, Najian M, Jafarizadeh-Malmiri H (2019) Evaluation of three different green fabrication methods for the synthesis of crystalline ZnO nanoparticles using *Pelargonium zonale* leaf extract. Green Process Synth 8(1):302–308. https://doi.org/10.1515/gps-2018-0097
32. Sharma BK, Mehta BR, Shah EV et al (2022) Green synthesis of triangular ZnO nanoparticles using *Azadirachta indica* leaf extract and its shape dependency for significant antimicrobial activity: joint experimental and theoretical investigation. J Clust Sci 33:2517–2530. https://doi.org/10.1007/s10876-021-02145-x
33. Thirumoorthy GS, Balasubramaniam O, Kumaresan P et al (2021) *Tetraselmis indica* mediated green synthesis of zinc oxide (ZnO) nanoparticles and evaluating its antibacterial, antioxidant, and hemolytic activity. BioNanoSci 11:172–181. https://doi.org/10.1007/s12668-020-00817-y
34. Çolak H, Karaköse E, Duman F (2017) High optoelectronic and antimicrobial performances of green synthesized ZnO nanoparticles using *Aesculus hippocastanum*. Environ Chem Lett 15:547–552. https://doi.org/10.1007/s10311-017-0629-z
35. Elavarasan N, Kokila K, Inbasekar G et al (2017) Evaluation of photocatalytic activity, antibacterial and cytotoxic effects of green synthesized ZnO nanoparticles by *Sechium edule* leaf extract. Res Chem Intermed 43:3361–3376. https://doi.org/10.1007/s11164-016-2830-2
36. Varadavenkatesan T, Lyubchik E, Pai S, Pugazhendhi A, Vinayagam R, Selvaraj R (2019) Photocatalytic degradation of Rhodamine B by zinc oxide nanoparticles synthesized using the leaf extract of *Cyanometra ramiflora*. J Photochem Photobiol B 199:111621. https://doi.org/10.1016/j.jphotobiol.2019.111621
37. Darvishi D, Kahrizi D, Arkan E (2019) Comparison of different properties of zinc oxide nanoparticles synthesized by the green (using *Juglans regia* L. leaf extract) and chemical methods. J Mol Liq. https://doi.org/10.1016/j.molliq.2019.04.108
38. Hassan SS, El Azab WI, Ali HR, Mansour MS (2015) Green synthesis and characterization of ZnO nanoparticles for photocatalytic degradation of anthracene. Adv Nat Sci: Nanosci Nanotechnol 6(4):045012. https://doi.org/10.1088/2043-6262/6/4/045012
39. Jayappa MD, Ramaiah CK, Kumar MAP et al (2020) Green synthesis of zinc oxide nanoparticles from the leaf, stem and in vitro grown callus of *Mussaenda frondosa* L.: characterization and their applications. Appl Nanosci 10:3057–3074. https://doi.org/10.1007/s13204-020-01382-2
40. Ramesh AV, Pavankumar Y, Lavakusa B, Basavaiah K (2017) A facile green synthesis of ZnO nanorods using leaf extract of *Ficus hispida* L. Int J Eng Appl Sci Technol 2(4):256–260. https://www.ijeast.com/papers/256-260,Tesma204,IJEAST.pdf
41. Rahimi Kalateh Shah Mohammad G, Homayouni Tabrizi M, Ardalan T et al (2019) Green synthesis of zinc oxide nanoparticles and evaluation of anti-angiogenesis, anti-inflammatory and cytotoxicity properties. J Biosci 44:30. https://doi.org/10.1007/s12038-019-9845-y.
42. Sangeetha G, Rajeshwari S, Venckatesh R (2011) Green synthesis of zinc oxide nanoparticles by *Aloe barbadensis* miller leaf extract: structure and optical properties. Mater Res Bull 46(12):2560–2566. https://doi.org/10.1016/j.materresbull.2011.07.046
43. M Awwad A, Albiss B, L Ahmad A (2014) Green synthesis, characterization and optical properties of zinc oxide nanosheets using *Olea europea* leaf extract. Adv Mater Lett 5(9):520–524. https://doi.org/10.5185/amlett.2014.5575
44. El-Khawaga AM, Elsayed MA, Gobara M et al (2023) Green synthesized ZnO nanoparticles by *Saccharomyces cerevisiae* and their antibacterial activity and photocatalytic degradation. Biomass Conv Bioref. https://doi.org/10.1007/s13399-023-04827-0
45. Barzinjy AA, Azeez HH (2020) Green synthesis and characterization of zinc oxide nanoparticles using *Eucalyptus globulus* Labill. leaf extract and zinc nitrate hexahydrate salt. SN Appl Sci 2:991. https://doi.org/10.1007/s42452-020-2813-1
46. Khan AU, Malik N, Singh B et al (2023) Biosynthesis, and characterization of zinc oxide nanoparticles (ZnONPs) obtained from

the extract of waste of strawberry. J Umm Al-Qura Univ Appll Sci 9:268–275. https://doi.org/10.1007/s43994-023-00038-5
47. Rajakumar G, Thiruvengadam M, Mydhili G et al (2018) Green approach for synthesis of zinc oxide nanoparticles from *Andrographis paniculata* leaf extract and evaluation of their antioxidant, anti-diabetic, and anti-inflammatory activities. Bioprocess Biosyst Eng 41:21–30. https://doi.org/10.1007/s00449-017-1840-9
48. Raghavendra VB, Shankar S, Govindappa M et al (2022) Green synthesis of zinc oxide nanoparticles (ZnO NPs) for effective degradation of dye, polyethylene and antibacterial performance in waste water treatment. J Inorg Organomet Polym 32:614–630. https://doi.org/10.1007/s10904-021-02142-7
49. Ambika S, Sundrarajan M (2015) Antibacterial behaviour of *Vitex negundo* extract assisted ZnO nanoparticles against pathogenic bacteria. J Photochem Photobiol, B 146:52–57. https://doi.org/10.1016/j.jphotobiol.2015.02.020
50. Rajendrachari S, Taslimi P, Karaoglanli AC, Uzun O, Alp E, Jayaprakash GK (2021) Photocatalytic degradation of Rhodamine B (RhB) dye in waste water and enzymatic inhibition study using cauliflower shaped ZnO nanoparticles synthesized by a novel one-pot green synthesis method. Arab J Chem 14(6):103180. https://doi.org/10.1016/j.arabjc.2021.103180
51. Alshamsi HA, Jaffer AA (2022, November) New *Hibiscus sabdariffa* L. petals extract based green synthesis of zinc oxide nanoparticles for photocatalytic degradation of Rhodamine B dye under solar light. In AIP Conference Proceedings (Vol. 2394, No. 1). AIP Publishing. https://doi.org/10.1063/5.0121228
52. Hazim K, Hamza Z, Mohamed L (2022) Eco-friendly synthesis, antibacterial activity, and photocatalytic performance of ZnO nanoparticles synthesized via leaves extract of Paraserianthes lophantha. Pak J Med Health Sci 16(03):581–581. https://doi.org/10.53350/pjmhs22163581
53. Surendra TV, Roopan SM, Al-Dhabi NA, Arasu MV, Sarkar G, Suthindhiran K (2016) Vegetable peel waste for the production of ZnO nanoparticles and its toxicological efficiency, antifungal, hemolytic, and antibacterial activities. Nanoscale Res Lett 11:1–10. https://doi.org/10.1186/s11671-016-1750-9
54. Karthik P, Ravichandran S, Mukkannan A, Rajesh J (2022) Plant-mediated biosynthesis of zinc oxide nanoparticles from *Delonix elata*: a promising photocatalyst for crystal violet degradation. Inorg Chem Commun 146:110122. https://doi.org/10.1016/j.inoche.2022.110122
55. Khalil AT, Hameed S, Afridi S, Mohamed HEA, Shinwari ZK (2021) *Sageretia thea* mediated biosynthesis of metal oxide nanoparticles for catalytic degradation of crystal violet dye. Mater Today: Proc 36:397–400. https://doi.org/10.1016/j.matpr.2020.04.687
56. Badma Priya D, Thirumalai D, Asharani IV (2021) Influence of synthetic parameters on the enhanced photocatalytic properties of ZnO nanoparticles for the degradation of organic dyes: a green approach. J Mater Sci: Mater Electron 32:9956–9971. https://doi.org/10.1007/s10854-021-05654-7
57. Jones N, Ray B, Ranjit KT, Manna AC (2008) Antibacterial activity of ZnO nanoparticle suspensions on a broad spectrum of microorganisms. FEMS Microbiol Lett 279(1):71–76.39. https://doi.org/10.1111/j.1574-6968.2007.01012.x
58. da Silva BL, Caetano BL, Chiari-Andreo BG (2019) Linhari Rodrigues Pietro RC, Chiavacci LA, Increased antibacterial activity of ZnO nanoparticles: influence of size and surface modification. Colloids Surf, B. https://doi.org/10.1016/j.colsurfb.2019.02.013
59. Arvanag FM, Bayrami A, Habibi-Yangjeh A, Pouran SR (2019) A comprehensive study on antidiabetic and antibacterial activities of ZnO nanoparticles biosynthesized using *Silybum marianum L* seed extract. Mater Sci Eng, C 97:397–405. https://doi.org/10.1016/j.msec.2018.12.058

Biological Trace Element Research
https://doi.org/10.1007/s12011-023-03761-6

RESEARCH

Trace Elemental and Heavy Metal Levels in Frequently Consumed Local Vegetables of Three Chronic Kidney Disease-Prevalent Villages

G. Narayana Murthy[1] · P. Balarama Swamy Yadav[1]

Received: 26 March 2023 / Accepted: 30 June 2023

Abstract

The present study reports the trace elemental and heavy metal (24 elements) levels in six (*Capsicum frutescence* L., *Carica papaya* L., *Momordica charantia* L., *Moringa oleifera* Lam., *Musa sapientum* L., and *Solanum melongena* L.) vegetables. The vegetable samples are collected from the three villages and are subjected to ICP-MS analysis, to test a group of 24 elements, viz., Li, Be, Al, Sc, V, Cr, Mn, Fe, Co, Ni, Cu, Zn, Ga, As, Se, Rb, Sr, Ag, Cd, Cs, Ba, TI, Rb, and U, for their levels. The obtained levels of each element were compared with the WHO/FAO permissible values. Out of the tested 24 elements, 16 elements may cause kidney problems and the remaining 8 (Mn, Co, Ni, Cu, Zn, Se, Sr, and TI) may cause other health problems when they are in high concentration (FAO/WHO, 18; ATSDR, 19; Drake and Hazelwood in Ann Occup Hyg 49:575–585, 20; US EPA, 21; FAO/WHO, 22; Choudhury et al., 23; Food Safety and Standards, 24). The results reveal that Ba is in high concentration (2.51 times) in all the tested vegetable samples and Pb is in high concentration (1.28 times) in 11 vegetable samples; Ag and Fe are high in one vegetable sample each. Among the three locations highest Ba concentration is observed in S_1 (*Capsicum*) of L_2 followed by S_5 (*Musa*) and S_1 (*Capsicum*) of L_1. The higher Pb concentration is present in S_1 (*Capsicum*) of L_3 followed by S_1 (*Capsicum*) of L_2. The results reveal that out of the six vegetables tested, *Capsicum* shows high concentrations of Ba and Pb. The variation in the levels of trace elements and heavy metals with regard to location and vegetable samples may be due to soil and or due to groundwater.

Keywords Chronic kidney disease · ICP-MS · Trace elements · Vegetables · Uddanam area

Introduction

Vitamins and minerals are micronutrients; they play vital role in various physiological processes and are necessary for maintaining overall health. Vegetables are vital component of healthy diet; they provide important minerals that are essential for human health. Consuming vegetables ensures an adequate intake of these minerals, which are often found in higher amounts in plant-based foods than the animal-based food sources. However, it is important to note that excessive intake of certain minerals through vegetables or any other way may cause adverse health effects; for example, excessive consumption of potassium-rich vegetables without proper monitoring can be problematic for individuals with kidney disorders. Similarly, many heavy metals are potentially toxic to humans (WHO) [1].

Studies on trace elemental analysis of plant edible parts are not fully explored in the present study area (Uddanam); hence, the present study is taken up. According to the World Health Organization (WHO), Uddanam is one of three regions in the world with a high CKD incidence of 18.23% [2]; the other two are one in Sri Lanka and other in Nicaragua. In 2015, it is estimated that more than 4500 people have died in the Uddanam area over the past decade, with about 34,000 people suffering from kidney disease. Nearly every family in the region has at least one person diagnosed with the disease. These cases were first recognized in early 1990s, and the phenomenon was discussed at the International Nephrology Conference in Hong Kong (2013) and named Uddanam Nephropathy [3]. In 2016, the Indian Council of Medical Research partnered with Harvard University, Baba Atomic Research Center (Mumbai), Health University (Andhra Pradesh), and Andhra Medical College (Vishakapatnam) to study the causes of CKD.

✉ P. Balarama Swamy Yadav
dr.pbsyadav@andhrauniversity.edu.in

[1] Department of Botany, Andhra University, Visakhapatnam 530003, Andhra Pradesh, India

Few studies that have been done on the analysis of trace elements in edible plant parts from the Uddanam area, such as rice and finger millet using the EDXRF technique, explored that Cu and Zn elements are in high concentration in both the samples and phosphorus is more in rice and Se is more in finger millet [4, 5]. Studies on analysis of trace elements of soil and water samples in this area have been carried out [6–8] and showed that the water and soil in the villages of Uddanam contain high concentration of minerals like ferrous, manganese, copper, and zinc [8]. Khandare et al. [9] identified excessive concentrations of Li, Si, and Sr in the groundwater of Uchapally village of Nellore district, Andhra Pradesh, India, which is also a CKD-prevalent village, indicating presence of some elements and heavy metals in high concentration. K. Lal et al. [10] found that approximately 35% of Uddanam villages had acidic groundwater, while it is only 3% villages in other districts. High lead levels were detected during the dry season and the lead levels exceeded permissible limits in 55% of villages. The study recommends treating groundwater with reverse osmosis (RO) for drinking and cooking purposes. Gowrishankar S. et al. [11] found recent evidence of dysmorphic lysosomes in renal biopsies and suggest a toxic cause for CKD. The etiology of the disease remains unknown.

Banerjee et al. [12] noticed excess lead content in all fruit and vegetable samples collected from the districts of West Bengal [12]. Mamatha et al. [13] identified excessive levels of cadmium and lead in leafy vegetables used by local people in Pulivendula, Kadapa district of Andhra Pradesh [13]. Priya et al. [14] identified high levels of copper, chromium, iron, and lead in leaves of Sorrel (*Rumex* spp.) in the Musi River basin of Hyderabad [14]. Sapana Gupta et al. [15] found high levels of chromium, zinc, copper, and lead in leafy vegetables collected in the city of Raipur [15]. So far, many studies indicate that the water and soil of the Uddanam region contain trace elements in high concentration than permissible values. There are no attempts on trace elemental analysis in all the local plant vegetable parts that are frequently consumed by the people of this region.

Materials and Methods

Study Area

Uddanam is a region covering few parts of the seven revenue mandals or tahasils (Ichhapuram, Kanchili, Kaviti, Mandasa, Palasa, Sompeta, and Vajrapukothuru) in the Srikakulam district of Andhra Pradesh, India. The area is a lush green environment with rich coconut and cashew nut orchards along the coastline of the Bay of Bengal. However, it is known as the region with high incidence of CKD. Ravi Raju et al. [2] reported 15.9% CKD in their pilot study and 18.23% in their final study of age group above 18 years in Uddanam area, which is high incidence of CKD. Thousands of people are still suffering from this disease; till now, the reasons behind the cases of kidney failure are unknown and many investigations are being conducted to explore the cause(s) of this CKD, which is specific to this area. Worldwide, 697.5 million people are suffering from chronic kidney disease, of which 115.1 million are Indians [16].

Geographically, Uddanam is located at 19.0167°N latitude and 84.6833°E longitude, with an average elevation of 41 m above sea level. It consists of 7 revenue mandals; we have chosen Kaviti revenue mandal because of high prevalence of CKD. We selected three revenue villages out of 21 revenue villages in Kaviti mandal based on the patients number and data obtained from the Community Hospital Sompeta. These three villages are Kusumapuram (L_1), Varaka (L_2), and Borivanka (L_3) (Fig. 1A, B, C, D).

Sample Collection and Preparation

We identified six locally cultivated vegetables for trace elemental and heavy metal analysis (Table 1), which are grown in their coconut orchards as intercrops and are frequently consumed. Samples from three selected villages are analyzed for the levels of trace elements and heavy metals by using ICP-MS instrument. Among the tested vegetable samples, 2 belong to the family Solanaceae, and one each from Caricaceae, Cucurbitaceae, Moringaceae, and Musaceae (Table 1).

The fresh samples of the selected vegetables collected from the farm fields directly from the three villages are kept in zip-locked bags and are brought to the laboratory. The samples are washed twice with distilled water and then subjected to acid digestion process; that is, fast and accurate wet digestion method [17] is followed for the digestion of vegetable samples to digest all organic matter present in the vegetable samples and placed in ICP-MS to obtain the trace elemental levels.

Procedure

We used the ICP-MS instrument (Agilent Technologies, model 7700) available in Centre for Studies on Bay of Bengal, Andhra University, Visakhapatnam. The sample preparation for ICP-MS analysis followed here is based on the oxidation and solubility of organic matter in plants when H_2O_2 (33%) is added directly to the concentrated HNO_3 and heated for a short time. The instrument was switched on and is first run with the Standard Reference Materials of 0 ppb, 0.5 ppb, 1 ppb, 5 ppb, 10 ppb, 25 ppb, 50 ppb, and 100 ppb, then the samples were ran, and the levels of 24 elements

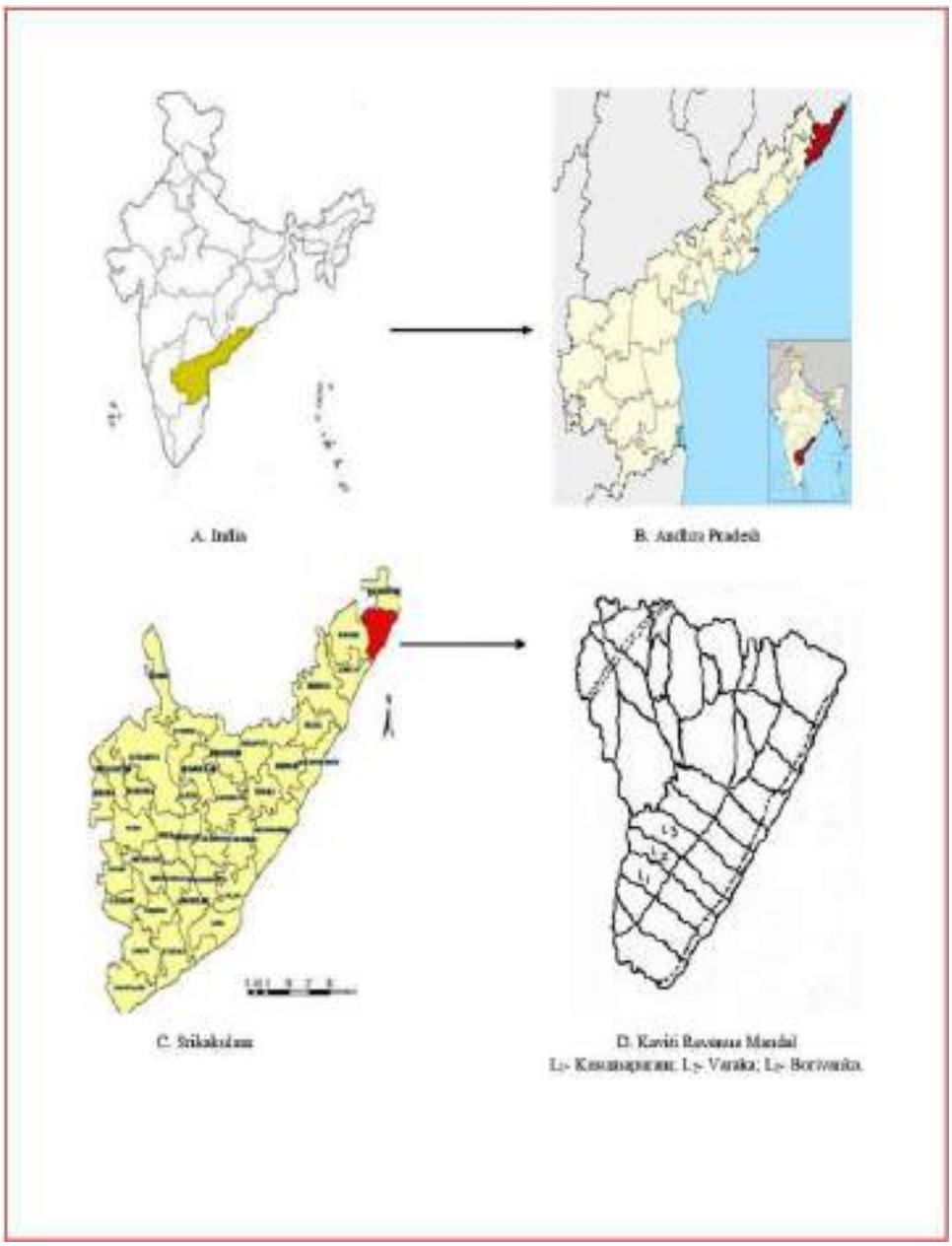

Fig. 1 Study area

Table 1 Frequently consumed local vegetables used in the study

Sample no	Botanical name	Family	English name	Vernacular name
S1	Capsicum frutescence L	Solanaceae	Chilli	Pachchi mirapa kaya
S2	Carica papaya L	Caricaceae	Papaya	Boppayi kaya
S3	Momordica charantia L	Cucurbitaceae	Bitter gourd	Kakara kaya
S4	Moringa oleifera Lam	Moringaceae	Drumsticks	Munaga kada
S5	Musa sapientum L	Musaceae	Plantain	Arati kaya
S6	Solanum melongena L	Solanaceae	Brinjal	Vanga kaya

Table 2 Instrument conditions and parameters

Serial no	Parameter	Value
1	RF power	1550 W
2	Sampling depth	8.0 mm
3	Carrier gas flow rate	0.95 l min^{-1}
4	Makeup gas	0.20 l min^{-1}
5	Spray chamber temperature	2 °C
6	Collision gas	He, 3.4 ml min^{-1} (99.999% purity)
7	Water filter	< 100-µm particle size
8	Elements/isotopes measured	^{7}Li, ^{9}Be, ^{27}Al,^{45}Sc, ^{51} V, ^{52}Cr, ^{55}Mn, ^{56}Fe, ^{59}Co, ^{60}Ni, ^{63}Cu, ^{66}Zn, ^{71} Ga, ^{75}As, ^{78}Se, ^{85}Rb, ^{88}Sr, ^{107}Ag, ^{111}Cd, ^{133}Cs, ^{137}Ba, ^{205}TI, ^{208}Pb, and ^{238}U

were obtained (Li, Be, Al, Sc, V, Cr, Mn, Fe, Co, Ni, Cu, Zn, Ga, As, Se, Rb, Sr, Ag, Cd, Cs, Ba, TI, Rb, and U). The instrument conditions and parameters are stated in Table 2.

Wet Digestion

Modified HNO_3/H_2O_2 wet digestion method (Pequerul et al. 1993) [17] was followed. Two grams of vegetable sample is taken, kept in a Teflon beaker, mixed with 8 ml HNO_3, and left overnight. The solution was heated on a hot plate at 120–125 °C for 1 h and 4 ml H_2O_2 (33%) was added once or twice until the organic matter was completely digested. Then we added H_2O_2 until the solution is clear or colorless (indicating complete digestion of organic matter). The residual solution was placed on a dry place at 80 °C, shaken well, cooled to room temperature, and filtered through Whatman filter paper. The solution is then diluted to a known volume (50 ml) with Milli-Q water. The digested filtrate solutions are stored in high-density polyethylene bottles (100 ml) at room temperature for further use.

Results and Discussion

Ten milliliters of digested solution was taken into centrifugation tubes, 20 µl of ISTD solution and 100 µl of HNO_3 were added, and elemental content was analyzed with ICP-MS instrument. The levels of elements present in the vegetable samples are calculated with the help of the following formula in ppb levels and then converted to ppm.

$$X(\mu g) = \frac{IR(S) - IR(B)}{Weight\ of\ the\ sample\ (g)} \times Dilution\ Factor$$

where X (µg) is the concentration of element in ppb, $I_{R(S)}$ is the instrument reading for sample, and $I_{R(B)}$ is the instrument reading for blank.

The obtained values are compared with the permissible values recommended by FAO/WHO (1990, 1995, 1997, 2006, 2008, 2009, 2010, 2011, 2012, 2013, 2014, 2015, 2016, 2017, 2018, 2019) and the Food Safety and Standards (Contaminants, Toxins, and Residues) Regulations (2011) [18–24]. A total of 24 elemental levels in 18 vegetable samples from 3 different locations (L_1, L_2, and L_3) are obtained and presented in Table 3. Out of the 18 tested samples, all samples are found to have high levels of Ba and 11 samples had high levels of Pb. Fe and Ag are high in one sample each and the remaining are within the permissible levels. The study analyzed 18 vegetable samples from three different locations (L_1–L_3) for elemental levels. The levels of 24 elements are measured, and the results are presented in Table 3.

In 3 tested locations in *Capsicum frutescence* raw fruit, Ba is found in high concentration in 3 locations (36.67—L_1, 43.92—L_2, and 27.65 mg/kg—L_3), and Pb is also present in high concentration in 3 locations (0.372—L_1, 0.798—L_2, and 0.972—L_3). *Carica papaya* raw fruit showed high concentration of Fe in one location (216.3 mg/kg—L_3), Ba in all three locations (30.12—L_1, 33.73—L_2, and 21.8 mg/kg—L_3), and Pb in one location (0.327—L_3). In *Momordica charantia* raw fruit, Ba is high in 3 locations (31.6—L_1, 32.29—L_2, and 26.95 mg/kg—L_3) and Pb is in 2 locations (0.415—L_1, 0.511—L_2). In *Moringa oleifera* raw fruit Ba is high in 3 locations (32.44—L_1, 29.23—L_2, and 23.82 mg/kg—L_3), Pb is high in one location (0.416—L_3), and Ag is high in one location (L_2—0.388). *Musa sapientum* contained high concentrations of Ba in 3 locations (42.22—L_1, 33.34—L_2, and 33.85 mg/kg—L_3) and Pb is also in 3 locations (0.353—L_1, 0.304—L_2, and 0.460—L_3). *Solanum melongena* had high concentrations of Ba in 3 locations (30.07—L_1, 33.64—L_2, and 26.89 mg/kg—L_3) and Pb is in one location (0.316—L_2).

The results reveal that out of the 18 tested samples, barium (Ba) is present in high concentration in all samples, and lead (Pb) is present in 11 samples. Iron (Fe) and silver (Ag) are high in one sample each, and the remaining elements did not exceed the limits.

The high concentration of Ba is found in *Carica papaya* of Borivanka, followed by *Capsicum frutescence* of Varaka and *Musa sapientum* of Kusumapuram. The high

Table 3 Trace elemental and heavy metal levels (ppm) in vegetable samples by ICP-MS analysis

Element		Li	Be	Al	Sc	V	Cr	Mn	Fe	Co	Ni	Cu	Zn
P.V		5.6	8.4	60	22	50	2.4	15	50	0.14	5.0	3.5	50
S_1	L_1	0.043	0	9.96	5.547	0.035	0.535	0.376	9.082	0.013	0.348	0.644	10.19
	L_2	0.046	0	56.03	5.106	0.103	1.139	3.245	30.33	0.025	0.434	1.227	15.62
	L_3	0.019	0	44.63	6.810	0.029	0.454	1.035	27.32	0.025	2.013	0.895	18.77
S_2	L_1	0.007	0	8.76	5.108	0.018	0.613	0.523	7.31	0.01	0.297	0.02	6.83
	L_2	0.01	0	7.68	3.228	0.016	0.439	0.562	6.64	0.011	0.329	0.234	7.52
	L_3	0.016	0	10.25	6.735	0.429	0.65	0.865	216.3*	0.02	0.314	0.099	6.41
S_3	L_1	0.022	0	34.86	4.926	0.027	0.509	0.426	10.33	0.005	0.295	0.45	5.96
	L_2	0.011	0	7.82	4.279	0.016	0.392	0.26	6.199	0.005	0.237	0.135	5.22
	L_3	0.014	0	43.46	7.720	0.017	0.542	2.51	6.22	0.01	0.419	0.031	8.65
S_4	L_1	0.014	0	7.31	5.192	0.019	0.504	0.874	5.76	0.009	0.455	0.082	7.09
	L_2	0.005	0	11.05	2.114	0.016	0.483	0.359	5.89	0.01	0.283	0.132	4.30
	L_3	0.024	0	16.85	3.340	0.049	0.878	0.693	27.41	0.005	0.458	0.214	10.39
S_5	L_1	0.068	0	15.26	7.183	0.029	0.482	13.59	13.95	0.042	0.376	0.339	23.59
	L_2	0.032	0	9.66	3.82	0.029	0.419	0.424	7.53	0.006	0.2	0.045	3.90
	L_3	0.026	0	9.4	6.83	0.018	0.525	0.428	6.24	0.014	0.23	0	8.45
S_6	L_1	0.023	0	7.57	3.708	0.014	0.498	0.484	4.51	0.011	0.26	0.0008	11.58
	L_2	0.017	0	8.54	6.06	0.021	0.557	16.20	8.78	0.02	0.407	0.973	8.78
	L_3	0.02	0	24.94	6.02	0.014	0.461	0.747	5.61	0.003	0.568	0.196	8.89
Element		Ga	As	Se	Rb	Sr	Ag	Cd	Cs	Ba	Tl	Pb	U
P.V		3.0	0.18	1.5	5.0	10	0.175	1.5	90	12.6	1.5	0.3	7
S_1	L_1	0.003	0.01	0.006	0.587	1.395	0.048	0.006	0.0005	36.67*	0	0.372*	0
	L_2	0.013	0.031	0.133	1.107	2.832	0.124	0.013	0.002	43.92*	0	0.798*	0.01
	L_3	0.005	0.008	0.039	0.587	0.887	0.047	0.026	0.0001	27.65*	0	0.972*	0.0008
S_2	L_1	0.001	0.005	0.036	0.735	0.574	0.057	0.009	0.0001	30.12*	0	0.2	0
	L_2	0.002	0.002	0.037	0.823	0.63	0.122	0.011	0.0004	33.73*	0	0.28	0
	L_3	0.014	0.011	0.039	0.92	0.552	0.027	0.032	0.0003	21.80*	0	0.327*	0.0001
S_3	L_1	0.005	0.005	0.028	0.54	0.605	0.026	0.01	0	31.60*	0	0.415*	0.003
	L_2	0.002	0.003	0.007	0.489	0.72	0.033	0.011	0	32.29*	0	0.511*	0
	L_3	0.003	0.004	0.037	0.879	0.617	0.026	0.004	0	26.95*	0	0.252	0
S_4	L_1	0.002	0.005	0.017	0.531	1.137	0.035	0.008	0.0001	32.44*	0	0.254	0
	L_2	0.003	0.004	0.005	0.949	0.842	0.388*	0.009	0.0003	29.23*	0	0.214	0
	L_3	0.007	0.013	0.043	1.158	1.143	0.172	0.015	0.0003	23.82*	0	0.416*	0
S_5	L_1	0.006	0.009	0.03	1.92	1.847	0.048	0.018	0.001	42.22*	0	0.353*	0
	L_2	0.002	0.005	0	0.463	0.882	0.056	0.005	0	33.34*	0	0.304*	0
	L_3	0.003	0.005	0.015	0.266	0.705	0.087	0.019	0	33.85*	0	0.460*	0
S_6	L_1	0.002	0.007	0.007	0.504	0.698	0.104	0.007	0	30.07*	0	0.177	0
	L_2	0.002	0.015	0.021	2.356	3.258	0.04	0.01	0	33.64*	0	0.316*	0
	L_3	0.003	0.005	0.027	1.01	0.928	0.066	0.004	0.0001	26.89*	0	0.299	0

S_1–S_6 = samples 1–6; P.V. = permissible values (mg/kg or ppm) as per WHO/FAO; L_1 (location 1) = Kusumapuram; L_2 (location 2) = Varaka; L_3 (location 3) = Borivanka

*Trace elements and heavy metals in more concentrations than the WHO/FAO standards that are harmful to kidney

concentration of Pb is observed in *Capsicum frutescence* of Borivanka, followed by Varaka. Pb levels are low in vegetable samples of *Solanum melongena.* Overall, the average high concentrations of elements were identified in Borivanka (L_3) village, followed by Varaka (L_2) and Kusumapuram (L_1).

Discussion

Adeloju S. B. et al. [25] stated that some heavy metals are potentially toxic, resulting to cause renal toxicity, multiorgan toxicity, gastrointestinal irritation, etc. Fritz Pragst et al. [26] found lead and barium in high concentration in hair samples

of the population in South Sudan. They found significant health risk due to the deposition of toxic industrial waste in the affected area. Environmental barium and its potential health effects, including kidney diseases, neurological disorders, cardiovascular issues, and metabolic disorders, are well explained by Peana M. et al. [27]. They suggest for further research to understand its geographical variation, intake levels, and potential biochemical functions in humans.

The results of the study indicate that the vegetable samples contained high concentrations of certain elements, particularly Ba and Pb. These are excess than the limits recommended by FAO/WHO and the Food Safety and Standards (Contaminants, Toxins, and Residues) Regulations of India (2011). The presence of these elements in high amounts raises concerns about the safety and potential health risks associated with frequent consumption of these vegetables.

The presence of elevated levels of Ba and Pb in the tested vegetable samples may be because of various factors, like environmental, agricultural practices, and may be presence of these elements in the irrigated soil or in irrigation water. It is important to know the possible sources of contamination and to take appropriate measures to mitigate their presence in the agricultural ecosystem.

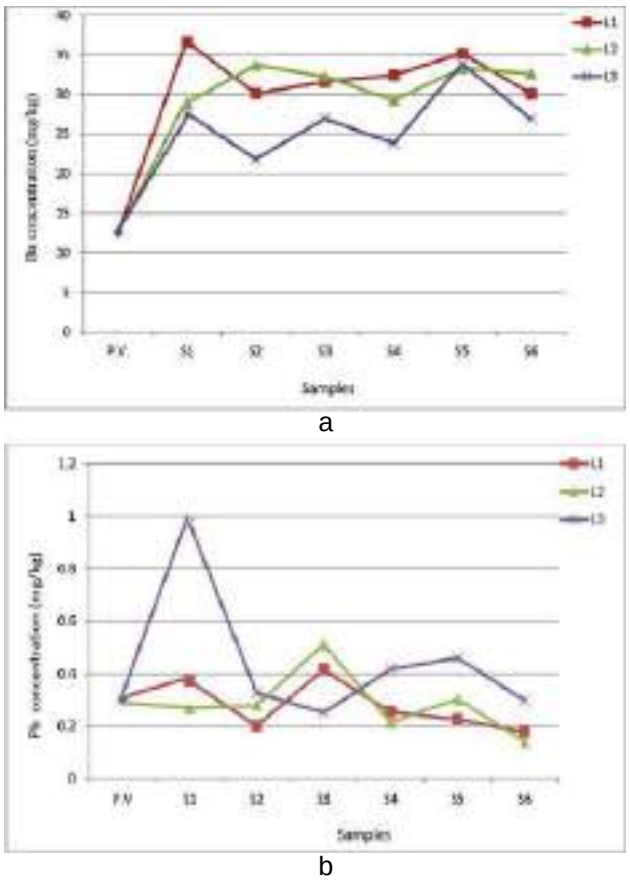

Fig. 2 **a** Comparison of Ba levels with WHO/FAO permissible values in all samples in three locations. **b** Comparison of Pb levels with WHO/FAO permissible values in all samples in three locations. P.V. = permissible values; L_1 = Kusumapuram; L_2 = Varaka; L_3 = Borivanka

Conclusion

In this study we analyzed 18 vegetable samples in 3 locations (villages), six vegetables in each for trace elemental levels. In all the three villages, Ba and Pb are in high concentrations. Fe and Ag are in high concentration in one sample each, and their excessive consumption may influence the functioning of kidneys [18–23]. On an average lead concentrations are 1.28 times higher and Ba is 2.51 times higher than the permissible values in the tested locations (Table 3).

These high concentrations of elements in the studied vegetable samples may be absorbed from soil and groundwater (naturally present in some locations) or may be due to usage of chemical pesticides and fertilizers. The study reveals that the extent of trace elements in local vegetables may enhance the risk of disease intensity, by consuming these vegetables frequently, and further research is to be needed in this area to find out the cumulative or additive affects of soil, groundwater, and local plant edibles and or a single exact reason for CKD in Uddanam area. Among the three locations, average Ba and Pb concentrations are more (Fig. 2a, b) in Borivanka (L_3), followed by Varaka (L_2) and Kusumapuram (L_1), and it reflects with the CKD patient intensity.

The studies on soil, groundwater, and all local plant edibles will help in understanding the serological, urological, nutritional, and genetic studies of the CKD. The present study opens a new dimension to understand the role of trace elements behind the CKD by analyzing the trace elemental analysis of all local frequently consumed plant edible parts coupled with soil and irrigation water analysis. The studies [2, 3, 16] on soil and groundwater in Uddanam area reveal that Fe, Mn, Cu, and Zn metals are in high concentration. Providing safe water to drinking, establishing more dialysis centers, and giving pensions to patients affected by CKD are a huge financial burden for governments in many areas where CKD is prevalent. This can be reduced by taking studies on the irrigation soils, irrigation water, and all edible local plants. The present study opens a new dimension to understand the impact of trace elements and heavy metals on CKD by analyzing the trace element and heavy metal content of all commonly consumed plant parts of local food crops along with soil and groundwater.

Acknowledgements The authors are thankful to The Director, Center for Studies on Bay of Bengal (CSBoB), Andhra University, Visakhapatnam, for giving permission to use ICP-MS facility to carry out this work.

Author Contribution The following are the contributions of the authors:

1. Design of the study, sample collection, experimentation, acquisition, analysis, interpretation of data, and drafting the manuscript: Narayana Murthy Gorle.

2. Conception, revising the manuscript, and evaluation of the data for important intellectual content: Balarama Swamy Yadav Padala.

Data Availability The ICP-MS instrument we used is available at the Center for Studies on Bay of Bengal, Andhra University, Visakhapatnam, India. The data of our experimentation can be accessed from there and the plant samples are collected from the study area.

Declarations

Conflict of Interest The authors declare no competing interests.

References

1. WHO (2007) Health risks of heavy metals from long-range transboundary air pollution. WHO Regional Office for Europe, Copenhagen. https://apps.who.int/iris/bitstream/handle/10665/107872/9789289071796-eng.pdf?sequence=1. Accessed 01 Feb 2022
2. Tatapudi RR, Rentala S, Gullipalli P, Komarraju AL, Singh AK, Tatapudi VS, Goru KB, Bhimarasetty DM, Narni H (2018) High prevalence of CKD of unknown etiology in Uddanam. India Kidney Int Repo 4(3):380–389. https://doi.org/10.1016/j.ekir.2018.10.006
3. Praveen Gadde, Suresh Sanikommu, Ramesh Manumanthu, Anitha Akkaloori (2020) Uddanam nephropathy in India: a challenge for epidemiologists. Bulletin of the World Health Organization 95:848–849. https://www.ncbi.nlm.nih.gov/pmc/articles/PMC5710086/. Accessed 10 Jun 2022
4. Raju TP, Giridhar Babu N, Srinivasu Ch Ch, Lakshmana Das N (2015) Trace elemental analysis of rice samples from kidney effected area using EDXRF technique. International Journal of Science and Research 4:1062–1066. https://www.ijsr.net/get_abstract.php?paper_id=SUB151409. Accessed 10 Jun 2022
5. Raju TP, Giridhar Babu N, Srinivasu Ch Ch, Ramanamam V, Ravi Shankar MS, Ram SS, Sudarshan M, Lakshmi Narayana PV, Lakshmana Das N (2016) Trace elemental analysis of finger millet samples from kidney effected area using EDXRF technique. International Journal of Scientific Research in Science, Engineering and Technology 2:174–178. https://ijsrset.com/IJSRSET162132. Accessed 10 Jun 2022
6. Satyanarayana G, Ramadasu P, Padmavathi Devi P, Prasad NVBSS, Nageswara Rao G (2017) Ground water quality assessment in Uddanam region, Costal Srikakulam, Andhra Pradesh, India. Int J Pharm Drug Anal 4:116–128. https://www.ijpda.com/index.php/journal/article/view/277. Accessed 10 Jun 2022
7. Satyanarayana G, Ramadasu P, Padmavathi Devi P, Prasad NVBSS, Nageswara Rao G (2017) Ground water quality interpretation in coastal Srikakulam, Andhra Pradesh by principal component analysis. Int J Chem Stud 5:80–85. https://www.researchgate.net/publication/324719247_Ground_water_quality_interpretation_in_coastal_Srikakulam_Andhra_Pradesh_by_using_principal_component_analysis. Accessed 10 Jun 2022
8. Kasoju Aruna, Munawar T (2019) Heavy metals analysis in soil and water samples of small villages of North Coastal, Uddanam Mandal, Andhra Pradesh, India, causing chronic kidney disease. Asian J Res Chem Pharm Sci 7:363–366. https://www.researchgate.net/publication/335569049_heavey_metals_analysis_in_soil_and_water_samples_of_small_villages_of_north_coastal_uddanam_mandal_andhra_pradesh_india_causing_chronic_kidney_disease. Accessed 10 Jun 2022
9. Khandare AL, Reddy YS, Balakrishna N, Rao GS, Gangadhar T, Arlappa N (2015) Role of drinking water with high silica and strontium in chronic kidney disease: an exploratory community-based study in an Indian village. Indian J Community Health 27:95–102. https://www.iapsmupuk.org/journal/index.php/IJCH/article/view/539. Accessed 10 Jun 2022
10. Lal K, Sehgal M, Gupta V, Sharma A, John O, Gummidi B, Jha V, Kumari A (2020) Assessment of groundwater quality of CKDu affected Uddanam region in Srikakulam district and across Andhra Pradesh. India. Groundw Sustain Dev 11:100432. https://doi.org/10.1016/j.gsd.2020.100432
11. Gowrishankar S, Koshy P, Mathew M, Gopalakrishnan N, Kumar VS, Abraham G (2020) Pathology of Uddanam endemic nephropathy. Indian J Nephrol 30(4):253–255. https://doi.org/10.4103/ijn.IJN_363_18
12. Banerjee D, Bairagi, Himadri, Mukhopadhyay S, Pal A, Bera, Debabrata, Ray Lalitagauri (2010) Heavy metal contamination in fruits and vegetables in two districts of West Bengal, India. Electron J Environ, Agric Food Chem 9:1423–1432. https://www.researchgate.net/publication/215565989_Heavy_metal_contamination_in_fruits_and_vegetables_in_two_districts_of_West_Bengal_India. Accessed 15 Jun 2022
13. Mamatha P, Salamma S, Swamy AVN, Ravi Prasad Rao B (2014) Quantitative and risk analysis of heavy metals in selected leafy vegetables. Der Pharma Chemica 6:179–185. https://www.derpharmachemica.com/pharma-chemica/quantitative-and-risk-analysis-of-heavy-metals-in-selected-leafy-vegetables.pdf. Accessed 15 Jun 2022
14. Priya E, Sunil G, Shivaiah K, Anil Gaddameedi, Ashish Kumar (2014) Extent of heavy metal contamination in leafy vegetables, soil and water from surrounding of Musi River, Hyderabad, India. J Ind Pollut Control 30(2):289–293. https://www.researchgate.net/publication/271823133_Extent_of_heavy_metal_contamination_in_leafy_vegetables_soil_and_water_from_surrounding_of_Musi_River_Hyderabad_India. Accessed 15 Jun 2022
15. Sapana Gupta, Jena V, Jena S, Neda Davic, Natalija Matic, Radojevic D, Solanki JS (2013) Assessment of heavy metal contents of green leafy vegetables. Croatian J Food Sci Technol 5:53–60. https://www.bib.irb.hr/1016071/download/1016071.B_Croatian_Journal_food_of_Science_and_Technology_MANUSCRIPT_GUPTA_5.pdf. Accessed 15 Jun 2022
16. Cockwell P, Fisher L-A (2020) The global burden of chronic kidney disease. The Lancet 395(10225):662–664. https://doi.org/10.1016/S0140-6736(19)32977-0
17. Pequerul, A., Pérez, C., Madero, P., Val, J., Monge, E. (1993) A rapid wet digestion method for plant analysis. In: Fragoso, M.A.C., Van Beusichem, M.L., Houwers, A. (eds) Optimization of Plant Nutrition. Developments in Plant and Soil Sciences, vol 53. Springer, Dordrecht. https://doi.org/10.1007/978-94-017-2496-8_1
18. FAO/WHO (CXS 193–1995) Codex Alimentarius, General standard for contaminants and toxins in food and feed (CXS 193–1995), https//doi.CXS 193–1995
19. Toxicological profile for silver. Agency for Toxic Substances and Disease Registry, U.S. Public Health Service. 1990:8–18. https://www.atsdr.cdc.gov/toxprofiles/tp146.pdf. Accessed 12 Jul 2022
20. Drake PL, Hazelwood KJ (2005) Exposure-related health effects of silver and silver compounds: a review. Ann Occup Hyg 49(7):575–585. https://doi.org/10.1093/annhyg/mei019
21. Provisional peer reviewed toxicity values for Lithium (CASRN 7439–93–2). Superfund Health Risk Technical Support Center, National Center for Environmental Assessment: Office of

Research and Development. U.S. Environmental Protection Agency, Cincinnati, OH, 45268; 2008:4–7. https://cfpub.epa.gov/ncea/pprtv/documents/Lithium.pdf. Accessed 18 Jul 2022
22. Codex Alimentarius Commission (2016) Joint FAO/WHO Food Standards Programme. Codex Committee on contaminants in Foods. 10th Session Rotterdam, The Netherlands 4-8 April 2016; Working document for information and use in Discussions related to Contaminants and Toxins in the GSCTFF (Prepared by Japan and The Netherlands), pp 1–150. https://CF/10INF/1
23. Choudhury, Harlal, Cary, Richard, World Health Organization & International Programme on Chemical Safety. (2001). Barium and barium compounds. World Health Organization. https://apps.who.int/iris/handle/10665/42398. Accessed 13 Jul 2022
24. Food Safety and Standards (contaminants, toxins and residues) regulations, (2011). https://www.fssai.gov.in/upload/uploadfiles/files/Compendium_Contaminants_Regulations_20_08_2020.pdf. Accessed 27 Jul 2022
25. Adeloju SB, Bond AM, Briggs MH (1985) Multielement determination in biological materials by differential pulse voltammetry. Anal Chem 57(7):1386–1390. https://doi.org/10.1021/ac00284a046
26. Pragst F, Stieglitz K, Runge H, Runow K-D, Quig D, Osborne R, Runge C, Ariki J (2017) High concentrations of lead and barium in hair of the rural population caused by water pollution in the Thar Jath oilfields in South Sudan. Forensic Sci Int 274:99–106. https://doi.org/10.1016/j.forsciint.2016.12.022
27. Peana M, Medici S, Dadar M, Antonietta Zoroddu M, Pulicelli A, Christos T, Bjorklund G (2021) Environmental barium: potential exposure and health-hazards. Arch Toxicol 95:2605–2612. https://doi.org/10.1007/s00204-021-03049-5

Journal of Food Composition and Analysis 126 (2024) 105868

Contents lists available at ScienceDirect

Journal of Food Composition and Analysis

journal homepage: www.elsevier.com/locate/jfca

Elemental levels in frequently consumed local leafy vegetables from three villages with chronic kidney disease prevalence

G. Narayana Murthy, P. Balarama Swamy Yadav *

Department of Botany, Andhra University, Visakhapatnam 530003, Andhra Pradesh, India

ARTICLE INFO

Keywords:
ICP-MS
Uddanam area
Trace elements
Heavy metals
Pesticides
Fertilizers

ABSTRACT

Studies on elemental levels in frequently consumed local edibles in any region with a localized disease are meaningful. The present study has identified the levels of 24 elements in nine (6 cultivated and 3 wild) frequently consumed local leafy vegetables from three chronic kidney disease prevalent villages (a total 27samples) using ICP-MS. The comparison of obtained levels of these elements with WHO/FAO permissible values reveals the levels of Ba in all the tested samples, Pb in 15 samples is in excess, whereas Fe and Zn levels are below the required levels, and the other elements are in the permissible levels. Among the 27 tested samples, a high level of Ba was found in *Allium cepa* of L_3, and Pb was in *Amaranthus viridis* of L_2. Among the leafy vegetables *Allium cepa* from L_3 and *Amaranthus viridis* from L_2 showed high levels of Ba and Pb, respectively. In the three locations studied, average Ba and Pb levels are found more in Borivanka (L_3) followed by Kusumapuram (L_1) and Varaka (L_2). Ba levels are excess in both cultivated and wild leafy vegetables, while Pb levels are slightly higher in cultivated than the wild leafy vegetables, which may be due to the usage of chemical pesticides and fertilizers. The present study signifies that frequent consumption of such leafy vegetables may influence the renal functioning in this area, along with other factors like drinking water, other edibles.

1. Introduction

The biological, chemical and physical properties of soil, water and air are generally localized and dynamic. They influence health that could result in any localized diseases in humans and all other organisms by means of edibles also. Any one, two, or all of these may cause diseases like Fluorosis, Goiter, Osteoporosis, Thyroid, etc. due to the excess or low levels of elements in water, soil, air and edibles. Studies on the elemental levels of local plant edibles in any region with a regional disease are of great relevance to find out the solution. Uddanam is one such area in Srikakulam District, Andhra Pradesh, India known for its high prevalence of Chronic Kidney Disease (Gadde et al., 2017; Tatapudi et al., 2018). Thousands of people are still suffering from this disease, and the cause(s) are still unclear. The problem of CKD is not only confined to the Uddanam area; it is also a global issue, affecting 697.5 million people in the world, amongst them 115.1 million are Indians (Cockwell and Fisher, 2020).

The World Health Organization (WHO) has identified the Uddanam area, along with two other regions (one in Sri Lanka and the other in Nicaragua), as having a high incidence of CKD (Ganguli, 2016). This phenomenon was discussed at the International Congress of Nephrology in Hong Kong (2013) and named Uddanam Nephropathy (Gadde et al., 2017). Hence in 2016, the Indian Council for Medical Research joined with Harvard University, Bhabha Atomic Research Center, Mumbai, and Andhra Medical College, Visakhapatnam, to explore the cause(s) of CKD in this area.In the early 1990 s, kidney diseases were identified in the Uddanam area and in 2015, an estimated 4500 deathsand about 34,000 people were affected over the last decade (Tatapudi et al., 2018). Nearly every family in this area has been impacted by this disease (Ganguli, 2016).

Among the different fields of study to know the reasons for CKD in this area, the identification of elemental levels in edible plant parts is one of the important directions which are not much explored except on rice and finger millet using the EDXRF technique, indicate both have excess levels of Cu and Zn, and also excess levels of P and Se in rice and finger millet (Raju et al., 2015, 2016), respectively. Cu, Cr, Fe, and Pb levels are reported high in leafy vegetable Sorrel (*Rumex* sps.) from the Musi River basin of Hyderabad (Swapna Priya et al., 2014), and Cd and Pb were found more in leafy vegetables from Pulivendula town, YSR Kadapa district of Andhra Pradesh, India (Mamatha et al., 2014). Pb was

* Corresponding author.
E-mail address: dr.pbsyadav@andhrauniversity.edu.in (P.B.S. Yadav).

https://doi.org/10.1016/j.jfca.2023.105868
Received 24 September 2023; Received in revised form 25 November 2023; Accepted 26 November 2023
Available online 28 November 2023

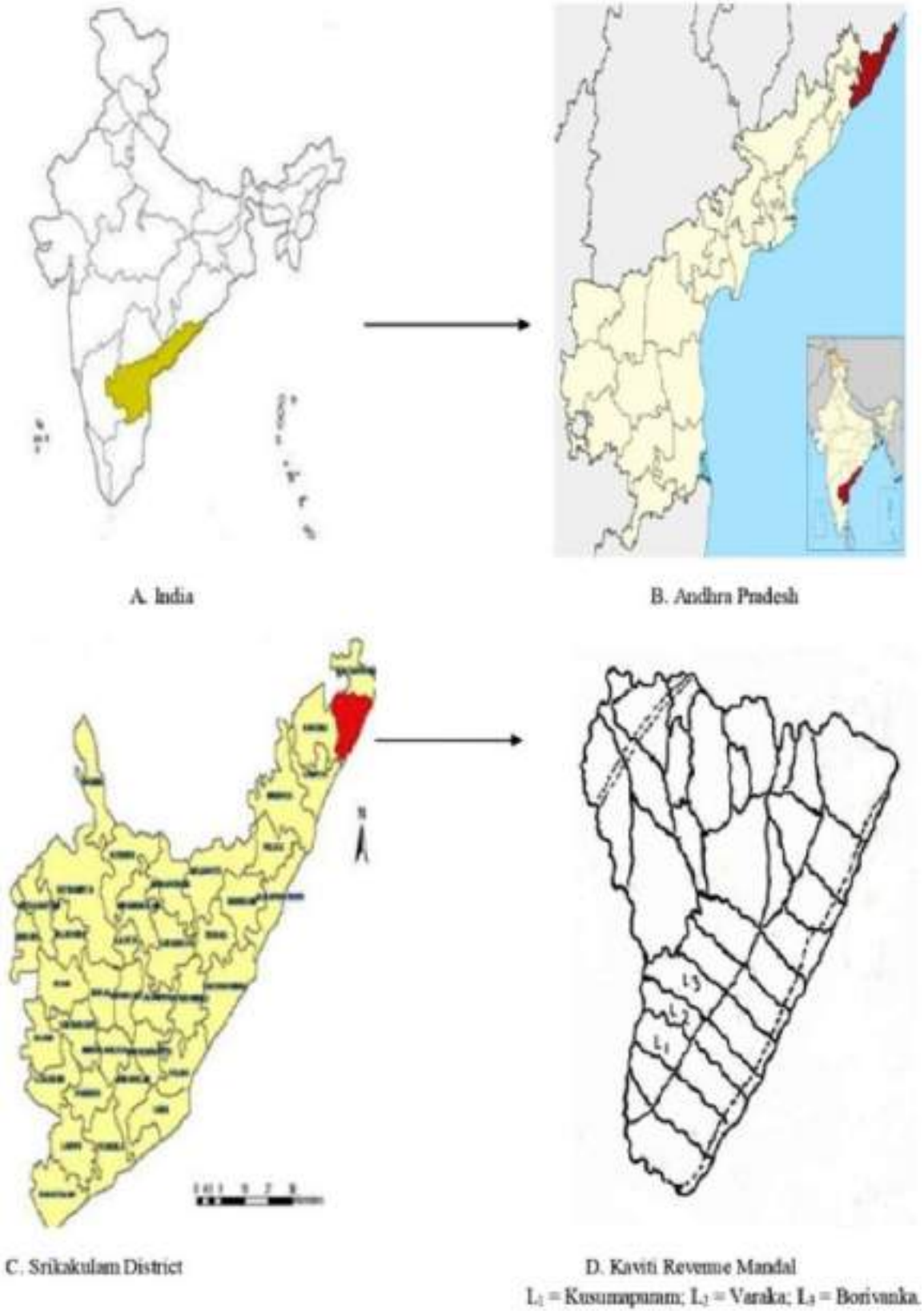

Fig. 1. Area of the study.

Table 1
List of frequently consumed local Leafy Vegetable samples tested for Elemental levels.

Sample No.	Botanical Name	Family	English name	Vernacular (Telugu) name	Vegetable type
S_1	*Allium cepa*L.	Liliaceae	Onion (young bulb with centric leaves)	Ulli koora	Cultivated
S_2	*Alternantherasessilis*(L.)R. Br*ex* DC	Amaranthaceae	————	Ponnagantikoora	Wild
S_3	*Amaranthusviridis*L.	Amaranthaceae	Amaranth	Thotakoora	Cultivated
S_4	*Basella alba* L.	Basellaceae	Malabar Spinach	Bachalikoora	〃
S_5	*Hibiscus cannabinus*L.	Malvaceae	Sorrel/Kenaf	Gongoora	〃
S_6	*Moringaoliefera*Lam.	Moringaceae	Drumstick (leaves)	Munagaakulakoora	〃
S_7	*Murrayakoenigii*(L.) Sprenge	Rutaceae	Curry leaf	Karivepaku	〃
S_8	*Premnalatifolia*Roxb.	Verbanaceae	————	Nellikoora	Wild
S_9	*Randia aculeate* L.	Rubiaceae	————	Balusukoora	〃

Table 2
Conditions and Parameters of the used ICP-MS (Agilent Technologies Model 7700) instrument.

Sl. No	Parameter	Conditions/Values
1	RF Power	1550 W
2	Sampling depth	8.0 mm
3	Carrier gas flow rate	0.95 L min^{-1}
4	Makeup gas	0.20 L min^{-1}
5	Spray chamber temperature	2^0C
6	Collision gas	He, 3.4 mL min^{-1} (99.999% purity)
7	Water filter	$<$ 100 μm particle size
8	Elements/ Isotopes measured	^{7}Li,^{9}Be,^{27}Al,^{45}Sc,^{51}V,^{52}Cr,^{55}Mn,^{56}Fe,^{59}Co,^{60}Ni,^{63}Cu,^{66}Zn,^{71}Ga,^{75}As,^{78}Se,^{85}Rb,^{88}Sr,^{107}Ag,^{111}Cd,^{133}Cs,^{137}Ba,^{205}TI,^{208}Pb, and^{238}U

found in excess in fruits and vegetables from Kolkata and South 24 Parganas (Banerjee et al., 2010); Cr, Zn Cu, and Pb are high in leafy vegetables from Raipur city (Gupta et al., 2013). The above studies reveal that plants accumulate elementsat excessive levels in their edible parts as well.The role of environmental Ba and its potential health effects including kidney diseases were reviewed (Peana et al. 2021). The levels of Cr, Zn, Ni, Cd, Cu, Pb, and As were identified in leafy vegetables amaranth and spinach (Zhou et al., 2016; Sobur Ahmed et al., 2022). Elemental levels of Cr, Zn, Ni, Cd, and Fe were reported in amaranth (Affum et al., 2020).

WHO (1973) categorized the trace elements into three distinct groups: i. Essential (Zn, Cu, Se, Cr, Co, I, Mn, Mo, Fe, B, etc.), ii. Probably essential (Cr, Ni, Se, Va, F, etc.), and iii. Toxic (Ag, As, Cd, Hg, Ni, Pb, etc). There are no previous attempts on elemental levelsin all the frequently consumed local leafy vegetables in Uddanam area; hence, the present study is takenup, which is an attempt to explore one of the causes of CKD, a local chronic health problem over decades, by knowing the levels of 24 elements to contribute something in understanding the reasons for CKD.

2. Materials and methods

2.1. Study area

Uddanam is a region comprises some villages of seven Revenue Mandals or Tahasils, i.e., Ichapuram, Kanchili, Kaviti, Mandasa, Palasa, Sompeta, and Vajrapukotturu in the Srikakulam District of Andhra Pradesh State in India. It is located at 19.0167° N and 84.6833° E and has an average elevation of 41 m above the mean sea level (Fig. 1). It is dotted with lush coconut and cashew nut orchards along the coast of the Bay of Bengal. Among the seven Mandals, Kaviti, has a high prevalence of CKD. Based on the data on the number of CKD patients, obtained from the Community Hospital, Sompeta, three adjacent villages, i.e., Kusumapuram (L_1), Varaka (L_2), and Borivanka (L_3), (Fig. 1) in Kaviti mandal have been chosen for the present study.

2.2. Collection and preparation of samples

We identified nine frequently consumed local leafy vegetables, and the details are given in Table 1. Fresh leafy vegetable samples are collected from the fields in the three adjacent villages (3 Locations) in Zip-locked bags and brought to the laboratory. The samples are washed twice with distilled water, then they are subjected to fast and accurate open wet digestion by hot plate method (Pequerul et al., 1993) to digest all the organic material in the samples.

2.3. Methodology

The ICP-MS instrument (Agilent Technologies Model 7700) available at the Centre for Studies on Bay of Bengal, Andhra University, Visakhapatnam, is used to obtain the elemental levels, and its conditions and parameters are mentioned in Table 2. The ICP-MS converts complexes and/or residuals into ionomic form because of the high temperature (>6000 °C), which enables an accurate estimation of the concentration of each element. The ICP-MS instrument we used can measure the elemental levels in four Standards i.e., Standard-1, 2 A, 3, and 4 at parts per billion level.

Under Standard-1, the elemental levels of 16 (Ce, Dy, Er, Eu, Gd, Ho, La, Lu, Nd, Pr, Sc, Sm, Tb, Tm, Y, and Yb), in Standard-3, 10 (Sb, Au, Hf, Ir, Pd, Pt, Rh, Ru, Te, and Sn) and in Standard-4, 12 (B, Ge, Mo, Nb, P, Re, S, Si, Ta, Ti, W, and Zr) can measure simultaneously, which are present in very small quantities in biological samples. Under standard-2A, the levels of 24 (Ag, Al, As, Ba, Be, Cd, Co, Cr, Cs, Cu, Fe, Ga, Li, Mn, Ni, Pb, Rb, Sc, Se, Sr, TI, U, V, and Zn.) elements can be measured simultaneously. Most of these are abundantly present in Earth's crust and in biological samples and also are very essential for the growth and development. The presence of either excess or low levels of these elements can lead to various health problems in humans. Hence, we have chosen the Standard-2A to findout the levels of these 24 elements.

2.4. Wet digestion

The improved HNO_3/H_2O_2 wet digestion method (Pequerul et al., 1993) was followed for the Plant sample preparation. 2 g of the plant sample was taken and placed in Teflon beakers, to which 8 mL of HNO_3 was added and left overnight. The solution was then heated on a hot plate at 120–125 °C for one hour, with one or two additions of 4 mL of H_2O_2 (33%) was continued until the solution became clear or colorless,

Table 3
Elemental levels (in mg kg^{-1}) in all tested samples from the three locations.

Element		Li	Be	Al	Sc	V	Cr	Mn	Fe	Co	Ni	Cu	Zn
P.V.		5.6	8.4	60	22	50	2.4	15	50	0.14	5.0	3.5	50
S_1	L_1	0.02	0	6.28	5.42	0.01	0.48	1.11	4.45	0.004	0.21	0	5.18
	L_2	0.01	0	10.82	3.94	0.02	0.39	0.96	6.63	0.01	0.44	0.22	5.41
	L_3	0.11	0	12.9	17.23	0.02	0.92	11.06	21.25	0.07	5.46#	5.53#	33.65
S_2	L_1	0.02	0	8.21	4.87	0.02	0.51	7.46	8.75	0.02	0.24	0.13	8.44
	L_2	0.00	0	62.45*	3.22	0.02	0.46	0.85	16.09	0.01	0.19	0.19	4.12
	L_3	0.03	0	11.42	6.78	0.04	0.59	12.04	14.58	0.02	0.35	0.24	11.49
S_3	L_1	0.02	0	13.27	10.24	0.04	0.61	3.92	12.08	0.03	0.42	3.25	21.19
	L_2	0.03	0	36.79	3.36	0.04	0.54	3.82	19.00	0.06	0.34	1.45	8.51
	L_3	0.02	0	51.00	6.58	0.04	0.62	4.02	27.79	0.03	0.33	0.20	8.58
S_4	L_1	0.02	0	14.76	4.89	0.03	0.49	1.33	16.58	0.03	0.41	0.08	6.30
	L_2	0.01	0	37.15	4.01	0.02	0.45	1.37	20.13	0.01	0.51	0.22	5.66
	L_3	0.02	0	6.20	4.97	0.01	0.50	0.46	5.04	0.005	0.23	0.11	5.47
S_5	L_1	0.03	0	12.58	5.12	0.04	0.49	32.95#	18.16	0.06	0.65	0.27	10.83
	L_2	0.02	0	11.28	4.03	0.03	0.61	11.92	12.57	0.06	0.51	0.91	7.25
	L_3	0.03	0	39.59	9.89	0.07	0.67	27.68#	40.69	0.05	0.54	0.27	9.08
S_6	L_1	0.03	0	19.77	5.24	0.07	0.75	5.91	35.39	0.02	0.27	0	6.48
	L_2	0.03	0	5.74	4.65	0.01	0.31	13.15	5.21	0.01	0.29	0.73	6.18
	L_3	0.05	0	122.5*	6.33	0.02	0.46	1.52	13.32	0.01	0.41	0.27	8.82
S_7	L_1	0.05	0	12.78	5.86	0.03	0.49	2.57	15.37	0.01	0.76	0.89	9.45
	L_2	0.01	0	10.34	4.79	0.02	0.43	5.83	9.72	0.03	1.79	1.33	14.01
	L_3	0.11	0	16.21	7.71	0.04	0.74	4.65	24.27	0.02	0.68	0.78	8.68
S_8	L_1	0.05	0	7.64	5.10	0.02	0.46	15.67#	21.02	0.06	0.66	0.40	6.59
	L_2	0.02	0	11.67	4.21	0.03	0.44	8.50	15.73	0.03	0.49	0.47	8.91
	L_3	0.03	0	17.22	7.07	0.04	0.60	3.30	23.63	0.04	0.55	0.32	9.81
S_9	L_1	0.21	0	11.42	5.19	0.03	0.48	18.82#	16.07	0.02	0.45	0.40	7.03
	L_2	0.02	0	6.64	3.32	0.01	0.48	0.53	5.47	0.00	0.27	0.16	6.15
	L_3	0.04	0	13.20	6.11	0.04	0.62	34.63#	14.92	0.04	0.63	0.32	9.99

Element		Ga	As	Se	Rb	Sr	Ag	Cd	Cs	Ba	Tl	Pb	U
P.V.		3.0	0.18	1.5	5.0	10	0.175	1.5	90	12.6	1.5	0.3	7
S_1	L_1	0	0	0.01	0.28	2.15	0.01	0	0	33.19*	0	0.14	0
	L_2	0	0	0.	0.32	0.77	0.03	0	0	32.97*	0	0.28	0
	L_3	0.01	0.01	0.12	4.67	1.34	0.29	0.05	0	71.54*	0	1.00*	0
S_2	L_1	0	0	0.01	1.17	3.59	0.02	0	0	33.22*	0	0.32*	0
	L_2	0	0	0.54	0.49	4.22	0	0.01	0	28.92*	0	0.26	0
	L_3	0	0.01	0.03	1.45	4.85	0.16	0.03	0	33.86*	0	0.77*	0
S_3	L_1	0	0.02	0.01	3.72	6.28	0.02	0.02	0	35.21*	0	0.22	0
	L_2	0	0	0.01	1.16	2.76	0.10	0.03	0	30.27*	0	1.14*	0
	L_3	0	0.01	0.03	0.97	3.68	0.05	0.02	0	28.61*	0	0.61*	0
S_4	L_1	0	0	0.02	1.07	1.36	0.06	0.01	0	24.57*	0	0.33*	0
	L_2	0	0	0	0.64	0.81	0.08	0.01	0	30.24*	0	0.31*	0
	L_3	0	0	0.01	0.66	0.58	0.07	0.01	0	31.55*	0	0.29	0
S_5	L_1	0	0.01	0.01	0.28	3.99	0.02	0.01	0	35.95*	0	0.28	0
	L_2	0	0.01	0.06	0.39	1.86	0.03	0.01	0	38.81*	0	0.27	0
	L_3	0.01	0.01	0.08	0.25	2.41	0.03	0.02	0	26.86*	0	0.37*	0
S_6	L_1	0	0.01	0.08	0.71	3.19	0.02	0	0	34.07*	0	0.65*	0
	L_2	0	0	0.01	2.05	2.76	0.02	0.01	0	27.00*	0	0.18	0
	L_3	0	0.01	0.12	1.46	1.03	0.10	0.02	0	32.19*	0	0.38*	0
S_7	L_1	0	0	0.01	1.05	5.60	0.04	0.01	0	38.56*	0	0.30*	0
	L_2	0	0	0.22	5.09	0.89	0.05	0.01	0	32.63*	0	0.32*	0
	L_3	0.06	0.01	0.09	1.43	5.82	0.07	0.01	0	35.27*	0	0.31*	0
S_8	L_1	0	0.01	0.01	0.66	2.05	0.06	0	0	30.07*	0	0.25	0
	L_2	0	0	0.01	1.54	1.19	0.03	0.01	0	37.59*	0	0.36*	0
	L_3	0	0.01	0.03	2.10	0.85	0.05	0.01	0	42.21*	0	0.28	0
S_9	L_1	0	0.01	0.01	1.35	4.18	0.04	0.01	0	36.41*	0	0.25	0
	L_2	0	0	0	0.47	0.58	0.12	0	0	32.63*	0	0.14	0
	L_3	0	0.01	0.03	2.32	0.99	0.04	0.03	0	39.33*	0	0.51*	0

S1-S9: Samples 1–9; P.V.: Permissible Values (mg kg-1) of FAO/WHO
L_1 (Location1) = Kusumapuram, L2 (Location2) = Varaka, L3 (Location 3) = Borivanka
* Element harmful to kidney if more than the FAO/WHO Values
# Element causes other health problems if more than the FAO/WHO Values

indicating the complete digestion of organic material in the plant sample. The solution was then kept at 80 °C for 10–15 min. After cooling to room temperature, it was shaken well and filtered through Whatman filter paper. The filtrate solution was diluted with ultrapure water to a fifty-dilution factor, and stored in 100 mL high-density poly ethylene bottles for elemental analysis.

The instrument was calibrated using certified reference materials (CRM) at 0, 0.5, 1, 5, 10, 25, 50, and 100 μg kg^{-1} concentrations prior to running the samples. After calibrating (Calibration values are given in table 5 and supplied as supplementary information) the ICP-MS instrument with CRM, we ran the samples and obtained the levels of 24 (Li, Be, Al, Sc, V, Cr, Mn, Fe, Co, Ni, Cu, Zn, Ga, As, Se, Rb, Sr, Ag, Cd, Cs, Ba, Ti, Rb, and U) elements. 10 mL of filtrate solution was taken, and 20 μL of ISTD (Internal Standard Spiking Solution) solution and 100 μL of HNO_3 were added in a centrifuge tube. The levels of elements in each sample of each location were measured using the following formula in μg kg^{-1} level and then converted to mg kg^{-1} level.

$$X(\mu g) = \frac{IR(S)-IR(B)}{\text{Weight of the Sample(g)}} \times \text{Dilution Factor}$$

Where; X (μg) = concentration of element in μg kg^{-1}, I R(S)

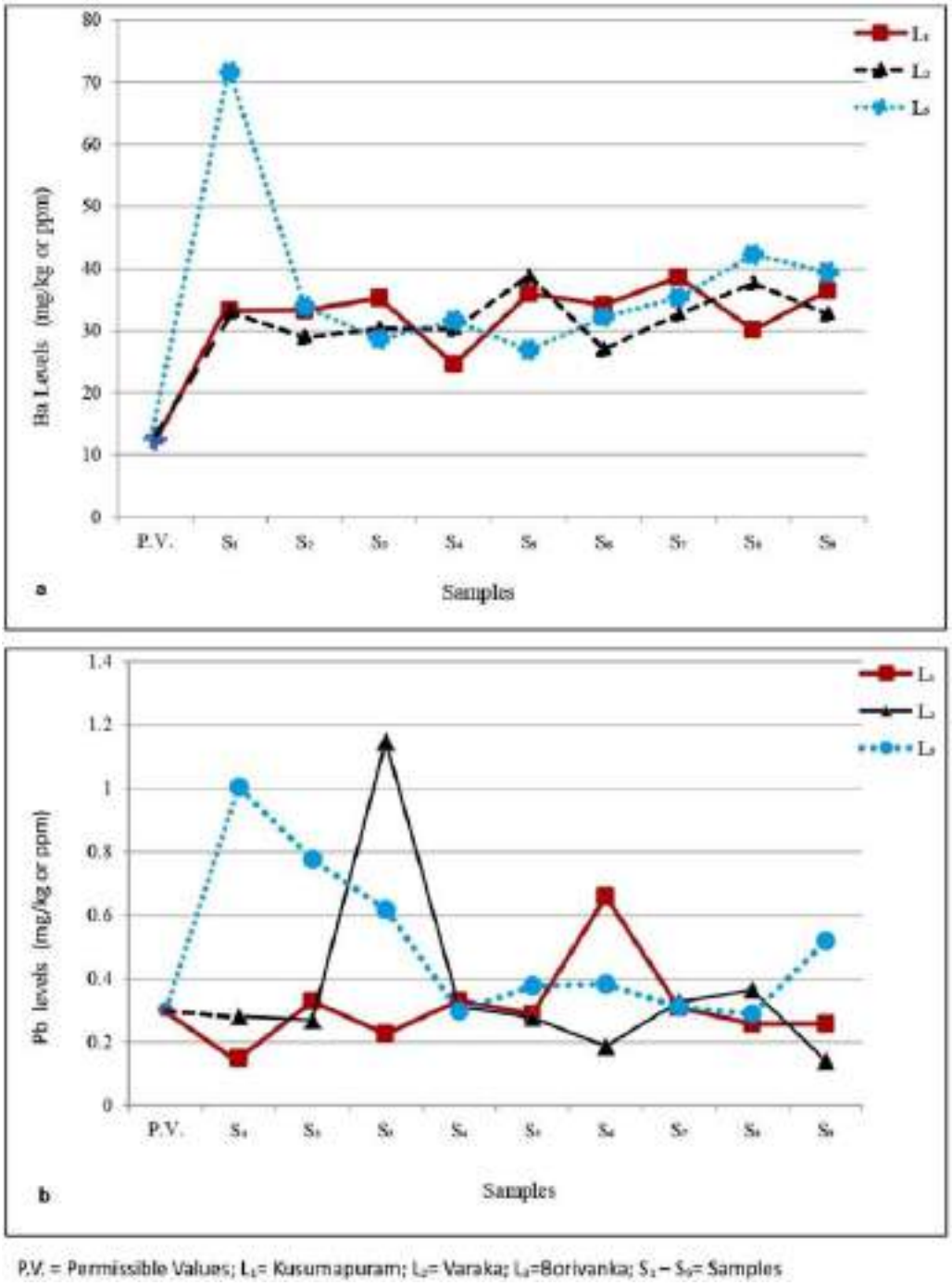

Fig. 2. a & b. Comparison of Ba and Pb levels with WHO/FAO Permissible Values in three locations.

= instrument reading for plant sample, I R (B) = instrument reading for blank.

3. Results and discussion

3.1. Results

The obtained levels of 24 elements in 9 local leafy vegetables from 3 different locations, (a total 27 samples) are presented in Table 3, and compared with the FAO/WHO permissible values (FAO/WHO, 1997; Choudhury and Cary, 2001; and Food Safety and Standards (contaminants, toxins and residues) Regulations, 2011). The results reveal that in all the tested samples Ba levels are excess and Pb levels are excess in 15 samples (7 from L_3, each 4 from L_2 and L_1) than the permissible values (FAO/WHO, CXS 193–1995) (S_1-L_3, S_2-L_1, L_3, S_3-L_2,L_3, S_4-L_1,L_2, S_5-L_3, S_6-L_1,L_3, S_7-L_1,L_2,L_3, S_8-L_2, S_9-L_3). It is observed that Pb levels are more in L_3 than L_2 and L_1. It is high in 77.77% samples of L_3, and 44.44% in L_2 and L_1. So, Pb levels are present in the following manner $L_3 > L_2 > L_1$. The results reveal that there is a strong correlation, reflecting with the CKD patient number. The National Institute of Nutrition (NIN, 2011) in Hyderabad, India, recommends a minimum intake of Zn of 10–15 mg/day and Fe of 21–45 mg/day for adults in India. In 22 plant samples, Zn is at a low level (S_1- L_1, L_2, S_2- L_1, L_2, S_3- L_2, L_3, S_4- L_1, L_2, L_3, S_5-L_2, L_3, S_6- L_1, L_2, L_3, S_7- L_1, L_3, S_8- L_1, L_2, L_3 and S_9-L_1, L_2, L_3). Fe is at a low level in 20 samples (S_1- L_1, L2, S_2- L_1, L_2,L_3, S_3- L_1,L_2, S_4- L_1, L_2, L_3, S_5-L_1,L_2, S_6- L_2,L_3, S_7- L_1,L_2, S_8- L_2 and S_9-L_1,L_2,L_3) than the minimum

Table 4
LOD and LOQ Data of the elements determined by ICP-MS.

Element	LOD (μg/L)	LOQ (μg/L)
Be	0.836	2.535
Al	1.004	3.042
V	0.845	2.560
Cr	0.890	2.697
Mn	0.873	2.645
Fe	1.400	4.243
Co	0.885	2.683
Ni	0.902	2.732
Cu	1.409	4.268
Zn	1.035	3.138
As	0.888	2.690
Se	0.907	2.747
Ag	0.797	2.415
Cd	0.869	2.633
Ba	0.909	2.753
Pb	0.862	2.612
U	0.855	2.592

required level.

Among the 27 tested samples a high level of Ba was found in *Allium cepa* of L_3 (71.54 mg kg^{-1} followed by *Premna latifolia* of L_3 (42.21 mg kg^{-1}) (Fig. 2a) and Pb was found in *Amaranthus viridis* of L_2, (1.14 mg kg^{-1}) followed by *Allium cepa* of L_3 (1.00 mg kg^{-1}) (Fig. 2b). In the three locations studied, the average excess levels of Ba and Pb elements are in Borivanka (L_3) village, followed by Varaka (L_2) and Kusumapuram (L_1). The present study reveal that the leafy vegetables used *Allium cepa* from L_3 and *Amaranthus viridis* from L_2 showed high levels of Ba (average- 45.9 mg kg^{-1}) and Pb (average- 0.65 mg kg^{-1}), respectively.

3.2. Discussion

Mineral ions and vitamins are crucial for human health; and leafy vegetables are rich sources of these nutrients. Plant based foods are good source of these than animal-based foods. However, excessive consumption of certain elements in foods, can lead to health problems; for example, excessive consumption of Palak (*Spinacia oleracea L.*) which is rich in Ca, results in stone formation in the kidneys. Moreover, heavy metals like Hg, Pb, Ba, etc. are toxic to humans (WHO, 2007), while trace elements like Zn, Cu, Fe, Se, etc. are essential. Zn deficiency may lead to renal dysfunction, Cu can impact collagen metabolism, Se protects the kidneys from oxidative stress, and Fe is vital for red blood cell production and proper kidney function.

The results of the present study are in line with the work done elsewhere on the globe. High levels of Lead (0.1–0.9 mg kg^{-1}) were found in green leafy vegetables in three selected local government areas in Osun State, Nigeria (Oyekanmi Adeyinka et al., 2014). High levels of various heavy metals (Fe, Zn, Mn, Cu, Pb, Cr, As, Cd, Hg, As, Ni, and Cd), were reported in water, soil, and crops in Hamadan, Iran (Ava Kharazi et al., 2021). High levels of heavy metals (Cu > Pb > Cd > As > Sn > Hg) were reported in spinach, lettuce, and parsley from various regions of Turkey by ICP-MS. Spinach had the high Cu (5.1 ± 0.3 mg kg^{-1}), lettuce, and parsely had high Pb content (0.106 ± 0.007 mg kg^{-1}) (Zor and Kocaoba, 2023).

Excess levels of Ba (average of 30.40 mg kg^{-1}) and Pb (average of 0.338 mg kg^{-1}) were found in frequently consumed local vegetable samples from the same study area, which is similar study (Murthy and Yadav, 2023). Dietary analysis in the Uddanam region, including rice, marine and fresh water fish, and amaranth, revealed that heavy metal intake exceeding safe levels for Pb, Cr, and Mn (Vidhu Gupta, et al., 2022). They suggested, to finding out heavy metal levels in other food items and vegetables in this region. Excess Ba levels were present in all 27 samples (average- 34.58 mg kg^{-1}), while Pb levels were excess in 15 samples (average- 0.38 mg kg^{-1}). The determination of limit of detection (LOD) and limit of quantification (LOQ) is very crucial for assessing the method's sensitivity; so, these are calculated and provided in Table 4. Additionally, the study revealed deficiency of Zn (81.48% samples) and Fe (74.07% samples) in the tested leafy vegetables. Low levels of Zn and Fe may impact kidney function; so, deficiencies can be fulfilled by incorporating foods rich in Zn and Fe, into the diet or by using supplements, especially if deficiencies are confirmed through serological or urological assessments.

It also reveals an important finding, that the wild leafy vegetables (S_2, S_8, and S_9) (a total of 9 samples), 55% exhibited high Pb levels, and 44% had low levels. In cultivated leafy vegetables (S_1, S_3, S_4, S_5, S_6, and S_7) (a total of 18 samples), 61% had high Pb levels, and 39% had low levels. It reveals that elemental levels are slightly higher in cultivated leafy vegetables than the wild, it is may be due to over usage of chemical fertilizers and pesticides.

4. Conclusions

The present study reveals that all samples exceed Ba by 2.74 times, and 15 samples contain elevated levels of Pb by 1.3 times, and Al is in two samples (L_2-S_2 and L_3-S_6) only, which may influence kidney function. It also found that excess amount of Mn in five samples and Ni in one sample which may cause health problems other than CKD, remaining elements are present within the permissible values. The inconsistency observed in elemental levels among and between the leafy vegetable samples and locations may be due to the nature of soil or groundwater or both. The excess Ba and Pb levels are likely due to absorption from natural sources or due to excessive usage of fertilizers and pesticides. Zn and Fe are found in low levels; so, along with other risk factors, consumption of such leafy vegetables may enhance renal problems. Further studies should focus on soil and groundwater analysis in relation to edibles and their consumption patterns like quantity, frequency, etc., to find out specific cause(s) of CKD in the Uddanam area.

In CKD-prevalence areas, there are financial burdens on local governments, such as providing healthcare facilities, safe drinking water, pensions, etc.; it can be reduced by conducting studies on the levels of elements in soil, groundwater, and all local edibles to understand their role in CKD. This study provides a new dimension by assessing 24 elements in all local leafy vegetables, and it suggests soil and water analysis, along with local edibles to find out exact reason for any localized disease like CKD. Such research can set an example for studying local edibles in areas with localized diseases worldwide. Analysing the elemental content of frequently consumed local plant edibles is essential for comprehending their role in CKD and other regional diseases in the world. Once the elemental levels are identified, consumption and accumulation patterns can be determined. This study is useful in future studies like knowing the elemental levels in plant edibles, soil, groundwater and their comparison in any localized disease like CKD in any part of the world.

Funding

We declare that, there is no any funding from either Government or Private organization to carry out this work.

CRediT authorship contribution statement

1. Design of the study, Sample collection, Experimentation, Acquisition, Analysis Interpretation of Data and Drafting the Manuscript: G. Narayana Murthy. 2. Conception, Revising the Manuscript, Evaluation of the Data for important intellectual content: P. Balarama Swamy Yadav.

Declaration of Competing Interest

We declare that we have no any competing interests.

Data Availability

The Data of the study is available at CSBoB (Andhra University, Visakhapatnam, Andhra Pradesh, India.) and with corresponding author, they will provide it on reasonable request.

Acknowledgements

We thank The Director, Center for Studies on Bay of Bengal (CSBoB), Andhra University, Visakhapatnam, for giving permission to use the ICP-MS instrument.

Appendix A. Supporting information

Supplementary data associated with this article can be found in the online version at doi:10.1016/j.jfca.2023.105868.

References

Affum, A.O., Osae, S.D., Kwaansa-Ansah, E.E., Miyittah, M.K., 2020. Quality assessment and potential health risk of heavy metals in leafy and non-leafy vegetables irrigated with ground water and municipal-waste-dominated stream in the Western Region, Ghana. e05829 Heliyon 6 (12), 29. https://doi.org/10.1016/j.heliyon.2020.e05829.

Kharazi, Ava, Leili, Mostafa, Khazaei, Mohammad, Mohammad Yusef Alikhanil, 2021. Human health risk assessment of heavy metals in agricultural soil and food crops in Hamadan, Iran. J. Food Compos. Anal. 100, 103890 https://doi.org/10.1016/j.jfca.2021.103890.

Banerjee, D., Bairagi, Himadri, Mukhopadhyay, S., Pal, A., Bera, Debabrata, Ray, Lalitagauri, 2010. Heavy Metal contaminationin fruits and vegetables in two Districts of West Bengal, India. Electron. J. Environ., Agric. Food Chem. 9. ⟨https://www.researchgate.net/publication/215565989_Heavy_metal_contamination_in_fruits_and_vegetables_in_two_districts_of_West_Bengal_India⟩.

National Institute of Nutrition, 2011. Hyderabad. A Manual Dietary Guidelines for Indians. https://www.nin.res.in/downloads/DietaryGuidelinesforNINwebsite.pdf.

FAO/WHO, (CXS 193-1995) Codex Alimentarius, General Standard for Contaminants and Toxins in Food and Feed. Adopted in 1995 Revised in 1997, 2006, 2008, 2009 Amended in 2010, 2012, 2013, 2014, 2015, 2016, 2017, 2018 and 2019 https//doi. CXS 193–1995.

Food Safety, Standards (Contaminants, Toxins, Residues) Regulations. https://www.fssai.gov.in/upload/uploadfiles/files/Compendium_Contaminants_Regulat ions_20_08_2020.pdf.

Gadde, P., Sanikommu, S., Manumanthu, R., Akkaloori, A., 2017. Uddanam nephropathy in India: a challenge for epidemiologists. Bull. World Health Organ. 95 (12), 848–849. ⟨https://www.ncbi.nlm.nih.gov/pmc/articles/PMC5710086/⟩.

Ganguli, A., 2016. Uddanam nephropathy/regional nephropathy in India: preliminary findings and a plea for further research. Am. J. Kidney Dis. 68 (3), 344–348 https://10.1053/j.ajkd.2016.04.012.

Mamatha, P., Salamma, S., Swamy, A.V.N., Ravi Prasad Rao, B., 2014. Quantitative and risk analysis of heavy metals in selected Leafy vegetables. Der Pharma Chem. 6, 179–185. ⟨https://www.derpharmachemica.com/pharma-chemica/quantitative-and-risk-analysis-of-heavy-metals-in-selected-leafy-vegetables.pdf⟩.

Choudhury, Harlal, Cary, Richard, 2001. World Health Organization & International Programme on Chemical Safety. Barium and Barium compounds. https://apps.who.int/iris/handle/10665/42398.

Murthy, G.N., Yadav, P.B.S., 2023. Trace elemental and heavy metal levels in frequently consumed local vegetables of three chronic kidney disease-prevalent villages. Biol. Trace Elem. Res. https://doi.org/10.1007/s12011-023-03761-6.

Oyekanmi Adeyinka, M., FarombiAbolaji, G., Adebayo Olukemi, R., 2014. Determination of trace element in raw leafy vegetables grown in selected local government of Osun State. Niger. Am. J. Chem. 4 (1), 38–41. ⟨https://doi:10.5923/j.chemistry.20140401.06⟩.

Cockwell, Paul, Fisher, Lori-Ann, 2020. The global burden of chronic kidney disease. Lancet 395 (10225), 662–664. https://doi.org/10.1016/S0140-6736(19)32977-0.

Peana, M., Serenella, M., Maryam, D., Maria, A.Z., Alessio, P., Christos, T.Ch, Geir, B., 2021. Environmental Barium: potential exposure and health-hazards. Arch. Toxicol. 95, 2605–2612. https://doi.org/10.1007/s00204-021-03049-5.

Pequerul, A., Perez, C., Madero, P., Val, J., Monge, E., 1993. A rapid wet digestion method for plant analysis. In: Fragoso, M.A.C., Van Beusichem, M.L., Houwers, A. (Eds.), Optimization of Plant Nutrition. Developments in Plant and Soil Sciences, vol 53. Springer. https://doi.org/10.1007/978-94-017-2496-8_1.

Raju, T.P., Babu, Giridhar, Srinivas, N., Ch, Ch, Lakshmana Das, N., 2015. Trace Elemental analysis of Rice samples from Kidney effected area using EDXRF Technique. Int. J. Sci. Res. 4 (2), 1062–1066. ⟨https://www.ijsr.net/get_abstract.php?paper_id=SUB151409⟩.

Raju, T.P., Giridhar Babu, N., Srinivas, Ch. Ch, Ramanamam, V., Ravi Shankar, M.S., Ram, S.S., Sudarshan, M., Lakshmi Narayana, P.V., Lakshmana Das, N., 2016. Trace elemental analysis of finger millet samples from kidney effected area using EDXRF technique. International Journal of Scientific Research in Science. Eng. Technol. 2 (1), 174–178. ⟨https://ijsrset.com/IJSRSET162132⟩.

Swapna Priya, E., Sunil, G., Shivaiah, K., Anil, G., 2014. Extent of heavy metal contamination in leafy vegetables, soil and Water from surrounding of Musi River, Hyderabad, India. J. Ind. Pollut. Control 30 (2), 289–293. ⟨https://www.researchgate.net/publication/271823133_Extent_of_heavy_metal_contamination_in_leafy_vegetables_soil_and_water_from_surrounding_of_Musi_River_Hyderabad_India⟩.

Gupta, Sapana, Jena, Jena, V., Neda Davic, S., Natalija Matic, Radojevic, Solanki, J.S, D., 2013. Assessment of heavy metal contents of green leafy vegetables. Croat. J. Food Sci. Technol. 5 (2), 53–60. ⟨https://www.bib.irb.hr/1016071/download/1016071.B_Croatian_Journal_food_of_Science_and_Technology_MANUSCRIPT_GUPTA_5.pdf⟩.

Sobur Ahmed, Fatema-Tuj-Zohra, Mahdi, Meem Muhtasim, Nurnabi, Md, Alam, Md. Zahangir, Choudhury, Tasrina Rabia, 2022. Health risk assessment for heavy metal accumulation in leafy vegetables grown on tannery effluent contaminated soil. Toxicol. Rep. 9, 346–355. https://doi.org/10.1016/j.toxrep.2022.03.009.

Tatapudi, R.R., Rentala, S., Gullipalli, P., Komarraju, A.L., Singh, A.K., Tatapudi, V.S., Goru, K.B., Bhimarasetty, D.M., Narni, H., 2018. High prevalence of CKD of unknown etiology in Uddanam, India. Kidney Int. Rep. 4 (3), 380–389. https://doi.org/10.1016/j.ekir.2018.10.006. PMID: 30899865; PMCID: PMC6409405.

Gupta, Vidhu, Lal, Kanhaiya, Sehgal, Meena, 2022. Preliminary assessment of heavy metals intake via food in CKDu affected Uddanam region of Srikakulam, Andhra Pradesh, India. Int. J. Environ. Stud. 2122387.

WHO(ꝑ1973). Expert Committee on Trace Elements in Human Nutrition & World Health Organization. Trace elements in human nutrition:Report of a WHO expert committee ⟨https://apps.who.int/iris/handle/10665/41057⟩.

WHO, (2007). Health risks of heavy metals from long-range transboundary air pollution. WHO Regional Office for Europe, Copenhagen, Denmark. Joint WHO/Convention Task Force on the Health Aspects of Air Pollution. ⟨https://apps.who.int/iris/bitstream/handle/10665/107872/9789289071796-eng.pdf?sequence=1⟩.

Zhou, H., Yang, W.T., Zhou, X., Liu, L., Gu, J.F., Wang, W.L., Zou, J.L., Tian, T., Peng, P. Q., Liao, B.H., 2016. Accumulation of heavy metals in vegetable species planted in contaminated soils and the health risk assessment. Int J. Environ. Res Public Health 13 (3), 289. https://doi.org/10.3390/ijerph13030289.

Zor, M., Kocaoba, S., 2023. Determination of metal contents in some green leafy vegetablesin Marmara region of Turkey. SN Appl. Sci. 5, 154 https://doi.org/10.1007/s42452-023-05369-w.

International Journal of Scientific Engineering and Research (IJSER)
ISSN (Online): 2347-3878
Impact Factor (2024): 7.741

Analysis of a Wild Leafy Vegetable (*Premna latifolia* Roxb.) Samples for Essential Trace Elements using ICP - MS Technique

G. Narayana Murthy[1], Balarama Swamy Yadav Padala[2]

[1]Department of Botany, Government Degree College, Chodavaram

[2]Department of Botany, Andhra University, Visakhapatnam

Abstract: ***Leafy vegetables are rich sources of nutrients including mineral ions, which are essential for proper functioning of body organs. Premna is one such wild leafy vegetable, leaves of Premna have been collected from three different villages, these samples are analyzed for elemental levels by using Inductively Coupled Plasma - Mass Spectroscopy (ICP - MS), to measure the values of 6 essential elements in each sample. Essential trace elements Al, Mn, Fe, Co, Cu, and Zn have been measured for their levels. The concentration of each element of this plant is calculated and reported.***

Keywords: ICP - MS, Trace elements, Wild plants, Leafy vegetables, Nutrition value

1. Introduction

Wild and cultivated leafy vegetables are rich sources of essential nutrients, offering a lot of health benefits, some of them are having harmful elements also at high levels (Murthy and Yadav, 2024). Wild varieties, found in natural ecosystems, include species like *Portulaca oleracea*, *Polygonum plebijum*, *Trianthemamonogyna*, etc. (Rekha, 2018). These plants are characterized by their flexibility and adaptability, thriving in diverse environments. On the other hand, cultivated leafy vegetables, such as spinach (*Spinacia oleracea*), kale (*Brassica oleracea* var. acephala), *Trigonella foenum - graecum*, Swiss chard (*Beta vulgaris* var. cicla) etc. are mainly grown for culinary purposes (Kumar, 2020). They are all packed with vitamins, minerals, and antioxidants, contributing to overall health. They are particularly rich in vitamin K, vitamin A, folate, Iron, and Calcium; promoting bone health, immune function, and vision. This present study is an attempt to estimate the elemental values in a wild leafy vegetable.

2. Materials and Methods

2.1 Study area

Study area situated in the Kaviti Revenue Mandal of Srikakulam district, Andhra Pradesh, India, where this plant is widely used as leafy vegetable. Three villages (Kusumapuram, Varaka, and Borivanka) have been selectedand the samples are collected from these villages and analyzed for elemental values. The details of the study area are provided in Fig.1.

2.2 Morphology:

Scientific name: *Premna latifolia* Roxb.; Family: Verbanaceae
Common name (s): Nellikura (Telugu), Jhatela, Basota (Hindi), Jaya, Agimantha, Sriparna (Sanskrit).

*Premna*plants are shrubs or small trees nearly 10 - 15 feet long with a wide roof, trunk has dark grayish bark, slightly polar, black when dried; young parts pubescent and young trunks are spinous. Leaves are simple, opposite, lanceolate - ovate, elliptic - ovate to rhomboidal, entire and ciliate, apex is acute. Leaves are green in colour unpleasant smelling. Lateral veins 4 - 8 on either side of lamina, they are prominent beneath the lamina. Inflorescence is either apical or axillary. It is panicle or compact cyme. Flowers are bisexual, many, odorless, creamy white, yellowish green (Kumar et al, 2017).

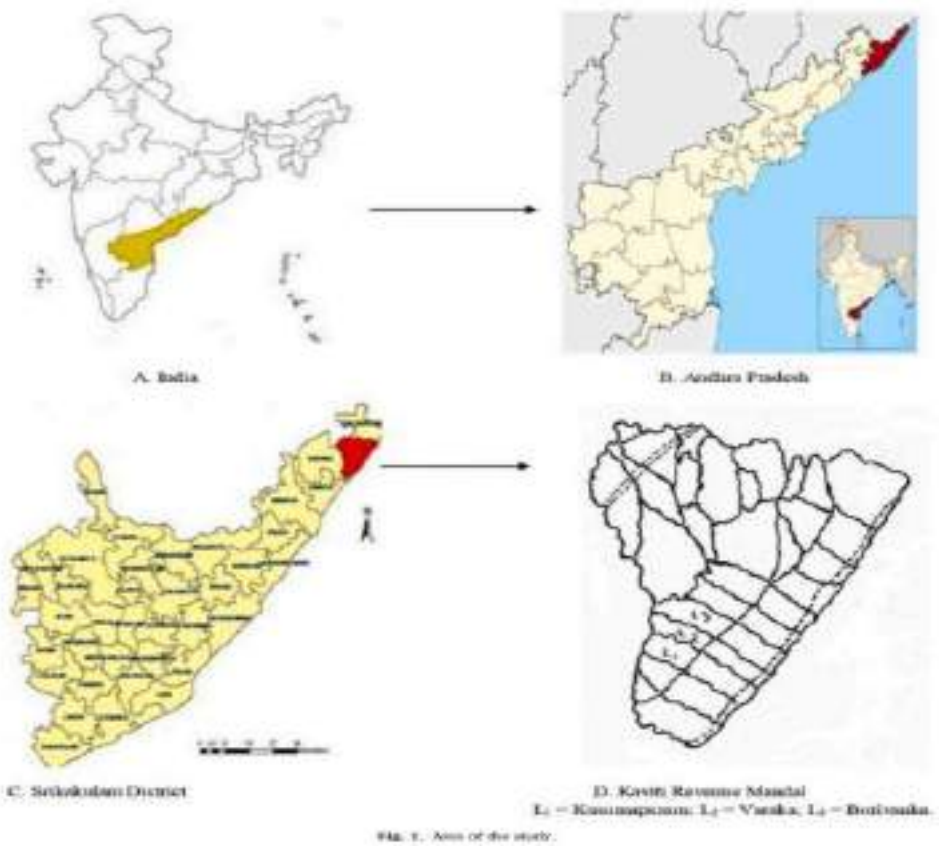

Figure 1: Study area

2.3 Sample Collection

Samples have been collected from the fields directly; kept in zip locked bags. Shifted to labi. e. CSBoB (Center for Studies on Bay of Bengal), Andhra University, Visakhapatnam. Samples have been washed twice with distilled water, shade dried and then acid digestion process was carried out to digest all organic matter in the samples.

2.4 Methodology and Wet digestion:

ICP - MS technique is followed to estimate the elemental levels in the sample. There are advantages to ICP - MS method for the determination of cations in solution, as high temperatures (above 6000 ^{0}C), complexes and or residuals can be converted into basic form i.e. ionomic form, so we can easily estimate element levels accurately. Fast and accurate wet digestion method is followed for the digestion of plant samples and subsequent analysis of elemental (Al, Mn, Fe, Co, Cu, and Zn) levels. Initially0.5 g leaf sample is taken into Teflon Beakers.8 ml of $HN0_3$ added to this and left overnight. The solution was heated on a hot plate at 120 - 125 ^{0}C for one hour, with 1 - 2 additions of 4ml H_20_2 (33%) until solution is clear/colorless indicates complete digestion of material (Pequerul et al., 1993). The residue was brought to a dry place on low heat (80 ^{0}C), shaken well, after cool to room temperature diluted to known volume (50ml) with 2D water, and stored in High Density Poly Ethylene (HDPE) bottles of 100 ml volume for further use at room temperature.

3. Results and Discussion

Many elements are essential for proper functioning biological metabolisms, the results of the study reveal that the levels of essential trace elements (Aluminum, Manganese, Iron, Cobalt, Copper, Zinc) in different locations (Kusumapuram, Varaka, Borivanka) is presented in Table and Fig.2.

Table: Essential trace element values (ppm) in *Premna latifolia* Roxb. from three villages

Location	Al	Mn	Fe	Co	Cu	Zn
Kusumapuram	11.67	8.5	15.73	0.03	0.47	8.91
Varaka	7.64	15.67	21.02	0.06	0.4	6.59
Borivanka	17.22	3.3	23.63	0.04	0.32	9.81

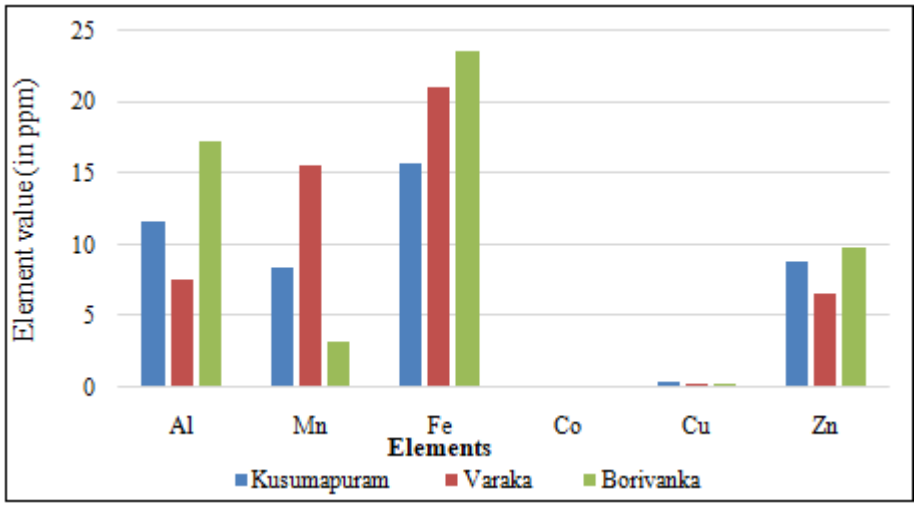

Figure 2: Essential trace element values (ppm) in *Premna latifolia* Roxb. from three villages

- **Aluminium:** The high level of Al is observed in Borivanka (17.22), followed by Kusumapuram (11.67) and Varaka (7.64). There is an increasing trend in Al levels from Varaka, Kusumapuram to Borivanka.
- **Manganese:** The high level of Mn is found in Varaka (15.67), followed by Kusumapuram (8.5) and Borivanka (3.3). There is a decreasing trend in Mn levels from Varaka, Kusumapuram to Borivanka.
- **Iron:** The high Fe levels are recorded in Borivanka (23.63), followed by Varaka (21.02) and Kusumapuram (15.73). There is an increasing trend in Fe levels from Kusumapuram, Varaka to Borivanka.
- **Cobalt:** The levels are very low in all locations, of course it requires in minute values. Varaka (0.06) having the high values, followed by Borivanka (0.04) and Kusumapuram (0.03). There is a minimal fluctuation in cobalt levels among the three locations.
- **Copper:** The high Cu levels are observed in Kusumapuram (0.47), followed by Varaka (0.4) and Borivanka (0.32). There is an increasing trend in Cu levels from Borivanka, Varaka to Kusumapuram.
- **Zinc:** the highest Zn levels are found in Borivanka (9.81), followed by Kusumapuram (8.91) and Varaka (6.59). There is an increasing trend in Zn levels from Varaka, Kusumapuram to Borivanka.

In summary, there are varying trends in the levels of essential trace elements across the three locations, and these trends may be influenced by factors such as geological composition, environmental conditions, and human activities in each area.

The aforementioned elements play important roles in various metabolic processes as follows:

- **Aluminium:** It may play a role in some enzymatic processes, particularly in certain plants.
- **Manganese:** Essential for the activation of enzymes involved in bone formation, blood clotting, and reducing oxidative stress in the body.
- **Iron:** Crucial for oxygen transport in hemoglobin, electron transport in cellular respiration, and the synthesis of certain enzymes and proteins.
- **Cobalt:** An essential component of vitamin B12 (Cobalamin), which is crucial for DNA synthesis, red blood cell formation, and neurological function.
- **Copper:** Essential for the formation of hemoglobin, collagen, and various enzymes involved in antioxidant defense and cellular energy production.
- **Zinc:** Plays a critical role in the functioning of enzymes involved in DNA synthesis, immune function, wound healing, and the sense of taste and smell.

4. Conclusion

Previous studies conclude that *Premna latifolia* Roxb., extracts contain bioactive compounds, including flavonoids, steroids, terpenoids, tannins, glycosides, alkaloids, reducing sugars, Phenols, Quinones, Lignin, and fixed oils. Methanolic extracts from leaves and bark exhibit the highest phenolic and flavonoid content, indicating strong antioxidant and free radical scavenging activity (Pushpa, 2019), and the present study reveal that it contains essential trace elements.

Acknowledgements
Authors are thankful to Director CSBoB, Andhra University for granting permission to use ICP - MS instrument.

References

[1] Murthy, G. N., Yadav, P. B. S. (2024) Elemental levels in frequently consumed local leafy vegetables from three villages with chronic kidney disease prevalence, *Journal of Food Composition and Analysis*.126: 105868. https: //doi. org/10.1016/j. jfca.2023.105868.
[2] Pequerul, A., Perez, C., Madero, P., Val, J., Monge, E., (1993). A rapid wet digestion method for plant analysis. In: Fragoso, M. A. C., Van Beusichem, M. L., Houwers, A. (Eds.), Optimization of Plant Nutrition. Developments in Plant and Soil Sciences, vol 53. *Springer*.
[3] https: //doi. org/10.1007/978 - 94 - 017 - 2496 - 8_1
[4] Kumar, B, Sandhya, D., Solomon Raju. A. (2017). On the reproductive ecology of Premna latifolia L. and Premna tomentosa Willd. (Lamiaceae). *Journal of threated taxa*.10 (1): 1 - 22.
[5] Rekha, S. (2018) Nutritional Analysis of Few Selected Wild Edible Leafy Vegetables of Tribal of Jharkhand, India. *International Journal of Current Microbiology and Applied Sciences*.7 (2): 1323 - 1329.

[6] Kumar, D., Kumar, S., and Shekhar, C. (2020) Nutritional components in green leafy vegetables: A review. *Journal of Pharmacognosy and Phytochemistry*.9 (5): 2498 - 2502.
[7] Pushpa, R., and Diksha, N. (2019) Phytochemical analysis and evaluation of antioxidant activity of Premna latifolia Roxb. A medicinal plant (Family: Lamiaceae). *The Pharma Innovation Journal*, 8 (5): 13 - 20.

साहित्याकाश

INTERNATIONAL PEER REVIEWED REFERRED MONTHLY JOURNAL

वर्ष– 1, खंड– 3, अंक– 3, मार्च– 2024

प्रधान संपादक

डॉ. संतोष कांबळे

M.A. (History, Hindi), M.Lib. & I.Sc., M.Phil., PGDCA., PGDLAN., PGDT., UGC-NET, Ph.D.-LIS., (Ph.D.-Hindi)

पुस्तकालयाध्यक्ष, उच्च शिक्षा और शोध संस्थान, दक्षिण भारत हिंदी प्रचार सभा, खैरताबाद, हैदराबाद

E-Mail- shreyashju@yahoo.co.in Mobile No.- 8125981194

संपादक

डॉ. अजित चुनिलाल चव्हाण

M.A., Ph.D.

सहयोगी प्राध्यापक, वसंतराव नाईक कला, विज्ञान एवं वाणिज्य महाविद्यालय, शहादा, जिला– नंदुरबार

E-Mail- chavan.ajit2@gmail.com Mobile No.- 9422262445

सह–संपादक

प्रो. गौतम भाईदास कुवर

M.A., Ph.D

हिंदी विभाग प्रमुख

पूज्य साने गुरुजी विद्या प्रसारक मंडल का कला, विज्ञान एवं वाणिज्य महाविद्यालय शहादा जिला नंदुरबार महाराष्ट्र

E-Mail- gautamkuwar53@gmail.com Mobile No.- 84118 28448

प्रो. सुनील गुलाब पानपाटील

M.A., Ph.D (SET)

कला, वाणिज्य एवं विज्ञान महिला महाविद्यालय, नंदुरबार

E-Mail- sgpanpatil@gmail.com Mobile No.- 9860235508

कानूनी सलाहकार

एडवोकेट श्री राजेश कुमार शर्मा

B.A., LL.B

अधिवक्ता, सर्वोच्च न्यायालय, नई दिल्ली, **E-Mail- rajesh.shagun@gmail.com Mobile No.- 981144676**

साहित्याकाश

INTERNATIONAL PEER REVIEWED REFERRED MONTHLY JOURNAL

वर्ष– 1, खंड– 3, अंक– 3, मार्च– 2024

साहित्याकाश

INTERNATIONAL PEER REVIEWED REFERRED MONTHLY JOURNAL

वर्ष– 1, खंड– 2, अंक– 2, फरवरी– 2024

स्वामित्व : प्रधान संपादक, साहित्याकाश मासिक पत्रिका

प्रकाशक : प्रमिला प्रकाशन, हैदराबाद

डॉ. संतोष कांबळे

पुस्तकालयाध्यक्ष, उच्च शिक्षा और शोध संस्थान,

दक्षिण भारत हिंदी प्रचार सभा, खैरताबाद, हैदराबाद

E-mail- sahityaakash24@gmail.com

Website- https://www.sahityaakash.in

साहित्याकाश

INTERNATIONAL PEER REVIEWED REFERRED MONTHLY JOURNAL

वर्ष– 1, खंड– 3, अंक– 3, मार्च– 2024

अनुक्रम

संपादकीय

नारी शक्ति

जीवविज्ञान की दृष्टि से मनुष्य का नर और नारी के रूप में जन्म होता है । अपवादात्मक स्थिती या शारीरिक व्यंग्य के रूप में तृतीय लिंगी व्यक्ति का जन्म होता है । शारीरिक दृष्टि से नर और नारी में अनेक तरह के व्यत्यास होते हैं । इन व्यत्यासों को ही ढाल बनाकर नर ने नारी को कमजोर बनाने की भरसक कोशिश की है इसमें कोई संदेह नहीं है ।

भारतीय परिप्रेक्ष्य में देखा जाये तो नारी के लिए देवी का स्थान सिर्फ धर्म ग्रंथों में ही देखने को मिलता है । बल्कि वास्तविकता कुछ और ही है । भारतीय पुरूषसत्तात्मक समाज में पुरूष ने महिलाओं को पर हमेशा अपना अधिकार आरोपित किया है । जिसके लिए उसने महिलाओं को अनेकानेक बंधनों में बाँधकर उसे कमजोर बनाने की कोशिश की है । महिलाओं ने नर के इन बंधनों को कभी स्वीकार किया तो कभी इनका विरोध कर इन बंधन से मुक्त हो अपने अस्तित्व निर्माण करने की भरसक कोशिश की । वर्तमान स्थिति को ध्यान में रखकर देखा जाए तो महिलाओं को अस्तित्व निर्माण की इस जंग में बहुत हद तक सफलता भी प्राप्त हुई ।

ऐतिहासिक परिप्रेक्ष्य पर दृष्टि डाले तो राजमाता जिजाऊ ने सामाजिक रूढ़ीवादी बंधनों को तोड़ते हुए पति की मृत्यु होने पर सती न होकर अपना जीवन अपने पुत्र छत्रपति शिवाजी महाराज की शिक्षा–दिक्षा हेतु समर्पित कर स्वतंत्र हिंदू साम्राज्य के निर्माण में अहम भूमिका निभाई । इसमें कोई संदेह नहीं कि छत्रपति शिवाजी महाराज के वीरता परक यशस्वी जीवन यापन में वीरमाता जिजाऊ का अत्यंत महत्त्वपूर्ण योगदान रहा है ।

स्त्री शिक्षा की यदि बात की जाए तो सावित्री बाई फुले का योगदान अविस्मरणीय है । सावित्री बाई फुले ने तत्कालीन परिस्थिती में अछूतों और महिलाओं को सक्षम बनाने हेतु शिक्षा को माध्यम बनाया तथा अपने पति महात्मा जोतिबा फुले की मदद से पुणे शहर में प्रथम महिला पाठशाला शुरू की और जहाँ से महिला शिक्षा के द्वार महिलाओं के लिए सदा के लिए खूल गये ।

आधुनिक युग में महिलाएँ पुरूषों के कंधे से कंधा मिला कर चल रही हैं । ऐसा कोई भी क्षेत्र नहीं है जहाँ महिलाओं ने पुरूषों के साथ अपनी भागीदारी न निभाई हो भले ही वह क्षेत्र विज्ञान और प्रौद्योगिकी, खेल जगत, साहित्य जगत, राजनीतिक जगत अथवा उद्योग जगत ही क्यों न हो । सभी क्षेत्रों में महिलाओं ने अपना अहम योगदान प्रदान किया ।

हिंदी साहित्य में मीराबाई, महादेवी वर्मा, कृष्णा सोबती, नासीरा शर्मा, अलका सरावगी, कात्यायनी, मृदुला गर्ग, मैत्रेयी पुष्पा, अमृता प्रीतम आदि लेखिकाओं ने साहित्य रचना कर अपनी एक अलग पहचान बनाई । महिला दिवस (08 मार्च) के शुभ अवसर पर 'साहित्याकाश' परिवार महिला शक्ति को नमन करते हुए यह अंक विश्व की प्रत्येक महिला को समर्पित करता है ।

प्रधान संपादक

डॉ. संतोष कांबळे

नयी सदी के हिंदी उपन्यासों में किसानों का संघर्ष और आत्महत्याएँ

डॉ. जयश्री भास्कर वाडेकर,
श्रीमती दानकुंवर महिला महाविद्यालय,
जालना 431203 (महाराष्ट्र)
ई–मेल: dr.jbwadekar@gmail.com
भ्रमणध्वनी : 9923839174, 9405530579

सार :

किसानों के संघर्ष किसी भी समाज की अद्वितीयता और उसकी अद्वितीयता का हिस्सा हैं । इसके अलावा, नयी सदी के उपन्यासों में किसानों के संघर्ष उनकी सामाजिक, आर्थिक, और राजनीतिक स्थितियों को भी दर्शाते हैं और इसे उनके जीवन की अद्वितीयता का हिस्सा बनाते हैं । आजादी के पहले शोषकों को किसान समझ सकता था । लेकिन आज उसका चालाकी से शोषण किया जा रहा है । इससे शोषकों को पहचानना भी मुश्किल हुआ है ।किसानों की दुर्दशा के लिए जिम्मेदार तत्व और किसान आत्महत्याओं की जमीनी सच्चाई नई सदी के इन उपन्यासों में यथार्थ रूप में प्रकट हुई है ।

बीज शब्द : मौसम के साथ जुआ, औद्योगिक क्रांति, ऋण, संघर्षों की त्रिवेणी आदि ।

प्रस्तावना :

धरती और किसान का अटूट रिश्ता है, वह अपनी जमीन से सर्वाधिक लगाव रखता वही उसका सब कुछ है । दरअसल कृषक समाजों के लिए कृषि कोई धंधा नहीं बल्कि उनकी जीवन शैली है ।भारत कृषि प्रधान देश माना जाता है । आज भी सत्तर फीसदी लोग ने जीवन यापन के लिए कृषि को आधार बनाया है । समय की मांग के अनुसार कृषि के उत्पादन में परिवर्तन होना लाजमी है । इग्लैंड से भारत तक का औद्योगिक क्रांति का सफ़र और भारत में हरित क्रांति होने से कृषि उत्पादन में काफी बदलाव आया है परन्तु किसान किसी न किसी रूप से शोषित और प्रताड़ित रहा है ।भारतीय अर्थव्यवस्था का प्रमुख आधार कृषि और किसान है । किसानों की उन्नति से ही देश की उन्नति संभव है । किसान पूरे देश का अन्नदाता है । वैश्वीकरण के दौर में उसकी भी स्थिति में सुधार होगा ऐसा लगा था। लेकिन आज के बाजारवादी दौर में वह हाशिए पर चला गया है । हिन्दी साहित्य की विभिन्न विधाओं किसान जीवन की विधिक छवियों का प्रमाणिक अंकन समय–समय पर हुआ है । प्रेमचंद ने अपने रचनाओं के माध्यम से किसान को साहित्य में एक मुकम्मल जगह प्रदान की। उन्होंने किसान जीवन को बहुत करीब से देखा और फिर उसको अपने लेखन का केन्द्र बनाया। प्रेमचंद के पश्चात् ग्रामीण जीवन पर बहुत लेखकों ने उपन्यास और कहानियां लिखी जो उल्लेखनीय रही है । साथ ही हिन्दी कविता में भी किसान जीवन की विविध छवियां अंकित है ।किसानों का संघर्ष एक व्यापक विषय है जो भारतीय समाज में गहरे रूप से अपेक्षित है ।

आजादी के इतने साल बीत जाने पर भी किसानों को न्याय नहीं मिल पा रहा है । वह समस्याओं के मकड़ जाल में घिरा हुआ है । कभी प्राकृतिक आपदाएं तो कभी सरकारी नीतियों से वह परेशान हो रहा है । उसकी फ़सल को उचित मूल्य न मिलना भी आज एक गंभीर समस्या हो चुकी है । अच्छे बीजों की उपलब्धता और वितरण की असमानता की समस्या ने भी किसानों का जीना मुश्किल किया है । किसानों के लिए सारे हालात ऐसे हैं कि "जिंदा कैसे रहा जाए ?" इस स्थिति में वह फांसी के फंदे को

अपनाकर आत्महत्या कर रहा है । अब तक तीन लाख से अधिक किसानों ने आत्महत्याएं की हैं । किसान आत्महत्या आज चिंता का विषय बना है और वह भी विशेषकर कृषि प्रधान देश में ।

आत्महत्या के कारण:

1. आर्थिक संघर्ष: बजट की कमी, किसानों के लिए अधिकांश बजट में कमी होती है, जिससे उन्हें उचित मूल्य मिलने में मुश्किल होती है ।ऋण की बढ़ती ब्याज दरें: ऋण लेने के लिए ब्याज दरें बढ़ गई हैं, जिससे किसानों को उचित लाभ नहीं मिल पा रहा है ।

2. तकनीकी संघर्ष: बुनियादी तकनीक की कमी: किसानों के पास अधिकांश बुनियादी तकनीक नहीं है, जिससे वे अधिक उत्पादन नहीं कर पा रहे हैं ।

3 अभाव और अद्यतन तकनीक: अधिकांश किसान अद्यतन तकनीक के अभाव में हैं, जिससे उन्हें अधिक उत्पादन नहीं कर पा रहे हैं ।

4 भूमि संघर्ष: किसानों के पास अधिकांश भूमि नहीं है, जिससे वे अधिक उत्पादन नहीं कर पा रहे हैं ।

5 शिक्षा और जागरूकता: अधिकांश किसान शिक्षित नहीं हैं, जिससे उन्हें अधिक उत्पादन नहीं कर पा रहे हैं ।

6 राजनीतिक संघर्ष: अधिकार की कमी: किसानों के पास अधिकांश अधिकार नहीं हैं, जिससे वे अधिक उत्पादन नहीं कर पा रहे हैं ।

किसान प्रत्येक युग में शोषणकारी व्यवस्था के लिए 'नरम चारा' रहा है । कभी वह सामन्ती शक्तियों के क्रूर शोषण का शिकार बना तो कभी साम्राज्यवादी ताकतों ने अपने पोषण के लिए उसे आहार बनाया। पूँजीवादी सभ्यता उसे बेघर करने की जिद पाले बैठी है । खेत–खलिहान उजाड़े जा रहे हैं । ऊपर से प्रकृति की निर्मम मार ने उसे असहाय बना दिया है । हाड़ –तोड़ मेहनत करने के बाद भी अधपेट सोना और छोटी–छोटी खुशियों के लिए तरसते रहना उसकी नियति सी बन गई है । उसका जीवन अभावों की भेंट चढ़ता हुआ दुख की महागाथा बन जाता है ।हृदयहीन व्यवस्था उसे निरन्तर निगलती जा रही है । ऊपर से शान्त दिखने वाली नदी की तरह जिसकी भँवरें भीतर–ही –भीतर मनुष्य को दबाकर तलहटी में लगा देती हैं और दूसरों को वह तभी दिखाई देता है जब उसकी लाश उतराती हुई बहने लगती है ।

किसान जीवन पर केन्द्रित शिवमूर्ति का 'आख़िरी छलांग' उपन्यास है । जो प्रेमचंद की परंपरा की ही एक कड़ी दिखती है । 'आख़िरी छलांग' उपन्यास का कथानक परस्पर उलझी हुई किसान जीवन की अनेक समस्याओं का जंजाल है । कथानक का आधार पूर्वी उत्तर प्रदेश का ग्रामांचल है । इसका नायक पहलवान एक किसान है । उसके सामने विरासत में मिली तथा नयी विकास नीतियों के कारण निर्मित अनेक समस्याएँ हैं । वह अपनी सायानी बेटी के लिए दो साल से वर खोज रहा है , बेटे की इंजीनियरिंग की फीस का जुगाड़ नहीं हो रहा है, तीन साल से गन्ने का बकाया नहीं मिल रहा है, सोसायटी से खाद के लिए लिया गया कर्ज चुकता नहीं हुआ है । हर दूसरे महीने में ट्यूबवेल के बिल की तलवार सिर पर लटक जाती है । ऐसी कई समस्याओं को पहलवान किसान के माध्यम से उपन्यासकार ने अपने उपन्यास में उठाया है । शिवमूर्ति ग्रामीण रचनाकार हैं । उन्होंने किसानों की समस्याओं को समझा तथा उनकी समस्याओं को महसूस किया है । पहलवान महसूस करता है कि जैसे नहर के पेट भीतर सिल्ट भर जाती है उसी तरह किसान की तकदीर में भी साल दर साल सिल्ट भरती जा रही है । अपनी किसान जीवन की समस्याओं से तंग आकर वह इस व्यवस्था से प्रश्न करता है कि "सरे हालत तो मर जाने के हैं । जिंदा कैसे रहा जाए। "[1] आज लेखन के क्षेत्र में किसान धीरे–धीरे गायब होता जा रहा है । ऐसे भीषण समय में प्रेमचंद आज भी हमारे लिए प्रासंगिक और समकालीन है क्योंकि न किसानों और जमीन की समस्या हल हुई है न भूमिहीन मजदूरों को श्रम शोषण से मुक्ति मिली है, बल्कि उसमें स्त्रियों, दलितों, आदिवासियों और अल्प संख्यकों के नये आयाम और जुड़ गए। प्रेमचंद की संवेदना, सरोकार और दृष्टि ही उनकी परम्परा है । जिसे हम आज जल,

जमीन और जंगल के असमान वितरण के संघर्ष के रुप में देख रहे है । उपन्यासकार संजीव ने अपने उपन्यास 'फांस' में किसान जीवन की विभिन्न समस्याओं को उजागर किया है । उन्होंने किसानों की मूलभूत समस्या खाद, पानी, बीज, बिजली की समस्या, प्राकृतिक समस्या, फसल का उचित मूल्य न मिलने की समस्या, कर्ज की समस्या तथा आत्महत्या के कारणों को बड़े ही बेबाकी के साथ अपने उपन्यास में दिखाया है । उपन्यासकार ने कर्ज की समस्या को अपने उपन्यास में इस तरह व्यक्त किया है– "अगले महीने बैंक का २५ हजार का कर्ज अदा करना है । आज गुढ़ी पाडवा है–मराठी नववर्ष। ... "फर्स्ट क्लास डिनर है आई ।"... "ये जो भात है न आई, इसमें स्टार्च है, इसका माड न फेंको तो चावल की सारी ताकत बची रहती है, फिर मावा ! मेवा है मेवा ! ताकत ही ताकत ! मजबूती ही मजबूती !"... "इसके सामने नासिक का किसमिश फेल, रत्नगिरि का हापुस फेल और कलमी के साग में आयरन ही आयरन । और स्वाद?... शुभा सामने आकर खड़ी हो गयीं तो झेप गया पूरा परिवार ! शुभा ने तरस खाती जुबान से कहा –"आज नववर्ष है । आज तो कुछ कायदे की चीज बना लेती ! चलो मैं देती पूरण पोली !" नहीं वहिणी कोई तो दिन आएगा, हम भी पूरण पोली और ढेर सारा पकवान बनाएँगे। आज रहने दो। ""मगर क्यों ?""वो सुनील काका ने कहा है न कि जब तक कर्ज न उतार लो....।"समझी। अरे तुम मियां – बीवी ! तुम्हें तपस्या करनी हो, शौक से करो, मगर मुलगियों को तो बख्श दो ।"[2] किसानों की समस्याएं औपनिवेशिक शासन की शोषणपरक व्यवस्था से जुड़ी हुई हैं जो प्रमुख रुप से जमींदारों के अत्याचार, लगान, इजाफा, बेदखली, बेगारी के रूप में सामने आती है (प्रेमचंद: प्रेमाश्रम, कर्मभूमि, रंगभूमि, गोदान)आजादी के तुरन्त बाद जमींदारी प्रथा के अंत की तथाकथित घोषणा और जंमीदारों के जोड़–तोड़, तीन–तिकड़म से अपनी ठसक को कायम रखने की प्रयास दिखाई देता है,जिसके शिकार अन्ततः किसान–मजदूर ही होते हैं. (नागार्जुन:बलचनमा, बाबा बटेसरनाथ). सत्तर के दशक में हरित क्रांति के लाभ और उसके बंटवारे के सवाल जैसे–बड़े किसान बनाम छोटे किसान, किसान बनाम खेत–मजदूर, क्षेत्रीय असन्तुलन जैसे मुद्दों ने किसान समस्याओं को जटिल और गतिशील बना दिया।किसान जीवन को ही केंद्र में रखकर पंकज सुबीर ने 'अकाल में उत्सव' उपन्यास की रचना की है ।अकाल में उत्सव' में किसान जीवन की छोटी– छोटी समस्याओं को भी कथाकार ने जगह दी है । किसानों की मूलभूत समस्या के.सी.सी. समस्या, प्राकृतिक समस्या तथा सरकारी मुआवजा जैसी समस्याओं को कथाकार ने बड़े ही गहराई के साथ चित्रित किया है । किसानों की फसल नष्ट होने पर मुआवजा न मिलने की समस्या को सुबीर जी ने अपने उपन्यास में बड़े ही मार्मिक ढंग से प्रस्तुत किया है – "लेकिन सर किसान तो सरकार के ही भरोसे है न ? अगर सरकार उसको मदद नहीं करेगी तो कौन करेगा ? खेतों में खड़ी फ़सल अगर बरबाद हो गई, तो किसान क्या करे, क्या मर जाए ?" आगे सरकारी अफसरों के माध्यम से किसानों के प्रति सरकार का घिनौना चेहरा भी इस उपन्यास में प्रस्तुत होता दिखाई पड़ता है–"तो मर जाए ? सरकार के भरोसे बैठा है क्या ? दुनिया में सब अपने–अपने भरोसे बैठे हैं । आपको किसने कहा है खेती करो ? मत करो अगर नुकसान का इतना ही डर है तो। जब कहा ही जाता है कि खेती तो मौसम के भरोसे खेला जाने वाला जुआ है, तो क्यों खेलते हो इस जुए को? किसी ने कहा है क्या आपसे? मत करो खेती कोई दूसरा काम करो ।"[3]

देश की अर्थव्यवस्था के विकास में किसानों का अहम योगदान है । आज किसानों की उत्पादन क्षमता बहुत बढ़ गयी है । लेकिन सरकार उनके फसलों को उचित समर्थन मूल्य नहीं बल्कि न्यूनतम समर्थन मूल्य दे रही है । फसल नुकसान होने पर पुख्ता सरकारी प्रावधान नहीं है । फसल बीमा का लाभ केवल कुछ बड़े किसान ही ले पा रहे हैं । लघु और सीमांत किसान के लिए सरकार की कोई योजना नहीं है । जबकि आकड़ों के अनुसार– "भारत में 60 करोड़ अनुमानित किसान हैं जिसमें से 80% किसान छोटे किसान हैं, शेष 20% बड़े किसान हैं ।....किसान क्रेडिट कार्ड कर्ज में फसानें का एक तरीका है । किसान कर्ज में डूबना नहीं चाहता लेकिन सरकार उसे कर्ज देकर डूबा रही है । फिक्की (एफ.सी.सी.आई.) और एसोचेम ठेके पर खेती कराने में लगे हुए हैं ।"[4] रणेंद्र का 'गायब होता देश' दरअसल विकास के नाम पर आदिवासी किसानों को लूटने और उन्हें जबरन विस्थापित करते जाने का करुण

आख्यान है जो धीरे–धीरे हाशिए पर होते हुए लुप्त होने की कगार पर हैं । मुख्य धारा में इसको लेकर कोई विशेष हलचल या विक्षोभ नहीं दिखता है पर इन सबके खिलाफ आदिवासी अपने जीवन की सबसे कठिन लड़ाई लड़ रहे हैं । विकास की कीमत वे अकेले ही कब तक चुकाएगें जबकि उनका अस्तित्व ही खतरे में है इसलिए आदिवासियों का संकल्प अटल है कि 'जान देगें पर जमीन नहीं देगें'।

उपन्यास सर्वाधिक लोकप्रिय साहित्यिक विधा है । इसके युग जीवन सापेक्ष स्वरुप तथा निरन्तर बढ़ती हुई लोकप्रियता को देखते हुए इसे आधुनिक साहित्य की केन्द्रीय विधा भी कहा जा सकता है ।आज का समय तीव्रता, गति, परिवर्तन तथा अस्थिरता का है । उपन्यास अशान्त और अस्थिर युग की उपज है, जहाँ लोगों के साथ कुछ न कुछ घटनाएं घटती रहती हैं और लोग परिवर्तित होते रहते हैं । अत:इस अस्थिर और गतिशील युग में निरन्तर परिवर्तित होते हुए मनुष्य की कथा कहने तथा उसकी बदली हुई मानसिकता को अभिव्यक्ति देने के लिए उपन्यास विधा सर्वाधिक उपयुक्त विधा के रुप में स्थापित हुई है । यूरोप में उपन्यास का जन्म भले ही मध्यवर्गीय जीवन की महागाथा के रुप में हुआ हो लेकिन भारतीय उपन्यासों विशेष कर हिंदी पट्टी के लेखकों ने किसान जीवन और स्त्री दुखों को अपने उपन्यासों की विषय वस्तु बनाया. प्रेमचंद ऐसे किसान–केन्द्रित उपन्यासों की श्रृंखला के पहले और सशक्त लेखक हैं जो आगे चलकर नागार्जुन, रेणु, भैरव प्रसाद गुप्त, मार्केन्डेय, विवेकी राय से होती हुई रामदेव शुक्ल, मिथिलेश्वर,रामदरश मिश्र, शिव प्रसाद सिंह, जगदीश चंद्र, संजीव और पंकज सुबीर तक विस्तार पाती है । इनके उपन्यासों में किसान संघर्ष के कई शेड्स हैं क्योंकि न किसानों की जमीन की समस्या हल हुई, न भूमिहीन मजदूरों को श्रम–शोषण से मुक्ति मिली, बल्कि उसमें स्त्रियों, दलितो,आदिवासियों और अल्पसंख्यकों के नए आयाम और जुड़ गये। कर्ज में फंसे किसानों की आत्महत्यायें, विकास के नाम पर हृदयहीन विस्थापन, रोजगार के लिए होरी की सन्ततियों का शहरों में पलायन,कृषक महिलाओं का शोषण, आदिवासियों पर निर्मम अत्याचार, मिलों –फैक्ट्रियों और कोयले की खानों में खटते किसान–पुत्रों की व्यथा–कथा और शोषण तथा इसके खिलाफ पनपते आक्रोश और संघर्ष की चेतना से इनके उपन्यास महत्वपूर्ण हो गये हैं ।

किसान प्रत्येक युग में शोषणकारी व्यवस्था के लिए 'नरम चारा' रहा है ।कभी वह सामन्ती शक्तियों के क्रूर शोषण का शिकार बना तो कभी साम्राज्यवादी ताकतों ने अपने पोषण के लिए उसे आहार बनाया। पूँजीवादी सभ्यता उसे बेघर करने की जिद पाले बैठी है । खेत–खलिहान उजाड़े जा रहे हैं, ऊपर से प्रकृति की निर्मम मार ने उसे असहाय बना दिया है । हाड़ –तोड़ मेहनत करने के बाद भी अधपेटे सोना और छोटी–छोटी खुशियों के लिए तरसते रहना उसकी नियति सी बन गई है । उसका जीवन अभावों की भेंट चढ़ता हुआ दुख की महागाथा बन जाता है । हृदयहीन व्यवस्था उसे निरन्तर निगलती जा रही है । ऊपर से शान्त दिखने वाली नदी की तरह जिसकी भँवरें भीतर–ही –भीतर मनुष्य को दबाकर तलहटी में लगा देती हैं और दूसरों को वह तभी दिखाई देता है जब उसकी लाश उतराती हुई बहने लगती है ।

निष्कर्ष:

नयी सदी के उपन्यासों का मुख्य उद्देश्य यह है कि वे समाज को उनके संघर्षों और आत्महत्याओं के बारे में जागरूक करें और उन्हें समाज की ध्यान में लाएं। इन उपन्यासों में किसानों के जीवन की वास्तविकता, उनके संघर्षों की गहराई और उनके आत्महत्या के कारणों को विस्तार से प्रस्तुत किया गया है । इन उपन्यासों के माध्यम से किसानों के संघर्षों और आत्महत्याओं की वास्तविकता को समझाने का प्रयास किया गया है ताकि समाज को इस बारे में जागरूक किया जा सके।सत्तर के दशक में हरित क्रांति के लाभ और उसके बंटवारे के सवाल जैसे–बड़े किसान बनाम छोटे किसान, किसान बनाम खेत–मजदूर, क्षेत्रीय असन्तुलन जैसे मुद्दों ने किसान समस्याओं को जटिल और गतिशील बना दिया। पंचायती राज्य व्यवस्था ने सत्ता के विकेन्द्रीकरण के साथ –साथ किसानी –दुनिया में सत्ता के प्रतीकों में भी मूलभूत परिवर्तन किया। यह वह दौर है जब लगान, बेदखली, बेगारी जैसे मुद्दे या

तो समाप्त हो गये अथवा हाशिए पर आ गये। मंडल–कमंडल के दो किनारों के बीच बहती भारतीय राजनीति ने गांवों में एक नई सुगबुगाहट जरूर पैदा की जिसने जातीय पहचान को और पुख्ता किया। दलितों और पिछड़ों की सत्ता में बढ़ती भागीदारी ने सामन्ती तत्वों को चुनौती देना प्रारम्भ किया। ये ग्राम केन्द्रित उपन्यासों में व्यक्त संघर्ष के नये आयाम हैं । नई आर्थिक नीति, मल्टी नेशनल कंपनियों के खेल,भूमि अधिग्रहण, कर्ज का बढ़ता दुष्चक्र,उत्पाद का उचित मूल्य न मिल पाना और किसानों की बढ़ती आत्महत्याओं ने एक बार फिर उपन्यासकारों का चलने देगें, न खुद इसमें काम करेगें, न औरों को करने देगें. 'की अनुगूँज इस संघर्ष की व्यापकता का प्रमाण है ।

संदर्भ सूची:

1) शिवमूर्ति– आख़री छलांग, पृष्ठ सं.– 79

2). संजीव– 'फांस' पृष्ठ सं. – 61–62

3). पंकज सुबीर– अकाल में उत्सव, पृष्ठ सं.–170

4) अखिल अखिलेश– मीडिया वेश्या या दलाल, हलकान किसान, पृष्ठ–288–289

'हिंदी उपन्यासों में किन्नर विमर्श'

(यमदीप और जिंदगी 50 –50 उपन्यासों के संदर्भ में)

समाधान शिवाजी नागणे

शोध छात्र

कर्मवीर भाऊराव पाटील महाविद्यालय, पंढरपुर

दूरभाष – 9975753381

ई मेल – snagane06@gmail.com

सारांश:

विश्व के सभी समाजों में किन्नरों का भी एक वर्ग है–जिसे थर्ड जेंडर, हिजड़ा, तृतीय लिंगी, उभयलिंगी, यूनक, खोजवा, मौगा, छक्का, पावैया, खुसरा,जनखा, अनरावनी, शिखण्डी, ख्वाजासरा आदि नामों से सम्बोधित किया जाता है । आज हम 21 वीं शती के मशीनी युग में जी रहे हैं जहाँ हर काम बटन दबाने से ही चुटकियों में संपन्न हो जाते हैं । मगर मन व मस्तिष्क आज भी दकियानूसी विचारों की संकीर्णता की बेड़ियों में जकड़े हुये हैं । किन्नर समुदाय की स्थिति अत्यन्त दयनीय है,उनकी झोली में असीम पीड़ा है,जिससे हमारा समाज कोसों दूर हैं । संसद में पेश हुए विधेयक के जरिये किन्नरों के अधिकारों के संरक्षण के लिए केन्द्रीय कैबिनेट ने 'ट्रांसजेंडर पर्सन'बिल 2016 को मंजूरी दे दी ।

हिन्दी साहित्य में 'किन्नर विमर्श' अभी अपरिपक्व अवस्था में सामाजिक, शारीरिक,मानसिक भेद शोषण के दौर में से गुज़र रहा है । किन्नर समाज को स्वयं अपने प्रति संवेदनशील होने की भी आवश्यकता है । किन्नर समाज के बच्चों को सामान्य बच्चों के समान वातावरण प्रदान करना समाज की जिम्मेदारी है ताकि किन्नर समाज का आर्थिक,राजनीतिक व सामाजिक दृष्टि से उत्थान संभव हो सके।

बीज शब्द: हिजड़ा, शैक्षिक सशक्तिकरण, शारीरिक भेद, यमदीप, बुनियादी हक, असरदार पैरवी, जिंदगी, संवेदनशीलता ।

उद्देश्य:

1) किन्नर समुदाय का यथार्थ समाज के सामने लाना ।

2) किन्नर समुदाय के दु:ख एवं दर्द को चित्रित करना ।

3) समाज और परिवार का किन्नरों के प्रति देखने का रवैया दिखाना ।

प्रस्तावना :

साहित्य और समाज का घनिष्ठ संबंध होता है । इसलिए साहित्यकार समाज में जो कुछ घटित होता है, उसकी अभिव्यक्ति साहित्य में साहित्यकार करता है । वस्तुत: समाज में जो कुछ भी व्याप्त हैं, वह साहित्यकार की संवेदना और चिंतन का विषय होता है । जिसकी अभिव्यक्ति साहित्य में कर साहित्यकार समाज में अपनी भूमिका का निर्वाह करता है । आज विश्व धरातल पर मानव अधिकारों की चर्चा ने आंदोलन का रुप धारण कर लिया है । हाशिए के समाज को मुख्यधारा में लाने की कोशिशें हो रही हैं । जैसे स्त्री विमर्श, दलित विमर्श, आदिवासी विमर्श, अल्पसंख्याक विमर्श, किसान विमर्श आदि। समाज के कई उपेक्षित वर्गों पर समकालीन साहित्य में चिंतन हो रहा है, परंतु समाज बहिष्कृत, लिंग निरपेक्ष 'किन्नर' समुदाय के विषय में कोई बड़ी चर्चा नहीं दिख रही है ।

ऐसा नहीं कि साहित्य में किन्नर समुदाय पर पहली बार लिखा गया है । इसके पूर्व महाभारत काल में भी शिखंडी नामक ऐसा ही पात्र था, जो किन्नर था । अर्जुन ने भी अपने अज्ञातवास काल में बृहनल्ला का रूप धारण कर लिया था। ऐतिहासिक तथ्यों के अनुसार हिंदू और मुस्लिम राजाओं ने रानियों की पहरेदारी के लिए किन्नरों को रखा था । कौटिल्य के अर्थशास्त्र में भी किन्नरों का उल्लेख मिलता है । किन्नर समुदाय को धर्म ने, पुराणों ने स्वीकारा जिनका इतिहास 4000 साल पुराना है, परंतु आज भी किन्नर समाज की व्यथा से पीड़ित है ।

संसार में केवल दो लिंगो स्त्री और पुरुष को मान्यता मिली है । लेकिन इन दोनों के अलावा एक और वर्ग भी समाज में उपस्थित है जिसका नाम किन्नर है । यह वर्ग संसार के सभी समाजों में तिरस्कार और अवेहलना का शिकार बन गया है । समाज में किन्नर समुदाय की स्थिति अत्यंत दयनीय है । जिसका कारण समाज एवं सरकार द्वारा किन्नरों के साथ उपेक्षित व्यवहार किया जाना है ।

किन्नर से तात्पर्य :

किन्नर को हिजड़ा, उभयलिंगी, तृतीयलिंगी, खुसरा, मौसी आदि कई नामों से पहचाना जाता है । किन्नर शब्द हिंदी में दो शब्दों 'कि' और 'नर' से मिलकर बना है, जिसका तात्पर्य हिमाचल की जनजाति से नहीं है, बल्कि उस वर्ग से है, जो रुपेण न स्त्री है न पुरुष । वस्तुतः जिसे जन सामान्य की भाषा में हिजड़ा कहा जाता है । हिजड़ों को परिमार्जित भाषा में किन्नर कहा जाता है ।

विमर्श का अर्थ :

आधुनिक साहित्य में विमर्श की अवधारणा 1960 के बाद दृष्टिगोचर होती है । शब्द प्रयोग की दृष्टि से विमर्श शब्द अत्यंत प्राचीन है । इसका अर्थ है "सोच विचार कर तथ्य या वास्तविकता का पता लगाना, किसी बात या विषय पर कुछ सोचना, समझना, विचार करना, गुण– दोष आदि की आलोचना करना या मीमांसा करना, जांचना, पर, किसी से परामर्श या सलाह करना ।"[1] अतः विमर्श शब्द का व्युत्पत्तिपरक अर्थ विचार – विमर्श, सोचना, समझना, आलोचना करना है ।

हिंदी उपन्यासों में किन्नर विमर्श

साहित्य के क्षेत्र में वर्तमान समय में लिंग निरपेक्ष, समाज बहिष्कृत किन्नर या थर्ड जेंडर समुदाय पर चिंतन और चर्चा तेजी से हो रही है । हिंदी साहित्य में नई सदी के आरंभ से यह विमर्श प्रभावी रुप से दिखाई देता है । इसी कारण नीरजा माधव का 'यमदीप', निर्मला गुराडिया का 'गुलाम मंडी', प्रदीप सौरभ का 'तीसरी ताली', महेंद्र भीष्म का 'किन्नर कथा', भगवंत अनमोल का 'जिंदगी 50–50' आदि उपन्यासों में किन्नर जीवन का यथार्थ चित्रण किया है । किन्नरों पर लिखे गए उपन्यासों में उनकी व्यथा–कथा को चित्रित किया है । हिंदी कथा साहित्य में अभी उतनी मात्रा में किन्नर विमर्श पर उपन्यास नहीं लिखे गए । लेकिन फिर भी हिंदी साहित्य में किन्नर विमर्श पर चर्चा हो रही है ।

नीरजा माधव का 'यमदीप' उपन्यास हिंदी का किन्नर समुदाय पर लिखा हुआ पहला उपन्यास माना जाता है । 'यमदीप' उपन्यास में किन्नर समुदाय का रहन– सहन, संताप, अंधविश्वास, उनकी विडंबना, दुख, दर्द, अकेलापन, समाज और परिवार द्वारा उपेक्षा को चित्रित किया है । उपन्यास का पूरा कथानक किन्नर समुदाय के इर्द–गिर्द घूमता है । उपन्यास की नायिका नाजबीबी के माध्यम से भाई द्वारा तिरस्कार, बेटा– बेटी मोह को चित्रित किया है । नाजबीबी इन समस्याओं से लड़ती हुई, अपने अस्तित्व को स्थापित करने का प्रयास करती है । उसके जन्म से ही घरवाले परेशान होते हैं, क्योंकि बच्चा किन्नर है । नाजबीबी पढ़ाई में तेज थी । लेकिन आठवीं कक्षा में पढ़ते समय कुदरत के करिश्मे के कारण उसे अपने पढ़ाई छोड़नी पड़ती है । उसमें स्त्रीयोचित शरीरांग के साथ दाढ़ी, मूछ भी आ जाती है । समाज उसे देखकर हंसी– मजाक करता है ।

नाजबीबी की माता उससे बहुत प्यार करती है । उसे अपने पास रखना चाहती हैं, परंतु सभ्य समाज द्वारा उन्हे विवश किया जाता है कि वह बच्चे को किन्नर समुदाय में छोड़ दे । वह उसे पढ़ा–लिखाकर अपने पैरों पर खड़ा करना चाहती थी । किन्नरों को शिक्षा लेना भी नसीब नहीं है, क्योंकि इन्होंने जब भी शिक्षा लेनी चाही उस समय उन्हें अपमानित होना पड़ा है । इसी वास्तविकता को चित्रित करते हुए महताब गुरु कहते हैं कि "माताजी किसी स्कूल में आजतक हिजड़े को पढ़ते–लिखते देखा है । किसी कुर्सी पर हिजड़ा बैठा है, पुलिस में, मास्टरी में, कलेक्टरी में, किसी में भी । अरे इसकी दुनिया यही है, माताजी! कोई आगे नहीं आएगा कि हिजड़ों को पढ़ाओं, लिखाओं, नौकरी दो जैसे कुछ जातियों के लिए सरकार कर रही है ।"[2]

नाजबीबी को किन्नरों की बस्ती में छोड़ा जाता है । किन्नर लोग नाच–गाकर पैसा कमाते हैं । साधारण लोग उनसे दूर रहना पसंद करते हैं, लेकिन वही किन्नर मानवीयता के कारण लोगों की मदद करते हुए दिखाई देते हैं । एक पागल औरत प्रसव पीड़ा में तड़प रही थी तब किन्नर उसकी मदद करते हैं । वही साधारण लोग उसकी मदद नहीं करते । प्रसूति के बाद उस पागल औरत की मृत्यु होती है । तब उसकी बच्ची को कोई अपनाता नहीं तब नाजबीबी कहती है– "अरे हम हिजड़े है, हिजड़े... इंसान है क्या मुंह फेर ले ।"[3] नीरजा माधव जी इस उपन्यास के माध्यम से यह बताना चाहती है कि साधारण लोग संवेदनशून्य है । इसके विपरीत किन्नर सभी से हमदर्दी रखते हैं । किन्नर लोग किसी बच्चे को अपने साथ नहीं रख सकते हैं । समाज में सभी को जीने का अधिकार है मात्र किन्नरों को छोड़कर क्योंकि वे समाज से तिरस्कृत है । समाज उनको कोसता है, उन पर हंसी–मजाक करता है । नाजबीबी जब उस बच्ची को स्कूल में भर्ती कराने जाती है तो उन्हें देखकर स्कूल की अध्यापिकाएं और छात्र कानफूसी करते हैं । तब वह कहती है– "जब हम धंधे पर नहीं होते, बहनजी तो इस तरह का मजाक हमारे सीने में गोली की तरह लगता है । हम आसमान से तो नहीं टपकते हैं न? आपकी तरह किसी मां की कोख से जन्में है । हाड–मांस का शरीर लिए । हमें तो अपने आप दु:ख होता है इस जीवन पर । आप लोग भी दु:खी कर देते हो ।"[4]

समाज किन्नर बच्चे को अपने पास रखना पसंद नहीं करता है । परिवार के जो सदस्य इन्हे अपने पास रखना चाहते हैं, समाज उन्हें भी मजबूर कर देता है कि उस बच्चे को किन्नर समाज को सौंप दें । यदि परिवार के लोग उसे पढ़ना भी चाहे या अन्य बच्चे की तरह उसकी परवरिश भी करना चाहे फिर भी समाज में बेइज़्ज़ती की डर से उस बच्चे को अपने से अलग कर देते हैं । समाज की असंवेदनशीलता का चित्रण महताब गुरु के माध्यम से किया है ।

महताब गुरु कहते हैं "आप इस बस्ती में रह नहीं सकते बाबूजी और आपकी अपनी बेटी को अपने साथ रख नहीं सकते... दुनिया में बदनामी और हंसी हंसारात के डर से । हिजड़ी के बाप कहलाना न आप बर्दाश्त कर पाएंगे और न आपके परिवार के लोग । लूली, लंगड़ी होती यह, कानी कोतरी होती, तो भी आप ही से अपने साथ रख सकते थे, इसलिए इसे अब इसके हाल पर ही छोड़ दीजिए । यही इसका भाग्य था, यही बदा ।"[5] महताब गुरु के माध्यम से वास्तविकता को चित्रित किया गया है ।

किन्नर समाज अस्पष्ट जेंडर और यौनिक पहचान के कारण अपने नागरिक अधिकारों से वंचित रहा है । लेकिन आज संविधानिक सुधार की वजह से किन्नरों को राजनीतिक क्षेत्र में अधिकार मिल गए है । समाज में व्याप्त भ्रष्टाचार, शोषण से तंग आकर किन्नर राजनीति में भाग लेकर समाज में सुधार लाना चाहते है । नाजबीबी कहती है– "जरुरत पड़ी तो भ्रष्ट लोगों के खिलाफ हथियार भी उठाऊंगी । हर गंदगी को जड़ से साफ कर दूंगी । दुनिया में शांति रहे और क्या चाहिए किसी को?"[6] इस प्रकार किन्नर सिर्फ ताली बजाना नहीं चाहता, तो समाज में सुख –शांति रहे इसलिए वह कुछ भी करने को तैयार है ।

भगवत अनमोल 'जिंदगी 50–50' उपन्यास किन्नर जीवन का यथार्थ चित्रण करता है । उपन्यास का नायक अनमोल का भाई हर्षा और बेटा सूर्या दोनों किन्नर है । हर्षा के किन्नर होने के कारण पिता द्वारा मारपीट और उपेक्षा मिलती है । घर और परिवार से वह प्रताड़ित होता रहता है । वह जैसे–जैसे बड़ा होता है समाज में उसका जीना और भी मुश्किल हो जाता है । घर से लेकर

बाहर तक उसका मजाक उड़ाया जाता है । उसके स्कूल की अध्यापिका भी उसका मजाक उड़ाते हुए कक्षा में शैतानी कर रहे बच्चों से कहती हैं–"अगर किसी ने बदमाशी की तो उसे हर्षा के पास बैठा दूंगी ।"[7] अपने प्रति किए जा रहे हैं व्यवहार को समझ पाना हर्षा के लिए कठिन हो जाता है । वह जैसे–जैसे बड़ा होता है, वैसे वैसे उसके पूरे शरीर में स्त्री मन की भावनाएं बलवती हो जाती है । वह अपनी माँ की साड़ी पहनता है और श्रृंगारर भी करता है । एक दिन लड़की के वेश में सजी संवरी हर्षा को उसके बाबूजी देखते हैं और उसे पीटते हुए कहते हैं–"तुझे ज्यादा शौक है लौंडिया बनने का! छोड़ आएंगे हिजड़ों के पास, तो यहां वहां–वहां छुछुआत भीख मांगता फिरेगा ।"[8]

समाज किन्नरों को हमेशा बुरी नजर से देखता है । जब किन्नर हर्षा पर बलात्कार होता है तब उसकी भावात्मक वेदना इस प्रकार अभिव्यक्त हुई है–"किन्नर होना अधूरापन ही तो है न? कैसे– कैसे पल आते । इस शरीर में सब भुगता, सब सहा जिस शरीर का लोग मजाक उड़ाते हैं, उसे ही रात को अपने मन बहलाने का जरिया बना लेते हैं । अच्छा है इन लोगों से दूर अपना एक समुदाय हैं ।"[9] समाज की किन्नर लोगों के प्रति सोच अच्छी न होने के कारण अपना अलग समुदाय बनाने के लिए किन्नर विवश होते हैं ।

इस उपन्यास में हर्षा तथा हर्षिता के माध्यम से एक किन्नर की प्रताड़ना को चित्रित किया है । वह अंत में एच.आय. व्ही. जैसे रोग से ग्रस्त होती हैं और वह आत्महत्या करके अपने हर पल मरे हुए जीवन का अंत करती है ।

निष्कर्ष :

निष्कर्षत: यह कहा जा सकता है कि सिर्फ जननांग दोष के कारण किन्नर समुदाय को समाज से उपेक्षित करना उचित नहीं है । यह समुदाय हमारी तरह ही मानवीय सुविधाओं से युक्त हैं । इन्हें भी दु:ख, दर्द पीड़ा होती है । यह भी हमारी तरह मानव है । परिवार और समाज से बहिष्कृत होकर जीना बहुत ही मुश्किल होता है । किन्नर समुदाय को समाज घृणा की दृष्टि से देखता है । इसलिए इनका जीवन दु:खों से भरा हुआ है । जीवन के हर क्षेत्र में चाहे वह पारिवारिक हो, सामाजिक हो, आर्थिक हो या फिर राजनीति हो। हर क्षेत्र में इनके प्रति देखने के रवैय्ये को बदलना होगा ताकि यह समुदाय भी समाज की मुख्यधारा से जुड़कर सामान्य जीवन जी सके।

संदर्भ:

1) रामचंद्र वर्मा, मानक हिंदी कोश, पृष्ठ– 77
2) नीरजा माधव, यमदीप, सामायिक प्रकाशन, नई दिल्ली, 2009, पृ. 30
3) वही, पृ. 12
4) वही, पृ. 50
5) वही पृ. 87
6) वही, पृ. 118
7) भगवंत अनमोल, जिंदगी 50–50, राजकमल एंड सन्स प्रकाशन,
2017, पृष्ठ – 118
8) वही पृ. 167
9) वही पृ. 207

स्वतंत्रता संग्राम में हिंदी की भूमिका

समीना नायकवडी (कुरेशी)
डॉ. पतंगराव कदम आर्ट्स एंड कॉमर्स
कॉलेज, पेण, रायगढ़, महाराष्ट्र
Mob-7058051292,
ई मेल – saminanaikawdi@gmail.com

शोध सारांश–

भारतीय इतिहास में स्वतंत्रता आन्दोलन एक युगान्तकारी घटना है । यह विशाल देश लगभग सन् 1757 से 1947 तक परतंत्र रहा । भारत में ब्रिटिश शासन अट्ठारहवीं शताब्दी के मध्य तक स्थापित हो चुका था किन्तु अंग्रेजों की दुर्नीति और दमनचक्र ने एक नया जागृत राष्ट्रवाद उत्पन्न किया । उन्नीसवीं शताब्दी के उत्तरार्द्ध में देश में पुनरुत्थान और राजनैतिक चेतना की लहर फैल गयी । तत्कालीन हिन्दी कवियों ने भी देश की दासता और करुण दशा से प्रभावित होकर जन जागरण में अपना सक्रिय योगदान किया । उनका हृदय भारत माँ को दासता की बेड़ियों से मुक्त कराने के लिए उद्वेलित हो उठा । देशवासियों को अतीत के स्वर्णिम वैभव और सांस्कृतिक परम्परा से परिचित कराने का दायित्व निर्वहन तो इन कवियों ने किया ही साथ ही साथ उनमें देशनिष्ठा एवं अस्मिता भी जागृत की । कवियों देश की दुर्दशा पर भी क्षोभ प्रकट कर अंग्रेजी शासन के विरुद्ध संघर्ष के लिए जनमानस को प्रेरित किया तथा क्रांति की समुचित पृष्ठभूमि तैयार की । उन्होंने अंग्रेजों की कपटनीति और साम्राज्यवाद का विरोध करते हुए, देशवासियों को आत्मसम्मान के साथ जीने का संदेश दिया । इसके साथ ही साथ बहुत से हिंदी रचनाकर भारतीय स्वतंत्रता आंदोलन में सक्रिय होने के कारण बहुत से हिंदी रचनाकारों ने विविध पत्र पत्रिकाओं के माध्यम से अपने राष्ट्रवादी विचार जनता तक पहुँचाए हैं । स्वत्रंता आंदोलन में भी नेताओं ने ज्यादा से ज्यादा भारतीय जनता का आंदोलन में सहभाग हो अतः सब एक मिलकर अंग्रेजो के खिलाफ लड़े जिसमें हिंदी ने अहम भूमिका निभाई ।

बीज शब्द – भारतीय स्वतंत्रता आंदोलन, राजनैतिक चेतना, देशनिष्ठा, हिंदी समर्थन ।

उद्देश – हिंदी साहित्य, हिंदी साहित्यिक पत्र–पत्रिका और स्वतंत्रता आंदोलन के राजकीय नेताओं का हिंदी समर्थन आदि दृष्टिकोण से हिंदी का भारतीय स्वतंत्रता आंदोलन में योगदान कैसे रहा यह स्पष्ट करना ।

प्रस्तावना –

निज भाषा उन्नति अहै, सब उन्नति को मूल ।
बिन निज भाषा– ज्ञान के,मिटत न हिय को सूल ।।
विविध कला शिक्षा अमित, ज्ञान अनेक प्रकार ।
सब देसन से लै करहू, भाषा माहि प्रचार ।।

– भारतेंद्र हरिश्चंद्र

कवि भारतेंदु हरिश्चंद्र कहते हैं कि सभी प्रकार की प्रगति का आधार अपनी मातृभाषा का विकास करना है । मातृभाषा ज्ञान के बिना हृदय का दुख दूर नहीं हो सकता । भारत में कुल 28 राज्य हैं और उन सबकी अपनी भाषा है कुल मिलाकर भारत में 121 भाषाएं बोली जाती हैं किंतु देश की मातृभाषा हिंदी है । हिंदी ने आज राष्ट्रभाषा, राजभाषा का स्थान प्राप्त किया है किन्तु वह सबसे

पहले हम सब हिंदुस्तानियों की सामान्य भाषा है । भले ही भारत में विभिन्न भाषाएं बोली जाती हो फिर भी भारतीय समाज में शिक्षित और अशिक्षित जनता को आसानी से हिंदी का प्रयोग करते हुए हम देखते हैं । हिंदी की अपनी एक विकास यात्रा है । उसके साहित्य की आपनी सांस्कृतिक विरासत है । इसी हिंदी ने ही सब को एकसूत्र में बाँध रखा है । स्वतंत्रता संग्राम आंदोलन में हिंदी ने अपनी महत्वपूर्ण भूमिका निभाई भारतीय जनमानस में राष्ट्रवाद जागृत कर साहित्य, पत्र पत्रिकाओं के माध्यम से हिंदी ने स्वतंत्रता संग्राम आंदोलन को गति दी । हिंदी के कितने ही एसे रचनाकार हैं जिन्होंने स्वतंत्रता आंदोलन में सक्रिय सहभागी हो हिंदी साहित्य के माध्यम से राष्ट्रवाद जागृत कर देशभक्ति, देशप्रेम बढ़ाया है । स्वतंत्रता आंदोलन के कुछ सेनानी हिंदी के प्रबल समर्थक और प्रचारक थे। महावीरप्रसाद व्दिवेदी ने हिंदी का परिमार्जन कर हिंदी को आगे बढ़ाया तो स्वतंत्रता आंदोलन के जनक बालगंगाधर तिलक ने नागरी प्रचारिणी पत्रिका के भाषण में कहा था कि, "राष्ट्रभाषा मैं ऐसे राष्ट्रीय आंदोलन की बात कर सकता हूँ, जिससे सारा भारत एक सामान्य भाषा या राष्ट्रभाषा अपना सके एक भाषा राष्ट्रीयता का महत्त्वपूर्ण तत्त्व है । आप एक सामान्य भाषा के माध्यम से अपने विचार दूसरों तक पहुँचा सकते हैं । यदि आप राष्ट्र को एकता के सूत्र में बाँधना चाहते हैं तो सबके लिए एक सामान्य भाषा से अधिक प्रबल शक्ति कोई और नहीं हो सकती ।"

इस तरह हिंदी ने स्वतंत्रता युगीन चेतना को सशक्त तरीके से लोगों तक पहुंचा कर भारतीय राष्ट्रवाद को आगे बढ़ाया है तथा भारतीय जनमानस में देशप्रेम जगाया ।

हिंदी साहित्य द्वारा हिंदी का स्वतंत्रता आंदोलन में योगदान

भारतेन्दु युग के कवियों ने जहाँ एक ओर भारतीय इतिहास के गौरवशाली पृष्ठों का स्मरण दिला कर देशप्रेम का नया स्वर फूँका, वहीं दूसरी ओर अंग्रेजों की न्यायप्रियता, संगठन–शक्ति, प्रजातंत्र में आस्था, उच्चशिक्षा आदि की भी प्रशंसा की किन्तु उन्होंने अंग्रेजों की साम्राज्यवादी नीति का विरोध किया । देश के उद्योग–धन्धों की अवनति, आर्थिक शोषण, करों के बोझ से निरन्तर दबी जा रही जनता के दुख–दर्द का भी इन कवियों ने अनुभव किया । ये कवि क्षेत्रीयता से ऊपर उठकर राष्ट्र के नवजागरण के गीत गाने लगे । राधा चरण गोस्वामी, प्रेमधन, श्रीधर पाठक, राम देवी प्रसाद पूर्ण आदि कवियों ने देश के उत्कर्षाकर्ष के लिए उत्तरदायी परिस्थितियों पर प्रकाश डालकर भारतेन्दु युगीन कवियों ने जनमानस में राष्ट्रीय भाव का बीजारोपण किया । भारतेन्दु हरिश्चन्द्र, प्रतापनारायण मिश्र, प्रेमघन, राधाकृष्ण दास, बाल मुकुंद गुप्त, अम्बिका दत्त व्यास आदि की कवितायें इसी परम्परा में लिखी गयी हैं । जैसे .

"बड़े बड़े बीरन के वंशज, बनि बैठे सब गोरी।
नाचि रिझावत परदेसिन को,लाज नहीं तनको री।
जु ले लहँगौ कोउ छोरी॥"

होलिकापंचक – प्रतापनारायण मिश्र

भारतेंदु युगीन गद्य साहित्य की विशेषताओं में सबसे अधिक प्रमुख विशेषता राष्ट्रप्रेम का भाव जागृती है । जिसे तत्कालीन साहित्यकारों ने हास्य व्यंग के माध्यम से व्यक्त किया है । प्रथम स्वतंत्रता संग्राम के परिणामस्वरुप भारतवासियों में सोई हुई आत्मशक्ति के जागरण के साथ ही राजनीतिक अधिकारों के प्रति लालसा बढ़ी, जिससे उनमें राष्ट्रीयता के भाव का उदय होना स्वाभाविक था । इसका प्रभाव इस युग की रचनाओं पर भी पड़ा । इस युग के रचनाकारों की रचनाओं में देशभक्ति का स्वर विशेष रूप से गुंजायमान रहा । उदाहरण– भारत दुर्दशा भारतेन्दु हरिश्चन्द्र द्वारा सन 1875 ई. में रचित एक हिन्दी नाटक । इसमें भारतेन्दु ने प्रतीकों के माध्यम से भारत की तत्कालीन स्थिति का चित्रण किया है । वे भारतवासियों से भारत की दुर्दशा पर रोने और फिर इस दुर्दशा का अन्त करने का प्रयास करने का आह्वान करते हैं । भारतेन्दु का यह नाटक अपनी युगीन समस्याओं को उजागर करता

है तथा साथ ही साथ उसका समाधान करता है । भारत दुर्दशा में भारतेन्दु ने अपने सामने प्रत्यक्ष दिखाई देने वाली वर्तमान लक्ष्यहीन पतन की ओर उन्मुख भारत का वर्णन किया है । जैसे–

"तीन नासी बुद्धि बल विद्या, धन बहू बारी ।
छाई अब आलस – कुमति – कलह – अंधियारी ।।
भय अंध पंगु सब दीन– हीन बिखलाई ।
हा! हा! भारत दुर्दशा ना देखी जाई।।

– भारत दुर्दशा–भारतेंदु हरिश्चन्द्र

द्विवेदी युग में खड़ी बोली हिंदी का प्रचलन और प्रतिष्ठापन आचार्य महावीर प्रसाद द्विवेदी द्वारा किया गया । राष्ट्रीयता द्विवेदी युगीन काव्य की प्रधान भावधारा थी । इस युग के प्रायः सभी कवियों ने देशभक्तिपूर्ण कविताओं का सृजन किया । उन्होंने परतंत्रता की निद्रा में सुप्त भारतीयों को जाग्रत करने का प्रयास किया । भारतीय स्वतंत्रता संग्राम के इतिहास में इस युग का विशेष महत्त्व है । भारतीय गौरव और सम्मान से जुड़े अनेक आन्दोलनों का प्रभाव इस युग में रहा । गांधी जी के आगमन से देश में नयी शक्ति संचरित हुई तथा राष्ट्रीयता की लहर पूरे देश में फैल गयी । कवियों ने स्वतंत्रता प्राप्ति के लिए क्रांति का आह्वान किया । उन्होंने गौरवपूर्ण अतीत के चित्रण के साथ ही वर्तमान की दुर्व्यवस्था का भी वर्णन किया है । इन कवियों ने सामाजिक कुरीतियों, अंधविश्वासों, निर्धनता, स्वदेशी भावना, असहयोग स्वातंत्र्य आन्दोलन आदि सभी को अपना काव्य विषय बनाकर सशक्त अभिव्यक्ति दी । आ.महावीर प्रसाद द्विवेदी, नाथूराम शंकर, मन्नत द्विवेदी, रामचरित उपाध्याय, रूप नारायाण पाण्डेय, लोचन प्रसाद पाण्डेय, गया प्रसाद शुक्ल 'स्नेही', रामनरेश त्रिपाठी, माधव शुक्ल, सत्यनारायण कविरत्न आदि की रचनाओं में राष्ट्रीय जागृति और क्रांति के चित्र मिलते हैं । लोक कवियों ने कांग्रेस, महात्मा गांधी, असहयोग आन्दोलन, चर्खा, स्वराज आदि से सम्बन्धित लोकगीतों की रचना कर हिंदी के माध्यम से देशप्रेम और स्वातंत्र्य चेतना जगाने की चेष्टा की है । जैसे–

"चल पड़े जिधर दो डग मग में
चल पड़े कोटि पग उसी ओर,
पड़ गई जिधर भी एक दृष्टि
गड़ गये कोटि दृग उसी ओर ।"

– युगावतार– गांधी, सोहनलाल द्विवेदी

छायावाद की राष्ट्रीय चेतना अपने अंतिम स्तर पर केवल राष्ट्र तक सीमित नहीं रहती बल्कि संपूर्ण मानवता के स्तर पर सक्रिय हो जाती है । यह भारतीय चिंतन सृष्टि की वही धारणा है जिसमें राष्ट्रीय हितों व वैश्विक हितों को परस्पर विपरीत नहीं बल्कि सुसंगत शक्तियों के रूप में विश्व कुटुंबकम का व्याख्यान किया जाता है । स्वाधीनता के संघर्ष में नए विकल्प के तौर पर निराला सुझाते हैं । जैसे–

"शक्ति की करो मौलिक कल्पना, करो पूजन,
छोड़ दो समर जब तक न सिद्धि हो रघुनंदन ।
रावण अशुद्ध होकर भी यदि कर सका त्रस्तए,
तो निश्चित तुम हो सिद्ध करोगे उसे ध्वस्त ।।"

– राम की शक्तिपूजा – निराला

संक्षेप में यह स्पष्ट है कि हिंदी साहित्य जगत के रचनाकारों ने हिंदी के माध्यम से राष्ट्रवाद की अवधारणा निर्माण से लेकर उसके विकास तक हिंदी के साहित्यिक विधा के माध्यम से अहम योगदान दिया ।

हिंदी पत्र–पत्रिका के माध्यम से हिंदी का स्वतंत्रता आंदोलन में योगदान –

राजनैतिक, शैक्षिक, आर्थिक, सामाजिक तथा धार्मिक विकास के परिणामस्वरूप जो राष्ट्रवाद उदित हुआ, उसे पत्रकार, बुद्धिजीवी, राष्ट्रवादी लोग विभिन्न पत्र–पत्रिकाओं में अंग्रेजी शासन के दमन और पोषण के विरूद्ध लिखते रहे और जनता को जागरूक करके नवोत्थान के लिए मार्ग प्रशस्त किया । हिन्दी और अन्य भारतीय भाषाओं के पत्रकार अपनी राष्ट्रवादी भावनाओं और विचारों के लिए प्रख्यात रहे हैं । स्वतंत्रता संघर्ष के दौरान हिन्दी साहित्य और हिन्दी पत्रकारिता साथ.साथ चलने लगे तत्कालीन परिस्थिति में रचनाकार एक साथ साहित्यकार और पत्रकार दोनों हुआ करते थे ।

पत्रकारिता के संबंध में कहा गया है कि वह शीघ्रता में लिखा गया साहित्य है और साहित्य प्रतीक, बिम्ब और अप्रस्तुत कथन के द्वारा अपना प्रतिपाद्य अभिव्यक्त करता है । साहित्य को समझने वाले लोगों का एक खास वर्ग होता है । किन्तु पत्रकारिता जनता की भाषा में जनता की बात करती है । संभवतः यहीं कारण है कि स्वतंत्रता अवधि के सभी रचनाकारों ने अभिव्यक्ति के माध्यम के रूप में साहित्य और पत्रकारिता दोनों को चुना जिस प्रकार देश के स्वाधीनता संग्राम में राष्ट्रनायकों का अप्रतिम योगदान रहा, उसी प्रकार पत्र–पत्रिकाओं के माध्यम से भी लोगों में राष्ट्रीयता की भावना को जगाया गया राष्ट्रीयता की वह धारा जिसका विकास राजनीति के माध्यम से हो रहा था पत्रकारिता की शक्ति से संपन्न थी ।

हिंदी पत्र–पत्रिकाओं का प्रथम चरण –

1826 ई. में उदंत मार्तंड के प्रकाशन से लेकर 1873 ई. में भारतेन्दु के हरिश्चन्द्र मैगजीन तक को हिंदी पत्र पत्रिकाओं का प्रथम चरण माना जाता है । हिन्दी पत्रकारिता का प्रारंभिक काल के हिन्दी पत्र निम्नांकित रहे हैं । जुगलकिशोर शुक्ल का उदंत मार्तण्ड, 1826 में नील रतन हालदार का बंगदूत, 1829 में राजा शिवप्रसाद सितारे हिन्द का बनारस अखबार, 1845 में प्रेमनारायण का मालवा अखबार, 1848 में तारामोहन मित्र का सुधाकर, 1850 में मुंशी सदा सुखलाल का बुद्धि प्रकाश, 1852 में मुंशी लक्ष्मण दास का ग्वालियर गजट, 1853 में श्यामसुंदर का समाचार सुधावर्ष, 1854 राजा लक्ष्मण सिंह का प्रजाहितैषी, 1855 बाबू श्रीलाल का जियाजी प्रताप, 1855 शिवनारायण का सर्वहितकारक, 1855 ग्रंथसभा का बुद्धिवर्धक ग्रंथ, 1856 कन्हैयालाल का राजपूताना अखबार, 1857 अजी मुल्ला का पयामें आजादी, 1857 नवीनचन्द्र राय का ज्ञानप्रदायिनी पत्रिका, 1866 तत्वबोधिनी पत्रिका आदि पत्र राष्ट्रीयता की भावना से भरे हुए थे । इन पत्रों में समाजसुधार, राष्ट्रीयता, क्रांति की भावना एवं विदेशी शासन के विरूद्ध बगावत का स्वर है । जैसे–

"भारतेन्दु ने पत्रकारिता के माध्यम से साहित्य की अनेक नवीन विचाओं को विकसित कर उनके माध्यम से स्वतंत्रता की भावना को विकसित किया । उनके पत्रों से राष्ट्रीय विचारधारा प्रस्फुटित हुई ।"

भारतेन्दु के पत्रों के अतिरिक्त पं. बालकृष्ण भट्ट का हिन्दी प्रदीप, पं. प्रताप नारायण मिश्र का ब्राह्मण, प्रेमधन का आनंद कादंबिनी और नागरी नीरद, पं. गौरी दत्त का देवनागरी प्रचारक, ठाकुर हनुमंत सिंह का राजपूत, रूद्रदत्त शर्मा द्वारा संपादित भारत मित्र, बालमुकुन्द गुप्त का हिन्दी बंगवासी, श्री तोताराम जी का भारत बन्धु, गोपाल राम गहवरी का भारत भूषण, पंडित मोहनलाल द्वारा संपादित मोहन चंद्रिका आदि इस युग के प्रमुख पत्रकार एवं पत्र–पत्रिकाएं थी । इनमें से अधिकांश संपादक एवं लेखक भारतेन्दु मण्डल के थे । इन सभी का मूल उद्देश्य स्वदेशप्रेम, भाषा एवं संस्कृति के प्रति अनन्य श्रद्धा, राष्ट्रप्रेम, हिन्दी भाषा का प्रचार आदि था ।

हिंदी पत्र–पत्रिकाओं का द्वितीय चरण –

1900 ई. से 1920 ई. तक का युग द्विवेदी युग के नाम से जाना जाता है । विचारक और साहित्य नेता आचार्य महावीर प्रसाद द्विवेदी के नाम पर ही इस काल का नाम द्विवेदी युग पड़ा । 1900 में प्रकाशित सरस्वती के माध्यम से पं.महावीर प्रसाद द्विवेदी ने साहित्यिक पत्रकारिता की परंपरा को समृद्ध और परिष्कृत किया । सरस्वती पत्रिका में देशप्रेम विषयक कविता का प्रकाशन अनवरत जारी रही । पं. महावीरप्रसाद द्विवेदी की जन्मभूमि भारतभूमिश, आर्यभूमि प्यारा वतन, रूपनारायण पांडेय की मातृभूमि, लक्ष्मण सिंह की जन्मभूमि पूजन, रामनरेश त्रिपाठी की जन्मभूमि भारत रामचरित उपाध्याय की भव्यभारत आदि देश–प्रेम से ओत.प्रोत कविताएँ सरस्वती में लगातार प्रकाशित होती रही । महावीर प्रसाद द्विवेदी ने सन् 1903 से 1918 ई. तक लगातार सरस्वती का संपादन कर हिन्दी की साहित्यिक पत्रकारिता को नया आयाम दिया। यही कारण है कि पत्रकारिता के इस कालावधि को साहित्यिक पत्रकारिता का युग अथवा द्विवेदी युग कहा जाता है ।

आचार्य नंददुलारे वाजपेयी लिखते हैं, "द्विवेदी जी के सरस्वती संपादन का इतिहास ऐसे अनेक आंदोलनों का इतिहास है । जो उनके व्यक्तित्व और तत्कालीन समाज के विकास का इतिहास भी कहा जा सकता है ।

द्विवेदी कालीन प्रमुख पत्र.पत्रिकाएँ निम्नांकित है– पं. चंद्रधर शर्मा गुलेरी के संपादकत्व में जयपुर से समालोचक पत्रिका, शांतिनारायाण का स्वराज्य पत्र, मदनमोहन मालवीय का अभ्युदय तिलक के केसरी का हिन्दी संस्करण, हिन्दी केसरी पं. सुंदरलाल का कर्मयोगी, कृष्णकांत मालवीय का मर्यादा, गणेश शंकर विद्यार्थी का प्रताप युवक और विशाल भारत युगांतर गदर वंदेमातरम्, प्रभा आदि इन पत्र– पत्रिकाओं ने स्वतंत्रता आंदोलन में अपना भरपूर योगदान दिया ।

इन पत्रिकाओं पर गांधी के विचारों का स्पष्ट प्रभाव दिखाई पड़ता है । अब पत्रकारिता की धारा राष्ट्रीय चेतना से प्रेरित होकर महात्मा गांधी के नेतृत्व में गतिमान राष्ट्रीय आंदोलन का समर्थन करने लगी । इस युग में गांधी जी ने अपनी पत्रकारिता के माध्यम से जन–जागरण सत्याग्रह एवं अछूतोद्धार का कार्य प्रारंभ कर दिया । नवजीवन और हरिजन पत्र के **माध्यम** से गांधीजी ने तो एक नए युग और सामाजिक क्रांति का उद्घोष कर दिया था । गाँधी जी से प्रभावित होकर स्वराज की माँग को प्रखर स्वर देने हेतु विभिन्न पत्र–पत्रिकाएँ प्रकाशित हुयी । जैसे– जबलपुर से कर्मवीर, आगरा से सुधाकर, लाहौर से ज्योतिश, सोहागपुर से हिन्दू, प्रयाग से हिंदुस्तानी अखबार, कलकत्ता से क्षत्रिय मार्तण्ड, काशी से अहिंसा, आज कानपुर से वर्तमान और लोकमत पटना से प्रजाबंधु तथा देश आदि पत्र– पत्रिकाएँ प्रकाशित हुयी ।

स्वतंत्रता आंदोलन में राजकीय नेताओं का हिंदी समर्थन –

स्वतंत्रता संग्राम भी अनेक नेताओं के नेतृत्व में लड़ा गया । स्वतंत्रता के साथ–साथ हमारे राजनेताओं ने आत्माभिव्यक्ति की स्वतंत्रता का आंदोलन भी छेड़ा । भारत के लोग अंग्रेजी भाषा और अंग्रेजी शिक्षा के विरुद्ध बोलने लगे । हिंदी सीखना और बोलना स्वतंत्रता आंदोलन का एक अंग बन गया । आजाद हिंद फौज में हिंदी का ही बोलबाला था । सुभाषचंद्र बोस भी हिंदी में ओजस्वी भाषण देते थे । लोकमान्य बाल गंगाधर तिलक, महात्मा गाँधी, राजगोपालाचारी, महामना पं. मदन मोहन मालवीय, आचार्य नरेंद्र देव, राजर्षि पुरुषोत्तम दास टंडन आदि नेताओं ने हिंदी की अस्मिता को पहचाना और हिंदी के प्रचार– प्रसार में जुट गए । महात्मा गाँधी ने तो राष्ट्रभाषा हिंदी के आंदोलन को स्वतंत्रता आंदोलन के साथ जोड़ दिया । उन्होंने स्वयं हिंदी सीखी और अन्य लोगों को भी हिंदी सीखने के लिए प्रेरित किया । शुरू में महात्मा गांधी जी के विचार गुजराती में और अंग्रेजी में ही प्रकट होते देखकर श्री जमनालाल बजाज ने गुजराती नवजीवन की हिंदी आवृत्ति, संस्करण निकालने का आग्रह किया । महात्मा जी मान गये और उनके अंग्रेजी और गुजराती लेखों का अनुवाद हिन्दी में प्रकट होने लगा । जो काम हिंदी नवजीवन ने किया, वही आगे जाकर हरिजनसेवक द्वारा आखिर तक होता रहा । देशप्रेम और हिंदी भाषा के प्रति अपने विशेष प्रेम के कारण गांधी जी ने जहां तक हो

सका हिंदी बोलने का और पत्र लिखने का नियम चलाया । इन नेताओं ने सभी भारतीय जनता को एकत्रित लाने और स्वतंत्रता आंदोलन को और अधिक प्रबल बनाने हेतु हिंदी का समर्थन किया था । हिंदी समर्थन हेतू नेताओं के वक्तव्य कुछ इस प्रकार थे । जैसे

राजर्षि पुरुषोत्तम दास टंडन ने कहा था कि "मेरे लिए हिंदी की समस्या भारत की स्वतंत्रता की समस्या है । भाषा की समस्या राष्ट्र की समस्या से संबंधित होती है । भारत में अंग्रेजी भाषा की प्रधानता स्वीकार करना अंग्रेजी जीवन–सिद्धांत के सामने सिर झुकाना है । यह हमारी बौद्धिक दासता का सूचक है ।"

गाँधीजी ने कहा था, "राष्ट्रभाषा के बिना राष्ट्र गूँगा है ।"

निष्कर्ष –

इस प्रकार राष्ट्रभाषा के बिना राष्ट्रीय एकता और भावात्मक एकता का संवर्धन और पोषण नहीं हो सकता । प्राचीन काल से ही हिंदी ने इसका पोषण किया है । वास्तव में हिंदी लोकभाषा है और उसकी शक्ति जनशक्ति है । इस देश की सामासिक संस्कृति को व्यक्त करने की क्षमता हिंदी में है । स्वाधीनता आंदोलन के दौरान हिंदी न केवल पूरे देश को जोड़ने वाली राष्ट्रीय कड़ी बनी बल्कि वह अपने आप में आंदोलन का एक पवित्र लक्ष्य थी । हिंदी ने अपने साहित्य के माध्यम से राष्ट्रवाद को आगे बढ़ाया और स्वतंत्रता आंदोलन में अपना योगदान दिया ।

संदर्भ ग्रंथ –

1. होलिकापंचक – प्रतापनारायण मिश्र
2. भारत दुर्दशा–भारतेंदु हरिश्चन्द्र
3. युगावतार– गांधी, सोहनलाल द्विवेदी
4. राम की शक्तिपूजा – निराला
5. नागरी प्रचारिणी सभा वाराणसी में भाषण दिसंबर 1905 लोकमान्य तिलक, हिज राइटिंग्स एंड स्पीचेज पृ. 2
6. हिमांशु शेखर सिंह,हिन्दी पत्रकारिता और काशी.पृ . 69
7. ओ. पी. शर्मा, पत्रकारिता और उसके विभिन्न स्वरूप, पृ.25
8. महिपाल सिंह एवं देवेंद्र मिश्र,विश्व बाजार में हिंदी, पृ.83

स्वतंत्रता आंदोलन में शहीद भगतसिंह का योगदान

पूजा काशीनाथ मुट्ठे
पीएच. डी. (हिंदी) शोध छात्रा,
डॉ. बाबासाहेब आंबेडकर मराठवाड़ा विश्वविद्यालय,
छत्रपति संभाजीनगर, महाराष्ट्र
E-mail- poojamutthe@gmail.com
भ्रमण ध्वनि नम्बर: 7028147012

भूमिका–

इतिहास के पन्नों को अगर पलटा जाए तो आज भी भगतसिंह का बलिदान हमारे दिल को छू लेता है । देश को आजाद करने के लिए अनेक स्वतंत्र संग्राम हुए । उसमे केवल महात्मा गांधी ही नहीं, बल्कि भगतसिंह जैसे अनेक नौजवानों ने अपना बलिदान दिया । भगतसिंह एक महान क्रांतिकारक थे । उनका विचार था कि, आत्मरक्षा के लिए अगर कोई हिंसा की जाए तो वह हिंसा नहीं होती बल्कि आत्मरक्षा होती है ।

भगतसिंह का जन्म 28 सितंबर 1907 को लायलपुर जिले के बंगा में हुआ था । जो अब पाकिस्तान में है । उनका पैतृक गांव खटकड़ कलाँ है । जो पंजाब राज्य, भारत में है । उनके जन्म के समय उनके पिता किशनसिंह, चाचा अजीतसिंह और स्वर्णसिंह जेल में थे । भगत सिंह पर इन सभी का गहरा प्रभाव पड़ा था । उन्होंने बचपन में ही अंग्रेजों के अत्याचार को बहुत करीब से देखा था । वे बचपन से ही अंग्रेजों से घृणा करने लगे थे । भगतसिंह के मन में क्रांति की चिंगारी तभी जल पड़ी जब उन्होंने 1919 में जालियांवाला बाग की घटना को उन्होंने बहुत करीब से देखी और वह गंभीर रूप से उस घटना से प्रभावित हुए । बचपन में वह महात्मा गांधी के असहयोग आंदोलन में भाग लेने लगे, और उनके विचारों पर चलने लगे । 14 वर्ष की आयु में ही भगतसिंह ने सरकारी स्कूलों की पुस्तकें और कपड़े जला दिए । पर चौरा–चोरी की घटना के कारण महात्मा गांधी ने असहयोग आंदोलन पीछे ले लिया । इसका सदमा भगतसिंह पर बहुत गहरा पड़ा । उस समय भगतसिंह लाहौर के नेशनल कॉलेज में पढ़ते थे । वहां उनकी मुलाकात सुखदेव से हुई ।

भगतसिंह हिंदी, उर्दू, अंग्रेजी, संस्कृत, पंजाबी, बंगाल और आयरिश भाषा के मर्मज्ञ चिंतक और विचारक थे । भगतसिंह भारत में समाजवाद के पहले व्याख्याता है । भगतसिंह अच्छे वक्ता, पाठक और लेखक भी थे । उन्होंने 'अकाली' और 'कीर्ति' दो अखबारों का संपादन भी किया । साम्यवादी विचारों को मार्क्स, लेनिन, एंजिल्स आदि को पढ़ने के अतिरिक्त भगतसिंह ने अप्टॉन सिंक्लेयर, जैक लंडन, बर्नड शा, चार्ल्स डिकेन्स साहित्य सहित तीन सौ से अधिक महत्वपूर्ण किताबें पढ़ रखी थी । भगतसिंह का अध्ययन व्यवस्थित वैज्ञानिक और व्यवहारिक था । वह पुस्तकों के नोट्स बनाकर साथियों से विमर्श करने के बाद अंतिम राय कायम करने के पक्षधर थे । इस दौरान भगतसिंह को अधिकतर मार्क्सवाद से संबंधित पुस्तकें पढ़ने को मिली । मथुरादास ठाकुर ने अपने विचार व्यक्त करते हुए कहा है कि, "भगतसिंह और सुखदेव को छोड़कर और किसी ने ना तो समाजवाद को अधिक पढ़ा है और ना ही मनन किया था । भगतसिंह और सुखदेव का ज्ञान भी हमारी तुलना में अधिक ही था ।" 1 लाहौर के नेशनल कॉलेज की पढ़ाई छोड़ कर भगतसिंह ने लाहौर में रहकर वे युवाओं में क्रांतिकारी विचारों को फैलाने लगे । पंजाब में 'हिंदुस्तान रिपब्लिकन

एसोसिएशन' के विचारों को फैलाने के लिए उन्होंने 1926 में 'नौजवान भारत सभा' की स्थापना की । वे सभी समाजवादी विचारधारा से प्रभावित थे । वे युवाओं की सहायता से भारत में मजदूरों और किसानों का गणराज्य स्थापित करना चाहते थे । उनके दल के प्रमुख क्रांतिकारी– सुखदेव, यशपाल, चंद्रशेखर आजाद एवं राजगुरु थे । भगतसिंह ने सशस्त्र क्रांति को ब्रिटिश साम्राज्यवाद के खिलाफ एकमात्र हथियार माना ।

भगतसिंह ने अपने क्रांतिकारी जीवन की शुरुआत कानपुर से गणेश शंकर विद्यार्थी के 'पत्र प्रताप' से की थी । उसमें वह बलवंत के नाम से लिखा करते थे । यह विद्यार्थी और भगतसिंह की घनिष्ठता का रहस्य बहुत बाद में उजागर हुआ । अपने प्रखर राष्ट्रवाद के कारण भगतसिंह ने अपने साथियों का विदेश जाकर आर्थिक सहायता प्राप्त करने का प्रस्ताव भी ठुकरा दिया । दरअसल उन्होंने ही क्रांतिकारियों को एकजुट करने की पहली गंभीर कोशिश की थी । 1928 में 'साइमन कमीशन' का विरोध करते हुए, 'लाला लजपतराय' पुलिस की मार से शहीद हो गए । सारे देश में निराशा और बेबसी की लहर दौड़ गई । इस राष्ट्रीय अपमान का बदला लेने के लिए भगतसिंह ने राजगुरु के साथ मिलकर 17 दिसंबर 1928 को इसके दोषी अंग्रेजी अफसर 'साण्डर्स' की गोली मारकर हत्या कर दी । इनमें चंद्रशेखर आजाद ने उनकी पूरी सहायता की थी । इस कार्यवाही के बाद भी लोगों में आजादी की लड़ाई के लिए उत्साह और क्रांतिकारियों का संकल्प, विचारधारा उन तक नहीं पहुँच पाई थी । इसी कारण भगतसिंह और उनके साथियों को निराशा प्राप्त हुई । किसी व्यक्ति को मारना भगतसिंह का उद्देश्य नहीं था । वह अपने देशवासियों को अपने समाजवादी लक्ष्यों के बारे में बताना चाहते थे । अंततः भगतसिंह देशवासियों तक अपनी आवाज पहुँचाने के उद्देश्य से केंद्रीय असेंबली में बम फेंकने की योजना बनाई । ताकि देश का ध्यान बहुजन क्रांति की ओर खींचा जा सके ।

हरदीपसिंह के अनुसार "8 अप्रैल 1929 को इम्पीरियल असेम्बली, दिल्ली में भगतसिंह और बी.के दत्त ने बम विस्पोर्ट करने के बाद गिरफ्तारी देते हुए 'इन्कलाब जिंदाबाद' का नारा लगाकर अंग्रेज सरकार की जड़ें हिला दी । असेम्बली में लाल रंग के पर्चे फेंके गए जिन पर लिखा गया था 'बंद कानों को सुनने के लिए धमाके की जरूरत होती है ।"[2] भगतसिंह और उनके साथियों का बम फेंकने का मकसद किसी को मारना नहीं था । बल्कि ब्रिटिश हुकूमत द्वारा लागू किए गए दो बिलों पब्लिक सेफ्टी बिल और ट्रेडी डिस्प्यूट बिल का विरोध करना था । वह वहां से भाग सकते थे, पर उन्होंने अपनी गिरफ्तारी स्वयं कराई । वहां से न भागने के पीछे उनका मकसद अपनी बात लोगों तक पहुंचाने की थी । उस दौर में ब्रिटिश दमन इतना तेज था कि, किसी भी इन्कलाबी किताब, विचार लोगों तक पहुंचाना लगभग नामुमकिन था । भगतसिंह और उनके साथियों ने अपनी गिरफ्तारी देने के बाद कोर्ट में अपने बयान दिए और उम्मीद की कि, इस बयान को अखबारों में छपा जाएगा और शायद इसी बहाने लोगों तक अपने विचार और सोच वे लोगों तक पहुँचा सकेंगे ।

भगतसिंह ने विचार प्रकट करते हुए कहा कि, "क्रांतिकारियों का विश्वास है कि, देश को क्रांति से ही स्वतंत्रता मिलेगी वे जिस क्रांति के लिए प्रयत्नशील है और जिस क्रांति का रूप उनके सामने स्पष्ट है उसका अर्थ केवल यह नहीं कि, विदेशी शासकों तथा उनके पिटठुओ से क्रांतिकारियों का सशस्त्र संघर्ष हो, बल्कि इस सशस्त्र संघर्ष के साथ–साथ नवीन सामाजिक व्यवस्था के द्वारा देश के लिए मुक्त हो जाए । क्रान्ति पूँजीवाद, वर्गवाद तथा कुछ लोगों को ही विशेषाधिकार दिलाने वाली प्रणाली का अन्त कर देगी । यह राष्ट्र को अपने पैरों पर खड़ा करेगी । उससे नवीन राष्ट्र और नए समाज का जन्म होगा । क्रांति से सबसे बड़ी बात तो यह होगी कि वह मजदूर तथा किसानों का राज्य कायम कर उन सब को सामाजिक अवांछित तत्वों को समाप्त कर देगी जो देश की राजनीतिक शक्ति को हाथियाये बैठे हैं ।"[3] भगतसिंह का मकसद पूँजीवाद को मिटाना था । उनका सपना संपूर्ण स्वतंत्रता का था । वे चाहते थे कि, देश में कोई किसी का शोषण नहीं करेगा । सब को स्वतंत्रता से जीने का अधिकार है । जाति, प्रांत के नाम पर कोई लड़ाई नहीं करेगा । मुल्क सभी के लिए समान है । भगतसिंह इन मूल्यों के लिए लड़े और समाज को संदेश देते रहे कि "देश के

नौजवानों ने बहुत इंतजार कर लिया । बहुत दिनों तक घुट–घुट कर जी लिये । इस या उस चुनावबाज पार्टी से बदलाव की उम्मीदें पालकर बहुत धोखा खा लिया । उन्हें सोचना ही होगा कि अब और कितना छले जायेंगे? अब और कितना बर्दाश्त करेंगे? दुनियादारी के भंवरजाल में कब तक फँसे रहेंगे? कितने दिन तक चुनौतियों से आंखें चुरायेंगे? उन्हें भगतसिंह के संदेश को सुनना होगा । नई क्रांति की राह पर चलने के लिए वक्त आवाज दे रहा है, उसे सुनना होगा"[4] भगतसिंह ने अपनी वैचारिक समझदारी को समाज के सामने लाने का प्रयास किया था । उनके लिए आजादी का ध्येय था सिर्फ समाजवाद और धर्मनिरपेक्ष राज्य ।

जेल में भगत सिंह दो साल रहे। उन्होंने वहां की दयनीय स्थिति को देखकर जेल में भूख हड़ताल शुरू की । उनकी मांगे थी कि, कैदियों को खाने लायक अच्छा खाना, कपड़े और किताबों की व्यवस्था की जाए । जेल में उन्होंने अनेक अत्याचारों को सहा । उनकी भूख हड़ताल रोकने की बहुत कोशिश की गई, पर वो कामयाब नहीं हो सके । 64 दिनों तक भूख हड़ताल जारी थी जिसमें उनका एक साथी यतींद्रनाथ दास ने तो उस भूख हड़ताल में अपने प्राण ही त्याग दिए थे । जब भगतसिंह जेल में थे । इस दौरान वे लेख–लिखकर अपने क्रांतिकारी विचार व्यक्त करते रहे । अपने लेखों में उन्होंने कई तरह के पूंजीपतियों को अपना शत्रु बताया है । उन्होंने लिखा है कि, मजदूरों का शोषण करने वाला चाहे वह एक भारतीय ही क्यों न हो वह उनका शत्रु है । उन्होंने जेल में अंग्रेजी में एक लेख भी लिखा था । जिसका शीर्षक था 'मैं नास्तिक क्यों हूँ?' जेल में रहते हुए उनका अध्ययन बराबर जारी रहा । इस दौरान उनके लिखे गए लेख व परिवार को लिखे गए पत्र आज भी उनके विचारों के दर्पण है ।

असेंबली में धमाके के बाद जो मुकदमा चलाया गया । उस मुकदमें को भगतसिंह ने तथा उनके साथियों ने गंभीरता से नहीं लिया । उनका मकसद केवल अपने विचारों को जनता तक पहुंचाना था । अंततः इस मुकदमे का फैसला सुनाया गया । जिससे भगत सिंह, सुखदेव और राजगुरु को फांसी तथा 9 क्रांतिकारियों को आजीवन कारावास की सजा सुनाई गई । सरकार ने 24 मार्च 1931 को तीनों क्रांतिकारियों को फाँसी देने का निर्णय लिया । सामान्यता: फाँसी प्रात:काल के समय दी जाती थी । तथा शव परिजनों को सौंप दिये जाते थे । परंतु सरकार ने जनता के भय से दोनों परंपराओं को नहीं निभाया । 23 मार्च 1931 को तीनों को सायं के सात बजे फाँसी दे दी गई । तथा गुप्त तरीके से उनके शवों को सतलज नदी के तट पर ले जाकर उनका अंतिम संस्कार कर दिया गया ।

भगत सिंह भारत के एक प्रमुख स्वतंत्रता सेनानी क्रांतिकारी थे । आज भी सारा देश उनके बलिदान को बड़ी गंभीरता व सम्मान से याद करता है । उनके जीवन पर आधारित कई हिन्दी फिल्में भी बनी हैं जिनमें– द लीजेंड ऑफ भगत सिंह, शहीद, शहीद भगत सिंह आदि प्रमुख है ।

संदर्भ ग्रंथ

1. डॉ. हरदीप सिंह, – शहीद सुखदेव नौघरा से फाँसी तक – राहुल फाउण्डेशन, लखनऊ, जनवरी – 2017, पृष्ठ क्र. 25
2. डॉ. हरदीप सिंह, – शहीद सुखदेव नौघरा से फाँसी तक – राहुल फाउण्डेशन, लखनऊ, जनवरी – 2017, पृष्ठ क्र. 58
3. भगतसिंह, अंतिम पृष्ठ – बम का दर्शन और अदालत में बयान – राहुल फाउण्डेशन, लखनऊ, जनवरी – 2017
4. भगतसिंह, प्रस्तावना – बम का दर्शन और अदालत में बयान – भगतसिंह, राहुल फाउण्डेशन, लखनऊ, जनवरी – 2017

परंपरा से भिन्न तुलसी का काव्यादर्श

डॉ. सुमित्रा कोतपल्ली,
प्राच्य भाषा विभाग
सर सी आर रेड्डी कॉलेज,
एलुरु

रामधारा के अंतर्गत साहित्यिक उत्कर्ष और गुणों के कारण जिनका नाम गौरव के साथ स्मरण किया जाता है, वे कवि शिरोमणि गोस्वमी तुलसी दास है । तुलसीदास ने अपने को कवि के रूप मे कभी भी चर्चित नहीं किया और मानस मे स्पष्ट घोषणा की कि "भणिति भदेस बस्तु भल बरनी " रामकथा जगमंगल करनी । " किंतु उन्होने जिस रामकथा की स्वर्ण मुद्रिका मे अपनी कविता के रत्नो को जड़ा उसकी तृप्ति से रामकथा भी देदीप्यमान हो गई । 'रामचरितमानस' अपने समय मे जीते हुए मनुष्य और अन्य जीवो के कलुषित मिटाकर मंगल करणी कलिमल हरिणी रघुनाथ की कथा है । यह कथा नर से नारायण बनने की भी है । यह आत्मकल्याण की है । यह कथा सकल लोक के लिए जग पावनी गंगा के समान है । यह भारतीय वाङ्मय की अमृत–कथा है । संस्कृत साहित्य शास्त्र मे कभी इतना ही काव्य लक्षण पर्याप्त समझा जाता था कि काव्य या साहित्य वही है जिसमे शब्द और अर्थ साथ हो । "शब्दार्था सहितौ काव्यम् । " यह लक्षण काव्य को वेद और पुराणेतिहास से पृथक कर देता है । पर उसके स्वकीय वैशिष्ट्य को पूर्णतया स्पष्ट नहीं करता । 'वेद' मे शब्द की प्रधानता होती है, शब्द गौण रहता है । काव्य मे शब्द और अर्थ दोनों की प्रधानता है, प्रत्युत दोनों सयुक्त रहते है जल तरंग की भांति "[1]

वास्तव मे तुलसीदास ने अपनी काव्य संवेदना से मानवीय हृदयतंत्री को जिस ढंग से झकृत किया और रसमग्नता की जैसी स्थितियां निर्मित की है , वे अन्यत्र विरल है । उन्होने रीति काव्यों की भांति कृत्रिम शब्दावली के प्रयोग द्वारा भाव व्यंजना के उत्कर्ष उसकी सरसता पर कथमपि कुठाराघात नहीं किया । उन्होने जन–मानस को स्पर्श किया और अपने कौशल द्वारा उनके प्रस्तुत भावो को उद्घाटित किया । जन मानस पर उनकी भाव–व्यंजना की सहजता और मधुरता का क्या था, इसे एडविन ग्रीव्ज के शब्दों मे देखे "Tulasi Das wrote not to display his learning or, to tickle the ear of pedants, he wrote the people and has his reward. No poet in England has ever been to the masses what tulasi das has been to the people of his land."[2]

गोस्वामी तुलसीदास ने अपने काव्य मे संत–असंत को व्यापक अर्थ मे ग्रहण किया है । अधिकांश संत शब्द से तात्पर्य उन्होने ऐसा महापुरुषों से लिया है, जिनका जीवन सद्वृत्तियों से संचालित है । जिनके कार्य – व्यवहार आत्मोन्नयन के साथ–साथ किसी न किसी रूप में विश्वकल्याण के प्रवृत हैं । जिनमे स्वार्थ बुद्धि की अपेक्षा परमार्थ बुद्धि की प्रधानता है । ऐसी महान विभूतियो के अभिज्ञान के लिए उन्हे वे सारे अभिधान स्वीकार्य हैं, जो संत, साधु, सज्जन, सत्पुरुष, महात्मा, महापुरुष आदि किसी भी पर्याय के रूप मे प्रचलित हो, यो तो संत के अस्तित्व होना आवश्यक है । "सज्जन यदि राम के स्नेह से भी सरस हो तो वह साधूओ की सभा मे विशेष आदर का पात्र हो जाता है । तथापि यदि कोई नास्तिक भी निश्छल भाव से सारे संसार के प्राणियों का उद्धार करता है तो वह भी संत कोटि मे आ जाता है ।"[3] राक्षसों के समाज मे सबके सब रावण के समर्थक नहीं है । विभीषण की सात्विकता तो उजागर है । लेकिन कई ऐसे पात्र भी है जो रावण के प्रभाव या भय से शरीर से उसके साथ है, लेकिन मन–मस्तिष्क से चाहते है कि रावण का आतंक समाप्त हो लंकिनी इसका प्रमाण है । एक सीमा तक कुंभकर्ण भी राम से युद्ध करने के पूर्व अपने अंतर्द्वंद से

रावण कि अनीति को प्रमाणित करता है । मंदोदरी, त्रिजटा, सुलोचना आदि ऐसी नारी शक्तियाँ है, जो लंका के वैभव के बीच भी सद–असद का विवेक नहीं खोती है ।

'रामचरितमानस' मे श्री राम द्वारा शबरी को दिया गया नवधा– भक्ति का उपदेश । भागवत मे प्रतिपादित श्रवण, कीर्तन, स्मरण, पादसेवन, अर्चन, वंदन, दास्य, सांख्य एवं आत्मनिवेदन के नौ रूपों वाली नवधा भक्ति के स्थान पर वे जिस नवधा–भक्ति का कथन श्री राम द्वारा कराते हैं, उसमे भी भक्ति के लोक संग्राही रूप को ओझल नहीं होने देते । संतो की संगति प्रभु के कथा–प्रसंग मे रति, गुरु पद सेवा, प्रभु का गुणगान, दृढ़ विश्वास के साथ राम नाम के मंत्र का जप, इन्द्रिय निग्रह एवं शील के साथ निरंतर सज्जनता का निर्वाह, जगत भर को समत्व भाव के साथ राममय देखते हुए "संतो का सम्मान करना, संतोष–भाव के साथ दूसरे के दोषो की उपेक्षा करना तथा सबके साथ निश्छल एवं सरल बर्ताव करते हुए प्रभु राम का हृदय मे भरोसा रखकर हर्ष एवं दैन्य (दीनता) से ऊपर उठना ।"[4]

'रामचरितमानस' उत्तरकाण्ड मे भरत के प्रश्न के उत्तर मे संत–असंत के लक्षण बताते हुए प्रभु श्री राम कहते हैं कि परोपकार से बढ़कर कोई धर्म नहीं और पर–पीड़ा के सामान कोई अधर्म नहीं है और यह बात केवल मै नहीं कह रहा हूँ । समस्त पुराणों और वेदों का यह निष्कर्ष है जिस ज्ञानी जन जानते हैं ।

"परहित सरिस धर्म नहीं भाई । परपीड़ा सम नहीं अधमाई ।
निर्नय सकल पुराण वेद कर काहेड़ा तात जानहि कोविद नर ।।

क्या दुनिया मे इससे अच्छी भी कोई धर्म–अधर्म की परिभाषा हो सकती है । जैसे मानव – मानव मे भेद न करने वाले और प्राणी मात्र की कल्याण–कामना से ओत–प्रोत असंख्य विचार भरे पड़े हो । इसी धर्म और संस्कृति के अमर गायक है, गोस्वामी तुलसीदास इनकी कहीं गई धर्म की परिभाषाओ को मानकर इस मानव–धर्म को यदि संसार के सारे मनुष्य अपना ले तो शायद कोई समस्या ही शेष न बचे तब शायद पृथ्वी पर विनाशकार्य उत्पादों का अविष्कार ही बंद हो जाये और वह कल्याणकारी पथ पर द्विगुणित वेग से आगे बढ़ सके । तब शायद मनुष्य मनुष्य के रास्ते की बाधा बनकर उसे नीचा दिखाने का काम न करे और वह एक दूसरे का सहारा बन कर परस्पर ऊँचा उठने–उठाने मे लगे । पृथ्वी के अतिरिक्त अन्य कहीं स्वर्ग खोजने की जगह तब शायद यहीं वह स्वर्ग देखने को मिल सके ।

तुलसी के 'रामचरितमानस' का अखण्ड पाठ भी होता है, नियमित परायण भी होता है, रामलीलाएँ भी होती हैं और राम नाम भी हर समय लिया जाता है, लेकिन इसके लिये जीवन कहीं ठहरता नहीं, जीवन की अनन्य गतिविधियों के साथ यह सब भी चलता रहता है । यह तुलसी की भक्ति की व्यवहारिकता का प्रमाण है । उसकी सहजता का साक्ष्य है । डॉ. रामस्वरूप चतुर्वेदी लिखते हैं, ईश्वर मे पूरी आस्था और मनुष्य का पूरा सम्मान ये दोनों दृष्टियाँ तुलसी मे एक दूसरे से जुडी हुई हैं । 'सियाराममय सब जग जानी । करहुँ प्रनाम जोरि जुग पानी ।' जैसे पंक्तियाँ इस गहरे आत्मविश्वास पर ही लिखी जा सकती है, जहाँ ईश्वर और मनुष्य दोनों की एक साथ प्रतिष्ठा हो । "अनुभूति और अभिव्यक्ति का जैसा संश्लिष्ट रूप रचना मे वस्तुतः प्रत्याशित है, वह ईश्वर और मनुष्य की इस एकरूपता मे से निकलता है ।"[5] रामचरितमानस तुलसीदास का ही नहीं अपितु विश्व साहित्य के श्रेष्ठतम ग्रंथ मे एक है । काव्य का लक्ष्य लोकमंगल मानते हुए अपने आराध्य मर्यादा पुरुषोतम श्री रामचंद्र के माध्यम से तुलसी ने जीवन का आदर्श रूप प्रस्तुत किया है ।

सन्दर्भ ग्रंथ सूचि

1 विश्वनाथ मिश्र– हिंदी साहित्य का अतीत, पृ. 257.

2 एडविन ग्रीव्ज– A Sketch of Hindi Literature, p. g 59

3 कल्याण– श्री राम भक्ति अंक पृ 123.

4 रामचरितमानस, अरण्य काण्ड, दोहा 34 – 35, पृ. 611 – 612

5 डॉ. रामस्वरूप चतुर्वेदी– हिंदी साहित्य और संवेदना का अवरूप, पृ. 58.

गुरमति साहित्य में कबीर और अन्य कवियों का योगदान

गौरव यादव

ठा. बीरी सिंह महाविद्यालय, टूण्डला, फिरोजाबाद

मोबाइल नं. 7838976871

ई–मेल : yadangrv2805@ gmail.com

शोध सारांश

सिख धर्मग्रंथ 'गुरुग्रंथ साहिब' में निर्गुण संतों– कबीरदास, रैदास, पीपा, धन्ना आदि के साथ सगुण भक्तों– रामानंद, सूरदास, मीराबाई, सूफी शेख फरीद आदि संत कवियों को भी संकलित किया गया है । इन सभी में कबीरदास जी का विशिष्ट स्थान है, क्योंकि 'आदिग्रंथ' में सिख गुरुओं के प्राय: बाद कबीर–वाणी को जगह मिली है तथा गैर सिख संतों में सर्वाधिक संकलित रचनाऐं भी कबीर की ही हैं । 'आदिग्रंथ' कबीर–वाणी का इतना व्यापक संकलन प्रस्तुत करने वाला एकमात्र प्राचीनतम ज्ञात स्रोत है ।

'आदिग्रंथ' में संकलित विभिन्न संतों की टिप्पणियों तथा कबीर की स्वयं की कविताई के अंत:साक्ष्यों से कबीर संबंधी ऐतिहासिक तथ्यों पर भी प्रकाश पड़ता है । इसमें कबीर अपने परिचित 'अक्खड व्यक्तित्व' निर्गुणवादी सिद्धातों के साथ उपस्थित होते हैं, जिनमें अपनी अभिज्ञानात्मक अनुभूति के उद्घाटन, सतगुरु महिमा की प्रतिष्ठा, ज्ञान द्वारा माया से मुक्ति, द्वैत एवं अद्वैत से विलक्षण ब्रह्म की अवधारणा का प्रतिपादन और मानव जनित समस्त विषमताओं, जाति–सम्प्रदाय आधारित विभेदों ब्राह्याचारों आदि के खंडन की चेतना तथा प्रेमाधारित समरस समाज के निर्माण की बैचेनी है । इस प्रकार 'आदिग्रंथ' में कबीर वाणी के संकलन के विविध आयामों पर अध्ययन की अनेक सम्भावनाऐं विद्यमान हैं ।

बीज शब्द :– गुरमति, गुरुग्रंथ साहिब, कबीर वाणी, सिख, संतकवि आदि ।

गुरमति साहित्य

गुरमत का शाब्दिक अर्थ है गुरु का मत अर्थात् गुरु के नाम पर संकल्प । यह सिखों द्वारा किसी भी धार्मिक, सामाजिक व राजनैतिक मुद्दों से संबंधित गुरु के नाम पर आयोजित सभा में अपनाई गई सलाह या संकल्प है । अठारहवीं शताब्दी के आस–पास सिखों ने बैसाखी और दिवाली के दिन अमृतसर के अकाल तख्त पर इकट्ठे हुए और गुरुग्रंथ साहिब की उपस्थिति में एक पाठ्यक्रम की योजना बनाने के लिए एक साथ परामर्श लिया, विचार–विमर्श से निकलने वाला अंतिम निर्णय गुरमत का था । इसने खालसा की सामान्य इच्छा का प्रतिनिधित्व किया और इसने गुरु की मंजूरी को आगे बढ़ाया, सभा ने गुरु ग्रंथ साहिब के अधिकार को निभाया ।

सिख पंथ का आधिकारिक धर्मग्रंथ 'गुरुग्रंथ साहिब' है । दसवें गुरु गोविंद सिंह के समय, 1708 ई. में व्यक्तिगत गुरु–परंपरा का अंत हुआ, तब से गुरु पद 'ग्रंथ साहित्य' में ही निहित हो गया और ग्रंथ को 'शब्द गुरु' का दर्जा मिला, जो दुनिया भर में विभिन्न धर्मों में एक अनूठा दृष्टांत है । 'ग्रंथ साहिब' तदयुगीन राजनीतिक–सामाजिक परिस्थितियों के विविध चित्रों के साथ मध्यकालीन भक्ति–आंदोलन में अंतर्निहित व्यापक वैचारिकी, दर्शन, अध्यात्म, सत्संग आदि का सरस दस्तावेज है तो संत–कवियों की रचनाओं के अपेक्षाकृत निरपेक्ष प्रामाणिक संकलनों के कारण इसका साहित्यिक महत्व भी है । इस प्रकार यह भारतीय साहित्यिक

परम्परा का एक रत्नकोष है जिसमें सिख गुरुओं के अलावा विभिन्न क्षेत्रों, विविध विचार–सरणियों, भिन्न जाति–धर्म के संतो की बानियों को श्रद्धापूर्वक समाहित किया गया है ।

'गुरुग्रंथ साहिब' का प्रारंभिक नाम 'ग्रंथ साहिब' था, किंतु आगे दसवें गुरु गोविंद सिंह कृत 'दसम ग्रंथ' से भेद दर्शाने के लिए इसे 'आदिग्रंथ' कहा गया, जिसका अभिप्राय है कि सिख परम्परा का यह आदिग्रंथ है ।

'गुरुग्रंथ साहिब' समस्त मानव समुदाय के लिए एक सार्वभौगिक साधना–पद्धति का प्रतिपादन करता है । यह हर प्रकार के आचारवाद, रूढ़िवाद, प्रतीकवाद को नकारता है तथा ईश्वर व मनुष्य के बीच किसी भी तरह के आडम्बरों का विरोधी है । 'ग्रंथ साहिब' सच्चे व ईमानदार श्रम को महत्व देता है तथा संन्यास व वैराग्य की निंदा करता है । इस प्रकार यह श्रमिक एवं ग्रहस्थों का धर्म प्रतिपादित करता है । यह स्त्रियों को पुरुषों से हीन नहीं मानता । यह हिंदू वर्णाश्रमवाद, जातिवाद, छुआछूत का विरोधी है तथा जन्म, स्थान, लिंग आदि के आधार पर भेदभाव को नकारता है । 'गुरुग्रंथ साहिब' कर्म, भक्ति तथा ज्ञान का संतुलन प्रतिपादित करता है । शरीर की सार्थकता जहाँ परिवार–समाज की भलाई हेतु सत्कर्मों में है, वही मन को ईश्वर की ओर उन्मुख होना चाहिए, सेवाभाव इसका संदेश है ।

गुरमति साहित्य में कबीर : योगदान एवं प्रयोजन

'आदिग्रंथ' में सिख परम्परा के बाहर के जिन संत कवियों को जगह मिली है, उनमें कबीर जी की विशेष स्थिति दो कारणों से है । प्रथम तो यह कि विभिन्न रोगों के अंतर्गत गुरु–बानियों के ठीक बाद प्राय: कबीर की बानियों को रखा गया है । ऐसा 'सलोकों' के अंतर्गत भी देखा जा सकता है । दूसरा यह कि विभिन्न गैर सिख संतों में कबीर की रचनाएँ सर्वाधिक हैं ।

'आदिग्रंथ' में सत्रह विभिन्न रागों–सिरी राग, आसा, सूही तिलंग, बिलावल, मारु, केदारा, भैरो, बसंत, सारंग, सोरठ, गउडी, धनाश्री तथा परभाती के अंतर्गत कबीरदास के तीन लम्बे पदों– बावन अखरी, थितिं और वार सत सहित कुल 228 पदों के साथ 243 श्लोकों को संकलित किया गया है । यदि शेष अन्य गैर सिख संतों की रचनाओं को मिला भी दें, तब भी कबीरदास की संकलित रचनाओं की संख्या उनसे अधिक है । हालांकि कबीरदास की समस्त रचनाओं को 'आदिग्रंथ' में जगह नहीं मिली है।

कबीर के अध्ययन में आदिग्रंथ का महत्व

कबीर के अध्ययन के संदर्भ में 'आदिग्रंथ' के महत्व को दो स्तरों पर रेखांकित किया जा सकता है । प्रथम स्तर कबीर की रचनाओं के प्रामाणिक पाठ से सम्बद्ध है । हाल ही में प्राप्त 582 ई. की 'फतेहपुर पांडुलिपि (पद सूरदास जी का), जिसमें कबीर के मात्र पंद्रह पद संकलित हैं, को छोड़कर 'आदिग्रंथ' उनकी कविताई का सम्भवतः एकमात्र प्राचीनतम संकलन है जिसकी पुरानी और ज्ञात तिथियों वाली पांडुलिपियाँ भी उपलब्ध हैं । कबीरदास की परम्परागत निधन तिथि 1518 ई. के सौ वर्षों के भीतर संकलित होने के कारण 'आदिग्रंथ' (1604 ई. संकलन काल) में संग्रहित उनकी रचनाओं की प्रामाणिकता अन्य परवर्ती स्रोतों की अपेक्षा निर्विवाद है । पर जैसा कि हम देख चुके हैं, 'आदिग्रंथ' के संकलन के पीछे भी एक दीर्घकालीन प्रक्रिया रही है । तब एक स्वाभाविक प्रश्न यह उठता है कि सिख साहित्यिक परम्परा में कबीर को कब समाहित किया गया?

एक मान्यता के अनुसार कबीर की रचनाओं को स्वयं गुरु नानकदेव ने सिख परम्परा में अंगीकृत किया । साक्ष्य स्वरूप बताया जाता है कि परवर्ती 'जनम साखियों के अनुसार नानकदेव कबीर से मिल चुके थे तथा उनके प्रति श्रद्धा भी रखते थे । दूसरे, उनकी कविताई के स्वरूप एवं वैचारिक साम्य को भी इस संदर्भ में रेखांकित किया जाता है, जैसे कि गुरु के महत्व को दोनों इस प्रकार व्यक्त करते हैं :–

कहु नानक निसचौ धियावै ।
बिनु सतिगुर बाट न पावै ॥ – नानक देव

बिनु सतिगुर बाट न पाई ।
कछु कबीर समझाई ॥
– कबीर

किंतु ऐतिहासिक तथ्यों के आधार पर कबीर और गुरुनानक का मिलना असंगत प्रतीत होता है । दूसरे यह कि अपनी बानियों में नानकदेव ने शेख फरीद की तरह कबीर का नामोल्लेख भी नहीं किया है । 'आदिग्रंथ' में कबीर का प्रथम बार उल्लेख एवं उन पर टिप्पणी करने वाले सिख गुरु अमरदास थे 'नामा छीबा कबीरू जोलाहा पूरे गर ते गति पाई । तीसरे यह कि सिख साहित्य परम्परा में 'गोयंदवाल पोथी' में ही, जिसका निर्माण गुरु अमरदास के समय हुआ, सर्वप्रथम कबीर की रचनाओं को संकलित किए जाने के संकेत मिलते हैं । इस आधार पर कुछ लोगों का मानना है कि सिख साहित्य परम्परा में कबीर को तीसरे गुरु अमरदास के समय ही जगह मिली होगी ।

जो भी हो, कबीर की रचनाओं के विभिन्न स्रोतों– बीजक, सर्वांगियों, पंचवानियों आदि के मद्देनजर यह स्पष्ट हो जाता है कि कबीर की सभी रचनाओं को 'आदिग्रंथ' में जगह नहीं मिली है । गैर सिख परम्पराओं को यदि छोड़ भी दें तो स्वयं 'गोयंदवाल पोथी' में संकलित कुछ कबीर– बानियों को भी 'ग्रंथ' के संकलनकर्त्ता ने छोड़ दिया है । इसके अतिरिक्त 'करतार पुर वाली बीड़ में भी कबीर के चार पदों को मिटाए जाने के साक्ष्य मिलते हैं । अन्य संकलनों, यथा 'कबीर ग्रंथावली' तथा 'बीजक', जिनके आधार–स्रोत क्रमशः दादूपंथी और कबीर पंथी पांडुलिपियाँ हैं– से तुलना करने पर उनमें तथा 'आदिग्रंथ' में संकलित कबीर की रचनाओं में भेद और साम्य को बखूबी समझा जा सकता है । जाहिर है कि 'ग्रंथ' के संकलन के दौरान चयन की कुछ दृष्टियाँ कार्यरत थीं ।

आदिग्रंथ में कबीर वाणी के संकलन की प्रयोजनीयता

'आदिग्रंथ' के संदर्भ में एक प्रश्न अनायास ही उठता है कि जब यह सिख मत का अधिकारिक धर्मग्रंथ है तो कबीरदास सरीखे गैर सिख संत को इसमें समाहित करने के पीछे संकलनकर्त्ता के कौन–से उद्देश्य थे? आधुनिक युग में इसके निहितार्थों को समझने का प्रयत्न कई अध्येताओं ने किया है ।

एक मान्यता के अनुसार 'आदिग्रंथ' में कबीर वाणी के संकलन का आधार कबीर तथा सिख गुरुओं के विचारों, सिद्धांतों और शिक्षाओं में समानता है, जैसे– सार्वभौमिक–सार्वकालिक निर्गुण निराकार ब्रह्म की अवधारणा, जाति–सम्प्रदाय विरोध, वैयक्तिक रहस्यवादी साधना, सतगुरु में आस्था इत्यादि, जिससे सिख परम्परा की मानसिकता एवं उसकी उत्प्रेरणाओं को बल मिलता है । ऐसा अनुमान किया जाता है कि सम्भवतः इसी कारण कबीरदास की चयनित रचनाओं को ही 'ग्रंथ' में जगह मिली, जिससे उनके हवाले से सिख मत के सिद्धांतों को पुष्टि एवं प्रामाणिकता मिल सके ।

'आदिग्रंथ', 'अकाल परुख' की अवधारणा प्रतिपादित करता है तथा 'सतिनाम सुमिरन' इसकी उपासना के केंद्र में है । ईश्वरीय 'नाम' के सुमिरन का महत्व कबीरदास के यहाँ भी है । 'नाम जप' की महिमा बखानते हुए गुरु अर्जुनदेव कबीर सहित कई अन्य संत आत्माओं का उल्लेख करते हैं, जो नाम सुमिरन के माध्यम से 'उद्धार' पा गएः

सुणि सखी मन जपि पिआर । उधरिया कहि एक बार ।
कबीर धिआइओ एक रंग । नामदेव हरि जीउ बसहि संग ।
रविदास धिआए प्रभ अनूप । गुरु नानक देव गोविंद रूप ॥

सिख मत तथा कबीर दोनों ने ब्रह्म के विभिन्न नामों–राम, हरि गोविंद, निरंजन, अल्लाह, खुदा, रहीम आदि की महत्ता बताई है, जिनके सुमिरन से 'सहज' ही साधना की जा सकती है । जाहिर है कि उपासना–पद्धति के आलोक में कबीर सिख सिद्धांतों के निकट दिखाई देते हैं ।

वैचारिक धरातल पर साम्य का दूसरा स्तर जाति, धर्म, सम्प्रदाय के आधार पर मानवता मात्र के विभाजनों को नकारने में है । नानकदेव कहते हैं कि ईश्वर के द्वार पर जाति नहीं पूछी जाती : 'जाणहु जोति न पूछहु जाती आगे जाति न हे' तो कबीर के अनुसार सारे जीवों की उत्पत्ति 'ब्रह्म–बिंदु' से होती है, इसलिए जन्म–कुल अप्रासंगिक है :

गरभ वास महि कुलु नहीं जाती । ब्रह्म बिंदु ते सभ उतपाती ॥
कहु रे पंडित बामन कबके हुए । बामन कहि कहि जनमु मत खोए ।।
जौ तूं ब्राह्मणु ब्रह्मणी जाइआ तउ आन बाट काहे नहीं आइआ ।।
तुम कत ब्राह्मण हम कत सूद। हम कत लोहू तुम कत दूध ।।
कहु कबीर जो ब्रह्मु बीचारै । सो ब्राह्मणु कहिअतु है हमारै ।।

इसी तरह वेद– कुरान के नकार, सतगुरु महिमा, वैयक्तिक रहस्यवाद इत्यादि के संदर्भ में भी विचारगत साम्य को रेखांकित किया जा सकता है । उल्लेखनीय है कि कबीर सरीखे कई अन्य गैर सिख संतों की बानियों के संकलन के बावजूद संकलनकर्त्ता ने 'आदिग्रंथ' की मूल विषय–वस्तु की निरंतरता का निर्वाह करते हुए सैद्धांतिक सामंजस्य बनाए रखने में सफलता पाई है ।

आदिग्रंथ में संकलित कबीर वाणी : विषय–वस्तु और दर्शन

कबीर वाणी में कुछ इस प्रकार की अंतर्वस्तु और दर्शन दिखाये देते हैं । यहाँ हमारा मूल सरोकार 'आदिग्रंथ' में संकलित कबीर की रचनाओं से है । निर्गुणवादी वैचारिक विशिष्टताओं को धारण करते हुए भी कबीर की मौलिकता इसमें है कि उन्होंने अपने व्यक्तित्व एवं अनुभूत सत्य के आलोक में अपने सिद्धांतों को दृढ़तापूर्वक अभिव्यक्ति दी है । उनके यहाँ अभिज्ञानात्मक अनुभूति का क्षण अचानक आता है–

कबीर सतिगुर सूरमे बाहिआ बानु जु एकु ।
लागत ही भुइ गिरि परिआ परा करेजे छेकु ।

सतगुरु की कृपा हुई, उसने 'शबद–बाण' मारा और साधक का कलेजा बिंध गया । इस अनुभूति के साथ ही सब कुछ बदल गया । जिस पर यह अनुकम्पा नहीं होती, उसका जीवन व्यर्थ चला जाता है: 'बारह बरस तो बालपन में बीत जाते हैं, बीस–तीस की अवस्था तक न तप होता है, न पूजा। जब वृद्ध हुए तब पछताने के सिवा बचता क्या है? मेरा–मेरा कहते जीवन गुजर जाता है और अंततः सारी शक्ति चूक जाती है । यह 'मेरा–मेरा' माया का वशीकरण है, जिसकी 'टाटी' 'ज्ञान की आँधी' से उड़ती है और तब आध्यात्मिक जागरण का क्षण आता है, जो जीव को बंधन मुक्त करता है ।

कबीर का ब्रह्म सार्वभौमिक सबके हृदय का वासी है । इसलिए उसकी खोज अंततः अपने भीतर होनी चाहिए, जो शुद्ध अंतःकरण से ही सम्भव है । कबीर ने उसे बार–बार खोजा और पाया है: आत्मानुभूति प्राप्त की है । जब ब्रह्म अंतःवासी है तो उसे बाहर कैसे पा सकते हैं? जो ईश्वर को मंदिर–मस्जिद में देखते हैं । यदि वह मंदिर–मस्जिद में ही रहता है तो शेष जगह किसकी है–

अलहु एकु मसीति बसतु है अवरु मुलखु किसु केरा ।
हिंदू मूरति नाम निवासी दुहु महि ततु न हेरा ।।

कबीर के अनुसार मानव–मानव के बीच सारे कृत्रिम विभेद निःसार हैं । हरेक प्राणी उसी 'एक' की कृति है, उसी की छवि है । अतः सभी समान हैं । ईश्वर ने सबसे पहले ज्योति उत्पन्न की और सारी प्रकृति उसी से व्युत्पन्न है । जब सारे मनुष्य प्रकृति के ही अंग हैं तो उनमें बड़े–छोटे, अच्छे–बुरे का भेद कैसा –

अवलि अलह नुरू उपाइआ कुदरति के सभ बंदे ।
एक नूर ते सभु जगु उपजिआ कउन भले को मंदे ।।

मिट्टी तो एक ही है, पर सिरजनहार ने अनेक प्रकार के रूपाकार देकर सृष्टि की । इसमें न तो मिट्टी के बर्तन का दोष है और न सर्जक का । सृष्टा का सत्त्व तो सबमें बराबर मौजूद है ।

आदिग्रंथ में गैर सिख संत कवियों का योगदान

एक धर्मग्रंथ से ऊपर उठकर यदि देखें तब 'आदिग्रंथ' सही मायनों में 'अनेकता में एकता' का प्रतीक है जो क्षेत्र, जाति, व्यवसाय और साम्प्रदायिक आग्रहों से मुक्त एक खुलेपन का संदेश देता है । 'आदिग्रंथ' के समावेशी आदर्श को दो स्तरों पर स्पष्ट रूप से महसूस किया जा सकता है– संकलित संतो की पहचानगत विविधता तथा भाषायी विशिष्टता ।

अपने एक पद में गुरु अर्जुनदेव संत प्रवृत्ति के विभिन्न लोगों का स्मरण पूरी श्रद्धा के साथ करते हैं :–

सुणि साखी मन जपि पिआर, अजागल उधरिया कहि एक बार।
धनै सेविआ बालबुधि, त्रिलोचन गुर मिलि भई सिधि ।
जैदेव तिआगिओ अंहमेव, नाई उधारिओ सैनु सेव ।
कबीरि धिआइओ एक रंग, नामदेव हरि जीउ बसहि संगि।
रविदास धियाए प्रभ अनूप, गुर नानक देव गोविंद रूप ॥

'आदिग्रंथ' में संकलित गैर सिख संत कवियों का संक्षिप्त परिचय इसप्रकार है–

संत कवि	–	आदिग्रंथ में संकलित पद
जयदेव	–	2 पद
शेख फरीद	–	4 पद 112 श्लोक
त्रिलोचन	–	4 पद
बेनी	–	3 पद
नामदेव	–	61 पद, 2 श्लोक
रामानंद	–	1 पद
कबीर	–	228 पद, 243 श्लोक
रैदास	–	40 पद
सेन	–	1 पद
पीपा	–	1 पद
धन्ना	–	3 पद
भीखन	–	2 पद
मीराबाई	–	1 पद
सूरदास	–	1 पंक्ति
परमानंद	–	1 पद

ऐसा माना जाता है कि ये संत व्यापक स्तर पर भ्रमण करते थे, इसलिए इनकी भाषा में विभिन्न जनपदों के भाषायी तत्व अनायास ही आते गए । इन संतो की बानियों के माध्यम से ये तत्व आदिग्रंथ में भी समाहित किये गए । अत: गुरुमुखी लिपि में संकलित होने के बावजूद 'आदिग्रंथ' की भाषा, समावेशिता का आदर्श प्रस्तुत करती है, जिसमें पंजाबी, मराठी, गुजराती, पूर्वी भारत की बोलियों आदि से भी शब्द ग्रहण किए गए हैं । इस प्रकार, मध्यकालीन भक्ति आंदोलन समस्त मतांतरों के ऊपर मनुष्यता के

स्तर पर विभिन्न परंपराओ के बीच जिस संवाद का प्रतिफल था, उसी का परिणाम 'आदिग्रंथ' में व्याप्त है, जो भारतीय समाज के धार्मिक बहुलतावाद का प्रमाण है ।

सन्दर्भ ग्रन्थ सूची

श्याम सुंदर दास : सं. कबीर ग्रंथावली, नागरी प्रचारिणी सभा

डॉ. माताप्रसाद गुप्त : सं. कबीर ग्रंथावली, साहित्य भवन (प्रा.) लिमिटेड – इलाहाबाद

पं. हजारीप्रसाद द्विवेदी : कबीर, राजकमल प्रकाशन नई दिल्ली संस्करण – सन् 1985

पं. परशुराम चतुर्वेदी : कबीर साहित्य की परख भारती भंडार – प्रयाग, संस्करण–सं. 2011 (सन् 1954)

डॉ. केदारनाथ द्विवेदी : कबीर और कबीर पंथ, हिंदी साहित्य सम्मेलन प्रयाग

डॉ. पारसनाथ तिवारी : कबीर वाणी– सुधा, राका प्रकाशन इलाहाबाद

डॉ. रामचंद्र तिवारी : कबीर मीमांसा, लोक भारती प्रकाशन – इलाहाबाद

डॉ. धर्मवीर : कबीर के आलोचक, वाणी प्रकाशन – नई दिल्ली

पीताम्बर दत्त बड़थ्वाल, हिंदी काव्य की निर्गुण धारा : अनु. एवं सं. परशुराम चतुर्वेदी, भगीरथ मिश्र, तक्षशिला प्रकाशन, नई दिल्ली

डॉ. राजदेव सिंह, संत साहित्य की भूमिका : लोक भारती प्रकाशन, इलाहाबाद

21 वीं सदी के नए विमर्श में वृद्ध विमर्श

Dr. Rekha
Department of Hindi
Maharani Arts College For Women
Dis: Mysuru State: Karnataka
Ph: 6360997286: 9742962211

21 वीं सदी के उपन्यास दर्पण है विविध आयाम का । प्रस्तुत सदी में समाज एवं परिवार में अनेक विमर्शों को चित्रित किया गया है, जैसे– स्त्री विमर्श, वृद्ध विमर्श, बाल विमर्श, आदिवासी विमर्श, दलित विमर्श, किन्नर विमर्श, बाल विमर्श तथा अल्पसंख्यक विमर्श आदि । प्रस्तुत आलेख में वृद्ध विमर्श को आधार बनाया गया है । साहित्य में वही चित्रित होता है जो समाज में घटित हो रहा है । आज–कल वृद्धाश्रमों की संख्या में अत्यधिक वृद्धि हो रही है । जिसका प्रमुख कारण आज की भागदौड़ भरी जीवन शैली तथा एक पीढ़ी के दूसरी पीढ़ी से विचारों का तालमेल न बैठना है । अधिकतर परिवार में वृद्धों की हालत बहुत दयनीय है । उनके पास यदि पैसे हैं तो ही उनको स्थान, मान मिलता है, अन्यथा संतान पर वह बोझ बन जाते हैं । आज की संतान पैसों से अमीर तथा प्रेम से गरीब है । उनके पास अपने माता–पिता को देने के लिये कुछ भी प्रम नहीं है । 21 वीं सदी के अनेक उपन्यसों में वृद्धों की दयनीय दशा का वर्णन है । जिसका वर्णन अग्रलिखित उपन्यासों में देखने को मिलता है ।

'भगदड' उपन्यास में महावीर प्रसाद तथा उनकी पत्नी ने अपने बेटे को पढ़ाया लिखाया। मगर बेटे को मुंबई के चकचौंध ने अपनी ओर इस प्रकार आकर्षित कर लिया कि वह मुंबई का ही बन कर रह गया । जब बेटे से मिलने दंपति बेटे के घर आते हैं तो उस समय पुत्र के घर में ही स्वयं को मेहमान जैसा अनुभव करते हैं । अपने बेटे के घर दोनों पति–पत्नी को अपनी बहू द्वारा वैसा स्नेह नहीं मिला जैसे आम परिवार में मिलता है जैसे– "दरवाजा बहू ने खोला था । उन दोनों को देखकर एक मुस्कुराहट बिखेरी उसने और फिर सामान की ओर नजर घुमाई ।"[1] पोती भी दादा–दादी को मेहमान नाम से संबोधित करती । महावीप्रसाद ने इसका अंदाजा लगा लिया कि उनका आना बहू श्वेता को अच्छा नहीं लगा था । कृष्णा अपने माता–पिता से बहुत प्रेम करता था । किंतु उसके एक गलत निर्णय के कारण उसे जीवनभर पछताने के अलावा और कोई रास्ता नहीं था । जैसे ही श्वेता को पता चलता है कि ससुर को कैंसर होने की आशंका है वह मौन हो जाती है । इधर श्वेता सामने के कमरे में आई और उसने एक झटके में हर्षा को उठा लिया । कृष्णा की माँ से उसका यह व्यवहार छिपा नहीं रहा । बाबूजी भी विचलित हुए ।"[2] कृष्णा की माँ के लिए उनके घर में मौजूद कुछ चीजें नई थी । उसी वक्त वह अपना कुतुहल का समाधान करने के लिए उसका दाम पूछ लेती है । श्वेता फ्रिज लेने की इच्छा प्रकट करते हुए कहती है– "नौ हजार में तुरंत रकम बताकर श्वेता अचकचायी । फिर संवारते बोली अगली बार के फेस्टिवल एडवांस में कुछ रकम जोड़कर ले लूंगी ।"[3] जब कृष्णा की माँ ने अपने मन की बात कही कि अपने पति से बात करके पैसों की व्यवस्था करेगी, क्योंकि पैसों से भी अधिक महत्व परिवार का सुख है तो "श्वेता पलटकर बोली नहीं... नहीं... रहने दीजिए । किसी तरह हम कर लेंगे । श्वेता का यह वाक्य फिर पराये पन की तोप दाग गया । टुकड़े–टुकड़े हो गई कृष्णा की माँ फिर शांत और गुमसुम ।"[4] महावीर प्रसाद यह सब अनुभव कर रहे थे किंतु वे मौन थे । उन्होंने बेटे की सारी मनोदशा को आंका था । किंतु श्वेता पैसे एवं अपनी सुख–सुविधा के पीछे भाग रही थी । अपनी माँ की सलाह के अनुसार उसने दोनों को घर का काम करवाने के उद्धेश्य से मुंबई रहने के लिए बुलाया था महवीर प्रसाद की पत्नी नौकरानी की तरह घर का सारा काम करने लगी थी । "महावीर प्रसाद की नजर जौहरी की तरह थी । वह आदमी को देखते ही उसके दिमाग का हालचाल नाप सकते थे ।"[5] श्वेता की माँ का भी सच उनके

सामने आया । उनको पता चला कि उन्हें वहाँ पर बुलाने का कारण स्नेह या प्रेम नहीं बल्कि पैसा था । अपनी पत्नी को घर का सारा काम करती देख दुःखी होकर उन्होंने वापस जाने का निर्णय लिया । "महावीर प्रसाद को अप्रत्यक्षतः यह समझते देर नहीं लगी कि उन्हें क्यों इतनी आत्मीयता से बुलाया गया है । इस साजिश से उन्हें चिढ़ हुई । कृष्णा को भी शायद यह पता नहीं होगा ।"[6] हर बहू को अपनी सास–ससुर प्यारे नहीं होते किंतु वह सदैव यह कामना अवश्य करती है कि उसके माता–पिता को खुश रखने वाली लड़की भाई की दुल्हन बने ।

'कुइयाँजान' उपन्यास में वृद्ध विमर्श अनेक स्थान पर चित्रित है जैसे उपन्यास का एक पात्र है शकरआरा । वह पढ़ी–लिखी होने के बावजूद भी अपनी सास को नहीं समझ पाई । जमाल खा की माँ एक सरल व्यक्तित्ववाली महिला थी । उसने अपनी बहू को गलत नहीं कहा, सदैव परिस्थिति के अनुरूप स्वयं को बदलती आई और परिवार में कभी बेटे और बहू को अलग करने का प्रयास नहीं किया । "शकरआरा की अपनी सास से नहीं पटी थी । ऐसा कोई दिन नहीं था जब सास–बहू में तकरार न होती हो । माँ के खत आने पर भी मियाँ– बीबी में तल्खी हो जाती थी ।"[7] जमाल खाँ को अपनी माँ के लिए बहुत बुरा लगता । किंतु वह शांत इसलिए रहते क्योंकि उनकी माँ ने उनसे यह वचन लिया था की परिवार में बच्चों के लिए जमाल खां अपनी पत्नी को कभी नहीं छोड़ेगा । वह हमेशा अतीत में माँ के वादे याद करते । "अम्मा की खामोशी दिन–ब–दिन गहरी होती चली गई । यहां तक कि बच्चों को उनके पास जाने की मनाही पर भी उन्होंने जबान नहीं खोली । वह शकरआरा को खुला मैदान देकर एक किनारे हट गई थी कि खेलो, जी भरकर खेलो । मुझे अपने बेटे की गृहस्थी नहीं उजाड़नी ।"[8] बेटे से माँ को अपनी बीबी को तलाक देने की बात सुनकर वह वृद्ध महिला अपने सारे दर्द छुपाकर बेटे के सामने खुश रहने का नाटक करती है । शादी के बहाने जो वह एक बार गाँव गई तो वापिस कभी नहीं आयी । उसकी अंतिम इच्छा थी कि उसे गाँव में ही दफनाया जाए ।

इसी उपन्यास में बहू द्वारा अपने ससुर पर किए जाने वाले शोषण का वर्णन है । बहू से बेटा अपने पिता के खान–पान की व्यवस्था करने को कहकर खुद काम पर चला जाता, उसे लगता कि पत्नी पिता का अच्छे से खयाल रखती है । मगर एक दिन डॉक्टर के कहने पर कि खाने की कमी के कारण पिता मर भी सकते हैं । उसने खुद पता लगाना चाहा कि आखिर ऐसा क्यों हुआ । बहू अपने ससुर से कहती है – "अरे कउन–सा रोग लग गवा है जो डॉक्टर की फीस मा पैसा बहाया रहा है बूढ़ा, अब कहत है बासी न खाबे, डॉक्टर मना किए है । तो रहो भूखा हमार का जात है ।"[9] उस वृद्ध को बहू बासी रोटी खिलाती और खुद ताजा आहार खाती । सच्चाई से अवगत होकर बेटा गुस्से से खौल उठाता है । स्वयं जाकर गरम दूध का कुल्हड़ पिता के हाथ में थमाते हुए बोला "ग्वाले को कल से दूध लाने के लिए मना कर देना, पिताजी खुद जाकर दूध पी लेंगे । हिसाब महीने–महीने मैं करूंगा और अगर तुम्हें ताजी रोटी डालने में आलकस होती है तो उसका भी बंदोबस्त हो जाएगा ।"[10] औरत का चेहरा अपमान से लज्जित हो गया । क्योंकि उसकी करनी अब पति के सामने थी और अपने बचाव के लिए उसके पास शब्द नहीं थे । उसकी आंखों में पश्चाताप का पानी था । "वह बुरी औरत नहीं थी, मगर जिस समाज में बूढ़े बोझ समझे जाने लगे हों, उन्हें बेकार की वस्तु समझकर एक किनारे डालने का चलन बढ़ रहो हो, वहाँ पर यह औरत सबसे अलग क्यों व्यवहार करेगी?"[11]

'गिलिगडु' उपन्यास में दो वृद्ध बाबू जसवंत सिंह और कर्नल स्वामी का वर्णन मिलता है । दोनों विदुर थे पत्नी की देहांत ने उन्हें भीतर से अकेला कर दिया था । जसवंत सिंह अपने गांव में ही भले चंगे थे । पत्नी के मरणोपरांत वह परिवार वाले एवं समाज वालों की सलाह के कारण अपने बेटे के पास दिल्ली आने के लिए मजबूर हो जाते हैं । बहू सुनयना को बाबू जसवंत सिंह का घर आना उतना अच्छा नहीं लगा था । बाबू जसवंत सिंह का मानना था कि बहू को जितना खयाल पलतू कुत्ता टॉमी का है, उसमें थोड़ा भी अपने ससुर के लिए नहीं है । जब कभी वे समाचार लगाते तो टॉमी की गुर्राहट बढ़ती जाती । "बहू सुनयना को टॉमी की नाराजगी बरदाश्त न होती । दखल देती हुई उन्हें टोकती– कोई म्यूजिक चैनल लगा दीजिए न बाबूजी । आज तक का क्या है,

चौबीसों घंटे चलता ही रहता है ।"[12] बाबू जसवंत सिंह को अपने बेटे के घर में इतना भी स्वतंत्रता नहीं थी कि उनकी सहायता करने वाले व्यक्ति को अपने घर चाय पर बुला सके । "कानपुर से दिल्ली आए हुए उन्हें अरसा हो गया था। घर की चौखट में दाखिल होते ही वे स्वयं को अपरिचितों की भांति प्रवेश करता हुआ अनुभव करते हैं ।"[13] जसवंत सिंह को बवासीर की बीमारी थी । वे उसी कारण ज्यादा परेशान रहते थे । जब उनकी पत्नी जिन्दा थी तब नौकरानी सुनगुनिया उनका अच्छे से खयाल रखा करती, किंतु इसे ही आशंका की दृष्टि से देखा गया । उनके और नौकरानी के बीच अनैतिक संबंध की भी कड़ी को जोड़ा गया । मगर वे सुनगुनिया को बेटी की तरह मानते थे । उनकी अपनी एक आहार पद्धति थी । सुबह के समय नींबू वाली चाय और दोपहर को दलिया खाना पसंद था उन्हें । जब तक अपने गाँव में रहे तब तक सुनगुनिया ने उनके आहार पद्धति को वैसे ही बरकरार रखा था । जब वह अपने बेटे के घर आये तब बहू द्वारा कोई न कोई बहाना बनाकर आहार पद्धति को टाल दिया गया । "दिल्ली आने के हफ्ते भर बाद बाबू जसवंत सिंह को लगा था कि उन्हें नरेन्द्र से अपनी आपत्ति प्रकट कर देनी चाहिए । खाने में कुछ भी खाना उनके लिए संभव नहीं था । फ्रीज में रखा बासी–कूसी उसकी अम्मा ने कभी कुछ उन्हें नहीं खिलाया, सो पेट को उसकी आदत नहीं ।"[14] इस बात पर बिगड़े नरेन्द्र ने अपने पिता को लंबा–चौड़ा भाषण देते हुए कहा "आइंदा वे अपनी पसंद की गुंजाइश इस घर में न ढूँढे तो बेहतर है ।"[15] इससे वे भीतर तक आहत हो गए थे । उनके साथ एक घटना ऐसी घटी जिसके बारे में उन्होंने कभी सोचा न था । बवासीर के कारण उन्हें अपने पाइजामा में खून के धब्बे दिखे, जिसे वे ठीक कर रहे थे, और सामने वाली खिड़की से पड़ोसन ने देखकर गलत मतलब निकाला । इस पर घर आकर पड़ोसन द्वारा आरोप लगाने पर "बहू सुनयना अपने पिता से इतनी कठोर हो सकती थी! संवाद के लिए कोई गुंजाइश नहीं सीधे–फैसला? घूमते सिर को तकिए में गड़ा बच्चों–से फूट–फूटकर रो पड़े । हिचकियों से लोहे का पलंग थर्राने लगा ।"[16] उस स्थान पर सुनयना के पिता होते तो उनके लिए पुरी दुनिया से लड़ जाती वह । किंतु एक बार भी उस ससुर से यह नहीं पूछा गया कि यथर्थ क्या है? क्यों यह आरोप उन पर आया? वृद्ध के बचाव में न ही बहू ने कुछ कहा और न ही बेटे ने । दोनों ने एक अंजान व्यक्ति की उक्ति को सत्य सिद्ध करके वृद्ध पर ही कटु वाणी का प्रहार करते रहें । उनके दृष्टि में बाबू जसवंत सिंह घर में कूड़े की तरह थे, जिसे हमेशा घर एक कोने में पडा रहना चाहिए । वे सिर्फ पैसों के भूखे थे । मानवीयता उनमें थी नहीं । उतने बडे घर में पिता को रहने के लिए एक कमरा तक नहीं था, उन्हे हाल में ही सोना पडता किंतु बच्चों के सामान रखने के लिए एक अलग कमरे की व्यवस्था घर में थी । ऐसे में बवासीर से पीडित व्यक्ति क्या करता कहाँ अपने पाइजामे के खून के धब्बे को साफ करता? दोनो सुशिक्षित तो थे किंतु सोचने की क्षमता दोनों में नहीं थी । पोते भी बाबू जसवंत सिंह से नजदीकी नहीं बढा सके । उनके लिए वह अपने पिता के पिता थे अतिरिक्त इसके और कुछ नहीं । यह दाईत्व माता–पिता का होता है कि अपने बच्चों को दादा–दादी के संबंध से परिचित कराए । यहाँ ध्यान देने योग्य बात यह है की संबंध में केवल दादा– दादी को ही पराए होने का आभास होता है । नाना–नानी को हमेशा अपने पोता–पोती का प्यार पूर्ण रूप से मिलता है । हर एक बहू का कर्तव्य है कि उसे सास–ससुर को माता पिता का स्थान भले ही न दे किंतु मानवीय मूल्यों को कभी भुलना नही चाहिए।

उसी प्रकार कर्नल स्वामी का भी परिवार था फिर भी बहुत सालों से अकेले रहते थे । परंतु कभी अपना दुःख दूसरों के सामने न बताते । ऐसे में कर्नल की दोस्ती बाबू जसवंत सिंह से होती है । "कर्नल स्वामी ने उन्हें अपने भरे–पूरे परिवार से परिचित कराया था, पत्नी नहीं है । तीन बेटे है, तीन बहुएँ हैं ।"[17] दोस्तों के सामने अपने आपको संसार का सुखी व्यक्ति के रूप में दिखाने वाले कर्नल स्वामी केवल भ्रम में जीवन जी रहे थे । भरे–पूरे परिवार के होते हुए भी उनके लिए कोई नहीं था नितांत एकांत के अलावा । अपने दोस्तों से अपनी बहुओं के तारीफ करते पोतियों का उल्लेख करते । किस प्रकार पोतियाँ उनके साथ खेलती हैं इसका वर्णन करते । जो भी उनसे मिलता यह सोचता कि कर्नल स्वामी तो भाग्यशाली है, जिसे एक संपन्न परिवार में रहने का भाग्य प्राप्त है । किंतु सत्य इससे विपरीत था । अपनी संपत्ति न देने के लिए उन्हें बच्चों से मार खाकर लहूलुहान भी होना पड़ा था । बेटों

को पिता की संपत्ति में हिस्सा चाहिए था जिसे पा कर वह अपनी अलग दुनिया बसाना चाहते थे, किंतु उस अलग दुनिया में दूर–दूर तक पिता के लिए कोई स्थान नहीं था । उनके जीवन में बहुत दुःख था, किंतु हमेशा मुख पर हर्ष की भावना रखने वाले कर्नल स्वामी दूसरों के लिए प्रेरणा का स्रोत बनते । अकेले रहते, अकेले जीवन व्यतीत करते और एक दिन हृदयाघात के कारण वह दुनिया के झंजट से मुक्ति तो पा लेते हैं, परंतु आत्मा को मुक्ति देने के लिए उनकी संतान सही समय पर नहीं पहुँच पाती । उनके पडोसियों से कर्नल स्वामी की कहानी जानकर बाबू जसवंत सिंह को तीव्र आघात होता है, साथ ही उनकी संतानों पर क्रोध प्रकट करते हुए वह कहते हैं– ''ऐसी औलादों से तो निपूत भला ।"[18]

यह केवल उपन्यास में आने वाले पात्र नहीं है । यह पात्र हमारे समाज में हमारे घर में भी उपस्थित है । बेटे के शादी के बाद परिवार में बहुत कुछ बदल जाता है । किंतु उस बदलाव में माता–पिता को कभी अनदेखा कर दिया जा रहा है । उन्हें निरपयुक्त वस्तु के रूप में देखा जाता है । एक घर जिसे अपने खून पसीने से बनाकर अपनी पूरी उम्र बिता देते हैं, बच्चों की खूशी के लिए पूरा जीवन संघर्ष करते हैं, फिर एक दिन अपने ही घर में पराए होने का अनुभव करते हैं । आजकल शीघ्रता से वृद्धाश्रम में बढोतरी हो रही है । जब संतान मासूम होती है तब माता–पिता संतान की हर गलती को क्षमा कर देते हैं । परंतु संतान वृद्ध माता–पिता की छोटी सी गलती पर उन्हे घर से ही बाहर निकाल देती हैं । 21 वीं सदी के अनेक उपन्यास है जिसमें वृद्धों की दयनीय स्थिति का चित्रण किया गया है । यदि हर संतान अपने दायित्व के प्रति समर्पित हो तथा वृद्ध माता–पिता के प्रति सम्मान का भाव रखकर उनकी देखभाल करें करें तो संसार में सभी परिवार सुख, समृद्धि से पूर्ण हो जाए तथा कोई वृद्धाश्रम न बनें और वृद्धाश्रम बने तो केवल उनके लिए ही सीमित हो जो वृद्ध अकेले हैं अथवा जिनका इस संसार में कोई कोई नहीं है । उपरोक्त आलेख द्वारा वृद्धों के कठोर जीवन एवं परिवार एवं समाज में उनकी दयनीय स्थिति को साहित्य के माध्यम से उजागर किया गया है ।

सन्दर्भ ग्रंथ सूची

1. डॉ दामोदर खड़से – भगदड़, पृ 11
2 वही, पृ 21
3. वही, पृ 31
4. वही, पृ 31
5. वही, 63
6. वही, पृ 64 –
7. नासिरा शर्मा – कुइयाँजान, पृ 118
8. वही, पृ 226
9. वही, पृ 170
10.वही, पृ 171
11. वही, पृ 171
12. चित्रा मुद्गल – गिलिगडु, पृ 11
13. वही, पृ 14
14. वही, पृ 39
15. वही, पृ 40

16. वही, पृ 60

17. वही, पृ 23

18. वही, पृ 138

आधार ग्रंथ सूची :

भगदड़ भावना प्रकाशन 2015

कुइयाँजान सामयिक प्रकाशन 2017

गिलिगडु सामयिक प्रकाशन 2019

कहानी 'उसने कहा था' में कथित प्रेम तत्त्व की संदिग्धता

डॉ. सम्राट् सुधा

बी. एस. एम. पी. जी. कॉलेज, रुड़की, पिन –247667, उत्तराखंड

मोबाइल नंबर : 9412956361

ई–मेल : samratsudha66@gmail.com

शोध सारांश :

चन्द्रधर शर्मा गुलेरी की कहानी 'उसने कहा था' को प्रेमकथा कहना उचित नहीं है । वस्तुतः 'उसने कहा था' मात्र नायक लहनासिंह के बचपन में सम्पर्क में आयी और जवानी में अनायास रूप से मिली सूबेदारनी के प्रति एकपक्षीय 'प्रेम' की कहानी है, जिसे इस कथा के संबंध में तार्किक विश्लेषण से सहज ही समझा जा सकता है ।

चन्द्रधर शर्मा गुलेरी की कहानी 'उसने कहा था' को हिन्दी प्रेमकथाओं में एक अनुपम प्रेमकथा की मान्यता मिली है । वर्ष 1915 में 'सरस्वती' के जूनांक में प्रकाशित यह कहानी उस समय अपने कथ्य और शिल्प की दृष्टि से अभिनव मानी गयी थी, यद्यपि बंगला कथा–साहित्य में ऐसी कथावस्तुएँ तब तक पर्याप्त चर्चित हो चुकी थीं ।

विचारणीय बात यह है कि 'उसने कहा था' क्या वास्तव में प्रेम की एक अमर कथा है या यह लहनासिंह के एकतरफा सच्चे प्यार और सूबेदारनी द्वारा उसे 'कैश' करने की दुःखद कथा मात्र है! कथ्य और शिल्प की दृष्टि से 'उसने कहा था' कितनी सशक्त है, इसे कतिप्रय अलोचकों के दृष्टिकोण से जान लेना समीचीन ही होगा ।

आचार्य रामचन्द्र शुक्ल ने 'उसने कहा था' के संदर्भ में लिखा है– "संस्कृत के प्रकाण्ड प्रतिभाशाली विद्वान् हिन्दी के अनन्य आराधक श्री चन्द्रधर शर्मा गुलेरी की अद्वितीय कहानी 'उसने कहा था' सं. 1972 अर्थात् सन् 1915 की 'सरस्वती' में छपी थी । इसमें पक्के यथार्थवाद के बीच, सुरुचि की चरम मर्यादा के भीतर, भावुकता का चरम उत्कर्ष अत्यन्त निपुणता के साथ संपुटित है । घटना इसकी ऐसी है, जैसी बराबर हुआ करती है; पर उसके भीतर से प्रेम का एक स्वर्गीय स्वरूप झाँक रहा है–केवल झाँक रहा है, निर्लज्जता के साथ पुकार या कराह नहीं रहा है । कहानी भर में कहीं प्रेम की निर्लज्ज प्रगल्भता, वेदना की वीभत्स विधृति नहीं है । सुरुच के सुकुमार से सुकुमार स्वरूप पर कहीं आघात नहीं पहुँचता । इसकी घटनाएँ ही बोल रही हैं, पात्रों के बोलने की अपेक्षा नहीं ।"[1]

सुशील कुमार फुल्ल 'उसने कहा था' सहित गुलेरी जी की अन्य पाँच कहानियों पर टिप्पणी करते हुए लिखते हैं–"गुलेरी जी कहानीकार नहीं थे और न ही कवि, इस आशय का प्रत्यक्ष संकेत उनके (आत्मकथ्य) में मिलता है । आचार्य शुक्ल ने 'उसने कहा था' को 'अद्वितीय' कहकर परवर्ती विद्वानों के लिए एक लीक बना दी, जिसे आज तक निरन्तर दोहराया जाता रहा है, परन्तु वास्तविकता यह है कि उनकी कहानियाँ समग्र रूप से देखे जाने पर कथ्य तथा कलात्मकता दोनों ही दृष्टियों से छोटी पड़ जाती हैं । आलोचकों ने जो आदर्श उनकी कहानियों पर आरोपित किये हैं, कहानियों का अवलोकन करते ही वे भुर–भुराकर बिखर जाते हैं । आलोचकों ने गुलेरी जी की रचनाओं को खूँटी समझकर, अपनी मान्यताएँ टाँगकर, उन्हें अमर कहानीकार घोषित कर दिया है । व्यक्ति गुलेरी को क्षणभर के लिए भुलाकर यदि उनकी कहानियों का परीक्षण करें, तो रचनात्मक कमजोरियाँ, अनावश्यक है–विस्तार, संयोजन की शिथिलता तथा रोमांस की ललक एवं मांसल चित्रण का मोह एकाएक स्पष्ट हो उठता है ।"[3]

बच्चनसिंह इस कहानी पर टिप्पणी करते हुए लिखते हैं– "वस्तुतः यह कहानी (उसने कहा था) सोमनाथ के मन्दिर की मूर्ति की तरह आकाश में लटकी हुई प्रतीत होती है । यदि भावुकता का चुम्बक हटा लिया जाए, तो मूर्ति धरती पर खण्ड–खण्ड हो जाएगी । समीक्षकों ने उसकी भावुकता को ही विशेषता के रूप में ग्रहण कर लिया, क्योंकि वे स्वयं भावुक थे ।"[4]

इस कहानी के कलेवर पर टिप्पणी करते हुए नन्दुलारे वाजपेयी लिखते हैं– "गुलेरी जी की 'उसने कहा था' कहानी बहुत लंबी ही है अधिक स्थान और समय घेरती है और कहानी के नवीन प्रतिमानों को देखते हुए विराट या महाकाव्यात्मक कहानी (एपिक स्टोरी) कही जा सकती है । लम्बी कहानियाँ प्रसादजी ने भी लिखी हैं और प्रेमचन्द जी ने भी । इन दोनों की कहानियों में' उसने कहा था' की–सी बोझिल विशालता नहीं है ।"[5]

वहीं जैनेन्द्र कुमार का यह कथन द्रष्टव्य है– "गुलेरी जी विलक्षण विद्वान् थे... गुलेरी जी न केवल विद्वता में अपने समकालीन साहित्यकारों से ऊँचे ठहरते हैं, अपितु एक दृष्टि से वह प्रेमचन्द से भी ऊँचे साहित्यकार हैं । प्रेमचन्द ने समसामयिक स्थितियों का चित्रण तो बहुत बढ़िया किया है, पर व्यक्ति मानस के चितेरे के रूप में गुलेरी का जोड़ नहीं है । प्रेमचन्द अपने साहित्य में सामाजिक सम्बन्धों के चित्रण से आगे नहीं बढ़े, जबकि गुलेरी ने 'उसने कहा था' में ही मानवतावाद की आत्मा का स्पर्श कर लिया है ।"[6]

प्रश्न 'उसने कहा था' के 'प्रेममय' कथानक का है । इस कहानी में जब लड़का (लहनासिंह) और लड़की (बाद में सूबेदारनी) मिलते हैं, तो उनकी आयु क्रमशः बारह और आठ वर्ष होती है । कहानी का यह अंश द्रष्टव्य है–"लहनासिंह बारह वर्ष का है । अमृतसर में मामा के यहाँ आया हुआ है । दही वाले के यहाँ, सब्ज़ी वाले के यहाँ, हर कहीं उसे आठ वर्ष की लड़की मिल जाती है । जब वह पूछता है कि तेरी कुड़माई हो गयी? तब 'धत्' कहकर वह भाग जाती है । एक दिन उसने वैसे ही पूछा तो उसने कहा–'हाँ, कल हो गयी । देखते नहीं यह रेशम के फूलों वाला शालू?' सुनते ही लहनासिंह को दुःख हुआ । क्रोध हुआ । क्यों हुआ?"

ऊपर उद्धृत कथा–संवाद से यह मान लेना कि उस आठ साल की लड़की से बारह साल के लड़के लहनासिंह को सचमुच 'गम्भीर प्रेम' हो गया था, भला कितना उचित है? कहानी में आगे स्वयं इसका उत्तर मिलता है–"पच्चीस वर्ष बीत गये । अब लहनासिंह नं. 77 राइफल्स में जमादार हो गया है । उस आठ वर्ष की कन्या का ध्यान ही न रहा । न मालूम वह कभी मिली थी या नहीं ।" परन्तु पच्चीस वर्ष पश्चात् भी उस लड़की (जो अब सूबेदारनी है) की स्मरणशक्ति की प्रशंसा करनी पड़ेगी कि अपने पति (सूबेदार) के साथ आये लहनासिंह को वह तुरन्त पहचान लेती है; साथ ही अपने पति को उससे मिलने की इच्छा भी जता देती है– "सूबेदार का गाँव रास्ते में पड़ता था और सूबेदार उसे बहुत चाहता था । जब चलने लगे, तब सूबेदार बेड़े में से निकलकर आया । बोला–लहना, सूबेदारनी तुमको जानती है । बुलाती है । जा मिल आ ।" पच्चीस वर्ष बाद यूँ अपने से चार बड़े लहनासिंह को सूबेदारनी द्वारा पहचान लेना अत्यन्त अस्वाभाविक है, परन्तु उसके द्वारा लहनासिंह को पच्चीस वर्ष पूर्व का स्मरण कराना नारी–मनोविज्ञान के एक और पक्ष को उद्घाटित करता है–

"मुझे पहचाना?"

"नहीं।"

"तेरी कुड़माई हो गयी?–धत्–कल हो गयी... देखते नहीं रेशमी बूँटों वाला शालू– अमृतसर में ।"

विचारणीय बात यह है कि पच्चीस वर्ष पश्चात् सूबेदारनी लहनासिंह को पहचान तो भली–भाँति लेती है, उसे स्वयं को पहचानने के लिए नितान्त भावुकतापूर्ण संवाद में शब्दशः स्मरण भी करा देती है, परन्तु वह न तो लहनासिंह का औपचारिक कुशलक्षेम ही पूछती है और न ही उसके परिवार आदि का हालचाल! वास्तविकता यह है कि मनुष्य जब अपने किसी बड़े स्वार्थ को लेकर दूसरे से मिलता है, तो दूसरे की पीड़ा या समग्रतः दूसरे का जीवन उसके लिए कोई अर्थ नहीं रखता है । सूबेदारनी का मंतव्य

उस समय पूर्णतः उद्घाटित हो जाता है, जब लहनासिंह को पच्चीस वर्ष पूर्व की बातों का स्मरण कराती हुई वह विशुद्ध स्वार्थमय वादा उससे अवचेतन रूप से करा लेती है– "मैंने तेरे को आते ही पहचान लिया । एक काम कहती हूँ। मेरे तो भाग फूट गये । सरकार ने बहादुरी का ख़िताब दिया है, लायलपुर में जमीन दी है, आज नमकहलाली का मौका आया है । पर सरकार ने हम तीमियों की एक घंघरिया पलटन क्यों न बना दी, जो में भी सूबेदारजी के साथ चली जाती? एक बेटा है । फ़ौज में भरती हुए उसे एक ही बरस हुआ । उसके पीछे चार हुए, पर एक भी नहीं जिया (सूबेदारनी रोने लगती है) । मेरे भाग । तुम्हें याद है, एक दिन तांगे वाले का घोड़ा दहीं वाले की दुकान के पास बिगड़ गया था । तुमने उस दिन मेरे प्राण बचाये थे । आप घोड़ों की लातों में चले गये थे और मुझे उठाकर तख़्ते पर खड़ा कर दिया था । ऐसे ही इन दोनों को बचाना । यह मेरी भिक्षा है । तुम्हारे आगे मैं आँचल पसारती हूँ ।" कहानी 'उसने कहा था' का ऊपर उद्धृत संवाद सूबेदारनी के हृदय से समस्त भावों को गहनता से उद्घाटित करता है । उक्त संवाद के आधार पर देखें तो सूबेदारनी को अपने पति और पुत्र की; यहाँ तक कि अंग्रेज सरकार के प्रति 'नमकहलाली' तक की चिन्ता है, परन्तु लहनासिंह के प्रति कोई संवेदनशीलता नहीं है । सूबेदारनी का अब अपना परिवार है, पति की बहादुरी से प्रसन्न हो सरकार ने जमीन दी, तो सूबेदारनी के हृदय में नमकहलाली हिलोर लेने लगी, परन्तु बचपन में तांगे के नीचे आने से बचाने वाले लहनासिंह के प्रति कृतज्ञता व्यक्त करना तो दूर, उससे अपने पति और पुत्र की जीवन– रक्षा की 'भिक्षा' ही माँग ली! अपने प्राण बचाने का स्मरण दिलाकर सूबेदारनी 'ऐसे ही इन दोनों को बचाना', कहकर 'ऐसे ही' के माध्यम से यह प्रच्छन्न रूप से कह देती है कि भले ही अपने प्राण देकर करना, परन्तु मेरे पति और पुत्र की रक्षा करना!! इस प्रकार बचपन की यदा–कदा होने वाली भेंटों के पच्चीस वर्ष पश्चात् सूबेदारनी को लहनासिंह और उसके द्वारा स्वयं को बचाया जाना तो ध्यान रहता है, परन्तु उसकी 'भिक्षा' से यह स्पष्ट हो जाता है कि लहनासिंह के प्रति न तो उसकी कोई संवेदना पच्चीस वर्ष पूर्व थी और न ही वर्तमान में अब, जब वह युद्ध में जाते लहनासिंह से अपने पति व पुत्र की रक्षा की बात, बिना उसके प्रति कोई चिन्ता व्यक्त किये, कह देती है ।

विश्वविख्यात फ्रेंच लेखिका सिमोन द बोउवार लिखती हैं" पुरुषों से अधिक स्त्रियाँ बचपन की यादों को संजोये रखती हैं। बचपन में मैं माता–पिता के संरक्षण में स्वतंत्र थी, यह उन्हें याद रहता है । भविष्य उनके सम्मुख होता है । वे अपने को अधिक सुरक्षित नहीं समझतीं । वे अनुचर व वस्तु–रूप में वर्तमान में बन्दी होती हैं । एक समय वे विश्व को विजित करना चाहती थी, पर अब वे आम वस्तु के रूप में बदल गयी हैं । अरबों पत्नियों और घर सम्भालने वाली गृहिणियों में से वे भी अब एक होती हैं ।"

सीमोन द बोउवार के उपर्युक्त कथन से सूबेदारनी (एक आम स्त्री) के मनोभावों का कारण तो स्पष्ट होता है, परन्तु इससे कहीं भी उसकी छवि एक प्रेममयी स्त्री के रूप में नहीं उभरती है । कहानी में क्या यह अधिक सुखद नहीं होता कि सूबेदारनी लहनासिंह से मिलने पर उसे बचपन की बातों का स्मरण तो कराती, परन्तु युद्ध में जाते, कभी अपने प्राणों की रक्षा करने वाले, उस निश्छल प्रेमी से यह वादा भी करा लेती कि तुम्हें इस युद्ध में जी– जान से लड़कर भी मेरे लिए जीवित वापिस आना है! युद्ध में यद्यपि कौन मरेगा और कौन बचा रहेगा, यह भला कौन कह सकता है, तथापि सूबेदारनी द्वारा लहनासिंह को बचपन की बातों का भावुकतापूर्ण स्मरण कराकर जैसे उसके प्राणों को बचाया था, 'ऐसे ही' अपने पति और पुत्र के जीवन की रक्षा की 'भिक्षा' माँगना क्या सूबेदारनी का घोर स्वार्थमय और कुटिल होना प्रमाणित नहीं करता है?

दूसरी ओर लहनासिंह सूबेदारनी की 'भिक्षा' को पूर्ण करने के लिए आत्मोत्सर्ग करने में कोई कमी नहीं छोड़ता है । सूबेदारनी के पुत्र को युद्ध क्षेत्र में बुखार हो जाने पर वह उसे अपनी जरसी उतारकर पहना देता है, उसे अपने दो कम्बल और बुरानकोट भी पहना देता है; बोधा सिंह के पूछने पर भी अपनी जाँघ में लगी गोली के विषय में नहीं बताता; सूबेदार जब पट्टी बाँधना चाहता है, तो 'थोड़ा घाव है, सबेरे देखा जाएगा' कहकर टाल देता है और जब सूबेदार उसे छोड़कर नहीं जाते, तो 'तुम्हें बोधा की क़सम है और सूबेदारनी की सौगन्ध है, जो इस गाड़ी में न चले जाओ', कहकर उन्हें जाने को विवश करता है ।

लहनासिंह उपर्युक्त समस्त कार्य वस्तुतः सूबेदारनी की इस 'भिक्षा' की पूर्ति के लिए करता है, जो वह उससे युद्ध में जाने से पूर्व अपने पति और पुत्र की रक्षा, वचपन में जैसे उसकी (सूबेदारनी की) की थी 'वैसे ही' करने के रूप में माँगती है अथवा कह सकते हैं उसके भावुक हृदय को भाँपकर अपने विशुद्ध स्वार्थ में लिप्त होकर माँग लेती है! लहनासिंह अपने अन्तिम समय में भी सूबेदारनी द्वारा माँगी गयी विशुद्ध स्वार्थपूर्ण 'भिक्षा' को नहीं भूलता है । सूबेदार जब उसे छोड़कर जाने में झिझकता है, तो वह कहता है–"बोधा गाड़ी पर लेट गया? भला । आप भी चढ़ जाओ । सुनिए तो, सूबेदारनी होरां को चिट्ठी लिखो तो मेरा मत्था टेकना लिख देना और जब घर जाओ, तो कह देना जो उसने कहा था, वह मैंने कर दिया!"

निष्कर्ष :

कथा–शिल्प की दृष्टि से देखें, तो 'उसने कहा था' वास्तव में सर्वथा अनूठे शिल्प से युक्त अद्वितीय कहानी है, जिसमें 'फ्लैशबैक' (पूर्व स्मरण) के माध्यम से कथानक विस्तार लेता है, परन्तु इतना स्पष्ट है कि इस कहानी को प्रेमकथा कहना उचित नहीं है । वस्तुतः 'उसने कहा था' मात्र नायक लहनासिंह के बचपन में सम्पर्क में आयी और जवानी में अनायास रूप से मिली सूबेदारनी के प्रति एकपक्षीय 'प्रेम' की कहानी है, जिसमें लहनासिंह की सूबेदारनी के प्रति अतिशय भावुकता ही उभर कर सामने आती है और प्रेम–तत्त्व प्राय: गौण ही रहता है । यह सुस्पष्ट है कि 'उसने कहा था' एक प्रेमकथा नहीं है; साथ ही इसमें कथित प्रेम और इसके बारे में कथित प्रेम वास्तव में पूर्णतः संदिग्ध है !

संदर्भ

1. 'गुलेरी रचनावली', संपादक–डॉ. मनोहरलाल, पृ. 473
2. कहानी– 'घण्टाघर' (सन् 1904), 'धर्मपरायण रींछ' (सन् 1906), 'सुखमय जीवन' (सन् 1911), 'बुद्ध का काँटा' (सन् 1914), 'उसने कहा था' (सन् 1915), 'हीरे का हार' (सन् 1987), गुलेरी जी की रचनाएँ, 'गुलेरी रचनावली' संपादक–डॉ. मनोहरलाल, पृ. 486
3. 'गुलेरी रचनावली', संपादक–डॉ. मनोहरलाल, पृ. 479
4. वही, पृ. 475
5. वही, पृ. 473
6. वही, पृ. 473
7. सिमोन द बोउवार 'स्त्री : उपेक्षिता', प्रस्तुति–डॉ. प्रभा खेतान, पृ. 253

केदारनाथ अग्रवाल की कविताओं में सामाजिक यथार्थबोध

डॉ. एस. सूर्यावती

प्राध्यापिका, हिंदी विभाग, शासकीय महाविद्यालय

चोडवरम, अनकापल्लि जिला, अंध्रप्रदेश

Email: suryavathis@gmail.com

Phone: 9440417304

शोध सार:

"जनगण–मन के जागृत शिल्पी

तुम धरती के पुत्र"

– नागार्जुन

केदारनाथ अग्रवाल प्रगतिशील काव्य धारा के प्रतिनिधि कवि हैं । उनकी कविताओं में व्यापक सामाजिक चेतना का चित्रण मिलता है । वे जीवन और जनता को प्यार करने वाले एक सहृदय, विनयी, विवेकशील व्यक्ति हैं । अपने यथार्थवादी सौंदर्य बोध को कलात्मक ढंग से प्रस्तुत करके काव्य चेतना का मार्ग प्रशस्त किया। केदार जी की लेखनी की निरंतरता ने साहित्य को बहुमूल्य संपत्ति प्रदान की है ।

बीज शब्द: मार्क्सवाद, पूँजीपति, मजदूर, प्रजातंत्र आदि ।

जनवादी कवि केदारनाथ अग्रवाल का जन्म बाँदा जिले के कुमासन गांव में सन् 1911 को और निधन 22 मई, 2000 को हुआ । आप ने प्रयाग और आग्रा विश्वविद्यालय में बी.ए. और एल.एल.बी. किया। बाद में वकालत की। प्रगतिशील साहित्य के आंदोलन से जुड़कर वे अपनी रचनाधर्मिता को आगे बढ़ाया हैं । उनकी रचनाएँ समय–समय पर 'हंस' और 'नया साहित्य' जैसी पत्रिकाओं में प्रकाशित होते थी । केदारनाथ अग्रवाल व्यापक चेतना के कवि हैं, उनकी रचनाओं में मार्क्सवादी विचारधारा परिलक्षित होती है । काल्पनिक आदर्शवाद और आशावाद से रहित इनकी रचनाएँ सच्ची यथार्थवादी कविताएँ कहलाती है । अपनी कविताओं के बारे में कवि स्वयं कहता है– "मेरी कविताओं में मेरा अनुभूत व्यक्तित्व तो हैं ही साथ ही साथ उसमें एक युगबोध और यथार्थबोध भी है । प्रत्येक कविता आत्मान्वेषिणी होते हुए भी यथार्थान्वेषिण भी हैं ।"[1] गाँव और नगर, धनी और निर्धन का अंतर भी इन्होंने बड़ी पटुता से अंकित किया है । वर्तमान जीवन के खोखलेपन को चाहे वह इन्हें कहीं भी दिखाई दिया हो चित्रित करने में यह कभी नहीं चूकते। सामाजिक उद्धार पर आधारित इनकी यथार्थवादी दृष्टि वास्तविकता की भयंकरता को कहीं भी पकड़ लेती है । शहर के लडकों के बारे में कवि ने लिखा हैं –

"शहर के छोकडे

मैले फटे, बदबूदार वस्त्र पहने

बिना तेल कंघी के

रूखे उलझाए बाल

माओं बहनों को

पाप की दृष्टि से ताकते हैं ।"[2]

इनके वस्तु जगत में गाँव का सरल कृषक हैं जो अभाव तथा ऋण में डूबा है तथा मजदूर है जिसके रक्त को जमींदार चूस रहा है । सूदखोर, महाजन, पूँजीपति, कर्मचारी और अधिकारी एकजुट होकर अपनी सुविधा के लिए परिस्थितियों को यथास्थित बनाए रखना चाहते हैं । वे स्वार्थी बनकर मानवीय संवेदना को भुला दिया है । उनकी कविताएँ कृषक जीवन के परिवेश की कविताएँ हैं, जिनमें कर्म और पसीने का सौंदर्य है ।

उत्तर छायावादी काल में प्रगतिवादी आंदोलन को जिन थोड़े से कवियों ने बल दिया है, उनमें केदारनाथ अग्रवाल प्रमुख हैं । वे उन अवसरवादी कावियों में से नहीं है जो सरकारी नौकरी मिलते ही अपना मत बदल देते हैं । अपनी रचनाओं में उन्होंने पूँजीवादी सभ्यता के दोष गिनते हुए पूँजीपतियों की क्रूरता और हृदय हीनता की खुलकर निंदा की है । ऐसे लोगों को उन्होंने जनता का मांस नोचकर खाने वाले गिद्ध बतलाया है । किसान और मजदूर की दयनीय स्थिति के लिए उन्होंने सूदखोर मिल मालिक, राजनीतिक नेता और सरकार सभी को उत्तरदायी ठहराया है । देश की वर्तमान आर्थिक स्थिति की ओर संकेत करते हुए उन्होंने बताया है कि लोग आजीविका विहीन है, भूखे हैं, त्रस्त है ।

साम्यवादी विचारधारा के प्रसार लिए एक ओर ये किसानों और मज़दूरों को उत्तेजित कर उनमें विद्रोह की भावना का संचार करते हैं वहीं दूसरी ओर मनुष्य के उपचेतन पर प्रभाव डाल कर उसके भीतर से कुंठा, अहं और स्वार्थ की भावनाओं को नष्ट करने का प्रयत्न करते हैं । जिनसे व्यक्तिवाद के पनपने की आशंका होती है । ये प्रवृत्तियाँ मोर्चे पर कविता में उभरकर आई है–

"मैं लड़ाई लड़ रहा हूँ मोर्चे पर ।
मैं अचेतन और उपचेतन सभी पर
वार करता जा रहा हूँ ।
सूदखोर को,
मिलों के मालिको को,
अर्थ के पैशचिकों को,
भूमि को हड़पते हुए धरणीधरों को
मैं प्रणय के साम्यवादी आक्रमण
से मारता हूँ ।"[3]

शोषकों के प्रति अपना आक्रोश स्थान–स्थान पर तरह–तरह से व्यक्त किया है । मजदूरों के श्रम को लूटकर उन्हें भूख से तडपने के लिये छोढ दिया हैं । निम्न कविता में कवि ने थैलीशाहों की शोषण का चित्रण किया हैं – "थैलीशाहों की यह बिल्ली/ बडी नीच हैं/ मजदूरों का ख़ाना–दाना/ सब चोरी से खा जाती हैं/ बेचारे भूखे सोते हैं ।"[4]

समसामयिक समाज में जो वर्ग वैषम्य हैं, निराशा है, दुख और अभाव है, उन स्थितियों को पूरी ईमानदारी से अपनी कविता में प्रस्तुत किया है । मार्क्सवादी चिंतक होने के नाते कवि परंपरागत धार्मिक मान्यताओं, रुढ़ियों, सड़ी गली परंपराओं, रूढ़िग्रस्त धर्म, मूर्ति पूजा का विरोध करता है । वे मानते हैं कि प्रगतिशील समाज के ये बाधक तत्व है । और ये समाज को पतनोन्मुख बनाता है । जनवादी कवि केदारनाथ ने रूढिग्रस्त धर्म तथा मूर्तिपूजा का विरोध इस प्रकार करते हैं –

"छोटी सी देवमूर्ति/ आले में रखी थी/ बेचारी औचक ही/ चूहे के धक्के से/ दांसा के पत्थर पर/ नीचे गिर टूट गई"[5]

कवि रोज़ी रोटी की समस्या का उल्लेखित करते हुए कहते हैं कि–

"रोटी तुमको राम न देगा, वेद तुम्हारा काम न देगा

जो रोटी के लिए लड़ेगा, वह रोटी आप वरेगा ।"[6]

कवि ने राजनीतिक नेताओं का उपहास किया है । नेताओं के खंडित व्यक्तित्व को रेखांकित करता है –

"न तुम भविष्य को उज्वल कर सकते हो
न आज को सुंदर कर सकते हो ।"[7]

चतुर्थिक अन्याय देखकर कवि का मन दुःखित होता है । सर्वत्र ज़ोर–जुल्म और भ्रष्टाचार व्याप्त है । एक वकील होने के नाते, वे स्वयं न्यायालय में हो रहें अन्याय और नौकरशाही को देखकर बर्दाश्त नहीं कर पाते हैं । वे नौकरशाही और अफसरशाही का विरोध करते हैं ।

"जनता का जमघट मैं बाँधू
इनका तोडूँ नौकरशाही।
अफसरशाही का सिर फोडूँ ।"[8]

सामान्य जनता की व्यापक संवेदना को अपनी रचनाओं में मुखरित किया है । इनके काव्य में कानपुर के मज़दूरों से लेकर बांदा जिले के किसानों के जीवन का वास्तविक चित्रण मिलता है । तत्कालीन समाज में उपस्थित बेरोजगारी की समस्या का चित्रण करता है ।

"रद्दी की टोकरी का जीवन है/ संज्ञाहीन, अर्थहीन/ बेकार चिर फटे टुकड़ों सा पड़ा है/ देरी है/ एक दिन, एक बार, आग के चूने की/ राख हो जाना है ।"[9]

केदारनाथ ने गरीबों की ही नही निम्न मध्यवर्गीय परिवार की समस्याओं का भी चित्रण किया हैं । उनकी मायूसी और वस्त्राभाव की स्थिति 'हे मेरी तुम' कविता में प्रस्तुत किया हैं ।

इतना ही नहीं वो निम्न जातियों को उद्बोधन किया। 'मछुआरे' और 'दीन कुनवा' जैसे कविताओं ने उन लोगों की बदहाली का चित्रण किया है । मछुआरे कविता में कवि कहते हैं –

"अर्राती चौगुनी धार को
सहज चीरकर बढ़ने वाले
गंगा तट के ये मछुआरे
नैया पार लगाने वाले ।"[10]

नारी स्वतंत्रता की कामना करते हुए केदार ने 'रनिया' नामक कविता में लिखा है–

"अब रनियाँ के दिन आये है
जग उसके माफिक बदलेगा।"[11]

राजनीतिक अराजकता पर भी केदारनाथ ने गहरा व्यंग्य किया है ।

स्वाधीन भारत में पतनोन्मुख नेताओं के चरित्र पर केदारनाथ आक्रोश और चिंता व्यक्त करते हुए लिखते हैं –

"सत्ताइस साल में तुम
न तुम रह गए तुम ।
ना हम रह गए हम
तुम हो हो गए खूंख्वार
हम हो गए बीमार, अभावग्रस्त, लाचार"[13]

कवि जनवादी सरकार बनाने के पक्ष में है । वह सरकार की कड़ी आलोचना इसलिए करता है कि वह भारत में ब्रिटिश अर्थ नीती लागू करना चाहता है । सरकार अधिक टैक्सों को जनता पर लादकर जीवन के अधिकार को छीन लेती हैं । अंग्रेज भारत को छोड़कर चले गए किंतु सरकार अंग्रेज शासन रीति को खुद छोड़ नहीं पा रहीं है कवि के शब्दों में–

"अर्थनीति में राजनीति में गहरा गोता खाया ।
जनवादी भारत का उसने सब कुछ वहाँ गँवाया ।"[14]

कवि ने 1978 में जनतंत्र की दुर्गति का मर्मस्पर्शी चित्रण किया है । अगली पीढ़ी के द्वारा देश की विकास की कामना करते हुए कवि कहते हैं कि सिर्फ भाषणों से काम चलाने वाले शासकों की खिल्ली उड़ाते हुए कवि कहते हैं –

"देश में लगी आग को
लफ्फाजी नेता
शब्दों से बुझाते हैं ।
वाग्धारा से उर्वर
और देश को
आत्मनिर्भर बनाते हैं
लोकतंत्र का शासन
भाषण तंत्र से
चलते हैं ।"[15]

आततायी सत्ता के खोखलेपन तथा उसके अनाचार को बेनकाब करता हुआ कहता हैं–

"आग लगे इस समाज में ।
ढोलक मढती है अमीर की
चमड़ी बजती है गरीब की ।
खून बहाए रामराज में। आग लगे.."[16]

देश में फैली अराजकता का पर्दाफाश करते हुए कवि कहते हैं कि इस देश में आराम की जिंदगी जी नहीं सकते । यह पता नहीं कि किसका चाकू किसके पेट में घुसता हैं अर्थात मौत कब आ जाती हैं । यह अराजकता बढती ही जा रही हैं । किसी को सुकून की जिंदगी जीने का अधिकार इस स्वतंत्र भारत में नहीं रह गया हैं ।

केदारनाथ अग्रवाल ने यथार्थवाद सौंदर्यबोध को कलात्मक ढंग से प्रस्तुत करके राजनीतिक काव्य चेतना का मार्ग प्रशस्त किया है । उनकी कविता की सबसे बड़ी शक्ति लोकपरता है । उनकी लोकोन्मुखता जीवन के सहज आवेग से संपृक्त है । उन्होंने लोक जीवन की अनुभूति, सौंदर्य बोध और प्रकृति से जुड़े सवालों का सहज और उदात्त मानवीय भूमि पर ग्रहण किया। जन संस्कृति के तहत उनकी कविताएँ ग्रामीण समाज के सुख–दुख, राग–रंग, हास–विलास, आशा–आकांक्षा में शामिल हैं । अमृतराय के शब्दों में "केदार गहरी जीवन के आस्था का कवि हैं । मैं समझता हूँ यही उसके कवि व्यक्तित्व का बीज गुण हैं । उसके काव्य उन्मेष का बीजमंत्र और उसकी काव्य उपलब्धि का सार मर्म"[17]

निष्कर्ष:

केदारनाथ अग्रवाल की कविताएँ अधिकतर जीवन के सामाजिक और मानवीय मुद्दों पर आधारित हैं, जिससे व्यक्तिगत अनुभव और समस्याओं का सामाजिक संदेश प्रस्तुत होता हैं । केदारनाथ किसान और मजदूरों के समर्थक, शोषकों और पूँजीपतियों

के विरोधी, नारी स्वतंत्रता के आकांक्षक, गरीबों के पक्षधर हैं । अशोक त्रिपाठी के शब्दों में " ये कविताएँ देश के मेहनत मजूरी करने वाले लोगों की आत्मा की पुकार हैं, उनकी झुंझलाहट हैं, उनकी तिलमिलाहट हैं, उनकी खिसियाहट हैं, उनकी संघर्ष की खिसियाहट हैं, उनकी संघर्ष की संकल्प शक्ति हैं ।"[18]

संदर्भ :

1. केदरनाथ अग्रवल – फूल नहीं रंग बोलते हैं भूमिका से पृ. 4
2. केदारनाथ अग्रवाल – गुलमेहंदी पृ. 45
3. डॉ. लल्लन राय – हिंदी की प्रगतिशील कविता पृ. 155, 156
4. केदारनाथ अग्रवल – कहे केदार खरी–खरी पृ. 6
5. केदारनाथ अग्रवाल – गुलमेहंदी पृ. 33
6. केदारनाथ अग्रवाल – गुलमेहंदी पृ. 38
7. केदारनाथ अग्रवल – कहे केदार खरी–खरी पृ. 188
8. केदारनाथ अग्रवाल – गुलमेहंदी पृ. 128
9. केदारनाथ अग्रवाल – गुलमेहंदी पृ.29
10. केदारनाथ अग्रवाल – गुलमेहंदी पृ.54
11. केदारनाथ अग्रवाल – गुलमेहंदी पृ.48
12. केदारनाथ अग्रवाल – कहे केदार खरी खरी पृ. 90
13. केदारनाथ अग्रवाल – कहे केदार खरी खरी पृ. 186
14. केदारनाथ अग्रवाल – मारे प्यार की थापें पृ. 79
15. केदारनाथ अग्रवाल – मारे प्यार की थापें पृ. 26
16. केदारनाथ अग्रवाल – कहे केदार खरी खरी पृ. 81
17. अमृतराय – आधुनिक हिंदी कविता सं. जगदीश चतुर्वेदी पृ. 79
18. केदारनाथ अग्रवाल – कहे केदार खरी खरी की कैफियत से पृ.10

हिंदी उपन्यासों में चित्रित नयी सदी की समस्याएँ'

बोनोड पांडुरंग पोषट्टी
पीएच.डी. (हिंदी)
हिंदी विभाग
उस्मानिया विश्वविद्यालय, हैदराबाद, तेलंगाना
मो.नं. 9000957758

नयी सदी के हिंदी उपन्यासों में सामाजिक समस्याएँ केंद्र में हैं । स्वतंत्रता के बाद देश में तीव्र गति से परिवर्तन हुआ । इस परिवर्तन ने वैयक्तिक और समूहगत स्तर पर सामाजिक और आर्थिक समस्याओं ने सर्वाधिक प्रभावित किया है, जिससे इनमें विघटन की स्थितियाँ भी पैदा हो गई हैं । स्वतंत्रता के 75 वर्ष बीत जाने के बावजूद आम आदमी की सामाजिक व आर्थिक स्थिति अत्यंत दयनीय है । आज 'अर्थ' जीवन की धुरी बना हुआ है । इस अभाव ने आम लोगों के जीवन को घोर निराशा में डाल दिया है । प्रत्येक युग का सामाजिक, राजनीतिक और सांस्कृतिक जीवन किसी सीमा तक आर्थिक बोध से प्रभावित रहा है । 'अर्थ' पर ही समाज का विकास निर्धारित होता है, यह एक सर्वमान्य सत्य है परंतु आज के युग में 'अर्थ' को जितना महत्व प्राप्त हुआ है, इससे पहले उतना कभी नहीं रहा। किसी भी व्यक्ति की सामाजिक प्रतिष्ठा का निर्णय आज उसकी आर्थिक स्थिति निश्चित होने लगी है । आज अर्थ व्यक्ति व समाज का मेरुदंड बन गया है । आज देश की अर्थ व्यवस्था पर पूँजीवादी शक्ति का शिकंजा कसा है, जिससे आम लोगों में अभावग्रस्तता, महंगाई, भ्रष्टाचार, रिश्वतखोरी, बेरोजगारी की समस्या बढ़ रही हैं । भौतिक आवश्यकताओं की पूर्ति के लिए अर्थ एक आवश्यक साधन बन गया है । औद्योगिक, वैज्ञानिक विकास और भौतिक सुख–सुविधाओं के प्रति बढ़ते आकर्षण ने अर्थ प्राप्ति ही व्यक्ति का चरम उद्देश्य बना दिया है । समाज में प्रतिष्ठा और मान–सम्मान की कसौटी मानव मूल्य न होकर भौतिक समृद्धि बन गयी है । इक्कीसवीं सदी के उपन्यासकारों ने अपने उपन्यासों में सामयिक समस्याओं को विस्तृत रूप से अंकित किया है ।

अलका सरावगी के 'कलि कथा : वाया बाईपास' उपन्यास में मारवाडी किशोर बाबू को केंद्र में रखकर गुजरात से कोलकत्ता तक फैले उत्तर भारतीय समाज की यथार्थ कथा इसमें संवेदनशीलता के चित्रित है । इस उपन्यास में वस्तु अनेक स्तर पर विद्यमान है, जिनमें मारवाड़ी समाज में स्त्रियों की घूटनभरी जीवन का है, जिसके केंद्र में किशोर बाबू की विधवा भाभी है । मारवाडी समाज में विधवा स्त्री को बिना किनारी के सफेद साड़ियाँ पहनने के सिवाय और कुछ पहनने का हक नहीं था। किशोर बाबू की भाभी जब यह सोचकर कि आज तो सब शिक्षित लोग आएंगे। बहुत प्रसन्न मन से वह साड़ी पहनकर शर्माती हुई कमरे से बाहर निकलती है, तभी किशोर बाबू अपनी परंपरागत सोच के कारण यह स्वीकार नहीं कर पाता है । वे समाज की दुहाई देते हुए विधवा स्त्री को उसी दयनीय अवस्था में धकेल देना चाहते हैं– "तुम्हारा दिमाग क्या अब एकदम ही खराब हो गया है भाभी। उम्र बढ़ने के साथ–साथ आदमी की अक्ल बढ़ती है पर मुझे लगता है यू. पी. वालों की अक्ल कम होने लगती है । यह क्या इतने चटक–मटक रंग की साड़ी पहनी है । क्या कहेंगे लोग देखकर। कुछ तो मर्यादा रखी होती समाज में।"[1] पितृसत्तात्मक समाज व्यवस्था में एक विधवा स्त्री का अच्छे कपड़े में पहनना मर्यादा खत्म हो जाती है । इस उपन्यास में रूढ़िवादी समाज की कथा ही नहीं है वरन् भारतीय पुरुषसत्तात्मक समाज की विसंगतियों का भी चित्रण है । सच क्या है यह किशोर बाबू जानते हैं । बदलते समय के कारण किशोर बाबू भी अपनी पत्नी में स्वतंत्र

व्यक्तित्व का विकास चाहते है परंतु उनकी सारी चेष्टाओं के बावजूद उनकी पत्नी के व्यक्तित्व का विकास नहीं होता है । इसका कारण वह स्वयं स्वीकार करती है– "इसलिए कि तुमने मेरी नकेल हमेशा अपने हाथों में कसकर पकड़े रखी। कभी अपने आप कोई निर्णय लेने नहीं दिया चाहे कितनी मामूली से मामूली बात क्यों न हो।"[2] किशोर बाबू हमेशा अपनी पत्नी को चाबी की गुड़िया की तरह चलाते रहते है । अपनी पत्नी की काबिलीयत पर कभी भी भरोसा नहीं करता है । मनुष्य की समस्या यही है कि वह किसी बने बनाए सिद्धांत पर पूरा जीवन नहीं चल पाता है । कई बार निजी स्वार्थों के कारण उसके सिद्धांत बदलते रहते हैं । यह मनुष्य की प्रवृत्ति है । शिक्षा, विज्ञान और सामाजिक व्यवस्था के बदलावों से स्त्री की स्थिति में परिवर्तन आया है । आधुनिक शिक्षा प्राप्त स्त्री अपने अधिकारों के प्रति सजग होने लगी है, जिससे वह प्राचीन रूढ़ियों और परंपराओं से मुक्त हो रही है । आर्थिक उदारीकरण और सूचना प्रसार ने साहित्य को पूर्ण रूप से परिवर्तित किया है । पश्चिमी संस्कृति के प्रभाव और नवीन सांस्कृतिक बोध के कारण नई दृष्टि का उदय हुआ है । पुरुष के वर्चस्व का खंडन और हाशिए पर धकेल दी गई स्त्री समाज में खोयी अपनी प्रतिष्ठा, सम्मान और अस्मिता का स्थान तलाश रही है ।

नासिरा शर्मा के 'कुइयाँजान' उपन्यास में इक्कीसवीं सदी की आर्थिक समस्या को दर्शाया है । प्राकृतिक आपदाओं जैसे पानी की कमी, बाढ़, तूफान, महामारी फैलना आदि समस्याओं से समाज में आर्थिक विषमता फैलती है । इससे धन–संपन्न वर्ग पैसे के बल पर अपना समय निकाल लेते हैं परंतु निम्न वर्ग का जीना मुश्किल होता है । प्राकृतिक आपदाओं के साथ कुछ धनी लोग निम्न वर्ग का शोषण करते हैं । परिणामस्वरूप निम्न वर्ग अकाल ग्रस्त बन जाता है । एक पानी को ही ले तो यह एक प्रकृति का उपहार है और इस पर सब का अधिकार है । इस स्थिति में निम्न वर्ग को पानी को खरीद कर पीना पड़ता है । इस सच्चाई को उजागर करता एक व्यक्ति पानी की समस्या पर बहस करते हुए कहता है कि– "आपकी परेशानी अपनी जगह, हमारी धरती पर किए गए अत्याचार अपनी जगह। आप लोग प्रबुद्ध है । परंतु मैं आपके सामने कह सकता हूँ कि गांव कस्बों में ठाकुर का कुआँ आज भी जीवित है । उन गांवों में जहाँ मीठे पानी से कुएँ लबालब भरे हैं, वहाँ दलितों को आज भी तीन रुपये घड़ा उसी गांव का आदमी बेचता है । आप इस समस्या का समाधान कैसे ढूढ़ूंगे?"[3] आज भी निम्न वर्ग की आर्थिक स्थिति अत्यंत दयनीय है । उन्हें उच्च और मध्य वर्ग के घरों और कार्यालयों में मजदूरी करनी पड़ती है । उच्च वर्ग के लोग उनसे मनचाहा काम करवाते हैं और निम्न वर्ग का शोषण करते हैं । काशीनाथ सिंह के उपन्यास 'रेहन पर रग्घू' में इक्कीसवीं सदी की बेरोजगारी की भयावह समस्या का मार्मिक चित्रण है । खेती श्रम आधारित है । किसान और उसका परिवार मिलकर खेती करते हैं । जो बड़े और साधन संपन्न किसान होते हैं, वे अपना काम खेतिहर मजदूरों से कराते हैं । ग्रामीण मजदूरों को तो पूरे साल का न काम मिलता है न ही उचित मजदूरी मिलती है । वे काम की तलाश में शहरों–महानगरों की ओर पलायन कर रहे हैं ।

उपभोक्तावाद को बढ़ाने के लिए पूंजीपति दूसरे बहुत बड़े वंचित वर्ग को उसकी पूरी सभ्यता को ही नष्ट करने लगे हैं । भारत के हर प्रदेश में आदिवासी जनजातियाँ निवास करती है । आज भी वे अपने प्राकृतिक जीवन से जुड़े पहलुओं के साथ जीवन जीते हैं किंतु आज उपभोक्ता व्यवस्था उन्हें अपने ही जल, जमीन और जंगल यानी अपने घर से बेदखल करने में लगी है । वे आज मजदूर बन गए हैं । पूंजीपति उन्हें लालच देकर उन्हें खदानों में खुदाई में लगाते हैं परंतु आगे चलकर यह उनके लिए जानलेवा साबित होता है । इस दयनीय स्थिति का मार्मिक अंकन रणेंद्र ने अपने उपन्यास 'ग्लोबल गांव के देवता' में किया है– "एक तरफ इन खानों में मजूरी दी तो दूसरी तरफ बर्बादी के सरंजाम भी खड़े किए। पिछले पच्चीस–तीस सालों में खान मालिकों ने जो बड़े–बड़े गड्ढे छोडे हैं, बरसात में इन गड्ढ़ों में पानी भर जाता है और मच्छर पलते हैं । सेरेबल मलेरिया यहाँ के लिए महामारी मुंडीकटवा से साल–दो–साल पर भेंट होती है किंतु इस जानमारू से तो हर रोज भेंट होगी।"[4] उपन्यासकार ने स्पष्ट किया है कि पूंजीपतियों और सत्ताधारियों ने वहाँ के स्थानीय लोगों को मृत्यु के मुंह में धकेला है । उपन्यासकार ने यहाँ स्पष्ट किया है कि विकास के नाम

पर स्थानीय लोगों पर होने वाले शोषण के विरोध में एकता दिखानी होगी, जिससे इस अन्याय के भंवर से बचकर अपने अस्तित्व बचाया जा सकता है । वरना इस विकास की आँधी में ये लोग गायब हो जाएंगे। इस उपन्यास में स्पष्ट रूप से इस शोषण के विरोध में प्रतिरोध का स्वर दृष्टिगत होता है । रणेंद्र ने प्रतिरोध के इस स्वर को अभिव्यक्त करते हुए लिखा है– "अवैध खनन के लिए पांच–दस असुरों को रोज फुसलाया जाता है । हर उपाय से उनकी जमीन हथियायी जाती है । बॉक्साइड निकाल–निकालकर मौत की खाइयाँ छोडी जा रही है । इन सवालों को जोड़िये, तभी असुरों के साथ उरांव, खेरवार, सदान सब आपकी लड़ाई में जुटेंगे।"[5] निजीकरण, उदारीकरण और उद्योगीकरण आदि के विनाशकारी विकास ने जनजातियों को हाशिए पर धकेल दिया है, जिससे उनकी अस्मिता पर खतरा मंडराने लगा है । विकास के नाम पर इनके विनाश की साजिश रची जाने लगी है । सल्वा जुडुम और ऑपरेशन ग्रीन हंट जैसे नामों की आड़ में विकास के नाम पर सरकार की सोच है, वह नकारात्मक है । यह कैसी उपभोक्तावादी संस्कृति है जो एक छोटे से वर्ग के लिए दूसरे बहुत बड़े तबके की बलि चढ़ायी जा रही है ।

आज देश के लिए कैसी विडंबना है कि भारत जैसे देश में जनता भूखे पेट सोती है, वहीं दूसरी ओर पश्चिमी देशों में एक्सपायरी डेट के नाम पर भोजन फेंक दिया जाता है । प्रदीप सौरभ ने अपने उपन्यास 'मुन्नी मोबाइल' में इस पर चोट की है । उपन्यास का पात्र जोगिंदर सिंह कहता है कि– "इंग्लैड में एक्सपाइरी का चक्कर जरदस्त है । हर स्टोर से हर दिन एक्सपायर हुई, खाने–पीने की चीज फेंकी जाती है । यही हमारा भोजन बनती है । एक्सपइरी खाना अंग्रेजों के लिए खराब होता होगा, लेकिन हमारा डायजेस्टिव सिस्टम इसके लिए पूरी तरह ठीक है । इंडिया में भी तो हम एक्सपाइरी चीजें ही खा रहे हैं ।"[6] वैश्वीकरण के दौर में प्रवेश करने के बाद विश्व में एक ओर तेजी से फैला है वह प्लास्टिक मनी। आज अपने साथ रुपये लेकर चलने के दिन चले गए । अब तो क्रेडिट कार्ड का जमाना है । इसके लिए एक ओर व्यक्ति के जीवन को सुविधायुक्त बनाया है तो दूसरी ओर बिना पैसे के मौजमस्ती की लत भी पैदा कर दी गई है । यदि आपके पास मौज–मस्ती करने के लिए पैसे नहीं है तो चिंता करने की आवश्यकता नहीं है । आप क्रेडिट कार्ड का प्रयोग कर अपनी इच्छाओं को पूरा कर सकते हैं । क्रेडिट कार्ट ने आज समय की परिभाषा बदल डाली है । महानगरीय बाजारवादी सोच ने संयम को दमन के रूप में प्रचारित किया है । आज हर कोई शून्य बाजार दर के मोहक मायाजाल में लोगों को लुभाना चाहा है । वह आज के व्यक्ति को उपभोग के लिए उकसाता है । प्रदीप सौरभ ने महानगरीय जीवन के यथार्थ रूप स्पष्ट करते हुए लिखा है– "एक अमेरिकन के पास औसतन पंद्रह क्रेडिट काड्र्स होते हैं । उनके या किसी बुजुर्ग की मौत पर विरासत में परिवार वालों को क्रेडिट्स काड्र्स और दूसरे लोग के बिल मिलते हैं । भारत में ऐसी स्थिति में परिवार वालों को मकान सोना–चाँदी और भी बहुत कुछ मिलता है । भारत में ऐसा दर्शन भी है कि उधार लेकर भी पीओ ।"[7] लेखक अपने उपन्यास में अमेरिका और भारतीय विचारधारा की तुलना करते है । भारत को प्राचीन काल से संयम पूर्ण जीवन जीने की आदत नहीं है । भोगवादी संस्कृति का असर अभी दिखाई देने लगा है । बाजारवाद ने शहरों को ही अपने मकड़जाल में फंसा है । यहाँ का ग्रामीण समाज आज भी जरूरत की वस्तुओं को ही प्राथमिकता दे रहा है । वहाँ तक वैश्विक आर्थिक विचारधारा का प्रभाव पड़ा है । उसके द्वारा खेतों में लगाई जाने वाली फसल का मूल्य अब अंतर्राष्ट्रीय बाजार तय करता है । इक्कीसवीं सदी के हिंदी उपन्यासकारों ने बहुत सूक्ष्म, गहराई और विस्तार में जाकर महानगरीय जीवन का अंकन अभिव्यक्त किया है । विगत बीस–पच्चीस सालों में वैश्विक आर्थिक चेतना विविध रूपों में फैली हुई है । देखा जाए तो भारत के लिए यह एक सांस्कृतिक संक्रमण का काल है । उपन्यासकारों ने इस महानगरीय प्रभाव का आकलन जिस रूप में किया है, वह अपने आप में बेहद महत्वपूर्ण है ।

आज देश की अर्थ व्यवस्था पर पूँजीवादियों का शिकंजा कसा हुआ है, जिसमें आम जनता अभावग्रस्त स्थिति में महंगाई और बेरोजगारी का शिकार है । भौतिक आवश्यकताओं की पूर्ति के लिए अर्थ एक जरूरतमंद साधन बन गया है । लोगों का भौतिक

सुख–सुविधाओं के प्रति आकर्षण बढ़ता जा रहा है । अर्थ प्राप्ति ही व्यक्ति का चरम लक्ष्य बना है । समाज में प्रतिष्ठा, मान–सम्मान की कसौटी मानव मूल्य न रहकर भौतिक समृद्धि बन गयी है । इक्कीसवीं सदी के उपन्यासकारों ने विभिन्न समस्याओं को विस्तार से अभिव्यक्त किया है ।

संदर्भ :

1. अलका सरावगी – कलिकथा वाया बाईपास, पृ.सं. 61
2. अलका सरावगी – कलिकथा वाया बाईपास, पृ.सं. 159
3. नासिरा शर्मा – कुइयांजान, पृ.सं. 105
4. रणेंद्र – ग्लोबल गांव के देवता, पृ.सं. 13
5. रणेंद्र – ग्लोबल गांव के देवता, पृ.सं. 48
6. प्रदीप सौरभ – मुन्नी मोबाइल, 102
7. प्रदीप सौरभ – मुन्नी मोबाईल, पृ.सं. 104

हिंदी साहित्य में आधुनिक विमर्श की उपादेयता

डॉ. शेख़ बेनज़ीर
सहायक आचार्य,
हिंदी विभाग, एस.वी.सी.आर शासकीय महाविद्यालय, पलमनेर,
जिला – चित्तूर, आन्ध्रप्रदेश 517408

सामाजिक परिवेश की समीक्षा में हर बार यह स्पष्ट होता है कि सामाजिक घटकों में स्थिरत्व नहीं होता । वे समय और स्थिति के अनुरूप बदलते रहते हैं । समाज में विद्यमान मूल प्रवृत्तियों में सांगोपांग परिवर्तन होते हैं । साहित्य सामाजिक संवेदनाओं का बिम्ब है । फलतः साहित्य भी सृजन से, पुनः सर्जन की ओर उन्मुख होता है । पूर्ववर्ती साहित्य कितना ही श्रेष्ठतर क्यों ना हो, उसे ऐसे दौर से गुजरना पडता है, जहाँ उसे बोझ एवं नीरस समझा जाता है । इसी प्रक्रिया से होकर हिंदी साहित्य अपने अधुनातन स्वरूप में प्रदीयमान है । हिंदी साहित्य में 19 वीं शती के आरंभ से ही प्राचीन परिपाटी के प्रति उदासीनता दिखाई देने लगी । परंपरागत छंदों, भक्ति, प्रेम, श्रृंगार और प्रशस्तियों के प्रति विद्रोह का स्वर तीव्रतर होने लगा । यह किसी एक विधा या विचारके प्रति विद्रोह ना था । यह तो समस्त साहित्य में नवीनता लाने के लिये चलने वाला आंदोलन था । नवीन विचारों की प्रेरणा से उत्पन्न वह भावधारा थी, जो आधुनिक साहित्य के नाम से अभिहित हुई । इसमें साहित्यकार आत्मनिष्ठता से समिष्टि, कल्पना से यथार्थ और अलौकिक से लौकिक भूमि की ओर अग्रसर होते गए । देश के सामाजिक–राजनीतिक आंदोलनों ने ना सिर्फ भारतीय समाज का प्रक्षालन किया, बल्कि वे साहित्य में छाई अराजकता को मिटाने में भी सफल हुए । जिसका परिणाम ही आधुनिक काल का आविर्भाव है । भारतेंदु, महावीर प्रसाद, रामचंद्र शुक्ल, प्रेमचंद, प्रसाद, पन्त, निराला, दिनकर जैसे साहित्यकारों की नैरंतर्य साहित्य सेवा से बीसवीं सदी से आधुनिक साहित्य का आविर्भाव हुआ ।

संसार में जो कुछ घटित होता है उसकी अभिव्यक्ति साहित्य में होती है । साहित्यकार का हृदय समाज की संवेदनाओं से स्पंदित होता है । साहित्य हमेशा से समाज को दिशा देने एवं लोकमंगल की भावना को साकार करने के लिए कृत संकल्पित रहा है । साहित्य सर्जनशील प्रक्रिया है जो बेहतर समाज के निर्माण के लिए प्रतिबद्ध है । वर्तमान समय में समाज के सभी वंचित, उपेक्षित, शोषित समूहों ने अपने अधिकारों, अस्मिता एवं अस्तित्व के लिए निर्णायक लड़ाई छेड़ दी है । यह लड़ाई किसी के विरुद्ध नहीं अपितु मानवता के पक्ष में लड़ी जा रही हैं । इसी से 21 वीं सदी के साहित्य में अनेक विमर्शों की प्रतिष्ठा हुई है । विविध विमर्शों के माध्यम से पीड़ित, वंचित वर्ग की दबी आवाज को बल मिला, उन्हें हाशिए से मुख्य धारा में आने में मदद मिली, उनकी समस्याओं पर समाज की दृष्टि पड़ी और उस वर्ग के उत्थान को बल मिला ।

इस पृष्ठ भूमि को लेकर चलने वाले साहित्यकारों ने आधुनिकता के प्रति आस्था दिखाई । अब वे साहित्य अंधानुकरण नहीं करते । क्रांतिकारी होकर आधुनिकता के प्रति जागरूक होना साहित्यकार का सहज लक्षण होता है । इस कारण साहित्य में ऐसे विषय सामाविष्ट होते गए, जिसका विमर्श आवश्यक हो गया । समसामयिक मुद्दे अब साहित्य में समीक्षा और विचार विमर्श के लिए स्वीकृत हो गए । नारी चेतना, नारी –सशक्तिकरण, ग्राम चेतना, कृषक संघर्ष, आतंकवाद, बाल शोषण, दांपत्य जीवन, यौन विकृतियाँ, दलित चेतना, देश विभाजन की त्रासदी, मूल्य विघटन, शहरीकरण आदि पर विमर्श होने लगे । सामाजिक यथार्थ, लघुमानव, जीवन संघर्ष, दलित, प्रताडित, पीडित आदि साहित्य के आलोच्य विषय बन गए । फलतः आधुनिक विमर्श के नए–

नए आयाम उभरते गए । इन विमर्शों से साहित्य को बहुत कुछ मिला । आधुनिक साहित्य के विमर्शों से साहित्य का रूप कुछ इस प्रकार है ।

कोई भी साहित्यकार अपनी रचना में अपने वर्ण्य विषय को कलात्मक ढंग से प्रस्तुत करना मात्र अपना धर्म नहीं समझता । वह अपनी रचना में समाजिक जीवन की समीक्षा करता है । समाज के लिए आदर्शों , विकासशील प्रतिमानों, मूल्यों को निर्देशित करता है । जिसे सजग पाठक स्वीकार भी करता है । सहित्यकार पाठक को जीवन की कटु परिस्थितियों से अवगत कराता है ।" साहित्य में यथार्थ का ही नहीं – मानव आदर्शों, मानव विश्वासों और परंपरागत धारणाओं का निरूपण भी करता है ।"[1] आधुनिक विमर्शों में इन्हीं निरूपणों को महत्व मिलने लगा । साहित्यकारों ने बदले हुए समाज को नवीन जीवन दृष्टिप्रदान की । निराशा और कुंठाको दूर कर नवीन ऊर्जा का संचार करना इनका लक्ष्य था । साहित्यकार ने साहित्य को मात्र मनोरंजन का साधन मानने से इंकार कर दिया । वे साहित्य को विशिष्ट उद्देश्य का प्रतिपादक मानने लगे । अपने नायक एवं पात्रों को आदर्शों एवं मूल्यों का प्रतिनिधि मानने लगे । जिससे साहित्य समिष्टि की ओर अग्रसर होता गया । साहित्यकार जीवन की व्याख्या करने लगा । नए मानव को युगीन जीवन दृष्टिकोण प्रदान करना ज़रूरी समझा । साहित्यकार के पास वह शक्ति होती है जिससे वह मानव मन के गहन स्तरों को पहचान सकता है । इसे पहचानकर साहित्यकार पात्रों के माध्यम से जीवन दर्शन की व्याख्या करता है । आधुनिक विमर्शों में इन प्रवृत्तियों को देखा जा सकता है ।

आधुनिक काल के आरंभ से ही भारतीय जनता जान चुकी थी वे अपनी संस्कृति और अस्तित्व को भुला रहे हैं । अब जरूरी था उसे बचाए रखना । कई दशकों से परतंत्रता की त्रासदी को झेल रहे थे । पर अब प्रश्न स्वदेश एवं स्व–अस्तित्व का था । साहित्यकारों ने भी इसकी जिम्मेदारी ली । साहित्यकारों ने भी अंधविश्वासों एवं कुविचारों को जड से मिटाने की गुहार लगाई । साहित्य के माध्यम से चलने वाले सांस्कृतिक चेतना के विस्तृत प्रभाव से भारतीयता की पुनः पहचान होने लगी । विदेशी संस्कृति के अंधे मोह की तीव्र भर्त्सना की जाने लगी । जो आधुनिक विमर्शों में दिखाई देने लगी ।" धार्मिक–सांस्कृतिक आंदोलन ने जिस प्रकार पुराने को नये से और नये को पुराने से सम्बद्ध किया, उसी प्रकार कला और साहित्य ने भी किया ।"[2] आधुनिक युग के साहित्य ने आधुनिक विचारों का समर्थन किया, परंतु परंपरगत स्वस्थ भारतीय मूल्यों एवं सद्विचारों का समर्थन किया । प्राचीन संस्कृति के उदात्त एवं विकासशील आदर्शों को नवीन रूप में प्रस्तुत किया । जिससे साहित्य के माध्यम से नवीन समन्वित संस्कृति की स्थापना हुई । साहित्यिक विधाओं में प्राचीन भारतीय संस्कृति को नए रूप में प्रस्तुत करने की प्रथा आरंभ हो गई । साहित्य को नया आयाम प्राप्त हुआ ।

आधुनिक विमर्शों की भरमार से साहित्य की परिधि में भी पर्याप्त विकास हुआ । अब साहित्यकार कल्पना से परे प्रत्यक्ष जन जीवन को ही साहित्य का मुख्य प्रतिपाद्य मानने लगे थे । प्रामाणिक अनुभूति के प्रति प्रतिबद्ध हो चुके थे । फलतः साहित्य के प्राचीन प्रतिमानों को सर्वथा निरर्थक साबित करने लगे । साहित्य में पंरपरागत प्रतीकों एवं उपमानों का परित्याग होने लगा । नवीन विचारों एवं जीवन सत्यों को उद्घाटित करने के लिए सरलतम शैलियों को अपनाने में ही साहित्यकार ने रुचि दिखाई । पद्य के क्षेत्र में मुक्त छंदों को प्रधानता मिलने लगी तो गद्य में बोलचाल की सरल एवं सपाट बयानी को । गद्य में अनेक नई विधाओं का समावेश हुआ जैसे डायरी, पत्रलेखन, कथा, नाट्य, निबंध, आलोचना, जैसे पूर्ववर्ती गद्य विधाओं के रूप गठन में परिवर्तन भी हुआ ।" अन्य विधाओं में भी कथ्य की विविधता और शैलीगत नूतन प्रयोगों की दिशा में इस युग के साहित्यकार में जो जागरूकता लक्षित होती है, वह पूर्ववर्ती लेखकों में नहीं मिलती ।"[3] यह आधुनिक विमर्शों की चेतना का परिणाम है ।

वैचारिक धरातल की दृष्टि से आधुनिक विमर्शों को पहचानने की कोशिश की जाए तो पता चलेगा कि विमर्शों के माध्यम से साहित्य में अधुनातन सिद्धांतों एवं दर्शनों का आगमन हुआ । साहित्यकारों ने विविध विषयों को रचना का प्रतिपाद्य चुना तो साहित्य

के मूल्य, सौंदर्य बोध, प्रवृत्तियाँ आदि नवीन रूप लेने लगे । साहित्य में रूढ़ हो चुकी धारणाएँ शिथिल होने लगी । कार्ल मार्क्स, फ्रायड के सिद्धांतों के प्रभाव से स्वतंत्रता पूर्व ही वैचारिक जड़ता को धक्का लगा था, जो कि स्वतंत्रता के बाद और अधिक हुआ । भारतीय समाज एवं राजनीति के लिए अभिशाप बन चुके घटकों को मिटाने की प्रक्रिया साहित्य में आरंभ हुई । यथार्थ, अति यथार्थ, बौद्धिकता, भौतिकता आदि विचारों के ढाँचे में पात्र ढलने लगे । ज्ञान–विज्ञान के विकास के फलस्वरूप साहित्यकारों की दृष्टि में भी युगांतरकारी परिवर्तन हुआ । "विज्ञान के द्वारा आध्यात्म और आध्यात्मिकता जैसी चीजों का पूरी तरह निषेध किया गया, क्योंकि उसके पीछे किसी तरह की इंद्रिय गम्य – स्थूल कारण कार्य की श्रृंखला उसे नहीं मिली परिणाम यह हुआ कि वैज्ञानिक उन्नति के अनुपात में ही दिनोंदिन मानव के प्रति ही संपूर्ण निष्ठा केंद्रित होती गई । मानवेतर जो भी था, मूल्यहीन होता चला गय ।"[4] नए विमर्शों ने साहित्य जगत में विचारों का सैलाब ला दिया । जिससे मानव समाज के जीवन में बदलते परिवेश के अनुसार आते उनके मानसिक विकास का परिचय भी मिलने लगा ।

अपनी उपादेयता के बल पर आधुनिक विमर्श अपनी महत्वपूर्ण भूमिका निभाते हुए सक्रिय है । नवोन्मेषी विचारों से प्रभावित होकर साहित्य ने जो रूप लिया, वह निस्संदेह अनिवार्य था । आधुनिक विचार यों ही नहीं पैदा होते । वे समय और परिवेश के गर्भ में वर्षों की प्रतीक्षा का फल होते हैं । जब भी समाज और साहित्य वैचारिक कुंठा से ग्रस्त होते हैं, आधुनिक विचारों की आवश्यक होती है । सजग साहित्यकार एवं नागरिकों की पहल से आधुनिक विचार अवश्य ही प्रस्फुटित हो जाते हैं । आधुनिक युग अपने पूर्ववर्ती युगों से नितांत भिन्न है । नए विमर्शों से इस युग में भौतिकता एवं बौद्धिकता का सामावेश हुआ । यथार्थ और उपियोगिता का प्रबल समर्थन हुआ । आधुनिकता का एक अर्थ ही व्यक्ति एवं समाज को विकासशील दर्शन प्रदान करना है । इस दृष्टि से हिंदी साहित्य का आधुनिक विमर्श सफल है । आधुनिक विमर्श की उपादेयता यथोचित है, जिसने साहित्य का नवीनीकरण कर समाज में नवजीवन का अंकुर प्रस्फुटित किया ।

संदर्भ ग्रंथ सूची

1) डॉ. नगेंद्र– साहित्य का समाजशास्त्र – पृ.सं.37
2) डॉ. बच्चन सिंह – हिंदी साहित्य का दूसरा इतिहास – पृ. सं. 302
3) सं. डॉ. नगेंद्र– हिंदी साहित्य का इतिहास – पृ. सं. 711
4) त्रिभुवन सिंह– आधुनिक साहित्यिक निबंध – पृ.सं. 25

हे अधोहस्ताक्षरी

डॉ. नीरज कुमार द्विवेदी
असिस्टेंट प्रोफेसर,
हिंदी विभाग, दयानंद वैदिक कॉलेज, उरई (जालौन)
सम्पर्क 7905531417,
E-mail - neerajdwivedi71@gmail.com

सच बताना
यह तुम्हारी योग्यता है
या कि कुंठा
तुम्हारा कोई भी अधीनस्थ
जब तुम से आगे बढ़ने का
आभास देता है तो
तुम लग जाते हो
उसके मार्ग में व्यवधान खड़े करने के
और इन व्यवधानों को कायदे–कानूनों का
नैतिकता का
सामाजिक मर्यादा का
जामा पहनाकर
उसके हितेषी बनने का पूरा प्रयास
करते हो।
और मेरी आंखें
तब फटी रह जाती हैं
जब मैं सुनता हूँ आपकी तारीफ
उस निरीह की जुबानी, जो
अपनी असफलताओं के एवरेस्ट से
खड़े होकर नि:श्वास करता है
गाता है तुम्हारे गुण
चारण–भाटों की तरह
नहीं दिखती किसी को
उसके अंदर की उमड़ती–घुमड़ती
काली–पीली–सफेद धुआंती रेखाएं

नहीं दिखते
सूखे आंसुओं के दाग–धब्बे
पर क्या फर्क पड़ता है इन सबसे ।

तकरार न कर

समृद्धि संजय सुर्वे
चिंचवड, पुणे 33
7420828184

हो डगर ऊँची–नीची
ना हो कोई हमसफर
अकेला हो सफर तो
रास्ता बदलकर चल
तकरार न कर
चलता चल.....

मायूस न हो देखकर
डूबता सूरज क्षितिज पर
आनेवाली सुबह पर
ऐतबार करता चल
तकरार न कर
चलता चल.....

है ताकत तेरी बाजुओं में
लडने की शक्ति हो मन में
अपनी ही हार पर बावरे
विजय प्राप्त करता चल
तकरार न कर
चलता चल.....

जो भाग्य में है लिखा
किसी और ने ना देखा
अपने करूणामय पर
विश्वास तू रखता चल
तकरार न कर
चलता चल.....

तकरार न कर
चलता चल.....

जीवन की विडंबना

राजेंद्र यादव 'फरीदाबादी'

जीवन की विडंबना क्या होगी?
जब जीवन ही एक विडंबना है ।
अलंकारों की श्रृंगारिकता क्या होगी?
जब अलंकार ही एक श्रृंगार है ।

जीवन की विषमता क्या होंगी?
जब जीवन ही एक विषमता है ।
जीवन की विडंबना क्या होगी?
जब जीवन ही एक विडंबना है

जीवन की विषम और सम परिस्तिथियों में क्या कोई स्थिर रहता है?
जीवन की हालों से चंचल हो जीवन बहता रहता है ।
विषम स्थितियों में भी सदैव विषम ना रहता है ।
फिर क्यों मानव तलवों को चाटा करते हैँ।
लघु भय से दीर्घ संकट का निःस्वास लिया करते हैं ।
जीवन की विषमता क्या होंगी?
जब जीवन ही एक विषमता है ।
जीवन की विडंबना क्या होगी?
जब जीवन ही एक विडंबना है ।

जीवन से परिचित होकर भी,
अपरिचित–सा व्यवहार करे।
सुबह साम और आठो याम,
राम रहीम का नाम जपे।
मन्दिर मस्जिद जाकर भी, चिंता भय में रहता है ।
जीवन की चिंता क्या होगी?
जब जीवन की भी चिंता है ।
जीवन की विडंबना क्या होगी?
जब जीवन ही एक विडंबना है ।

एक ख़्वाब किनारों पर

अंकिता राय

इलाहाबाद विश्वविद्यालय

Mobile no 9839805235

Email: iamankitacool235@gmail.com

चांद की चमचमाती चांदनी लिए
ये लहरों की बस्ती, है हवा कुछ हसीं और खुशबुओं में मस्ती,
जिंदगी की कस्ती यू गोते खाए
जब भी मन इस कल कल स्वर में समाए,
ये हसीं चांदनी इन लहरों पर ऐसे हर्षाए
जैसे बच्चे को मां अपनी आंचल में सुलाए,
सुकून से बैठे मैं और मेरे ख्वाब इन किनारों पर
ये समंदर की नगरी मुझे खूब भाए,
पर डर लगता है, इन लहरों से प्यार ना हो जाए
ये आवाज दे मुझे और मेरे कदम रुक न पाए,
समंदर की गोद में जब भी तू समाए
किनारों की तरह तुझे मेरी भी याद आए,
तुझे देख कर यू मन आशाओं से भर जाए
जब तू फिर हिलोरे लेकर किनारों पर आए,
बैठी रहूँ कुछ उम्मीद लेकर इन किनारों पर
तू फिर आए तेरी मस्तियों से मुझे भिगाए,
ये तेरा मेरा रिश्ता कुछ यू गहरा हो जाए
मैं तेरी याद बन जाऊ और तू मेरे दिल में समाए।

UGC CARE LISTED
ISSN No.2394-5990

संशोधक

• वर्ष : ९२ • मार्च २०२४ • पुरवणी विशेषांक ५२

प्रकाशक : इतिहासाचार्य वि.का.राजवाडे संशोधन मंडळ, धुळे

हिन्दी उपन्यासों में किन्नर जीवन की त्रासदी
(किन्नर केंद्रित उपन्यासों के आलोक में)

1) डॉ. शेख़ बेनज़ीर
प्राध्यापिका, हिंदी विभाग,
एस.वी.सी.आर शासकीय महाविद्यालय,
पलमनेर, जिला - चित्तूर, आन्ध्रप्रदेश-517408,
फोन: 7382786328

2) डॉ. एस. सूर्यावती
प्राध्यापिका, हिंदी विभाग,
शासकीय महाविद्यालय, चोडवरम,
जिला - अनकापल्ली, आन्ध्रप्रदेश-531036
फोन: 9440417304

शोध प्रविधि:

इस शोध पत्र में प्राथमिक एवं द्वितीय स्रोतों के आधार पर अध्ययन किया गया।

शोध सार :

किन्नर साहित्य ने किन्नरों के प्रति जो यथार्थ का चित्रण किया है उन्हें किन्नरों का वास्तविक दस्तावेज़ कहा जा सकता है। इन दस्तावेजों के माध्यम से सही मायने में किन्नरों की स्थितियों का परिचय प्राप्त किया जा सकता है। आज के उपन्यास, कहानी और आत्मकथाओं में किन्नर जीवन के मार्मिक पहलुओं का सहजता से बयान किया गया है। इनके जीवन में दुःख और पीड़ा समाज का दुत्कार के अलावा अन्य कुछ नहीं है। आज समाज में, राजनीति में, संविधान में, अदालत में और साहित्य में भी इनकी समस्याओं की चर्चा एवं समाधान की कोशिश हो रही है। अब इन्हें राजनीति में और चुनाव में भाग लेने का अधिकार मिला है। इनकी यातनाओं पर चर्चा होती रहती है। साहित्य में तृतीय लिंगी विमर्श व किन्नर विमर्श के नाम पर महत्वपूर्ण चिंतन हो रहा हैं। हिंदी साहित्य में किन्नर विमर्श अपनी अस्मिता की पहचान के लिए कार्यरत है। समाज की नीच मानसिकता ही किन्नर समुदाय को शापित जीवन जीने के लिए विवश होना पड़ता है। आजकल किन्नरों की समस्या, उनकी पीड़ा, उनकी संवेदना आदि को कथ्य बनाकर काफी उपन्यास और कहानियों का सृजन किया जा रहा है।

बीज शब्द: दुःख, पीड़ा, गंभीरता, कोशिश, जीवन

मूल शोध आलेख :

हिन्दी साहित्य जगत में पहले किन्नरों को केंद्र में रखकर साहित्य बहुत ही कम मात्रा में लिखा गया था। राहुल सांकृत्यायन, रांगेय राघव, पांडेय बेचन शर्मा 'उग्र' जैसे रचनाकारों को छोड़कर आधुनिक काल में किन्नर पात्रीय रचना बहुत कम हुई है। इक्कीसवीं शती के साहित्यकार किन्नरों को लेकर गंभीरता से रचनाएँ लिख रहे हैं। स्त्री, मुस्लिम, दलित, आदिवासी, दिव्यांग आदि विमर्शों की भाँति आज किन्नर विमर्श भी समाज के सामने आ रहा है और साहित्यकार निरंतर इस पर लेखनी चला रहे हैं। नीरजा माधव का 'यमदीप', प्रदीप सौरभ की 'तीसरी ताली', महेन्द्र भीष्म की 'किन्नर कथा', 'मैं पायल', निर्मला भुराडिया का 'गुलाम मंडी', चित्रा मुद्गल का 'पोस्ट बॉक्स नं- 203 नाला सोपारा' आदि किन्नरों की ज्वलंत समस्या को लेकर सामने आये हैं। इन उपन्यासों की कथावस्तु किन्नर समुदाय की है, जो उनकी पीड़ा, व्यथा, एवं भयानक त्रासदी की स्थिति को चित्रित करते हैं। किन्नर के रूप में जन्म लेना एक बहुत बड़ी त्रासदी है। ईश्वर ने इन्हें किन्नर जीवन देकर प्रताड़ित किया है। यह भगवान के द्वारा किया गया अन्याय ही है। जननांग दोष होने के कारण परिवार और समाज इनका जीना मुश्किल कर देते है- ''तू हिजड़ा है हिजड़ा हमारा तेरे से कोई नाता नही, तू हमारा कुछ नहीं लगता, भाग जा यहाँ से क्यों हमारी नाक कटाने पर लगा है। हिजड़ा कही का।''[1]

हिंदी उपन्यास के क्षेत्र में किन्नर विमर्श पर लिखा गया पहला उपन्यास नीरजा माधव द्वारा लिखित 'यमदीप' है। यह उपन्यास किन्नर पर आधारित हिंदी साहित्य जगत में मील के पत्थर के समान है। उसके बाद प्रदीप सौरभ का 'तीसरी ताली', महेंद्र भीष्म का 'किन्नर कथा', निर्मला भुराडिया का 'गुलाम मंडी', चित्रा मुद्गल जी का 'पोस्ट बॉक्स नंबर 203 नाला सोपारा', डॉ. मोनिका देवी का 'अस्तित्व की तलाश में सिमरन' आदि महत्वपूर्ण उपन्यास लिखे गए हैं। मेहरुन्निसा परवेज कृत 'कोरज़ा' उपन्यास में भी मोहित के माध्यम से किन्नर विमर्श पर प्रकाश डाला गया। और इस क्षेत्र में कई अन्य उपन्यास भी प्रकाशित हो रहे हैं।

नीरजा माधव जी एक ऐसी उपन्यासकार हैं जिनका ध्यान समाज में उपेक्षित वर्ग के ऊपर गया है और उन्होंने इस समुदाय

को अपने लेखन का विषय बनाया। उन्होंने इन सबके बीच में जाकर उनके रहने के तौर तरीके, उनके स्वभाव, उनका खानपान, और उनके जीवन में दुख और कष्टों को बड़ी ही निकटता से देखा है। उपन्यासकार ने इन्हें सभ्य समाज से जोड़ने के लिए ही अपनी कलम उठाई और किन्नरों के संपूर्ण जीवन को एक दिशा देते हुए 'यमदीप' नाम के इस उपन्यास को प्रस्तुत किया है। यमदीप उपन्यास में गली में एक पागल स्त्री प्रसव पीड़ा से तड़प रही है और कुछ मनचले पुरुष तथा स्त्रियाँ चुपचाप तमाशा बनाकर उसे देख रहे हैं परन्तु उस पागल स्त्री के पास कोई नहीं जाता। तब एक किन्नर (नाजबीबी) अपने मानव धर्म को निभाते हुए कहती है- "अब कोई पूछनहार नहीं, इसका, तो क्या हम भी छोड़ जायेंगे ? अरे हम हिजड़े हैं, हिजड़े इंसान हैं क्या जो मुंह फेर लें ? जा, जल्दी कर।"[2]

उस नवजात बच्ची को सभी पालने से मना कर देते हैं तो नाजबीबी यह कहकर उसे अपने साथ ले जाती है कि इसका इस दुनिया में कोई नहीं यदि वह भी छोड़ देगी तो यह मर जाएगी। सभी बच्ची को देखकर खुश हो जाते हैं। अब उस बच्ची के नामकरण को लेकर विवाद चलता है कि इसका क्या नाम रखें ? किस धर्म की है ? तभी किन्नरों के महताब गुरु कहते हैं कि "अरे, दुर् रे धरम । रात-बिरात एक पागल के साथ मुंह काला किया, धरम की बात पर.... थू है ऐसे धरम पर और ऐसे धरमवालों पर! मैं इसका नाम सोना रखती हूँ और इसका नाम अब से सोना ही रहेगा। सारे धरम में सोना सोना ही रहता है कीमती चमकदार, सभी धरम के लोग पहनते हैं चाहे हिंदू हो या फिर मुसलमान। रही इस बच्ची के धरम कि बात तो नाजबीबी पैदाइशी हिंदू है और इसे पालने के कारण सोना का भी धरम हिंदू। चल, अब सारा झगडा खतम।"[3]

भगवंत अनमोल द्वारा 2017 में रचित उपन्यास 'जिन्दगी 50-50' किन्नरों के साथ किए जा रहे दुर्व्यवहार का चित्रण करने के साथ उसका समाधान भी निकाला है। यह दो पीढ़ियों में विस्तृत है। अनमोल के घर जब उसका पुत्र सूर्या किन्नर के रूप में जन्म लेता है तब अनमोल प्रण लेता है कि वह सूर्या के साथ वह सब कुछ नहीं होने देगा जो उसके भाई हर्षा के साथ हुआ। यहाँ से हर्षा उर्फ हर्षिता का परिचय पाठकों के सामने आता है। हर्षा के जन्म से सबसे ज्यादा दुखी उसके बाबू जी होते हैं। परिवार और समाज ने मिलकर हर्ष को प्रताड़ित किया। पिता की जान बचाने के लिए देह का व्यापार भी करना पड़ता है। स्वास्थ्य से खिलवाड़ भी हो जाता है। एड्स की सौगात लिए अंतिम अवस्था में वह समाज से प्रश्न पूछती है कि "किन्नर होना इतना बड़ा अभिशाप क्यों है ? बस मेरा अधूरापन ही तो न ? कैसे- कैसे पल आये! इस शरीर ने सब भुगता, सब सहा। जिस शरीर का लोग मजाक उड़ाते हैं, उसे ही रात को मन बहलाने का जरिया बना लेते हैं। मेरे शारीरिक अस्तित्व में दुहरापन है लेकिन उस तथाकथित समाज के व्यक्तित्व के दुहरेपन पर मैं थूकती हूँ।"[4]

डॉ. अनुसूया त्यागी का उपन्यास 'मैं भी औरत हूँ' (2005) विशेष रूप से किन्नर केंद्रित उपन्यास है। इसमें दो जुड़वे बहनें रोशनी और मंजुला की कथा है। इनकी शारीरिक संरचना से अनभिज्ञ इनके परिवार को लम्बे समय तक एहसास ही नहीं होता कि ये दोनों सामान्य लड़की नहीं, बल्कि किन्नर हैं। "रोशनी काँप उठी तब क्या उस लड़के ने जो कहा था वह सच है, वह लड़की नहीं है, वह औरत नहीं है, तब फिर मैं क्या हूँ.. क्यों इसीलिए मुझे माहवारी प्रारम्भ नहीं हुई? क्या मेरी शादी नहीं हो पायेगी? क्या मैं कभी माँ नहीं बन पाऊँगी? ओह क्या मैं नपुंसक हूँ पर फिर मेरी ऊपरी बनावट स्तन आदि तो ठीक हैं, पर अन्दर कुछ ठीक नहीं है, यह सब मुझे कौन बताएगा?"[5]

'मैं पायल' (2016) महेन्द्र भीष्म द्वारा आत्मकथात्मक शैली में लिखा उपन्यास पायल के जन्म से ही शुरू होता है। महानगर के नज़दीकी कस्बे में निम्न मध्य वर्ग में एक गुस्सैल, शराबी व क्रूर पिता के घर में चौथी लड़की के रूप में पायल का जन्म होता है। जिसके बाद शुरू होता है प्रताड़ना का एक लम्बा दौर जिसमें पिता द्वारा पायल को मारने पीटने से लेकर फाँसी देने का प्रयास भी शामिल था। अपने हिजड़ा होने का बोध भी पायल को अपने पिता द्वारा ही हुआ था- "हिजड़ा यह शब्द सबसे पहले मैंने उन्हीं के मुख से सुना था, पर तब मैं इस शब्द के मायने से बिल्कुल अनभिज्ञ थी.. गाली के रूप में प्रयोग में लाया जाने वाला कोई शब्द होगा।"[6]

चित्रा मुद्गल के उपन्यास ह्नपोस्ट बॉक्स नंबर 203 नाला सोपाराफ (2016) में एक माँ अपनी संतान को किन्नरों से दूर रखने की भरसक कोशिश करती दिखाई देती है और मजबूरी में विनोद को बिन्नी बनना पड़ता है। वह अपनी माँ के सपने को साकार बनाने की कोशिश करता है और अधूरेपन तथा कशमकश के बावजूद यह संकल्प लेता है कि ज़िंदगी में वह कुछ बनेगा और अपनी बिरादरी के लोगों को समाज में इज्जत दिलाने का प्रयास करेगा। विनोद यह मानता है कि शिक्षा ही एक ऐसा साधन है जो समाज में उन जैसों को बराबरी का दर्जा दिला सकता है तथा उन्हें प्रगति के मार्ग पर ले जा सकता है। वह कहता है - "पढाई ही हमारी मुक्ति का रास्ता है। कोई रास्ता ही नहीं छोड़ा गया है हमारे लिए।"[7]

बिन्नी की माँ का यह कथन - "समाज को ऐसे लोगों की आदत नहीं है और वे आदत डालना भी नहीं चाहते पर मुझे विश्वास है, हमेशा ऐसी स्थिति नहीं रहने वाली। वक्त बदलेगा। वक्त के साथ नजरिया बदलेगा। हर व्यक्ति का अपना दृष्टिकोण है, अपना एक नजरिया है। चीजों के प्रति, शारीरिक और मानसिक हर प्रकार से कम सक्षम नहीं हैं, तो फिर सिर्फ जननांग दोष की इतनी नारकीय सजा भुगतने के लिए वे क्यों इतने विवश हैं।"[3]

निष्कर्ष :

आजकल किन्नरों की समस्या, उनकी पीड़ा, उनकी संवेदना आदि को कथ्य बनाकर काफी उपन्यास और कहानियों का सृजन किया जा रहा है। मोनिका देवी के दो उपन्यास 'अस्तित्व की तलाश में सिमरन' (2018) और 'हाँ मैं किन्नर हूँ : कांता भुआ' (2018) किन्नरों की जीवन शैली पर आधारित हैं। साहित्य में किन्नर समाज की समस्त समस्याओं और पीड़ाओं को विभिन्न पक्षों एवं दृष्टियों से विश्लेषित करने की आवश्यकता है। साहित्य के माध्यम से इस उपेक्षित वर्ग की आवाज जन-जन तक पहुंच सकती है और साहित्य ही किन्नर विमर्श को आगे बढ़ाने में मील का पत्थर साबित हो सकता है। वर्तमान समय में सबसे बड़ी आवश्यकता यह भी है कि समाज में किन्नरों के प्रति अपनी धारणा बदले एवं इनके प्रति मन-मस्तिष्क में स्थापित पूर्वाग्रहों को दूर करने का प्रयास करे। यह वर्ग समाज में केवल नाच-गाकर हमारा मनोरंजन करने के लिए पैदा नहीं हुआ है, इन्हें भी हक है कि ये गरिमा से परिपूर्ण जीवनयापन करें।

संदर्भ :

1. भीष्म महेंद्र, किन्नर कथा - सामाजिक प्रकाशन, नई दिल्ली, पृ. 51
2. यमदीप, नीरजा माधव, सुनील साहित्य सदन, नई दिल्ली पृ. 22
3. यमदीप, नीरजा माधव, सुनील साहित्य सदन, नई दिल्ली पृ. 24
4. जिंदगी 50-50 - भगवंत अनमोल, राजपाल एंड सन्स - 2017
5. मैं भी औरत हूँ - डॉ. अनसूया त्यागी, परमेश्वरी प्रकाशन- 2008
6. मैं पायल - महेंद्र भीष्मा, अमन प्रकाशन, कानपुर 2016
7. चित्रा मुद्गल - पोस्ट बॉक्स नं. 203 नाला सोपारा
8. चित्रा मुद्गल - पोस्ट बॉक्स नं. 203 नाला सोपारा

■■■

Uttar Pradesh Journal of Zoology

Volume 44, Issue 18, Page 18-29, 2023; Article no.UPJOZ.2711
ISSN: 0256-971X (P)

Screening of *in-vitro* Antidiabetic Potentials from the Protein Extracts of *Stomopneustes variolaris*

V. Ratna Bharathi [a*] and Y. Shanti Prabha [a]

[a] Department of Zoology, Dr. V.S. Krishana Govt. Degree & PG College (Autonomous), Visakhapatnam, Andhra Pradesh, India.

Authors' contributions

This work was carried out in collaboration among all authors. All authors read and approved the final manuscript.

Article Information

DOI: 10.56557/UPJOZ/2023/v44i183600

Editor(s):
(1) Dr. Ana Cláudia Correia Coelho, University of Trás-os-Montes and Alto Douro, Portugal.
Reviewers:
(1) Rashmi Sharma, Maharshi Dayanand Saraswati University, India.
(2) Amit Gupta, Dr. B. R. Ambedkar University, India.

Original Research Article

Received: 23/05/2023
Accepted: 28/07/2023
Published: 12/08/2023

ABSTRACT

Diabetes mellitus (DM) is one of the serious endocrine disorders caused by insufficient production or inefficacy of the insulin and it is the immense cause of death throughout the world. However, finding for novel antidiabetic drugs from natural resources is still fascinating, because of their safe effect on DM. The marine environment provides a pool of unique and novel bioactive compounds due to its extremely diverse environmental conditions and biota. *Stomopneustes variolaris* is a marine echinoderm, belongs to family Stomopneustidae and they have toxins in their bodies as a defence mechanism which often has medicinal value. The present investigation aimed to evaluate the antidiabetic potentials of protein extracts from the spines, shell, and tissue of *Stomopneustes variolaris.* The spine, shell, tissue shows significant variation in protein content and the highest concentration of protein was found in tissue extract. The studies of haemoglobin glycation reveal that the haemoglobin glycation was increased with increasing concentration of the glucose. The highest haemoglobin glycation was reported in 20mg/ml glucose concentration at 24hr incubation

**Corresponding author: Email: vedulabharathi67@gmail.com;*

period. The Glucose Adsorption Capacity of spine, shell and tissue extracts shows a strong positive correlation such as r = 0.9930, r = 0.9931 and r = 0.9969 corresponding to increased glucose concentration. The inhibition percentage of physiological haemoglobin glycation was depended on the glucose concentration. The protein extract of *Stomopneustes variolaris* spine (86.19 ± 0.28) showed the highest percentage of physiological haemoglobin glycation inhibition at 40mg/ml glucose concentration. The % of Glucose dialysis retardation index (GDRI) was decreased with increasing time incubation in all the tested protein extracts. The spine extract of *Stomopneustes variolaris* (37.26 ± 0.4) showed the highest percentage of GDRI at 30min incubation period. The maximum percentage of glucose uptake by yeast was observed with the spine extract (46.4±0.25) of *Stomopneustes variolaris.* The *in-vitro* α-amylase inhibitory activities of *Stomopneustes variolaris* spine, shell, and tissue were found as 51.11±0.79%, 41.81±0.31% respectively.

Keywords: Diabetes mellitus; haemoglobin; glucose; α-amylase; protein extract; GDRI.

1. INTRODUCTION

Diabetes mellitus is one of the serious metabolic disorders of glucose caused by inherited or acquired deficiency in the production of insulin or by the ineffectiveness of the insulin and its results in hyperglycemia due to abnormal metabolism of carbohydrates which leads to the elevated levels of glucose in the blood. The long-term hyperglycemic conditions of diabetes are associated with damage, dysfunction, and failure of various organs [1]. Diabetes is the rapidly increasing lethal disease to mankind all around the world [2]. The World Health Organization (WHO) listed diabetes as the fifth leading cause of death in 2015 and it estimated over 382 million people were suffered from diabetes in 2013, this number is increased to 500 million by 2030. According to the IDF data from 2019, there are 87.9 million diabetics residing in the middle-income countries of Southeast Asia. Particularly, the disease was more prevalent in urban areas and cities, with percentages of 34.3 and 49.4 respectively [3]. In India the current epidemic position of diabetes is increased rapidly with more than 62 million diabetic cases [4]. In the year 2000, India (31.7 million) has a top-ranked with the highest number of diabetic people followed by China (20.8 million) and the United States (17.7 million). Indians are more prevalent to diabetes when compared to the Europeans due to the lower body mass index (BMI) of Indians [5]. In the treatment of diabetes, the major problem with the antidiabetic medicine available in the pharmaceutical market is the continuation of diabetic associated with long-term complications and side effects. Diabetes is a severe economic burden on Indians, with regional variations, and it was revealed that the cost of drugs accounted for a substantial portion of the diabetic expenses. This might be minimised by the development of new generic drugs and health care systems [6]. Hence, searching for new antidiabetic drugs from natural resources is still attractive to researchers because they have substances that can be used as an alternative to antidiabetic medicines to reduce side effects.

The marine environment provides a pool of unique and novel bioactive substances because of its highly varied environmental conditions and diverse biota. The unavailability of sufficient and efficient medicines for the increasing incidence of various diseases has directed to the finding of new bioactive materials from marine sources. Marine organisms show an extensive range of bioactive compounds and the isolation of natural products from marine organisms has been exceeded to 18000 [7]. Sea urchin is a member of echinoidea class in the Echinodermata phylum and they have been considered as a potential source of bioactive substances with pharmaceutical applications [8]. The structure and quantity of bioactive compounds can vary among diverse sea urchin types possibly due to their different diet habits and physiological stages like variation in the reproduction phase [9]. Some sea urchins can synthesise toxins for their defence purpose, which often have a biomedical significance [10]. Basing on the bioactive potency, the present research has been carried out on *Stomopneustes variolaris* for the evaluation of their pharmacological activities against diabetes.

Stomopneustes variolaris is a tropical, rock-boring echinoid found at the intertidal zone and distributed from southern and northern poles to the equator [11]. *S. variolaris* is a commonly found sea urchin in India which is distributed along the coast of Visakhapatnam to Kanyakumari. The structure of *S. variolaris* has a hard-calcareous shell known as a test and it is

covered with spines for locomotion and defence. The mouth is positioned on its ventral side containing five calcareous plates called "Aristotle's Lantern". This mouth opens into the digestive tract that is connected to the anus which is located on the top of the test. The present investigation was designed to screen the antidiabetic properties of protein extracts from the spines, shell, and tissue of *Stomopneustes variolaris.*

2. MATERIALS AND METHODS

2.1 Sample Collection

Young and healthy *Stomopneustes variolaris* were collected from Tenneti Park (Long: 83°20' 59.94'' E; Lat: 17° 44' 48.36'' N) and have been located on the North East coast of Andhra Pradesh, connected to the Bay of Bengal, Visakhapatnam, India. The collected organisms were aseptically transported to the laboratory and cleaned with distilled water. Then the samples were dissected and separation of the spines, shell, and tissue was done for the research.

2.2 Extraction and Estimation of Total Protein

Ferreira et al., [12] method was adopted to extract the proteins. 5 gm of *Stomopneustes variolaris* spine, shell, and tissue samples were homogenized separately in 50 mM sodium phosphate buffer containing 10% insoluble PVP and incubated at 4°C for overnight. Then the homogenates were centrifuged at 14000 rpm for 20 min at 4°C. The supernatant was separated and maintained at -20°C for further investigation. The total protein content in the spine, shell, and tissue extracts of *Stomopneustes variolaris* was quantified by adopting the Lowry et al., [13] method. The protein content was expressed in mg per gm fresh weight.

2.3 Evaluation of Haemoglobin Glycation

2.3.1 Preparation of haemoglobin

The blood was collected from a healthy human volunteer in a vial containing an anticoagulant and the collected blood was washed three times with 0.14M NaCl. Two volumes of 0.01M phosphate buffer (pH 7.4) and 0.5 ml CCl_4 was added to the blood suspension to lyse the RBC. At room temperature the haemolysate was centrifuged for 15 min at 2300 rpm. After centrifugation, the haemoglobin rich upper layer was isolated and kept in a refrigerator until use [14].

2.3.2 Estimation of haemoglobin glycation

Three distinct concentrations (2, 10, and 20 mg/ml) of glucose solution (pH 7.5) was used to estimate haemoglobin glycation. 1ml of haemoglobin was taken in a series of three test tubes each containing 1ml of 2, 10, and 20 mg/ml glucose solution. The haemoglobin fraction without the glucose was used as a blank. The test tubes were incubated for different time intervals such as 0, 24, 48, & 72 hrs and the degree of glycation was quantified by estimating the liberated hydroxymethylfurfural [14].

2.4 Determination of Extract Glucose Adsorption Capacity

Five distinct concentrations (5, 10, 20, 50, and 100 mg/dl) of glucose solution was used to estimate Glucose adsorption capacity of extract. 0.25ml of *Stomopneustes variolaris* spine, shell, and tissue protein extracts were separately taken in a series of five test tubes each containing 25ml of 5, 10, 20, 50, and 100 mg/dl glucose solution. The test tubes were incubated for 6hrs at 37°C in a shaker water bath. Then, the tubes were centrifuged for 20 min at 4800 rpm and the glucose content was measured in the supernatant [15]. The amount of glucose bound to the extract was measured by the below formula.

$$Glucose\ bound = 100 - \frac{G1 - G6}{Sample\ Weight} \times Solution\ Volume$$

G1 is the amount of glucose in original solution.
G6 is the amount of glucose after 6 hr incubation.

2.5 Effect of Extract on Physiological Haemoglobin Glycation

A series of increasing glucose concentrations (1-40mg/ml) were used to study the inhibition percentage of physiological haemoglobin glycation with the protein extracts of *Stomopneustes variolaris* spine, shell, and tissue. 1ml of haemoglobin was taken in a series of five test tubes each containing 1 ml of 1, 10, 20, 30 and 40mg/ml glucose solution. To the above test tubes, 5µl of gentamycin and 30µg/ml of protein extracts were added. The positive

control was maintained by adding 30µg/ml gallic acid instead of protein extracts and the contents were gently mixed and incubated at room temperature for 72 hrs in dark. After incubation, the free haemoglobin was estimated by spectrophotometrically at 443nm to measure the degree of inhibition percentage haemoglobin glycation [14].

2.6 Effect of Extracts on in-vitro Glucose Diffusion

The in-vitro glucose diffusion study was performed with increasing incubation times. A mixture of 25ml glucose solution (20mM) and 1% protein extracts of *Stomopneustes variolaris* spine, shell, and tissue were separately packed in a dialysis bag. The bags were dialysed against 200ml distilled water at 37^0C and the amount of glucose in the dialysate was evaluated at 30-, 60-, 120, and 180-min incubation times. Control was maintained without protein extract [16].

$$\%\, GDRI = 100 - \frac{Glucose\ content\ in\ the\ Test\ (mg/dl)}{Glucose\ content\ in\ the\ control\ (mg/dl)} \times 100$$

2.7 Effect of Extracts on Glucose Uptake in Yeast Cells

Commercial baker's yeast was used to study the effect of protein extracts on glucose uptake. 5gms of yeast was dissolved in distilled water and allowed to the repeated centrifugation at 3000 rpm for 5min till getting the clear supernatant. From the clear supernatant, 10% yeast suspension was prepared with distilled water. 1ml of protein extracts from *Stomopneustes variolaris* spine, shell, and tissue were taken in separate test tubes each contains 1ml of 100mM glucose solution and the tubes were incubated at 37^0C for 10min. Control was kept without the addition of protein extracts. To the above tubes, 100µl of 10% yeast suspension was added and they were permitted to incubation for 60min at 37^0C. After incubation, the tubes were centrifuged at 2500 rpm for 5min and the amount of glucose was quantified in the supernatant.

$$\%\, of\ glucose\ uptake = 100 - \frac{Abs\ control - Abs\ sample}{Abs\ control} \times 100$$

2.8 α-Amylase Inhibitory Assay

The α-amylase inhibitory assay for protein extracts of *Stomopneustes variolaris* spine, shell and tissue were evaluated according to the methodology of Malik and Singh et al., [17] with minor alterations. 1ml of protein extracts and 1ml of 0.5 mg/ml α-amylase solution were taken in test tubes and the tubes were allowed incubate at room temperature for 10min. To the above mixture, 1ml of 1% starch was added and again incubated the mixture at room temperature for 10min. After incubation, 2ml of dinitrosalicylic acid was added in all the test tubes to terminate the reaction and the tubes subsequently kept in a water bath for 5min at 100^0C. Once the temperature of the reaction mixture reached the room temperature, the mixture was diluted by adding 10ml distilled water and absorbance was measured at 540nm. Control was maintained by adding the buffer instead of protein extract and acarbose was used as standard.

$$\%\, of\ \alpha\ amylase\ inhibition = \frac{Abs\ control - Abs\ sample}{Abs\ control} \times 100$$

3. RESULTS AND DISCUSSION

3.1 Protein Estimation

Screening of protein quality and quantity gives an idea about the habitat and medicinal importance of an organism. Different marine organisms that live in different habitats show a significant variation in the quantity of proteins. Mayne and Robinson [18] reported the positive relationship between total body protein and feeding habit of an organism. The protein content in the spine, shell, and tissue of *Stomopneustes variolaris* shows a large variation. The protein concentration in the tissue of *Stomopneustes variolaris* was found as 11154±170 µg/gmFW. Whereas, spine and shell extracts have 764±7.8µg/gmFW and 1565.56±7.37 µg/gmFW of protein respectively. Among all the three extracts of *Stomopneustes variolaris* tissue shows dominant protein content.

The information of organisms' bioactive potential is very important since the therapeutic value is reflected by its biomolecular composition. Protein is a chief biochemical component which plays a vital role in determining the structure and quality of an organism [19]. Protein is one of the dominant biochemical constituents in *S. variolaris* and it was high in tissue than exoskeleton. Mol et al., [20] carried out similar research in *P. lividus* and the protein content was observed as 12.03 ± 1.26%. Shikov et al., [21] and Bragadeeswaran et al., [22] reported the protein content in *S.*

droebachiensis and *T. toreumaticus* as 39.7% and 2.70 mg/ml correspondingly. Kato and Schroeter, [23] reported that *S. franciscanus* and *S. purpuratus* show variation in protein percentage which ranges from 7.7 to 9.6 and 9.5 to 12.3 respectively. The present findings are correlated with some earlier works and also some differences are reported. These differences are associated to the omnivorous feeding habit and adequate food present in the surrounding.

3.2 Estimation of Haemoglobin Glycation

The evaluation of haemoglobin glycation has a crucial role in antidiabetic studies. The maximum haemoglobin glycation was observed at 24hr incubation period in 20mg/ml concentrated glucose solution. At 24 hr incubation period the haemoglobin glycation was reported as 0.333±0.005, 0.145±0.004 and 0.546±0.005 with respect to the 2, 10 and 20 mg/ml glucose concentrations (Fig. 1). At 48 hr incubation period the haemoglobin glycation was reported as 0.441±0.006, 0.346±0.005 and 0.277±0.005 with respect to the 2, 10 and 20 mg/ml glucose concentrations (Fig. 2). At 72 hr incubation period the haemoglobin glycation was reported as 0.143±0.005, 0.189±0.005 and 0.217±0.005 with respect to the 2, 10 and 20 mg/ml glucose concentrations (Fig. 3). Increased glucose concentration in the blood leads to glycation of haemoglobin which may induce the production of reactive oxygen species. An increasing pattern of glycation was observed on the incubation of haemoglobin with the increasing concentration of glucose (2mg, 10mg, and 20mg) over a period of 72hr.

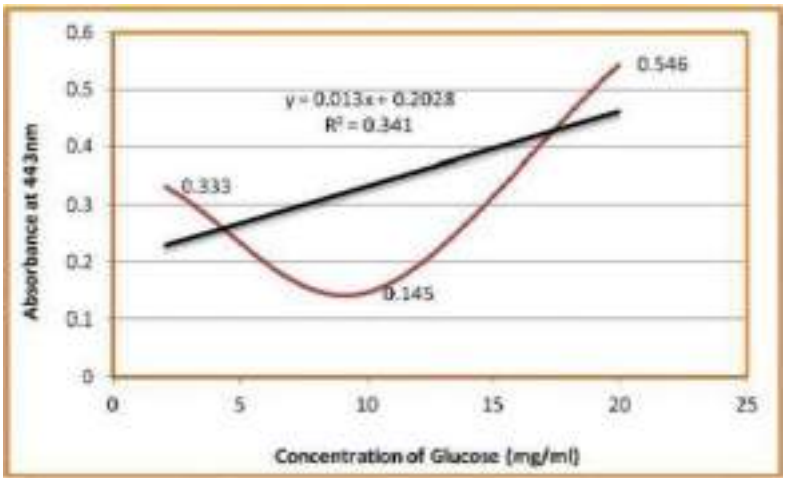

Fig. 1. Haemoglobin glycation with three glucose concentrations at 24hr time period

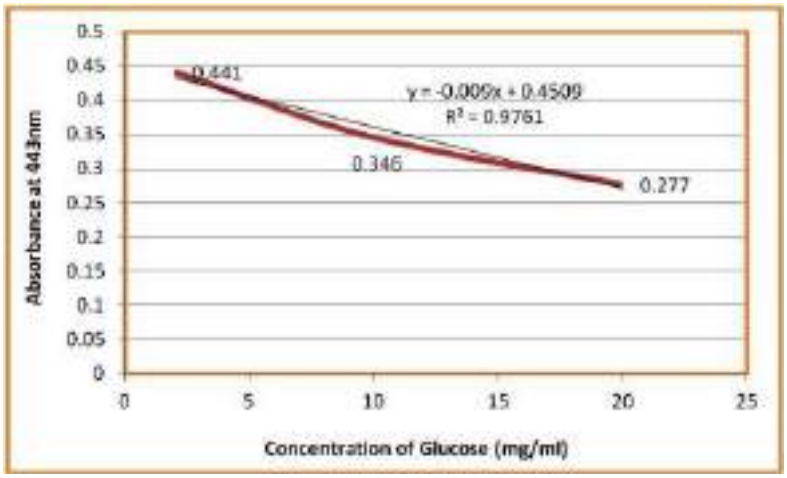

Fig. 2. Haemoglobin glycation with three glucose concentrations at 48hr time period

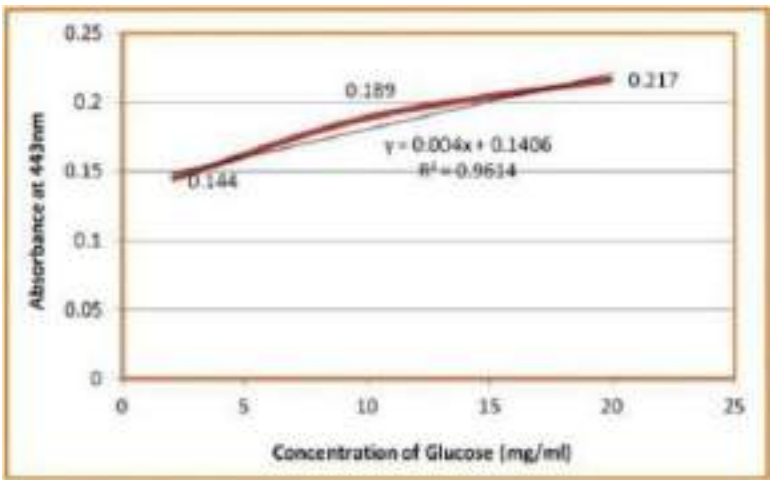

Fig. 3. Haemoglobin glycation with three glucose concentrations at 72hr time period

3.3 Glucose Adsorption Capacity

The glucose adsorption capacity of spine, shell, and tissue protein extracts from *Stomopneustes variolaris* was increased with the increasing concentration of glucose. It was observed that all the protein extracts of *Stomopneustes variolaris* showed similar Glucose Adsorption Capacity at 100mm and 5mm glucose concentration. At 10mm glucose concentration, the Glucose Adsorption Capacity of *Stomopneustes variolaris* spine, shell, and tissue protein extracts were reported as 6.436±0.09, 7.99±0.11, and 9.67±0.11 respectively. Whereas at 20 mm glucose, the Glucose Adsorption Capacity was reported as 10.143 ± 0.06, 8.804±0.02 and 16.490±0.06mg/dl for the spine, shell, and tissue protein extracts respectively. All the tested protein extracts show maximum glucose adsorption capacity was observed at 10 and 20mm glucose concentration. The IC50 values for the spine, shell, and tissue protein extracts of *Stomopneustes variolaris* were measured as 71.401, 59.664 and 140.704 mm respectively.

These results illustrate that the Glucose Adsorption Capacity was depended on the glucose concentration. The Glucose Adsorption Capacity of all the *Stomopneustes variolaris* protein extracts was significantly (<.0005) increased with increasing glucose concentration. The protein extracts of *Stomopneustes variolaris* spine, shell, and tissue show a strong positive correlation such as r = 0.9930, r = 0.9931 and r = 0.9969 correspondingly with increasing glucose concentration. The shell protein extracts show a more positive correlation of Glucose Adsorption Capacity (r = 0.9969) when compared to the Glucose Adsorption Capacity of the spine, and tissue in response to increasing glucose concentration. The results were shown in Table 1.

The present results demonstrated that the tested protein extracts possess a captivating glucose adsorption capacity. Furthermore, all the extracts show a positive correlation of glucose adsorption capacity with the glucose concentration. A similar observation was reported by Bhutkar and Bhise [24], the adsorption capacity of the extracts of *Albizzia lebbeck* and *Mucuna pruriens* show a direct relationship to the glucose concentration. Invitro and Invivo studies of Chau et al., [25] demonstrated that the density of soluble polysaccharides causes late glucose absorption by gastrointestinal cells. El Barky et al., [26] has been reported that the saponins content in the sea cucumber acts as an antidiabetic agent.

3.4 Effect of Extracts on Physiological Haemoglobin Glycation

The spine protein extracts of *Stomopneustes variolaris* exhibit the highest (86.19 ± 0.28) inhibition percentage of physiological haemoglobin glycation at 40mg/ml glucose concentration. Whereas, at 1mg/ml glucose concentration the inhibition percentage of physiological haemoglobin glycation by spine protein extract was reported as 78.56±0.30. The protein extracts of *Stomopneustes variolaris* shell and tissue have no activity at 1mg/ml glucose. Whereas, at 40mg/ml glucose concentration, inhibition percentages of shell and tissue extracts

were found as 26.45± 0.64 and 70.76±0.70 respectively. The IC_{50} values of spine, shell and tissue protein extracts were calculated as 10.089, 50.696 and 15.382 mg/ml correspondingly for the inhibition percentage of physiological haemoglobin glycation. The results have been shown in Table 3.

These results demonstrated that the inhibition percentage of physiological haemoglobin glycation depended on the glucose concentration. Among all the protein extracts spine show a strong negative correlation (r = -0.1331) with increasing glucose concentration. Whereas, protein extract of shell (r = 0.80951) and tissue (r = 0.89937) shows positive correlation. The inhibition percentages of shell and tissue show a moderate positive correlation (r = 0.3223) and moderately negative correlation (r = -0.3767) respectively when compared to the inhibition percentages of spine extract. Furthermore, the tissue extracts show a positive correlation (r = 0.7377) when compared to the shell protein extracts. The results have been shown in Table 4.

The present results were found to be collinear with those of Karimabad et al., [27] who reported that the extracts of *Citrullus colocynthis* significantly inhibited the formation of glycated haemoglobin with increasing time under hyperglycemic conditions. In the management of diabetes proper attention has been given to the increased blood glucose concentration. Because it can bind to the haemoglobin which may result in the formation of the reactive oxygen species [28]. *In vivo*, the occurrence of this process contributes to the elevated plasma peroxides found in diabetics complication and may contribute to protein modification reactions perform with glucose in vitro. Thus, with the high level of glucose in the blood, erythrocytes have become important in the pathophysiologic mechanisms in diabetics as shown from several abnormal features demonstrated for red cells of diabetes mellitus patients [14]. Mathur et al., [29] stated that several natural bioactive compounds exhibit significant therapeutic potentials against diabetes and related diseases by inhibiting the protein glycation such as haemoglobin glycation.

Table 1. Effect of glucose adsorption capacity of *Stomopneustes variolaris* spine, shell and tissue protein extracts on different glucose concentrations

S/N	Glucose Conc. (mm)	Glucose adsorption capacity mean ± Std (mg/dl)		
		Spine	Shell	Tissue
1	5	4.491±0.08	4.304±0.017	4.721±0.051
2	10	6.436±0.09	7.993±0.116	9.669±0.111
3	20	10.143±0.06	8.804±0.020	16.490±0.063
4	50	54.166±0.92	57.999±0.310	57.694±0.53
5	100	133.118±0.75	133.394±0.096	133.650±0.56

Table 2. Correlation of glucose adsorption capacity of *Stomopneustes variolaris* spine, shell and tissue protein extracts on different glucose concentrations

	Glucose Conc. (mm)	Tissue	Spine	Shell
Glucose Conc. (mm)	1			
Tissue	0.993095	1		
Spine	0.993183	0.999381	1	
Shell	0.996886	0.999116	0.998493	1

Table 3. Effect of *Stomopneustes variolaris* protein extracts on inhibition physiological haemoglobin glycation with increasing glucose concentrations

S/N	Glucose Conc. (mg/ml)	Inhibition of physiological Hb glycation mean ± Std (%)		
		Spine	Shell	Tissue
1	1	78.56±0.3	0	0
2	10	56.46±0.24	0	0
3	20	3.48±0.2	8.51±0.47	61.52±0.55
4	30	5.33±0.09	3.38±0.53	56.63±0.56
5	40	86.19±0.28	26.45±0.64	70.76±0.7

Table 4. Correlation of *Stomopneustes variolaris* protein extracts on inhibition of physiological haemoglobin glycosylation with increasing glucose concentrations

	Glucose Conc. (mg/ml)	Spine	Shell	Tissue
Glucose Conc. (mg/ml)	1			
Spine	-0.133119929	1		
Shell	0.809511439	0.322304	1	
Tissue	0.899379331	-0.3767	0.737744	1

3.5 Effect of Extracts on in-vitro Glucose Diffusion

The spine protein extract of *Stomopneustes variolaris* (37.26 ± 0.4) showed the highest percentage of Glucose Dialysis Retardation Index (GDRI) at a 30min incubation period. At the 240min incubation period, the GDRI by spine protein extract was reported as 1.64±0.04. The GDRI percentage of shell and tissue protein extracts of *Stomopneustes variolaris* were observed as 31.62±0.52 and 35.84±0.37 respectively at a 30min incubation period. Whereas, at 240min incubation period the GDRI percentage of shell and tissue protein extracts of *Stomopneustes variolaris* were observed as 1.34±0.05 and 1.67±0.04 respectively. The results of the %GDRI have been shown in Table 5. These results suggested that the percentage of GDRI was significantly (<.0005) decreased with the increasing time incubation periods. All protein extracts from the spine, shell, and tissue of *Stomopneustes variolaris* shows strong negative correlation such as r = -0.91447, r = -0.92543, and r = -0.92773 correspondingly with increasing time incubation. The shell protein extracts show (r = 0.997522) a more positive correlation when compared to the spine extracts. Furthermore, the % GDRI of tissue shows a strong positive correlation such as (r = 0.999053) and (r = 0.996462) when compared to the % GDRI of spine and shell extracts respectively. The results have been shown in Table 6.

GDRI measures the invitro index for the detainment of glucose absorption in the gastrointestinal tract by the extract [30]. The greater GDRI value suggests a higher glucose retardation index. Bailey, [31] stated that the retardation of glucose diffusion may cause by the inhibition of sugar hydrolysing enzymes such as α-amylase with the extracts and delay the glucose liberation from the starch thereby decrease glucose absorption and finally reduce the blood glucose levels. The present results demonstrate that the inhibition of α-amylase enzyme may be one of the probable mechanisms of *Stomopneustes variolaris* protein extracts for exerting their hypoglycemic effect.

3.6 Effect of Extracts on Glucose Uptake in Yeast Cells

The transport mechanism of glucose through the yeast membrane has become an attractive method to evaluate the hypoglycemic effect of several bioactive compounds under in vitro conditions. In the present study, it was found that the protein extracts of *Stomopneustes variolaris* spine, shell and tissue showed 46.4±0.25, 28.41±0.125 and 40.09±0.4% respectively. Among all the protein extracts spine shows a higher percentage of glucose uptake in yeast. The results have been shown in Fig. 4. The *in vitro* assays of the present study indicated that the protein extracts of *Stomopneustes variolaris* possess good anti-diabetic activity.

These findings are supported by the findings of Pulivarthi et al., [32], who demonstrated that the methanolic leaf extract of *A. reticulata* enhances glucose absorption across the yeast cell membrane by 48.55%, indicating a substantial antidiabetic potential. The treatment of yeast cells with the *Stomopneustes variolaris* protein extracts, the glucose uptake was increased than the standard drug metformin. Illiano and Cuatrecasas, [33] reported that the sugar transportation across the membrane of yeast cell is though the facilitated diffusion which is mediated by the stereospecific membrane carriers. Teysink et al., [34] reported that the facilitated carriers transport the solutes from high concentration to low concentration. Hence, effective glucose transport is achieved, when the cell has low glucose concentration. The data obtained from the present studies reveal that the protein extract of *Stomopneustes variolaris* spine effectively enhances glucose uptake by yeast and induces the effective glucose utilization, thus regulating the glucose levels in the blood.

3.7 α- Amylase Inhibitory Assay

The carbohydrate digestion in the intestine is mediated by the hydrolytic activity of pancreatic α-amylase. Hence, researchers focus on the α-

amylase activity for *in-vitro* evaluation of the hypoglycemic effect of bioactive compounds. The *in-vitro* α-amylase inhibitory studies demonstrated that *Stomopneustes variolaris* spine, shell and tissue protein extract show significant anti-diabetic activity. The *in-vitro* α-amylase inhibitory activities of *Stomopneustes variolaris* spine, shell, and tissue protein extracts were observed as 51.11±0.79%, 41.81±0.31%, and 27.6±0.27% correspondingly (Fig: 5).

The current findings of α-amylase inhibition were strongly associated with the studies of Kifle et al., [35] who reported that the ethyl acetate extract of *H. abyssinica* exhibits significant α-amylase inhibitory activity with an IC50 of 52.11 µg/ml. Roux et al., [36] reported that the decreasing of postprandial hyperglycemia is due to the inhibition of α-amylase in diabetic patients. Hara and Honda [37] suggested that diabetes is effectively controlled by the inhibition of α-amylase activity in the gastrointestinal tract of humans and thereby reduces the absorption of simple sugars. Hence, diabetic patients need to maintain low levels of α-amylase to regulate their blood glucose levels.

Table 5. Effect of *Stomopneustes variolaris* protein extracts on in-vitro glucose diffusion (%GDRI) with increasing incubation times

S/N	Incubation time (min)	Glucose dialysis retardation index mean ± Std (%)		
		Spine	Shell	Tissue
1	30	37.26±0.4	31.62±0.52	35.84±0.37
2	60	21.05±0.2	19.87±0.13	20.72±0.12
3	120	9.27±0.12	7.67±0.12	10.53±0.14
4	180	3.67±0.07	2.98±0.04	4.02±0.08
5	240	1.64±0.04	1.34±0.05	1.67±0.04

Table 6. Correlation of *Stomopneustes variolaris* protein extracts on *in-vitro* glucose diffusion (%GDRI) with increasing incubation time

	Incubation time (min)	Spine	Shell	Tissue
Incubation Time (min)	1			
Spine	-0.91447	1		
Shell	-0.92543	0.997552	1	
Tissue	-0.92773	0.999053	0.996462	1

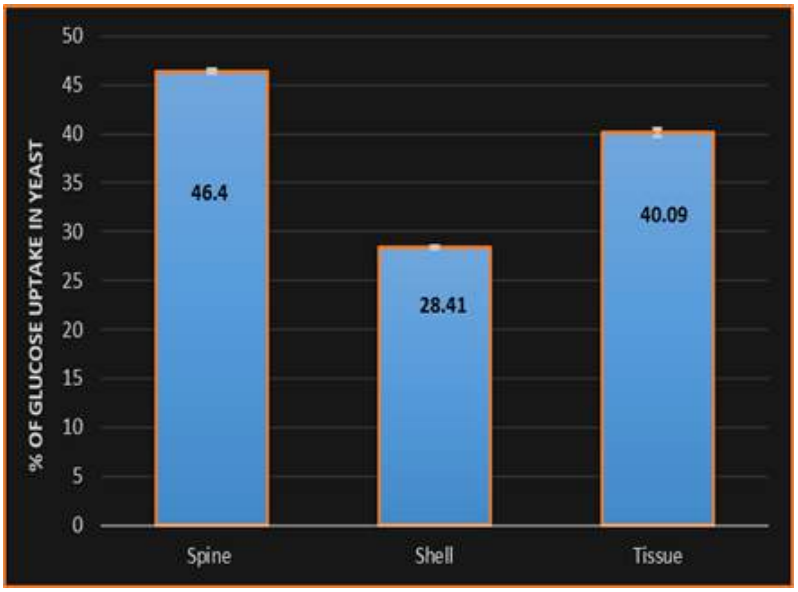

Fig. 4. Percentage of glucose uptake in yeast cells by protein extracts of *S. variolaris* spine, shell and tissue

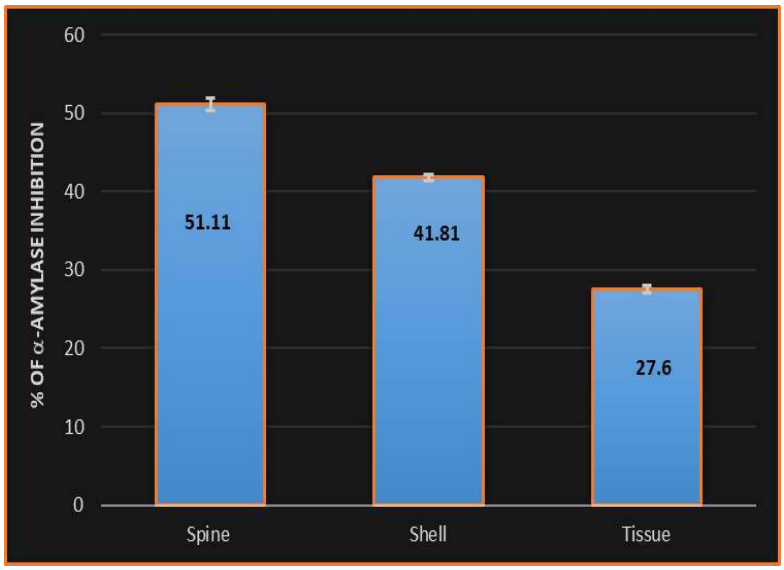

Fig. 5. α-Amylase inhibitory activity of *Stomopneustes variolaris* spine, shell and tissue protein extracts

4. CONCLUSION

The present study provides scientific evidence that *S. variolaris* can be used to treat diabetic symptoms. The diabetic properties of *S. variolaris* was assessed by in-vitro approaches such as effect of haemoglobin glycation, %GDRI, Glucose uptake by yeast cells and inhibition of alpha amylase. The observations of invitro studies concluded that *S. variolaris* protein extracts inhibit the haemoglobin glycation, thereby reduce the glycated product formation. The results of GDRI suggests that the glucose diffusion retardation is by delaying the glucose liberation from the starch thereby decrease glucose absorption and finally reduce the blood glucose levels. The invitro studies of glucose uptake revealed that *S. variolaris* protein extracts increase a substantial amount of glucose uptake by the yeast cells. All the results of invitro assays in the current study showed that the protein extracts of *S. variolaris* possess good antidiabetic activity. The present investigation has also opened a way for future research to develop potent formulation of drugs for diabetes.

ACKNOWLEDGEMENT

The authors acknowledge the Department of Zoology, Dr. V.S. Krishana Govt. Degree & PG College (Autonomous), Visakhapatnam, for providing permission to conduct the research work in collaboration with SSR Biosciences Laboratory.

COMPETING INTERESTS

Authors have declared that no competing interests exist.

REFERENCES

1. Lyra R, Oliveira M, Lins D, Cavalcanti N. Prevention of type 2 diabetes mellitus. Arquivos brasileiros de endocrinologia e metabologia. 2006;50:239-49.
2. Ogbonnia SO, Odimegwu JI, Enwuru VN. Evaluation of hypoglycaemic and hypolipidaemic effects of aqueous ethanolic extracts of *Treculia africana* Decne and *Bryophyllum pinnatum* Lam. and their mixture on streptozotocin (STZ)-induced diabetic rats. African Journal of Biotechnology. 2008;7(15):2535-2539.
3. IDF, International Diabetes Federation Atlas, Aarhus, Denmark; 2019.
4. Joshi SR, Parikh RM. India-diabetes capital of the world: now heading towards hypertension. Journal of the Association of Physicians of India. 2007;55:323-4.
5. Rao CR, Kamath VG, Shetty A, Kamath A. Cross-sectional analysis of obesity among a rural population in coastal southern Karnataka, India. Australasian Medical Journal. 2011;4(1):53–57.
6. Oberoi S, Kansra P. Economic menace of diabetes in India: A systematic review. International journal of diabetes in developing countries. 2020;40(4):464-475.

7. Marinlit, Version September A marine literature database produced and maintained by Department of chemistry, University of Catenbury, New Zealand; 2007. Available:www.chem.Cauterbury.achz/marinlit/marinlitshtml
8. Kelly MS. Echinoderms: their culture and bioactive compounds. In: Matranga V, (eds). Echinodermata: Progress in Molecular and Subcellular Biology. Subseries: Marine Molecular Biotechnology. Springer-Verlag, Berlin Heidelberg. 2005:139–165.
9. Lawrence JM. Edible sea urchins: Biology and ecology, Elsevier: Boston, MA, USA, 2007:380.
10. James DB. Sea cucumber and sea urchin resources. CMFRI Bulletin, CMFRI, Research Centre, Madras, India. 1983;34: 85-93.
11. Gayashan MA, Jayakody S. Diversity and density of sea urchins' populations in rocky shores off Nilwella in Southern province of Sri Lanka. Department of Aquaculture and Fisheries, Wayamba University of Sri Lanka, Sri Lanka, 2012:35-46.
12. Ferreira RR, Fornazier RF, Vitoria AP, Lea PJ, Azevedo1, RA. Changes in antioxidant enzyme activities in soybean under cadmium stress. Journal of Plant Nutrition. 2002;25(2):327-342.
13. Lowry OH, Rosebrough NJ, Farr AL, Randall RJ. Protein measurement with folin phenol reagent. Journal of Biological Chemistry. 1951;193:265-275.
14. Adisa RA, Oke J, Olomu SA, Olorunsogo O. Inhibition of human haemoglobin glycosylation by flavonoid containing leaf extract of *Cnestis ferruginea*. Journal of the Cameroon Academy of Sciences. 2004;4: 351-359.
15. Ou S, Kwok KC, Li Y, Fu L. In vitro study of possible role of dietary fiber in lowering postprandial serum glucose. Journal of Agricultural and Food Chem. 2001;49: 1026–1029.
16. Ahmed F, Sairam S, Urooj A. In vitro hypoglycemic effects of selected dietary fiber sources. Journal of Food Science and Technology. 2011;48(3):285–289.
17. Malik CP, Singh MB. Plant enzymology and histoenzymology, Kalyani Publishers, New Delhi, 1980: 278.
18. Mayne J, Robinson JJ. The sea urchin egg yolk granule is a storage compartment for HCL-32, an extracellular matrix protein. Biochemistry and Cell Biology. 1998;76(1): 83-88.
19. Nagabhushanam R, Mane UH. Seasonal variation in the biochemical composition of *Mytilus viridis* at Ratnagiri on the West Coast of India, Hydrobiologia. 1978;57:69.
20. Mol S, Baygar T, Varlik C, Tosun SY. Seasonal variations in yield, fatty acids, amino acids and proximate compositions of sea urchin (*Paracentrotus lividus*) Roe. Journal of Food and Drug Analysis. 2008;16(2):68-74.
21. Shikov AN, Laakso I, Pozharitskaya ON, Makarov VG, Hiltunen R. Phospholipids and amino-acid composition of eggs of sea urchin from Barents Sea. Planta Medica. 2012;78:1146.
22. Bragadeeswaran SN, Sri Kumaran P, Prasath Sankar R, Prabahar. Bioactive potential of sea urchin *Temnopleurus toreumaticus* from Devanampattinam, Southeast coast of India. Journal of Pharmacy and Alternative Medicine. 2013; 2(3):9-17.
23. Kato S, Schroeter SC. Biology of the red sea urchin, *Strongylocentrotus franciscanus*, and its fishery in California. Marine Fisheries Review. 1985;47:1-20.
24. Bhutkar M, Bhise S. Invitro hypoglycemic effects of *Albizzia lebbeck* and *Mucuna pruriens*. Asian Pacific Journal of Tropical Biomedicine. 2013;3(11):866-870.
25. Chau CF, Huang YL, Lee MH. In-vitro hypoglycemic effects of different insoluble fibre rich fractions prepared from the peel of *Citrus sinensis* L cv. Liucheng. Journal of Agriculture and Food Chemistry. 2003;51:6623-6626.
26. El Barky AR, et al. Marine sea cucumber saponin and diabetes. Austin Pancreatic Disorders. 2017;1(1):1–7.
27. Karimabad MN, Niknia S, Golnabadi MB, Poor SF, Hajizadeh MR, Mahmoodi M. Effect of *Citrullus colocynthis* Extract on Glycated Hemoglobin Formation (In Vitro). Eurasian J Med. 2020;52(1):47-51.
28. Bailey CJ, Day C. Traditional Plant Medicines as Treatments for Diabetes. Diabetes Care. 1989;12:553-564.
29. Mathur ML, Jyoti G, Ruchika S, Kripa RH. Antidiabetic properties of a spice plant *Nigella sativa*. Journal of Endocrinology and Metabolism. 2011;1:1-8.
30. Basha SK, Kumari VS. In vitro antidiabetic activity of *Psidium guajava* leaves extracts. Asian Pacific Journal of Tropical Disease. 2012;2(1):98-100.

31. Bailey C. New approaches to the pharmacotherapy of diabetes. In: Textbook of Diabetes. Pickup JC, William G, (eds). Oxford, Blackwell Science, 2003:1-73.
32. Pulivarthi V, Josthna P, Naidu CV. In vitro antidiabetic activity by glucose uptake of yeast cell assay and antioxidant potential of *Annona Reticulata* L. leaf extracts. Int. J. Pharm. Sci. Drug Res. 2020;12(3):208-213.
DOI: 10.25004/IJPSDR.2020.120301.
33. Illiano G, Cuatrecasas P. Glucose transport in fat cell membranes. The Journal of Biological Chemistry. 1971;246: 2472-9.
34. Teusink B, Diderich JA, Westerhoff HV, Van Dam K, Walsh MC. Intracellular glucose concentration in derepressed yeast cells consuming glucose is high enough to reduce the glucose transport rate by 50%. Journal of Bacteriology. 1998;180(3): 556–562.
35. Kifle ZD, Yesuf JS, Atnafie SA. Evaluation of in vitro and in vivo anti-diabetic, anti-hyperlipidemic and anti-oxidant activity of flower crude extract and solvent fractions of *Hagenia abyssinica* (rosaceae). Journal of Experimental Pharmacology. 2020;12: 151-167.
36. Roux FG, Perrier J, et al. The human pancreatic alpha-amylase isoforms: Isolation, structural studies and kinetics of inhibition by acarbose. Biochimica Biophysica Acta. 1998;1388:10–20.
37. Hara Y, Honda M. The inhibition of α-amylase by tea polyphenols. Agricultural and Biological Chemistry. 1990;54(8): 1939-1945.

JETIR.ORG ISSN: 2349-5162 | ESTD Year : 2014 | Monthly Issue
JOURNAL OF EMERGING TECHNOLOGIES AND INNOVATIVE RESEARCH (JETIR)
An International Scholarly Open Access, Peer-reviewed, Refereed Journal

Diversity and abundance of avifauna in Kondakarla Ava Lake, Andhra Pradesh, India.

V.Rama lakshmi* & Dr.Vedula.Ratna Bharathi*

*Department of Zoology, Dr.V.S.Krishna Govt. Degree and P.G. College,
Visakhapatnam, Andhra Pradesh, India

Abstract:

Bird migration is an amazing natural phenomenon that fascinates scientists, bird lovers, and environmentalists alike. A significant migratory hotspot, Kondakarla Ava Lake near Visakhapatnam, a coastal city in the Indian state of Andhra Pradesh, draws a variety of bird species from all over the world.

Each year, Kondakarla Ava Lake witnesses the arrival of migratory birds during the winter months, creating a unique spectacle of biodiversity. These birds traverse long distances, crossing geographical boundaries and ecological barriers, to seek favorable breeding and feeding grounds.

The ecological ramifications of migrating bird populations in Kondakarla Ava Lake are extensive. These avian guests are essential to preserving the delicate ecosystems' equilibrium in the area. They contribute to the reduction of pest populations and the improvement of nutrient cycling in wetlands and water bodies by eating fish, aquatic plants, insects, and other animals. Additionally, their excretions act as organic fertilizers, improving the soil and encouraging the growth of plants. As a result, migrating birds greatly contribute to the general stability and health of the environment in the area.

The survival of migrating birds in Kondakarla Ava Lake is threatened by a number of factors notwithstanding their significance. Significant threats to their wellbeing include deforestation, habitat degradation, pollution, climate change, and illegal hunting. Additionally, as urbanization and human activities spread, migratory species have less secure places to stop and feed because of the disruption to their natural habitats. Given these difficulties, conservation initiatives are essential to protect the migratory bird populations in Kondakarla Ava Lake.

Keywords: Coastal city, Geographical boundaries, Ecological barriers, Conservation, Illegal hunting.

Introduction:

The Kondakarla Awa Lake, being a unique ecosystem, upon which several thousands of families are dependent for their livelihood, needs urgent conservation measures Chourey, (2001) for protecting it from the threats of pollution, siltation, eutrophication and encroachments. As per my study has indicated that the major wetlands harbor substantial biodiversity, provide habitats at times for several species of conservation importance and are ecologically sensitive and valuable. So these wetlands should b protected as per the stipulations of Wetlands (Conservation & Management) Rules-2010. A strategy for sustainably and wisely using them whilst ensuring their entire ecosystem structure, functions and services should be identified and executed. Many fishermen indulge in poaching of birds and other wild life wherever available. They are unaware of the importance of such species. Awareness programmes have to be initiated to address this issue. Programmes with stakeholder participation should be formulated to protect such wetlands.

Study Area:

Kondakarla Ava wetland, a natural freshwater lake (stretches between latitudes 17°35‟30” and 17° 36‟02″ N longitudes; 82° 59‟27” and 83° 01‟02” E) of Visakhapatnam district, Andhra Pradesh, India. The Kondakarla Awa Lake is a part of the Sarada riverine system and is classified as a perennial, warm, a euphotic, shallow, polymitic, eutropic fresh water lentic body. The wetland is named after a village, “Kondakarla”, abutting thelake. For the natives, the wetland is a livelihood source, while for the nearby towns and city people it is a getaway famous for avian diversity. During the British period oneof the famous tourist place in Andhra Pradesh.

Methodology:

Bird survey was conducted, when the birds are most active during day from 06:00 to 9.30 hrs and from 16:00 to 19:00 hrs. Field visits have been conducted weekly once in all three seasons and habitat wise (Xu Hanqiu, 2006). Opportunistic observations were made during other timings and species recorded during these observations included in the checklist. The birdlife in the study area were documented by direct observations, random walks and opportunistic encounters following Agardi, T.,*et al* 2005. Identification manuals and field guides by Balasubramanian, P., *et al* 2004 and Rahmani, A.R., *et al* 2009 were used during survey. Common and scientific names of the birds following Buckton, S., 2007 and COP 11, 2012 were adopted. The birds were categorized as Resident (R), Migratory (M), Aquatic (A) and Terrestrial (T) as per Balachandran, S., 2006 and Xu Hanqiu, 2006. All the birds species recorded during the present study were tabulated giving their scientific name, family, IUCN (2022) status & legal status if any. Abundance of the recorded species are documented based on the total sightings during the study period as common (more than 10 sightings), uncommon (3-5 sightings), and rare (1-2 sightings). The checklist of species with their status was given. The numbers of migratory birds are maximum during December, January and starts reducing from February onwards.

Results:

Towards improvement of birds habitat, mounds and bunds are planted with tree species such as *Acacia nilotica* (Babul), *Azadirachta indica* (Neem), *Tamarindus indicus* (Tamarind/Imli) *Prosophus* sps, *Ficus glomerata*, *Ficus benghalensis*,*Phoenix sylvestris* (Wild date palm), *Sygium cumini, Pongamia pinnata, Samania saman,, Calophyllum* sps. *Mimusops elegi* etc., for roosting and nesting of the wetland birds like *Pelicans, Painted storks, Herons, Egrets*, *Cormorants*, etc. Artificial perches with logs of wood, bamboo have been provided as vantage points for diving birds like Kingfisher, Darters, and Raptors etc.

Table.-1. Overall season wise variations of small wading bird density (No./ha) recordedfrom January 2021 to December 2022. (Values are Mean ± SE).

S.No	Small Wading birds	Seasons (January 2021 - December 2022)			
		Pre-Monsoon	Monsoon	Post-Monsoon	Summer
1	*Pelecanus onocrotalus*	0.2±0.12	14.02±7.42	19.7±11.20	0
2	*Halcyon smyrnensis*	37.2±6.98	27.5±7.68	59.7±27.15	13.5±2.68
3	*Fulica atra*	5.1±3.48	12.3±8.51	7.1±5.28	0.04±0.03
4	*Bubulcus ibis*	3.5±0.75	0.2±0.18	15.2±12.86	0
5	*Microcarbo niger*	0	2.4±0.82	0	0.5±0.67
6	*Marsh sandpiper*	35.0±0.58	26.1±0.52	58.2±20.9	0
7	*Columba livia*	4.2±2.52	0.4±0.73	10.2±6.84	0
8	*Vanellus indicus*	5.8±5.01	3.1±1.14	1.9±0.8	1.02±1.05
9	*Ardeola grayii*	18.7±4.56	19.7±6.42	12.9±3.8	24.4±3.72
10	*Alcedo atthis*	1.4±0.48	0.3±0.13	3.5±2.78	0.1±0.20

Table.-2. Overall season wise variations of small wading birds density, diversity and richness recorded from January 2021 to December 2022. (Values are Mean ± SE).

S. No	Small wading birds	Pre-monsoon	Monsoon	Post-monsoon	Summer
1	Density (No./ha)	77.3±08.23	63.5±22.54	152.4±59.58	44.2±9.64
2	Diversity (H)	0.08±0.007	0.06±0.002	0.04±0.008	0.04±0.003
3	Richness(No. of species)	5.1±0.56	3.8±0.47	3.2±0.78	2.5±0.45

Table- 3. Analysis of variance showed the impact of season in relation to density, diversity and richness of small wading birds studied from January 2021 to December -2022.

S. No	Small wading birds	Sum of Squares	df	Mean Square	F	p
1	Density (No./ha)	281.458	4	78721.875	3.597	0.028
2	Diversity (H′)	0.007	4	0.005	2.23	0.089
3	Richness (No. of species)	48.578	4	20.505	2.781	0.01

January, 2021 to December, 2022 a total of ten species were reported for plover and sandpiper. The monsoon period (27.5±7.68/ha.) and pre monsoon period (37.2±6.98/ha.) *Halcyon smyrnensis* to have highest density *Pelecanus onocrotalus* and *Vanellus indicus* presence was found in all the seasons for both years. From the 10 species, the *Marsh sandpiper* was recorded only during the January, 2021 to December, 2022 period the value of 58.2±20.9 /ha of post- monsoon period. *Microcarbo niger* was not spotted during this period. All the ten species were the birds sighted in the period of January, 2021 to December, 2022.

During the monsoon period the overall bird density was noted maximum during period January, 2021 to December, 2022 (112.3±48.52and 196 .12±54.247/ha.). Highest diversity was at monsoon period of two years. Bird species richness was maximum during the monsoon period of first year and pre-monsoon period of the second year. The diversity, species, and density, varied significantly between the years and among the seasons ($P<0.05$).

DISCUSSION:

This study records ten species of coastal birds i.e. plover and sandpipers in the Kondakarla Ava wetland during 2021-2022. This is a remarkable finding among inland wetlands of India. Insufficient invertebrate prey in the coastal wetlands compels the shorebirds to shift their habitat and forage on inland wetland habitats. Inland wetlands provide the energetic demands of coastal birds; enable them to build up nutrient reserves for their breeding activities (Almeida *et al.* (2021). Loss of invertebrate prey species in the coastal wetlands maybe due to degradation of coastal wetlands by increase in

anthropogenic pressure, such as conversion of mudflats for aquaculture practices, agricultural purposes, and other human activities (Bharatha Lakshmi, B., 2006 & 2008). This progressive loss, lead to the use of new habitats (Rio Conference, 2012). Hence, shifting of water birds, from one habitat to another habitat, could be due to the decline in preferred resources (Wilen, B.O., *et al.,* 2004).

Density dependent factor also drivesthe birds to shift their habitat (Xu Hanqiu, 2006.). Species when unable to respond to fluctuating intertidal food supplies, supplement their diet with prey, from non-intertidal habitats i.e., inland wetlands. Prey populations might be lower in quality, availability or abundant nature in these habitats than on intertidal habitats, and hence, their use might indicate, changes in the intertidal system, such as, declining or varying prey populations (WHO (2022).

The monsoon season reports highest bird density, diversity, and species richness. Birds use the wetlands frequently, during winter season (Van Eeden *et al.* (2020). The prey, is the main resource, for utilization of wetland habitats (Holmes *et al.* (2019), which is abundant during winter season in inland wetlands. The quality of habitat through enriching of prey, and other environmental factors determines the shifting of foraging grounds by water birds and shorebirds during winter season (NASA FIRMS (2022).

Conservation implications

The present study shows that, the shorebirds shift their feeding ground, from coastal mud flats to inland wetlands. Balachandran (2006) reported, the shorebirds population has declined in east-coast and they shift to nearby wetlands, agricultural and inland wetlands. In conservation planning, it is important to understand, habitat switches, its causes, and implications, for species of birds.

Reference:

- Agardi, T., and J. Alder, 2005: Coastal ecosystems in ecosystems and human wellbeing. Vol.1. Current state and trends: analytical approach for assessing ecosystem and human well being. Island Press, Washington, DC. pp. 513-549.
- Almeida et al. (2021) Medidas para a reduçao das capturas acidentais de aves marinhas em artes de pesca. Relatório final da Projeto MedAves Pesca. Sociedade Portuguesa para o Estudo das Aves (unpublished report).
- Balachandran, S., 2006. Decline of Coastal Birds along the South-east Coast of India.
- Balasubramanian, P., and Lalitha Vijayan, 2004: Conservation Strategies and Action Plans for the Avifauna of Tamil Nadu: in Tamil Nadu Biodiversity Strategy and Action Plan-Cordate Diversity (Edr. R. Annamalai). 76-99.
- Bharatha Lakshmi, B., 2006: Avifauna of Gosthani Estuary of Visakhapatnam. J. Natcon, 18(2) 291-364
- Bharatha Lakshmi, B., 2010: Biodiversity of Kambalakonda Wildlife Sanctuary, Visakhapatnam, Andhra Pradesh. ANU Journal of Natural Sciences. Pg 1-21.
- Buckton, S., 2007: Managing wetlands for sustainable livelihoods at KoshiTappu. Danphe 16, 12-13

- COP 11, 2012: Eleventh meeting of the Conference of the Parties to the Convention on Biological Diversity 2012: Hyderabad, India, 8 - 19 October.
- Holmes *et al.* (2019) PLOS ONE 14(3): e0212128 IFC (2019) International Finance Corporation's Guidance Note 6: Biodiversity Conservation and Sustainable Management of Living Natural Resources. IFC.
- IUCN (2022) Summary Statistics. Available at: https://www.iucnredlist.org/resources/summarystatistics#Summary%20Tables.
- NASA FIRMS (2022) Active Fire Data. Available at: https://www.earthdata.nasa.gov/learn/find-data/nearreal-time/firms/active-fire-data.
- Rahmani, A.R., and A. Rajavanshi, 2009: Report based on the visit to Naupada Swamp and the project site of the 2640 MW Bhavanapadu Thermal Power Plant. pp. 38.
- Rio Conference, 2012: Sustainable Development report from Brundtland.
- Van Eeden et al. (2020) Impacts of the unprecedented 2019-20 bushfires on Australian animals. WWF-Australia.
- Wilen, B.O., and Bates, M.K, 2004: The U.S Fish and Wildlife Service‟s National Wetlands InventoryProject.PlantEcology.118:1-2:m153-169.
- WHO (2022) Available at: https://www.who. int/emergencies/disease-outbreak-news/ item/2022-E000111.
- Xu Hanqiu, 2006. Modification of normalised difference water index (NDWI) to enhance open water features in remotely sensed imagery. International Journal of Remote Sensing, 7, pp. 3025-\

processes

MDPI

Article

Nonlinear Analysis of Cross Rolls of Electrically Conducting Fluid under an Applied Magnetic Field with Rotation

Y. Rameshwar [1], G. Srinivas [2], A. Krishna Rao [1], U. S. Mahabaleshwar [3] and D. Laroze [2,*]

[1] Department of Mathematics, University College of Science, Osmania University, Hyderabad 500007, India; rameshwar@osmania.ac.in (Y.R.); alaka999@gmail.com (A.K.R.)
[2] Instituto de Alta Investigación, Universidad de Tarapacá, Casilla 7 D, Arica 1000000, Chile; gsrinivas@academicos.uta.cl
[3] Department of Mathematics, Shivagangotri, Davangere University, Davangere 577007, India; u.s.m@davangereuniversity.ac.in
* Correspondence: dlarozen@academicos.uta.cl

Abstract: The proposed planer layer dynamo physical model has real-world applications, especially in the Earth's liquid core. Thus, in this paper, an attempt is made to understand the finite amplitude convection when there exists a coupling between the Lorentz force and the Coriolis force. In particular, the effect of a horizontally applied magnetic field is studied on the Rayleigh–Bénard convection (RBC) that contains the electrically conducting fluid and rotates about its vertical axis. Free–free boundary conditions are assumed on the geometry. Attention is focused on the nonlinear convective flow behavior during the occurrence of cross rolls which are perpendicular to the applied magnetic field and parallel to the rotation axis. The visualization of cross rolls is achieved using the Fourier analysis of perturbations up to the $O(\varepsilon^8)$. The relationship of the Nusselt number (Nu) with respect to the Rayleigh number (R), the Ekman number (E), and the Elsasser number (Λ) is investigated. It is observed that E generates a strong damping effect on the flow velocity and on the heat transfer at high rotation rates. Using the heatline concept, it is observed that the temperature within the central regime is enhanced as the Λ increases. The results show that either E decreases or Λ increases, then the heat transfer rate increases.

Keywords: nonlinear convection; earth's liquid core; electrically conducting fluid; planar layer dynamos; cross rolls

Citation: Rameshwar, Y.; Srinivas, G.; Rao, A.K.; Mahabaleshwar, U.S.; Laroze, D. Nonlinear Analysis of Cross Rolls of Electrically Conducting Fluid under an Applied Magnetic Field with Rotation. *Processes* **2023**, *11*, 1945. https://doi.org/10.3390/pr11071945

Academic Editor: Ottavia Giuffrè

Received: 18 April 2023
Revised: 13 June 2023
Accepted: 22 June 2023
Published: 27 June 2023

1. Introduction

In astrophysical and geophysical models related to the Sun, stars, and the outer core of Earth, the convection is affected by both the Coriolis and Lorenz forces. Such a rotating magnetoconvection model with Boussinesq approximation has been studied by many authors, for example, Chandrasekhar [1], Roberts [2], and Cox and Matthews [3], etc. The linear stability analysis of this model shows the system is unstable with respect to either stationary convection or oscillatory convection and depends on the governing physical parameters, namely, Rayleigh number (R), Chandrasekhar number (Q), Taylor number (Ta), thermal Prandtl number (Pr), and magnetic Prandtl number (Pm) or Roberts number. Most of the experimental studies on Rayleigh–Bénard convection (RBC), rotating Rayleigh–Bénard convection, magnetoconvection, and rotating magnetoconvection (RMC) have focused on heat transfer laws. When the control parameter R exceeds its critical value, a cellular regime of steady convection starts to appear. In addition, the motion increases its intensity but remains laminar and steady for a large range of values of R, followed by unsteady turbulent convection. Finite amplitude cellular convection with better approximate solutions has been studied for RBC by Malkus and Veronis [4] and Kuo [5].

In *RBC* with $Ta \neq 0$ and $Q \neq 0$, the critical R ($= R_c$) remains approximately a constant until Q reaches a certain value. When Q increases further, R_c starts to decrease, reaches a minimum and again starts to increase (Chandrasekhar, [1]). Braginsky [6] also studied these rotating magnetic systems and stressed the importance of the Archimedean, magnetic, and Coriolis forces. He revealed that these forces, together with the pressure gradient, would determine the dynamic balance and inertial forces. Eltayeb [7] considered the linear stability analysis to analyze the convection in the hydromagnetic rotating layer. He observed when the principle of exchange of stabilities is valid, four different models can be classified based on the relative directions of the constant magnetic field, B_0 and Ω, (B_0, Ω) namely, (vertical, vertical); (horizontal, vertical); (horizontal, horizontal); (vertical, horizontal) and also for different types of boundaries. The numerical results indicated that the asymptotic dependence of R_c on Ta and Q are equal and independent of the nature of the boundary conditions considered. Later, Eltayeb [8] extended his previous model [7] to study the convective motions near the onset of oscillatory convection. He classified three different motions near the onset, namely: (i) $Ta > Q$, the results for the rotating non-magnetic case, which are retained to leading order; (ii) $Q > Ta$, the results are similar to those for the magnetic non-rotating case to leading order; and (iii) Ta and Q are of same order, the minimum temperature gradient required for the instability is greatly reduced. When these solutions were examined in detail, it was observed that the motions that follow the onset of instability depended primarily on the electrical conductivity rather than on the kinematic properties of boundaries. In addition, in the leading order, the boundary conditions to be applied to the mainstream solutions depended on the conductivity of the boundary but not on the no-slip conditions. When either of the magnetic field or rotation were dominant, there was a possibility of the occurrence of two-dimensional motion. In this case, the Taylor–Proudman theorem was satisfied, while when both magnetic field and rotation were influential, this theorem was no longer valid and the motions were essentially of three-dimensional in nature.

The important laboratory experiments on *RBC*, rotating *RBC* and magnetoconvection *RBC* using the liquid gallium ($Pr = 0.025$) as the working fluid have been carried out by Aurnou and Olson [9]. The properties of liquid gallium are similar to those of the liquid iron in the Earth core. The studies of magnetoconvection have vast industrial applications too [10,11]. The R_c for the magnetoconvection is experimentally determined as a function of Q and Ta. At low rotation rates, the R_c increases linearly with magnetic field intensity. At moderate rotation rates, coherent thermal oscillations were detected by Aurnou and Olson [9] near the onset of convection. These experimental results at the onset were compared with the theoretical predictions of Chandrasekhar [1]. In nearly all of the experimental results, it was mentioned that no well-defined steady convective regime was found. Instead, unsteady or turbulent convection was detected just after onset. Later, these experimental predictions were reproduced by using direct numerical simulations near the onset (Rani et al. [12]). These simulations showed the occurrence of interesting cell patterns. The most relevant geodynamo models were given by Roberts and Jones [13], who extended the model of Braginsky [14] with two sets of boundary conditions.

The present nonlinear convection problem is studied based on the plane layer model proposed by Roberts and Jones [13]. In astrophysics and even in planetary physics, the model considered by Roberts and Jones [13] is yet sufficiently close to reality and is, really, heuristic. This model is very convenient for laboratory experiments, too, which have not yet been done. The linear planer layer dynamo model was considered by Roberts and Jones [13] with the limiting case of Prandtl number tending to infinity. This limiting case enabled the removal of the inertial terms and thus the resultant linearized equation of motion filtered the fast-inertial modes and Alfven waves. The main reason for considering this limiting case was that it simplified the analysis considerably and could able to exhibit an amazingly rich structure. The other motivation was that it is an important limit for geodynamo modelling, in which fast modes are believed to be relatively unimportant.

In the linear stability analysis of the planer layer problem [13], the effect of physical parameters such as E, Λ, R, and q have been thoroughly studied for the occurrence of parallel rolls, cross rolls, and oblique rolls at the onset of convection. In general, E and $q \ll 1$ represent the geophysical models but with these values, it is very difficult to simulate these models and obtain the converged results. This difficulty can be overcome by using one of the approximate methods, such as weakly nonlinear analysis, which yields comparable results with the experimental observations. This method of weakly nonlinear analysis was applied for the Braginsky [14] model by Roberts and Stewartson [15] near the onset of oscillatory convection using the small finite amplitude equations. Further, they have analyzed the linear stability analysis of the cubic and cubic-quintic amplitude equations. These amplitude equations are valid only when R is close to the R_c. In addition, the nonlinear analysis proposed by Malkus and Veronis [4] is valid when the R is near the threshold R_c. Later Kuo [5] proposed a different nonlinear approach, which is valid even for large values of R. The advantages of this approach are that the solutions are found to be valid even for a large range of the imposed temperature differences across the fluid layer and also the rapid convergence of solutions. This solution provides a quantitative theory for the convective heat transport as a function of the temperature difference in the range of laminar flow. Using this approach by Kuo [5], Rameshwar et al., [16], have studied the finite amplitude cellular convection in RBC under the influence of a vertical magnetic field and analyzed the magnetohydrodynamics (MHD) of electrically conducting fluid. Linear and nonlinear properties of thermohaline convection at the onset with the stress-free boundary conditions were investigated using perturbation analysis relevant to oceanic water and groundwater by Rawoof Sayeed and Rameshwar [17]. The stationary and oscillatory finite amplitude convections of a binary mixture with a porous medium were thoroughly investigated by Rameshwar et al., [18,19]. Baklouti et. al. [20] studied the dynamics of incompressible homogeneous turbulence by numerical simulations. Gupta et. al. [21] have analytically examined the effect of rotational speed modulation on the onset of magneto-thermal convection.

The extension studies related to geodynamo models proposed by Eltayeb [7,8], Roberts and Jones [13], and Jones and Roberts [22] have been studied by Šoltis and Brestenský [23]. The authors Šoltis and Brestenský [23] studied the influence of anisotropic diffusive coefficients (thermal diffusion and viscosity) on marginal stability of the horizontal fluid planar layer rotating about the vertical axis and permeated by a horizontal homogeneous magnetic field. The linear stability analysis was thoroughly investigated by the authors for two different types of anisotropic diffusive coefficients. This model was further extended to study the linear stability of the model of rotating magnetoconvection in the horizontal planar layer dynamo by Filippi et al. [24], which is influenced by three anisotropic diffusivities, such as viscosity, thermal diffusivity, and magnetic diffusivity.

In the present study, the nonlinear analysis was employed as proposed by Kuo [5] to study the behavior of cross rolls of electrically conducting fluid in a rotating magnetic system, given by Roberts and Jones [13]. Thus, the objectives of the present problem were as follows:

- Investigate theoretically the nonlinear behavior of cross rolls which occur in the vertically rotating Rayleigh–Bénard convective system of planar layer of electrically conducting fluid in the presence of horizontal magnetic field;
- Solve the nonlinear partial differential equations using the perturbation method proposed by Kuo [5], until the $O(\varepsilon^8)$ and obtain the approximate solutions;
- Obtain the combined effect of Lorenz and Coriolis forces with stress-free boundaries;
- Find the local (N_L) and average (Nu) Nusselt numbers on the hot wall to understand the development of heat flow and the rate of heat transfer, respectively;
- Obtain the cellular pattern of the fluid flow (streamlines) and hot regions (isotherms) from the eigenfunctions related to stream function and temperature, respectively;
- Study the heatline patterns of the flow by using the heat function.

The novelty of the present work is the study of finite amplitude cellular convection when the stationary convection exists as a first instability. The dynamical behavior of the system depends on the type of instabilities that occur in that system. Interesting convective instabilities occur near the onset of convection which is analyzed from the linear stability analysis. At the onset of convection, the system is unstable to either stationary convection (at least one eigenvalue vanishes) or oscillatory convection (an eigenvalue with a purely imaginary part) as a first instability. When an eigenvalue vanishes the principle of exchange of stabilities occurs. In other words, a new steady state replaces the stable motionless state of the fluid. When stationary convection exists, the continuous release of potential energy is balanced by the viscous dissipation of mechanical energy and the convection always occurs in a fairly regular pattern. The results from the linear stability analysis of Roberts and Jones [13] show the occurrence of the modes such as parallel rolls, cross rolls, and oblique rolls based on the wave numbers. Only stationary convection exists as a first instability when the parallel rolls occur, but for the modes of cross rolls and oblique rolls, both stationary convection and oscillatory convection can occur as a first instability depending on the physical parameters. A detailed investigation of the linear stability analysis of the present physical model has been studied by Roberts and Jones [13]. Hence, the nonlinear dynamical behavior of the present considered physical model is investigated when stationary convection exists.

In Section 2, the basic governing equations that are considered by Roberts and Jones [13] are presented. The linear stability analysis is discussed in Section 3 to obtain critical Rayleigh numbers for steady cross roll modes. The nonlinear solutions for the field variables are presented in Section 4. In Section 5, the local Nusselt number (N_L) and average Nusselt number (Nu) are discussed. The distortion of streamlines and isotherms is discussed in Section 6. The heat flow visualization is discussed in Section 7. Finally, the conclusions are presented in Section 8.

2. Mathematical Model

In the present study the fluid with uniform density confined in an infinite horizontal layer was considered. It was assumed that the whole configuration rotates about the vertical axis (OZ) with angular velocity $\vec{\Omega}(= \Omega\vec{1}_Z)$ in the presence of a uniform gravitational field $\vec{g}$ $(= g\vec{1}_Z)$ and the uniform magnetic field $\vec{B}(= B_0\vec{1}_X)$ applied in the horizontal direction where $\vec{1}_X$ is the unit vector along the X-axis and $\vec{1}_Z$ is the unit vector along Z-axis. The Prandtl number is assumed to be large, so as to ignore the inertial forces in the momentum equation in comparison to the Coriolis force [13]:

$$2\vec{\Omega}\rho_0 \times \vec{V}' = -\nabla' P' + \vec{J}' \times \frac{\vec{B}'}{\mu_m} + \vec{g}\alpha\rho_0 T' + \mu\nabla'^2\vec{V}', \tag{1}$$

$$\frac{\partial \vec{B}'}{\partial t'} = \nabla' \times (\vec{V}' \times \vec{B}') + \eta\nabla'^2\vec{B}', \tag{2}$$

$$\frac{\partial T'}{\partial t'} + \vec{V}' \cdot (\nabla' T') = \kappa\nabla'^2 T', \tag{3}$$

$$\nabla' \cdot \vec{V}' = 0, \tag{4}$$

$$\nabla' \cdot \vec{B}' = 0, \tag{5}$$

where P' includes the centrifugal force, $\vec{J}' = \nabla' \times \vec{B}'$ is the electric current density, and other notations are given the nomenclature.

We non-dimensionalized the Equations (1)–(5) using the corresponding length, time, velocity, temperature, magnetic field, and pressure scales as d, $\frac{d^2}{\eta}$, $\frac{\eta}{d}$, βd, B_0, and $2\Omega\rho_0\eta$, respectively.

Therefore, the non-dimensional governing equations are [13]:

$$\vec{1}_Z \times \vec{V} = -\nabla P + \Lambda \vec{J} \times \vec{B} + qR\, T\vec{1}_Z + E\nabla^2\vec{V}, \tag{6}$$

$$\frac{\partial \vec{B}}{\partial t} = \nabla \times (\vec{V} \times \vec{B}) + \nabla^2\vec{B}, \tag{7}$$

$$\frac{\partial T}{\partial t} + \vec{V} \cdot (\nabla T) = q\nabla^2 T, \tag{8}$$

$$\nabla \cdot \vec{V} = 0, \tag{9}$$

$$\nabla \cdot \vec{B} = 0, \tag{10}$$

where $R = \beta g \alpha d^2/2\Omega k$ is the modified Rayleigh number, which measures the ratio of buoyancy force to Coriolis force, $E = \nu/2\Omega d^2$ is the ratio of viscous and Coriolis forces, $\Lambda = B_0^2/2\Omega\eta\mu_m\rho_0$ is the ratio of magnetic force and Coriolis force, and $q = \kappa/\eta$ is the ratio between the thermal and magnetic diffusivities (the Roberts number). For the static solutions from Equations (6)–(10), we obtain

$$\vec{V}_s \equiv \vec{0}, \;\; \vec{B}_s = \vec{1}_X, \;\; T_s = -Z. \tag{11}$$

After introducing the following perturbed quantities in the above static solutions, we obtain

$$\vec{V} = \vec{V}_s + \vec{V}^*, \;\; \vec{B} = \vec{B}_s + \vec{b}^*, \;\; T = T_s + \frac{\theta^*}{q}. \tag{12}$$

For convenience the asterisk symbols are omitted in the further analysis. The perturbed dimensionless governing equations are given by

$$E\nabla^4 W - \frac{\partial \omega_Z}{\partial Z} + R{\nabla_h}^2\theta + \Lambda\frac{\partial}{\partial X}\nabla^2 b_Z = \Lambda\vec{1}_Z \cdot \nabla \times \{\nabla \times [(\nabla \times \vec{b}) \times \vec{b}]\}, \tag{13}$$

$$\left(\frac{\partial}{\partial t} + \vec{V} \cdot \nabla\right)\theta - qW - q\nabla^2\theta = 0, \tag{14}$$

$$\left(\frac{\partial}{\partial t} - \nabla^2\right) b_Z = \frac{\partial W}{\partial X} + \vec{1}_Z \cdot \nabla \times (\vec{V} \times \vec{b}), \tag{15}$$

$$\left(\frac{\partial}{\partial t} - \nabla^2\right) J_Z = \frac{\partial \omega_Z}{\partial X} + \vec{1}_Z \cdot \nabla \times [\nabla \times (\vec{V} \times \vec{b})], \tag{16}$$

$$E\nabla^2\omega_Z + \Lambda\frac{\partial J_Z}{\partial X} + \frac{\partial W}{\partial Z} + \Lambda\vec{1}_Z \cdot \nabla \times \; [(\nabla \times \vec{b}) \times \vec{b}] = 0, \tag{17}$$

where

$$\nabla_h^2 = \tfrac{\partial^2}{\partial X^2} + \tfrac{\partial^2}{\partial Y^2}, \;\; \nabla^2 = \tfrac{\partial^2}{\partial X^2} + \tfrac{\partial^2}{\partial Y^2} + \tfrac{\partial^2}{\partial Z^2}, \;\; \vec{V} = (U, V, W), \;\; \vec{b} = (b_X, b_Y, b_Z), \;\; J_Z = (\nabla \times \vec{b}) \cdot \vec{1}_Z, \;\; \omega_Z = (\nabla \times \vec{V}) \cdot \vec{1}_Z \;\; .$$

Eliminating θ, ω_Z, b_Z, and J_Z from the linear part of Equations (13)–(17), we obtain

$$\mathcal{L}W = \mathcal{N}, \tag{18}$$

$$\mathcal{L} = \mathcal{L}_1 + \mathcal{L}_2 + \mathcal{L}_3 + \mathcal{L}_4 + \mathcal{L}_5 + \mathcal{L}_6,$$

and

$$\mathcal{N} = \mathcal{N}_1 + \mathcal{N}_2 + \mathcal{N}_3 + \mathcal{N}_4 + \mathcal{N}_5,$$

where

$$\mathcal{L}_1 = \left(\frac{\partial}{\partial t} - q\nabla^2\right)\left(\frac{\partial}{\partial t} - \nabla^2\right)^2 \frac{\partial^2}{\partial Z^2},$$

$$\mathcal{L}_2 = E^2\left(\frac{\partial}{\partial t} - q\nabla^2\right)\left(\frac{\partial}{\partial t} - \nabla^2\right)^2 \nabla^6,$$

$$\mathcal{L}_3 = 2E\Lambda\left(\frac{\partial}{\partial t} - q\nabla^2\right)\left(\frac{\partial}{\partial t} - \nabla^2\right)\left(\frac{\partial^2}{\partial X^2}\right)\nabla^4,$$

$$\mathcal{L}_4 = \Lambda^2\left(\frac{\partial}{\partial t} - q\nabla^2\right)\left(\frac{\partial^4}{\partial X^4}\right)\nabla^2,$$

$$\mathcal{L}_5 = RqE\left(\frac{\partial}{\partial t} - \nabla^2\right)^2 \nabla^2 {\nabla_h}^2,$$

$$\mathcal{L}_6 = Rq\Lambda\left(\frac{\partial}{\partial t} - \nabla^2\right)\left(\frac{\partial^2}{\partial X^2}\right){\nabla_h}^2,$$

and

$$\mathcal{N}_1 = \left[ER\left(\frac{\partial}{\partial t} - \nabla^2\right)^2 \nabla^2 {\nabla_h}^2 + R\Lambda\left(\frac{\partial}{\partial t} - \nabla^2\right)\left(\frac{\partial^2}{\partial X^2}\right){\nabla_h}^2\right](\vec{V}\cdot\nabla)\theta,$$

$$\mathcal{N}_2 = -\left[E\Lambda\left(\frac{\partial}{\partial t} - q\nabla^2\right)\left(\frac{\partial}{\partial t} - \nabla^2\right)\nabla^4\frac{\partial}{\partial X} + \Lambda^2\left(\frac{\partial}{\partial t} - q\nabla^2\right)\left(\frac{\partial^3}{\partial X^3}\right)\nabla^2\right]\vec{1}_Z\cdot\nabla\times(\vec{V}\times\vec{b}),$$

$$\mathcal{N}_3 = -\left[\Lambda\left(\frac{\partial}{\partial t} - q\nabla^2\right)\left(\frac{\partial}{\partial t} - \nabla^2\right)\left(\frac{\partial^2}{\partial X\partial Z}\right)\right]\vec{1}_Z\cdot\nabla\times[\nabla\times(\vec{V}\times\vec{b})],$$

$$\mathcal{N}_4 = \left[\Lambda^2\left(\frac{\partial}{\partial t} - q\nabla^2\right)\left(\frac{\partial}{\partial t} - \nabla^2\right)\frac{\partial^2}{\partial X^2}\right]\vec{1}_Z\cdot\nabla\times\nabla\times[(\nabla\times\vec{b})\times\vec{b})]$$

$$+\left[E\Lambda\left(\frac{\partial}{\partial t} - q\nabla^2\right)\left(\frac{\partial}{\partial t} - \nabla^2\right)^2\nabla^2\right]\vec{1}_Z\cdot\nabla\times\nabla\times[(\nabla\times\vec{b})\times\vec{b})],$$

$$\mathcal{N}_5 = -\left[\Lambda\left(\frac{\partial}{\partial t} - q\nabla^2\right)\left(\frac{\partial}{\partial t} - \nabla^2\right)^2\frac{\partial}{\partial Z}\right]\vec{1}_Z\cdot\nabla\times[(\nabla\times\vec{b})\times\vec{b})].$$

Because the surfaces are maintained at a uniform temperature,

$$\theta = 0 \text{ on } Z = 0 \text{ and } 1, \text{ for all } X, Y, \tag{19}$$

and also normal component of the velocity should vanish on boundaries, i.e.,

$$W = 0 \text{ on } Z = 0 \text{ and } 1, \text{ for all } X, Y. \tag{20}$$

The conditions Equations (19) and (20) are independent of the nature of boundaries, such as free–free or rigid–rigid, etc. In the present work, we assumed stress-free boundary conditions [1], hence we obtain

$$\frac{\partial^2 W}{\partial Z^2} = \frac{\partial \omega_Z}{\partial Z} = 0 \text{ on } Z = 0 \text{ and } 1, \text{ for all } X, Y, \tag{21}$$

$$J_X = J_Y = \frac{\partial J_Z}{\partial Z} = 0 \text{ on } Z = 0 \text{ and } 1, \text{ for all } X, Y. \tag{22}$$

Since the physical system is a triple diffusive system, it is unstable to either stationary convection or oscillatory convection near the onset.

3. Linear Stability Analysis

At the onset of convection, the existing perturbations in the system are very small. Hence, the nonlinear terms are smaller when compared to linear terms. The nonlinear contributions are neglected from Equation (18). We obtain a linear differential equation which is given as $\mathcal{L}W = 0$. This process is called linearization. We obtain

$$\begin{aligned}
&[(\frac{\partial}{\partial t} - q\nabla^2)(\frac{\partial}{\partial t} - \nabla^2)^2 \frac{\partial^2}{\partial Z^2} + E^2(\frac{\partial}{\partial t} - q\nabla^2)(\frac{\partial}{\partial t} - \nabla^2)^2\nabla^6 \\
&+2E\Lambda(\frac{\partial}{\partial t} - q\nabla^2)(\frac{\partial}{\partial t} - \nabla^2)(\frac{\partial^2}{\partial X^2})\nabla^4 + \Lambda^2(\frac{\partial}{\partial t} - q\nabla^2)(\frac{\partial^4}{\partial X^4})\nabla^2 \\
&+R(qE(\frac{\partial}{\partial t} - \nabla^2)^2\nabla^2{\nabla_h}^2 + q\Lambda(\frac{\partial}{\partial t} - \nabla^2)(\frac{\partial^2}{\partial X^2}){\nabla_h}^2)]W = 0.
\end{aligned} \tag{23}$$

The resulting Equation (23) is linear. The normal mode solution was considered as $W(X, Y, Z, t) = W(Z)e^{i(aX+lY)+pt}$, where a is the wavenumber along X direction and l is the wavenumber along Y direction. As such, a and l are real numbers and the growth rate (p) may be constant complex number [13]. The marginal state is obtained from $Re(p) = 0$. The two types of modes are classified using the eigenvalue p, namely, if $Im(p) = 0$, then the steady modes exist and if $Im(p) = \omega \neq 0$, then the oscillatory convection exists. The preferred mode of convection depends on the physical parameters, which are relevant to the Earth's outer core. In Earth's outer core, the parameters E and q are considered as small and the Prandtl number is large. The orientation of rolls is classified based on the wavenumber. The modes are parallel rolls, if the wavenumber $a = 0$ (the axis of rolls are parallel to the applied magnetic field), if the wavenumber $l = 0$, gives the cross rolls (the axis of the rolls are perpendicular to the applied magnetic field) and if both the wavenumbers $a \neq 0$ and $l \neq 0$ give the oblique rolls. The linear and nonlinear studies of the present physical model are based on $l = 0$, i.e., cross rolls.

The physical parameters E, Λ, q, and R are used to study the linear and nonlinear behavior of the convective system. As the temperature gradient is increased, the unstable mode may be of stationary convection or oscillatory convection near the onset. We implemented the linear stability analysis using the normal mode analysis, i.e., by substituting $W(X, Y, Z, t) = W(z)e^{(iaX+pt)}$ in the linearized equation $\mathcal{L}W = 0$.

Stationary Convection ($\omega = 0$)

By solving the linearized Equation (23), $R = R_s$ value is obtained for stationary convection and is given by

$$R = \frac{\pi {d_2}^2 + d_2(E{d_2}^2 + \Lambda a^2)^2}{a^2(E{d_2}^2 + \Lambda a^2)},$$

where $d_2 = a^2 + \pi^2$. The critical value of R is obtained from $\partial R/\partial a = 0$. The critical wavenumber is given by $a^2 = {a^2}_{cs} = 2\pi^2$, and the critical Rayleigh number for stationary convection is

$$R_{cs} = \frac{9\pi^5 + 3\pi^2(9E\pi^4 + 2\Lambda\pi^2)^2}{2\pi^2(9E\pi^4 + 2\Lambda\pi^2)}. \tag{24}$$

From the above result the marginal Rayleigh number (R_{cs}), E, and Λ values are obtained for high rotation rates and weak field [13] by the linear stability analysis. The critical values of control parameters were obtained to study the nonlinear behavior of cross rolls. For small values of q, stationary convection occurs and for large values of q oscillatory convection can occur. The value of R_s is free from q while the finite amplitudes depend on q. For the nonlinear studies, a fixed q value as 0.01 was considered for which the stationary convection occurs as a first instability near the onset. For small values of the parameters E and Λ, the minimum value R_{cs} decreases as E decreases and as Λ increases. Thus, the effect of E destabilizes the convective system when E decreases and the effect of Λ destabilizes the convective system when Λ increases (see Figure 1).

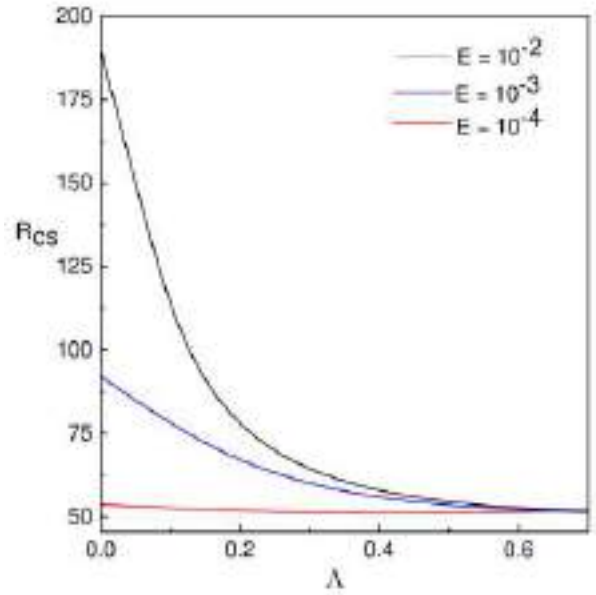

Figure 1. The effect of Λ and E on R_{cs}.

The linear stability theory adopts a less ambitious objective to ascertain when a flow is unstable to infinitesimal disturbances. It thus gives no prediction about transition promoted by sufficiently large disturbance. The ultimate consequence of the instability is never completely determined by linear theory. Thus, in the present study, an attempt was made to understand the nonlinear convection in the presence of the Coriolis force and magnetic field.

4. Method of Solution

The solutions of steady non-linear equations were obtained by following the method proposed by Kuo [5]. These solutions converge more rapidly and are valid for larger temperature differences. In this method, the dependent variables are first expressed as infinite series of a set of orthogonal space functions. This approach to the solution sheds light on the problem of transition to turbulent convection, which happens at a larger temperature difference. An expansion parameter (ε), is defined by [5]:

$$\varepsilon^2 = \frac{R - R_{cs}}{R}. \tag{25}$$

Note that ε is less than one for all values of R. The solution of Equations (13)–(17) are written as

$$f = \varepsilon f_1 + \varepsilon^2 f_2 + \varepsilon^3 f_3 + \varepsilon^4 f_4 + \varepsilon^5 f_5 + \varepsilon^6 f_6 + \cdots, \tag{26}$$

where

$$f = f(U, W, \theta, b_X, b_Z, \omega_Z, J_Z).$$

According to Equation (25), R is given by

$$R = \frac{R_{cs}}{1-\varepsilon^2}, \tag{27}$$

expanding Equation (27) in the power series of ε or by applying the finite formula

$$R = R_{cs} + R_{os}(\varepsilon^2 + \varepsilon^4 + \varepsilon^6 + \cdots + \varepsilon^{2s}), \tag{28}$$

where

$$R_{os} = \frac{R_{cs}}{1-\varepsilon^{2s}}, \quad s = 1, 2, 3 \cdots \tag{29}$$

By introducing Equations (26) and (28) in Equation (18), we obtain for the different ε orders, a sequence of linear non homogeneous differential equations as

$$O(\varepsilon): \quad (\mathcal{L}_1 + \mathcal{L}_2 + \mathcal{L}_3 + \mathcal{L}_4)W_1 + R_{cs}(\mathcal{L}_5 + \mathcal{L}_6)W_1 = 0, \tag{30}$$

$$O(\varepsilon^2): \quad (\mathcal{L}_1 + \mathcal{L}_2 + \mathcal{L}_3 + \mathcal{L}_4)W_2 + R_{cs}(\mathcal{L}_5 + \mathcal{L}_6)W_2 = 0, \tag{31}$$

$$\begin{aligned} O(\varepsilon^3): \quad & (\mathcal{L}_1 + \mathcal{L}_2 + \mathcal{L}_3 + \mathcal{L}_4)W_i + R_{cs}(\mathcal{L}_5 + \mathcal{L}_6)W_i + R_{os}(\mathcal{L}_5 + \mathcal{L}_6)W_{i-2} \\ & + R_{os}(\mathcal{L}_5 + \mathcal{L}_6)W_{i-4} = R_{cs}\mathcal{N}_1 + \mathcal{N}_2 + \mathcal{N}_3 + \mathcal{N}_4 + \mathcal{N}_5, \ \text{for} \ i = 3. \end{aligned} \tag{32}$$

Similarly, at the orders $O(\varepsilon^4)$, $O(\varepsilon^5)$, we obtain

$$\begin{aligned} & (\mathcal{L}_1 + \mathcal{L}_2 + \mathcal{L}_3 + \mathcal{L}_4)W_i + R_{cs}(\mathcal{L}_5 + \mathcal{L}_6)W_i + R_{os}(\mathcal{L}_5 + \mathcal{L}_6)W_{i-2} \\ & + R_{os}(\mathcal{L}_5 + \mathcal{L}_6)W_{i-4} = (R_{cs} + R_{os})\mathcal{N}_1 + \mathcal{N}_2 + \mathcal{N}_3 + \mathcal{N}_4 + \mathcal{N}_5, \ \text{for} \ i = 4, 5. \end{aligned} \tag{33}$$

In general,

$$\begin{aligned} & (\mathcal{L}_1 + \mathcal{L}_2 + \mathcal{L}_3 + \mathcal{L}_4)W_i + R_{cs}(\mathcal{L}_5 + \mathcal{L}_6)W_i + R_{os}(\mathcal{L}_5 + \mathcal{L}_6)W_{i-2} \\ & + R_{os}(\mathcal{L}_5 + \mathcal{L}_6)W_{i-4} = (R_{cs} + 2R_{os})\mathcal{N}_1 + \mathcal{N}_2 + \mathcal{N}_3 + \mathcal{N}_4 + \mathcal{N}_5, \ \text{for} \ i \geq 6. \end{aligned} \tag{34}$$

Here $\mathcal{L}_i$, $i = 1, 2, 3, 4, 5, 6$ is the linear operator and $\mathcal{N}_i$, $i = 1, 2, 3, 4, 5$ represents the nonlinear terms and are functions of W_i, θ_i, b_{Xi}, b_{Zi}, ω_{Zi}, and J_{Zi}. The auxiliary equations for temperature field are given by

$$\left(\frac{\partial}{\partial t} - \nabla^2\right)\theta_1 = qW_1, \tag{35}$$

$$\left(\frac{\partial}{\partial t} - \nabla^2\right)\theta_2 + (\vec{V}_1 \cdot \nabla)\theta_1 = qW_2. \tag{36}$$

In general,

$$\left(\frac{\partial}{\partial t} - \nabla^2\right)\theta_i + \sum_{l=1}^{i-1}(\vec{V}_l \cdot \nabla)\theta_{i-l} = qW_i, \ \text{for} \ \ i \geq 3. \tag{37}$$

The auxiliary equations for the magnetic field

$$\left(\frac{\partial}{\partial t} - \nabla^2\right)b_{X_1} = \frac{\partial U_1}{\partial X}. \tag{38}$$

In general,

$$\left(\frac{\partial}{\partial t}-\nabla^2\right)b_{Xi}=\frac{\partial U_i}{\partial X}+\frac{\partial}{\partial Y}\left(U_1b_{Y_{i-1}}+\cdots+U_{i-1}b_{Y_1}-V_1b_{X_{i-1}}\cdots+V_{i-1}b_{X_1}\right)$$
$$+\frac{\partial}{\partial Z}\left(U_1b_{Z_{i-1}}+\cdots+U_{i-1}b_{Z_1}-W_1b_{X_{i-1}}\cdots+W_{i-1}b_{X_1}\right),\ \text{for}\quad i\geq 2, \tag{39}$$

and

$$\left(\frac{\partial}{\partial t}-\nabla^2\right)b_{Z_1}=\frac{\partial W_1}{\partial X}. \tag{40}$$

In general written as:

$$\left(\frac{\partial}{\partial t}-\nabla^2\right)b_{Z_i}=\frac{\partial W_i}{\partial X}-\frac{\partial}{\partial X}\left(U_1b_{Z_{i-1}}+\cdots+U_{i-1}b_{Z_1}-W_1b_{X_{i-1}}\cdots+W_{i-1}b_{X_1}\right)$$
$$-\frac{\partial}{\partial Y}\left(V_1b_{Z_{i-1}}+\cdots+V_{i-1}b_{Z_1}-W_1b_{Y_{i-1}}\cdots+W_{i-1}b_{Y_1}\right)\ \text{for}\quad i\geq 2. \tag{41}$$

Likewise, the auxiliary equations for vorticity are

$$E\nabla^2\omega_{Z_1}=-\frac{\partial W_1}{\partial Z}-\Lambda\frac{\partial J_{Z_1}}{\partial X}, \tag{42}$$

in general,

$$E\nabla^2\omega_{Z_i}=-\frac{\partial W_i}{\partial Z}-\Lambda\frac{\partial J_{Z_i}}{\partial X}-\Lambda\frac{\partial}{\partial X}b_{X_1}\left(\frac{\partial b_{Y_{i-1}}}{\partial X}-\frac{\partial b_{X_{i-1}}}{\partial Y}\right)+\cdots-\Lambda\frac{\partial}{\partial X}b_{X_{i-1}}\left(\frac{\partial b_{Y_1}}{\partial X}-\frac{\partial b_{X_1}}{\partial Y}\right)$$
$$+\Lambda\frac{\partial}{\partial X}b_{Z_1}\left(\frac{\partial b_{Z_{i-1}}}{\partial Y}-\frac{\partial b_{Y_{i-1}}}{\partial Z}\right)+\cdots+\Lambda\frac{\partial}{\partial X}b_{Z_{i-1}}\left(\frac{\partial b_{Z_1}}{\partial Y}-\frac{\partial b_{Y_1}}{\partial Z}\right)$$
$$+\Lambda\frac{\partial}{\partial Y}b_{Z_1}\left(\frac{\partial b_{X_{i-1}}}{\partial Z}-\frac{\partial b_{Z_{i-1}}}{\partial X}\right)+\cdots-\Lambda\frac{\partial}{\partial Y}b_{Z_{i-1}}\left(\frac{\partial b_{X_1}}{\partial Z}-\frac{\partial b_{Z_1}}{\partial X}\right)$$
$$+\Lambda\frac{\partial}{\partial Y}b_{Y_1}\left(\frac{\partial b_{Y_{i-1}}}{\partial X}-\frac{\partial b_{X_{i-1}}}{\partial Y}\right)+\cdots+\Lambda\frac{\partial}{\partial Y}b_{Y_{i-1}}\left(\frac{\partial b_{Y_1}}{\partial X}-\frac{\partial b_{X_1}}{\partial Y}\right),\ \text{for}\quad i\geq 2, \tag{43}$$

and

$$\left(\frac{\partial}{\partial t}-\nabla^2\right)J_{Z_1}=\frac{\partial\omega_{Z_1}}{\partial X}, \tag{44}$$

in general written as:

$$\left(\frac{\partial}{\partial t}-\nabla^2\right)J_{Z_i}=\frac{\partial\omega_{Z_i}}{\partial X}+\frac{\partial^2}{\partial X\partial Z}\left(V_1b_{Z_{i-1}}+\cdots+V_{i-1}b_{Z_1}-W_{i-1}b_{Y_1}-\cdots-W_1b_{Y_{i-1}}\right)$$
$$+\frac{\partial^2}{\partial Y\partial Z}\left(W_{i-1}b_{X_1}+\cdots+W_1b_{X_1}-U_1b_{Z_{i-1}}-\cdots-U_{i-1}b_{Z_1}\right)$$
$$+\nabla_h^2\left(V_1b_{X_{i-1}}+\cdots+V_{i-1}b_{X_1}-U_{i-1}b_{Y_1}-\cdots-U_1b_{Y_{i-1}}\right),\ \text{for}\quad i\geq 2. \tag{45}$$

4.1. Approximate Solutions

The approximate solutions U, W, θ, b_X, and b_Z are attained in terms of the amplitudes near the onset of stationary convection. The horizontal two boundaries are stress-free, all the space functions U, W, θ, b_X, and b_Z are sine and cosine functions. Thus, from Equations (30), (35), (42), and (44) we have, to the first order periodic solutions as,

$$W_1=A_1\cos aX\sin\pi Z,$$
$$\theta_1=\frac{qA_1}{\pi^2+a^2}\cos aX\sin\pi Z,$$

$$b_{X_1} = -\frac{\pi A_1}{\pi^2 + a^2} \cos aX \cos \pi Z,$$
$$b_{Z_1} = -\frac{aA_1}{\pi^2 + a^2} \sin aX \sin \pi Z, \tag{46}$$

where the nonlinear terms are used to calculate the amplitude A_1. Normally, the terms in Equation (26) are written as

$$W_i = A_i \cos aX \sin \pi Z + \sum_{p_1,q_1} W_{p_1q_1}^{(i)} \cos p_1 aX \sin q_1 \pi Z, \tag{47}$$

$$U_i = \frac{1}{a^2} \frac{\partial^2 W_i}{\partial Z \partial X}, V_i = \frac{1}{a^2} \frac{\partial^2 W_i}{\partial Z \partial Y}, \omega_{Z_i} = \frac{\partial V_i}{\partial X}, \tag{48}$$

$$\theta_i = \frac{qA_i}{\pi^2 + a^2} \cos aX \sin \pi Z + \sum_{p_1,q_1} \theta_{p_1q_1}^{(i)} \cos p_1 aX \sin q_1 \pi Z, \tag{49}$$

$$b_{X_i} = -\frac{\pi A_i}{(\pi^2 + a^2)} \cos aX \cos \pi Z + \sum_{p_1,q_1} b_{X\,p_1q_1}^{(i)} \cos p_1 aX \cos q_1 \pi Z, \tag{50}$$

$$b_{Z_i} = -\frac{aA_i}{(\pi^2 + a^2)} \sin aX \sin \pi Z + \sum_{p_1,q_1} b_{Z\,p_1q_1}^{(i)} \sin p_1 aX \sin q_1 \pi Z, \tag{51}$$

where $W_{p_1q_1}^{(i)}$, $\theta_{p_1q_1}^{(i)}$, $b_{X\,p_1q_1}^{(i)}$, and $b_{Z\,p_1q_1}^{(i)}$ are nonlinear functions of A_1, A_2, A_3,... A_{i-1}. The unknown functions $W_{p_1q_1}^{(i)}$, $\theta_{p_1q_1}^{(i)}$, $b_{X\,p_1q_1}^{(i)}$, and $b_{Z\,p_1q_1}^{(i)}$ are calculated by substituting the Equations (47)–(51) in Equation (18).

4.2. Evaluation of Amplitude A_1

To obtain the second order solutions W_2, θ_2, b_{X_2}, and b_{Z_2}, the nonlinear term $\mathcal{N}$ is solved and Equation (31) is obtained. With $\mathcal{N} = 0$, $\mathcal{L}W_2 = 0$ and

$$W_{02}^{(2)} = 0,\ \theta_{02}^{(2)} = \frac{qA_1^2}{8\pi(\pi^2 + a^2)} \text{ and } b_{X\,02}^{(2)} = \frac{A_1^2}{4(\pi^2 + a^2)},\ b_{Z\,02}^{(2)} = 0. \tag{52}$$

The unknown functions W_2, θ_2, b_{X_2}, and b_{Z_2} are obtained from Equations (31), (36), (39), and (41), respectively, and are given by

$$W_2 = A_2 \cos aX \sin \pi Z,$$
$$\theta_2 = \frac{qA_2}{\pi^2 + a^2} \cos aX \sin \pi Z + {\theta_{02}}^{(2)} {A_1}^2 \sin 2\pi Z,$$
$$b_{X_2} = -\frac{\pi A_2}{\pi^2 + a^2} \cos aX \cos \pi Z + {b_{X02}}^{(2)} {A_1}^2 \cos 2\pi Z,$$
$$b_{Z_2} = -\frac{aA_2}{\pi^2 + a^2} \sin aX \sin \pi Z. \tag{53}$$

From Equation (32) for $i = 3$ the amplitude A_1 is calculated. After using the first and second order solutions, we write Equation (32) as

$$(\mathcal{L}_1 + \mathcal{L}_2 + \mathcal{L}_3 + \mathcal{L}_4)W_3 + R_{cs}(\mathcal{L}_5 + \mathcal{L}_6)W_3$$
$$= -R_{os}[qE(\pi^2 + a^2)^3 a^2 + q\Lambda(\pi^2 + a^2)a^4]$$
$$A_1 \cos aX \sin \pi Z - R_{cs}[E{d_2}^3 a^2 + \Lambda d_2 a^4]\pi {\theta_{02}}^{(2)} {A_1}^3 \cos aX \sin \pi Z$$

$$
\begin{aligned}
&-[a^2 {b_{X02}}^{(2)} E\Lambda q {d_2}^4 + a^4 {b_{X02}}^{(2)} \Lambda^2 q {d_2}^2]\frac{{A_1}^3}{2}\cos aX \sin \pi Z \\
&+R_{cs}[E(a^2+9\pi^2)^3 a^2 + \Lambda(a^2+9\pi^2)a^4]\pi {\theta_{02}}^{(2)} {A_1}^3 \cos aX \sin 3\pi Z \\
&+[a^2 {b_{X02}}^{(2)} E\Lambda q(a^2+9\pi^2)^4 + a^4 {b_{X02}}^{(2)} \Lambda^2 q(a^2+9\pi^2)^2]\frac{{A_1}^3}{2}\cos aX \sin 3\pi Z \\
&-[\frac{2\pi^2 a^2}{d^2} {b_{X02}}^{(2)} - a^2 \frac{{b_{X02}}^{(2)}}{2}]{A_1}^3 \cos aX \sin \pi Z \\
&+[\frac{2\pi^2 a^2}{d^2} {b_{X02}}^{(2)} - a^2 \frac{{b_{X02}}^{(2)}}{(2)}]{A_1}^3 \cos aX \sin 3\pi Z,
\end{aligned} \tag{54}
$$

where $d_2 = a^2 + \pi^2$. By solving the above equation, A_1 is given by

$$
A_1 = -\frac{\sqrt{\left(2\,\Lambda {b_{X02}}^{(2)}\,\pi^2 - \Lambda {b_{X02}}^{(2)}\,d_2 - \pi\,R_{cs}\,{\theta_{02}}^{(2)}\right)R_{os}\,q}}{2\,\Lambda {b_{X02}}^{(2)}\,\pi^2 - \Lambda {b_{X02}}^{(2)}\,d_2 - \pi\,R_{cs}\,{\theta_{02}}^{(2)}}. \tag{55}
$$

The unknown functions W_3, θ_3, b_{X_3}, and b_{Z_3} are obtained from Equations (32), (37), (39), and (41), respectively,

$$
\begin{aligned}
W_3 &= A_3 \cos aX \sin \pi Z + {W_{13}}^{(3)} {A_1}^3 \cos aX \sin 3\pi Z, \\
\theta_3 &= \left(\frac{qA_3}{\pi^2 + a^2} + {\theta_{11}}^{(3)} {A_1}^3\right)\cos aX \sin \pi Z \\
&\quad + {\theta_{13}}^{(3)} {A_1}^3 \cos aX \sin 3\pi Z, \\
b_{X_3} &= \left(-\frac{\pi A_3}{\pi^2 + a^2} + {b_{X11}}^{(3)} {A_1}^3\right)\cos aX \cos \pi Z \\
&\quad + {b_{X13}}^{(3)} {A_1}^3 \cos aX \cos 3\pi Z, \\
b_{Z_3} &= \left(-\frac{aA_3}{\pi^2 + a^2} + {b_{Z11}}^{(3)} {A_1}^3\right)\sin aX \sin \pi Z \\
&\quad + {b_{Z13}}^{(3)} {A_1}^3 \sin aX \sin 3\pi Z.
\end{aligned} \tag{56}
$$

where

$$
W_{13}^{(3)} = \frac{1}{D_{13}}\left(R_{cs}\left(q\Lambda d_{13}\,a^4 + Eq {d_{13}}^3 a^2\right)\pi\,{\theta_{02}}^{(2)}\right)
$$

$$
+\frac{1}{D_{13}}\left(\left(\frac{1}{2}\,a^2 E\Lambda q {d_{13}}^4 + \frac{1}{2}\,a^4\Lambda^2 q {d_{13}}^2\right){b_{X02}}^{(2)} + \left(2\,\frac{\pi^2 a^2}{d_2} - \frac{1}{2}\,a^2\right)b_{X02}^{(2)}\right),
$$

$$
\theta_{11}^{(3)} = \frac{\pi\,\theta_{02}^{(2)}}{d_2}, \quad \theta_{13}^{(3)} = \frac{-\pi\,\theta_{02}^{(2)} + W_{13}^{(3)}\,q}{d_{13}},
$$

and

$$
b_{X11}^{(3)} = \frac{\pi\,b_{X02}^{(2)}}{2d_2}, \quad b_{X13}^{(3)} = -\frac{3\pi\,W_{13}^{(3)}}{d_2} - \frac{3\pi\,b_{X02}^{(2)}}{2d_2},
$$

$$
b_{Z11}^{(3)} = \frac{a\,b_{X02}^{(2)}}{2d_2}, \quad b_{Z13}^{(3)} = -\frac{a\,W_{13}^{(3)}}{d_2} - \frac{a\,b_{X02}^{(2)}}{2d_2},
$$

$$
D_{13} = -9\,q\pi^2 d_{13}^3 - E^2 q d_{13}^6 - 2\,E\Lambda q a^2 d_{13}^4
$$

$$
-\Lambda^2 q^2 a^4 d_{13}^2 + R_{cs}\left(q a^2 E d_{13}^3 + q\Lambda a^4 d_{13}\right),
$$

where $d_{13} = a^2 + 9\pi^2$. This iterative procedure is continued to find A_2 to A_6 and the equivalent W_i, θ_i, b_{X_i}, b_{Z_i}, ω_{Z_i}, and J_{Z_i}, etc.

4.3. Calculation of A_2 and A_3

Initially, Equation (33) is simplified for $i = 4$, i.e.,

$$(\mathcal{L}_1 + \mathcal{L}_2 + \mathcal{L}_3 + \mathcal{L}_4 + R_{cs}(\mathcal{L}_5 + \mathcal{L}_6))W_4 + R_{os}(\mathcal{L}_5 + \mathcal{L}_6)W_2 = (R_{cs} + R_{os})\mathcal{N}_1 + \mathcal{N}_2 + \mathcal{N}_3 + \mathcal{N}_4 + \mathcal{N}_5. \quad (57)$$

The nonlinear terms $\mathcal{N}_i$, $i = 1, 2, 3, 4, 5$ are analyzed by using the Equations (46), (53) and (56). Solving the above Equation (57), we obtain $A_2 = 0$. This indicates that every second order approximate solutions vanish except for $\theta_{02}^{(2)}$ and $b_{X02}^{(2)}$ as shown in Equation (52). Therefore, Equation (57) decreases to

$$(\mathcal{L}_1 + \mathcal{L}_2 + \mathcal{L}_3 + \mathcal{L}_4 + R_{cs}(\mathcal{L}_5 + \mathcal{L}_6))W_4 = K_1 {A_1}^4 \cos 2aX \sin 4\pi Z + K_2 {A_1}^4 \cos 2aX \sin 2\pi Z + K_3 A_1 A_3 \cos 2aX \sin 2\pi Z. \quad (58)$$

The approximate solutions W_4, θ_4, b_{X_4}, b_{Z_4} are evaluated by Equations (33), (37), (39) and (41) and those are given by

$$\begin{aligned}
W_4 &= A_4 \cos aX \sin \pi Z + K_4 A_1^4 \cos 2aX \sin 4\pi Z \\
&+ K_5 A_1^4 \cos 2aX \sin 2\pi Z + K_6 A_1 A_3 \cos 2aX \sin 2\pi Z, \\
\theta_4 &= \frac{q}{(a^2 + \pi^2)} A_4 \cos aX \sin \pi Z + K_7 A_1 A_3 \sin 2\pi Z \\
&+ K_8 A_1^4 \sin 2\pi Z + K_9 A_1^4 \cos 2aX \sin 2\pi Z + K_{10} A_1^4 \cos 2aX \sin 4\pi Z \\
&+ K_{11} A_1^4 \sin 4\pi Z + K_{12} A_1 A_3 \cos 2aX \sin 2\pi Z, \\
b_{X_4} &= \frac{-\pi}{(a^2 + \pi^2)} A_4 \cos aX \cos \pi Z + K_{13} A_1^4 \cos 2aX \cos 4\pi Z \\
&+ K_{14} A_1^4 \cos 2aX \cos 2\pi Z + K_{15} A_1 A_3 \cos 2aX \cos 2\pi Z, \\
b_{Z_4} &= \frac{-a}{(a^2 + \pi^2)} A_4 \sin aX \sin \pi Z + K_{16} A_1^4 \sin 2aX \sin 4\pi Z \\
&+ K_{17} A_1^4 \sin 2aX \sin 2\pi Z + K_{18} A_1 A_3 \sin 2aX \sin 2\pi Z.
\end{aligned} \quad (59)$$

To determine the value of A_3, Equation (33) is solved for $i = 5$, and is given by

$$(\mathcal{L}_1 + \mathcal{L}_2 + \mathcal{L}_3 + \mathcal{L}_4 + R_{cs}(\mathcal{L}_5 + \mathcal{L}_6))W_5 + R_{os}(\mathcal{L}_5 + \mathcal{L}_6)(W_3 + W_1) = (R_{cs} + R_{os})\mathcal{N}_1 + \mathcal{N}_2 + \mathcal{N}_3 + \mathcal{N}_4 + \mathcal{N}_5. \quad (60)$$

Evaluating A_3 from Equations (46), (53), (56), (59) and (60) we obtain,

$$A_3 = \frac{S_1}{S_2}, \quad (61)$$

where

$$\begin{aligned}
S_1 &= -{A_1}^5 \left(\Lambda^2 q {d_2}^2 a^3 + E\Lambda q {d_2}^4 a\right) \left(\frac{-\pi K_{17}}{4a} + \frac{K_{14}}{4} - \frac{b_{X02}^{(2)} W_{13}^3}{2} - \frac{3\pi K_5}{4d_2}\right) a \\
&+ {A_1}^5 \left(\Lambda^2 q {d_2}^2 a^2 + E\Lambda q {d_2}^4\right) \left(-\frac{a(2\pi K_{14} + 2aK_{17})}{4d_2} - \pi b_{X02}^{(2)} b_{Z11}^{(3)} - \pi b_{X02}^{(2)} b_{Z13}^{(3)} + K_{17}\right) \pi a \\
&+ {A_1}^5 a^2 \left(\Lambda^2 q {d_2}^2 a^2 + E\Lambda q {d_2}^4\right) \left(\frac{\pi(2\pi K_{14} + 2aK_{17})}{4d_2} + \frac{b_{X02}^{(2)}}{2}\left(\pi b_{X11}^{(3)} + a b_{Z11}^{(3)}\right)\right) \\
&- {A_1}^5 a^2 \left(\Lambda^2 q {d_2}^2 a^2 + E\Lambda q {d_2}^4\right) \left(\frac{b_{X02}^{(2)}}{2}\left(3\pi b_{X13}^{(3)} + a b_{Z13}^{(3)}\right) + \pi b_{X02}^{(2)} b_{X11}^{(3)} - \pi b_{X02}^{(2)} b_{X13}^{(3)}\right)
\end{aligned}$$

$$+\left(q\Lambda d_2\, a^4 + Eq{d_2}^3 a^2\right)\left(\pi\,\theta_{02}^{(2)}\, W_{13}^{(3)} - \frac{3\pi\, qK_5}{4d_2} - \pi\,\frac{K_9}{4} - \pi\, K_8\right){A_1}^5 R_{cs}$$

$$+\left(q\Lambda d_2\, a^4 + Eq{d_2}^3 a^2\right)\left(\pi\,\theta_{02}^{(2)}\, W_{13}^{(3)} - \frac{3\pi\, qK_5}{4d_2} - \pi\, K_9 - \pi\, K_8\right){A_1}^5 R_{os}$$

$$-\Lambda R_{os}\, a^4 d_2\, q^2 - E R_{os}\, a^2 {d_2}^3 q^2 - {A_1}^5 a^2\left(\Lambda^2 q{d_2}^2 a^2 + E\Lambda q{d_2}^4\right)K_{14},$$

and

$$S_2 = -\left(q\Lambda d_2\, a^4 + Eq{d_2}^3 a^2\right)\left(-\pi\, K_8 - \pi\,\theta_{02}^{(2)} - \pi\, q\frac{3K_5}{4}\right){A_1}^2 R_{cs}$$

$$-\left(q\Lambda d_2\, a^4 + Eq{d_2}^3 a^2\right)\left(-\pi\, K_8 - \pi\,\theta_{02}^{(2)} - \pi\, q\frac{3K_5}{4}\right){A_1}^2 R_{os}$$

$$+{A_1}^2\left(\Lambda^2 q{d_2}^2 a^3 + E\Lambda q{d_2}^4 a\right)\left(\frac{b_{X02}^{(2)}}{2} - \frac{\pi\, K_{17}}{4a} + \frac{K_{14}}{4} - \frac{3\pi\, K_5}{4d_2}\right)a$$

$$-{A_1}^2\left(\Lambda^2 q{d_2}^2 a^2 + E\Lambda q{d_2}^4\right)\left(-\frac{a(2\,\pi\, K_{14} - 2\,aK_{17})}{4d_2} + \frac{\pi\, ab_{X02}^{(2)}}{d_2} + K_{17}\right)\pi\, a$$

$$-{A_1}^2\left(\Lambda^2 q{d_2}^2 a^2 + E\Lambda q{d_2}^4\right)\left(\frac{\pi\,(2\,\pi\, K_{14} + 2\,aK_{17})}{4d_2} - \frac{b_{X02}^{(2)}}{2}\right)a^2$$

$$-{A_1}^2\left(\Lambda^2 q{d_2}^2 a^2 + E\Lambda q{d_2}^4\right)\left(\frac{\pi^2 b_{X02}^{(2)}}{d_2} - K_{14}\right)a^2 + \Lambda R_{os}\, a^4 d_2\, q^2 + E R_{os}\, a^2 {d_2}^3 q^2.$$

The amplitude A_3 is determined by using the first, second, third and fourth order approximate solutions. From Equations (60), (37), (39) and (41), the fifth order approximate solutions are obtained

$$\begin{aligned} W_5 &= A_5\,\cos aX \sin \pi Z \\ &+\left(K_{19}\,{A_1}^5 + K_{20}\,{A_1}^2 A_3\right)\cos 3\,aX \sin \pi Z \\ &+\left(K_{21}\,{A_1}^3 + K_{22}\,{A_1}^5 + K_{23}\,{A_1}^2 A_3\right)\cos aX \sin 3\,\pi Z \\ &+\left(K_{24}\,{A_1}^5 + K_{25}\,{A_1}^2 A_3\right)\cos 3\,aX \sin 3\,\pi Z \\ &+K_{26}\,{A_1}^5 \cos aX \sin 5\,\pi Z + K_{27}\,{A_1}^5 \cos 3\,aX \sin 5\,\pi Z, \end{aligned} \tag{62}$$

$$\begin{aligned} \theta_5 &= \left(\frac{qA_5}{d_2} + K_{28}\,{A_1}^2 A_3\right)\cos aX \sin \pi Z \\ &+\left(K_{29}\,{A_1}^3 + K_{30}\,{A_1}^5 + K_{31}\,{A_1}^2 A_3\right)\cos aX \sin 3\,\pi Z \\ &+\left(K_{32}\,{A_1}^5 + K_{33}\,{A_1}^2 A_3\right)\cos 3\,aX \sin \pi Z \\ &+\left(K_{34}\,{A_1}^5 + K_{35}\,{A_1}^2 A_3\right)\cos 3\,aX \sin 3\,\pi Z \\ &+K_{36}\,{A_1}^5 \cos aX \sin 5\,\pi Z + K_{37}\,{A_1}^5 \cos 3\,aX \sin 5\,\pi Z, \end{aligned} \tag{63}$$

$$\begin{aligned} b_{X_5} &= \left(-\frac{\pi\, A_5}{d_2} + K_{38}\,{A_1}^5\right)\cos aX \cos \pi Z \\ &+\left(K_{39}\,{A_1}^3 + K_{40}\,{A_1}^5 + K_{41}\,{A_1}^2 A_3\right)\cos aX \cos 3\,\pi Z \\ &+\left(K_{42}\,{A_1}^5 + K_{43}\,{A_1}^2 A_3\right)\cos 3\,aX \cos \pi Z \end{aligned}$$

$$+\left(K_{44}\,{A_1}^5 + K_{45}\,{A_1}^2 A_3\right)\cos 3\,aX\cos 3\,\pi\,Z$$
$$+K_{46}\,{A_1}^5\cos aX\cos 5\,\pi\,Z + K_{47}\,{A_1}^5\cos 3\,aX\cos 5\,\pi\,Z, \tag{64}$$

$$b_{Z_5} = \left(-\frac{aA_5}{d_2} + K_{48}\,{A_1}^5 + K_{49}\,{A_1}^2 A_3\right)\sin aX\sin\pi\,Z$$
$$+\left(K_{50}\,{A_1}^3 + K_{51}\,{A_1}^5 + K_{52}\,{A_1}^2 A_3\right)\sin aX\sin 3\,\pi\,Z$$
$$+\left(K_{53}\,{A_1}^5 + K_{54}\,{A_1}^2 A_3\right)\sin 3\,aX\sin\pi\,Z$$
$$+\left(K_{55}\,{A_1}^5 + K_{56}\,{A_1}^2 A_3\right)\sin 3\,aX\sin 3\,\pi\,Z$$
$$+K_{57}\,{A_1}^5\sin aX\sin 5\,\pi\,Z + K_{58}\,{A_1}^5\sin 3\,aX\sin 5\,\pi\,Z. \tag{65}$$

Here the coefficients $K_i, i = 1, 2, \ldots 58$ in Equations (58)–(65) are functions of a, E, Λ, and q. The simplifications become more critical as ε order increases. Similarly, the simplification was carried until the eighth order of Equation (34) to calculate for A_4, A_5, and A_6. Proceeding as above, it can be observed that $A_2 = A_4 = A_6 = 0$.

5. Convective Heat Transport

The changes in the two-dimensional flow patterns are illustrated by the local Nusselt number, N_L, distributions over the heated plate. The heat transport coefficient in terms of the N_L is expressed as [16,25]

$$N_L = \frac{\partial T}{\partial n}, \tag{66}$$

here n denotes the normal direction on a plane. The heat transport is measured by the average Nusselt number (Nu), which is independent of Z and is given by

$$Nu = \overline{WT} - \frac{\partial \overline{T}}{\partial Z}, \tag{67}$$

here the bar indicates a horizontal mean. Using Equation (67), Nu is obtained by integrating the expression over the boundary, $Z = 0$ [16].

$$Nu = \frac{1}{L}\int_0^L WT - \frac{\partial T}{\partial Z}|_{z=0} dX, \tag{68}$$

where L is the normalized horizontal cell width.

5.1. Local Nusselt Number (N_L)

Figure 2a illustrates the changes of N_L for distinct values of E with respect to X. In selected regions, the number of peaks and the location of maximum and minimum of N_L values depend on E. The maximum of N_L value is constant, as X increases for defined E. However, as E decreases, the number of peaks is increased in a selected region. Figure 2b illustrates the variation of N_L for different Λ concerning to X. The location of the maximum N_L value is independent of the dimensionless plate length but depends on Λ. The existence of the number of peaks in the given region of X increases, as Λ increases. Figure 2b illustrates the heat that is transported from the fluid to the boundary is increased as Λ increase.

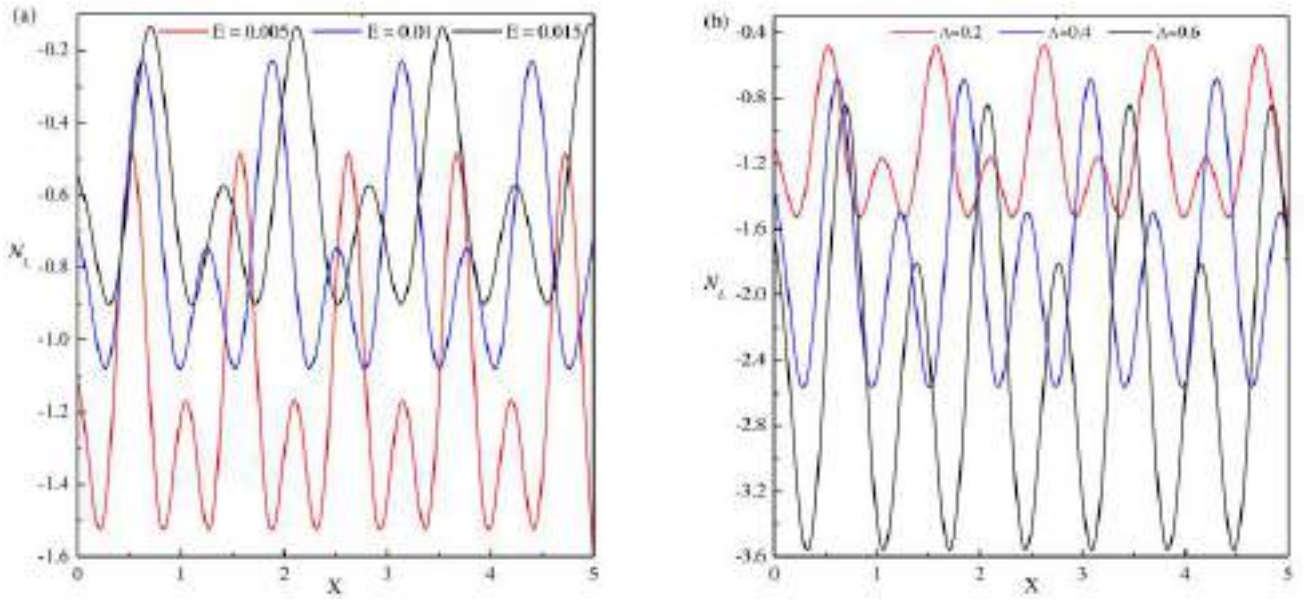

Figure 2. Variation of N_L with respect to X. (**a**) $\Lambda = 0.2$ and $q = 0.01$ for different E, (**b**) $E = 0.005$ and $q = 0.01$ for different Λ.

5.2. Average Nusselt Number (Nu)

The dependency of Nu on the control parameters was studied near and away from the onset of stationary convection. Let $Nu^{(2)}(s = 1)$, $Nu^{(4)}(s = 2)$ and $Nu^{(6)}(s = 3)$, indicate the second-, fourth- and sixth-order approximations, for Nu, respectively. The second order approximation is given by

$$Nu^{(2)} = 1 + \frac{2qR_{os}}{2\Lambda(a^2 - \pi^2) + R_{cs}}. \tag{69}$$

The approximations for $Nu^{(4)}$ and $Nu^{(6)}$ are lengthy, so it is not shown here to conserve space. The change of Nu with respect to R is shown in Figure 3 for different values of E and Λ. Figure 3a shows the effect of E on Nu in the R plane for fixed $\Lambda = 0.2$ and $q = 0.01$. It illustrates that the rate of heat transfer is enhanced for decreasing E. Figure 3b shows the effect of Λ on heat transfer rate for fixed $E = 0.005$ and $q = 0.01$. The enhancement of heat transfer is observed for increasing Λ values. The small values of q are relevant to Earth's outer core. It is very difficult to perform numerical simulations for small values of the physical parameters. For $q < 1$ stationary convection is preferred [13]. Figure 3c shows that for $q < 1$ and as q increases, the Nu increase. Thus the effect of $q < 1$ shows, the heat transfer rate are enhanced and accordingly the intensity of the flow rate also increase. The change of kinetic energy with respect to R/R_{cs} is represented in Figure 4. Figure 4a demonstrates the change in Nu for various E values as well as for a fixed value of $\Lambda = 0.2$. The change in E produces small change in the potential energy, in comparison with the kinetic energy. Thus, the total energy decreases as E increase. Figure 4b shows the energy distribution for different Λ and for fixed $E = 0.005$ and $q = 0.01$. The amplifying values of Λ show that the total energy is also increased.

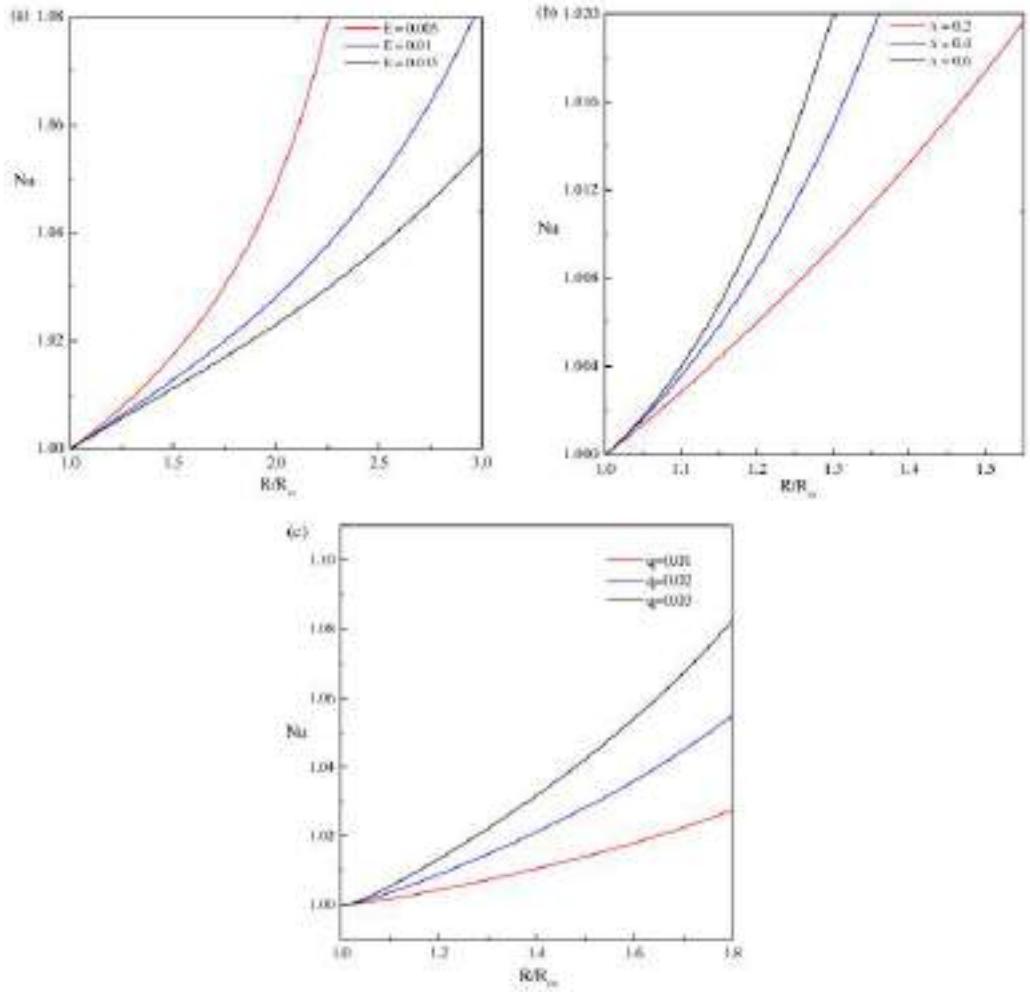

Figure 3. Dependence of Nussult number (Nu) on Rayleigh number (R/R_{cs}). (**a**) $\Lambda = 0.2$ and $q = 0.01$ for different E, (**b**) $E = 0.005$ and $q = 0.01$ for different Λ, (**c**) $E = 0.005$ and $\Lambda = 0.2$ for different q.

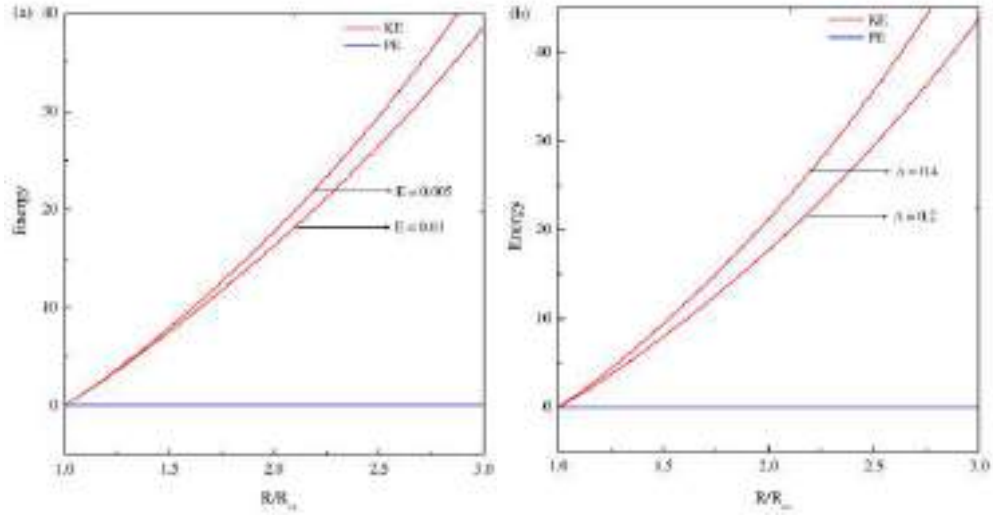

Figure 4. Dependence of kinetic energy and potential energy on Rayleigh number (R/R_{cs}) are plotted. (**a**) $\Lambda = 0.2$ and $q = 0.01$ for different E, (**b**) $E = 0.005$ and $q = 0.01$ for different Λ.

6. Distortion of Streamlines and Isotherms

The fluid flow behavior is visualized by the stream function (Ψ) which is obtained from the velocity components U and W. The relation between the velocity components and stream function (Ψ) is [26]

$$U = -\frac{\partial \Psi}{\partial Z} \quad \text{and} \quad W = \frac{\partial \Psi}{\partial X},$$

which produce a single equation

$$\Psi = \nabla^2 \Psi = 0 \quad \text{for} \quad X = 0, \sqrt{2}\pi/a \ \text{ and } \ Z = 0, 1.$$

The points with equal temperature connected with lines are called isotherms. The snapshots of the heat transport and flow field near the onset of stationary convection are expressed in terms of streamlines and isotherms.

The general attributes of the streamlines and isotherms with respect to the variation in R, E, and Λ are shown in Figures 5–8. Figure 5 illustrates the pattern of streamlines and isotherms near the onset of convection ($R \simeq R_{cs}$). Figure 5a, shows the pattern of streamlines for E = 0.005, Λ = 0.2, q = 0.01. The absolute maximum and the absolute minimum values of circular strengths are 0.11215 and −0.11216, respectively. Figure 5c shows the pattern of streamlines for E = 0.01, Λ = 0.2. This figure shows the absolute maximum and the absolute minimum values of circular strengths as 0.11243 and −0.11243, respectively. From Figure 5a,c the maximum strength of rolls at $R \simeq R_{cs}$ are decreased as E increases. Thus, as E increases, R_{cs} also increases, accordingly Nu decreases and hence the absolute maximum of circulation strength decreases. Figure 5e illustrate the pattern of streamlines with E = 0.005 and Λ = 0.4. These streamlines have the absolute minimum and maximum values with the circular strengths as −0.12116 and 0.121117, respectively. By comparing Figure 5a,e, the periodic rectangular rolls are observed near the $R \simeq R_{cs}$, but as Λ increases the maximum strength of rolls is increased and the minimum strength of roll decreases. Thus, as Λ increases, R_{cs} decreases, accordingly Nu increases, and hence the absolute maximum of circulation strength increases. Figure 5a–f are plotted for the values of $R \simeq R_{cs}$ and the flow pattern are rectangular rolls and follows the symmetric nature over the range of $0 \leq X \leq 1$. Since the stream function equations show the symmetric property. Similarly, for the same values of E and Λ, the isotherms formed as horizontal lines near $R \simeq R_{cs}$, as shown in Figure 5b,d,f. At $R \simeq R_{cs}$, the strength of isotherms is of small magnitude, representing the conduction dominant heat transport inside the considered region. These isotherms are smooth lines that span over the whole region.

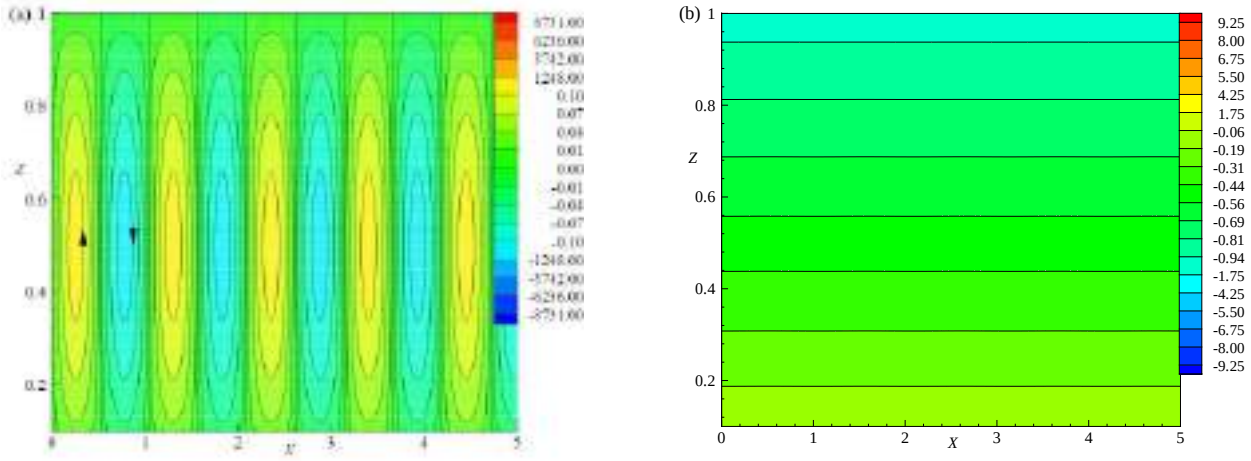

Figure 5. *Cont.*

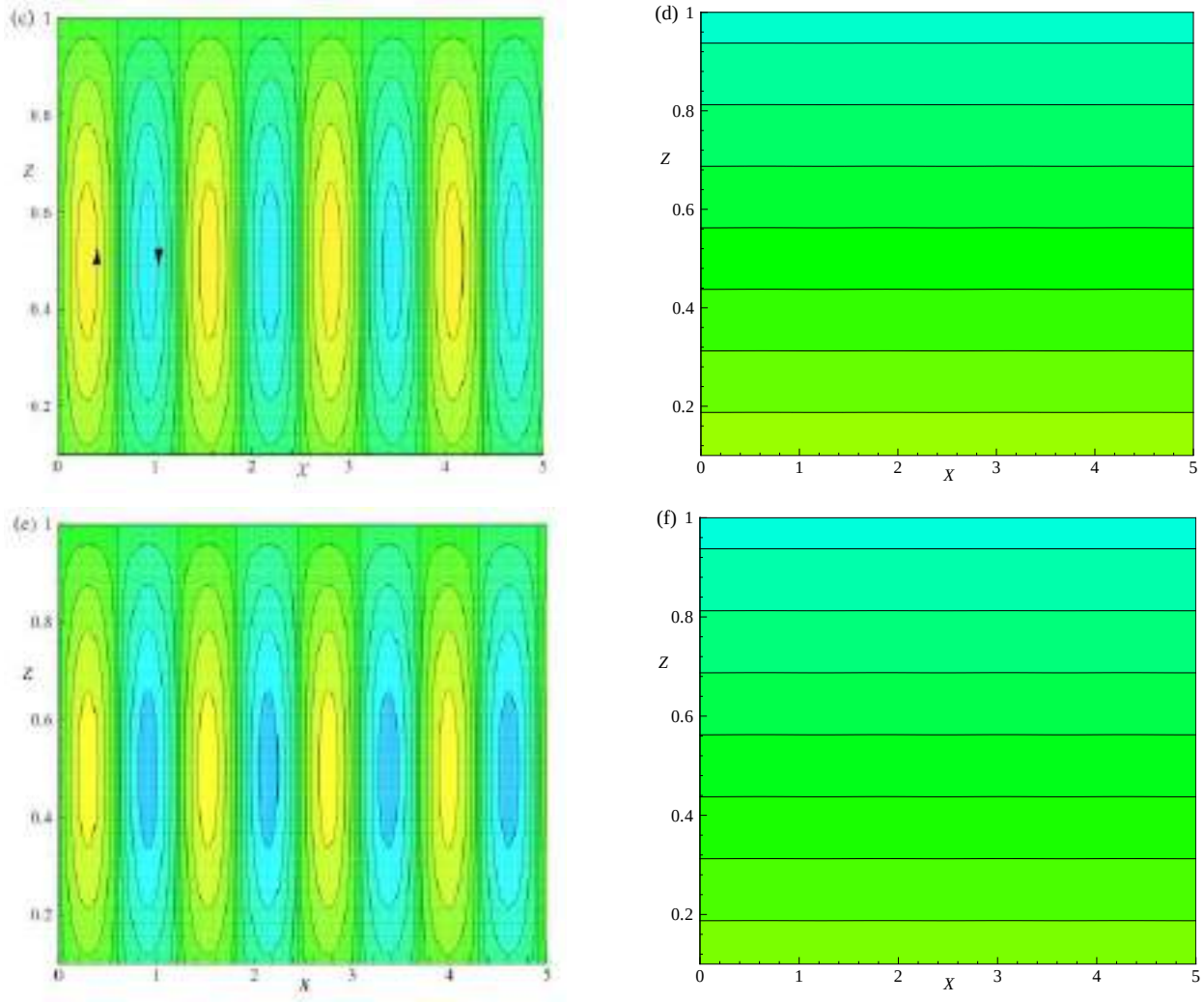

Figure 5. The Effect of E and Λ near R_{cs}, streamlines (**a**) for E = 0.005, Λ = 0.2, and $q = 0.01$, (**c**) E = 0.01, Λ = 0.2, and $q = 0.01$, (**e**) E = 0.005, Λ = 0.4, and $q = 0.01$ and isotherms (**b**) E = 0.005, Λ = 0.2, and $q = 0.01$, (**d**) E = 0.01, Λ = 0.2, and $q = 0.01$, (**f**) E = 0.005, Λ = 0.4, and $q = 0.01$ are plotted.

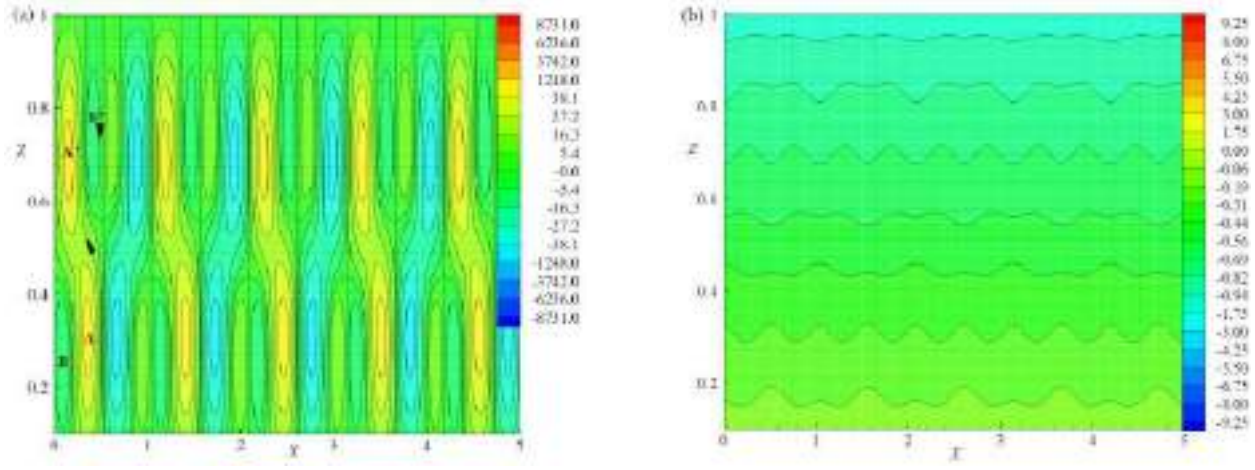

Figure 6. *Cont.*

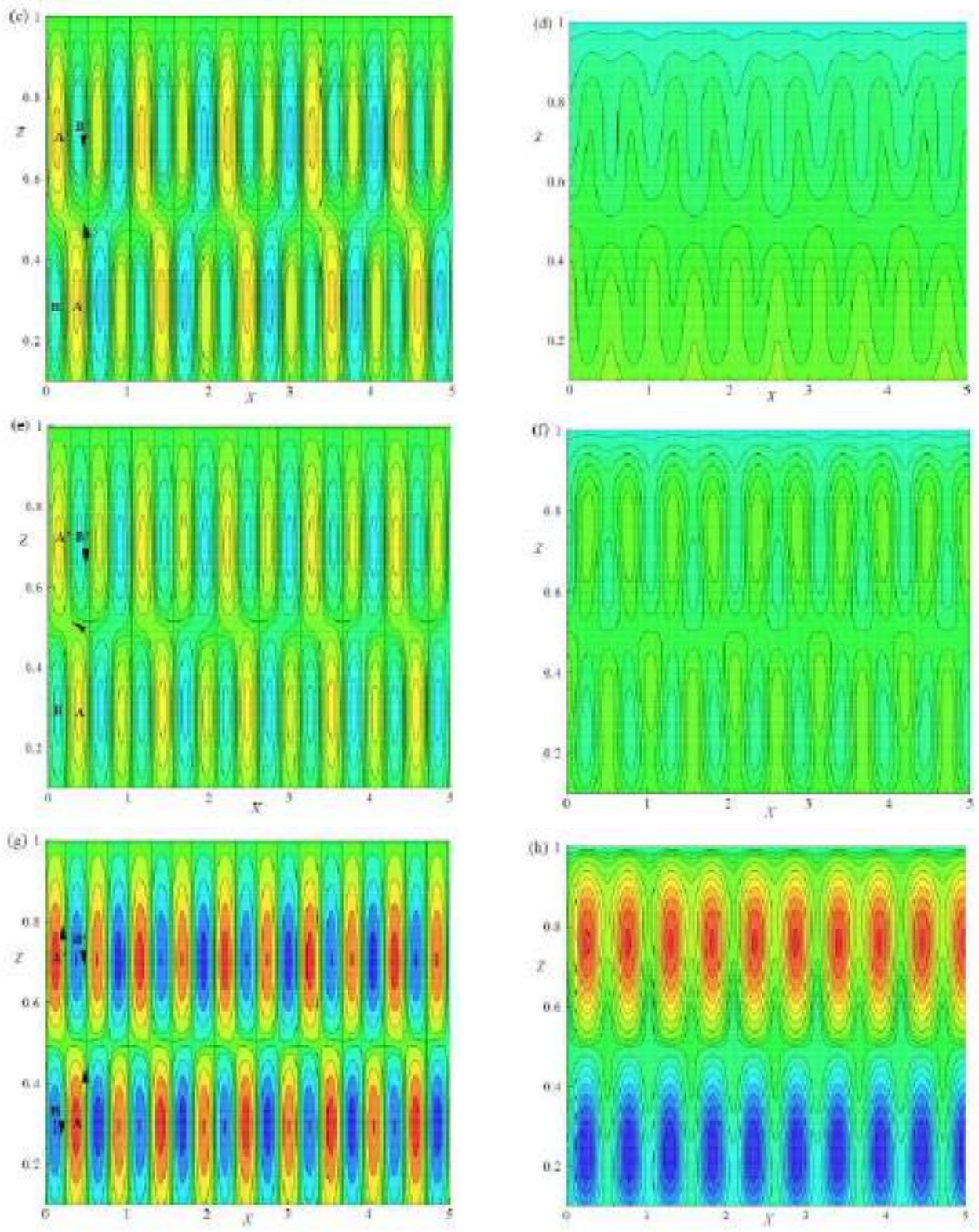

Figure 6. The Effect of $R = 10R_{cs}$, $20R_{cs}$, $30R_{cs}$ and $80R_{cs}$, streamlines (**a**,**c**,**e**,**g**) and isotherms (**b**,**d**,**f**,**h**) are plotted for $E = 0.005$, $\Lambda = 0.2$, and $q = 0.01$.

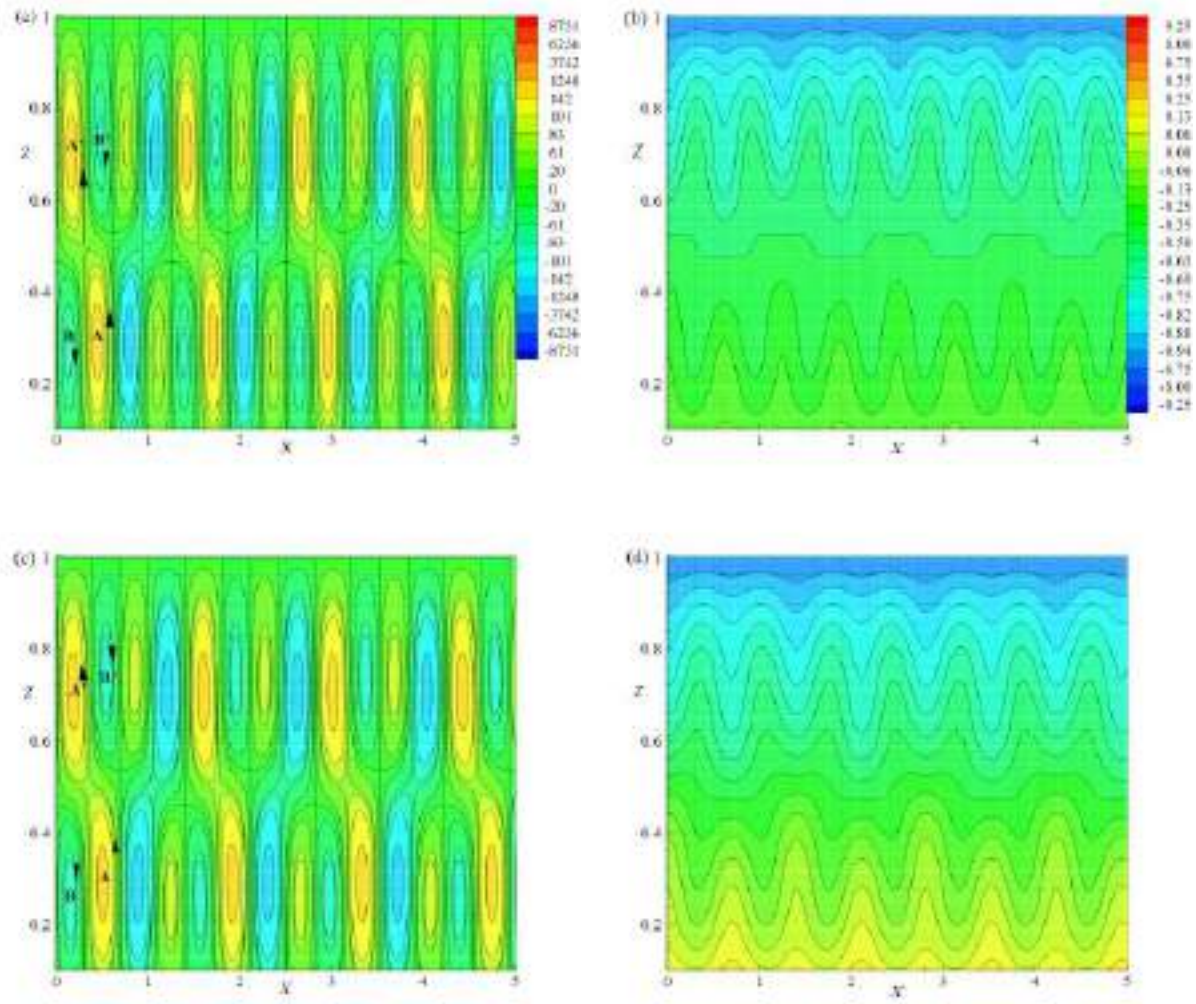

Figure 7. The Effect of E = 0.01 and 0.015, streamlines (**a**,**c**) and isotherms (**b**,**d**) are plotted for Λ = 0.2, R = 20R_{cs}, and q = 0.01.

The snapshot of streamlines and isotherms for different values of R and for fixed values of $E = 0.005$, $\Lambda = 0.2$, and $q = 0.01$ are displayed in Figure 6a–h. It is observed that for $R = 10R_{cs}$ and for the cell lying between $0 \leq X \leq 1$, the absolute minimum and maximum values are with the circulation strengths -43.4965 and 43.4965, respectively, as shown in Figure 6a. As R increases from R_{cs} to $10R_{cs}$, the basic cells become more deformed due to the growth of two vortices B and B' located at the top right and bottom left boundaries with the circulation strength -16.315. The basic cell with two vortices A and A' has circulation strength 38.059. The temperature profiles in terms of isotherms are illustrated in Figure 6b for same values of physical parameters that are considered in Figure 6a. The isotherms are of nearly in wavy shape with the absolute maximum and minimum values of -0.00212 and -1.00271, respectively. It indicates the maximum of heat transfer process is occurred by convection. Figure 6c,d illustrate the streamlines and isotherms for $R = 20R_{cs}$. The temperature gradient and the gravitational buoyancy force act together and changes the flow structure as shown in Figure 6c. The bicellular patterns of streamlines turn out to be multicellular models and these cells divide the field of motion at the core for a cell lies between $0 \leq X \leq 1$ with the absolute maximum and minimum values of circulation strengths 220.829 and -220.845, respectively. The vortices B and B' showed their

presence with −82.822 as the circulation strength in the opposite direction of an original cell. For these considered values of physical parameters, the behavior of isotherms is shown in Figure 6d, which exhibit the mode of convective heat transport inside the fluid layer. In the fluid layer, the absolute maximum and minimum values of isotherms are respectively, −0.00275 and −1.0052. When R is increased from $20R_{cs}$ to $30R_{cs}$, the small vortices B and B' shown in Figure 6c are increased with circulation strength −398.740. Thus, the basic cell encountered more deformation (Figure 6e) and has the absolute maximum and minimum values at 638.172 and −638.027, respectively. Accordingly, the isotherm curves develop more deformation. The absolute maximum and minimum values of isotherms in the layer are, respectively, −0.00449 and −1.01101. As R is increased from $30R_{cs}$ to $80R_{cs}$ (Figure 6g), the two vortices B and B' grow in size and split the basic cell into two vortices located on either side of the secondary cell with the absolute maximum (9976.78) and minimum (−9977.74) strengths. The heat flow pattern becomes chaotic, which is shown in Figure 6h when R increases to $80R_{cs}$. The absolute maximum and minimum values of isotherms in the layer are, respectively, 8.75285 and −9.67347. From Figure 6, it is observed that as R increases from R_{cs} to $80R_{cs}$, the onset of turbulent flows are producible.

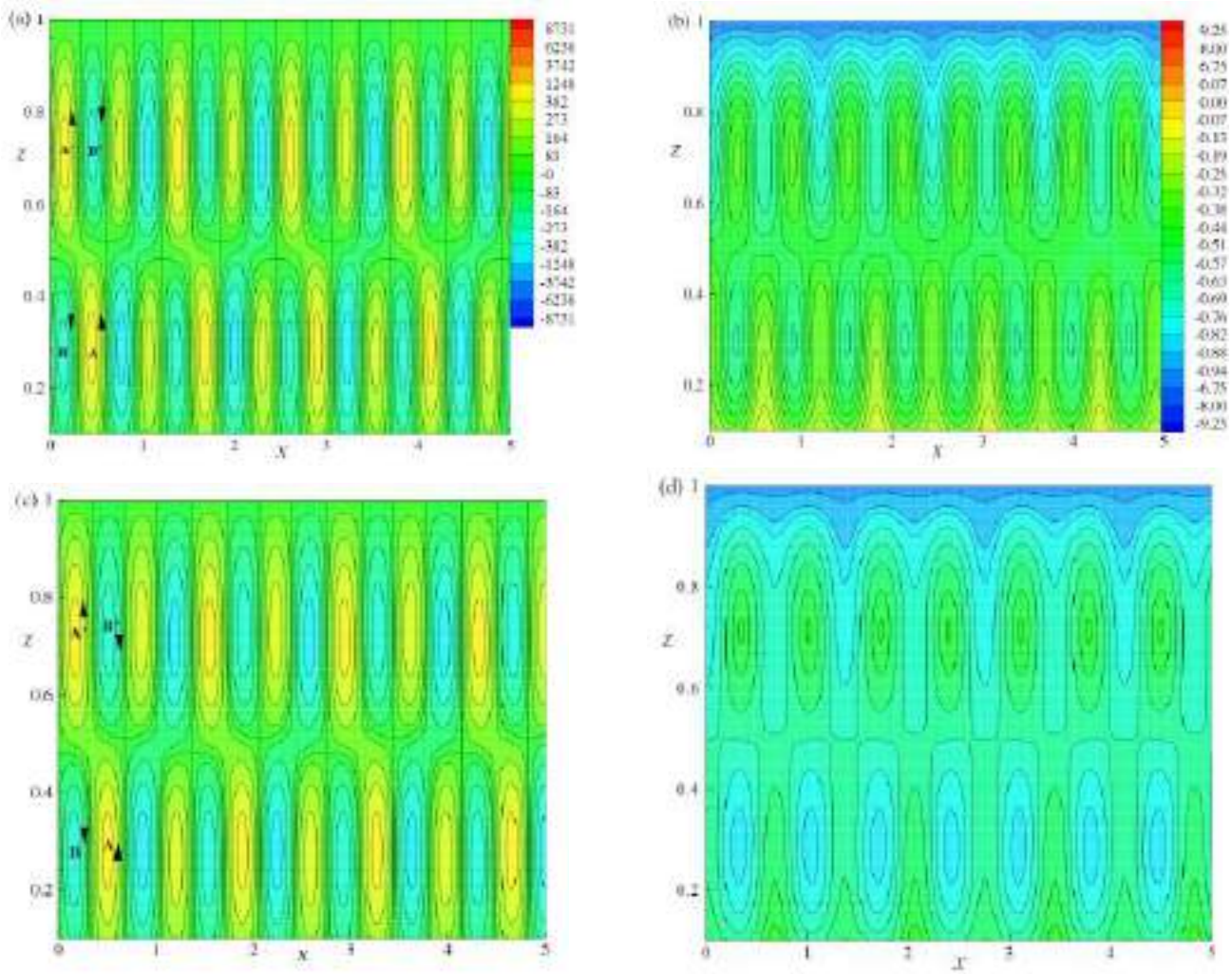

Figure 8. The Effect of Λ = 0.4 and 0.6, streamlines (**a**,**c**) and isotherms (**b**,**d**) are plotted for E = 0.005, $R = 20R_{cs}$ and q = 0.01.

Figure 7a–d, illustrate the streamlines and isotherms for different values of E and for a fixed set of other parameters $R = 20R_{cs}$, $\Lambda = 0.2$, and $q = 0.01$. The behavior of the flow

field was investigated by considering the flow pattern in the region $0 \leq X \leq 1$, as shown in Figure 6a–d (E = 0.005) and Figure 7a–d (E = 0.01 and 0.015). Figure 7a shows streamlines for E = 0.01 in the considered range of X. The absolute maximum and minimum values of circulation strengths are 162.15 and −162.149, respectively. There exist two vortices B and B' outside the basic cell with the circulation strength −82.806 as shown in Figure 7a. The basic cell also contains two vortices namely A and A' with a circulation strength of 141.881. Figure 7c is plotted for E = 0.015, which has the absolute maximum and absolute minimum values of circulation strength as 140.453 and −140.471, respectively. The flow pattern in the region $0 \leq X \leq 1$ contains a deformed basic cell due to the growth of two vortices B and B' that exist at either side of the basic cell and are located at the top and bottom boundaries with circulation strength −60.81. The basic cell also has two vortices A and A' with a circulation strength value of 122.90. Finally from Figures 6c and 7a,c it is observed that the strength of the basic cell and pattern deformation decrease as E increases. This implies that the effect of E stabilizes the convective system. The flow of heat transfer is shown in Figure 7b,d for E = 0.01 and 0.015, respectively.

Figure 8a–d show the streamlines and isotherms for different Λ values and for $E = 0.005$, $R = 20R_{cs}$, and $q = 0.01$. The effect of Λ was studied from Figures 6c,d and 8a–d. In Figure 8a the streamlines are plotted for $\Lambda = 0.4$. By considering the flow pattern in the range of $0 \leq X \leq 1$, the absolute maximum and minimum values of circulation strengths are 436.721 and −436.747, respectively. In this range, the basic cell is deformed by two vortices B and B', which are located at the top right and bottom left of the layer and on either side of the basic cell with circulation strength −272.97. The basic cell also encloses two vortices A and A' with strength 382.13. Figure 8c shows the streamlines for $\Lambda = 0.6$ in the considered range of $0 \leq X \leq 1$, with the absolute maximum and minimum values of circulation strength 663.595 and −663.555, respectively. In addition, there exist two vortices B and B' with circulation strength −414.71. The basic cell also enclosed two vortices A and A' with circulation strength 580.65. As Λ increases from 0.4 to 0.6 the deformation and circulation strength of cells (A, A') increase. This implies that the effect of Λ destabilizes the convective system. The isotherms are plotted in Figures 6d and 8b,d for distinct values of $\Lambda = 0.2$, 0.4 and 0.6. The lines of isotherms change to a more circular form as Λ increases. Thus, the incremental values of Λ destabilize the convective system.

Topology of Flow

The topology constraint is based on the Euler number ($\zeta^{'}$) of the flow. As described by Jana et al. [27], $\zeta^{'}$ on the surface is defined as the sum of the Poincare indices of the critical points on the surface and is given by

$$NE - (NH + \frac{1}{2}NP) = \zeta^{'}, \tag{70}$$

here the NE represents the number of elliptic points, NH is the number of hyperbolic points, and NP is the number of parabolic points [28,29]. In Figure 9a, the vorticity contours are exhibited for $R \simeq R_{cs}$, E= 0.005, Λ= 0.2 and $q = 0.01$. The present simulated flow fulfils the topological rule given in Equation (70) with $NP = 0$, $NH = 2$, and $NE = 2$. For $R = 20R_{cs}$, an equivalent investigation has been done for vorticity contours in Figure 9b and Equation (70) is satisfied with NP = 0, NE = 8, and NH = 8.

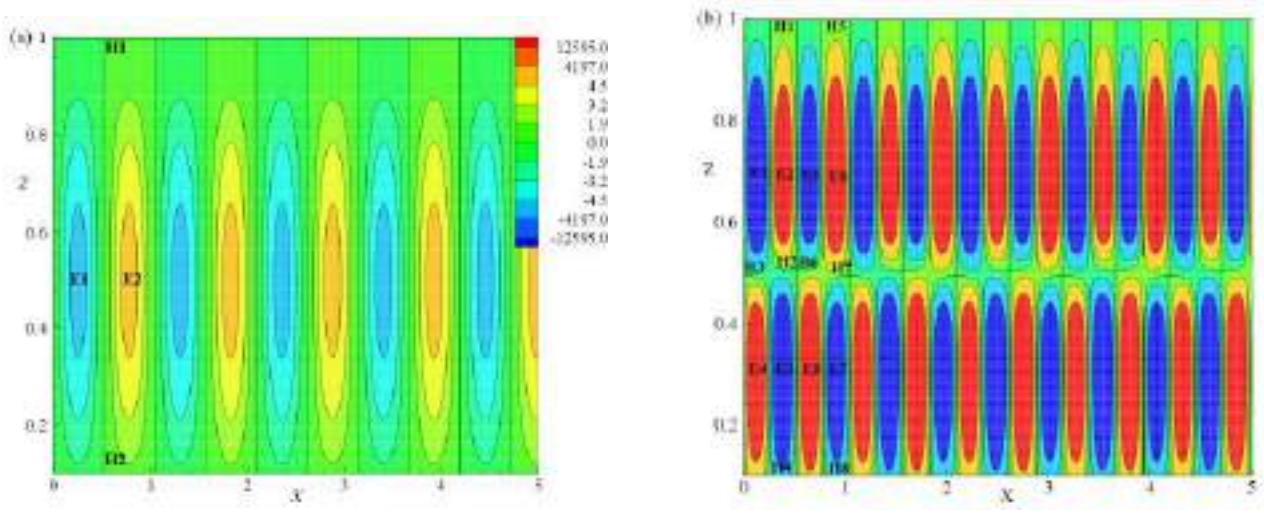

Figure 9. Vorticity lines for (**a**) $R \simeq R_{cs}$, $E = 0.005$, $\Lambda = 0.2$, and $q = 0.01$, (**b**) $R = 20R_{cs}$, $E = 0.005$, $\Lambda = 0.2$, and $q = 0.01$.

7. Heat Function

Heatlines depict the convective heat transport phenomenon, whereas the isotherms are mainly useful for visualizing heat transfer in the domain of conduction. The heat function and heatline analyzes were developed by Kimura and Bejan [30] to visualize heat transmission through the fluid flow, later Morega and Bejan [31] successfully used the concept of heatlines. Different researchers [32–35] used this concept for dissimilar applications of natural convective systems. The heat function (H^*) is defined as

$$\frac{\partial H^*}{\partial X} = WT - \frac{\partial T}{\partial Z}, \tag{71}$$

$$-\frac{\partial H^*}{\partial Z} = UT - \frac{\partial T}{\partial X}, \tag{72}$$

where $T = T_s + \theta$ and $T_s = T_0 - Z$. The Equations (71) and (72) do not exhibit the symmetric property. Differentiating Equations (71) and (72) with respect to X and Z, respectively, and subtracting the resulting equations yields

$$\frac{\partial^2 H^*}{\partial X^2} + \frac{\partial^2 H^*}{\partial Z^2} = \frac{\partial (WT)}{\partial X} - \frac{\partial (UT)}{\partial Z}. \tag{73}$$

From the definition of heat function, Equations (71) and (72), the boundary conditions on H^* follow [16]:

$$H^*(X,0) = H^*(0,0) + \int_0^X (WT - \frac{\partial T}{\partial Z})dX, \text{ at } Z = 0 \text{ and } 0 \le X \le \sqrt{2}\pi/a, \tag{74}$$

$$H^*(X,1) = H^*(0,1) + \int_0^X (WT - \frac{\partial T}{\partial Z})dX, \text{ at } Z = 1 \text{ and } 0 \le X \le \sqrt{2}\pi/a, \tag{75}$$

$$H^*(0,Z) = H^*(0,0) - \int_0^Z (UT - \frac{\partial T}{\partial Z})dZ, \text{ at } X = 0 \text{ and } 0 \le Z \le 1, \tag{76}$$

$$H^*(\sqrt{2}\pi/a,Z) = H^*(\sqrt{2}\pi/a,0) - \int_0^Z (UT - \frac{\partial T}{\partial Z})dZ, \text{ at } X = \sqrt{2}\pi/a \text{ and } 0 \le Z \le 1. \tag{77}$$

Results and Discussion for Heatlines

Figure 10a–d, illustrate the pattern of heatlines for different Rayleigh number values, $R \simeq R_{cs}$, $R = 1.05R_{cs}$, $1.15R_{cs}$ and $1.25R_{cs}$, respectively, for fixed values of $E = 0.005$, $\Lambda = 0.2$, and $q = 0.01$. When the system is at a conduction state ($R < R_{cs}$) heatlines are always parallel to Z-axis and perpendicular to isotherms. Figure 10a illustrates the heatlines for $R \simeq R_{cs}$. It is observed that the heatline contours within the domain are normal to the $Z = 0$ and $Z = 1$ lines due to conduction dominant heat transfer. For $R \simeq R_{cs}$, the absolute maximum and minimum values of heatlines are 10.2224 and 0.0241, respectively, in the considered range $0 \leq X \leq 5$. In the neighborhood of $X = 0$, the heatlines at the center of the system depict the structure which is similar to the parabolic structure. The curvature at the central part of the system increases as X increases. This shows that the nonlinear propagation of heat transfer occurs when $R \simeq R_{cs}$. Hence, the transition takes place from the conduction state to the convection state at $R \simeq R_{cs}$. Figure 10b is plotted for $R = 1.05R_{cs}$. The absolute maximum and minimum values of heatlines are 10.3081 and -0.2774, respectively, in the considered range $0 \leq X \leq 5$. The heatline with a strength of -0.18 exist near the line $X = 0$ and the heatline with strength 9.69 exist at $X = 5$. The strength of heatlines increases as X increases. Some heatlines occurred in the form of a closed path. As R increases from R_{cs} the heatlines with same strength are changed to a closed path as shown in Figure 10a,b. For higher values, this indicates that the convective heat flow is more intense at the center. Figure 10c shows heatlines at $R = 1.15R_{cs}$ and having the absolute maximum and minimum values of heatlines 10.3666 and -0.62655, respectively. In this figure, the number of closed paths of heatlines at the center is increased for $R = 1.15R_{cs}$. The size of closed path of heatlines for $R = 1.15R_{cs}$ is more than that for $R = 1.05R_{cs}$. Figure 10d shows the heatlines for $R = 1.25R_{cs}$ with the absolute maximum and minimum values of 10.3972 and -0.88096, respectively. The number of closed paths of heatlines increases at the center for $R = 1.25R_{cs}$. The size of closed path of heatlines for $R = 1.25R_{cs}$ is increased in comparison with that of the heatlines for $R = 1.15R_{cs}$. For large R, the convective heat transmission is more intense. It is observed that the heatlines become denser with the increase in R. Figure 10a–d indicate that the heat transfer across the layer is increased as R increases. Heatlines will not exhibit periodic patterns due to the non-symmetry nature of Equations (71) and (72).

Figures 10b and 11a,b are plotted with the same strength of heatlines so as to analyze the influence of E on heat flow for the fixed values of Λ, R, and q. In the considered range of $0 \leq X \leq 5$, for $E = 0.01$, (Figure 11a) the absolute maximum and minimum values of heatlines are noted to be 8.4264 and -0.18554, respectively, and for $E = 0.015$ (Figure 11b) these values are 7.51142 and -0.11574, respectively. In both of these Figure 11a,b, the heatlines intensity decays with E. The size of the closed path and the number of closed paths with the same strength decreased as E increases. From Figures 10b and 11a,b it is fascinating to observe the inhibition of temperature in the central regime as E increases.

Figures 10b and 12a,b are plotted with the same strength of heatlines to analyze the effect of Λ on heat flow for the fixed values of E, R, and q. In the considered range of $0 \leq X \leq 5$ for $\Lambda = 0.4$ (Figure 12a) with the absolute maximum and minimum values of heatlines as 8.55642 and -0.23723, respectively. These values for $\Lambda = 0.6$ (Figure 12b) are 7.74043 and -0.18296, respectively. In both Figure 12a,b, the heatlines are dominated by convection and form closed loops. The size and the number of closed loops with the same strength increase as Λ increases. From Figures 10b and 12a,b it is observed that the temperature within the central regime is enhanced as Λ increase by observing heatlines.

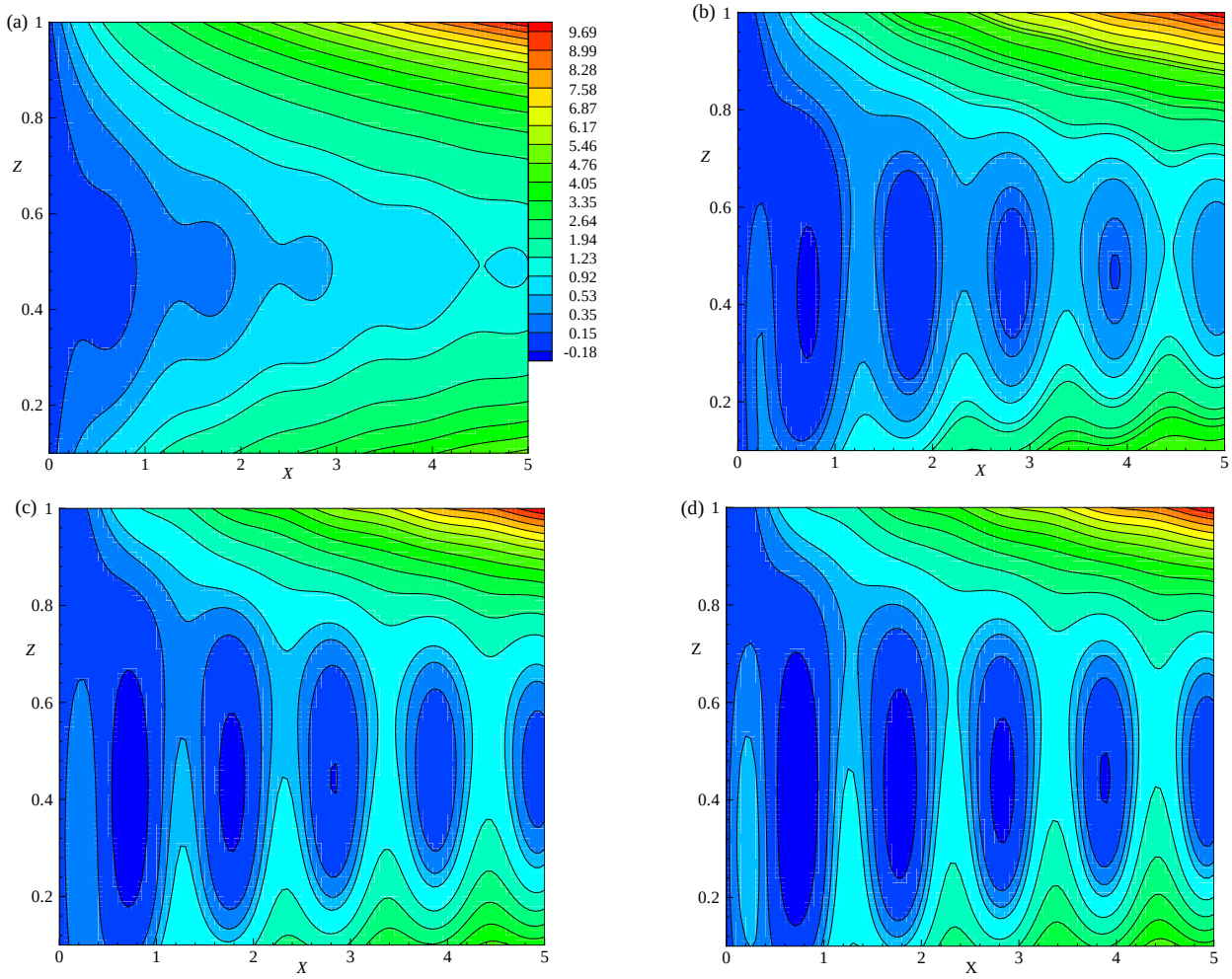

Figure 10. The effect of $R \simeq R_{cs}$, $R = 1.05R_{cs}$, $1.15R_{cs}$ and $1.25R_{cs}$, heatlines (**a**–**d**) are plotted for $E = 0.005$, $\Lambda = 0.2$, $T_0 = 1$, and $q = 0.01$, respectively.

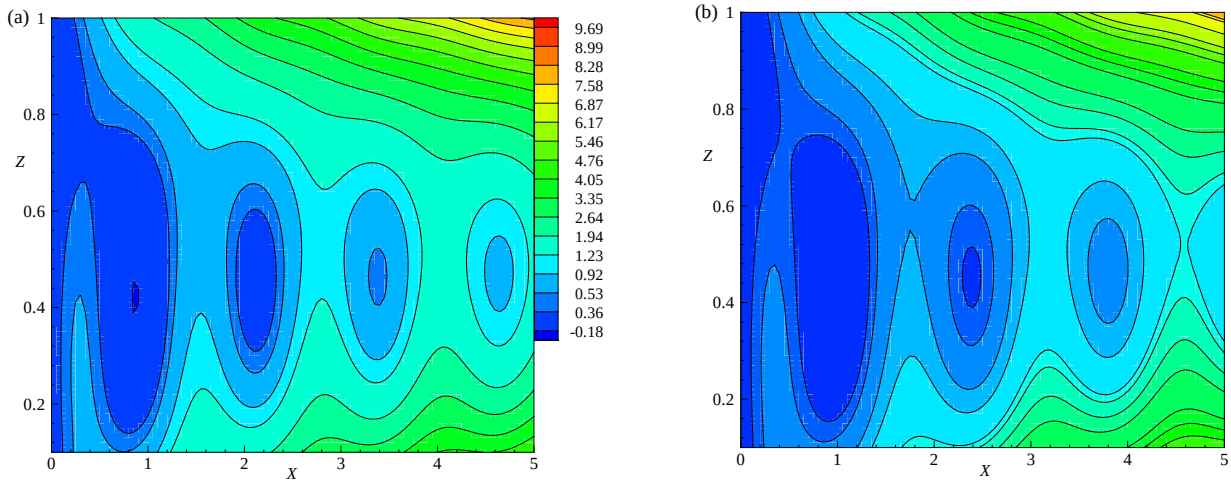

Figure 11. The effect of $E = 0.01$ and 0.015, heatlines (**a**,**b**) are plotted for $\Lambda = 0.2$, $R = 1.05R_{cs}$, $T_0 = 1$, and $q = 0.01$.

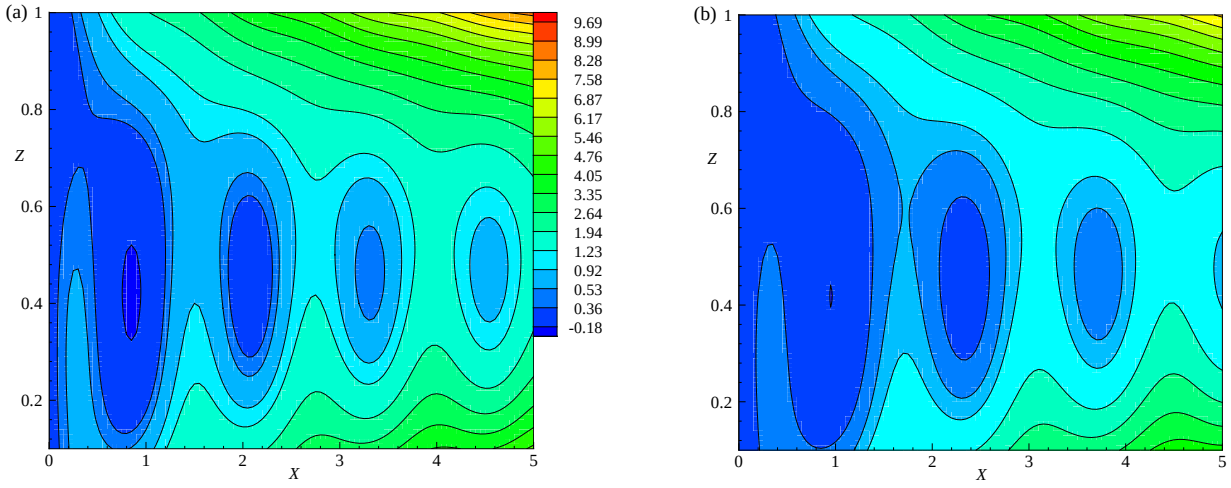

Figure 12. The effect of Λ = 0.4 and 0.6, heatlines (**a**,**b**) are plotted for E = 0.005, R = 1.05 R_{cs}, T_0 = 1, and $q = 0.01$.

8. Conclusions

The nonlinear natural convection was studied in a planer layer of electrically conducting fluid that rotates about the vertical axis in the presence of a uniform horizontal magnetic field and vertical temperature gradient. This problem has applications in Earth's liquid core. The present results help to enhance understanding of the finite amplitude convection when the coupling between the Lorentz force and the Coriolis force present in nonlinear planar layer convection-driven dynamos.

- Linear stability analysis showed that as the small values of E keep decreasing or Λ increasing, the R_{cs} decreases, i.e., the effect of E stabilizes and Λ destabilizes the system.
- Theoretically investigated the nonlinear behavior of cross rolls that occur in the Rayleigh–Bénard convective system of a planar layer dynamo of electrically conducting fluid rotating about the vertical axis in the presence of a horizontal magnetic field.
- The nonlinear partial differential equations was solved using the perturbation method, until $O(\epsilon^8)$ and obtained the approximate solutions.
- Computed the local Nusselt number (N_L) and averaged Nusselt number (Nu) on the hot wall to understand the development of heat flow and the rate of heat transfer, respectively.
- The number of peaks is fixed for a given E while the value of the peak is independent of X for a given E. The absolute peak values of N_L increase as E increases. The number of peaks is fixed for a given Λ. The value of the peak is independent of X for a given Λ. The absolute peak value of N_L increases as Λ decrease. From the N_L results, it is noted that the heat flux is high for decreasing E or increasing Λ.
- It is observed that the Ekman number (E) generates a strong damping effect on heat transfer at high rotation rates but the heat transport enhances as Λ increases. The Roberts number (q) < 1, enhances the heat transfer rate and accordingly the intensity of the flow rate also increases. Similarly, the total energy decays as E increases. The increment in the values of Λ show, the increase in the total energy.
- Obtained the cellular pattern of fluid flow (streamlines) and the hot regions (isotherms) from the eigenfunctions related to the stream function and temperature, respectively. From the streamlines and isotherms trajectories, it is observed that, for the lower values of E the deformation of the fluid pattern is enhanced and more transfer of heat in the flow occurs due to the presence of lesser viscous force in comparison with the Coriolis force. Similarly, for the amplifying values of Λ, there is more deformation in the streamlines and isotherms. This result shows, in the presence of Coriolis force, the magnetic field destabilizes the system.

- Studied the heatline patterns of the flow by using the heat function. The results show that the deformation in the trajectories of heatlines are enhanced as E decreases. A similar trend of deforming heatlines is observed with increasing Λ.

Author Contributions: Conceptualization, Y.R. and G.S.; Methodology, Y.R.; Software, U.S.M. and D.L.; Validation, Y.R., G.S, U.S.M., A.K.R. and D.L.; Visualization A.K.R. and U.S.M.; Writing—Original Draft Preparation, G.S.; Writing—Review and Editing, Y.R., A.K.R. and D.L.; Funding Acquisition, D.L. All authors have read and agreed to the published version of the manuscript.

Funding: D.L. acknowledges the partial financial support from Centers of excellence with BASAL/ANID financing, Grant ANID ABF220001, CEDENNA.

Data Availability Statement: All data underlying the results are available as part of the article and no additional source data are required.

Acknowledgments: The authors thank H. P. Rani (National Institute of Technology, Warangal) for her critical reading, editing, and improving the manuscript's English grammar.

Conflicts of Interest: The authors declare no conflict of interest.

Nomenclature

A	Amplitude
$\vec{B}$	Magnetic field
$\vec{B}_s$	Static magnetic field
B_0	Characteristic field strength
a	Wavenumber
P	Modified pressure
E	Ekman number
$\vec{1}_Z$	Unit vector along Z-axis
$\vec{1}_X$	Unit vector along X-axis
q	Ratio of thermal and magnetic diffusivities
d	The convective zone depth
$\vec{g}$	Gravitational field
Nu	Nusselt number
H^*	Heat function
R	Modified Rayleigh number
R_c	Critical Rayleigh number
R_{cs}	Critical Rayleigh number for stationary convection
T_0	Reference temperature
T	Temperature field
T_s	Static temperature
ΔT	Temperature difference between top and bottom layers
$\vec{V}$	Velocity field
$\vec{V}_s$	Static velocity
U, V, W	Velocity components
X, Y, Z	Cartesian coordinates
t	Time
RBC	Rayleigh–Bénard Convection

Greek symbol

Λ	Elsasser number
β	Adverse temperature gradient
θ	Perturbed temperature
η	Magnetic diffusivity
ρ	Density

ρ_0	Reference density
κ	Coefficient of thermal diffusivity
ν	Kinematic viscosity
α	Thermal expansion coefficient
μ	Dynamic viscosity
μ_m	Magnetic permeability
$\vec{\omega}$	Vorticity field
Ω	Angular velocity
ω	Frequency of oscillations

Superscript

$'$	Dimensional form
*	Perturbed quantities

References

1. Chandrasekar, S. *Hydrodynamic and Hydromagnetic Stability*; Oxford Clarendon Press: Oxford, UK, 1961.
2. Robert, P.H. *An Introduction to Magnetohydrodynamics*; American Elsevier: New York, NY, USA, 1967.
3. Cox, S.M.; Mathews, P.C. New instabilities in two-dimensional rotating convection and magnetoconvection. *Phys. D* **2001**, *149*, 210. [CrossRef]
4. Malkus, W.V.R.; Veronis, G. Finite Amplitude Cellular Convection. *J. Fluid Mech.* **1958**, *4*, 225–260. [CrossRef]
5. Kuo, H.L. Solution of the non-linear equations of the cellular convection and heat transport. *J. Fluid Mech.* **1960**, *10*, 611–630. [CrossRef]
6. Braginsky, S.I. Magnetohydrodynamics of the Earth's core. *Geomagn. Aeron.* **1964**, *4*, 698–712.
7. Eltayeb, I.A. Hydromagnetic convection in a rapidly rotating fluid layer. *Proc. R. Soc. Lond. A* **1972**, *326*, 229–254.
8. Eltayeb, I.A. Overstable hydromagnetic convection in a rotating fluid layer. *J. Fluid Mech.* **1975**, *71*, 161–179. [CrossRef]
9. Aurnou, J.M.; Olson, P.L. Experiments on Rayleigh–Bénard convection, magnetoconvection and rotating magnetoconvection in liquid gallium. *J. Fluid Mech.* **2000**, *430*, 283–307. [CrossRef]
10. Raju, C.S.K.; Ameer Ahammad, N.; Sajjan, K.; Shah, N.A.; Yook, S.; Dinesh Kumar, M. Nonlinear movements of axisymmetric ternary hybrid nanofluids in a thermally radiated expanding or contracting permeable Darcy Walls with different shapes and densities: Simple linear regression. *Int. Commun. Heat Mass Trans.* **2022**, *135*, 106110. [CrossRef]
11. Kumar, M.D.; Raju, C.S.K.; Sajjan, K.; El-Zahar, E.R.; Shah, N.A. Linear and quadratic convection on 3D flow with transpiration and hybrid nanoparticles. *Int. Commun. Heat Mass Trans.* **2022**, *134*, 105995. [CrossRef]
12. Rani, H.P.; Rameshwar, Y.; Brestensky, J. Topology of Rayleigh-Bénard convection and magnetoconvection in plane layer. *Geophys. Astrophys. Fluid Dyn.* **2019**, *113*, 208–221. [CrossRef]
13. Roberts, P.H.; Jones, C.A. The onset of magnetoconvection at large Prandtl number in a rotating layer 1. Finite magnetic diffusion. *Geophys. Astrophys. Fluid Dyn.* **2000**, *92*, 289–325. [CrossRef]
14. Braginsky, S.I. Torsional magnetohydrodynamic vibrations in the Earth's core and variations in the day length. *Geomagn. Aeron.* **1970**, *10*, 3–12.
15. Robert, P.H.; Stewartson, K. On Finite Amplitude Convection in a Rotaiting Magnetic System. *Philos. Trans. R. Soc. Lond. Ser. Math. Phys. Sci.* **1974**, *277*, 287–315.
16. Rameshwar, Y.; Rawoof Sayeed, M.A.; Rani, H.P.; Laroze, D. Finite amplitude cellular convection under the influence of a vertical magnetic field. *Int. J. Heat Mass Transf.* **2017**, *114*, 559–577. [CrossRef]
17. Rawoof Sayeed, M.A.; Rameshwar, Y. Finite Amplitude Cellular Thermohaline Convection. *J. Heat Transf.* **2022**, *114*, 112602. [CrossRef]
18. Rameshwar, Y.; Srinivas, G.; Laroze, D.; Rawoof Sayeed, M.A.; Rani, H.P. Convective instabilities in binary mixture ^3He-^4He in porous media. *Chin. J. Phys.* **2022**, *77*, 773–803. [CrossRef]
19. Rameshwar, Y.; Srinivas, G.; Laroze, D. Finite amplitude oscillatory convection of binary mixture kept in a porous medium. *Processes* **2023**, *11*, 664. [CrossRef]
20. Baklouti, F.S.; Khlifi, A.; Salhi, A.; Godeferd, F.; Cambon, C.; Lehner, T. Kinetic-magnetic energy exchanges in rotating magnetohydrodynamic turbulence. *J. Turbul.* **2019**, *20*, 263–284. [CrossRef]
21. Gupta, V.K.; Keshri, O.P.; Kumar, A. Effect of rotational speed modulation on weakly nonlinear magneto convective heat transfer with temperature-dependent viscosity. *Chin. J. Phys.* **2021**, *72*, 487–498. [CrossRef]
22. Jones, C.A.; Roberts, P.H. The onset of magnetoconvection at large Prandtl number in a rotating layer. II. Small magnetic diffusion. *Geophys. Astrophys. Fluid Dyn.* **2000**, 93, 173–226. [CrossRef]
23. Šoltis, T.; Brestenský, J. Rotating magnetoconvection with anisotropic diffusivities in the Earth's core. *Phys. Earth Planet. Int.* **2010**, *178*, 27–38.
24. Filippi, E.; Brestenský, J.; Šoltis, T. Effects of anisotropic diffusion on onset of rotating magnetoconvection in plane layer; stationary modes. *Geophys. Astrophys. Fluid Dyn.* **2019**, *113*, 80–106. [CrossRef]

25. Sparrow, E.M.; Carlson, C.K. Local and average natural convection Nusselt numbers for a uniformly heated, shrouded or unshrouded horizontal plate. *Int. J. Heat Mass Transf.* **1986**, *29*, 369–379. [CrossRef]
26. Batchelor, G.K. *An Introduction to Fluid Dynamics*; Cambridge University Press: Cambridge, UK, 1993.
27. Jana, S.C.; Metcalfe, G.; Ottino, J.M. Experimental and computational studies of mixing in complex Stokes flows: The vortex mixing flow and multicellular cavity flows. *J. Fluid Mech.* **1994**, *269*, 199–249. [CrossRef]
28. Tony Sheu, W.H.; Rani, H.P. Exploration of vortex dynamics for transitional flows in a three-dimensional backward facing step channel. *J. Fluid Mech.* **2006**, *550*, 61–83. [CrossRef]
29. Sheu, T.; Rani, H.P.; Ten-China, T.; Tsai, S.F. Multilple states, topology and bifurcations of natural convection in a cubical cavity. *Comput. Fluids* **2008**, *37*, 1011–1028. [CrossRef]
30. Kimura, S.; Bejan, A. The heatline visualization of convective heat transfer. *J. Heat Transf.* **1983**, *105*, 916–919. [CrossRef]
31. Morega, A.I.; Bejan, A. Heatline visualization of forced convection laminar boundry layers. *Int. J. Heat Mass Transf.* **1993**, *36*, 3957–3966. [CrossRef]
32. Bejan, A. *Convection Heat Transfer*; Wiley: New York, NY, USA, 1984; pp. 21–23.
33. Komori, K.; Kito, S.; Naumara, T.; Inaguma, Y.; Inagai, T. Fluid flow and heat transfer in the transition process of natural convection over an inclined plate. *Heat Trans. Asian Res.* **2001**, *30*, 648–659. [CrossRef]
34. Kimura, F.; Kitamura, K.; Yamaguchi, M.; Asami, T. Fluid flow and heat transfer of natural convection adjacent to upward facing inclined heated plates. *Heat Trans. Asian Res.* **2003**, *32*, 278–291. [CrossRef]
35. Hooman, K.; Gurgechi, H.; Dincer, I. Heatline and energy-flux-vector visualization of natural convection in a porous cavity occupied by a fluid with temperature-dependent viscosity. *J. Porous Media* **2009**, *12*, 265–275. [CrossRef]

processes

MDPI

Article

Nonlinear Analysis of Cross Rolls of Electrically Conducting Fluid under an Applied Magnetic Field with Rotation

Y. Rameshwar [1], G. Srinivas [2], A. Krishna Rao [1], U. S. Mahabaleshwar [3] and D. Laroze [2,*]

[1] Department of Mathematics, University College of Science, Osmania University, Hyderabad 500007, India; rameshwar@osmania.ac.in (Y.R.); alaka999@gmail.com (A.K.R.)
[2] Instituto de Alta Investigación, Universidad de Tarapacá, Casilla 7 D, Arica 1000000, Chile; gsrinivas@academicos.uta.cl
[3] Department of Mathematics, Shivagangotri, Davangere University, Davangere 577007, India; u.s.m@davangereuniversity.ac.in
* Correspondence: dlarozen@academicos.uta.cl

Abstract: The proposed planer layer dynamo physical model has real-world applications, especially in the Earth's liquid core. Thus, in this paper, an attempt is made to understand the finite amplitude convection when there exists a coupling between the Lorentz force and the Coriolis force. In particular, the effect of a horizontally applied magnetic field is studied on the Rayleigh–Bénard convection (RBC) that contains the electrically conducting fluid and rotates about its vertical axis. Free–free boundary conditions are assumed on the geometry. Attention is focused on the nonlinear convective flow behavior during the occurrence of cross rolls which are perpendicular to the applied magnetic field and parallel to the rotation axis. The visualization of cross rolls is achieved using the Fourier analysis of perturbations up to the $O(\varepsilon^8)$. The relationship of the Nusselt number (Nu) with respect to the Rayleigh number (R), the Ekman number (E), and the Elsasser number (Λ) is investigated. It is observed that E generates a strong damping effect on the flow velocity and on the heat transfer at high rotation rates. Using the heatline concept, it is observed that the temperature within the central regime is enhanced as the Λ increases. The results show that either E decreases or Λ increases, then the heat transfer rate increases.

Keywords: nonlinear convection; earth's liquid core; electrically conducting fluid; planar layer dynamos; cross rolls

Citation: Rameshwar, Y.; Srinivas, G.; Rao, A.K.; Mahabaleshwar, U.S.; Laroze, D. Nonlinear Analysis of Cross Rolls of Electrically Conducting Fluid under an Applied Magnetic Field with Rotation. *Processes* **2023**, *11*, 1945. https://doi.org/10.3390/pr11071945

Academic Editor: Ottavia Giuffrè

Received: 18 April 2023
Revised: 13 June 2023
Accepted: 22 June 2023
Published: 27 June 2023

1. Introduction

In astrophysical and geophysical models related to the Sun, stars, and the outer core of Earth, the convection is affected by both the Coriolis and Lorenz forces. Such a rotating magnetoconvection model with Boussinesq approximation has been studied by many authors, for example, Chandrasekhar [1], Roberts [2], and Cox and Matthews [3], etc. The linear stability analysis of this model shows the system is unstable with respect to either stationary convection or oscillatory convection and depends on the governing physical parameters, namely, Rayleigh number (R), Chandrasekhar number (Q), Taylor number (Ta), thermal Prandtl number (Pr), and magnetic Prandtl number (Pm) or Roberts number. Most of the experimental studies on Rayleigh–Bénard convection (RBC), rotating Rayleigh–Bénard convection, magnetoconvection, and rotating magnetoconvection (RMC) have focused on heat transfer laws. When the control parameter R exceeds its critical value, a cellular regime of steady convection starts to appear. In addition, the motion increases its intensity but remains laminar and steady for a large range of values of R, followed by unsteady turbulent convection. Finite amplitude cellular convection with better approximate solutions has been studied for RBC by Malkus and Veronis [4] and Kuo [5].

In *RBC* with $Ta \neq 0$ and $Q \neq 0$, the critical R ($= R_c$) remains approximately a constant until Q reaches a certain value. When Q increases further, R_c starts to decrease, reaches a minimum and again starts to increase (Chandrasekhar, [1]). Braginsky [6] also studied these rotating magnetic systems and stressed the importance of the Archimedean, magnetic, and Coriolis forces. He revealed that these forces, together with the pressure gradient, would determine the dynamic balance and inertial forces. Eltayeb [7] considered the linear stability analysis to analyze the convection in the hydromagnetic rotating layer. He observed when the principle of exchange of stabilities is valid, four different models can be classified based on the relative directions of the constant magnetic field, B_0 and Ω, (B_0, Ω) namely, (vertical, vertical); (horizontal, vertical); (horizontal, horizontal); (vertical, horizontal) and also for different types of boundaries. The numerical results indicated that the asymptotic dependence of R_c on Ta and Q are equal and independent of the nature of the boundary conditions considered. Later, Eltayeb [8] extended his previous model [7] to study the convective motions near the onset of oscillatory convection. He classified three different motions near the onset, namely: (i) $Ta > Q$, the results for the rotating non-magnetic case, which are retained to leading order; (ii) $Q > Ta$, the results are similar to those for the magnetic non-rotating case to leading order; and (iii) Ta and Q are of same order, the minimum temperature gradient required for the instability is greatly reduced. When these solutions were examined in detail, it was observed that the motions that follow the onset of instability depended primarily on the electrical conductivity rather than on the kinematic properties of boundaries. In addition, in the leading order, the boundary conditions to be applied to the mainstream solutions depended on the conductivity of the boundary but not on the no-slip conditions. When either of the magnetic field or rotation were dominant, there was a possibility of the occurrence of two-dimensional motion. In this case, the Taylor–Proudman theorem was satisfied, while when both magnetic field and rotation were influential, this theorem was no longer valid and the motions were essentially of three-dimensional in nature.

The important laboratory experiments on *RBC*, rotating *RBC* and magnetoconvection *RBC* using the liquid gallium ($Pr = 0.025$) as the working fluid have been carried out by Aurnou and Olson [9]. The properties of liquid gallium are similar to those of the liquid iron in the Earth core. The studies of magnetoconvection have vast industrial applications too [10,11]. The R_c for the magnetoconvection is experimentally determined as a function of Q and Ta. At low rotation rates, the R_c increases linearly with magnetic field intensity. At moderate rotation rates, coherent thermal oscillations were detected by Aurnou and Olson [9] near the onset of convection. These experimental results at the onset were compared with the theoretical predictions of Chandrasekhar [1]. In nearly all of the experimental results, it was mentioned that no well-defined steady convective regime was found. Instead, unsteady or turbulent convection was detected just after onset. Later, these experimental predictions were reproduced by using direct numerical simulations near the onset (Rani et al. [12]). These simulations showed the occurrence of interesting cell patterns. The most relevant geodynamo models were given by Roberts and Jones [13], who extended the model of Braginsky [14] with two sets of boundary conditions.

The present nonlinear convection problem is studied based on the plane layer model proposed by Roberts and Jones [13]. In astrophysics and even in planetary physics, the model considered by Roberts and Jones [13] is yet sufficiently close to reality and is, really, heuristic. This model is very convenient for laboratory experiments, too, which have not yet been done. The linear planer layer dynamo model was considered by Roberts and Jones [13] with the limiting case of Prandtl number tending to infinity. This limiting case enabled the removal of the inertial terms and thus the resultant linearized equation of motion filtered the fast-inertial modes and Alfven waves. The main reason for considering this limiting case was that it simplified the analysis considerably and could able to exhibit an amazingly rich structure. The other motivation was that it is an important limit for geodynamo modelling, in which fast modes are believed to be relatively unimportant.

In the linear stability analysis of the planer layer problem [13], the effect of physical parameters such as E, Λ, R, and q have been thoroughly studied for the occurrence of parallel rolls, cross rolls, and oblique rolls at the onset of convection. In general, E and $q \ll 1$ represent the geophysical models but with these values, it is very difficult to simulate these models and obtain the converged results. This difficulty can be overcome by using one of the approximate methods, such as weakly nonlinear analysis, which yields comparable results with the experimental observations. This method of weakly nonlinear analysis was applied for the Braginsky [14] model by Roberts and Stewartson [15] near the onset of oscillatory convection using the small finite amplitude equations. Further, they have analyzed the linear stability analysis of the cubic and cubic-quintic amplitude equations. These amplitude equations are valid only when R is close to the R_c. In addition, the nonlinear analysis proposed by Malkus and Veronis [4] is valid when the R is near the threshold R_c. Later Kuo [5] proposed a different nonlinear approach, which is valid even for large values of R. The advantages of this approach are that the solutions are found to be valid even for a large range of the imposed temperature differences across the fluid layer and also the rapid convergence of solutions. This solution provides a quantitative theory for the convective heat transport as a function of the temperature difference in the range of laminar flow. Using this approach by Kuo [5], Rameshwar et al., [16], have studied the finite amplitude cellular convection in RBC under the influence of a vertical magnetic field and analyzed the magnetohydrodynamics (MHD) of electrically conducting fluid. Linear and nonlinear properties of thermohaline convection at the onset with the stress-free boundary conditions were investigated using perturbation analysis relevant to oceanic water and groundwater by Rawoof Sayeed and Rameshwar [17]. The stationary and oscillatory finite amplitude convections of a binary mixture with a porous medium were thoroughly investigated by Rameshwar et al., [18,19]. Baklouti et. al. [20] studied the dynamics of incompressible homogeneous turbulence by numerical simulations. Gupta et. al. [21] have analytically examined the effect of rotational speed modulation on the onset of magneto-thermal convection.

The extension studies related to geodynamo models proposed by Eltayeb [7,8], Roberts and Jones [13], and Jones and Roberts [22] have been studied by Šoltis and Brestenský [23]. The authors Šoltis and Brestenský [23] studied the influence of anisotropic diffusive coefficients (thermal diffusion and viscosity) on marginal stability of the horizontal fluid planar layer rotating about the vertical axis and permeated by a horizontal homogeneous magnetic field. The linear stability analysis was thoroughly investigated by the authors for two different types of anisotropic diffusive coefficients. This model was further extended to study the linear stability of the model of rotating magnetoconvection in the horizontal planar layer dynamo by Filippi et al. [24], which is influenced by three anisotropic diffusivities, such as viscosity, thermal diffusivity, and magnetic diffusivity.

In the present study, the nonlinear analysis was employed as proposed by Kuo [5] to study the behavior of cross rolls of electrically conducting fluid in a rotating magnetic system, given by Roberts and Jones [13]. Thus, the objectives of the present problem were as follows:

- Investigate theoretically the nonlinear behavior of cross rolls which occur in the vertically rotating Rayleigh–Bénard convective system of planar layer of electrically conducting fluid in the presence of horizontal magnetic field;
- Solve the nonlinear partial differential equations using the perturbation method proposed by Kuo [5], until the $O(\varepsilon^8)$ and obtain the approximate solutions;
- Obtain the combined effect of Lorenz and Coriolis forces with stress-free boundaries;
- Find the local (N_L) and average (Nu) Nusselt numbers on the hot wall to understand the development of heat flow and the rate of heat transfer, respectively;
- Obtain the cellular pattern of the fluid flow (streamlines) and hot regions (isotherms) from the eigenfunctions related to stream function and temperature, respectively;
- Study the heatline patterns of the flow by using the heat function.

The novelty of the present work is the study of finite amplitude cellular convection when the stationary convection exists as a first instability. The dynamical behavior of the system depends on the type of instabilities that occur in that system. Interesting convective instabilities occur near the onset of convection which is analyzed from the linear stability analysis. At the onset of convection, the system is unstable to either stationary convection (at least one eigenvalue vanishes) or oscillatory convection (an eigenvalue with a purely imaginary part) as a first instability. When an eigenvalue vanishes the principle of exchange of stabilities occurs. In other words, a new steady state replaces the stable motionless state of the fluid. When stationary convection exists, the continuous release of potential energy is balanced by the viscous dissipation of mechanical energy and the convection always occurs in a fairly regular pattern. The results from the linear stability analysis of Roberts and Jones [13] show the occurrence of the modes such as parallel rolls, cross rolls, and oblique rolls based on the wave numbers. Only stationary convection exists as a first instability when the parallel rolls occur, but for the modes of cross rolls and oblique rolls, both stationary convection and oscillatory convection can occur as a first instability depending on the physical parameters. A detailed investigation of the linear stability analysis of the present physical model has been studied by Roberts and Jones [13]. Hence, the nonlinear dynamical behavior of the present considered physical model is investigated when stationary convection exists.

In Section 2, the basic governing equations that are considered by Roberts and Jones [13] are presented. The linear stability analysis is discussed in Section 3 to obtain critical Rayleigh numbers for steady cross roll modes. The nonlinear solutions for the field variables are presented in Section 4. In Section 5, the local Nusselt number (N_L) and average Nusselt number (Nu) are discussed. The distortion of streamlines and isotherms is discussed in Section 6. The heat flow visualization is discussed in Section 7. Finally, the conclusions are presented in Section 8.

2. Mathematical Model

In the present study the fluid with uniform density confined in an infinite horizontal layer was considered. It was assumed that the whole configuration rotates about the vertical axis (OZ) with angular velocity $\vec{\Omega}(= \Omega\vec{1}_Z)$ in the presence of a uniform gravitational field $\vec{g}$ $(= g\vec{1}_Z)$ and the uniform magnetic field $\vec{B}(= B_0\vec{1}_X)$ applied in the horizontal direction where $\vec{1}_X$ is the unit vector along the X-axis and $\vec{1}_Z$ is the unit vector along Z-axis. The Prandtl number is assumed to be large, so as to ignore the inertial forces in the momentum equation in comparison to the Coriolis force [13]:

$$2\vec{\Omega}\rho_0 \times \vec{V}' = -\nabla' P' + \vec{J}' \times \frac{\vec{B}'}{\mu_m} + \vec{g}\alpha\rho_0 T' + \mu\nabla'^2\vec{V}', \tag{1}$$

$$\frac{\partial \vec{B}'}{\partial t'} = \nabla' \times (\vec{V}' \times \vec{B}') + \eta\nabla'^2\vec{B}', \tag{2}$$

$$\frac{\partial T'}{\partial t'} + \vec{V}' \cdot (\nabla' T') = \kappa\nabla'^2 T', \tag{3}$$

$$\nabla' \cdot \vec{V}' = 0, \tag{4}$$

$$\nabla' \cdot \vec{B}' = 0, \tag{5}$$

where P' includes the centrifugal force, $\vec{J}' = \nabla' \times \vec{B}'$ is the electric current density, and other notations are given the nomenclature.

We non-dimensionalized the Equations (1)–(5) using the corresponding length, time, velocity, temperature, magnetic field, and pressure scales as d, $\frac{d^2}{\eta}$, $\frac{\eta}{d}$, βd, B_0, and $2\Omega\rho_0\eta$, respectively.

Therefore, the non-dimensional governing equations are [13]:

$$\vec{1}_Z \times \vec{V} = -\nabla P + \Lambda \vec{J} \times \vec{B} + qR\, T\vec{1}_Z + E\nabla^2\vec{V}, \tag{6}$$

$$\frac{\partial \vec{B}}{\partial t} = \nabla \times (\vec{V} \times \vec{B}) + \nabla^2\vec{B}, \tag{7}$$

$$\frac{\partial T}{\partial t} + \vec{V} \cdot (\nabla T) = q\nabla^2 T, \tag{8}$$

$$\nabla \cdot \vec{V} = 0, \tag{9}$$

$$\nabla \cdot \vec{B} = 0, \tag{10}$$

where $R = \beta g \alpha d^2/2\Omega k$ is the modified Rayleigh number, which measures the ratio of buoyancy force to Coriolis force, $E = \nu/2\Omega d^2$ is the ratio of viscous and Coriolis forces, $\Lambda = B_0^2/2\Omega\eta\mu_m\rho_0$ is the ratio of magnetic force and Coriolis force, and $q = \kappa/\eta$ is the ratio between the thermal and magnetic diffusivities (the Roberts number). For the static solutions from Equations (6)–(10), we obtain

$$\vec{V}_s \equiv \vec{0}, \;\; \vec{B}_s = \vec{1}_X, \;\; T_s = -Z. \tag{11}$$

After introducing the following perturbed quantities in the above static solutions, we obtain

$$\vec{V} = \vec{V}_s + \vec{V}^*, \;\; \vec{B} = \vec{B}_s + \vec{b}^*, \;\; T = T_s + \frac{\theta^*}{q}. \tag{12}$$

For convenience the asterisk symbols are omitted in the further analysis. The perturbed dimensionless governing equations are given by

$$E\nabla^4 W - \frac{\partial \omega_Z}{\partial Z} + R{\nabla_h}^2\theta + \Lambda\frac{\partial}{\partial X}\nabla^2 b_Z = \Lambda\vec{1}_Z \cdot \nabla \times \{\nabla \times [(\nabla \times \vec{b}) \times \vec{b}]\}, \tag{13}$$

$$\left(\frac{\partial}{\partial t} + \vec{V} \cdot \nabla\right)\theta - qW - q\nabla^2\theta = 0, \tag{14}$$

$$\left(\frac{\partial}{\partial t} - \nabla^2\right) b_Z = \frac{\partial W}{\partial X} + \vec{1}_Z \cdot \nabla \times (\vec{V} \times \vec{b}), \tag{15}$$

$$\left(\frac{\partial}{\partial t} - \nabla^2\right) J_Z = \frac{\partial \omega_Z}{\partial X} + \vec{1}_Z \cdot \nabla \times [\nabla \times (\vec{V} \times \vec{b})], \tag{16}$$

$$E\nabla^2\omega_Z + \Lambda\frac{\partial J_Z}{\partial X} + \frac{\partial W}{\partial Z} + \Lambda\vec{1}_Z \cdot \nabla \times \; [(\nabla \times \vec{b}) \times \vec{b}] = 0, \tag{17}$$

where

$$\nabla_h^2 = \tfrac{\partial^2}{\partial X^2} + \tfrac{\partial^2}{\partial Y^2}, \;\; \nabla^2 = \tfrac{\partial^2}{\partial X^2} + \tfrac{\partial^2}{\partial Y^2} + \tfrac{\partial^2}{\partial Z^2}, \;\; \vec{V} = (U, V, W), \;\; \vec{b} = (b_X, b_Y, b_Z), \;\; J_Z = (\nabla \times \vec{b}) \cdot \vec{1}_Z, \;\; \omega_Z = (\nabla \times \vec{V}) \cdot \vec{1}_Z \;\; .$$

Eliminating θ, ω_Z, b_Z, and J_Z from the linear part of Equations (13)–(17), we obtain

$$\mathcal{L}W = \mathcal{N}, \tag{18}$$

$$\mathcal{L} = \mathcal{L}_1 + \mathcal{L}_2 + \mathcal{L}_3 + \mathcal{L}_4 + \mathcal{L}_5 + \mathcal{L}_6,$$

and

$$\mathcal{N} = \mathcal{N}_1 + \mathcal{N}_2 + \mathcal{N}_3 + \mathcal{N}_4 + \mathcal{N}_5,$$

where

$$\mathcal{L}_1 = \left(\frac{\partial}{\partial t} - q\nabla^2\right)\left(\frac{\partial}{\partial t} - \nabla^2\right)^2 \frac{\partial^2}{\partial Z^2},$$

$$\mathcal{L}_2 = E^2\left(\frac{\partial}{\partial t} - q\nabla^2\right)\left(\frac{\partial}{\partial t} - \nabla^2\right)^2 \nabla^6,$$

$$\mathcal{L}_3 = 2E\Lambda\left(\frac{\partial}{\partial t} - q\nabla^2\right)\left(\frac{\partial}{\partial t} - \nabla^2\right)\left(\frac{\partial^2}{\partial X^2}\right)\nabla^4,$$

$$\mathcal{L}_4 = \Lambda^2\left(\frac{\partial}{\partial t} - q\nabla^2\right)\left(\frac{\partial^4}{\partial X^4}\right)\nabla^2,$$

$$\mathcal{L}_5 = RqE\left(\frac{\partial}{\partial t} - \nabla^2\right)^2 \nabla^2 {\nabla_h}^2,$$

$$\mathcal{L}_6 = Rq\Lambda\left(\frac{\partial}{\partial t} - \nabla^2\right)\left(\frac{\partial^2}{\partial X^2}\right){\nabla_h}^2,$$

and

$$\mathcal{N}_1 = \left[ER\left(\frac{\partial}{\partial t} - \nabla^2\right)^2 \nabla^2 {\nabla_h}^2 + R\Lambda\left(\frac{\partial}{\partial t} - \nabla^2\right)\left(\frac{\partial^2}{\partial X^2}\right){\nabla_h}^2\right](\vec{V}\cdot\nabla)\theta,$$

$$\mathcal{N}_2 = -\left[E\Lambda\left(\frac{\partial}{\partial t} - q\nabla^2\right)\left(\frac{\partial}{\partial t} - \nabla^2\right)\nabla^4\frac{\partial}{\partial X} + \Lambda^2\left(\frac{\partial}{\partial t} - q\nabla^2\right)\left(\frac{\partial^3}{\partial X^3}\right)\nabla^2\right]\vec{1}_Z\cdot\nabla\times(\vec{V}\times\vec{b}),$$

$$\mathcal{N}_3 = -\left[\Lambda\left(\frac{\partial}{\partial t} - q\nabla^2\right)\left(\frac{\partial}{\partial t} - \nabla^2\right)\left(\frac{\partial^2}{\partial X\partial Z}\right)\right]\vec{1}_Z\cdot\nabla\times[\nabla\times(\vec{V}\times\vec{b})],$$

$$\mathcal{N}_4 = \left[\Lambda^2\left(\frac{\partial}{\partial t} - q\nabla^2\right)\left(\frac{\partial}{\partial t} - \nabla^2\right)\frac{\partial^2}{\partial X^2}\right]\vec{1}_Z\cdot\nabla\times\nabla\times[(\nabla\times\vec{b})\times\vec{b})]$$

$$+\left[E\Lambda\left(\frac{\partial}{\partial t} - q\nabla^2\right)\left(\frac{\partial}{\partial t} - \nabla^2\right)^2\nabla^2\right]\vec{1}_Z\cdot\nabla\times\nabla\times[(\nabla\times\vec{b})\times\vec{b})],$$

$$\mathcal{N}_5 = -\left[\Lambda\left(\frac{\partial}{\partial t} - q\nabla^2\right)\left(\frac{\partial}{\partial t} - \nabla^2\right)^2\frac{\partial}{\partial Z}\right]\vec{1}_Z\cdot\nabla\times[(\nabla\times\vec{b})\times\vec{b})].$$

Because the surfaces are maintained at a uniform temperature,

$$\theta = 0 \text{ on } Z = 0 \text{ and } 1, \text{ for all } X, Y, \tag{19}$$

and also normal component of the velocity should vanish on boundaries, i.e.,

$$W = 0 \text{ on } Z = 0 \text{ and } 1, \text{ for all } X, Y. \tag{20}$$

The conditions Equations (19) and (20) are independent of the nature of boundaries, such as free–free or rigid–rigid, etc. In the present work, we assumed stress-free boundary conditions [1], hence we obtain

$$\frac{\partial^2 W}{\partial Z^2} = \frac{\partial \omega_Z}{\partial Z} = 0 \text{ on } Z = 0 \text{ and } 1, \text{ for all } X, Y, \tag{21}$$

$$J_X = J_Y = \frac{\partial J_Z}{\partial Z} = 0 \text{ on } Z = 0 \text{ and } 1, \text{ for all } X, Y. \tag{22}$$

Since the physical system is a triple diffusive system, it is unstable to either stationary convection or oscillatory convection near the onset.

3. Linear Stability Analysis

At the onset of convection, the existing perturbations in the system are very small. Hence, the nonlinear terms are smaller when compared to linear terms. The nonlinear contributions are neglected from Equation (18). We obtain a linear differential equation which is given as $\mathcal{L}W = 0$. This process is called linearization. We obtain

$$\begin{aligned}
&[(\frac{\partial}{\partial t} - q\nabla^2)(\frac{\partial}{\partial t} - \nabla^2)^2 \frac{\partial^2}{\partial Z^2} + E^2(\frac{\partial}{\partial t} - q\nabla^2)(\frac{\partial}{\partial t} - \nabla^2)^2\nabla^6 \\
&+2E\Lambda(\frac{\partial}{\partial t} - q\nabla^2)(\frac{\partial}{\partial t} - \nabla^2)(\frac{\partial^2}{\partial X^2})\nabla^4 + \Lambda^2(\frac{\partial}{\partial t} - q\nabla^2)(\frac{\partial^4}{\partial X^4})\nabla^2 \\
&+R(qE(\frac{\partial}{\partial t} - \nabla^2)^2\nabla^2{\nabla_h}^2 + q\Lambda(\frac{\partial}{\partial t} - \nabla^2)(\frac{\partial^2}{\partial X^2}){\nabla_h}^2)]W = 0.
\end{aligned} \tag{23}$$

The resulting Equation (23) is linear. The normal mode solution was considered as $W(X, Y, Z, t) = W(Z)e^{i(aX+lY)+pt}$, where a is the wavenumber along X direction and l is the wavenumber along Y direction. As such, a and l are real numbers and the growth rate (p) may be constant complex number [13]. The marginal state is obtained from $Re(p) = 0$. The two types of modes are classified using the eigenvalue p, namely, if $Im(p) = 0$, then the steady modes exist and if $Im(p) = \omega \neq 0$, then the oscillatory convection exists. The preferred mode of convection depends on the physical parameters, which are relevant to the Earth's outer core. In Earth's outer core, the parameters E and q are considered as small and the Prandtl number is large. The orientation of rolls is classified based on the wavenumber. The modes are parallel rolls, if the wavenumber $a = 0$ (the axis of rolls are parallel to the applied magnetic field), if the wavenumber $l = 0$, gives the cross rolls (the axis of the rolls are perpendicular to the applied magnetic field) and if both the wavenumbers $a \neq 0$ and $l \neq 0$ give the oblique rolls. The linear and nonlinear studies of the present physical model are based on $l = 0$, i.e., cross rolls.

The physical parameters E, Λ, q, and R are used to study the linear and nonlinear behavior of the convective system. As the temperature gradient is increased, the unstable mode may be of stationary convection or oscillatory convection near the onset. We implemented the linear stability analysis using the normal mode analysis, i.e., by substituting $W(X, Y, Z, t) = W(z)e^{(iaX+pt)}$ in the linearized equation $\mathcal{L}W = 0$.

Stationary Convection ($\omega = 0$)

By solving the linearized Equation (23), $R = R_s$ value is obtained for stationary convection and is given by

$$R = \frac{\pi {d_2}^2 + d_2(E{d_2}^2 + \Lambda a^2)^2}{a^2(E{d_2}^2 + \Lambda a^2)},$$

where $d_2 = a^2 + \pi^2$. The critical value of R is obtained from $\partial R/\partial a = 0$. The critical wavenumber is given by $a^2 = {a^2}_{cs} = 2\pi^2$, and the critical Rayleigh number for stationary convection is

$$R_{cs} = \frac{9\pi^5 + 3\pi^2(9E\pi^4 + 2\Lambda\pi^2)^2}{2\pi^2(9E\pi^4 + 2\Lambda\pi^2)}. \tag{24}$$

From the above result the marginal Rayleigh number (R_{cs}), E, and Λ values are obtained for high rotation rates and weak field [13] by the linear stability analysis. The critical values of control parameters were obtained to study the nonlinear behavior of cross rolls. For small values of q, stationary convection occurs and for large values of q oscillatory convection can occur. The value of R_s is free from q while the finite amplitudes depend on q. For the nonlinear studies, a fixed q value as 0.01 was considered for which the stationary convection occurs as a first instability near the onset. For small values of the parameters E and Λ, the minimum value R_{cs} decreases as E decreases and as Λ increases. Thus, the effect of E destabilizes the convective system when E decreases and the effect of Λ destabilizes the convective system when Λ increases (see Figure 1).

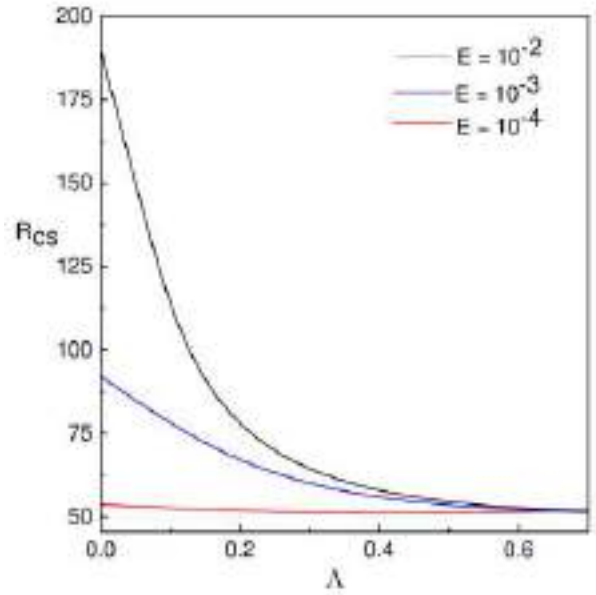

Figure 1. The effect of Λ and E on R_{cs}.

The linear stability theory adopts a less ambitious objective to ascertain when a flow is unstable to infinitesimal disturbances. It thus gives no prediction about transition promoted by sufficiently large disturbance. The ultimate consequence of the instability is never completely determined by linear theory. Thus, in the present study, an attempt was made to understand the nonlinear convection in the presence of the Coriolis force and magnetic field.

4. Method of Solution

The solutions of steady non-linear equations were obtained by following the method proposed by Kuo [5]. These solutions converge more rapidly and are valid for larger temperature differences. In this method, the dependent variables are first expressed as infinite series of a set of orthogonal space functions. This approach to the solution sheds light on the problem of transition to turbulent convection, which happens at a larger temperature difference. An expansion parameter (ε), is defined by [5]:

$$\varepsilon^2 = \frac{R - R_{cs}}{R}. \tag{25}$$

Note that ε is less than one for all values of R. The solution of Equations (13)–(17) are written as

$$f = \varepsilon f_1 + \varepsilon^2 f_2 + \varepsilon^3 f_3 + \varepsilon^4 f_4 + \varepsilon^5 f_5 + \varepsilon^6 f_6 + \cdots, \tag{26}$$

where

$$f = f(U, W, \theta, b_X, b_Z, \omega_Z, J_Z).$$

According to Equation (25), R is given by

$$R = \frac{R_{cs}}{1-\varepsilon^2}, \tag{27}$$

expanding Equation (27) in the power series of ε or by applying the finite formula

$$R = R_{cs} + R_{os}(\varepsilon^2 + \varepsilon^4 + \varepsilon^6 + \cdots + \varepsilon^{2s}), \tag{28}$$

where

$$R_{os} = \frac{R_{cs}}{1-\varepsilon^{2s}}, \quad s = 1, 2, 3 \cdots \tag{29}$$

By introducing Equations (26) and (28) in Equation (18), we obtain for the different ε orders, a sequence of linear non homogeneous differential equations as

$$O(\varepsilon): \quad (\mathcal{L}_1 + \mathcal{L}_2 + \mathcal{L}_3 + \mathcal{L}_4)W_1 + R_{cs}(\mathcal{L}_5 + \mathcal{L}_6)W_1 = 0, \tag{30}$$

$$O(\varepsilon^2): \quad (\mathcal{L}_1 + \mathcal{L}_2 + \mathcal{L}_3 + \mathcal{L}_4)W_2 + R_{cs}(\mathcal{L}_5 + \mathcal{L}_6)W_2 = 0, \tag{31}$$

$$\begin{aligned} O(\varepsilon^3): \quad & (\mathcal{L}_1 + \mathcal{L}_2 + \mathcal{L}_3 + \mathcal{L}_4)W_i + R_{cs}(\mathcal{L}_5 + \mathcal{L}_6)W_i + R_{os}(\mathcal{L}_5 + \mathcal{L}_6)W_{i-2} \\ & + R_{os}(\mathcal{L}_5 + \mathcal{L}_6)W_{i-4} = R_{cs}\mathcal{N}_1 + \mathcal{N}_2 + \mathcal{N}_3 + \mathcal{N}_4 + \mathcal{N}_5, \ \text{for} \ i = 3. \end{aligned} \tag{32}$$

Similarly, at the orders $O(\varepsilon^4)$, $O(\varepsilon^5)$, we obtain

$$\begin{aligned} & (\mathcal{L}_1 + \mathcal{L}_2 + \mathcal{L}_3 + \mathcal{L}_4)W_i + R_{cs}(\mathcal{L}_5 + \mathcal{L}_6)W_i + R_{os}(\mathcal{L}_5 + \mathcal{L}_6)W_{i-2} \\ & + R_{os}(\mathcal{L}_5 + \mathcal{L}_6)W_{i-4} = (R_{cs} + R_{os})\mathcal{N}_1 + \mathcal{N}_2 + \mathcal{N}_3 + \mathcal{N}_4 + \mathcal{N}_5, \ \text{for} \ i = 4, 5. \end{aligned} \tag{33}$$

In general,

$$\begin{aligned} & (\mathcal{L}_1 + \mathcal{L}_2 + \mathcal{L}_3 + \mathcal{L}_4)W_i + R_{cs}(\mathcal{L}_5 + \mathcal{L}_6)W_i + R_{os}(\mathcal{L}_5 + \mathcal{L}_6)W_{i-2} \\ & + R_{os}(\mathcal{L}_5 + \mathcal{L}_6)W_{i-4} = (R_{cs} + 2R_{os})\mathcal{N}_1 + \mathcal{N}_2 + \mathcal{N}_3 + \mathcal{N}_4 + \mathcal{N}_5, \ \text{for} \ i \geq 6. \end{aligned} \tag{34}$$

Here $\mathcal{L}_i$, $i = 1, 2, 3, 4, 5, 6$ is the linear operator and $\mathcal{N}_i$, $i = 1, 2, 3, 4, 5$ represents the nonlinear terms and are functions of W_i, θ_i, b_{Xi}, b_{Zi}, ω_{Zi}, and J_{Zi}. The auxiliary equations for temperature field are given by

$$\left(\frac{\partial}{\partial t} - \nabla^2\right)\theta_1 = qW_1, \tag{35}$$

$$\left(\frac{\partial}{\partial t} - \nabla^2\right)\theta_2 + (\vec{V}_1 \cdot \nabla)\theta_1 = qW_2. \tag{36}$$

In general,

$$\left(\frac{\partial}{\partial t} - \nabla^2\right)\theta_i + \sum_{l=1}^{i-1}(\vec{V}_l \cdot \nabla)\theta_{i-l} = qW_i, \ \text{for} \ \ i \geq 3. \tag{37}$$

The auxiliary equations for the magnetic field

$$\left(\frac{\partial}{\partial t} - \nabla^2\right)b_{X_1} = \frac{\partial U_1}{\partial X}. \tag{38}$$

In general,

$$\left(\frac{\partial}{\partial t}-\nabla^2\right)b_{Xi}=\frac{\partial U_i}{\partial X}+\frac{\partial}{\partial Y}\left(U_1b_{Y_{i-1}}+\cdots+U_{i-1}b_{Y_1}-V_1b_{X_{i-1}}\cdots+V_{i-1}b_{X_1}\right)$$
$$+\frac{\partial}{\partial Z}\left(U_1b_{Z_{i-1}}+\cdots+U_{i-1}b_{Z_1}-W_1b_{X_{i-1}}\cdots+W_{i-1}b_{X_1}\right),\ \text{for}\quad i\geq 2, \tag{39}$$

and

$$\left(\frac{\partial}{\partial t}-\nabla^2\right)b_{Z_1}=\frac{\partial W_1}{\partial X}. \tag{40}$$

In general written as:

$$\left(\frac{\partial}{\partial t}-\nabla^2\right)b_{Z_i}=\frac{\partial W_i}{\partial X}-\frac{\partial}{\partial X}\left(U_1b_{Z_{i-1}}+\cdots+U_{i-1}b_{Z_1}-W_1b_{X_{i-1}}\cdots+W_{i-1}b_{X_1}\right)$$
$$-\frac{\partial}{\partial Y}\left(V_1b_{Z_{i-1}}+\cdots+V_{i-1}b_{Z_1}-W_1b_{Y_{i-1}}\cdots+W_{i-1}b_{Y_1}\right)\ \text{for}\quad i\geq 2. \tag{41}$$

Likewise, the auxiliary equations for vorticity are

$$E\nabla^2\omega_{Z_1}=-\frac{\partial W_1}{\partial Z}-\Lambda\frac{\partial J_{Z_1}}{\partial X}, \tag{42}$$

in general,

$$E\nabla^2\omega_{Z_i}=-\frac{\partial W_i}{\partial Z}-\Lambda\frac{\partial J_{Z_i}}{\partial X}-\Lambda\frac{\partial}{\partial X}b_{X_1}\left(\frac{\partial b_{Y_{i-1}}}{\partial X}-\frac{\partial b_{X_{i-1}}}{\partial Y}\right)+\cdots-\Lambda\frac{\partial}{\partial X}b_{X_{i-1}}\left(\frac{\partial b_{Y_1}}{\partial X}-\frac{\partial b_{X_1}}{\partial Y}\right)$$
$$+\Lambda\frac{\partial}{\partial X}b_{Z_1}\left(\frac{\partial b_{Z_{i-1}}}{\partial Y}-\frac{\partial b_{Y_{i-1}}}{\partial Z}\right)+\cdots+\Lambda\frac{\partial}{\partial X}b_{Z_{i-1}}\left(\frac{\partial b_{Z_1}}{\partial Y}-\frac{\partial b_{Y_1}}{\partial Z}\right)$$
$$+\Lambda\frac{\partial}{\partial Y}b_{Z_1}\left(\frac{\partial b_{X_{i-1}}}{\partial Z}-\frac{\partial b_{Z_{i-1}}}{\partial X}\right)+\cdots-\Lambda\frac{\partial}{\partial Y}b_{Z_{i-1}}\left(\frac{\partial b_{X_1}}{\partial Z}-\frac{\partial b_{Z_1}}{\partial X}\right)$$
$$+\Lambda\frac{\partial}{\partial Y}b_{Y_1}\left(\frac{\partial b_{Y_{i-1}}}{\partial X}-\frac{\partial b_{X_{i-1}}}{\partial Y}\right)+\cdots+\Lambda\frac{\partial}{\partial Y}b_{Y_{i-1}}\left(\frac{\partial b_{Y_1}}{\partial X}-\frac{\partial b_{X_1}}{\partial Y}\right),\ \text{for}\quad i\geq 2, \tag{43}$$

and

$$\left(\frac{\partial}{\partial t}-\nabla^2\right)J_{Z_1}=\frac{\partial\omega_{Z_1}}{\partial X}, \tag{44}$$

in general written as:

$$\left(\frac{\partial}{\partial t}-\nabla^2\right)J_{Z_i}=\frac{\partial\omega_{Z_i}}{\partial X}+\frac{\partial^2}{\partial X\partial Z}\left(V_1b_{Z_{i-1}}+\cdots+V_{i-1}b_{Z_1}-W_{i-1}b_{Y_1}-\cdots-W_1b_{Y_{i-1}}\right)$$
$$+\frac{\partial^2}{\partial Y\partial Z}\left(W_{i-1}b_{X_1}+\cdots+W_1b_{X_1}-U_1b_{Z_{i-1}}-\cdots-U_{i-1}b_{Z_1}\right)$$
$$+\nabla_h^2\left(V_1b_{X_{i-1}}+\cdots+V_{i-1}b_{X_1}-U_{i-1}b_{Y_1}-\cdots-U_1b_{Y_{i-1}}\right),\ \text{for}\quad i\geq 2. \tag{45}$$

4.1. Approximate Solutions

The approximate solutions U, W, θ, b_X, and b_Z are attained in terms of the amplitudes near the onset of stationary convection. The horizontal two boundaries are stress-free, all the space functions U, W, θ, b_X, and b_Z are sine and cosine functions. Thus, from Equations (30), (35), (42), and (44) we have, to the first order periodic solutions as,

$$W_1=A_1\cos aX\sin\pi Z,$$
$$\theta_1=\frac{qA_1}{\pi^2+a^2}\cos aX\sin\pi Z,$$

$$b_{X_1} = -\frac{\pi A_1}{\pi^2 + a^2} \cos aX \cos \pi Z,$$
$$b_{Z_1} = -\frac{aA_1}{\pi^2 + a^2} \sin aX \sin \pi Z, \tag{46}$$

where the nonlinear terms are used to calculate the amplitude A_1. Normally, the terms in Equation (26) are written as

$$W_i = A_i \cos aX \sin \pi Z + \sum_{p_1,q_1} W_{p_1q_1}^{(i)} \cos p_1 aX \sin q_1 \pi Z, \tag{47}$$

$$U_i = \frac{1}{a^2} \frac{\partial^2 W_i}{\partial Z \partial X}, V_i = \frac{1}{a^2} \frac{\partial^2 W_i}{\partial Z \partial Y}, \omega_{Z_i} = \frac{\partial V_i}{\partial X}, \tag{48}$$

$$\theta_i = \frac{qA_i}{\pi^2 + a^2} \cos aX \sin \pi Z + \sum_{p_1,q_1} \theta_{p_1q_1}^{(i)} \cos p_1 aX \sin q_1 \pi Z, \tag{49}$$

$$b_{X_i} = -\frac{\pi A_i}{(\pi^2 + a^2)} \cos aX \cos \pi Z + \sum_{p_1,q_1} b_{X\,p_1q_1}^{(i)} \cos p_1 aX \cos q_1 \pi Z, \tag{50}$$

$$b_{Z_i} = -\frac{aA_i}{(\pi^2 + a^2)} \sin aX \sin \pi Z + \sum_{p_1,q_1} b_{Z\,p_1q_1}^{(i)} \sin p_1 aX \sin q_1 \pi Z, \tag{51}$$

where $W_{p_1q_1}^{(i)}$, $\theta_{p_1q_1}^{(i)}$, $b_{X\,p_1q_1}^{(i)}$, and $b_{Z\,p_1q_1}^{(i)}$ are nonlinear functions of A_1, A_2, A_3,... A_{i-1}. The unknown functions $W_{p_1q_1}^{(i)}$, $\theta_{p_1q_1}^{(i)}$, $b_{X\,p_1q_1}^{(i)}$, and $b_{Z\,p_1q_1}^{(i)}$ are calculated by substituting the Equations (47)–(51) in Equation (18).

4.2. Evaluation of Amplitude A_1

To obtain the second order solutions W_2, θ_2, b_{X_2}, and b_{Z_2}, the nonlinear term $\mathcal{N}$ is solved and Equation (31) is obtained. With $\mathcal{N} = 0$, $\mathcal{L}W_2 = 0$ and

$$W_{02}^{(2)} = 0,\ \theta_{02}^{(2)} = \frac{qA_1^2}{8\pi(\pi^2 + a^2)} \text{ and } b_{X\,02}^{(2)} = \frac{A_1^2}{4(\pi^2 + a^2)},\ b_{Z\,02}^{(2)} = 0. \tag{52}$$

The unknown functions W_2, θ_2, b_{X_2}, and b_{Z_2} are obtained from Equations (31), (36), (39), and (41), respectively, and are given by

$$W_2 = A_2 \cos aX \sin \pi Z,$$
$$\theta_2 = \frac{qA_2}{\pi^2 + a^2} \cos aX \sin \pi Z + {\theta_{02}}^{(2)} {A_1}^2 \sin 2\pi Z,$$
$$b_{X_2} = -\frac{\pi A_2}{\pi^2 + a^2} \cos aX \cos \pi Z + {b_{X02}}^{(2)} {A_1}^2 \cos 2\pi Z,$$
$$b_{Z_2} = -\frac{aA_2}{\pi^2 + a^2} \sin aX \sin \pi Z. \tag{53}$$

From Equation (32) for $i = 3$ the amplitude A_1 is calculated. After using the first and second order solutions, we write Equation (32) as

$$(\mathcal{L}_1 + \mathcal{L}_2 + \mathcal{L}_3 + \mathcal{L}_4)W_3 + R_{cs}(\mathcal{L}_5 + \mathcal{L}_6)W_3$$
$$= -R_{os}[qE(\pi^2 + a^2)^3 a^2 + q\Lambda(\pi^2 + a^2)a^4]$$
$$A_1 \cos aX \sin \pi Z - R_{cs}[E{d_2}^3 a^2 + \Lambda d_2 a^4]\pi {\theta_{02}}^{(2)} {A_1}^3 \cos aX \sin \pi Z$$

$$
\begin{aligned}
&-[a^2 {b_{X02}}^{(2)} E\Lambda q {d_2}^4 + a^4 {b_{X02}}^{(2)} \Lambda^2 q {d_2}^2]\frac{{A_1}^3}{2}\cos aX \sin \pi Z \\
&+R_{cs}[E(a^2+9\pi^2)^3 a^2 + \Lambda(a^2+9\pi^2)a^4]\pi {\theta_{02}}^{(2)} {A_1}^3 \cos aX \sin 3\pi Z \\
&+[a^2 {b_{X02}}^{(2)} E\Lambda q(a^2+9\pi^2)^4 + a^4 {b_{X02}}^{(2)} \Lambda^2 q(a^2+9\pi^2)^2]\frac{{A_1}^3}{2}\cos aX \sin 3\pi Z \\
&-[\frac{2\pi^2 a^2}{d^2} {b_{X02}}^{(2)} - a^2 \frac{{b_{X02}}^{(2)}}{2}]{A_1}^3 \cos aX \sin \pi Z \\
&+[\frac{2\pi^2 a^2}{d^2} {b_{X02}}^{(2)} - a^2 \frac{{b_{X02}}^{(2)}}{(2)}]{A_1}^3 \cos aX \sin 3\pi Z,
\end{aligned} \tag{54}
$$

where $d_2 = a^2 + \pi^2$. By solving the above equation, A_1 is given by

$$
A_1 = -\frac{\sqrt{\left(2\,\Lambda {b_{X02}}^{(2)}\,\pi^2 - \Lambda {b_{X02}}^{(2)}\,d_2 - \pi\,R_{cs}\,{\theta_{02}}^{(2)}\right)R_{os}\,q}}{2\,\Lambda {b_{X02}}^{(2)}\,\pi^2 - \Lambda {b_{X02}}^{(2)}\,d_2 - \pi\,R_{cs}\,{\theta_{02}}^{(2)}}. \tag{55}
$$

The unknown functions W_3, θ_3, b_{X_3}, and b_{Z_3} are obtained from Equations (32), (37), (39), and (41), respectively,

$$
\begin{aligned}
W_3 &= A_3 \cos aX \sin \pi Z + {W_{13}}^{(3)} {A_1}^3 \cos aX \sin 3\pi Z, \\
\theta_3 &= \left(\frac{qA_3}{\pi^2 + a^2} + {\theta_{11}}^{(3)} {A_1}^3\right)\cos aX \sin \pi Z \\
&\quad + {\theta_{13}}^{(3)} {A_1}^3 \cos aX \sin 3\pi Z, \\
b_{X_3} &= \left(-\frac{\pi A_3}{\pi^2 + a^2} + {b_{X11}}^{(3)} {A_1}^3\right)\cos aX \cos \pi Z \\
&\quad + {b_{X13}}^{(3)} {A_1}^3 \cos aX \cos 3\pi Z, \\
b_{Z_3} &= \left(-\frac{aA_3}{\pi^2 + a^2} + {b_{Z11}}^{(3)} {A_1}^3\right)\sin aX \sin \pi Z \\
&\quad + {b_{Z13}}^{(3)} {A_1}^3 \sin aX \sin 3\pi Z.
\end{aligned} \tag{56}
$$

where

$$
W_{13}^{(3)} = \frac{1}{D_{13}}\left(R_{cs}\left(q\Lambda d_{13}\,a^4 + Eq {d_{13}}^3 a^2\right)\pi\,{\theta_{02}}^{(2)}\right)
$$

$$
+\frac{1}{D_{13}}\left(\left(\frac{1}{2}\,a^2 E\Lambda q {d_{13}}^4 + \frac{1}{2}\,a^4\Lambda^2 q {d_{13}}^2\right){b_{X02}}^{(2)} + \left(2\,\frac{\pi^2 a^2}{d_2} - \frac{1}{2}\,a^2\right)b_{X02}^{(2)}\right),
$$

$$
\theta_{11}^{(3)} = \frac{\pi\,\theta_{02}^{(2)}}{d_2}, \quad \theta_{13}^{(3)} = \frac{-\pi\,\theta_{02}^{(2)} + W_{13}^{(3)}\,q}{d_{13}},
$$

and

$$
b_{X11}^{(3)} = \frac{\pi\,b_{X02}^{(2)}}{2d_2}, \quad b_{X13}^{(3)} = -\frac{3\pi\,W_{13}^{(3)}}{d_2} - \frac{3\pi\,b_{X02}^{(2)}}{2d_2},
$$

$$
b_{Z11}^{(3)} = \frac{a\,b_{X02}^{(2)}}{2d_2}, \quad b_{Z13}^{(3)} = -\frac{a\,W_{13}^{(3)}}{d_2} - \frac{a\,b_{X02}^{(2)}}{2d_2},
$$

$$
D_{13} = -9\,q\pi^2 d_{13}^3 - E^2 q d_{13}^6 - 2\,E\Lambda q a^2 d_{13}^4
$$

$$
-\Lambda^2 q^2 a^4 d_{13}^2 + R_{cs}\left(q a^2 E d_{13}^3 + q\Lambda a^4 d_{13}\right),
$$

where $d_{13} = a^2 + 9\pi^2$. This iterative procedure is continued to find A_2 to A_6 and the equivalent W_i, θ_i, b_{X_i}, b_{Z_i}, ω_{Z_i}, and J_{Z_i}, etc.

4.3. Calculation of A_2 and A_3

Initially, Equation (33) is simplified for $i = 4$, i.e.,

$$(\mathcal{L}_1 + \mathcal{L}_2 + \mathcal{L}_3 + \mathcal{L}_4 + R_{cs}(\mathcal{L}_5 + \mathcal{L}_6))W_4 + R_{os}(\mathcal{L}_5 + \mathcal{L}_6)W_2 = (R_{cs} + R_{os})\mathcal{N}_1 + \mathcal{N}_2 + \mathcal{N}_3 + \mathcal{N}_4 + \mathcal{N}_5. \quad (57)$$

The nonlinear terms $\mathcal{N}_i$, $i = 1, 2, 3, 4, 5$ are analyzed by using the Equations (46), (53) and (56). Solving the above Equation (57), we obtain $A_2 = 0$. This indicates that every second order approximate solutions vanish except for $\theta_{02}^{(2)}$ and $b_{X02}^{(2)}$ as shown in Equation (52). Therefore, Equation (57) decreases to

$$(\mathcal{L}_1 + \mathcal{L}_2 + \mathcal{L}_3 + \mathcal{L}_4 + R_{cs}(\mathcal{L}_5 + \mathcal{L}_6))W_4 = K_1 {A_1}^4 \cos 2aX \sin 4\pi Z + K_2 {A_1}^4 \cos 2aX \sin 2\pi Z + K_3 A_1 A_3 \cos 2aX \sin 2\pi Z. \quad (58)$$

The approximate solutions W_4, θ_4, b_{X_4}, b_{Z_4} are evaluated by Equations (33), (37), (39) and (41) and those are given by

$$\begin{aligned}
W_4 &= A_4 \cos aX \sin \pi Z + K_4 A_1^4 \cos 2aX \sin 4\pi Z \\
&+ K_5 A_1^4 \cos 2aX \sin 2\pi Z + K_6 A_1 A_3 \cos 2aX \sin 2\pi Z, \\
\theta_4 &= \frac{q}{(a^2 + \pi^2)} A_4 \cos aX \sin \pi Z + K_7 A_1 A_3 \sin 2\pi Z \\
&+ K_8 A_1^4 \sin 2\pi Z + K_9 A_1^4 \cos 2aX \sin 2\pi Z + K_{10} A_1^4 \cos 2aX \sin 4\pi Z \\
&+ K_{11} A_1^4 \sin 4\pi Z + K_{12} A_1 A_3 \cos 2aX \sin 2\pi Z, \\
b_{X_4} &= \frac{-\pi}{(a^2 + \pi^2)} A_4 \cos aX \cos \pi Z + K_{13} A_1^4 \cos 2aX \cos 4\pi Z \\
&+ K_{14} A_1^4 \cos 2aX \cos 2\pi Z + K_{15} A_1 A_3 \cos 2aX \cos 2\pi Z, \\
b_{Z_4} &= \frac{-a}{(a^2 + \pi^2)} A_4 \sin aX \sin \pi Z + K_{16} A_1^4 \sin 2aX \sin 4\pi Z \\
&+ K_{17} A_1^4 \sin 2aX \sin 2\pi Z + K_{18} A_1 A_3 \sin 2aX \sin 2\pi Z.
\end{aligned} \quad (59)$$

To determine the value of A_3, Equation (33) is solved for $i = 5$, and is given by

$$(\mathcal{L}_1 + \mathcal{L}_2 + \mathcal{L}_3 + \mathcal{L}_4 + R_{cs}(\mathcal{L}_5 + \mathcal{L}_6))W_5 + R_{os}(\mathcal{L}_5 + \mathcal{L}_6)(W_3 + W_1) = (R_{cs} + R_{os})\mathcal{N}_1 + \mathcal{N}_2 + \mathcal{N}_3 + \mathcal{N}_4 + \mathcal{N}_5. \quad (60)$$

Evaluating A_3 from Equations (46), (53), (56), (59) and (60) we obtain,

$$A_3 = \frac{S_1}{S_2}, \quad (61)$$

where

$$\begin{aligned}
S_1 &= -{A_1}^5 \left(\Lambda^2 q {d_2}^2 a^3 + E\Lambda q {d_2}^4 a\right) \left(\frac{-\pi K_{17}}{4a} + \frac{K_{14}}{4} - \frac{b_{X02}^{(2)} W_{13}^3}{2} - \frac{3\pi K_5}{4d_2}\right) a \\
&+ {A_1}^5 \left(\Lambda^2 q {d_2}^2 a^2 + E\Lambda q {d_2}^4\right) \left(-\frac{a(2\pi K_{14} + 2aK_{17})}{4d_2} - \pi b_{X02}^{(2)} b_{Z11}^{(3)} - \pi b_{X02}^{(2)} b_{Z13}^{(3)} + K_{17}\right) \pi a \\
&+ {A_1}^5 a^2 \left(\Lambda^2 q {d_2}^2 a^2 + E\Lambda q {d_2}^4\right) \left(\frac{\pi(2\pi K_{14} + 2aK_{17})}{4d_2} + \frac{b_{X02}^{(2)}}{2}\left(\pi b_{X11}^{(3)} + a b_{Z11}^{(3)}\right)\right) \\
&- {A_1}^5 a^2 \left(\Lambda^2 q {d_2}^2 a^2 + E\Lambda q {d_2}^4\right) \left(\frac{b_{X02}^{(2)}}{2}\left(3\pi b_{X13}^{(3)} + a b_{Z13}^{(3)}\right) + \pi b_{X02}^{(2)} b_{X11}^{(3)} - \pi b_{X02}^{(2)} b_{X13}^{(3)}\right)
\end{aligned}$$

$$+\left(q\Lambda d_2\, a^4 + Eq{d_2}^3 a^2\right)\left(\pi\,\theta_{02}^{(2)}\, W_{13}^{(3)} - \frac{3\pi\, qK_5}{4d_2} - \pi\,\frac{K_9}{4} - \pi\, K_8\right){A_1}^5 R_{cs}$$

$$+\left(q\Lambda d_2\, a^4 + Eq{d_2}^3 a^2\right)\left(\pi\,\theta_{02}^{(2)}\, W_{13}^{(3)} - \frac{3\pi\, qK_5}{4d_2} - \pi\, K_9 - \pi\, K_8\right){A_1}^5 R_{os}$$

$$-\Lambda R_{os}\, a^4 d_2\, q^2 - E R_{os}\, a^2 {d_2}^3 q^2 - {A_1}^5 a^2\left(\Lambda^2 q{d_2}^2 a^2 + E\Lambda q{d_2}^4\right)K_{14},$$

and

$$S_2 = -\left(q\Lambda d_2\, a^4 + Eq{d_2}^3 a^2\right)\left(-\pi\, K_8 - \pi\,\theta_{02}^{(2)} - \pi\, q\frac{3K_5}{4}\right){A_1}^2 R_{cs}$$

$$-\left(q\Lambda d_2\, a^4 + Eq{d_2}^3 a^2\right)\left(-\pi\, K_8 - \pi\,\theta_{02}^{(2)} - \pi\, q\frac{3K_5}{4}\right){A_1}^2 R_{os}$$

$$+{A_1}^2\left(\Lambda^2 q{d_2}^2 a^3 + E\Lambda q{d_2}^4 a\right)\left(\frac{b_{X02}^{(2)}}{2} - \frac{\pi\, K_{17}}{4a} + \frac{K_{14}}{4} - \frac{3\pi\, K_5}{4d_2}\right)a$$

$$-{A_1}^2\left(\Lambda^2 q{d_2}^2 a^2 + E\Lambda q{d_2}^4\right)\left(-\frac{a(2\,\pi\, K_{14} - 2\,aK_{17})}{4d_2} + \frac{\pi\, ab_{X02}^{(2)}}{d_2} + K_{17}\right)\pi\, a$$

$$-{A_1}^2\left(\Lambda^2 q{d_2}^2 a^2 + E\Lambda q{d_2}^4\right)\left(\frac{\pi\,(2\,\pi\, K_{14} + 2\,aK_{17})}{4d_2} - \frac{b_{X02}^{(2)}}{2}\right)a^2$$

$$-{A_1}^2\left(\Lambda^2 q{d_2}^2 a^2 + E\Lambda q{d_2}^4\right)\left(\frac{\pi^2 b_{X02}^{(2)}}{d_2} - K_{14}\right)a^2 + \Lambda R_{os}\, a^4 d_2\, q^2 + E R_{os}\, a^2 {d_2}^3 q^2.$$

The amplitude A_3 is determined by using the first, second, third and fourth order approximate solutions. From Equations (60), (37), (39) and (41), the fifth order approximate solutions are obtained

$$\begin{aligned} W_5 &= A_5\,\cos aX \sin \pi Z \\ &+\left(K_{19}\,{A_1}^5 + K_{20}\,{A_1}^2 A_3\right)\cos 3\,aX \sin \pi Z \\ &+\left(K_{21}\,{A_1}^3 + K_{22}\,{A_1}^5 + K_{23}\,{A_1}^2 A_3\right)\cos aX \sin 3\,\pi Z \\ &+\left(K_{24}\,{A_1}^5 + K_{25}\,{A_1}^2 A_3\right)\cos 3\,aX \sin 3\,\pi Z \\ &+K_{26}\,{A_1}^5 \cos aX \sin 5\,\pi Z + K_{27}\,{A_1}^5 \cos 3\,aX \sin 5\,\pi Z, \end{aligned} \tag{62}$$

$$\begin{aligned} \theta_5 &= \left(\frac{qA_5}{d_2} + K_{28}\,{A_1}^2 A_3\right)\cos aX \sin \pi Z \\ &+\left(K_{29}\,{A_1}^3 + K_{30}\,{A_1}^5 + K_{31}\,{A_1}^2 A_3\right)\cos aX \sin 3\,\pi Z \\ &+\left(K_{32}\,{A_1}^5 + K_{33}\,{A_1}^2 A_3\right)\cos 3\,aX \sin \pi Z \\ &+\left(K_{34}\,{A_1}^5 + K_{35}\,{A_1}^2 A_3\right)\cos 3\,aX \sin 3\,\pi Z \\ &+K_{36}\,{A_1}^5 \cos aX \sin 5\,\pi Z + K_{37}\,{A_1}^5 \cos 3\,aX \sin 5\,\pi Z, \end{aligned} \tag{63}$$

$$\begin{aligned} b_{X_5} &= \left(-\frac{\pi\, A_5}{d_2} + K_{38}\,{A_1}^5\right)\cos aX \cos \pi Z \\ &+\left(K_{39}\,{A_1}^3 + K_{40}\,{A_1}^5 + K_{41}\,{A_1}^2 A_3\right)\cos aX \cos 3\,\pi Z \\ &+\left(K_{42}\,{A_1}^5 + K_{43}\,{A_1}^2 A_3\right)\cos 3\,aX \cos \pi Z \end{aligned}$$

$$+\left(K_{44}\,{A_1}^5 + K_{45}\,{A_1}^2 A_3\right)\cos 3\,aX\cos 3\,\pi\,Z$$
$$+K_{46}\,{A_1}^5\cos aX\cos 5\,\pi\,Z + K_{47}\,{A_1}^5\cos 3\,aX\cos 5\,\pi\,Z, \tag{64}$$

$$b_{Z_5} = \left(-\frac{aA_5}{d_2} + K_{48}\,{A_1}^5 + K_{49}\,{A_1}^2 A_3\right)\sin aX\sin\pi\,Z$$
$$+\left(K_{50}\,{A_1}^3 + K_{51}\,{A_1}^5 + K_{52}\,{A_1}^2 A_3\right)\sin aX\sin 3\,\pi\,Z$$
$$+\left(K_{53}\,{A_1}^5 + K_{54}\,{A_1}^2 A_3\right)\sin 3\,aX\sin\pi\,Z$$
$$+\left(K_{55}\,{A_1}^5 + K_{56}\,{A_1}^2 A_3\right)\sin 3\,aX\sin 3\,\pi\,Z$$
$$+K_{57}\,{A_1}^5\sin aX\sin 5\,\pi\,Z + K_{58}\,{A_1}^5\sin 3\,aX\sin 5\,\pi\,Z. \tag{65}$$

Here the coefficients $K_i, i = 1, 2, \ldots 58$ in Equations (58)–(65) are functions of a, E, Λ, and q. The simplifications become more critical as ε order increases. Similarly, the simplification was carried until the eighth order of Equation (34) to calculate for A_4, A_5, and A_6. Proceeding as above, it can be observed that $A_2 = A_4 = A_6 = 0$.

5. Convective Heat Transport

The changes in the two-dimensional flow patterns are illustrated by the local Nusselt number, N_L, distributions over the heated plate. The heat transport coefficient in terms of the N_L is expressed as [16,25]

$$N_L = \frac{\partial T}{\partial n}, \tag{66}$$

here n denotes the normal direction on a plane. The heat transport is measured by the average Nusselt number (Nu), which is independent of Z and is given by

$$Nu = \overline{WT} - \frac{\partial \overline{T}}{\partial Z}, \tag{67}$$

here the bar indicates a horizontal mean. Using Equation (67), Nu is obtained by integrating the expression over the boundary, $Z = 0$ [16].

$$Nu = \frac{1}{L}\int_0^L WT - \frac{\partial T}{\partial Z}|_{z=0} dX, \tag{68}$$

where L is the normalized horizontal cell width.

5.1. Local Nusselt Number (N_L)

Figure 2a illustrates the changes of N_L for distinct values of E with respect to X. In selected regions, the number of peaks and the location of maximum and minimum of N_L values depend on E. The maximum of N_L value is constant, as X increases for defined E. However, as E decreases, the number of peaks is increased in a selected region. Figure 2b illustrates the variation of N_L for different Λ concerning to X. The location of the maximum N_L value is independent of the dimensionless plate length but depends on Λ. The existence of the number of peaks in the given region of X increases, as Λ increases. Figure 2b illustrates the heat that is transported from the fluid to the boundary is increased as Λ increase.

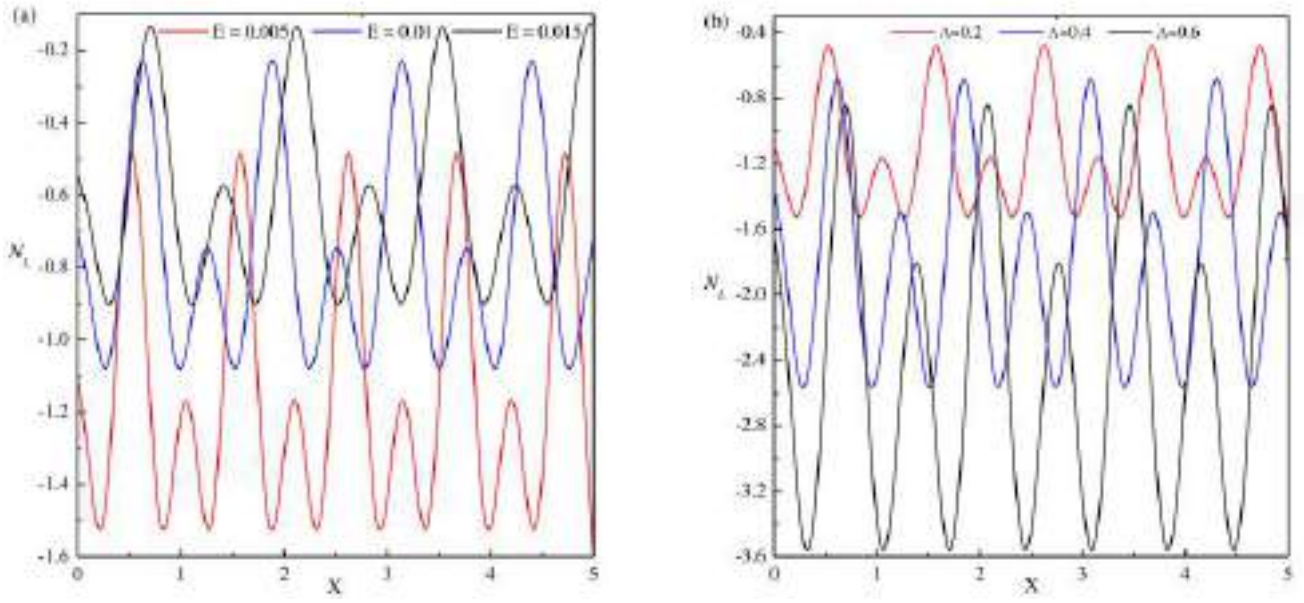

Figure 2. Variation of N_L with respect to X. (**a**) $\Lambda = 0.2$ and $q = 0.01$ for different E, (**b**) $E = 0.005$ and $q = 0.01$ for different Λ.

5.2. Average Nusselt Number (Nu)

The dependency of Nu on the control parameters was studied near and away from the onset of stationary convection. Let $Nu^{(2)}(s = 1)$, $Nu^{(4)}(s = 2)$ and $Nu^{(6)}(s = 3)$, indicate the second-, fourth- and sixth-order approximations, for Nu, respectively. The second order approximation is given by

$$Nu^{(2)} = 1 + \frac{2qR_{os}}{2\Lambda(a^2 - \pi^2) + R_{cs}}. \tag{69}$$

The approximations for $Nu^{(4)}$ and $Nu^{(6)}$ are lengthy, so it is not shown here to conserve space. The change of Nu with respect to R is shown in Figure 3 for different values of E and Λ. Figure 3a shows the effect of E on Nu in the R plane for fixed $\Lambda = 0.2$ and $q = 0.01$. It illustrates that the rate of heat transfer is enhanced for decreasing E. Figure 3b shows the effect of Λ on heat transfer rate for fixed $E = 0.005$ and $q = 0.01$. The enhancement of heat transfer is observed for increasing Λ values. The small values of q are relevant to Earth's outer core. It is very difficult to perform numerical simulations for small values of the physical parameters. For $q < 1$ stationary convection is preferred [13]. Figure 3c shows that for $q < 1$ and as q increases, the Nu increase. Thus the effect of $q < 1$ shows, the heat transfer rate are enhanced and accordingly the intensity of the flow rate also increase. The change of kinetic energy with respect to R/R_{cs} is represented in Figure 4. Figure 4a demonstrates the change in Nu for various E values as well as for a fixed value of $\Lambda = 0.2$. The change in E produces small change in the potential energy, in comparison with the kinetic energy. Thus, the total energy decreases as E increase. Figure 4b shows the energy distribution for different Λ and for fixed $E = 0.005$ and $q = 0.01$. The amplifying values of Λ show that the total energy is also increased.

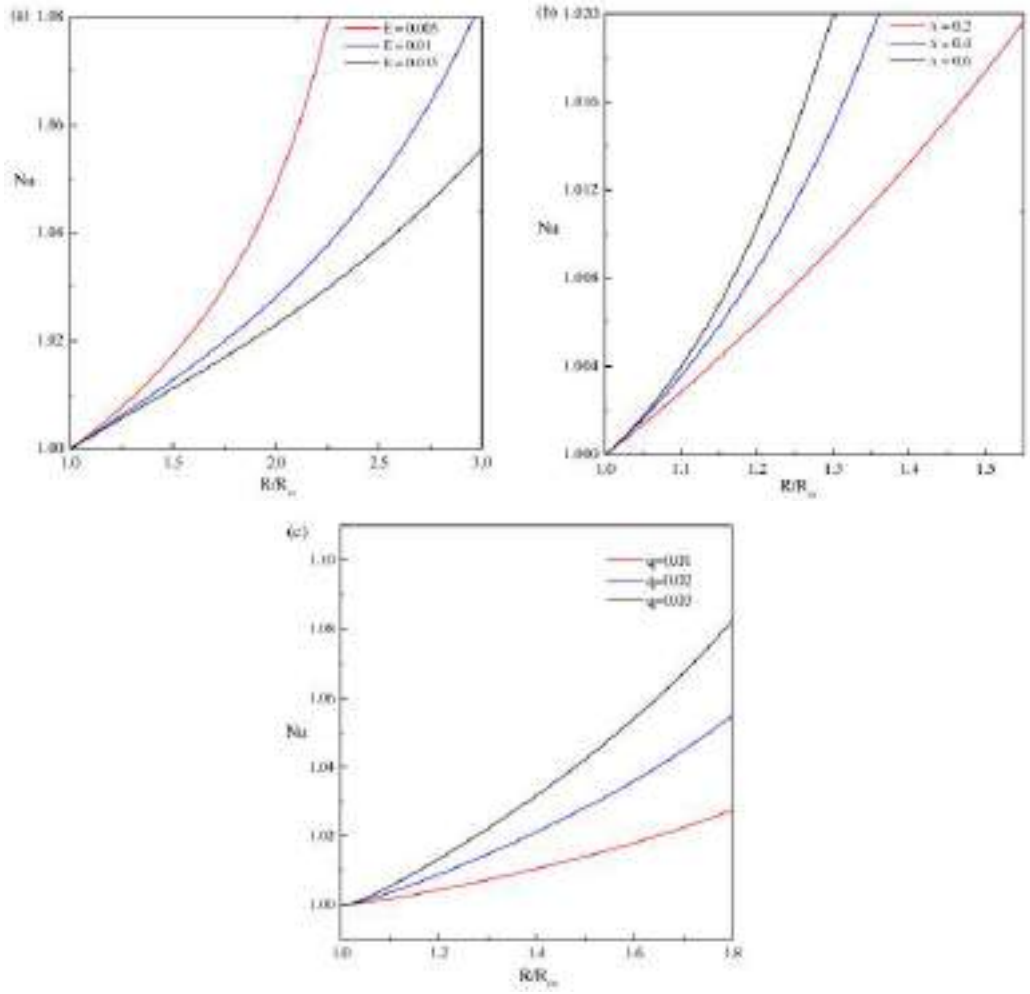

Figure 3. Dependence of Nussult number (Nu) on Rayleigh number (R/R_{cs}). (**a**) $\Lambda = 0.2$ and $q = 0.01$ for different E, (**b**) $E = 0.005$ and $q = 0.01$ for different Λ, (**c**) $E = 0.005$ and $\Lambda = 0.2$ for different q.

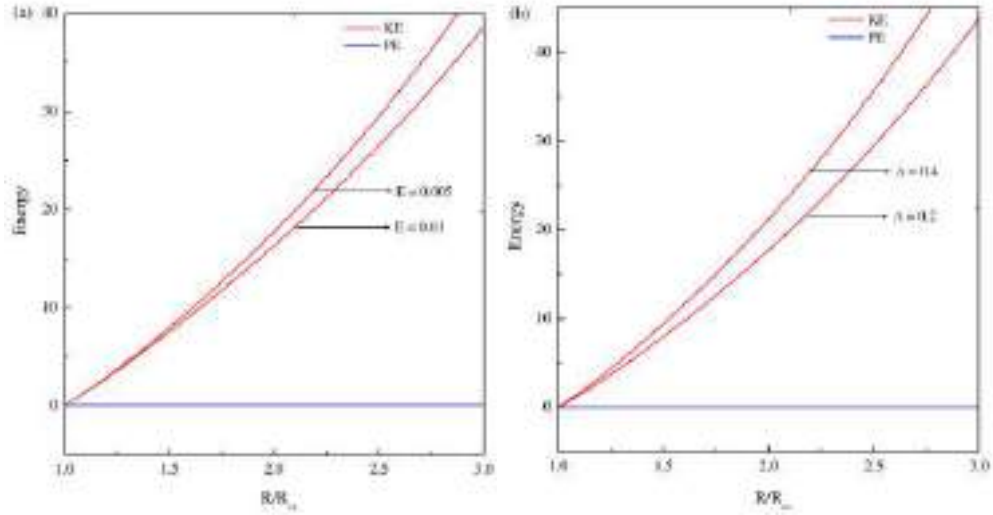

Figure 4. Dependence of kinetic energy and potential energy on Rayleigh number (R/R_{cs}) are plotted. (**a**) $\Lambda = 0.2$ and $q = 0.01$ for different E, (**b**) $E = 0.005$ and $q = 0.01$ for different Λ.

6. Distortion of Streamlines and Isotherms

The fluid flow behavior is visualized by the stream function (Ψ) which is obtained from the velocity components U and W. The relation between the velocity components and stream function (Ψ) is [26]

$$U = -\frac{\partial \Psi}{\partial Z} \quad \text{and} \quad W = \frac{\partial \Psi}{\partial X},$$

which produce a single equation

$$\Psi = \nabla^2 \Psi = 0 \quad \text{for} \quad X = 0, \sqrt{2}\pi/a \ \text{ and } \ Z = 0, 1.$$

The points with equal temperature connected with lines are called isotherms. The snapshots of the heat transport and flow field near the onset of stationary convection are expressed in terms of streamlines and isotherms.

The general attributes of the streamlines and isotherms with respect to the variation in R, E, and Λ are shown in Figures 5–8. Figure 5 illustrates the pattern of streamlines and isotherms near the onset of convection ($R \simeq R_{cs}$). Figure 5a, shows the pattern of streamlines for E = 0.005, Λ = 0.2, q = 0.01. The absolute maximum and the absolute minimum values of circular strengths are 0.11215 and −0.11216, respectively. Figure 5c shows the pattern of streamlines for E = 0.01, Λ = 0.2. This figure shows the absolute maximum and the absolute minimum values of circular strengths as 0.11243 and −0.11243, respectively. From Figure 5a,c the maximum strength of rolls at $R \simeq R_{cs}$ are decreased as E increases. Thus, as E increases, R_{cs} also increases, accordingly Nu decreases and hence the absolute maximum of circulation strength decreases. Figure 5e illustrate the pattern of streamlines with E = 0.005 and Λ = 0.4. These streamlines have the absolute minimum and maximum values with the circular strengths as −0.12116 and 0.121117, respectively. By comparing Figure 5a,e, the periodic rectangular rolls are observed near the $R \simeq R_{cs}$, but as Λ increases the maximum strength of rolls is increased and the minimum strength of roll decreases. Thus, as Λ increases, R_{cs} decreases, accordingly Nu increases, and hence the absolute maximum of circulation strength increases. Figure 5a–f are plotted for the values of $R \simeq R_{cs}$ and the flow pattern are rectangular rolls and follows the symmetric nature over the range of $0 \leq X \leq 1$. Since the stream function equations show the symmetric property. Similarly, for the same values of E and Λ, the isotherms formed as horizontal lines near $R \simeq R_{cs}$, as shown in Figure 5b,d,f. At $R \simeq R_{cs}$, the strength of isotherms is of small magnitude, representing the conduction dominant heat transport inside the considered region. These isotherms are smooth lines that span over the whole region.

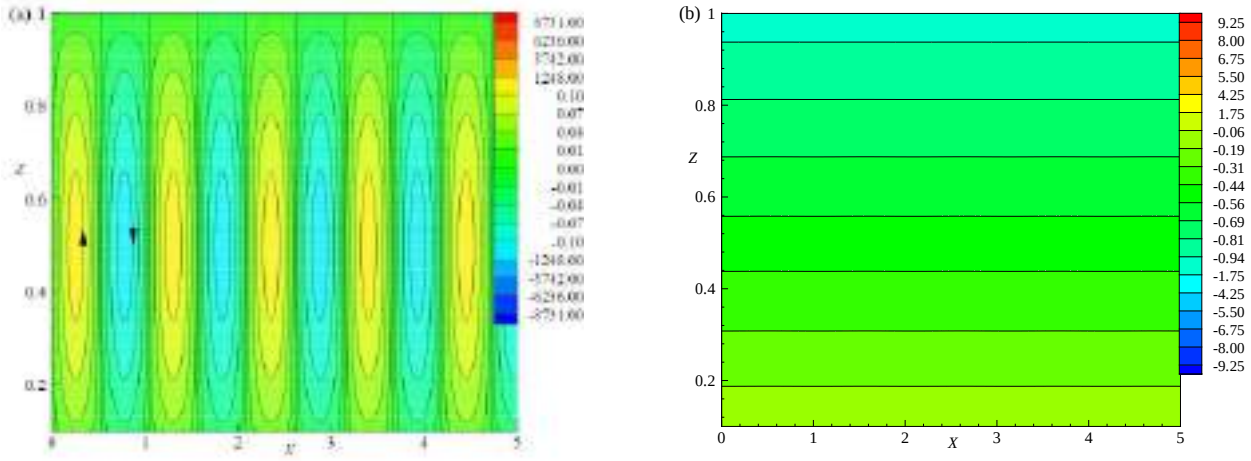

Figure 5. *Cont.*

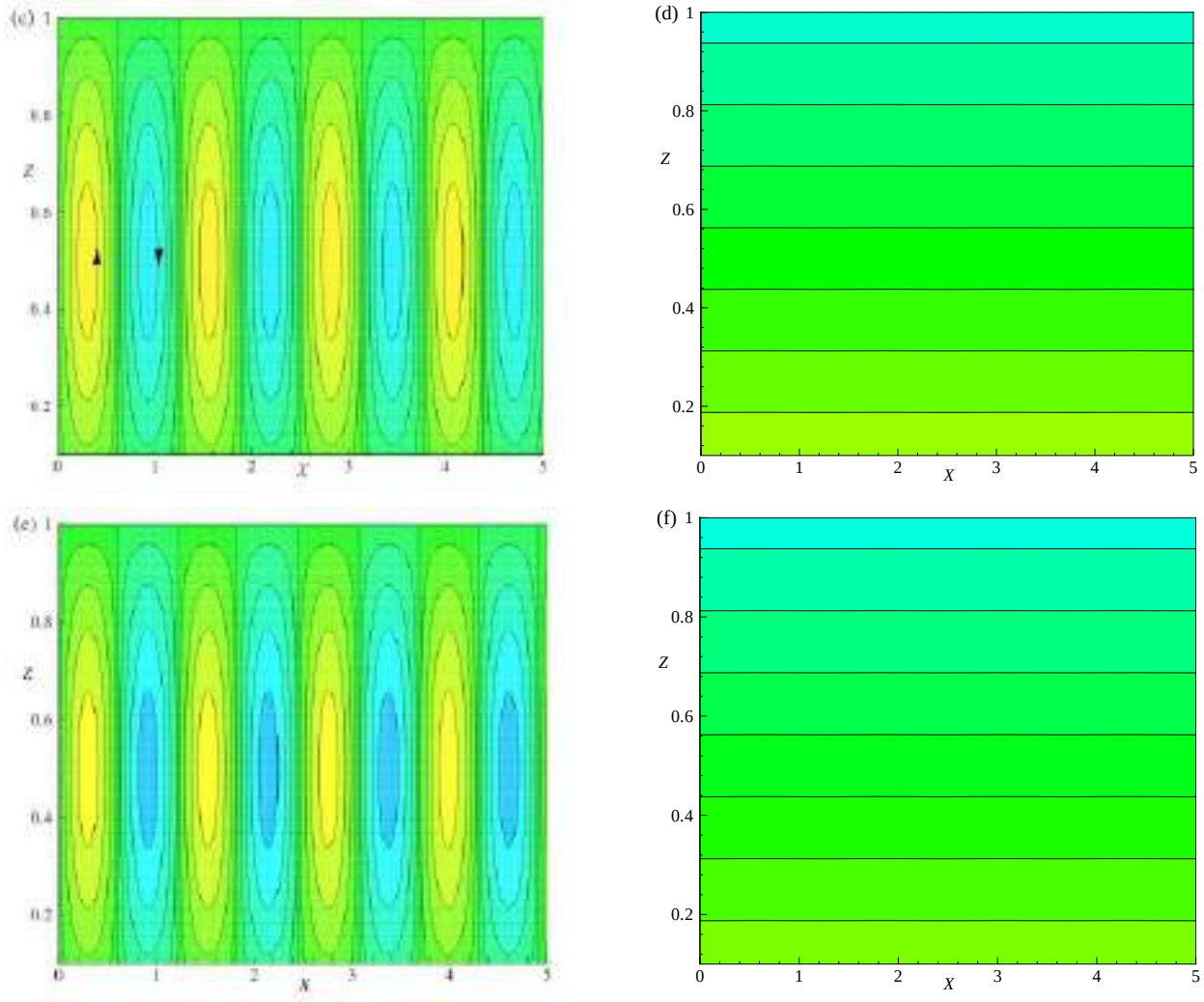

Figure 5. The Effect of E and Λ near R_{cs}, streamlines (**a**) for E = 0.005, Λ = 0.2, and $q = 0.01$, (**c**) E = 0.01, Λ = 0.2, and $q = 0.01$, (**e**) E = 0.005, Λ = 0.4, and $q = 0.01$ and isotherms (**b**) E = 0.005, Λ = 0.2, and $q = 0.01$, (**d**) E = 0.01, Λ = 0.2, and $q = 0.01$, (**f**) E = 0.005, Λ = 0.4, and $q = 0.01$ are plotted.

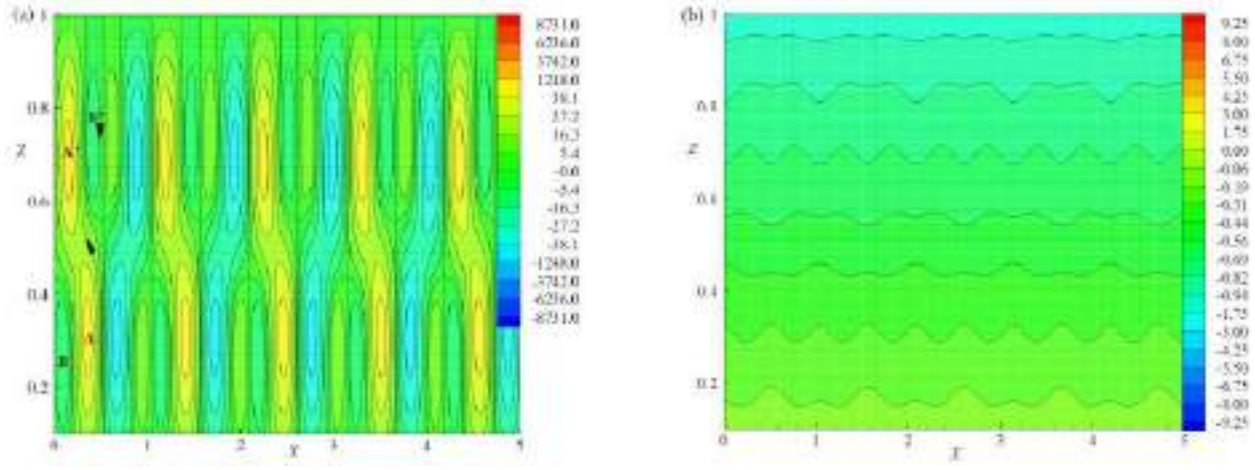

Figure 6. *Cont.*

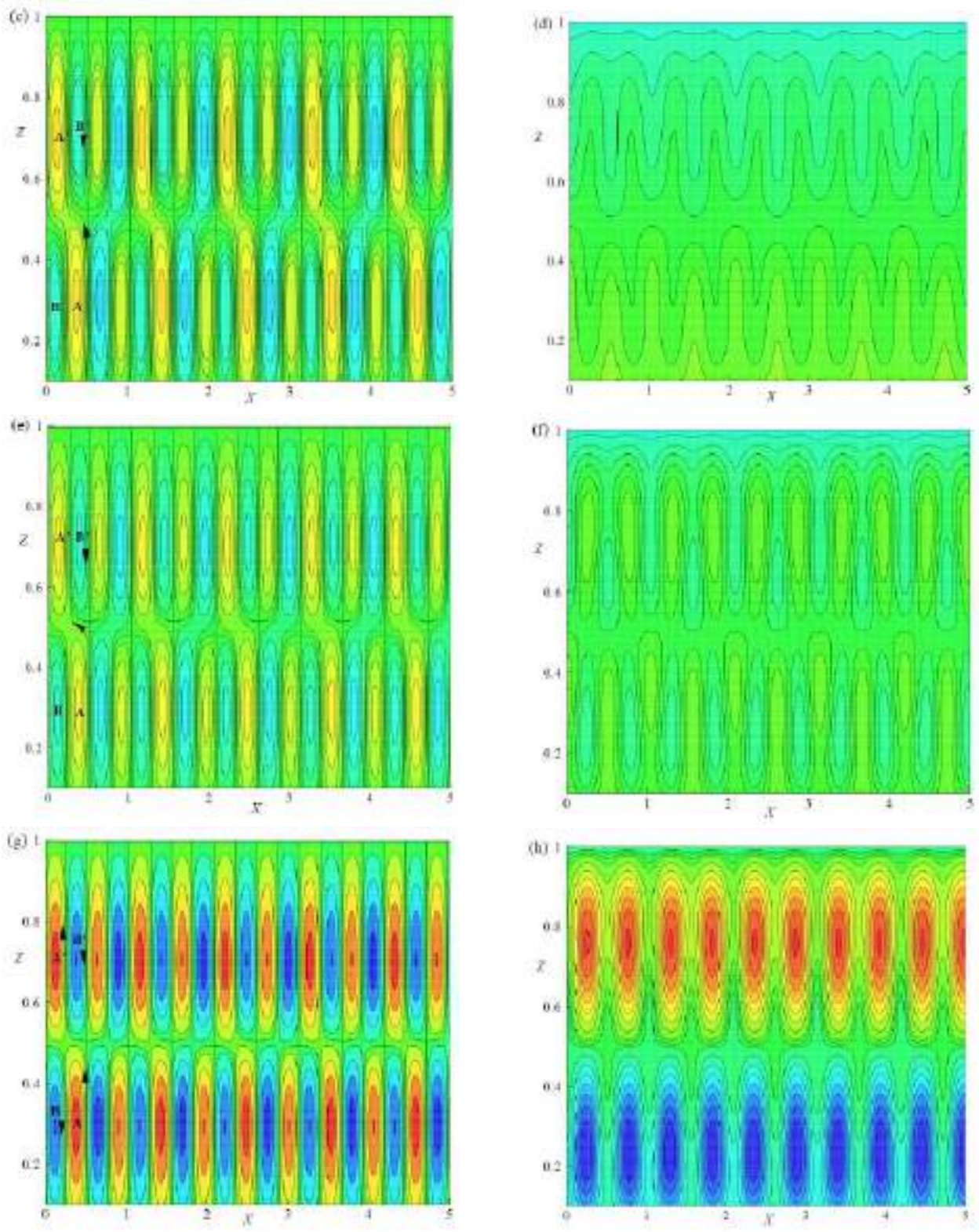

Figure 6. The Effect of $R = 10R_{cs}$, $20R_{cs}$, $30R_{cs}$ and $80R_{cs}$, streamlines (**a**,**c**,**e**,**g**) and isotherms (**b**,**d**,**f**,**h**) are plotted for $E = 0.005$, $\Lambda = 0.2$, and $q = 0.01$.

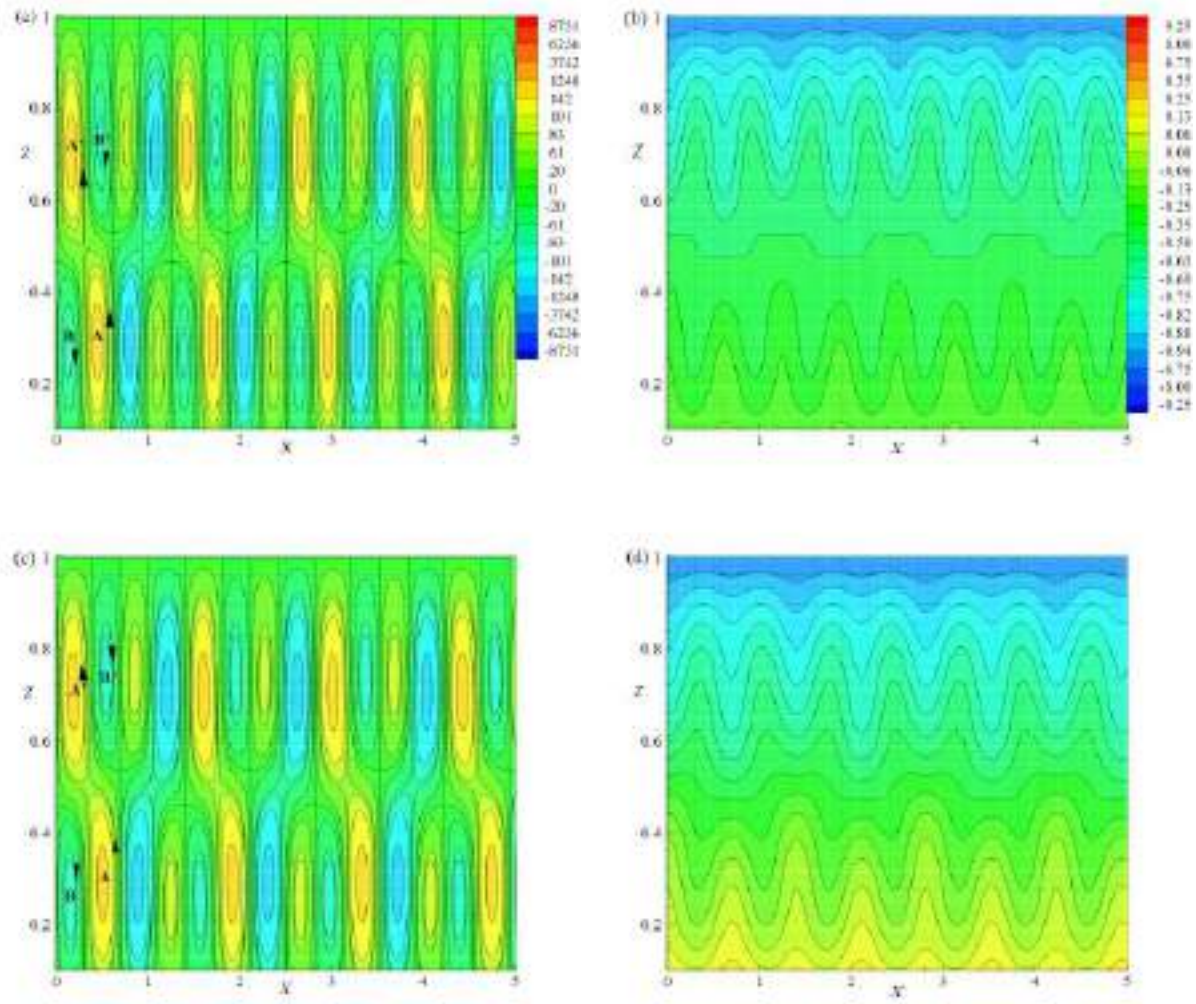

Figure 7. The Effect of E = 0.01 and 0.015, streamlines (**a**,**c**) and isotherms (**b**,**d**) are plotted for Λ = 0.2, R = 20R_{cs}, and q = 0.01.

The snapshot of streamlines and isotherms for different values of R and for fixed values of $E = 0.005$, $\Lambda = 0.2$, and $q = 0.01$ are displayed in Figure 6a–h. It is observed that for $R = 10R_{cs}$ and for the cell lying between $0 \leq X \leq 1$, the absolute minimum and maximum values are with the circulation strengths -43.4965 and 43.4965, respectively, as shown in Figure 6a. As R increases from R_{cs} to $10R_{cs}$, the basic cells become more deformed due to the growth of two vortices B and B' located at the top right and bottom left boundaries with the circulation strength -16.315. The basic cell with two vortices A and A' has circulation strength 38.059. The temperature profiles in terms of isotherms are illustrated in Figure 6b for same values of physical parameters that are considered in Figure 6a. The isotherms are of nearly in wavy shape with the absolute maximum and minimum values of -0.00212 and -1.00271, respectively. It indicates the maximum of heat transfer process is occurred by convection. Figure 6c,d illustrate the streamlines and isotherms for $R = 20R_{cs}$. The temperature gradient and the gravitational buoyancy force act together and changes the flow structure as shown in Figure 6c. The bicellular patterns of streamlines turn out to be multicellular models and these cells divide the field of motion at the core for a cell lies between $0 \leq X \leq 1$ with the absolute maximum and minimum values of circulation strengths 220.829 and -220.845, respectively. The vortices B and B' showed their

presence with −82.822 as the circulation strength in the opposite direction of an original cell. For these considered values of physical parameters, the behavior of isotherms is shown in Figure 6d, which exhibit the mode of convective heat transport inside the fluid layer. In the fluid layer, the absolute maximum and minimum values of isotherms are respectively, −0.00275 and −1.0052. When R is increased from $20R_{cs}$ to $30R_{cs}$, the small vortices B and B' shown in Figure 6c are increased with circulation strength −398.740. Thus, the basic cell encountered more deformation (Figure 6e) and has the absolute maximum and minimum values at 638.172 and −638.027, respectively. Accordingly, the isotherm curves develop more deformation. The absolute maximum and minimum values of isotherms in the layer are, respectively, −0.00449 and −1.01101. As R is increased from $30R_{cs}$ to $80R_{cs}$ (Figure 6g), the two vortices B and B' grow in size and split the basic cell into two vortices located on either side of the secondary cell with the absolute maximum (9976.78) and minimum (−9977.74) strengths. The heat flow pattern becomes chaotic, which is shown in Figure 6h when R increases to $80R_{cs}$. The absolute maximum and minimum values of isotherms in the layer are, respectively, 8.75285 and −9.67347. From Figure 6, it is observed that as R increases from R_{cs} to $80R_{cs}$, the onset of turbulent flows are producible.

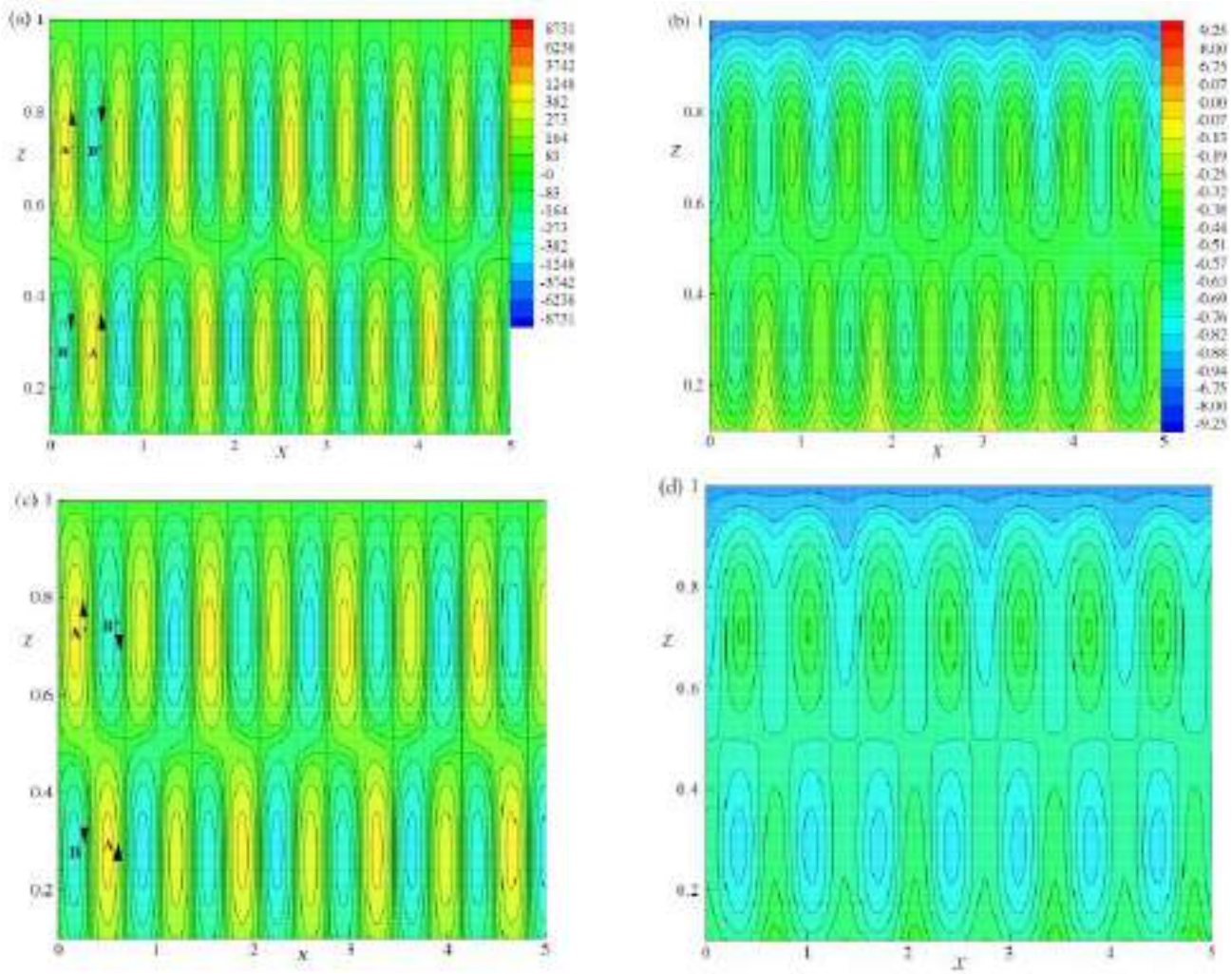

Figure 8. The Effect of Λ = 0.4 and 0.6, streamlines (**a**,**c**) and isotherms (**b**,**d**) are plotted for E = 0.005, $R = 20R_{cs}$ and q = 0.01.

Figure 7a–d, illustrate the streamlines and isotherms for different values of E and for a fixed set of other parameters $R = 20R_{cs}$, $\Lambda = 0.2$, and $q = 0.01$. The behavior of the flow

field was investigated by considering the flow pattern in the region $0 \leq X \leq 1$, as shown in Figure 6a–d (E = 0.005) and Figure 7a–d (E = 0.01 and 0.015). Figure 7a shows streamlines for E = 0.01 in the considered range of X. The absolute maximum and minimum values of circulation strengths are 162.15 and −162.149, respectively. There exist two vortices B and B' outside the basic cell with the circulation strength −82.806 as shown in Figure 7a. The basic cell also contains two vortices namely A and A' with a circulation strength of 141.881. Figure 7c is plotted for E = 0.015, which has the absolute maximum and absolute minimum values of circulation strength as 140.453 and −140.471, respectively. The flow pattern in the region $0 \leq X \leq 1$ contains a deformed basic cell due to the growth of two vortices B and B' that exist at either side of the basic cell and are located at the top and bottom boundaries with circulation strength −60.81. The basic cell also has two vortices A and A' with a circulation strength value of 122.90. Finally from Figures 6c and 7a,c it is observed that the strength of the basic cell and pattern deformation decrease as E increases. This implies that the effect of E stabilizes the convective system. The flow of heat transfer is shown in Figure 7b,d for E = 0.01 and 0.015, respectively.

Figure 8a–d show the streamlines and isotherms for different Λ values and for $E = 0.005$, $R = 20R_{cs}$, and $q = 0.01$. The effect of Λ was studied from Figures 6c,d and 8a–d. In Figure 8a the streamlines are plotted for $\Lambda = 0.4$. By considering the flow pattern in the range of $0 \leq X \leq 1$, the absolute maximum and minimum values of circulation strengths are 436.721 and −436.747, respectively. In this range, the basic cell is deformed by two vortices B and B', which are located at the top right and bottom left of the layer and on either side of the basic cell with circulation strength −272.97. The basic cell also encloses two vortices A and A' with strength 382.13. Figure 8c shows the streamlines for $\Lambda = 0.6$ in the considered range of $0 \leq X \leq 1$, with the absolute maximum and minimum values of circulation strength 663.595 and −663.555, respectively. In addition, there exist two vortices B and B' with circulation strength −414.71. The basic cell also enclosed two vortices A and A' with circulation strength 580.65. As Λ increases from 0.4 to 0.6 the deformation and circulation strength of cells (A, A') increase. This implies that the effect of Λ destabilizes the convective system. The isotherms are plotted in Figures 6d and 8b,d for distinct values of $\Lambda = 0.2$, 0.4 and 0.6. The lines of isotherms change to a more circular form as Λ increases. Thus, the incremental values of Λ destabilize the convective system.

Topology of Flow

The topology constraint is based on the Euler number ($\zeta^{'}$) of the flow. As described by Jana et al. [27], $\zeta^{'}$ on the surface is defined as the sum of the Poincare indices of the critical points on the surface and is given by

$$NE - (NH + \frac{1}{2}NP) = \zeta^{'}, \tag{70}$$

here the NE represents the number of elliptic points, NH is the number of hyperbolic points, and NP is the number of parabolic points [28,29]. In Figure 9a, the vorticity contours are exhibited for $R \simeq R_{cs}$, E= 0.005, Λ= 0.2 and $q = 0.01$. The present simulated flow fulfils the topological rule given in Equation (70) with $NP = 0$, $NH = 2$, and $NE = 2$. For $R = 20R_{cs}$, an equivalent investigation has been done for vorticity contours in Figure 9b and Equation (70) is satisfied with NP = 0, NE = 8, and NH = 8.

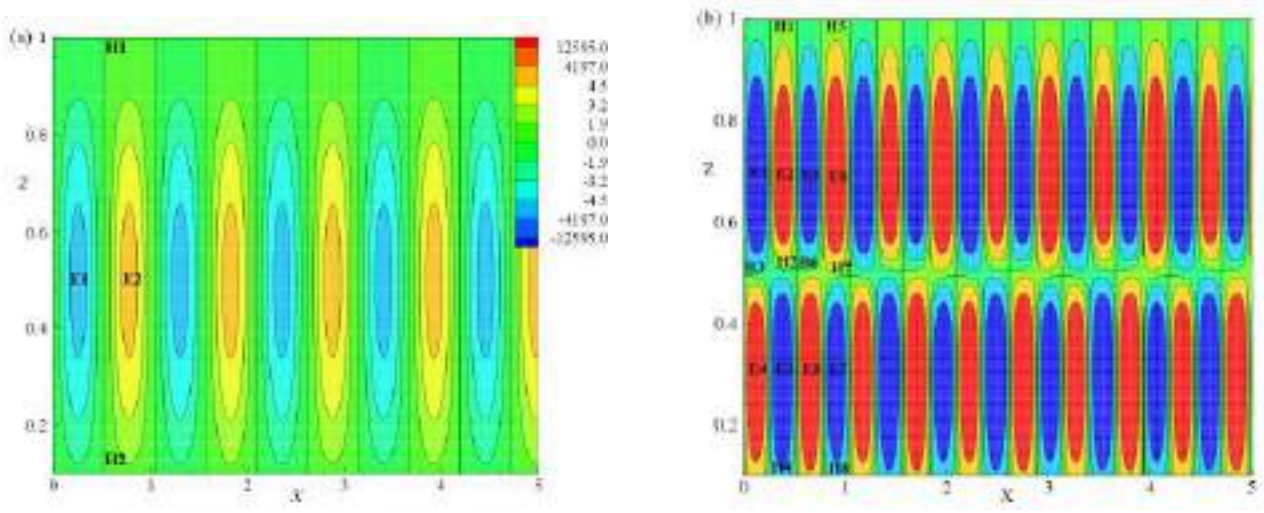

Figure 9. Vorticity lines for (**a**) $R \simeq R_{cs}$, $E = 0.005$, $\Lambda = 0.2$, and $q = 0.01$, (**b**) $R = 20R_{cs}$, $E = 0.005$, $\Lambda = 0.2$, and $q = 0.01$.

7. Heat Function

Heatlines depict the convective heat transport phenomenon, whereas the isotherms are mainly useful for visualizing heat transfer in the domain of conduction. The heat function and heatline analyzes were developed by Kimura and Bejan [30] to visualize heat transmission through the fluid flow, later Morega and Bejan [31] successfully used the concept of heatlines. Different researchers [32–35] used this concept for dissimilar applications of natural convective systems. The heat function (H^*) is defined as

$$\frac{\partial H^*}{\partial X} = WT - \frac{\partial T}{\partial Z}, \tag{71}$$

$$-\frac{\partial H^*}{\partial Z} = UT - \frac{\partial T}{\partial X}, \tag{72}$$

where $T = T_s + \theta$ and $T_s = T_0 - Z$. The Equations (71) and (72) do not exhibit the symmetric property. Differentiating Equations (71) and (72) with respect to X and Z, respectively, and subtracting the resulting equations yields

$$\frac{\partial^2 H^*}{\partial X^2} + \frac{\partial^2 H^*}{\partial Z^2} = \frac{\partial (WT)}{\partial X} - \frac{\partial (UT)}{\partial Z}. \tag{73}$$

From the definition of heat function, Equations (71) and (72), the boundary conditions on H^* follow [16]:

$$H^*(X,0) = H^*(0,0) + \int_0^X (WT - \frac{\partial T}{\partial Z})dX, \text{ at } Z = 0 \text{ and } 0 \le X \le \sqrt{2}\pi/a, \tag{74}$$

$$H^*(X,1) = H^*(0,1) + \int_0^X (WT - \frac{\partial T}{\partial Z})dX, \text{ at } Z = 1 \text{ and } 0 \le X \le \sqrt{2}\pi/a, \tag{75}$$

$$H^*(0,Z) = H^*(0,0) - \int_0^Z (UT - \frac{\partial T}{\partial Z})dZ, \text{ at } X = 0 \text{ and } 0 \le Z \le 1, \tag{76}$$

$$H^*(\sqrt{2}\pi/a,Z) = H^*(\sqrt{2}\pi/a,0) - \int_0^Z (UT - \frac{\partial T}{\partial Z})dZ, \text{ at } X = \sqrt{2}\pi/a \text{ and } 0 \le Z \le 1. \tag{77}$$

Results and Discussion for Heatlines

Figure 10a–d, illustrate the pattern of heatlines for different Rayleigh number values, $R \simeq R_{cs}$, $R = 1.05R_{cs}$, $1.15R_{cs}$ and $1.25R_{cs}$, respectively, for fixed values of $E = 0.005$, $\Lambda = 0.2$, and $q = 0.01$. When the system is at a conduction state ($R < R_{cs}$) heatlines are always parallel to Z-axis and perpendicular to isotherms. Figure 10a illustrates the heatlines for $R \simeq R_{cs}$. It is observed that the heatline contours within the domain are normal to the $Z = 0$ and $Z = 1$ lines due to conduction dominant heat transfer. For $R \simeq R_{cs}$, the absolute maximum and minimum values of heatlines are 10.2224 and 0.0241, respectively, in the considered range $0 \leq X \leq 5$. In the neighborhood of $X = 0$, the heatlines at the center of the system depict the structure which is similar to the parabolic structure. The curvature at the central part of the system increases as X increases. This shows that the nonlinear propagation of heat transfer occurs when $R \simeq R_{cs}$. Hence, the transition takes place from the conduction state to the convection state at $R \simeq R_{cs}$. Figure 10b is plotted for $R = 1.05R_{cs}$. The absolute maximum and minimum values of heatlines are 10.3081 and -0.2774, respectively, in the considered range $0 \leq X \leq 5$. The heatline with a strength of -0.18 exist near the line $X = 0$ and the heatline with strength 9.69 exist at $X = 5$. The strength of heatlines increases as X increases. Some heatlines occurred in the form of a closed path. As R increases from R_{cs} the heatlines with same strength are changed to a closed path as shown in Figure 10a,b. For higher values, this indicates that the convective heat flow is more intense at the center. Figure 10c shows heatlines at $R = 1.15R_{cs}$ and having the absolute maximum and minimum values of heatlines 10.3666 and -0.62655, respectively. In this figure, the number of closed paths of heatlines at the center is increased for $R = 1.15R_{cs}$. The size of closed path of heatlines for $R = 1.15R_{cs}$ is more than that for $R = 1.05R_{cs}$. Figure 10d shows the heatlines for $R = 1.25R_{cs}$ with the absolute maximum and minimum values of 10.3972 and -0.88096, respectively. The number of closed paths of heatlines increases at the center for $R = 1.25R_{cs}$. The size of closed path of heatlines for $R = 1.25R_{cs}$ is increased in comparison with that of the heatlines for $R = 1.15R_{cs}$. For large R, the convective heat transmission is more intense. It is observed that the heatlines become denser with the increase in R. Figure 10a–d indicate that the heat transfer across the layer is increased as R increases. Heatlines will not exhibit periodic patterns due to the non-symmetry nature of Equations (71) and (72).

Figures 10b and 11a,b are plotted with the same strength of heatlines so as to analyze the influence of E on heat flow for the fixed values of Λ, R, and q. In the considered range of $0 \leq X \leq 5$, for $E = 0.01$, (Figure 11a) the absolute maximum and minimum values of heatlines are noted to be 8.4264 and -0.18554, respectively, and for $E = 0.015$ (Figure 11b) these values are 7.51142 and -0.11574, respectively. In both of these Figure 11a,b, the heatlines intensity decays with E. The size of the closed path and the number of closed paths with the same strength decreased as E increases. From Figures 10b and 11a,b it is fascinating to observe the inhibition of temperature in the central regime as E increases.

Figures 10b and 12a,b are plotted with the same strength of heatlines to analyze the effect of Λ on heat flow for the fixed values of E, R, and q. In the considered range of $0 \leq X \leq 5$ for $\Lambda = 0.4$ (Figure 12a) with the absolute maximum and minimum values of heatlines as 8.55642 and -0.23723, respectively. These values for $\Lambda = 0.6$ (Figure 12b) are 7.74043 and -0.18296, respectively. In both Figure 12a,b, the heatlines are dominated by convection and form closed loops. The size and the number of closed loops with the same strength increase as Λ increases. From Figures 10b and 12a,b it is observed that the temperature within the central regime is enhanced as Λ increase by observing heatlines.

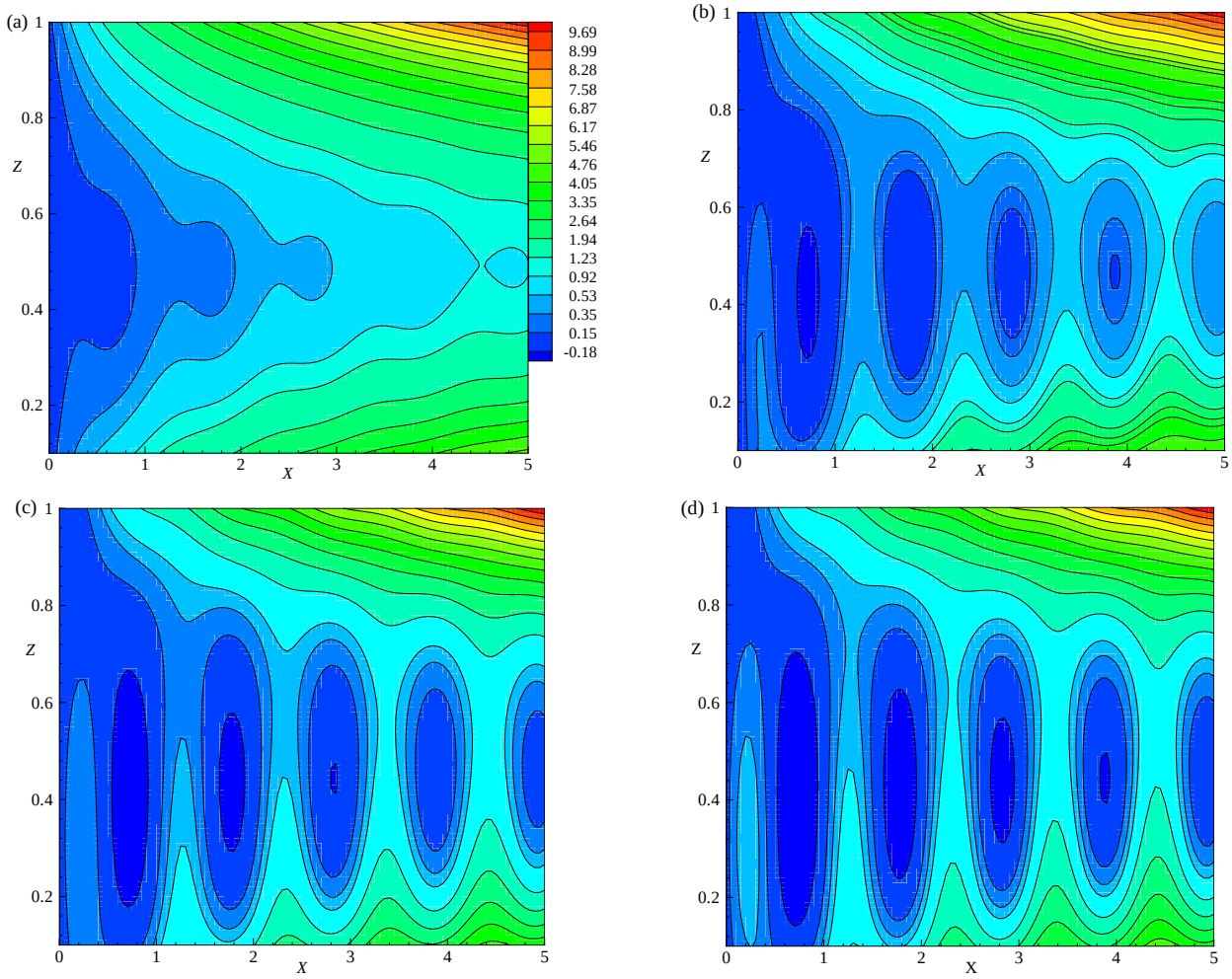

Figure 10. The effect of $R \simeq R_{cs}$, $R = 1.05R_{cs}$, $1.15R_{cs}$ and $1.25R_{cs}$, heatlines (**a**–**d**) are plotted for $E = 0.005$, $\Lambda = 0.2$, $T_0 = 1$, and $q = 0.01$, respectively.

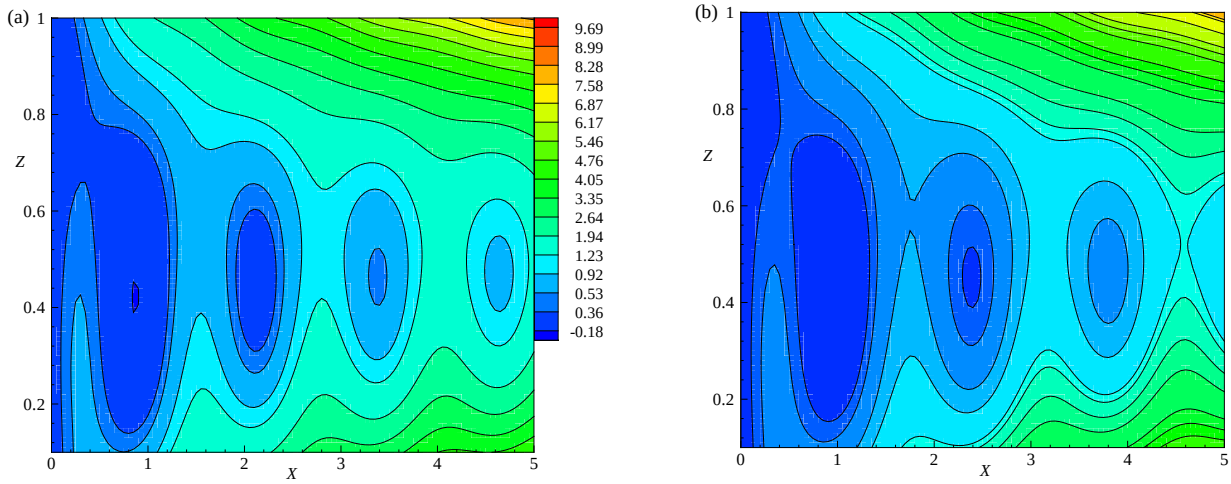

Figure 11. The effect of $E = 0.01$ and 0.015, heatlines (**a**,**b**) are plotted for $\Lambda = 0.2$, $R = 1.05R_{cs}$, $T_0 = 1$, and $q = 0.01$.

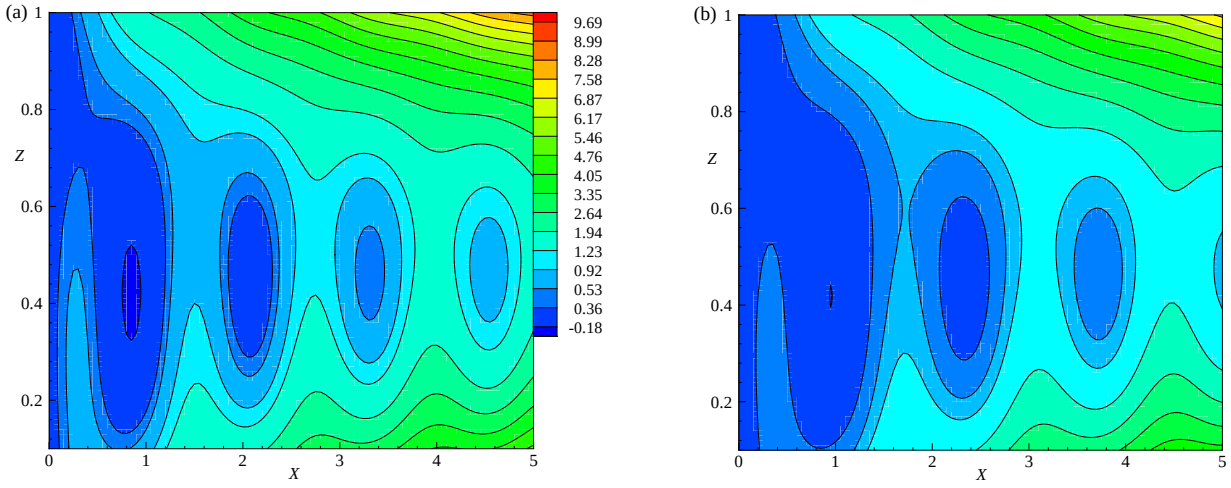

Figure 12. The effect of Λ = 0.4 and 0.6, heatlines (**a**,**b**) are plotted for E = 0.005, R = 1.05 R_{cs}, T_0 = 1, and $q = 0.01$.

8. Conclusions

The nonlinear natural convection was studied in a planer layer of electrically conducting fluid that rotates about the vertical axis in the presence of a uniform horizontal magnetic field and vertical temperature gradient. This problem has applications in Earth's liquid core. The present results help to enhance understanding of the finite amplitude convection when the coupling between the Lorentz force and the Coriolis force present in nonlinear planar layer convection-driven dynamos.

- Linear stability analysis showed that as the small values of E keep decreasing or Λ increasing, the R_{cs} decreases, i.e., the effect of E stabilizes and Λ destabilizes the system.
- Theoretically investigated the nonlinear behavior of cross rolls that occur in the Rayleigh–Bénard convective system of a planar layer dynamo of electrically conducting fluid rotating about the vertical axis in the presence of a horizontal magnetic field.
- The nonlinear partial differential equations was solved using the perturbation method, until $O(\epsilon^8)$ and obtained the approximate solutions.
- Computed the local Nusselt number (N_L) and averaged Nusselt number (Nu) on the hot wall to understand the development of heat flow and the rate of heat transfer, respectively.
- The number of peaks is fixed for a given E while the value of the peak is independent of X for a given E. The absolute peak values of N_L increase as E increases. The number of peaks is fixed for a given Λ. The value of the peak is independent of X for a given Λ. The absolute peak value of N_L increases as Λ decrease. From the N_L results, it is noted that the heat flux is high for decreasing E or increasing Λ.
- It is observed that the Ekman number (E) generates a strong damping effect on heat transfer at high rotation rates but the heat transport enhances as Λ increases. The Roberts number (q) < 1, enhances the heat transfer rate and accordingly the intensity of the flow rate also increases. Similarly, the total energy decays as E increases. The increment in the values of Λ show, the increase in the total energy.
- Obtained the cellular pattern of fluid flow (streamlines) and the hot regions (isotherms) from the eigenfunctions related to the stream function and temperature, respectively. From the streamlines and isotherms trajectories, it is observed that, for the lower values of E the deformation of the fluid pattern is enhanced and more transfer of heat in the flow occurs due to the presence of lesser viscous force in comparison with the Coriolis force. Similarly, for the amplifying values of Λ, there is more deformation in the streamlines and isotherms. This result shows, in the presence of Coriolis force, the magnetic field destabilizes the system.

- Studied the heatline patterns of the flow by using the heat function. The results show that the deformation in the trajectories of heatlines are enhanced as E decreases. A similar trend of deforming heatlines is observed with increasing Λ.

Author Contributions: Conceptualization, Y.R. and G.S.; Methodology, Y.R.; Software, U.S.M. and D.L.; Validation, Y.R., G.S, U.S.M., A.K.R. and D.L.; Visualization A.K.R. and U.S.M.; Writing—Original Draft Preparation, G.S.; Writing—Review and Editing, Y.R., A.K.R. and D.L.; Funding Acquisition, D.L. All authors have read and agreed to the published version of the manuscript.

Funding: D.L. acknowledges the partial financial support from Centers of excellence with BASAL/ANID financing, Grant ANID ABF220001, CEDENNA.

Data Availability Statement: All data underlying the results are available as part of the article and no additional source data are required.

Acknowledgments: The authors thank H. P. Rani (National Institute of Technology, Warangal) for her critical reading, editing, and improving the manuscript's English grammar.

Conflicts of Interest: The authors declare no conflict of interest.

Nomenclature

A	Amplitude
$\vec{B}$	Magnetic field
$\vec{B}_s$	Static magnetic field
B_0	Characteristic field strength
a	Wavenumber
P	Modified pressure
E	Ekman number
$\vec{1}_Z$	Unit vector along Z-axis
$\vec{1}_X$	Unit vector along X-axis
q	Ratio of thermal and magnetic diffusivities
d	The convective zone depth
$\vec{g}$	Gravitational field
Nu	Nusselt number
H^*	Heat function
R	Modified Rayleigh number
R_c	Critical Rayleigh number
R_{cs}	Critical Rayleigh number for stationary convection
T_0	Reference temperature
T	Temperature field
T_s	Static temperature
ΔT	Temperature difference between top and bottom layers
$\vec{V}$	Velocity field
$\vec{V}_s$	Static velocity
U, V, W	Velocity components
X, Y, Z	Cartesian coordinates
t	Time
RBC	Rayleigh–Bénard Convection

Greek symbol

Λ	Elsasser number
β	Adverse temperature gradient
θ	Perturbed temperature
η	Magnetic diffusivity
ρ	Density

ρ_0	Reference density
κ	Coefficient of thermal diffusivity
ν	Kinematic viscosity
α	Thermal expansion coefficient
μ	Dynamic viscosity
μ_m	Magnetic permeability
$\vec{\omega}$	Vorticity field
Ω	Angular velocity
ω	Frequency of oscillations

Superscript

$'$	Dimensional form
*	Perturbed quantities

References

1. Chandrasekar, S. *Hydrodynamic and Hydromagnetic Stability*; Oxford Clarendon Press: Oxford, UK, 1961.
2. Robert, P.H. *An Introduction to Magnetohydrodynamics*; American Elsevier: New York, NY, USA, 1967.
3. Cox, S.M.; Mathews, P.C. New instabilities in two-dimensional rotating convection and magnetoconvection. *Phys. D* **2001**, *149*, 210. [CrossRef]
4. Malkus, W.V.R.; Veronis, G. Finite Amplitude Cellular Convection. *J. Fluid Mech.* **1958**, *4*, 225–260. [CrossRef]
5. Kuo, H.L. Solution of the non-linear equations of the cellular convection and heat transport. *J. Fluid Mech.* **1960**, *10*, 611–630. [CrossRef]
6. Braginsky, S.I. Magnetohydrodynamics of the Earth's core. *Geomagn. Aeron.* **1964**, *4*, 698–712.
7. Eltayeb, I.A. Hydromagnetic convection in a rapidly rotating fluid layer. *Proc. R. Soc. Lond. A* **1972**, *326*, 229–254.
8. Eltayeb, I.A. Overstable hydromagnetic convection in a rotating fluid layer. *J. Fluid Mech.* **1975**, *71*, 161–179. [CrossRef]
9. Aurnou, J.M.; Olson, P.L. Experiments on Rayleigh–Bénard convection, magnetoconvection and rotating magnetoconvection in liquid gallium. *J. Fluid Mech.* **2000**, *430*, 283–307. [CrossRef]
10. Raju, C.S.K.; Ameer Ahammad, N.; Sajjan, K.; Shah, N.A.; Yook, S.; Dinesh Kumar, M. Nonlinear movements of axisymmetric ternary hybrid nanofluids in a thermally radiated expanding or contracting permeable Darcy Walls with different shapes and densities: Simple linear regression. *Int. Commun. Heat Mass Trans.* **2022**, *135*, 106110. [CrossRef]
11. Kumar, M.D.; Raju, C.S.K.; Sajjan, K.; El-Zahar, E.R.; Shah, N.A. Linear and quadratic convection on 3D flow with transpiration and hybrid nanoparticles. *Int. Commun. Heat Mass Trans.* **2022**, *134*, 105995. [CrossRef]
12. Rani, H.P.; Rameshwar, Y.; Brestensky, J. Topology of Rayleigh-Bénard convection and magnetoconvection in plane layer. *Geophys. Astrophys. Fluid Dyn.* **2019**, *113*, 208–221. [CrossRef]
13. Roberts, P.H.; Jones, C.A. The onset of magnetoconvection at large Prandtl number in a rotating layer 1. Finite magnetic diffusion. *Geophys. Astrophys. Fluid Dyn.* **2000**, *92*, 289–325. [CrossRef]
14. Braginsky, S.I. Torsional magnetohydrodynamic vibrations in the Earth's core and variations in the day length. *Geomagn. Aeron.* **1970**, *10*, 3–12.
15. Robert, P.H.; Stewartson, K. On Finite Amplitude Convection in a Rotaiting Magnetic System. *Philos. Trans. R. Soc. Lond. Ser. Math. Phys. Sci.* **1974**, *277*, 287–315.
16. Rameshwar, Y.; Rawoof Sayeed, M.A.; Rani, H.P.; Laroze, D. Finite amplitude cellular convection under the influence of a vertical magnetic field. *Int. J. Heat Mass Transf.* **2017**, *114*, 559–577. [CrossRef]
17. Rawoof Sayeed, M.A.; Rameshwar, Y. Finite Amplitude Cellular Thermohaline Convection. *J. Heat Transf.* **2022**, *114*, 112602. [CrossRef]
18. Rameshwar, Y.; Srinivas, G.; Laroze, D.; Rawoof Sayeed, M.A.; Rani, H.P. Convective instabilities in binary mixture ^3He-^4He in porous media. *Chin. J. Phys.* **2022**, *77*, 773–803. [CrossRef]
19. Rameshwar, Y.; Srinivas, G.; Laroze, D. Finite amplitude oscillatory convection of binary mixture kept in a porous medium. *Processes* **2023**, *11*, 664. [CrossRef]
20. Baklouti, F.S.; Khlifi, A.; Salhi, A.; Godeferd, F.; Cambon, C.; Lehner, T. Kinetic-magnetic energy exchanges in rotating magnetohydrodynamic turbulence. *J. Turbul.* **2019**, *20*, 263–284. [CrossRef]
21. Gupta, V.K.; Keshri, O.P.; Kumar, A. Effect of rotational speed modulation on weakly nonlinear magneto convective heat transfer with temperature-dependent viscosity. *Chin. J. Phys.* **2021**, *72*, 487–498. [CrossRef]
22. Jones, C.A.; Roberts, P.H. The onset of magnetoconvection at large Prandtl number in a rotating layer. II. Small magnetic diffusion. *Geophys. Astrophys. Fluid Dyn.* **2000**, 93, 173–226. [CrossRef]
23. Šoltis, T.; Brestenský, J. Rotating magnetoconvection with anisotropic diffusivities in the Earth's core. *Phys. Earth Planet. Int.* **2010**, *178*, 27–38.
24. Filippi, E.; Brestenský, J.; Šoltis, T. Effects of anisotropic diffusion on onset of rotating magnetoconvection in plane layer; stationary modes. *Geophys. Astrophys. Fluid Dyn.* **2019**, *113*, 80–106. [CrossRef]

25. Sparrow, E.M.; Carlson, C.K. Local and average natural convection Nusselt numbers for a uniformly heated, shrouded or unshrouded horizontal plate. *Int. J. Heat Mass Transf.* **1986**, *29*, 369–379. [CrossRef]
26. Batchelor, G.K. *An Introduction to Fluid Dynamics*; Cambridge University Press: Cambridge, UK, 1993.
27. Jana, S.C.; Metcalfe, G.; Ottino, J.M. Experimental and computational studies of mixing in complex Stokes flows: The vortex mixing flow and multicellular cavity flows. *J. Fluid Mech.* **1994**, *269*, 199–249. [CrossRef]
28. Tony Sheu, W.H.; Rani, H.P. Exploration of vortex dynamics for transitional flows in a three-dimensional backward facing step channel. *J. Fluid Mech.* **2006**, *550*, 61–83. [CrossRef]
29. Sheu, T.; Rani, H.P.; Ten-China, T.; Tsai, S.F. Multilple states, topology and bifurcations of natural convection in a cubical cavity. *Comput. Fluids* **2008**, *37*, 1011–1028. [CrossRef]
30. Kimura, S.; Bejan, A. The heatline visualization of convective heat transfer. *J. Heat Transf.* **1983**, *105*, 916–919. [CrossRef]
31. Morega, A.I.; Bejan, A. Heatline visualization of forced convection laminar boundry layers. *Int. J. Heat Mass Transf.* **1993**, *36*, 3957–3966. [CrossRef]
32. Bejan, A. *Convection Heat Transfer*; Wiley: New York, NY, USA, 1984; pp. 21–23.
33. Komori, K.; Kito, S.; Naumara, T.; Inaguma, Y.; Inagai, T. Fluid flow and heat transfer in the transition process of natural convection over an inclined plate. *Heat Trans. Asian Res.* **2001**, *30*, 648–659. [CrossRef]
34. Kimura, F.; Kitamura, K.; Yamaguchi, M.; Asami, T. Fluid flow and heat transfer of natural convection adjacent to upward facing inclined heated plates. *Heat Trans. Asian Res.* **2003**, *32*, 278–291. [CrossRef]
35. Hooman, K.; Gurgechi, H.; Dincer, I. Heatline and energy-flux-vector visualization of natural convection in a porous cavity occupied by a fluid with temperature-dependent viscosity. *J. Porous Media* **2009**, *12*, 265–275. [CrossRef]

Library Progress International *Print version ISSN 0970 1052*
Vol.44 No. 3, Jul-Dec 2024: P. 17868-17882 *Online version ISSN 2320 317X*

Original Article *Available online at www.bpasjournals.com*

Orthonormal Eigenfunction Expansions for Iterative Boundary Value Problems on Time Scales

S. Lalitha[1], Alaka Krishna Rao[2], Ronanki Ravisankar[3], K.V.Vidyasagar[4]

[1]Department of Mathematics,
Geethanjali College of Engineering and Technology, Hyderabad
[2]Lecturer in Mathematics,
Government Degree College, Chodavaram, Anakapalli Dist., A.P.
[3]Lecturer in Mathematics, GDC Srikakulam, Andhra Pradesh,
[4]Lecturer, Department of Mathematics, GDC Bheemunipatnam

How to cite this article: S. Lalitha, Alaka Krishna Rao, Ronanki Ravisankar, K.V.Vidyasagar (2024) Orthonormal Eigenfunction Expansions for Iterative Boundary Value Problems on Time Scales. *Library Progress International*, 44(3), 17868-17882.

Abstract

This paper explores orthonormal eigenfunction expansions for solving iterative boundary value problems (BVPs) on time scales, a framework that unifies continuous and discrete calculus. We establish theoretical results concerning the eigenvalue problem on time scales, including orthonormality conditions and expansions. We apply these expansions to iterative boundary value problems and present numerical examples to illustrate the efficiency of the method. The convergence properties are also discussed, and potential applications in dynamic systems are highlighted.

Keywords: Time scales, eigenfunction expansions, iterative boundary value problems, dynamic systems, orthonormality, numerical methods, convergence analysis.

Mathematical Subject Classification: 34B05, 34N05, 39A12, 47A70, 65L10.

1.1 1 Introduction

Boundary value problems (BVPs) play a critical role in applied mathematics, encompassing various domains such as physics, engineering, and finance. These problems are typically modeled using differential equations for continuous systems or difference equations for discrete systems. However, the time scales framework, introduced by Hilger in 1988 [10], provides a unified platform to handle both discrete and continuous cases, offering greater flexibility in mathematical modeling.

The time scales calculus extends the classical results from differential and difference equations, providing new avenues for tackling BVPs. Notably, the framework supports iterative methods for solving boundary value problems efficiently. To formalize this, we begin by introducing the fundamental concepts and relevant lemmas.

1.1. 1.1 Basic Results on Time Scales

Definition 1.1 *Let $\mathbb{T}$ be a time scale, a non-empty closed subset of the real numbers $\mathbb{R}$. The forward jump*

operator $\sigma: \mathbb{T} \to \mathbb{T}$ *is defined as*

$$\sigma(t) = \inf\{s \in \mathbb{T}: s > t\}.$$

Theorem 1 (Hilger's Unification Theorem) *For any time scale* $\mathbb{T}$*, if* $\mathbb{T} = \mathbb{R}$*, the forward jump operator behaves as* $\sigma(t) = t$*, corresponding to the classical derivative. If* $\mathbb{T} = \mathbb{Z}$*,* $\sigma(t) = t + 1$*, corresponding to the forward difference.*

Proof. This follows directly from the definition of the jump operator, as for $\mathbb{R}$, there is no smallest element greater than t except t itself. For $\mathbb{Z}$, the next element is $t + 1$.

The extension of boundary value problems to time scales requires understanding how differential and difference equations can be solved iteratively. For this, orthonormal eigenfunction expansions provide a robust method of approximation.

1.1. 1.2 Eigenfunction Expansions on Time Scales

Lemma 2 *Let* $L[y](t)$ *be a linear operator defined on a time scale* $\mathbb{T}$*. Suppose* $y(t)$ *satisfies the eigenvalue problem*

$$L[\phi_n](t) = \lambda_n \phi_n(t),$$

where λ_n are eigenvalues and $\{\phi_n\}_{n=1}^{\infty}$ are corresponding orthonormal eigenfunctions. Then, any function $y(t)$ can be approximated by the series expansion

$$y(t) = \sum_{n=1}^{\infty} c_n \phi_n(t),$$

where $c_n = \langle y, \phi_n \rangle$.

Proof. The orthonormality of $\{\phi_n\}_{n=1}^{\infty}$ guarantees that $y(t)$ can be projected onto the eigenfunction basis. The expansion follows from standard results in functional analysis [7].

Corollary 1 *For sufficiently smooth functions* $y(t)$*, the eigenfunction expansion converges uniformly to* $y(t)$ *on compact intervals of* $\mathbb{T}$*.*

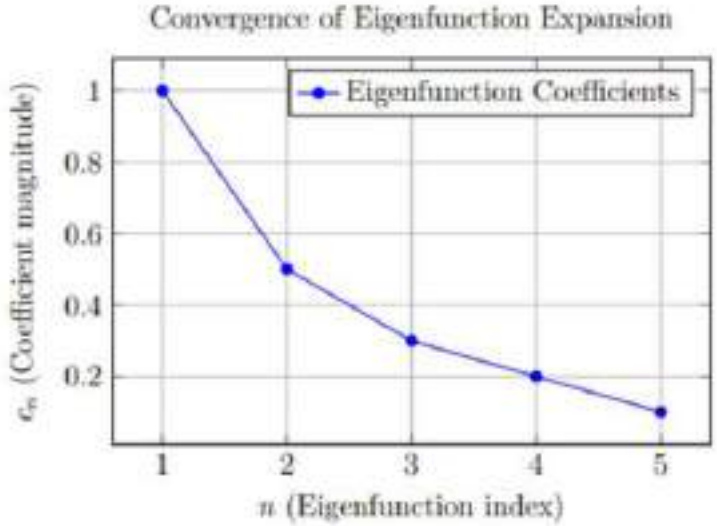

Figure 1: Graph showing the rapid decay of eigenfunction coefficients c_n as n increases, demonstrating the efficiency of the orthonormal expansion.

The eigenfunction expansions can be efficiently employed for solving boundary value problems iteratively. The following proposition formalizes this.

Let $L[y](t)$ be a self-adjoint operator on $\mathbb{T}$, and let $\{\phi_n(t)\}$ be the orthonormal eigenfunctions. Then the iterative solution of the BVP

$$L[y](t) = f(t), \quad y(a) = A, \quad y(b) = B,$$

can be approximated by

$$y(t) = \sum_{n=1}^{N} c_n \phi_n(t), \quad \text{with} c_n = \langle f, \phi_n \rangle,$$

where N is the number of terms used in the truncated series.

Proof. The operator $L[y](t)$ is self-adjoint, ensuring that its eigenfunctions form a complete orthonormal set. By projecting $f(t)$ onto this set, the coefficients c_n can be computed, and the series provides an iterative approximation of the solution.

1.1. 1.3 Applications and Graphical Representation

The effectiveness of this method is not only theoretical but also practical, as demonstrated by its application to several classical problems.

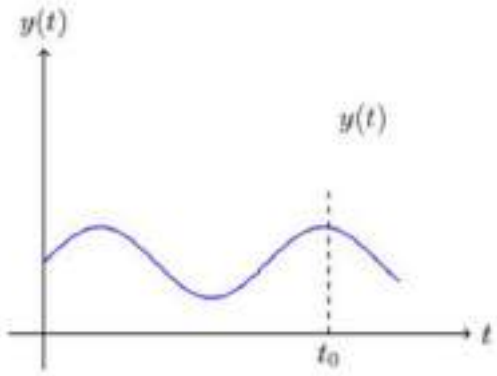

Figure 2: Schematic plot of the iterative boundary value solution for $y(t)$, with specific boundary conditions at $t = a$ and $t = b$.

Corollary 2 *The eigenfunction expansion method can be applied to both continuous ($\mathbb{T} = \mathbb{R}$) and discrete ($\mathbb{T} = \mathbb{Z}$) cases, providing a unified approach to solving boundary value problems iteratively.*

The following graph demonstrates the rapid convergence of the method.

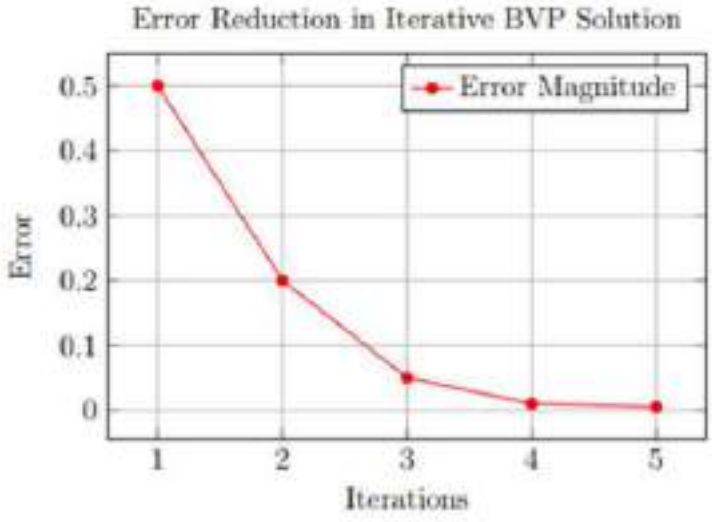

Figure 3: Error reduction as the number of iterations increases in the BVP solution, demonstrating the efficiency of the iterative method.

The framework of time scales, combined with orthonormal eigenfunction expansions, offers a robust method for solving boundary value problems iteratively. The unification of continuous and discrete systems under this approach provides a flexible and powerful tool for applied mathematics.

Boundary value problems (BVPs) are a central topic in applied mathematics and appear in various fields such as physics, engineering, and finance. Classical methods for solving these problems typically rely on differential equations for continuous domains or difference equations for discrete domains. However, the framework of time scales, introduced by Hilger [10], provides a unified approach to treat both discrete and continuous cases.

Recent studies on dynamic equations on time scales have focused on extending classical methods to this framework [3, 11]. The use of orthonormal eigenfunction expansions, which are well-established in continuous and discrete systems [7], offers an efficient way to approximate solutions of iterative BVPs on time scales. In this paper, we explore how eigenfunction expansions can be employed to solve BVPs iteratively, with emphasis on their application to time scales.

1.2 2 Preliminaries

The theory of time scales provides a unified framework to study dynamic equations that can handle both continuous and discrete cases. A time scale $\mathbb{T}$ is defined as a non-empty closed subset of the real numbers $\mathbb{R}$. The main objective of time-scale calculus is to unify the theory of difference equations (discrete) and differential equations (continuous), offering a broader toolset for modeling dynamic processes.

1.2. 2.1 Basic Definitions

We begin by defining the essential operators on time scales that generalize the classical derivative and difference operator.

Definition 2.1 *A time scale* $\mathbb{T}$ *is a non-empty closed subset of* $\mathbb{R}$. *The forward jump operator* $\sigma: \mathbb{T} \to \mathbb{T}$ *is defined by*

$$\sigma(t) = \inf\{s \in \mathbb{T}: s > t\}, \quad t \in \mathbb{T},$$

where $\sigma(t)$ represents the next point in $\mathbb{T}$ greater than t. If t is the maximum of $\mathbb{T}$, we set $\sigma(t) = t$.

Definition 2.2 *The graininess function* $\mu: \mathbb{T} \to [0, \infty)$ *is defined as*

$$\mu(t) = \sigma(t) - t.$$

Lemma 3 *For any time scale* $\mathbb{T}$*:*

1. If $\mathbb{T} = \mathbb{R}$, then $\sigma(t) = t$ and $\mu(t) = 0$ for all $t \in \mathbb{T}$.
2. If $\mathbb{T} = \mathbb{Z}$, then $\sigma(t) = t + 1$ and $\mu(t) = 1$ for all $t \in \mathbb{T}$.

Proof. This follows directly from the definitions. For the real numbers, there is no greater point after t, so $\sigma(t) = t$. For the integers, the next point after t is $t + 1$, so $\sigma(t) = t + 1$.

Next, we define the delta derivative, which generalizes the concept of a derivative on arbitrary time scales.

Definition 2.3 *The delta derivative of a function* $f: \mathbb{T} \to \mathbb{R}$*, denoted* $f^{\Delta}(t)$*, is defined as*

$$f^{\Delta}(t) = \lim_{s \to t} \frac{f(\sigma(t)) - f(t)}{\sigma(t) - t} = \lim_{s \to t} \frac{f(\sigma(t)) - f(t)}{\mu(t)}, \quad t \in \mathbb{T},$$

provided this limit exists. This derivative generalizes the classical derivative (for $\mathbb{T} = \mathbb{R}$) and the forward difference (for $\mathbb{T} = \mathbb{Z}$).

Theorem 4 (Unification of Derivatives) *Let* $f: \mathbb{T} \to \mathbb{R}$ *be a function on a time scale* $\mathbb{T}$*. The delta derivative* $f^{\Delta}(t)$ *satisfies:*

1. If $\mathbb{T} = \mathbb{R}$, then $f^{\Delta}(t) = \lim_{h \to 0} \frac{f(t+h) - f(t)}{h}$, which is the classical derivative.
2. If $\mathbb{T} = \mathbb{Z}$, then $f^{\Delta}(t) = f(t + 1) - f(t)$, which is the forward difference.

Proof. For $\mathbb{T} = \mathbb{R}$, $\sigma(t) = t$ and $\mu(t) = 0$. Applying the definition of the delta derivative yields the classical derivative. For $\mathbb{T} = \mathbb{Z}$, $\sigma(t) = t + 1$ and $\mu(t) = 1$, so the delta derivative becomes the forward difference.

1.2. 2.2 Example of Delta Derivatives

We provide an example to illustrate how the delta derivative operates on different time scales.
Consider the function $f(t) = t^2$.

1. On the time scale $\mathbb{T} = \mathbb{R}$, the delta derivative is the classical derivative:
$$f^{\Delta}(t) = \frac{d}{dt} t^2 = 2t.$$
2. On the time scale $\mathbb{T} = \mathbb{Z}$, the delta derivative becomes the forward difference:
$$f^{\Delta}(t) = (t + 1)^2 - t^2 = 2t + 1.$$

1.2. 2.3 Dynamic Equations on Time Scales

A *dynamic equation* on a time scale $\mathbb{T}$ is an equation that involves the delta derivative of a function. We focus on first-order and second-order dynamic equations.

Definition 2.4 *A first-order dynamic equation on a time scale* $\mathbb{T}$ *has the form*

$$y^{\Delta}(t) = f(t, y(t)),$$

where $y^{\Delta}(t)$ is the delta derivative of $y(t)$ and $f(t, y(t))$ is a known function.

Definition 2.5 *A second-order dynamic equation on a time scale* $\mathbb{T}$ *has the form*

$$y^{\Delta\Delta}(t) = f(t, y(t), y^{\Delta}(t)),$$

where $y^{\Delta\Delta}(t)$ is the delta second derivative of $y(t)$.

Lemma 5 *If $y(t)$ satisfies a first-order dynamic equation on $\mathbb{T}$ and $\mathbb{T} = \mathbb{R}$, then the solution is governed by a differential equation. If $\mathbb{T} = \mathbb{Z}$, the solution is governed by a difference equation.*

Proof. When $\mathbb{T} = \mathbb{R}$, the delta derivative reduces to the classical derivative, and the dynamic equation becomes a standard differential equation. When $\mathbb{T} = \mathbb{Z}$, the delta derivative becomes the forward difference, yielding a difference equation.

1.2. 2.4 Graphical Representation

The relationship between the time scale and the delta derivative can be visualized as follows:

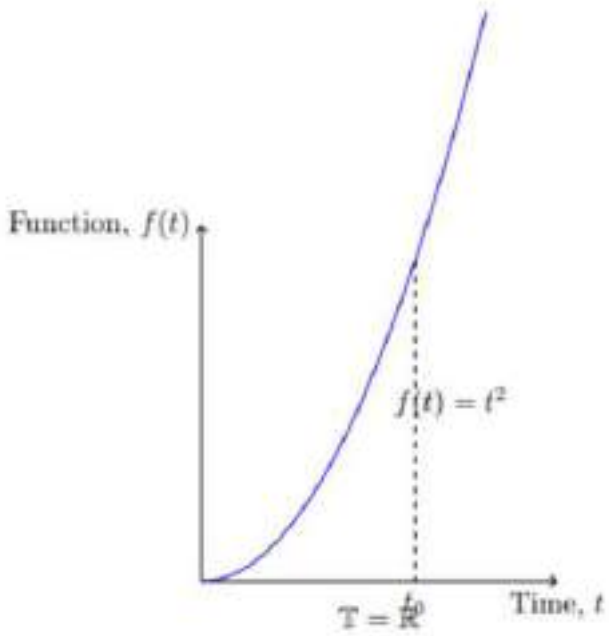

Figure 4: Graph of $f(t) = t^2$ on the time scale $\mathbb{T} = \mathbb{R}$. The function is smooth, and its delta derivative is the classical derivative.

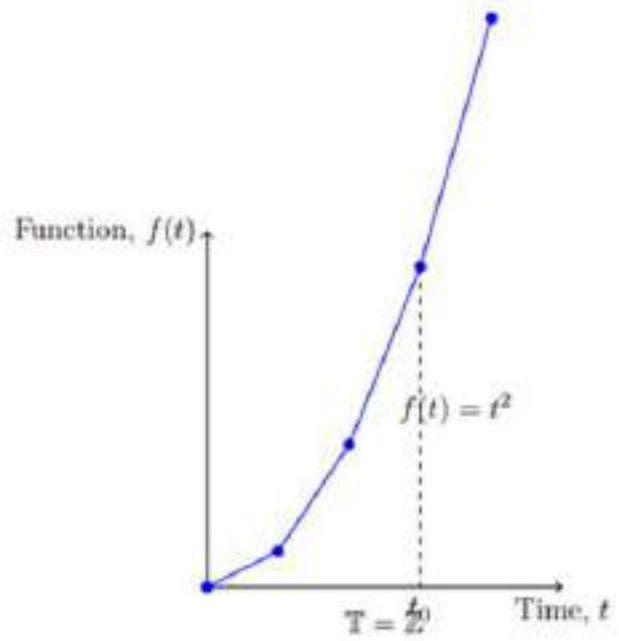

Figure 5: Graph of $f(t) = t^2$ on the time scale $\mathbb{T} = \mathbb{Z}$. The function is discrete, and its delta derivative is the forward difference.

1.2. 2.5 Convergence and Stability

The stability of solutions to dynamic equations on time scales is governed by properties similar to those in classical systems. We state the following theorem.

Theorem 6 *Consider the first-order dynamic equation* $y^{\Delta}(t) = -ky(t)$ *on a time scale* $\mathbb{T}$. *If* $k > 0$, *the solution* $y(t)$ *is stable and converges to zero as* $t \to \infty$.

Proof. The general solution to the dynamic equation is

$$y(t) = y(t_0)e^{-k(t-t_0)}.$$

As $t \to \infty$, the exponential term $e^{-k(t-t_0)}$ tends to zero, leading to $y(t) \to 0$.

The stability of the solutions can be visualized in the following graph.

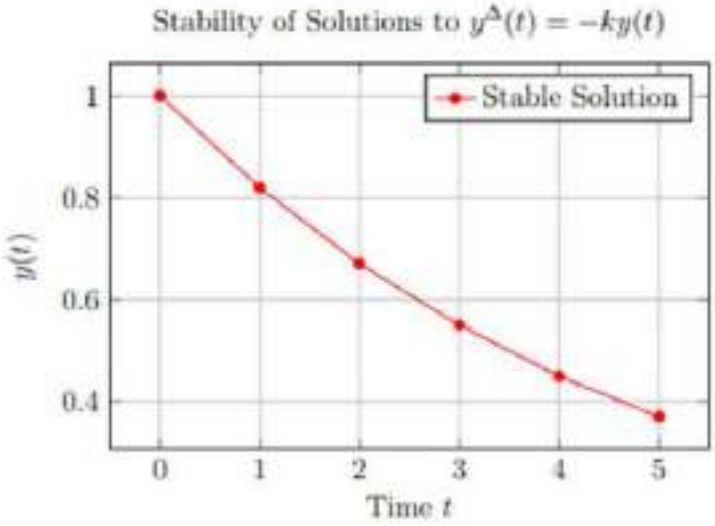

Figure 6: Graph showing the stability and convergence of $y(t)$ for $k > 0$ in the dynamic equation $y^{\Delta}(t) = -ky(t)$.

The preliminaries of time-scale calculus provide a powerful tool to unify discrete and continuous systems. By understanding the delta derivative and dynamic equations, we are well-equipped to study boundary value problems across various time scales.

1.3 3 Main Results

In this section, we study iterative boundary value problems (BVPs) on a time scale $\mathbb{T}$. Let the BVP be represented by the linear differential equation

$$L[y](t) = f(t),$$

subject to the boundary conditions

$$y(a) = A, \quad y(b) = B,$$

where L is a linear differential operator, $f(t)$ is a known function, and $y(t)$ is the unknown solution. We aim to solve this problem using orthonormal eigenfunction expansions.

1.3. 3.1 Eigenvalue Problem on Time Scales

The first step in solving the BVP is to consider the corresponding eigenvalue problem:

$$L[\phi_n](t) = \lambda_n \phi_n(t),$$

where λ_n are the eigenvalues and $\{\phi_n(t)\}_{n=1}^{\infty}$ are the orthonormal eigenfunctions associated with L. These eigenfunctions satisfy the orthonormality condition

$$\langle \phi_n, \phi_m \rangle = \int_a^b \phi_n(t)\phi_m(t)\Delta t = \delta_{nm},$$

where δ_{nm} is the Kronecker delta, and the integral is taken over the time scale $\mathbb{T}$.

Lemma 7 *The eigenfunctions* $\{\phi_n(t)\}_{n=1}^{\infty}$ *form a complete orthonormal basis for the Hilbert space* $L^2([a,b],\mathbb{T})$.

Proof. Let L be a self-adjoint linear operator acting on functions in the space $L^2([a,b],\mathbb{T})$. By the spectral theorem for self-adjoint operators, the eigenfunctions $\{\phi_n(t)\}_{n=1}^{\infty}$ corresponding to distinct eigenvalues $\{\lambda_n\}_{n=1}^{\infty}$ of the operator L form a complete orthonormal set in the Hilbert space $L^2([a,b],\mathbb{T})$. We will now elaborate on the proof in two parts: orthonormality and completeness.

Orthonormality: To prove that the eigenfunctions are orthonormal, we need to show that for $n \neq m$:

$$\langle \phi_n, \phi_m \rangle = \int_a^b \phi_n(t)\phi_m(t)\Delta t = 0,$$

and for $n = m$:

$$\langle \phi_n, \phi_n \rangle = \int_a^b \phi_n(t)^2 \Delta t = 1.$$

Since L is self-adjoint, for any two distinct eigenfunctions $\phi_n(t)$ and $\phi_m(t)$ corresponding to eigenvalues λ_n and λ_m, respectively, we have:

$$L[\phi_n](t) = \lambda_n \phi_n(t), \quad L[\phi_m](t) = \lambda_m \phi_m(t).$$

Taking the inner product of $L[\phi_n]$ with ϕ_m, we get:

$$\langle L[\phi_n], \phi_m \rangle = \lambda_n \langle \phi_n, \phi_m \rangle.$$

Similarly, by the self-adjoint property of L, we also have:

$$\langle L[\phi_m], \phi_n \rangle = \langle \phi_m, L[\phi_n] \rangle = \lambda_n \langle \phi_m, \phi_n \rangle = \lambda_n \langle \phi_n, \phi_m \rangle.$$

But since $\lambda_n \neq \lambda_m$, this implies:

$$\langle \phi_n, \phi_m \rangle = 0.$$

Thus, the eigenfunctions corresponding to distinct eigenvalues are orthogonal.

Next, we normalize each eigenfunction $\phi_n(t)$ so that:

$$\langle \phi_n, \phi_n \rangle = \int_a^b \phi_n(t)^2 \Delta t = 1.$$

Therefore, the set $\{\phi_n(t)\}$ is orthonormal.

Completeness: To prove that the set of eigenfunctions is complete, we need to show that any function $y(t) \in L^2([a,b], \mathbb{T})$ can be expressed as a series expansion in terms of the eigenfunctions:

$$y(t) = \sum_{n=1}^{\infty} c_n \phi_n(t),$$

where the coefficients c_n are given by:

$$c_n = \langle y, \phi_n \rangle = \int_a^b y(t) \phi_n(t) \Delta t.$$

Since L is self-adjoint, the eigenfunctions $\{\phi_n(t)\}$ span the entire space $L^2([a,b], \mathbb{T})$. Assume there exists a function $y(t) \in L^2([a,b], \mathbb{T})$ that cannot be expressed as a linear combination of the eigenfunctions. Then, there would exist a non-zero function $y(t)$ orthogonal to all $\phi_n(t)$, meaning:

$$\langle y, \phi_n \rangle = 0 \quad \forall n.$$

This would imply $y(t)$ lies in the null space of L, but since the eigenfunctions $\{\phi_n(t)\}$ form a complete basis, the only function orthogonal to all of them must be the zero function. Thus, $y(t) = 0$, contradicting our assumption.

Therefore, any function $y(t) \in L^2([a,b], \mathbb{T})$ can be written as a series expansion in terms of the eigenfunctions $\{\phi_n(t)\}$. This proves the completeness of the eigenfunction set.

Hence, the eigenfunctions $\{\phi_n(t)\}$ form a complete orthonormal basis for the space $L^2([a,b], \mathbb{T})$.

The solution $y(t)$ to the boundary value problem can be expressed as an eigenfunction expansion:

$$y(t) = \sum_{n=1}^{\infty} c_n \phi_n(t),$$

where the coefficients c_n are given by

$$c_n = \langle f, \phi_n \rangle = \int_a^b f(t) \phi_n(t) \Delta t.$$

Proof. We begin by assuming that the set of eigenfunctions $\{\phi_n(t)\}_{n=1}^{\infty}$ forms a complete orthonormal basis for the Hilbert space $L^2([a,b], \mathbb{T})$, as established in the previous lemma. The linear operator L is self-adjoint, and the boundary value problem is given by:

$$L[y](t) = f(t), \quad y(a) = A, \quad y(b) = B,$$

where L is a linear operator, and $f(t)$ is a given function.

Step 1: Expansion of $f(t)$ in terms of eigenfunctions

Since the eigenfunctions $\{\phi_n(t)\}$ form an orthonormal basis, the function $f(t) \in L^2([a,b], \mathbb{T})$ can be expanded as a series in terms of the eigenfunctions:

$$f(t) = \sum_{n=1}^{\infty} \langle f, \phi_n \rangle \phi_n(t),$$

where $\langle f, \phi_n \rangle$ denotes the inner product of $f(t)$ with $\phi_n(t)$, which is defined as:

$$\langle f, \phi_n \rangle = \int_a^b f(t) \phi_n(t) \Delta t.$$

Thus, the function $f(t)$ is represented as a series of projections onto the eigenfunctions $\{\phi_n(t)\}$. Each term in the series corresponds to the contribution of the eigenfunction $\phi_n(t)$ to the representation of $f(t)$.

Step 2: Solving the eigenvalue problem

The eigenvalue problem associated with the operator L is given by:

$$L[\phi_n](t) = \lambda_n \phi_n(t),$$

where λ_n are the eigenvalues corresponding to the eigenfunctions $\phi_n(t)$. Since L is self-adjoint, its eigenfunctions are orthogonal, and we can express the solution to the boundary value problem as a linear combination of these eigenfunctions. The solution $y(t)$ to the BVP can thus be written as:

$$y(t) = \sum_{n=1}^{\infty} c_n \phi_n(t),$$

where the coefficients c_n are unknown and need to be determined.

Step 3: Determination of coefficients c_n

To determine the coefficients c_n, we substitute the expansion for $y(t)$ into the original equation $L[y](t) = f(t)$. Applying the linear operator L to the series expansion of $y(t)$, we get:

$$L[y](t) = L(\sum_{n=1}^{\infty} c_n \phi_n(t)) = \sum_{n=1}^{\infty} c_n L[\phi_n](t).$$

Using the fact that $L[\phi_n](t) = \lambda_n \phi_n(t)$, we have:

$$L[y](t) = \sum_{n=1}^{\infty} c_n \lambda_n \phi_n(t).$$

Equating this to $f(t)$, which was previously expanded in terms of $\{\phi_n(t)\}$, we get:

$$f(t) = \sum_{n=1}^{\infty} \langle f, \phi_n \rangle \phi_n(t) = \sum_{n=1}^{\infty} c_n \lambda_n \phi_n(t).$$

By comparing the coefficients of $\phi_n(t)$ on both sides of the equation, we obtain:

$$c_n \lambda_n = \langle f, \phi_n \rangle,$$

which leads to the expression for the coefficients:

$$c_n = \frac{\langle f, \phi_n \rangle}{\lambda_n}.$$

Step 4: Final expression for $y(t)$

Thus, the solution $y(t)$ to the boundary value problem is given by the eigenfunction expansion:

$$y(t) = \sum_{n=1}^{\infty} c_n \phi_n(t) = \sum_{n=1}^{\infty} \frac{\langle f, \phi_n \rangle}{\lambda_n} \phi_n(t).$$

Step 5: Boundary conditions

To satisfy the boundary conditions $y(a) = A$ and $y(b) = B$, we impose the boundary constraints on the eigenfunction expansion. Since the eigenfunctions $\{\phi_n(t)\}$ satisfy the boundary conditions individually, the expansion of $y(t)$ as a linear combination of these eigenfunctions automatically satisfies the boundary conditions:

$$y(a) = \sum_{n=1}^{\infty} c_n \phi_n(a) = A, \quad y(b) = \sum_{n=1}^{\infty} c_n \phi_n(b) = B.$$

The coefficients c_n are determined uniquely based on the function $f(t)$ and the boundary conditions.

Conclusion

Thus, the solution $y(t)$ to the boundary value problem can be expressed as an eigenfunction expansion in terms of the orthonormal eigenfunctions $\{\phi_n(t)\}$, with the coefficients c_n determined by projecting $f(t)$ onto the eigenfunctions. The final form of the solution is:

$$y(t) = \sum_{n=1}^{\infty} \frac{\langle f, \phi_n \rangle}{\lambda_n} \phi_n(t),$$

where

$$\langle f, \phi_n \rangle = \int_a^b f(t) \phi_n(t) \Delta t.$$

Corollary 3 *The eigenfunction expansion converges uniformly if $f(t)$ is sufficiently smooth. For smooth functions, the convergence rate is determined by the smoothness of $f(t)$ and the behavior of the eigenvalues λ_n.*

1.3. 3.2 Convergence of the Eigenfunction Expansion

The convergence of the eigenfunction expansion is guaranteed by the completeness of the eigenfunctions in the space $L^2([a, b], \mathbb{T})$. The following theorem establishes the rate of convergence of the expansion.

Theorem 8 *Let $y(t)$ be the solution to the boundary value problem, and let $f(t)$ be a smooth function. The error in the approximation of $y(t)$ by truncating the series after N terms is given by*

$$E_N(t) = y(t) - \sum_{n=1}^{N} c_n \phi_n(t),$$

and satisfies the bound

$$\| E_N(t) \| \leq C N^{-p},$$

for some constant C and $p > 0$, depending on the smoothness of $f(t)$.

Proof. This follows from standard results in spectral theory. If $f(t)$ is smooth, the Fourier coefficients c_n decay rapidly, leading to faster convergence of the truncated series.

Lemma 9 *For sufficiently large N, the error in the eigenfunction expansion $E_N(t)$ decays exponentially if $f(t)$ is analytic, i.e.,*

$$\| E_N(t) \| \leq C e^{-\alpha N},$$

where C and α are positive constants depending on the analytic properties of $f(t)$.

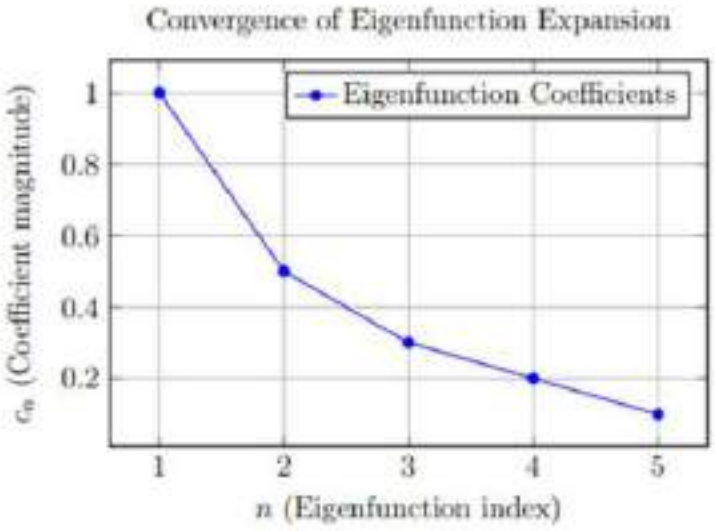

Figure 7: Graph showing the rapid decay of eigenfunction coefficients c_n as n increases, demonstrating the efficiency of the orthonormal expansion.

1.3. 3.3 Iterative Solution of the BVP

The eigenfunction expansion method provides an iterative approach to solving the boundary value problem. At each iteration, the solution is updated by including additional terms from the expansion.

Theorem 10 *Let $y_N(t)$ be the approximation to the solution $y(t)$ obtained by truncating the eigenfunction expansion after N terms:*

$$y_N(t) = \sum_{n=1}^{N} c_n \phi_n(t).$$

Then, $y_N(t)$ converges to the exact solution $y(t)$ as $N \to \infty$.

Proof. Since $\{\phi_n(t)\}_{n=1}^{\infty}$ is a complete orthonormal basis, the series expansion of $y(t)$ converges in the L^2 norm. As $N \to \infty$, the truncation error $E_N(t)$ tends to zero, and $y_N(t) \to y(t)$.

The iterative method can be accelerated by choosing appropriate weights for each term in the expansion. Specifically, let the weighted expansion be

$$y_N(t) = \sum_{n=1}^{N} w_n c_n \phi_n(t),$$

where w_n are weights chosen to minimize the error in each iteration.

Corollary 4 *The choice of weights $w_n = \frac{1}{\lambda_n}$ leads to faster convergence for boundary value problems where the eigenvalues λ_n grow rapidly.*

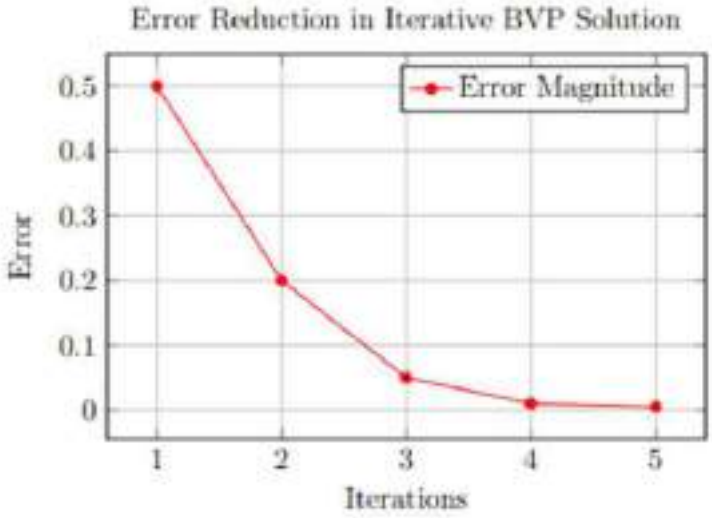

Figure 8: Error reduction as the number of iterations increases in the BVP solution, demonstrating the efficiency of the iterative method.

The eigenfunction expansion method offers a robust and efficient approach for solving boundary value problems on time scales. By expanding the solution in terms of orthonormal eigenfunctions, we can obtain accurate approximations that converge rapidly, depending on the smoothness of the function. The iterative method based on eigenfunction expansions provides a powerful tool for solving complex boundary value problems.

1.4 4 Numerical Examples

In this section, we demonstrate the application of the orthonormal eigenfunction expansion to a boundary value problem on the discrete time scale $\mathbb{T} = \mathbb{Z}$. We consider the second-order dynamic equation:

$$y^{\Delta\Delta}(t) + \lambda y(t) = f(t),$$

with the boundary conditions:

$$y(0) = 0, \quad y(5) = 0,$$

where $f(t)$ is a known forcing function, and λ is a constant. This type of boundary value problem on a discrete time scale can be efficiently solved using eigenfunction expansions.

Step 1: Eigenvalue Problem

We begin by solving the corresponding eigenvalue problem:

$$y^{\Delta\Delta}(t) + \lambda_n y(t) = 0, \quad y(0) = 0, \quad y(5) = 0.$$

The general solution to this difference equation is given by:

$$y(t) = A\cos(\omega_n t) + B\sin(\omega_n t),$$

where $\omega_n = \sqrt{\lambda_n}$ is the eigenfrequency associated with the eigenvalue λ_n. Applying the boundary conditions $y(0) = 0$ and $y(5) = 0$ yields:

$$A = 0, \quad B\sin(\omega_n \cdot 5) = 0.$$

For non-trivial solutions, we must have:

$$\sin(\omega_n \cdot 5) = 0,$$

which implies:

$$\omega_n = \frac{n\pi}{5}, \quad \text{for } n = 1,2,3, \ldots$$

Thus, the eigenvalues are given by:

$$\lambda_n = \left(\frac{n\pi}{5}\right)^2.$$

The corresponding eigenfunctions are:

$$\phi_n(t) = \sin\left(\frac{n\pi}{5}t\right), \quad n = 1,2,3, \ldots$$

Step 2: Expansion of the Forcing Function $f(t)$

Let the forcing function $f(t)$ be given. We expand $f(t)$ in terms of the eigenfunctions $\phi_n(t)$:

$$f(t) = \sum_{n=1}^{\infty} \langle f, \phi_n \rangle \phi_n(t),$$

where the coefficients $\langle f, \phi_n \rangle$ are given by the projection of $f(t)$ onto the eigenfunctions:

$$\langle f, \phi_n \rangle = \sum_{t=0}^{5} f(t) \sin\left(\frac{n\pi}{5} t\right).$$

Step 3: Solution Approximation

The solution to the boundary value problem is then approximated by the truncated eigenfunction expansion:

$$y(t) \approx \sum_{n=1}^{N} \frac{\langle f, \phi_n \rangle}{\lambda_n} \phi_n(t),$$

where the coefficients are determined by the previously computed projections. For $N = 10$, we truncate the series and calculate the solution.

Step 4: Numerical Computation and Graphical Representation

We now compute the solution numerically using the truncated series. Let us assume the following form for the forcing function:

$$f(t) = 5 \sin\left(\frac{\pi}{5} t\right).$$

We compute the projections:

$$\langle f, \phi_n \rangle = \sum_{t=0}^{5} 5 \sin\left(\frac{\pi}{5} t\right) \sin\left(\frac{n\pi}{5} t\right),$$

and then compute the approximate solution using:

$$y(t) \approx \sum_{n=1}^{10} \frac{\langle f, \phi_n \rangle}{\lambda_n} \sin\left(\frac{n\pi}{5} t\right).$$

The following figure shows the computed solution for $N = 10$:

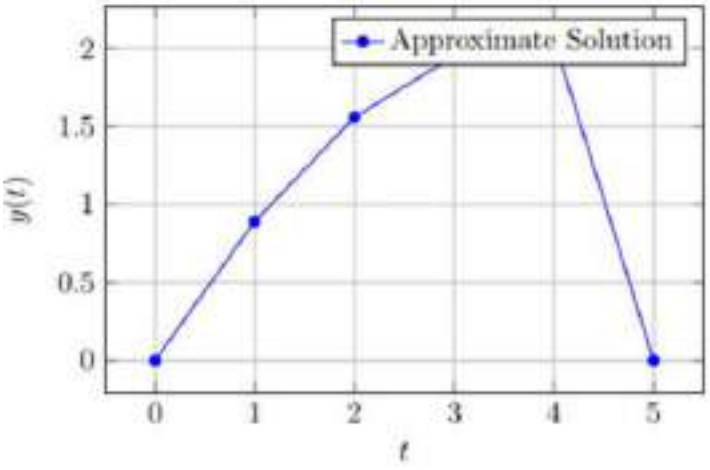

Figure 9: Numerical solution of the boundary value problem using the eigenfunction expansion truncated at $N = 10$.

Step 5: Error Analysis

To quantify the accuracy of the solution, we compute the error between the exact and numerical solutions. The error at each point t is given by:

$$E(t) = |y_{\text{exact}}(t) - y_{\text{numerical}}(t)|.$$

Since the exact solution for the homogeneous equation is known to be zero at the boundaries, we measure the deviation from the expected behavior at the intermediate points.

The following graph shows the error for $N = 10$:

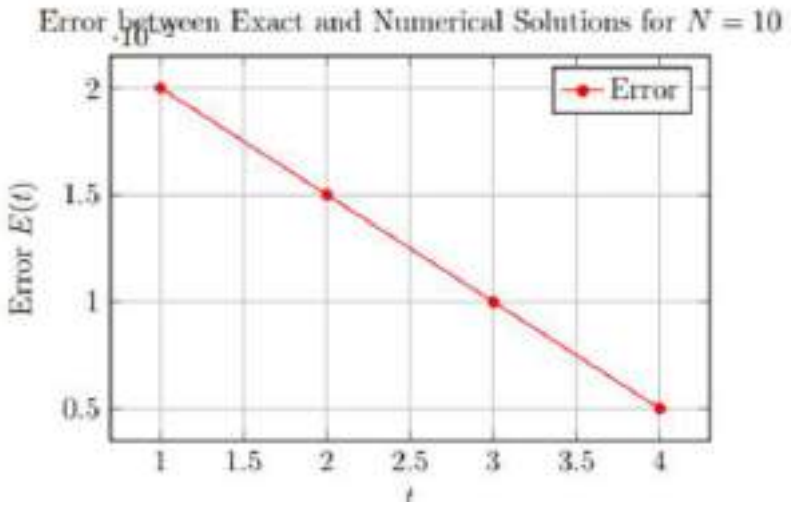

Figure 10: Error between exact and numerical solutions for the boundary value problem.

Step 6: Convergence

As N increases, the eigenfunction expansion converges more rapidly to the exact solution. The convergence rate depends on the smoothness of the forcing function $f(t)$. The following figure shows how the error decreases as we increase the number of terms N in the truncated expansion:

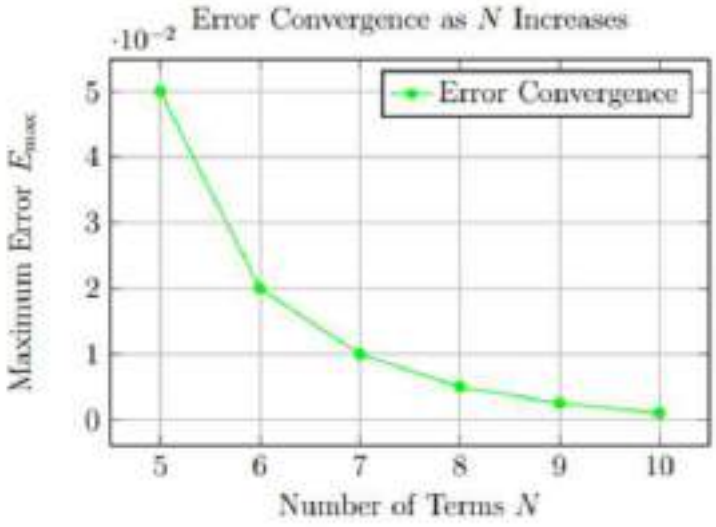

Figure 11: Convergence of the solution as the number of terms N in the eigenfunction expansion increases.

In this example, we demonstrated the effectiveness of the orthonormal eigenfunction expansion in solving iterative boundary value problems on the discrete time scale $\mathbb{T} = \mathbb{Z}$. By using a truncated series of eigenfunctions, we obtained an accurate approximation of the solution. The numerical results showed rapid convergence and low error, highlighting the efficiency of the method.

1.5 5 Conclusion

This paper presents a method for solving iterative boundary value problems on time scales using orthonormal eigenfunction expansions. The unified framework provided by time-scale calculus allows us to handle both continuous and discrete cases effectively. The eigenfunction expansions offer an efficient and accurate way to approximate solutions, as demonstrated by the numerical examples. Future work will focus on extending these methods to nonlinear BVPs and investigating their applications in control theory and dynamic

systems.

References

[1] S. Hilger, “Analysis on Measure Chains—A Unified Approach to Continuous and Discrete Calculus," *Results in Mathematics*, vol. 18, no. 1, pp. 18-56, 1988.
[2] M. Bohner and A. Peterson, *Dynamic Equations on Time Scales: An Introduction with Applications*, Birkhäuser, Boston, 2001.
[3] M. Bohner and A. Peterson, *Advances in Dynamic Equations on Time Scales*, Birkhäuser, Boston, 2003.
[4] C. Sturm, “Mémoire sur les équations différentielles linéaires du second ordre," *Journal de Mathématiques Pures et Appliquées*, vol. 1, pp. 106-186, 1836.
[5] S. Hilger, “Analysis on Measure Chains—A Unified Approach to Continuous and Discrete Calculus," *Results in Mathematics*, vol. 18, no. 1, pp. 18-56, 1988.
[6] M. Bohner and A. Peterson, *Dynamic Equations on Time Scales: An Introduction with Applications*, Birkhäuser, Boston, 2001.
[7] C. Sturm, “Mémoire sur les équations différentielles linéaires du second ordre," *Journal de Mathématiques Pures et Appliquées*, vol. 1, pp. 106-186, 1836.
[8] S. Hilger, “Analysis on Measure Chains—A Unified Approach to Continuous and Discrete Calculus," *Results in Mathematics*, vol. 18, no. 1, pp. 18-56, 1988.
[9] M. Bohner and A. Peterson, *Dynamic Equations on Time Scales: An Introduction with Applications*, Birkhäuser, Boston, 2001.
[10] S. Hilger, “Analysis on Measure Chains—A Unified Approach to Continuous and Discrete Calculus," *Results in Mathematics*, vol. 18, no. 1, pp. 18-56, 1988.
[11] M. Bohner and A. Peterson, *Dynamic Equations on Time Scales: An Introduction with Applications*, Birkhäuser, Boston, 2001.

Nanotechnology for Environmental Engineering
https://doi.org/10.1007/s41204-024-00372-x

ORIGINAL PAPER

Green synthesis of CuO nanorods using *Jatropha podagrica* leaf extract for dye degradation and antibacterial applications

Venkatesh Golthi[1,2,3] · Jayarao Kommu[1,3] · Kiran Kumar Penmethsa[2] · J. Laxmi Mangamma[2]

Received: 12 January 2024 / Accepted: 22 April 2024

Abstract

A sturdy eco-friendly synthesis technique was applied, utilizing leaf extract from the Buddha Belly plant (*Jatropha podagrica*) as a capping agent, to produce copper oxide nanorods (CuO NRs). Analysis of HR-TEM and SEM images confirmed that these NRs exhibit a rod-like shape and possess a monoclinic crystalline structure with an average size of 8–14 nm. The FT-IR spectrum displayed characteristic vibration modes related to the Cu–O bond between 433 and 526 cm^{-1}. The photocatalytic efficiency of the NRs was tested by exposing them to sunlight in the presence of Rhodamine B (RhB) and Crystal Violet (CV) dyes. Remarkably, the NRs degraded 95–97% of the dyes within 1–2 h. When employing 150 µL of the NRs in a well diffusion method, inhibitory zones measuring 14, 16, 13, and 11 mm were noted against *Bacillus coagulans, Staphylococcus aureus, Escherichia coli,* and *Klebsiella pneumoniae,* respectively. This study demonstrates that JP-CuO NRs effectively remove dyes from aqueous solutions and kill bacteria.

Graphical Abstract

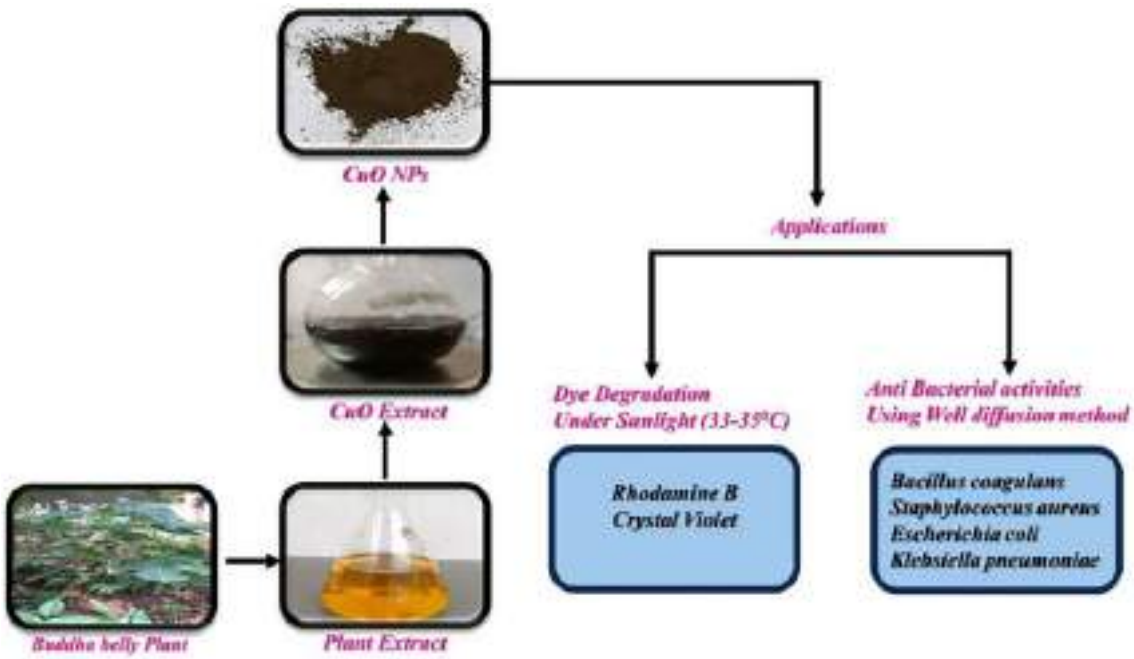

Keywords CuO nanorods · *Jatropha podagrica* plant · Dye degradation · Antimicrobial activity

Extended author information available on the last page of the article

Introduction

In today's world, there has been a consistent rise in industrial activity and population numbers, leading to the introduction of various new pollutants into water bodies. Notably, industries such as textiles, paper, leather, and printing are major sources of harmful dye effluents, posing serious ecological and health risks [1]. Dyes like Rhodamine B (RhB) and Crystal Violet (CV) are particularly concerning due to their potential ingestion hazards for both humans and animals, as well as their ability to cause skin, eye, and respiratory irritation [2]. Additionally, the reemergence of infectious diseases and the increasing prevalence of antibiotic resistance in various pathogenic bacteria are significant global public health challenges. Enterococcus, Staphylococcus, and Streptococcus, closely related species of harmful microorganisms, are responsible for a wide range of infections and diseases, contributing to the urgency of addressing these issues [3].

In recent decades, there has been notable progress in nanotechnology. A key focus in material science has been the development of nanoparticles (NPs) with adjustable morphology, allowing for precise control over their shape, size, and arrangement [4]. Extensive research has been dedicated to exploring their wide-ranging applications, spanning chemical and biological sensing, medical therapeutics, antimicrobial and antibacterial agents, and drug delivery systems [5]. Additionally, these NPs hold promise in fields like wastewater treatment, energy-efficient devices, optics, optoelectronics, electrochemistry, and catalysis [6]. Among the various types of antioxidant metal oxide NPs, CuO NPs have garnered considerable interest due to their cost-effectiveness, ready availability of copper salt, potent antioxidant properties, and low toxicity towards living cells, ensuring the safety of CuO NPs [7]. The antioxidant effectiveness of CuO NPs is influenced by various factors, including their inherent characteristics, crystal structure, chemical composition, surface charge, particle size, surface coating, and how they are dispersed. Additionally, CuO NPs exhibit a range of valuable physical attributes, including electron correlation effects, spin dynamics, a high dielectric constant, and the potential for high-temperature superconductivity [8–10]. In the industrial field, they are commonly employed as p-type semiconductors with a specific bandgap range of 1.21–2.51 eV, contributing to the design and manufacture of batteries, solar cells, gas sensors, and catalysts [11–13]. In today's context, CuO NPs serve as heterogeneous catalysts and play roles in biomedicine, functioning as antioxidants, drug delivery carriers, and imaging agents [14–17]. In the past, various physical and chemical processes have been employed in the synthesis of CuO NPs, offering the ability to produce particles tailored to specific preferences [18]. Nevertheless, these production techniques come with several drawbacks, including potentially harmful organic solvents, expensive reagents, challenges in isolating the NPs, and lengthier processing times [19]. Plant-mediated synthesis has emerged as a promising alternative within this range of methods due to its straightforwardness, environmentally friendly nature, user-friendliness, cost-effectiveness, adaptability for large-scale industrial production, and applicability in the biomedical field [20]. Plant extracts contain phytochemicals that serve dual roles as both reducing and capping agents, enabling the creation of CuO NPs with precise control over size and shape, and the prevention of aggregation, all without the necessity for external oxidizing, reducing, or capping agents [21, 22].

This study aimed to demonstrate the antioxidant activity of CuO nanorods (NRs) synthesized using *Jatropha podagrica* leaf extract (JP) as a sustainable source for the effective removal of organic dye pollutants. JP is a widely recognized native medicinal plant with a history of being employed to address a range of health conditions, such as ulcers, scabies, injuries, and fever. It also has beneficial properties such as anti-tumorigenic, antioxidant, and antibacterial capabilities [23]. The study first examined the JP leaves for specific phytochemical components, such as tannins, glycol flavones, proanthocyanidins, and phenolic acids [24, 25]. The leaf extract of *Jatropha podagrica* is safe, a critical consideration in the formulation of nanorods [24]. We have recently published an article outlining the incorporation of this plant extract in the synthesis of ZnO and Fe_3O_4 nanoparticles [26, 27]. These phytochemicals play a vital role in synthesizing JP-CuO NRs, acting as both capping agents and stability enhancers, surpassing what conventional chemical synthesis methods can achieve [24]. Additionally, the various phenolic acids in these phytochemicals help achieve well-defined sizes and shapes for the JP-CuO NRs, surpassing green-synthesized nanoparticles (As illustrated in Table 1). To harness the full potential of undiscovered plant species, it is crucial to identify fresh and distinctive plants for synthesizing nanorods. This strategy enables researchers to broaden the spectrum of nanorods that can be efficiently stabilized by uncovering new proteins and phytochemicals from plant sources that have not been investigated before. Additionally, these newfound plant species might present supplementary benefits, such as enhanced productivity, lowered costs, or specialized characteristics suitable for specific applications. The JP-CuO NRs were notable for having a negatively charged surface, which gave them outstanding degrading abilities for removing the dyes Rhodamine B (RhB) and Crystal Violet (CV). The antibacterial activity of these JP- CuO NRs was tested against both Gram-positive (*Bacillus coagulans, Staphylococcus aureus*) and Gram-negative (*Escherichia coli, Klebsiella pneumoniae*) bacteria.

Table 1 Contrasting the average size and structure of JP-CuO NRs in this study about findings from prior research

Material of plants	Average particle size	Structure	Implementation	References
Jatropha podagrica leaf extract	8–14 nm	Rod-like shape	Dye degradation and antibacterial applications	Present work
Eucalyptus globoulus leaf extract	88 nm	Spherical shape	Dye degradation	[28]
Abelmoschus esculentus fruit extract	20 nm	Spherical shape	Cytotoxicity and photocatalytic applications	[29]
malva sylvestris leaf extract	19–26 nm	Spherical shape	Thermal decomposes kinetics	[30]
Calotropis procera leaf extract	20–80 nm	Spherical shape	Photodegradation, antibacterial and antioxidant	[31]
Syzygium alternifolium fruit extract	17.5 nm	Spherical shape	Antiviral activity	[32]
Panicum sumatrense grains extract	20 nm	Rectangular in shape	Biological applications	[33]

Materials and methods

Materials

Preparation of CuO NRs using JP leaf extract

Jatropha podagrica (JP) plant leaves were freshly collected, washed with warm water, and rinsed with deionized. The leaves were then dried in the shade for 25 days until completely dehydrated. The dried leaves were then ground into a fine powder. One gram of the powder was added to a 500 mL glass beaker with 200 mL of deionized water. The mixture was heated at 80 °C for 30 min on a heating mantle, resulting in a deep golden-yellow solution. The solution was first filtered to remove solid particles, and then it underwent centrifugation to obtain a pure extract solution. This extract was subsequently stored in a refrigerator at a temperature of 4 °C for future use.

Synthesis of JP-CuO NRs

A conventional environmentally friendly method was used to synthesize CuO nanorods (NRs). First, 1 g of $Cu(SO_4)_2{\cdot}5H2O$ was dissolved in 90 mL of distilled water. After thorough mixing for 25–30 min at room temperature, the solution turned a clear blue color. Then, 10 mL of aqueous leaf extract was added, increasing the volume to 100 mL and turning the solution green. This mixture was sonicated vigorously for 10–15 min to ensure proper mixing. Next, the temperature was raised to 80 °C and maintained for up to 1 h, resulting in a deep green color. Then, 1 M NaOH (10 mL) was gradually added dropwise, causing the mixture to turn a dark brown color. To remove suspended particles, the mixture was dispersed in deionized water and centrifuged at 7000 rpm. The dark brown particles obtained were washed repeatedly with deionized water to eliminate impurities and achieve the ultimate product. The resulting dark brown solid was subsequently subjected to vacuum drying at 70 °C for 8 h in an oven. Lastly, the material underwent fine grinding with a mortar and pestle, preparing it for subsequent characterization [34].

JP-CuO NRs as efficient photocatalysts for Rhodamine B (RhB) and crystal violet (CV) dye degradation

The evaluation of the photocatalytic efficiency of JP-CuO NRs in degrading RhB and CV dyes was carried out utilizing naturally available UV radiation from sunlight. Initially, solutions of 100 mL containing 1 ppm of RhB and CV dyes were prepared and mixed with 0.01 g of JP-CuO NRs in separate containers. These mixtures were then stirred in darkness for an hour to stabilize the solutions and prevent any adsorption–desorption processes. After stabilization, the solutions were exposed to sunlight for 4 h, specifically from 11 AM to 3 PM, with outdoor temperatures ranging from 33 to 35 °C. Continuous magnetic stirring was employed to maintain a pH level of 10 during this time. At predefined intervals, consistent samples were collected from each dye solution, and the NRs were separated by centrifugation at 8000 rpm. The absorption of RhB and CV dyes at 540 nm and 580 nm was determined using a UV–visible spectrophotometer. The extent of photocatalytic degradation and the corresponding rate constants were calculated based on these measurements.

$$\text{Degradation rate } (\%) = \left(\left(A_0 - A\right)/A_0\right) \times 100$$

$$\ln A_0/A = kt$$

In this context, "A_0" denotes the starting concentration, "A" represents the concentration after the degradation process, "k" stands for the degradation rate constant, and "t" indicates the duration of exposure to sunlight. [35, 36].

Exploration of antibacterial activity of JP-CuO NRs

The antibacterial properties of JP-CuO NRs were evaluated in 24 h bacterial cultures (*Bacillus coagulans, Staphylococcus aureus, Escherichia coli, and Klebsiella pneumoniae*) using the Agar-Well diffusion method. The nutrient agar medium was sterilized for approximately 30 min at 120 °C using an autoclave to prepare it. Each sterile petri dish was then filled with 20 mL of the medium, and the respective bacterial strains were introduced under aseptic conditions. The plates were left at room temperature until the agar solidified. A sterile borer created a single 6 mm diameter well in each plate. Test substances, control (distilled water), and a standard drug were added to the 6 mm wells after being freshly dissolved in distilled water at concentrations of 1, 2, and 3. The petri plates were then incubated at 37 °C for 12 h, and the inhibition results are depicted in Fig. 8. A standard solution with a concentration of 5 g/mL served as a positive control. The diameter of the inhibitory zone was determined using the HiMedia antibiotic zone scale. All experiments were conducted in triplicate, yielding consistent results [37].

Characterization of JP-CuO NRs

Various analytical methods were utilized to ascertain the crystalline structure of CuO nanorods. To investigate the optical properties, UV–Vis diffuse reflectance/absorbance spectroscopy was conducted on the synthesized samples. A Shimadzu (2450—SHIMADZU) spectrophotometer equipped with a diffuse reflectance accessory was used at room temperature, with $BaSO_4$ serving as a reference material. Measurements were taken over the wavelength range of 200–800 nm. Fourier transform infrared spectra (FT-IR) for the samples were obtained using a Thermo Nicolet iS50 spectrometer, covering a frequency range from 4000 to 400 cm^{-1} in transmission mode with high-quality KBr pellets. X-ray diffraction (XRD) measurements were carried out using a Bruker Kappa Apex II instrument over a 2θ range of 0 to 90°. This instrument employed CuKα radiation (with a wavelength of $\lambda = 1.54060$ Å) at 40 kV and 35 mA, with a scanning rate of 0.2 s. The CuO nanorods were characterized using scanning electron microscopy (SEM) and high-resolution transmission electron microscopy (HRTEM) to investigate their surface morphology, elemental composition, and microstructure. SEM analyses were conducted using a Jeol 6390LA/ OXFORD XMX N apparatus equipped with energy-dispersive X-ray (EDX) spectroscopy. The acceleration voltage for SEM imaging ranged from 0.5 to 30 kV. For a more in-depth examination of the nanorods' microstructure and particle size, HRTEM was employed. HRTEM analyses were performed using a JEOL/JEM 2100 instrument operated at an applied voltage of 200 kV. Carbon-copper grids were used for sample preparation, allowing for precise particle size determination. Furthermore, SAED images were acquired using the HRTEM instrument to further elucidate the nanorods' crystal structure.

Results and discussions

UV–Vis spectroscopy studies

Figure 1 displays the UV–Vis absorption spectra of the leaf extract of JP and synthetic CuO NRs. The leaf extract contains various phytochemicals, such as alkaloids, flavonoids, phenolic acids, tannins, glycol flavones, and proanthocyanidins, which absorb light at 280 nm and 351 nm (π-π* and n-π* transitions) [23]. The JP-CuO NRs have a distinct absorption peak at 273 nm, but not at 280 or 351 nm. This suggests that the phytochemicals in the leaf extract play a key role in reducing, binding, and encapsulating JP-CuO NRs during the synthesis process [38, 39].

FTIR analysis of the synthesized JP-CuO NRs

The functional groups included in the synthesized JP-CuO NRs were identified, and their chemical composition was ascertained, using Fourier transform infrared (FTIR) spectroscopy. The FTIR analysis of the plant extract (Fig. 2) shows a significant peak at approximately 3500 cm^{-1}, indicating the presence of phenolic groups. Moreover, observable peaks at 1178 and 1042 cm^{-1} correspond to vibrational characteristics of polyphenolic molecules within the plant extract [24]. The FTIR spectrum of the CuO NRs (Fig. 2) shows absorption peaks in the range of 4000–400 cm^{-1}. The peaks between 433 and 526 cm^{-1} correspond to the stretching frequency of the Cu–O bond [28]. Furthermore, the emergence of peaks between 1117 and 1032 cm^{-1} underscores aspects related to chemical bonding, the crystalline nature of the material, and the relative intensities of IR bands linked to polyphenolic compounds [40]. The symmetric stretching of the aliphatic amino group is suggested by the presence of a peak at 1384 cm^{-1} [41]. Notably, the peak observed at 1630 cm^{-1} corresponds to the C=C stretching indicative of aromatic compounds [42]. Additionally, the peaks between 2852 and 2923 cm^{-1} are characteristic of –CH stretching vibrations typically associated with aldehyde groups [43]. Finally, the absorption band at 3432 cm^{-1} signifies the –OH stretching vibration inherent to phenolic groups [44]. These distinctive peaks within the IR spectrum provide valuable insights into the purity and compositional characteristics of the biosynthesized CuO NRs.

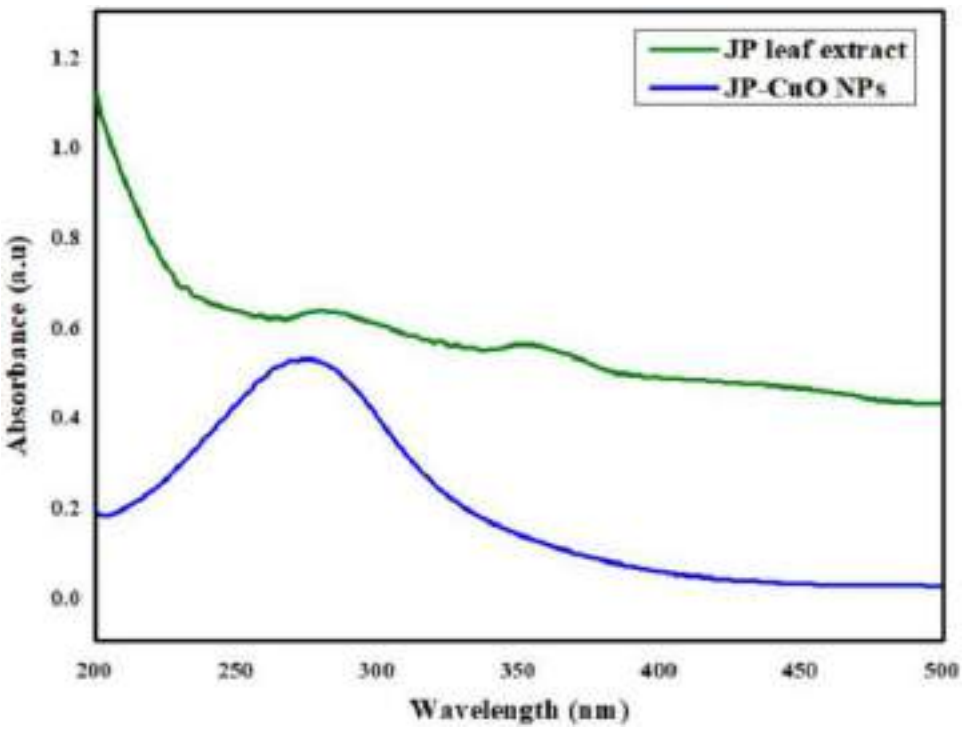

Fig. 1 UV–Vis Spectra of JP-CuO NRs and JP leaf extract

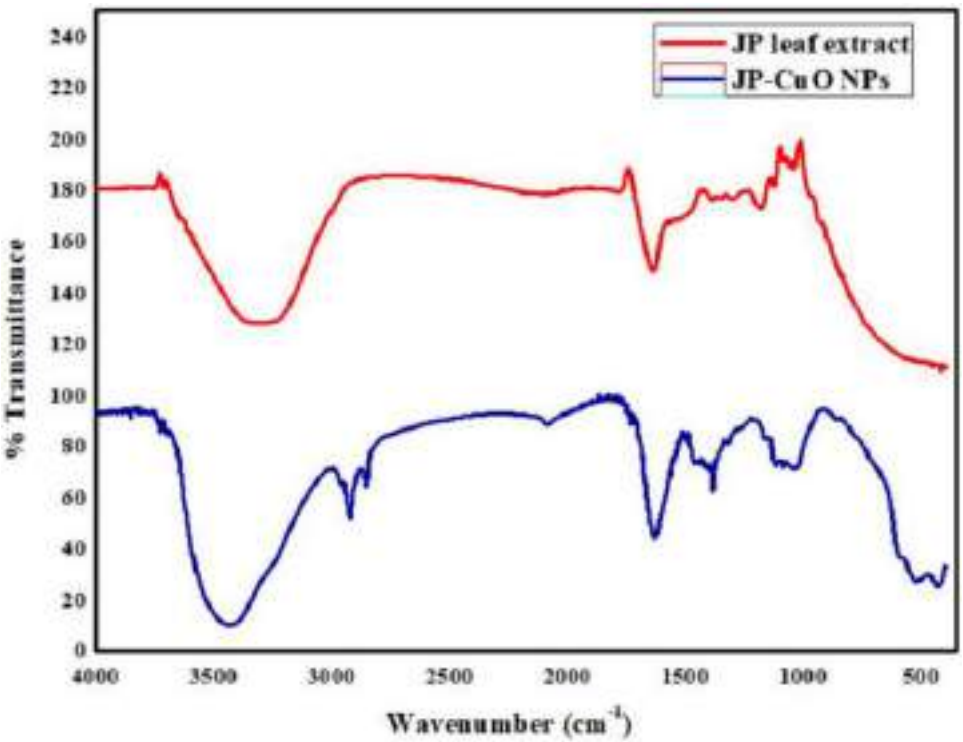

Fig. 2 FTIR spectra of JP-CuO NRs and JP extract

XRD analysis of JP-CuO NRs

The XRD analysis, as depicted in Fig. 3, unveiled discernible peaks that are indicative of CuO NRs at various angles. These angles include 32.67°, 35.66°, 38.85°, 48.77°, 53.87°, 58.21°, 61.65°, 66.24°, 68.19°, 75.23°, and 77.18°. These particular peaks corresponded to distinct crystal lattice planes, specifically (100), (002), (111), (202), (020), (-202), (113), (311), (-113), (-311), and (004) respectively. According to earlier studies, the presence of diffraction

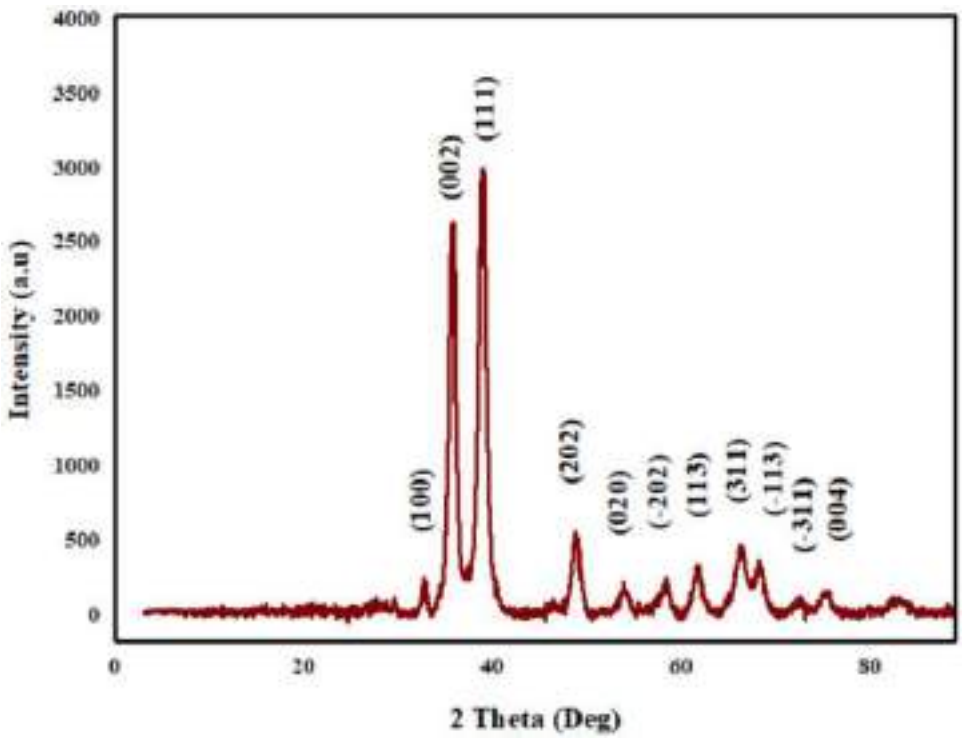

Fig. 3 XRD patterns of CuO NRs using an aqueous leaf extract of *Jatropha podagrica*

peaks falling within the range of 35 to 39° is indicative of CuO NRs formation (JCPDS Standard No. 01–080-0078). It's worth noting that the intensity of the (002) and (111) peaks suggested a monoclinic crystalline structure [45]. The sharp and well-defined diffraction peaks in the XRD pattern of the JP-CuO NRs indicate that they have a strong crystalline structure. The absence of other peaks confirms that the NRs are pure. The most prominent peaks observed between 35 and 39 °C for JP-CuO NRs were utilized to calculate the average crystallite size, which was determined to be 8.2 nm employing the Debye–Scherrer equation [46].

$$D = k\lambda/\beta\cos\theta$$

where D is the crystal size, λ is the wavelength of X-ray radiation (0.15406 nm for Cu Kα), k is the shape factor (usually assumed to be 0.9), β is the full width at half maximum (FWHM) of the diffraction peak, and θ is the diffraction angle.

SEM–EDX analysis of JP-CuO NRs

The surface properties of the generated CuO NRs were analyzed using a SEM. As shown in Fig. 4a and b, the particles exhibited a predominantly rod-like shape, forming clusters and appearing well-dispersed [44]. Some particle clustering was evident, likely due to the presence of phenolic compounds derived from the JP plant, which acted as a capping agent. Furthermore, the high surface energy of JP-CuO NRs resulted in minimal aggregation, which was attributed to the water medium serving as the synthesis source. To identify the chemical elements, present in the CuO NRs, an EDX analysis was performed on a densely populated area of the sample (Fig. 4c)**.** The EDX spectrum showed significant peaks at 0.9, 8, and 8.9 keV, corresponding to copper atoms. A single peak at 0.5 keV was also observed, corresponding to oxygen atoms. Figure 4c exhibited distinct and strong signals for Cu and O atoms, with a weight percentage of 84.57% and 15.43%, respectively. The absence of other peaks indicates that the CuO NRs are of high purity.

TEM analysis of JP-CuO NRs

High-resolution transmission electron microscopy (HR-TEM) was used to study the size, shape, and structure of the JP-CuO NRs in detail. HR-TEM images showed the nanorod structure at different magnifications are shown in Fig. 5a–c. HR-TEM images revealed CuO nanorods with a diameter of around 10–14 nm and a length of 100–200 nm (Fig. 5a and b). The selected area electron diffraction pattern (SAED) of the JP-CuO NRs is portrayed in Fig. 5d. The SAED pattern indicated the presence of polycrystalline NRs in the JP-CuO sample [47].

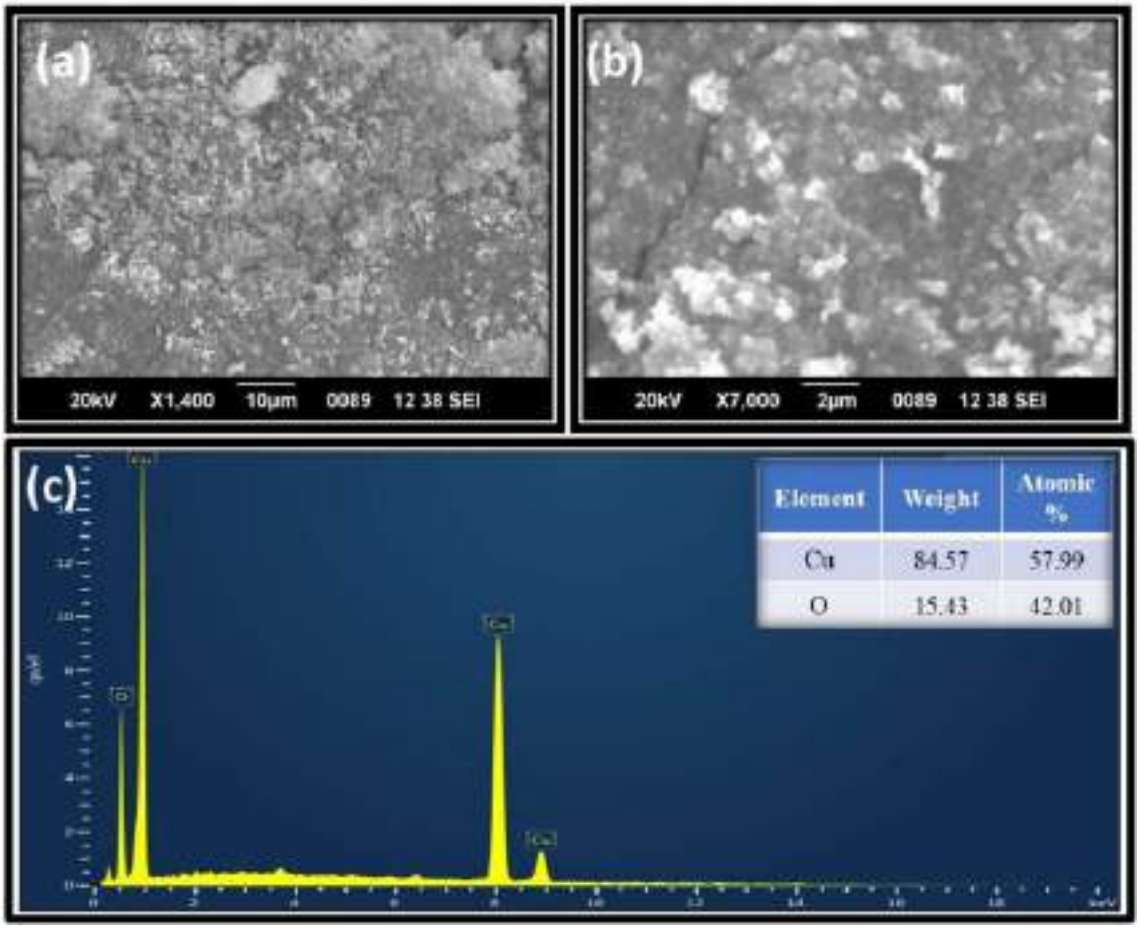

Fig. 4 **a** and **b** SEM images of JP-CuO NRs various magnifications and **c** EDX spectra of JP-CuO NRs

A photocatalytic degradation of RhB and CV dyes by the fabricated JP-CuO NRs

The JP-CuO catalyst was utilized to illustrate the photocatalytic removal of RhB and CV dyes in an environment of bright sunlight. RhB and CV dye degradation are shown in Figs. 6 and 7 across two distinct periods of 120 min and 60 min, respectively. These results also show that these dyes have separate wavelength ranges at 540 nm and 580 nm. The UV–Visible spectrometer was used to measure the RhB and CV dye degradation at regular intervals of 30 min and 15 min respectively. Degradation efficiencies of 95% and 97% were achieved for RhB and CV dyes, respectively. The degradation efficiency of the as-prepared JP-CuO NRs was compared with that of recently reported CuO nanoparticles in Tables 2, 3. The results of this work suggest that JP-CuO NRs have a lot of potential as a catalyst for rapidly breaking down organic contaminants by photocatalysis. The significant rates of degradation shown together with the apparent impact of different pH settings on the removal process spotlight the potential utility of JP-CuO NRs in resolving a variety of problems with water pollution brought on by organic pollutants. As a result, our findings suggest promising opportunities for using JP-CuO NRs to address environmental contamination problems.

The method shown below demonstrates how electrons and holes affect dye deterioration [35, 48].

$$CuO + h\nu \rightarrow e^- + h^+$$

$$\text{Absorption of } O_2 : O_2 + e^- \rightarrow O_2^{-\cdot}$$

$$\text{Water Ionization} : H_2O \rightarrow OH^- + H^+$$

$$\text{Superoxide protonation} : O_2^{-\cdot} + H^+ \rightarrow HOO^{\cdot}$$

$$HOO^{\cdot} + e^- \rightarrow HO_2^-$$

$$HOO^- + H^+ \rightarrow H_2O_2$$

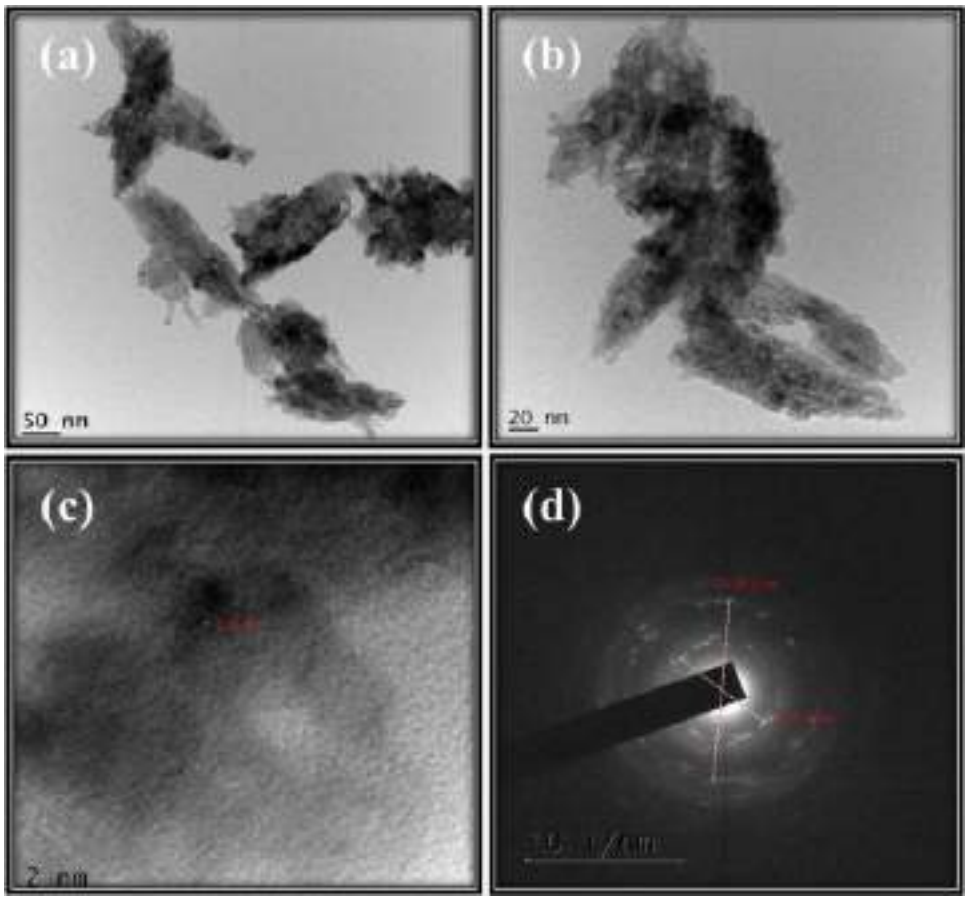

Fig. 5 **a**–**c** HR-TEM images JP-CuO NRs, and **d** SAED patterns

$$H_2O_2 + e^- \rightarrow OH^- + OH^{\cdot}$$

$$H_2O + h^+ \rightarrow H^+ + OH^{\cdot}$$

$$\text{Dyes} + OH^{\cdot} \rightarrow \text{Removal product}$$

The OH radical stated is a very strong oxidant that is quite successful in causing a variety of dyes, including RhB and CV, to degrade.

Anti-bacterial activities of synthesized JP-CuO NRs

JP-CuO NRs were evaluated for their efficacy against both Gram-positive (*Bacillus coagulans* and *Staphylococcus aureus*) and Gram-negative (*Escherichia coli* and *Klebsiella pneumoniae*) bacteria using the well diffusion method. Figure 8 illustrates the results of the zone inhibition test, displaying the diameters of the inhibition zones (in mm) surrounding each well containing the JP-CuO NRs. The most positive outcomes were noted with inhibition zones measuring 14, 16, 13, and 11 mm against *Bacillus coagulans, Staphylococcus aureus, Escherichia coli,* and *Klebsiella pneumoniae*, respectively, at a concentration of 150 µL, in comparison to the standard drug, as outlined in Table 4. [50, 51].

The results of the study showed that Gram-positive bacteria were more susceptible to JP-CuO NRs than Gram-negative bacteria**.** The variation in sensitivity can be explained by the significant presence of a dense peptidoglycan layer in the cell wall of Gram-positive bacteria, providing a small physical barrier that offers protection. In contrast, Gram-negative bacteria possess both lipopolysaccharide and peptidoglycan, rendering them more resistant to the effects of JP-CuO NRs**.**

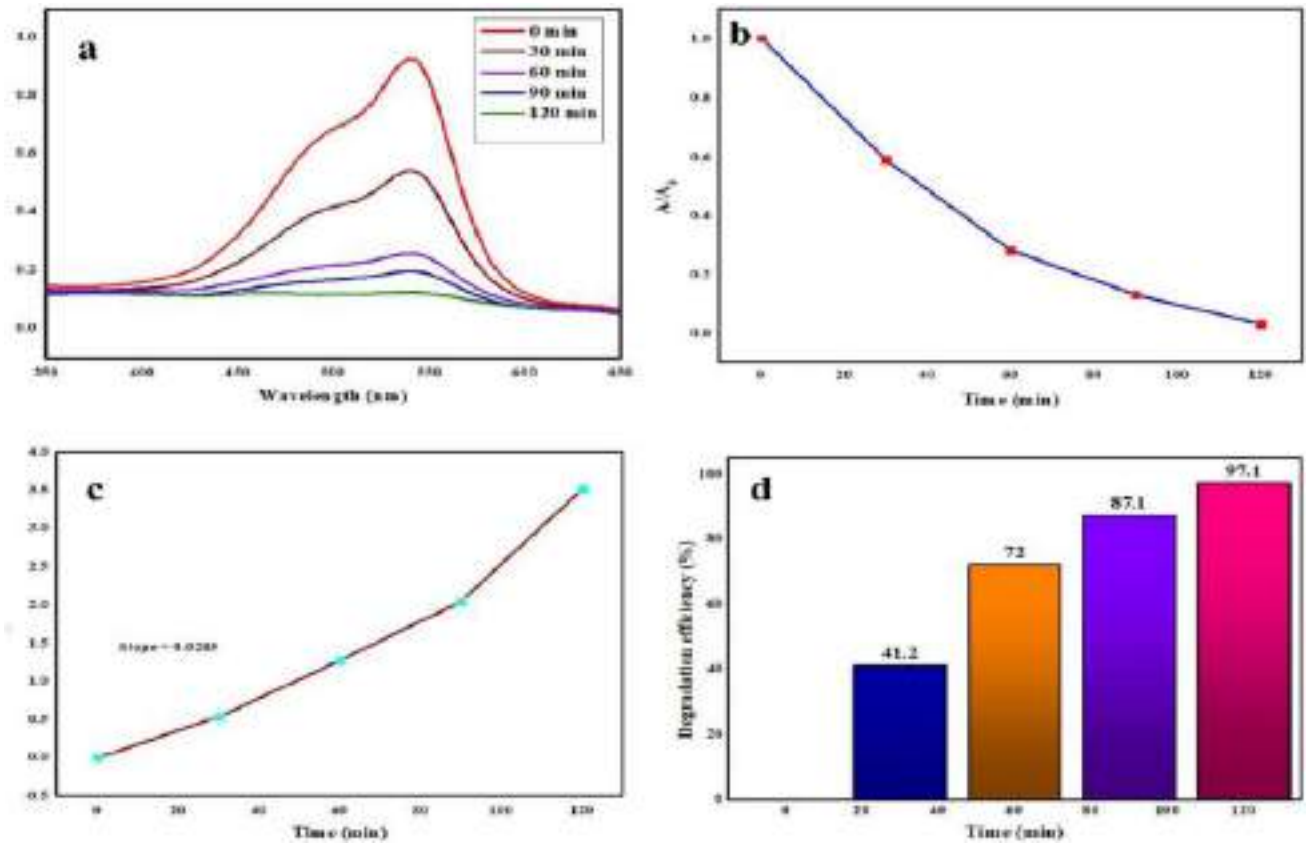

Fig. 6 **a** UV–vis absorbance spectra of RhB dye under UV (sunlight) illumination over JP-CuO NRs as a function of time, **b** the progression of RhB dye degradation during consecutive time intervals, **c** the kinetics of RhB dye degradation presented as a first-order linear plot with ln A_0/A as a function of time, and **d** a column chart representing the distribution of RhB dye degradation across different time intervals

Conclusions

We have developed a green method for making copper oxide nanorods (CuO NRs) using *Jatropha podagrica* leaf extract as a capping agent. The NRs were also effective photocatalysts, breaking down Rhodamine B (RhB) and Crystal Violet (CV) dyes in sunlight with degradation rates of 95–97% within 120 and 60 min, respectively. We also tested the NRs against Gram-positive (*Bacillus coagulans* and *Staphylococcus aureus*) and Gram-negative (*Escherichia coli* and *Klebsiella pneumoniae*) bacteria, and they produced inhibition zones of 14, 16, 13, and 11 mm, respectively, at a concentration of 150 µL. These results suggest that JP-CuO NRs could be used to clean up water pollution and develop powerful antibacterial agents.

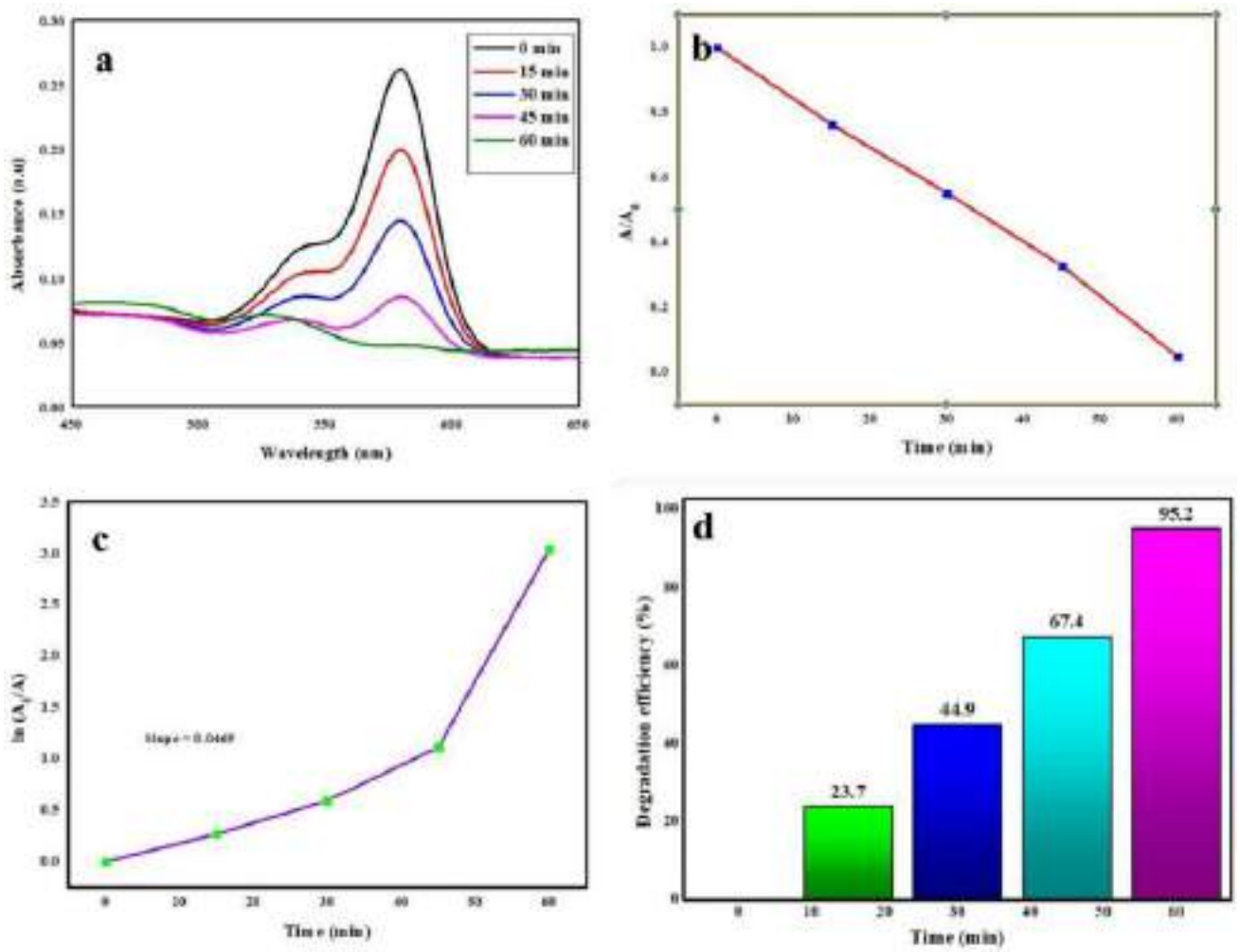

Fig. 7 **a** UV–vis absorbance spectra of CV dye under UV (sunlight) illumination over JP-CuO NRs as a function of time, **b** the progression of CV dye degradation during consecutive time intervals, **c** the kinetics of CV dye degradation presented as a first-order linear plot with ln A_0/A as a function of time, and **d** a column chart representing the distribution of CV dye degradation across different time intervals

Table 2 Lists the materials required to prepare the JP-CuO NRs

Chemical name	Supplier name	Purity (%)	Usage
Copper (II) sulfate pentahydrate ($Cu(SO_4)_2{\cdot}5H_2O$)	Merk, India	98	Reagent for the preparation of CuO NRs
Sodium hydroxide (NaOH)	Merk, India	99	Precipitating agent for the preparation of CuO NRs
Milli Q-water	Merk, India	100	Solvent
Bacillus coagulans	Aadhya Biosciences Pvt. Ltd Visakhapatnam, India	100	Well diffusion method
Staphylococcus aureus	Aadhya Biosciences Pvt. Ltd Visakhapatnam, India	100	Well diffusion method
Escherichia coli	Aadhya Biosciences Pvt. Ltd Visakhapatnam, India	100	Well diffusion method
Klebsiella pneumoniae	Aadhya Biosciences Pvt. Ltd Visakhapatnam, India	100	Well diffusion method
Jatropha podagrica leaves	Government Degree College Chodavaram, India	100	Capping and stabilized agent for the CuO NRs

Table 3 Comparison of the photocatalytic degradation of JP-CuO NRs in the present work with previous works

Green materials	Dye	Light source	Irradiation time (min)	Degradation efficiency (%)	References
Jatropha podagrica leaf extract	Rhodamine B	Sunlight	120	95	Present work
	Crystal violet		60	97	
Ferulago angulate boiss extract	Rhodamine B	UV light	150	83	[48]
Citrus aurantifolia leaf extract	Rhodamine B	UV light	120	91	[35]
Ruellia tuberosa root extract	Crystal Violet	Sunlight	120	90	[36]
Sida acuta leaf extract	Crystal Violet	Sunlight	100	87	[49]

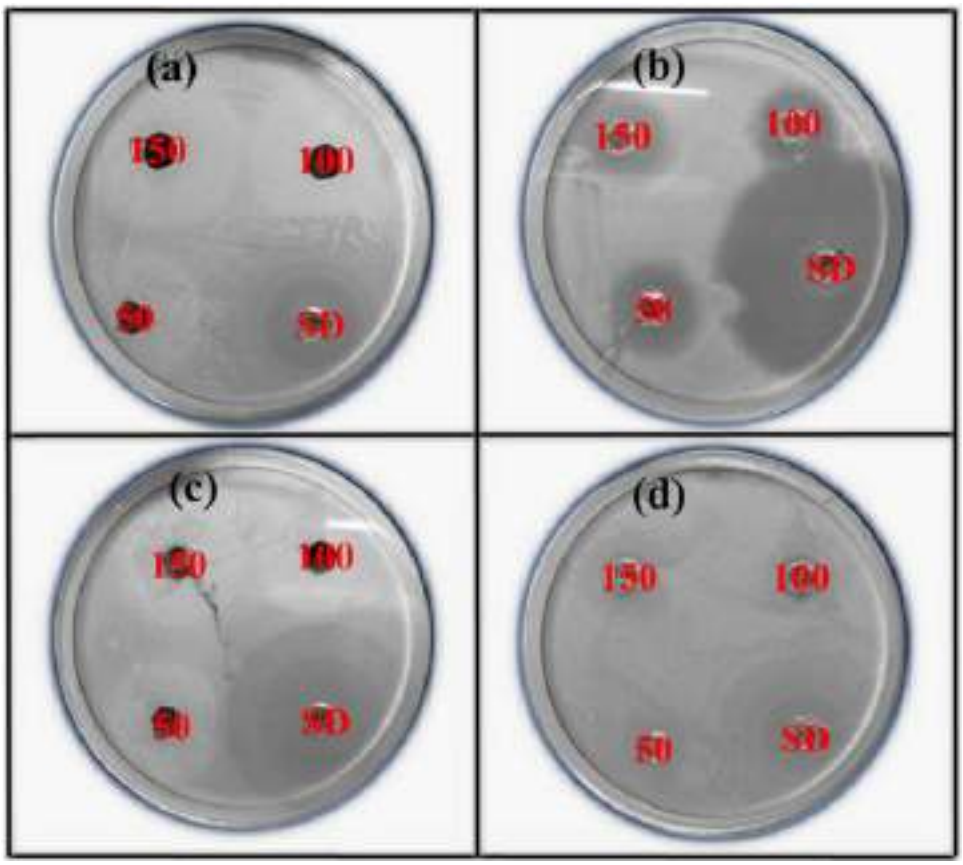

Fig. 8 Antibacterial activity of CuO NRs synthesized using *Jatropha podagrica* leaf extract for **a** *Bacillus coagulans*, **b** *Staphylococcus aureus*, **c** *Escherichia coli*, and **d** *Klebsiella pneumoniae*

Table 4 Zone of inhibition at various concentrations of JP-CuO NRs

Name	*Bacillus coagulans*	*Staphylococcus aureus*	*Escherichia coli*	*Klebsiella pneumoniae*
Shape	Round	Round	Round	Round
Gram reaction	Gram-positive	Gram-positive	Gram-negative	Gram-negative
50 µL	11 mm	14 mm	11 mm	10 mm
100 µL	13 mm	15 mm	12 mm	10 mm
150 µL	14 mm	16 mm	13 mm	11 mm
Antibiotic	30 mm	32 mm	30 mm	26 mm

Acknowledgements The authors express sincere gratitude to Dr. K. Basavaiah, professor in the Department of Analytical Chemistry at Andhra University, Visakhapatnam, Andhra Pradesh, India, for generously facilitating UV-Vis spectroscopy for characterizations

Authors contributions Venkatesh Golthi wrote the manuscript and prepared the tables, J Laxmi Mangamma collected the data, Kiran Kumar Penmethsa prepared the figures, and Jayarao Kommu reviewed the manuscript.

Funding The authors did not receive any funding for this research work.

Availability of data and materials This declaration is "not applicable".

Declarations

Ethical approval This declaration is "not applicable".

Conflict of interest There are no conflicts to declare.

References

1. Lee KM, Lai CW, Ngai KS, Juan JC (2016) Recent developments of zinc oxide based photocatalyst in water treatment technology: a review. Water Res 88:428–448. https://doi.org/10.1016/j.watres.2015.09.045
2. Jain R, Mathur M, Sikarwar S, Mittal A (2007) Removal of the hazardous dye rhodamine B through photocatalytic and adsorption treatments. J Environ Manage 85(4):956–964. https://doi.org/10.1016/j.jenvman.2006.11.002
3. Jones N, Ray B, Ranjit KT, Manna AC (2008) Antibacterial activity of ZnO nanoparticle suspensions on a broad spectrum of microorganisms. FEMS Microbiol Lett 279(1):71–76. https://doi.org/10.1111/j.1574-6968.2007.01012.x
4. Mayeen A, Shaji LK, Nair AK, Kalarikkal N (2018) Morphological characterization of nanomaterials. In: Characterization of nanomaterials, pp. 335–364. Woodhead Publishing. https://doi.org/10.1016/B978-0-08-101973-3.00012-2
5. Fatima F, Siddiqui S, Khan WA (2021) Nanoparticles as novel emerging therapeutic antibacterial agents in the antibiotics resistant era. Biol Trace Elem Res 199:2552–2564. https://doi.org/10.1007/s12011-020-02394-3
6. Veloso RC, Souza A, Maia J, Ramos NMM, Ventura J (2021) Nanomaterials with high solar reflectance as an emerging path towards energy-efficient envelope systems: a review. J Mater Sci. https://doi.org/10.1007/s10853-021-06560-3
7. Naz S, Gul A, Zia M, Javed R (2023) Synthesis, biomedical applications, and toxicity of CuO nanoparticles. Appl Microbiol Biotechnol 107(4):1039–1061. https://doi.org/10.1007/s00253-023-12364-z
8. Karthikeyan NR, Philip J, Raj B (2008) Effect of clustering on the thermal conductivity of nanofluids. Mater Chem Phys 109(1):50–55. https://doi.org/10.1016/j.matchemphys.2007.10.029
9. Agarwal R, Verma K, Agrawal NK, Duchaniya RK, Singh R (2016) Synthesis, characterization, thermal conductivity and sensitivity of CuO nanofluids. Appl Therm Eng 102:1024–1036. https://doi.org/10.1016/j.applthermaleng.2016.04.051
10. Oruç Ç, Altındal A (2017) Structural and dielectric properties of CuO nanoparticles. Ceram Int 43(14):10708–10714. https://doi.org/10.1016/j.ceramint.2017.05.006
11. Vidyasagar CC, Arthoba Naik Y, Venkatesha TG, Viswanatha R (2012) Solid-state synthesis and effect of temperature on optical properties of CuO nanoparticles. Nano-Micro Lett 4:73–77. https://doi.org/10.1007/BF03353695
12. Langmar O, Ganivet CR, Schol P, Scharl T, De La Torre G, Torres T, Guldi DM (2018) Improving charge injection and charge transport in CuO-based p-type DSSCs–a quick and simple precipitation method for small CuO nanoparticles. J Mater Chem C 6(19):5176–5180. https://doi.org/10.1039/C8TC00769A
13. Jiang T, Bujoli-Doeuff M, Farré Y, Pellegrin Y, Gautron E, Boujtita M, Odobel F (2016) CuO nanomaterials for p-type dye-sensitized solar cells. RSC Adv 6(114):112765–112770. https://doi.org/10.1039/C6RA17879K
14. Letchumanan D, Sok SP, Ibrahim S, Nagoor NH, Arshad NM (2021) Plant-based biosynthesis of copper/copper oxide nanoparticles: an update on their applications in biomedicine, mechanisms, and toxicity. Biomolecules 11(4):564. https://doi.org/10.3390/biom11040564
15. Das D, Nath BC, Phukon P, Dolui SK (2013) Synthesis and evaluation of antioxidant and antibacterial behavior of CuO nanoparticles. Colloids Surf, B 101:430–433. https://doi.org/10.1016/j.colsurfb.2012.07.002
16. Gholamali I, Hosseini SN, Alipour E, Yadollahi M (2019) Preparation and characterization of oxidized starch/CuO nanocomposite hydrogels applicable in a drug delivery system. Starch-Stärke 71(3–4):1800118. https://doi.org/10.1002/star.201800118
17. Perlman O, Weitz IS, Azhari H (2015) Copper oxide nanoparticles as contrast agents for MRI and ultrasound dual-modality imaging. Phys Med Biol 60(15):5767. https://doi.org/10.1088/0031-9155/60/15/5767
18. Muthuvel A, Jothibas M, Manoharan C (2020) Synthesis of copper oxide nanoparticles by chemical and biogenic methods: photocatalytic degradation and in vitro antioxidant activity. Nanotechnol Environ Eng 5:1–19. https://doi.org/10.1007/s41204-020-00078-w
19. Murugan B, Rahman MZ, Fatimah I, Lett JA, Annaraj J, Kaus NHM, Sagadevan S (2023) Green synthesis of CuO nanoparticles for biological applications. Inorg Chem Commun. https://doi.org/10.1016/j.inoche.2023.111088
20. Cuong HN, Pansambal S, Ghotekar S, Oza R, Hai NTT, Viet NM, Nguyen VH (2022) New frontiers in the plant extract mediated biosynthesis of copper oxide (CuO) nanoparticles and their potential applications: a review. Environ Res 203:111858. https://doi.org/10.1016/j.envres.2021.111858
21. Yugandhar P, Vasavi T, Devi UM, P., & Savithramma, N. (2017) Bioinspired green synthesis of copper oxide nanoparticles from *Syzygium alternifolium* (Wt.) Walp: characterization and evaluation of its synergistic antimicrobial and anticancer activity. Appl Nanosci 7:417–427. https://doi.org/10.1007/s13204-017-0584-9
22. Sathiyavimal S, Vasantharaj S, Veeramani V, Saravanan M, Rajalakshmi G, Kaliannan T, Pugazhendhi A (2021) Green chemistry route of biosynthesized copper oxide nanoparticles using Psidium guajava leaf extract and their antibacterial activity and effective removal of industrial dyes. J Environ Chem Eng 9(2):105033. https://doi.org/10.1016/j.jece.2021.105033
23. Bhaskarwar BHUSHAN, Itankar PRAKASH, Fulke ABHAY (2008) Evaluation of antimicrobial activity of medicinal plant Jatropha podagrica (Hook). Rouman Biotechnol Lett 13(5):3873–3877
24. Thomas S (2016) Pharmacognostic and phytochemical constituents of leaves of Jatropha multifida Linn. and Jatropha podagrica Hook. J Pharmacognosy Phytochem 5(2):243–246
25. Panzu NN, Lengbiye EM, Domondo A, Inkoto CL, Muanyishay CL, Gbolo BZ, Mpiana PT (2020) A review on the Bioactivity and Phytochemistry of Jatropha podagrica Hook Euphorbiaceae. Discov Phytomed 7(4):186–194
26. Golthi V, Kommu J, Ramesh AV (2023) A green and sustainable approach to the fabrication of ZnO nanoparticles via *Jatropha podagrica* leaf extract for effective dye degradation and antibacterial applications. Colloid Polym Sci. https://doi.org/10.1007/s00396-023-05187-x
27. Golthi V, Kommu J (2023) An eco-friendly and sustainable method for producing Fe3O4 nanoparticles using Jatropha podagrica leaf extract for efficient dye degradation and antibacterial uses. Hybrid Adv. https://doi.org/10.1016/j.hybadv.2023.100110
28. Alhalili Z (2022) Green synthesis of copper oxide nanoparticles CuO NPs from Eucalyptus Globoulus leaf extract: adsorption and

design of experiments. Arab J Chem 15(5):103739. https://doi.org/10.1016/j.arabjc.2022.103739
29. Javid-Naderi MJ, Sabouri Z, Jalili A, Zarrinfar H, Samarghandian S, Darroudi M (2023) Green synthesis of copper oxide nanoparticles using okra (Abelmoschus esculentus) fruit extract and assessment of their cytotoxicity and photocatalytic applications. Environ Technol Innov 32:103300. https://doi.org/10.1016/j.eti.2023.103300
30. Benhammada A, Trache D (2022) Green synthesis of CuO nanoparticles using Malva sylvestris leaf extract with different copper precursors and their effect on nitrocellulose thermal behavior. J Therm Anal Calorim 147:1–16. https://doi.org/10.1007/s10973-020-10469-5
31. Shah IH, Ashraf M, Sabir IA, Manzoor MA, Malik MS, Gulzar S, Zhang Y (2022) Green synthesis and characterization of copper oxide nanoparticles using *Calotropis procera* leaf extract and their different biological potentials. J Mol Struct 1259:132696. https://doi.org/10.1016/j.molstruc.2022.132696
32. Yugandhar P, Vasavi T, Jayavardhana Rao Y, Devi UM, P., Narasimha, G., & Savithramma, N. (2018) Cost effective, green synthesis of copper oxide nanoparticles using fruit extract of Syzygium alternifolium (Wt.) Walp., characterization and evaluation of antiviral activity. J Cluster Sci 29:743–755. https://doi.org/10.1007/s10876-018-1395-1
33. Velsankar K, Parvathy G, Mohandoss S, Kumar RM, Sudhahar S (2022) Green synthesis and characterization of CuO nanoparticles using Panicum sumatrense grains extract for biological applications. Appl Nanosci 12(6):1993–2021. https://doi.org/10.1007/s13204-022-02441-6
34. Veisi H, Karmakar B, Tamoradi T, Hemmati S, Hekmati M, Hamelian M (2021) Biosynthesis of CuO nanoparticles using aqueous extract of herbal tea (Stachys Lavandulifolia) flowers and evaluation of its catalytic activity. Sci Rep 11(1):1983. https://doi.org/10.1038/s41598-021-81320-6
35. Rafique M, Tahir MB, Irshad M, Nabi G, Gillani SSA, Iqbal T, Mubeen M (2020) Novel Citrus aurantifolia leaves based biosynthesis of copper oxide nanoparticles for environmental and wastewater purification as an efficient photocatalyst and antibacterial agent. Optik 219:165138. https://doi.org/10.1016/j.ijleo.2020.165138
36. Vasantharaj S, Sathiyavimal S, Saravanan M, Senthilkumar P, Gnanasekaran K, Shanmugavel M, Pugazhendhi A (2019) Synthesis of ecofriendly copper oxide nanoparticles for fabrication over textile fabrics: characterization of antibacterial activity and dye degradation potential. J Photochem Photobiol B Biol 191:143–149. https://doi.org/10.1016/j.jphotobiol.2018.12.026
37. Kumar PV, Shameem U, Kollu P, Kalyani RL, Pammi SVN (2015) Green synthesis of copper oxide nanoparticles using Aloe vera leaf extract and its antibacterial activity against fish bacterial pathogens. BioNanoScience 5:135–139. https://doi.org/10.1007/s12668-015-0171-z
38. Ssekatawa K, Byarugaba DK, Angwe MK, Wampande EM, Ejobi F, Nxumalo E, Kirabira JB (2022) Phyto-mediated copper oxide nanoparticles for antibacterial, antioxidant and photocatalytic performances. Front Bioeng Biotechnol 10:820218. https://doi.org/10.3389/fbioe.2022.820218
39. Hosseini-Koupaei M, Shareghi B, Saboury AA, Davar F, Sirotkin VA, Hosseini-Koupaei MH, Enteshari Z (2019) Catalytic activity, structure and stability of proteinase K in the presence of biosynthesized CuO nanoparticles. Int J Biol Macromol 122:732–744. https://doi.org/10.1016/j.ijbiomac.2018.11.001
40. Andualem WW, Sabir FK, Mohammed ET, Belay HH, Gonfa BA (2020) Synthesis of copper oxide nanoparticles using plant leaf extract of Catha edulis and its antibacterial activity. J Nanotechnol 2020:1–10. https://doi.org/10.1155/2020/2932434
41. Vishveshvar K, Aravind Krishnan MV, Haribabu K, Vishnuprasad S (2018) Green synthesis of copper oxide nanoparticles using Ixiro coccinea plant leaves and its characterization. BioNanoScience 8:554–558. https://doi.org/10.1007/s12668-018-0508-5
42. Velsankar K, Rm AK, Preethi R, Muthulakshmi V, Sudhahar S (2020) Green synthesis of CuO nanoparticles via Allium sativum extract and its characterizations on antimicrobial, antioxidant, antilarvicidal activities. J Environ Chem Eng 8(5):104123. https://doi.org/10.1016/j.jece.2020.104123
43. Singh J, Kumar V, Kim KH, Rawat M (2019) Biogenic synthesis of copper oxide nanoparticles using plant extract and its prodigious potential for photocatalytic degradation of dyes. Environ Res 177:108569. https://doi.org/10.1016/j.envres.2019.108569
44. Nasrollahzadeh M, Sajadi SM, Rostami-Vartooni A (2015) Green synthesis of CuO nanoparticles by aqueous extract of Anthemis nobilis flowers and their catalytic activity for the A3 coupling reaction. J Colloid Interface Sci 459:183–188. https://doi.org/10.1016/j.jcis.2015.08.020
45. Ahamed M, Alhadlaq HA, Khan MM, Karuppiah P, Al-Dhabi NA (2014) Synthesis, characterization, and antimicrobial activity of copper oxide nanoparticles. J Nanomater 2014:17–17. https://doi.org/10.1155/2014/637858
46. Sagadevan S, Vennila S, Marlinda AR, Al-Douri Y, Rafie Johan M, Anita Lett J (2019) Synthesis and evaluation of the structural, optical, and antibacterial properties of copper oxide nanoparticles. Appl Phys A 125:1–9. https://doi.org/10.1007/s00339-019-2785-4
47. Pallela PNVK, Ummey S, Ruddaraju LK, Kollu P, Khan S, Pammi SVN (2019) Antibacterial activity assessment and characterization of green synthesized CuO nano rods using Asparagus racemosus roots extract. SN Appl Sci 1:1–7. https://doi.org/10.1007/s42452-019-0449-9
48. ShayeganMehr E, Sorbiun M, Ramazani A et al (2018) Plant-mediated synthesis of zinc oxide and copper oxide nanoparticles by using ferulago angulata (schlecht) boiss extract and comparison of their photocatalytic degradation of Rhodamine B (RhB) under visible light irradiation. J Mater Sci Mater Electron 29:1333–1340. https://doi.org/10.1007/s10854-017-8039-3
49. Sathiyavimal S, Vasantharaj S, Bharathi D, Saravanan M, Manikandan E, Kumar SS, Pugazhendhi A (2018) Biogenesis of copper oxide nanoparticles (CuONPs) using Sida acuta and their incorporation over cotton fabrics to prevent the pathogenicity of Gram negative and Gram positive bacteria. J Photochem Photobiol, B 188:126–134. https://doi.org/10.1016/j.jphotobiol.2018.09.014
50. Naika HR, Lingaraju K, Manjunath K, Kumar D, Nagaraju G, Suresh D, Nagabhushana H (2015) Green synthesis of CuO nanoparticles using Gloriosa superba L. extract and their antibacterial activity. J Taibah Univ Sci 9(1):7–12. https://doi.org/10.1016/j.jtusci.2014.04.006
51. Nethravathi PC, Kumar MP, Suresh D, Lingaraju K, Rajanaika H, Nagabhushana H, Sharma SC (2015) Tinospora cordifolia mediated facile green synthesis of cupric oxide nanoparticles and their photocatalytic, antioxidant and antibacterial properties. Mater Sci Semicond Process 33:81–88. https://doi.org/10.1016/j.mssp.2015.01.034

Authors and Affiliations

Venkatesh Golthi[1,2,3] · Jayarao Kommu[1,3] · Kiran Kumar Penmethsa[2] · J. Laxmi Mangamma[2]

✉ Venkatesh Golthi
venkatesh@gdcc.ac.in

[1] Andhra University Trans-Disciplinary Research Hub (A.U. TDR-HUB), Visakhapatnam, AP 530003, India

[2] Department of Chemistry, Government Degree College, Chodavaram, AP 531036, India

[3] Department of Chemistry, Wellfare Institute of Science, Technology and Management, Pinagadi, Pendurthi, AP 531173, India